OBSERVATOIRE DE PARIS
NATIONAL & KAPODISTRIAN UNIVERSITY OF ATHENS

ECOLE DOCTORALE
ASTRONOMIE ET ASTROPHYSIQUE D' ILE-DE-FRANCE

Doctorat en co-tutelle
ASTRONOMIE ET ASTROPHYSIQUE

Anezina SOLOMONIDOU

COMPARATIVE STUDY OF THE DIACHRONIC EVOLUTION OF THE GEOLOGICAL AND VOLCANOLOGICAL ENVIRONMENTS OF THE EARTH WITH THE SATURNIAN SATELLITES TITAN AND ENCELADUS

Thesis Supervisors: Athena COUSTENIS
Konstantinos KYRIAKOPOULOS
Xenophon MOUSSAS

Date of Defence: 8 Novembre, 2013

Jury:

President: Stamatios KRIMIGIS
Rapporteurs: Pascal RANNOU
Ioannis DAGLIS
Examiners: Gabriel TOBIE
Jean-Pierre LEBRETON

Acknowledgements

For the completion of this thesis I am forever indebted to my supervisors, Dr. Athena Coustenis, Professor Xenophon Moussas and Professor Konstantinos Kyriakopoulos. I would like, specifically, to express my deepest gratitude towards my mentor, Dr. Athena Coustenis, for continuously motivating me, guiding and supporting me in every possible way. I would not have been able to complete this doctoral course without the time, ideas, scientific experience and encouragement offered and provided by my supervisors.

I would also like to thank the rapporteurs of my PhD thesis (Pascal Rannou and Ioannis Daglis) and the other members of the Jury, for reviewing the manuscript and providing me with comments and suggestions.

I am grateful for all the help and support that I received as a PhD student at the French laboratory of the Paris Observatory 'Laboratoire d'études spatiales et d'instrumentation en astrophysique' (LESIA) and from its Director, Dr. Pierre Drossart. I am proud of being a member of the scientific team of LESIA; to continue being in touch with the lab and its members is one of my top priorities. In addition, it was a great pleasure being a part of the 'Space Physics Group' of the Department of Physics at the University of Athens and I would like to thank my supervisor, Professor Moussas and the members of the group, for their guidance in Physics and the great experiences we shared throughout our Outreach activities. Also, I am thankful for their continuous help, efforts and assistance through this challenging times, in terms of bureaucracy on the 'co-supervision' PhD, to the Secretaries of the Department of Geology and Geoenvironment, Mrs. Evgenia Mastorou and Mrs. Kelly Chorafopoulou.

During this PhD, I worked closely with many scientific teams, and colleagues, from all over the world that helped me overpass problems I faced during my research, provided me with important data, enhanced my scientific background, and offered me the opportunity to work on diverse and exciting projects. For all these reasons, and their aid, I would like to express my sincere thanks to S. Rodriguez of AIM, K. Stephan, F. Sohl, R. Jaumann and. M. Knapmeyer of DLR, G. Tobie and. S. Le Mouélic of LPG, R. H. Brown of LPL, and. R. Lopes and C. Sotin of JPL.

At this point I feel the need to mention my friend and colleague. Mathieu Hirtzig for the countless hours he spent tutoring me and guiding me through the many aspects of my

research and especially for sharing his code and for his patience in helping me learn how to use it. He has my ardent gratitude. Moreover, my sincere thanks to my good friends and fellows, Dr. Karen Stamatelopoulou – Seymour, an inspiring professor of mine from the University of Patras and Mrs. M. Vekri from my school years, G. Bampasidis, E. Bratsolis, G. Xystouris, S. Stamogiorgos, N. Sergis Th. Kouloumvakos and E. Mitsakou with whom we have accomplished many projects as well as enjoyed memorable times.

Finally, I would like to thank my family and, considering this PhD being as a part of me, dedicate it to; my mother Chrysso, who nurtured me with love for science, nature and life, my father Babis, who always supported me spiritually throughout my life, and urged me to always follow my heart, my brother Zak, my amazing grandmother Aleka, and my lovely aunts, Despina and Natassa. I am also grateful for my non-related 'relatives'; the Kaoustou, Tsakiroglou, Katsadouri, Plavoukou and Chatzinikolaou families, who always took great care of me with their love and support.

Last, but certainly not least, particular thanks go out to my special friends and supporters Aspasia and Konstantina, my 'editor' Dimitris Plavoukos, my exceptional friend Dimitris Mouhthis and to all of my unique friends from Milos, Korydallos, Patras, and UCL.

This research has been co-financed by the European Union (European Social Fund – ESF) and Greek national funds through the Operational Program "Education and Lifelong Learning" of the National Strategic Reference Framework (NSRF) - Research Funding Program: Heracleitus II. Investing in knowledge society through the European Social Fund.

Abstract

This thesis presents on the study of the environment of Titan and Enceladus, Saturn's satellites observed by the Cassini-Huygens mission. Various aspects of the geology of Titan are presented focusing on the characteristics of the surface geological features and processes,the internal structure and the correlation with the atmosphere. The morphotectonic features are presented on the basis of terrestrial models. Moreover, Titan areas probably correlated with the interior are tested against a geophysical model of tidal distortion and found to conform with localisation and internal dynamics. We then study the surface albedo and composition of specific Titan areas (Hotei Regio, Tui Regio, Sotra Patera) –determined by the PCA method- based on data from Cassini/VIMS (0.4–5 μm) on which a radiative transfer code is applied with the most updated spectroscopic parameters. Monitoring of these areas showed surface albedo changes in the course of 1-3.5 yrs, implying dynamic exogenic-endogenic processes that affect the surface and compatible with cryovolcanism in the case of Sotra Patera. Processes that form the surface of Enceladus are also discussed. In addition, the analogies with the Earth's surface and possible internal processes on the icy satellites are being explored. The astrobiological implications of this work are discussed within the framework of the quest for habitable environments in our outer Solar system. These studies are related to the preparation of future space missions to the systems of Jupiter and Saturn and payload capability. Finally, public awareness and perspectives of this research are discussed.

Résumé

Cette thèse porte sur l'étude de l'environnement de Titan et Encelade, satellites de Saturne, observés par la mission Cassini -Huygens. On présente différents aspects de la géologie de Titan mettant l'accent sur les caractéristiques de la surface, les processus géologiques, la structure interne et la corrélation et échanges avec l'atmosphère. Les caractéristiques morphotectoniques sont présentées sur la base des modèles terrestres. Des zones de Titan probablement corrélées à l'intérieur sont étudiées avec un modèle géophysique de distorsion des marées et jugées conformes en localisation et dynamique interne. Ensuite on étudie l'albédo de surface et la composition des régions spécifiques sur Titan - déterminées par la méthode PCA - à partir des données de Cassini / VIMS (0,4 à 5 microns) sur lesquelles on applique un code de transfert radiatif mis à jour avec les paramètres spectroscopiques les plus récents. Le suivi temporel de ces zones a montré des changements de leur albédo de surface pendant 1 à 3,5 ans, ce qui implique des processus exogènes-endogènes dynamiques qui affectent la surface et qui est compatible avec du cryovolcanisme. Les processus qui forment la surface d'Encelade sont également discutés. Les analogies avec la surface terrestre et les processus internes possibles sur les satellites de glace sont explorés. Les implications astrobiologiques de ce travail sont discutées en ce qui concerne leur habitabilité. Ces études sont liées à la préparation de futures missions spatiales vers les systèmes de Jupiter et de Saturne et les possibilités de charge utile. Enfin, la sensibilisation du grand public et les perspectives de cette recherche sont discutés.

Περίληψη

Η παρούσα διδακτορική διατριβή αφορά τη μελέτη των περιβαλλόντων του Τιτάνα και του Εγκέλαδου, δορυφόρων του Κρόνου, μέσω της ανάλυσης δεδομένων που ανακτήθηκαν από τη διαστημική αποστολή Cassini-Huygens. Αρχικά παρουσιάζεται η επισκόπηση της γεωλογίας του Τιτάνα, με επίκεντρο τις γεωλογικές δομές και διεργασίες και το συσχετισμό μεταξύ της ατμόσφαιρας, της επιφάνειας και του εσωτερικού του δορυφόρου. Οι μορφοτεκτονικές δομές κατατάσσονται σε συγκεκριμένες κατηγορίες βάσει γήινων μοντέλων σχηματισμού. Επιφανειακές περιοχές του Τιτάνα, οι οποίες θεωρούνται συνδεδεμένες με το εσωτερικό, συγκρίθηκαν με γεωφυσικά μοντέλα παλιρροιακής στρέβλωσης και διαπιστώθηκε ότι συμπίπτουν σε σχέση με τη θέση, την επιφάνεια και την εσωτερική ενεργότητα. Ένα δεύτερο μέρος της διδακτορικής διατριβής παρουσιάζει την ενδελεχή ανάλυση συγκεκριμένων περιοχών του Τιτάνα –όπως αυτές καθορίζονται μέσω μιας στατιστικής μεθόδου– με επίκεντρο την επιφανειακή ανακλαστικότητα που παρουσιάζουν και τη χημική σύνθεση από την επεξεργασία δεδομένων του φασματογράφου Cassini/VIMS (εγγύς υπέρυθρη περιοχή του φάσματος από 0,4 έως 5 micron). Η εφαρμογή ενός εκσυγχρονισμένου και state-of-the-art κώδικα μεταφοράς ακτινοβολίας, επέδειξε τη φασματική συμπεριφορά και το εύρος της φωτεινότητας αυτών των περιοχών. Η έρευνα τριών σημαντικών περιοχών, που έχουν προταθεί ως υποψήφιες κρυοηφαιστειακές (Hotei Regio, Tui Regio και Sotra Patera), παρουσίασε ενδείξεις χρονικής μεταβολής της επιφανειακής ανακλαστικότητας για δύο από αυτές σε μια χρονική περίοδο από 1-3,5 χρόνια, υποδεικνύοντας δυναμικές εξωγενείς - ενδογενείς διεργασίες, οι οποίες επηρεάζουν την επιφάνεια και είναι συμβατές με φαινόμενα κρυοηφαιστεότητας στην περίπτωση της Sotra Patera. Επίσης, οι διαδικασίες που σχηματίζουν την επιφάνεια του Εγκέλαδου περιγράφονται λεπτομερειακά στη διατριβή. Σε ένα τρίτο μέρος, γήινα ανάλογα επιφανειακών εμφανίσεων καθώς και διεργασιών παρουσιάζονται εκτεταμένα, επισημαίνοντας ενδιαφέρουσες ομοιότητες και διαφορές μεταξύ της πυριτικής Γης και των παγωμένων δορυφόρων. Οι αστροβιολογικές συσχετίσεις αυτής της εργασίας διεξάγονται στο πλαίσιο της αναζήτησης περιβαλλόντων κατοικησιμότητας στο εξωτερικό ηλιακό σύστημα. Όλες οι προαναφερθείσες μελέτες συνδέονται με την προετοιμασία των μελλοντικών διαστημικών αποστολών και των οργάνων τους στα συστήματα του Κρόνου και του Δία. Τέλος, συζητούνται οι δυνατότητες εκλαΐκευσης της επιστήμης και οι προοπτικές που παρουσιάζει η συγκεκριμένη έρευνα.

Contents

Foreword

The Solar system and the Saturnian system in particular have been capturing my interest for many years now. My great interest in geology has been triggered since the early years of my life through observations of the environmental scenery of the island that I come from, Milos, which is in the most southwestern position of the islands in the Cyclades group, located in the Aegean Sea in Greece. Milos is a composite, high-enthalpy volcanic field, and is occupying the central part of the Quaternary (volcanic) Aegean Arc.

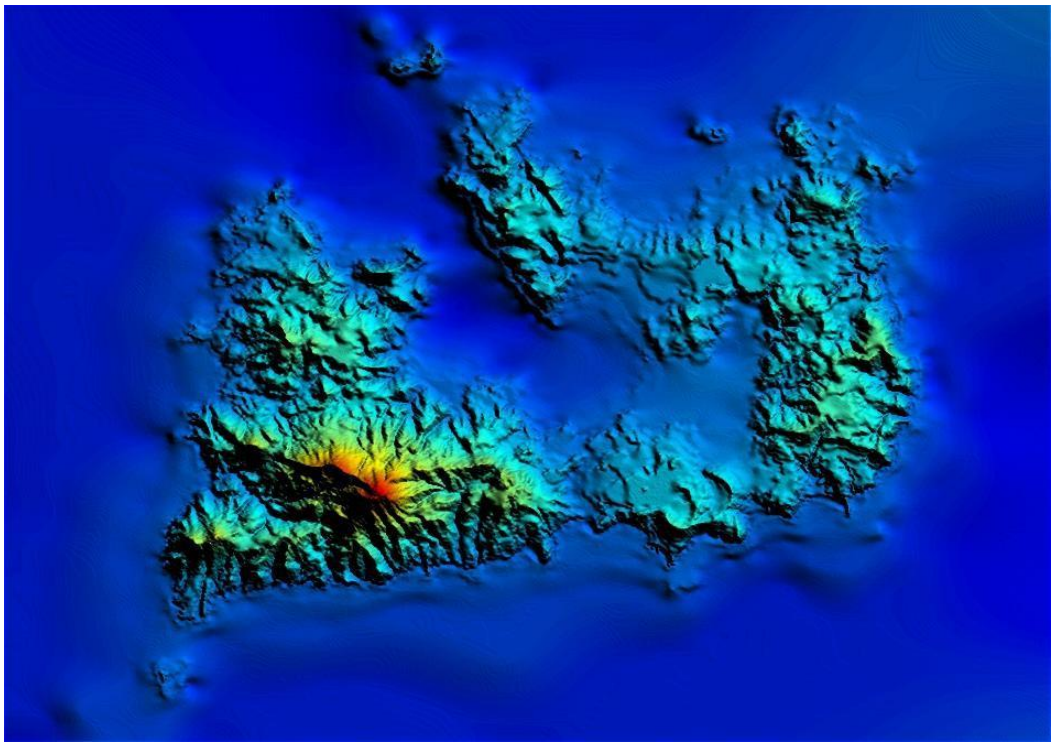

Milos, a volcanic island in the Aegean Sea, Greece. Digital Elevation Dem (DEM) representing the hypsometry of the island from satellite data showing the highest elevation at the mountain Prophet Elias (with red) (Image credit: Volcanology and Petrology Team of U. of Patras; Karen St. Seymour, George Papaioannou, Anezina Solomonidou, Dimitrios Zouzias, Yianna Tsiattalou).

Volcanic activity in the island started 2-3 Myr ago and ceased 90,000 years ago, forming a large variety of rocks and surface expressions. Hence, Milos being an excellent place for geological and volcanological investigations developed my scientific research interest towards this direction.

I obtained my Bachelor's degree in Greece in May 2007, from the University of Patras at the Department of Geology/Faculty of Science. The field that I had chosen, besides an in-depth study of general geology, was that of Volcanology, extended to planetary sciences. My BSc dissertation, resulting from more than 1.5 years of studies

and extensive field work, sample acquisition and laboratory analysis, was on *'Sedimentary and tectonic research of the Saraceneco Basin and the northern portion of Milos island (an integral part of the Apollonia Caldera System) based on the discovery of a caldera and the study of the volcanic activity',* under the supervision of Prof. Karen Stamatelopoulou-Seymour, an expert on Volcanology, Planetary geology and Mineralogy. This research provided me with skills such as field sampling, mapping, stratification modeling (Earth's interior), lab chemical analysis, use of specific software for geophysical analysis and many more.

Moon-like landscape at the Saraceneco bay in the Northern side of Milos. The area is made of volcanic sediments, pumice and fossils.

Prolonging my studies in planetological issues (2007-2008), I got a Master's degree in Science, 'MSc in Geoscience', at the University College London (UCL), UK, from the Department of Earth Sciences/Faculty of Mathematical and Physical Sciences. This Master degree concentration was on a synthesis of geological and planetological courses, in addition to weekly lectures by expert researchers of each field, and I focused on Planetary Geology applied to Saturn's moon, Titan, that presented potential interest for volcanism. One of the main reasons for choosing a 'target' planetary body for my dissertation was the synthesis and the conjecture of time between the great interests that Titan provides, concerning its geological environment (i.e. geology-volcanology, internal characteristics and atmospheric exchanges) and the arrival of Cassini-Huygens in 2004 that provided a wealth of data and unveiled many unknown aspects of Titan. By the time I had started my Master's course in 2007, Cassini and Huygens had already

collected a great number of images, spectroscopic and radar data that required study and extensive analysis.

My Master's dissertation is titled *'Modeling of Volcanic eruptions on Titan'*, under the supervision of Dr. Dominic Andrew Fortes who is an expert on planetary ices and the evolution of icy moons. During this research I investigated Titan's possible cryovolcanism in two isolated areas. I created several 'volcanic eruption' model scenarios in order to look at possible behaviors of the hypothesized cryomagma that covers -and thus forms- the areas. The results limited the number of possible volcanic sources in the areas, and at the same time provided plausible alternatives regarding the deposition of material onto Titan's surface. This study pushed my interest and enthusiasm further into exploring the geology of this satellite as well as other icy moons.

Since then I have pursued my studies of Titan, as well as of the other kronian moon, Enceladus, and their geology during a 4-year PhD program, started in 2009, in a framework of a co-tutelle (joint supervision). I present here my PhD thesis where I try to answer some of the current fundamental questions - arising from the Cassini-Huygens and ground-based observations. I focus mainly on Titan due to the larger amount of data available in respect to Enceladus as well as the many resemblances of Titan's geological features with that of Earth's.

I intend and desire to continue my research on the subject of icy moons of both Saturn and Jupiter in the course of a Post-doc position and to continue to explore the Milos environment during vacation…

Chapter 1

Introduction/context

In this introductory chapter I first provide a brief overview of the Solar system characteristics and formation, focusing on its outer part. I continue with a short presentation of the historical facts concerning the Saturnian system exploration, with an emphasis on Titan and Enceladus, and the related Earth-based observations of the pre-Cassini period. I follow that with a general description of the Cassini mission (with additional description in Chapter 2) and the major findings that have been collected and reached so far, describing briefly in particular, the major aspects of both Titan and Enceladus from measurements concerning their atmospheres, surfaces and interiors. In the chapters that follow in this manuscript, I present the aforementioned aspects in more analytical details.

1.1 Formation of the outer Solar system: Giant Planets and their icy moons

In a schematic and over-simplified representation, the Solar system consists of the Sun, the eight planets and their satellites in orbit around them and other planetary bodies such as asteroids and comets. The planetary system is divided into, the inner planets, which include bodies with rocky and metal composition, and the outer planets, which are mainly composed of gases and ices. The inner and outer planets are also referred as terrestrial planets and gas giants respectively. All four 'giant' planets are surrounded by ring systems, possibly made of debris from the original solar nebula, although only the Saturnian one is the largest and most visible from ground-based observations (Goldstein and Morris, 1973).

The understanding of the formation and evolution of the Solar system has been significantly and unexpectedly grown since the proposition of the nebula hypothesis in the 18th century by Emanuel Swedberg (1688-1772), Immanuel Kant (1724–1804) and later by Pierre-Simon de Laplace (1749–1827), that were based on the original idea put forward by Leucippus and his disciple Democritus back at the 5th century B.C.E., about a vortex of various atoms that rotate to form the Earth, a star or the cosmos, with the heavy atoms going in the centre and the astronomical body heating up as a result of that rotation. This understanding has been achieved from a great amount of Earth and space observations as well as from theoretical modeling based on the development of physics, chemistry, geology and more (e.g. Cameron, 1973; Nakagawa et al. 1986; Duncan et al. 1987; Cyr et al. 1998; Thommes et al. 1999; Grossman and Larimer, 2010). The aforementioned hypothesis[1] suggests that molecular hydrogen clouds (GMC) form the stars through gravitational forces and mutual interactions. A sun-like star formation could take almost 100 Myr. Such a formation process produces a gaseous protoplanetary disk around the newborn star that collapses, leading to the formation of planets, that revolve around the Sun mostly in circular orbits. This disk, during its accretion phase, forms small dust grains of rock and/or ice. The collision of these materials would gradually form the planetesimals[2] whose accretion from the disk's large mass produces the planets (100 Myr – 1 Byr). The planets are formed with a clear dichotomy of characteristics between the terrestrial and the giant planets, depending on their location.

[1] *Most of the information for the formation of the Solar system have been adapted from Coustenis and Ecrenaz (2013) and Montmerle et al. (2006)*

[2] *Dust and ice particles in the Solar nebula considered as building blocks of the planets and satellites*

The planets that are closer to the Sun are, Mercury, Venus, the Earth and Mars, that may have taken from 100 Myr to 1 Byr to form, with relatively small sizes, high densities, solid surfaces and very few satellites in contrast to the giant planets, Jupiter, Saturn, Uranus and Neptune, which are far away from the Sun, several times more massive than the terrestrials, with low densities, thick hydrogenous atmospheres and many satellites. For the formation of planets and their acquired elements, and thus composition, the distance from the Sun and the relative local temperatures based on that distance, played an important role.

Originally, in the protosolar disk, hydrogen was the most abundant element, followed by deuterium, helium, lithium and beryllium, while the heavier elements such as carbon, oxygen and nitrogen were the least in abundance. In the zone between the Sun and 5 Astronomical Units (AU) (frost line) (i.e. terrestrial planets) the temperature was approximately above 200 K and in such high temperatures the lighter elements vaporized, while the remaining rare materials, with high densities such as silicates, oxides and metals. Due to this shortage in material and heavy elements present, only planets similar to Earth's size or smaller could have been formed with thin atmospheres that for most of the terrestrial planet cases, developed further later on from outgassing processing.

The formation of the giant planets on the other hand, is hypothesized in the basic model (which does not consider migration) to have occurred beyond the frost line (5 AU) that is the distance in the Solar nebula from its center (protostar=Sun), where hydrogen, helium, oxygen, carbon and nitrogen compounds (such as water, ammonia and methane), could condense into solid ice grains (Mumma et al. 2003), at temperatures below 200 K. These elements were abundant enough to form large solid nuclei, larger than 10–15 Earth masses, with sufficiently strong gravity fields to pull in or accrete the surrounding nebula, and hence create planets with massive sizes and low densities, the so called the giant planets. These are divided into two different classes, the gas giants (with mass 318 times that of Earth), including Saturn and Jupiter, and the ice giants, Uranus and Neptune (with mass 95 times that of Earth). This distinction has been attributed, among other theories, to their migration in a Solar system 'region' far away from Jupiter and Saturn that the reduced density of the solar nebula and longer orbital times render their formation not possible.

The remaining planetesimals, after the formation of the Solar system as described above, interacted with the giant planets, causing changes in their orbits. In the case of Jupiter and Saturn, both planets were introduced to a 2:1 orbital resonance (see Fig. 1.4 and text) that created a gravitational push that caused Neptune to migrate after Pluto into a zone of dense planetesimals. In brief the scattering and interaction with planets of the planetesimals

managed the inward or outward moving of the giant planets, causing the outward migration of Uranus and Neptune and the inward migration of Jupiter and Saturn into their current positions. Hence, that far away location of Uranus and Neptune, in a less dense region of the disk, affected their accretion; they consist mostly of an icy core (ice giants). On the other hand, Jupiter and Saturn are made of their (primitive) protosolar gaseous components, hydrogen and helium (gas giants).

The giant planets most likely had flattened accretion disks (proto-nebulas), consisting of hydrogen, helium and solid bodies that accreted into the giant planets satellites (e.g. Korycansky et al. 1991). Thus, regular satellites were formed in the equatorial plane of the planets, and others were captured by the large gravity field of the big planetesimals which explains the large number of satellites orbiting the giant planets. Jupiter and Saturn in particular have the largest number of natural satellites (more than 60), while Uranus and Neptune have 27 and 14 respectively.

Hereafter we focus on the gas giants. Saturn is the sixth planet from the Sun in a distance of 10 AU from the Earth. It is the second largest after Jupiter. Saturn is mainly composed of hydrogen while its outer atmosphere contains 96.3% molecular hydrogen and 3.25% helium (e.g. Prinn et al. 1984) and its core is suggested to be small and rocky with many similarities with the Earth's core only denser (Guillot et al. 2009). The ring system that surrounds Saturn consists of nine main rings and three discontinuous arcs, composed mostly of ice particles (containing a few percent of refractory organic solid -tholin) and a small amount of dust rocky debris (e.g. Poulet and Cuzzi, 2002). The rings have been suggested to be composed of remnants from the original solar nebula, or from parts of a destroyed Saturnian moon. The source of the E-ring is attributed to the material exsoluted from the active geysers of Enceladus (see Chapter 8). The satellites of Saturn with confirmed orbits are 62 (confirmed until today). Their sizes range dramatically to less than 1-km (like the Alkyonides: Methone, Anthe, and Pallene), up to a satellite with larger size than that of an actual planet such as Mercury, Titan. The Saturnian moons' physical and orbital characteristics vary widely. Figure 1.1 shows the distances in scale of the major moons from Saturn.

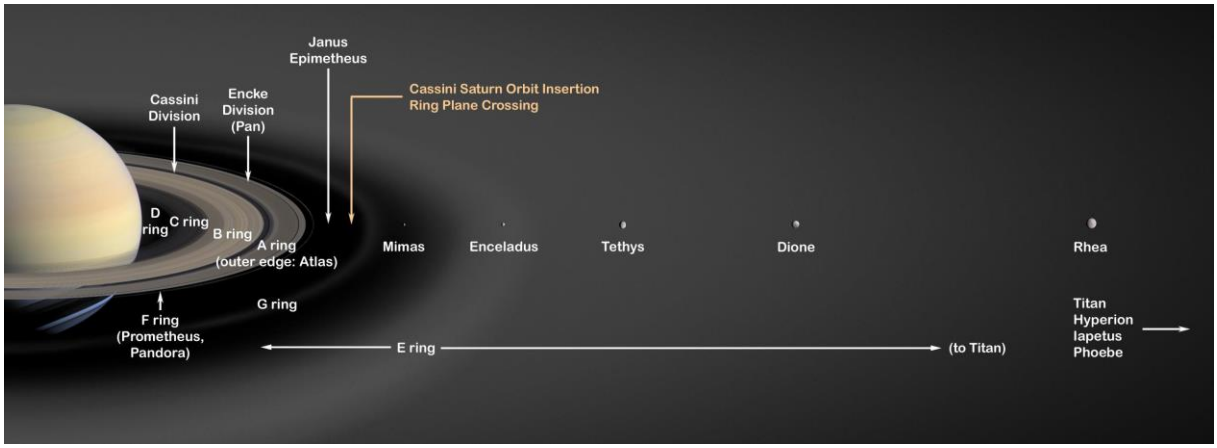

Fig. 1.1 - Schematic view of Saturn's rings and major icy moons (Image credit: NASA/JPL, PIA03550).

Jupiter, on the other hand, is the fifth planet from the Sun and one of its satellites, Ganymede, is the largest in the Solar system. Similar to Saturn, Jupiter also lacks a well-defined solid surface. It primarily consists of hydrogen and helium and a rocky core of heavy elements is hypothesized (Hubbard and Marley, 1989; Saumon and Guillot, 2004). Jupiter counts more satellites than Saturn up today, since the ones with confirmed orbits are 67. The most important ones, in terms of physical characteristics and observations, are the four Galilean satellites[3]. These four major satellites are Io, Europa, Ganymede and Callisto and they orbit in varied distances, orbital periods and inclinations around Jupiter (Fig. 1.2).

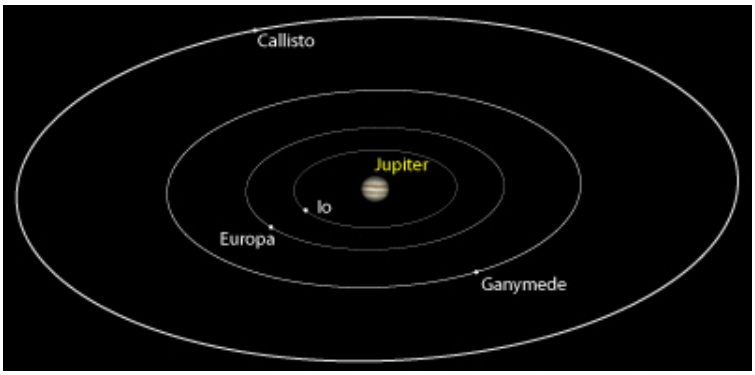

Fig. 1.2 - The orbits of the four Galilean satellites around Jupiter (Image credit: Nick Antony Fiorenza, www.lunarplanner.com).

The differences in composition between the terrestrial planets and the gas-ice giants are present in the compositions of their satellites as well. Thus, the surfaces of terrestrial planet

[3]*Discovered in 1610 by Galileo Galilei and were the first objects that found to orbit a body other than Earth and the Sun.*

satellites, such as the Martian satellite Phobos, on which spectroscopic evidence suggests the presence of a carbonaceous chondrite or phyllosilicate surface (Rivkin et al. 2002; Palomba et al. 2010), comprise mainly of silicates, while the outer Solar system satellites, of ices. Indeed, models of the formation of planetary bodies in our Solar system (4.5 Byr ago) confirm this classification, setting the orbit of Mars as the theoretical boundary between the rocky and icy materials of formation (Weidenschilling, 1977), as pre mentioned. In addition, the large distance of the outer planets from the Sun, in comparison to the distance of the inner ones, limits the amount of solar energy that reaches the surface of the planets and the satellites enabling the sustainability of ice on the surface (e.g. Johnson, 2004). Theoretical assumptions concerning the solar abundance of elements, modeling as well as data analysis, showed that the ice of the outer Solar system bodies will be water, ice, with volatiles such as ammonia, methane (hydrates, clathrates), CO_2 and N_2 (Calvin et al.1997; McCord et al. 1998; Gautier and Hersant, 2004). Thus, a satellite in orbit around a gas giant should be a combination of rock and water ice (Johnson, 2004).

Ground-based, spacecraft observations and data analysis have confirmed the aforementioned, with the only exception of Jupiter's Io. Hence the surface of the satellites of the outer planet system is covered by ice therefore is referred to as 'icy satellites' or 'icy moons'. Some of the major icy satellites are, Jupiter's; Ganymede, and Europa; Saturn's; Titan, Enceladus and Dione; and Neptune's, Triton (Fig. 1.3).

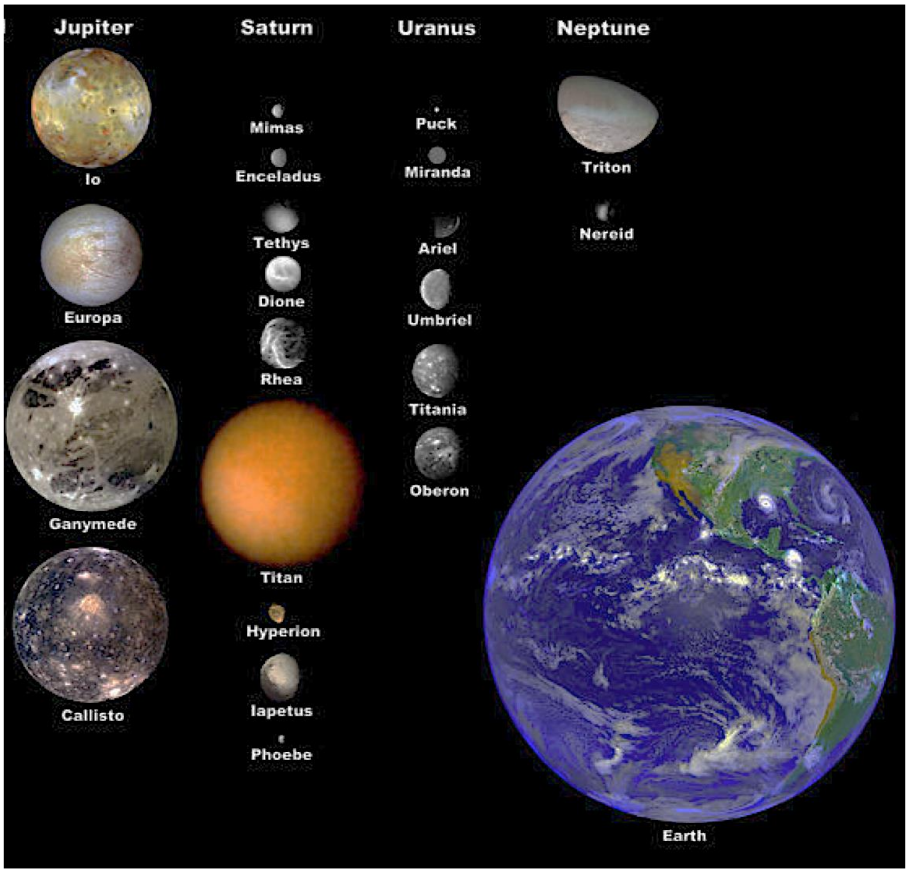

Fig. 1.3 - Major moons of Giant Planets scaled to Earth (Image credit: NASA).

Interior modeling and geophysical data of the icy moons suggest the presence of a compact rocky core, layers of ice, and also assume the presence of a subsurface liquid water ocean for some of the icy moons (e.g. Kargel, 1991; Zimmer et al. 2000). Heat in the interior of several of these bodies is mostly generated by tidal friction, caused by varying gravitational interactions with their hosting planet (Jupiter and Saturn) owing to eccentric orbits (Poirier et al. 1983; Moore and Schubert, 2000). Furthermore, tidal deformation can play an important role in the geological activity and surface formation of the icy moons (e.g. Stevenson, 1987; Schubert et al. 2010). Orbital resonances, such as the Laplace resonance between Io, Europa and Ganymede, or the resonance between Enceladus and Dione, can be a key role maintaining an elevated eccentricity over geological timescales.

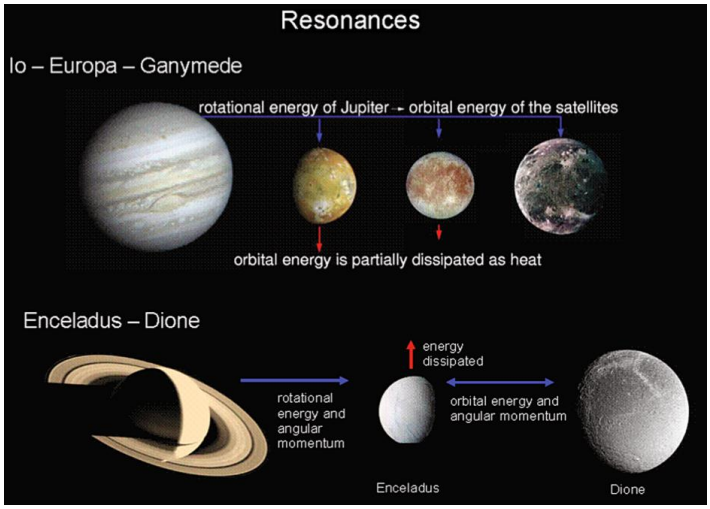

Fig. 1.4 - Orbital periods of Io, Europa and Enceladus locked in resonance involving internal heating due to resonance coupling, energy and angular momentum. The dissipation of heat as part of that energy is caused due to the presence of tidal flexing (Image credit: Schubert et al. 2010).

One distinguishable characteristic among the planets of our Solar system is the existence, or lack of, an atmosphere, and the properties that this veil might have. The same applies to the outer Solar system satellites, which mostly lack an atmosphere, with few exceptions, that of Io, Europa, Enceladus, Titan and Triton. Io has a very thin atmosphere, mainly dominated by sulfur dioxide (SO_2) that originates from the volcanic eruptions. This interaction between the volcanoes and the atmosphere sustain a continuous replenishment of the atmosphere with SO_2, which also supplies Jupiter's magnetosphere with plasma (e.g. Coustenis et al. 2010). In a similar fashion, Enceladus also has a dynamic but more significant atmosphere than Io's, produced by the jets of water vapor that emanates from its southern pole (Dougherty et al. 2006) (see Chapter 8). On the other hand, Europa's atmosphere is very thin and dominated by O_2 and unlike Enceladus and Io it is produced by intense radiation bombardment (e.g. Coustenis et al. 2010). Titan stands out very uniquely in terms of atmospheric properties among the icy satellites. It is the only satellite with a dense, nitrogen-rich and compositionally distinct atmosphere that resembles the terrestrial one in many ways (see § 1.2.1 and 1.4.1.1). Triton also possesses a nitrogen-rich atmosphere, but very teneous.

The main focus of the PhD thesis presented hereafter is the satellites of Saturn and in particular Titan and Enceladus. I have processed and analyzed data that regard specific aspects of both satellites but I also try to present a holistic review of their natural environments, setting the context. In addition, I investigate Jupiter's satellites Europa and Ganymede in terms of interior modeling and comparative planetology.

1.2 Pre-Cassini exploration from the ground and space missions

The gas giants were first observed from the Earth from Babylonian astronomers in the 7th or 8th century BC (Sachs, 1974) and later in 1610 from Galileo Galilei by a refracting telescope (e.g. MacLachlan, 1997). The giant planets Jupiter and Saturn were first viewed from a space mission by the Pioneer 10 spacecraft, which passed by Jupiter on December, 1973 at a distance of 130,000 km and acquired information regarding its atmosphere, radiation field and fluid state (e.g. Ingersoll and Porco, 1978). Pioneer 11[4] then passed by Saturn in September 1979 at a distance of 20,000 km and studied its properties, moons and rings.

After that, the twin spacecrafts Voyager 1 (V1) & 2[5] (V2) were sent to the outer Solar system for a dedicated and thorough investigation. The V1 spacecraft was launched in 1977 and passed by Jupiter, then Saturn, then Uranus and on August 2nd, 2013 reached a distance of 125 AU from the Sun.

Hereafter I concentrate on the early exploration of Titan and Enceladus.

1.2.1 Titan

Saturn's largest satellite, Titan, with a mean radius of 2,576 km (2/5 of the Earth's size), is the second in size among the satellites of our Solar system after Jupiter's Ganymede. This icy moon has been discovered by the Dutch astronomer Christiaan Huygens on March 25, 1655. Titan orbits Saturn at a distance of 1.2 million km (759,220 mi) in a synchronous rotation. It takes 15.6 days to complete a full orbit while 1 Titan year is almost equal to 30 terrestrial years. Titan receives 1% of sunlight in comparison to Earth. Its surface temperature is about −179.2 °C (94 K). The atmosphere is nearly free of water vapor since at this temperature water ice has an extremely low vapor pressure. However, water vapor was detected by the Infrared Space Observatory (ISO) in 1997 (Coustenis et al. 1998).

In our Solar system, Earth, Venus, Mars and Titan are the only planetary bodies that have both a solid surface and a substantial atmosphere. Therefore, Titan is the only natural large satellite in the Solar system that holds these characteristics, making it fascinating for investigation. The presence of Titan's substantial atmosphere was first reported back in 1908 when the Catalan astronomer Jose Comas i Solá observed a limb-darkening (Comas Solá,

[4] *A description on the Pioneer 11 mission can be found at Fimmel et al. (1974).*
[5] *Detailed description on Voyager 1 and 2 instruments can be found at Space Science Reviews, Special Voyager instrumentation issue, vol. 21(2): 75-232, 1977.*

1908). The thickness of the atmosphere, which is about 1.19 times as massive as Earth's in general, forces Titan to subtend 0.8 arcsec in the sky, something that in the early days of exploration mislead the astronomer John Herschel to name the satellite 'Titan' after the Greek primeval race of powerful deities which were children of Gaia (Goddess of Earth) and Uranus (God of the sky) and were distinguished due to their gigantic size. The Voyager mission clarified the situation by proving that Ganymede is a few kilometers larger (2,634 km –mean radius).

Titan's atmosphere resembles that of Earth's due to its major constituent of N_2 and of the general atmospheric environment that hosts a complex organic chemistry based on the photochemistry between N_2, CH_4, H_2 and more. The persistence of a dense atmosphere on Titan is a complex issue, especially due to the satellite's weak gravity and small size, which should have left Titan with a negligible atmosphere similar to that of Callisto or Ganymede. However, as stated by Sir James Jeans in 1925, Titan kept a substantial atmosphere due to the preservation of a number of constituents, which could have been present in the proto-solar nebula like ammonia, argon, neon, molecular nitrogen and methane (Jeans, 1925). Later studies showed that ammonia is absent from the atmosphere (converted to N_2 during Titan's warmer past) but present in its solid phase due to Titan's temperature. Nevertheless, the second most abundant constituent, which is methane (from 4.9% at the surface to 1.5% in the stratosphere, Niemann et al. 2010), is in gaseous phase at present Titan's atmospheric temperature range and, unlike molecular nitrogen, exhibits strong absorption bands in the infrared. Gerard Kuiper of Chicago University first detected these bands in 1944 (Kuiper 1944).

Before the Pioneer 11, Voyager 1 & 2, and Cassini-Huygens observations, two main atmospheric models existed. The first suggested methane instead of nitrogen as the most abundant component up to 90% and surface P, T surface conditions of 20 mbar and 86 K respectively (Danielson et al. 1973; Caldwell, 1977). The second, and more accurate, based on the later discoveries on the atmospheric composition, suggested the production of molecular nitrogen from the dissociation of ammonia with surface temperature at 200 K and pressure at 20 bars (Lewis, 1971, Hunten, 1977). The latter suggest the contribution of nitrogen into a global greenhouse effect. Sagan in 1973 indicates in his study, the significance of a greenhouse effect on Titan. Another climate phenomenon is also present on Titan, which is unique and only occurs in this Saturnian moon and concerns an anti-greenhouse effect. The greenhouse phenomenon keeps 90% of the energy at the surface of Titan as a result of the density of the atmosphere and the presence of nitrogen, methane and hydrogen while the anti-

greenhouse absorbs light in but prohibits infrared due to the presence of haze layers in the atmosphere (McKay et al. 1991).

Ground-based observations and modeling provided a first but essential knowledge regarding Titan, showing also the need for *in situ* exploration and study. During the next decades space missions would unveil the mystery of Saturn, its moons and rings.

The Pioneer 11[6] spacecraft passed by Titan on September 2, 1979 at a distance of 363,000 km and acquired information regarding its radius (Smith, 1980). After that, the V1 spacecraft had a closest approach to Titan (6,970 km) on November 12, 1980 (Fig. 1.5), while V2 flew over Titan nine months later at a much greater distance (663,400 km).

Fig. 1.5 - Titan's thick haze layer as captured by Voyager 1 VG ISS Narrow angle camera. The image was taken on November 12, 1980 at a distance of 435,000 km (Image credit: NASA/JPL –PIA02238).

As seen in Figure 1.5 the surface is not visible and the currently known and observed exciting world was covered, at that moment, under the dense and hazy atmosphere of Titan. Figure 1.6 shows image data from Pioneer 11, V1 and V2 missions, with the only visible difference throughout the globe being the detached haze layers, the dark polar hood and the brightness difference of the two hemispheres that is known as the north-south asymmetry (NSA). This asymmetry is possibly related to atmospheric circulation phenomena (Sromovsky et al. 1981).

[6] *A description on the Pioneer 11 mission can be found at Fimmel et al. (1974).*

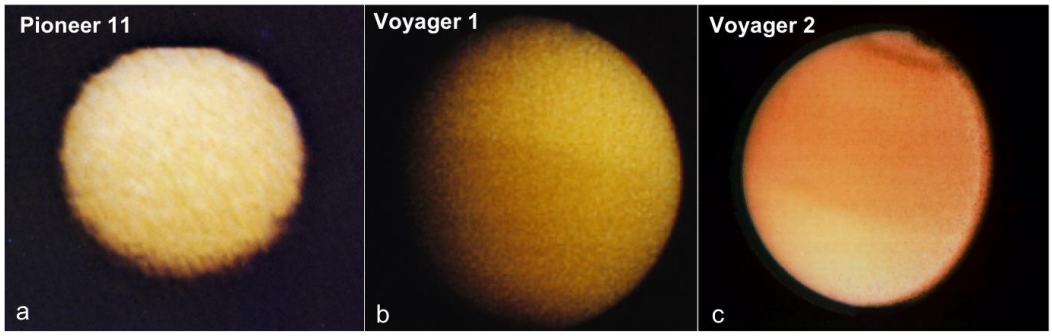

Fig. 1.6 - Images of Titan as captured by Pioneer 11 (1979), Voyager 1 (1980), and Voyager 2 (1981). (a) First close up image of Titan from the compilation of 5 images acquired by Pioneer 11 at a distance of 360,000 km on September 2, 1979. The only detection at that time was the possible existence of clouds (NASA). (b) Image in visible light from the cameras of Voyager 1 from a distance of 4,000 km in 1980 showing again only Titan's clouds (NASA). (c) Voyager 2 RGB composite of Titan, from a distance of 2.3 million km taken on August 23, 1981 (NASA). At this point, the extended haze, composed of submicron-size particles, surrounds the satellite's limb.

In addition to the images (Fig. 1.6) acquired during the first close up capturing of Titan, the radio-occultation experiment from the Radio Science Subsystem (RSS) and infrared spectrometer (IRIS) data from Voyager, provided information concerning the orbital and physical characteristics of the satellite (e.g. Hanel et al. 1981; Lindal et al. 1983), (Table 1.1). Titan's surface radius was found to be 2,575 ± 2 km, with a surface temperature of 94 ± 2 K and a pressure of about 1.44 bar, values that were later confirmed by the Cassini-Huygens measurements (e.g. Smith et al. 1982).

Table 1.1 - Orbital and Physical Parameters of Titan (Information from NASA/ESA[7]).

TABLE 1.1	**Titan's Orbital and Physical Characteristics**
Surface radius	2,575 km
Mass	1.35 × 1023 kg (= 0.022 × Earth)
Mean density	1880 kg m^{-3}
Distance from Saturn	1.2 x 10^6 km
Distance from Sun	9.5 AU
Orbital period	15.95 days
Revolution around Sun	29.5 years
Equatorial surface gravity	1.352 m/s²
Mean surface temperature	93.6 K
Surface pressure	1.467 bar
Inclination (degrees)	0.33
Eccentricity	0.0292

[7] *Information adapted from JPL HORIZONS solar system data and ephemeris computation service: http://ssd.jpl.nasa.gov/horizons.cgi#top.*

Additionally, Voyager 1 took IR measurements of the atmosphere of Titan detecting molecular N_2 as the major component, CH_4, C_4H_2, HC_3N, C_2N_2 and traces of hydrogen (e.g. Kunde et al. 1981; Lindal et al. 1983). Moreover, pre-Cassini models, Pioneer 11 and Voyager images indicated aerosol radii between 0.2-0.5 μm (e.g. Tomasko et al. 1982) and the presence of opaque haze layers (Fig. 1.5). Hence, from the beginning of Titan's exploration with spacecraft missions, it was known that the atmosphere is opaque at many wavelengths and a complete reflectance spectrum of the surface is impossible to acquire from orbit.

After the Pioneer 11 and the Voyager missions, ground-based and observatory measurements were acquired at the Canada France Hawaii Telescope (CFHT), the Very Large Telescope (VLT), the Hubble Space Telescope (HST), the ISO and the Keck Telescope providing complementary information on Titan's system. The Cassini-Huygens mission arrived 25 years after the Voyagers and stands as an extremely successful mission organized by ESA and NASA and 17 contributing countries (see § 1.3, 1.4, Chapter 2).

A missing methane reservoir that would have replenished the atmosphere, since its preservation limit is 10-30 Myr (Yung et al. 1984; Atreya et al. 2006; Atreya, 2010), hinted a presence of a surface global deep ocean, several kilometers in depth, consisting of dissolved ethane and nitrogen (Flasar 1983, Lunine et al. 1983). This assumption has been since then refuted by ground and spacecraft observations that showed that the surface of Titan is not covered by a global liquid ocean nor is homogenous as shown from the ground-based observations by the Very Large Array (New Mexico) radio-telescope, that indicated a significant surface variability with the main constituent being 'dirty' ice (Muhleman et al. 1990). The presence of 'dirty ice', meaning ice combined with tholins or other organic material, was confirmed by Griffith et al. (1991) at the Infrared Telescope Facility (IRTF) and modeled by Coustenis et al. (1995) at the CFHT, through the use of methane windows in the near infrared, which facilitate a probing of various atmospheric levels down to the surface (a detailed description on methane windows can been found at Chapter 6). Additional ground-based observations from the Hawaiian telescopes on Mauna Kea, confirmed the heterogeneity of the surface (Griffith, 1993, Coustenis et al. 1991, 1995, Combes et al. 1997), something that was further supported by HST observations (Smith et al. 1996). Albedo variations have also been reported by Steward Observatory and the Multiple Mirror Telescope data (Lemmon et al. 1993), while in 2001 and 2002 Arecibo data indicated areas of specular reflections, similar to small lake-like features (Campbell et al. 2003). Using these data, models concerning the presence of liquids on the surface have changed, suggesting the presence of

small surface liquid basins (Dermott and Sagan, 1995). Moreover, the CFHT acquired albedo data (1991-1996) showing the presence of a water-ice and tholins mixture on the surface of Titan (Coustenis et al. 1995), while the VLT suggested the presence of ammonia ice (Lellouch et al. 2003) (Fig. 1.7).

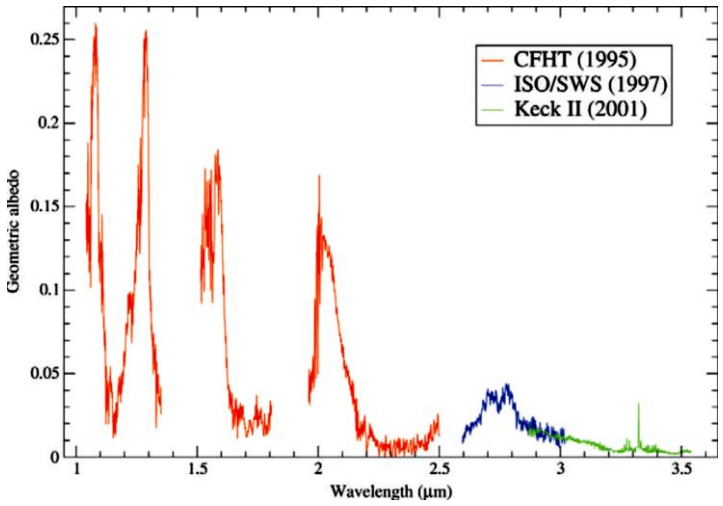

Fig. 1.7 - Titan's albedo as retrieved from data ground-based observatories from the Canada France Hawaii Telescope (CFHT) (red color), the Keck Telescope in Hawaii (green color), and ISO (blue color). The spectrum exhibits several strong methane absorption bands, but also 'windows' where the methane absorption is weak enough to allow for the lower atmosphere and surface to be probed (Graph credit: Negrao et al. (2006) and Coustenis et al. (2006)).

In chronological order observations from, the Hubble Space Telescope (HST) in 1994 (Smith et al. 1996) and 1997-1998 (Meier et al. 2000), the speckle interferometry from Keck Telescope in 1996-1998 (Gibbard et al. 1999, Gibbard et al. 2004) and adaptive optics from CFHT in 1998 (Coustenis et al. 2001), from VLT in Chile (VLT) in 2002 (Gendron et al. 2004), from combination of CFHT and VLT data during 2001-2004 (Coustenis et al. 2005) and from W.M. Keck II telescope within 2001-2003 (Roe et al. 2004), revealed the heterogeneous nature of the surface and showed that dark and bright regions consist of different ice components.

The surface of Titan has long been studied with various remote sensing instruments and ground-based adaptive optics systems (Coustenis et al. 2005). Images derived from the HST planetary camera through the methane windows at 0.94 and 1.08 μm, created the first near-infrared global maps of Titan showing for the first time the surface diversity (Fig. 1.8) (Smith et al. 1996). This diversity is reflected on the bright leading and the dark trailing sides, with a massive bright area (currently known as Xanadu) located at 114°E, 10°S and a number of, varied in size, distinct dark regions which are nowadays known to be hydrocarbon lakes (Smith et al. 1996).

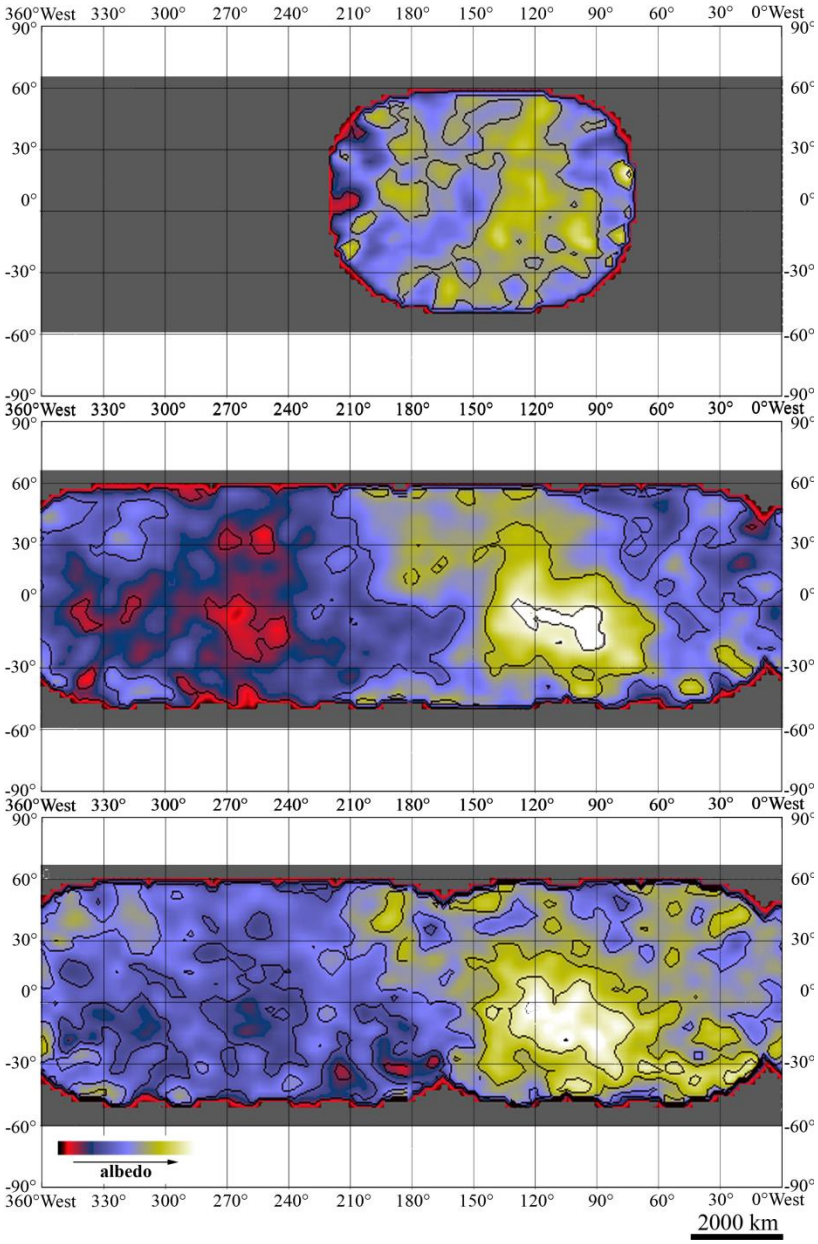

Fig. 1.8 - Albedo heterogeneities on Titan's surface as derived from HST observations. (upper) F673N use of filter; (center) F850LP, and (lower) F1042M, which are sensitive in the red light, as well as in the methane windows at 0.94 and 1.04 μm (Smith et al. 1996).

1.2.2 Enceladus

Enceladus is the sixth largest satellite of Saturn with a mean radius of 505 km. It was discovered by the German astronomer Frederick William Herschel in 1789 and named after the Giant Enceladus; the generator of earthquakes according to the Greek mythology. Even though it is a relatively small satellite, it presents an extremely interesting and rare phenomenon in the Solar system, such as internal activity expressed as water jets. Other than

Enceladus, the only observed recent eruptions in the Solar system are limited to Earth and two other locations: 1) Io, moon of Jupiter and 2) Triton, moon of Neptune.

Enceladus orbits Saturn at a distance of 238,000 km (147,886 mi) in a synchronous rotation and its orbital period is 1.37 days. The mean surface temperature reaches only -198 °C (75 K) because of Enceladus' visual geometric albedo of 1.38, which ranks it as the most reflective surface of a planetary body in the Solar system (Verbiscer et al. 2007).

Prior to the Space Age[8], a limited knowledge was offered from ground-based observations such as estimations of its density (~1.6 g/cm³), mass (~1.08 $\times 10^{20}$ kg), and albedo (~1). Enceladus' nearness to the bright rings and Saturn itself in addition to its faint apparent magnitude (11.7 m), hinders Earth-based observations (Herschel, 1795) and as a result, limits the amount of data and observations offered before the Voyager missions.

Unlike Titan, that possesses a thick and dense atmosphere difficult to penetrate for observation, Enceladus is airless (thin atmosphere). Due to that, the Voyager 1 spacecraft, which was the first to fly over Enceladus (November 12, 1980), provided images that even though of very poor spatial resolution, unveiled the general geological set of the moon that was greatly expanded later with the Cassini-Huygens mission. The Voyager 1 observations confirmed that Enceladus is enclosed in Saturn's E-ring (Terrile and Cook, 1981). This was also confirmed from Earth-based observations with a Charge Coupled Devices (CCD) system attached to the 1.8 m Perkins reflector at Lowell Observatory (Baum et al. 1981). Implications concerning the relation of Enceladus with the E-ring were concentrated on the inferred short lifetimes of the ring's particles, suggesting a geyser-like activity as the material source (Haff et al. 1983, Pang et al. 1984). Furthermore, the discovery of the Enceladus neutral OH cloud enhanced the theories in favor to exchange processes (Shemansky et al. 1993; Jurac et al. 2001).

Voyager 2, on August 26, 1981, approached Enceladus closer than Voyager 1 and captured higher-resolution images from the satellites but did not provide any information on its internal structure. These higher resolution images showed that the moon consists of various geological terrains with different ages (Fig. 1.9). Smith et al. (1982) after Voyager 2 image analysis stated that 'Enceladus' surface ranges from old, densely cratered terrain to relatively young, uncratered plains crossed by grooves and faults'. The authors of this study also noted the extremely high albedo of the moon's surface, the highest of any solid body in the Solar system. The youthful terrain, suggestive of active geological phenomena, was unexpected for

[8] *A website dedicated to the Space Age can be found here: http://www.nasa.gov/externalflash/SpaceAge/*

such small, frozen and airless planetary body and the results from Voyager 1 and mainly Voyager 2 came as a great surprise (Fig. 1.9).

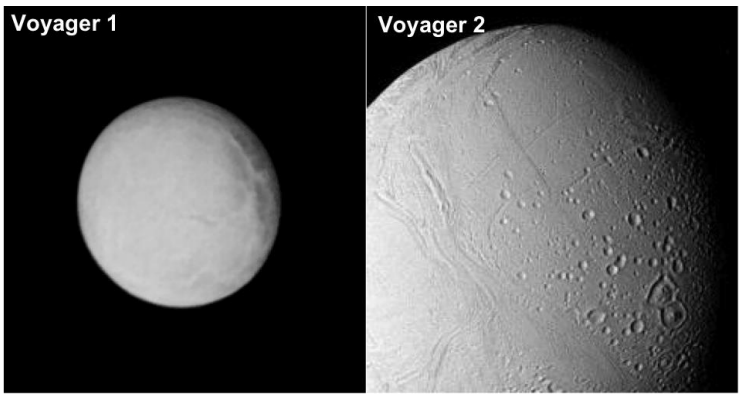

Fig. 1.9 - Voyager 1 & 2 images of Enceladus. (left) Voyager 1 images Enceladus from a distance of 202,000 km (125,500 mi) on November 12, 1980 (Image credit: NASA/JPL). (right) The Voyager 2 ISS narrow-angle camera highest-resolution image of Enceladus acquired on August 25, 1981 at a closer distance of 112,000 km (69,500 mi) showing the surface variability with rough (cratered) and smooth terrains (Image credit: NASA/JPL).

During the years of exploration from Voyager 1 to just before Cassini-Huygens, a wealth of data had been acquired and analyzed by a number of studies. The basic characteristics of the moon are presented in Table 1.2 while in § 8, I present a detailed description of the current state of the investigation of Enceladus.

Table 1.2 - Orbital and Physical Parameters of Enceladus (Information from NASA/ESA[9]).

TABLE 1.2	**Enceladus' Orbital and Physical Characteristics**
Surface radius	252 km
Mass	1.2 x 1020 kg (=1.8×10^{-5} Earths)
Mean density	1609 kg/m³
Distance from Saturn	237,378 km
Distance from Sun	9.5 AU
Orbital period	32.8 hours
Revolution around Sun	29.5 years
Equatorial surface gravity	0.114 m/s²
Mean surface temperature	75 K

[9]*Information adapted from "JPL HORIZONS solar system data and ephemeris computation service: http://ssd.jpl.nasa.gov/horizons.cgi#top.*

1.3 The Cassini mission

The information in regards to Titan and Enceladus from the ground-based observations, the Pioneer 11 and Voyager 1 & 2 missions, emerged the need for a more analytical and *in situ* exploration of these two fascinating planetary worlds. Based on the scientific questions that all the observations raised and the need for a future mission with more enhanced instrumentation than Voyagers' and more capabilities, the idea for the Cassini-Huygens[10] mission was born. This National Aeronautics and Space Administration (NASA), European Space Agency (ESA) and Agenzia Spaziale Italiana (ASI) mission, consisting of the Cassini orbiter and the Huygens probe, is designed, built and managed by teams from sixteen European countries and the United States. Table 1.3 summarizes the orbiter and probe instruments as per their name and main goal and more details on the instruments can be found in Chapter 2.

Table 1.3 - Cassini and Huygens instrumentation and their scientific goals (Information from ESA, NASA and Matson et al. 2012, Space Science Reviews 104:1–58, 2002).

The Cassini orbiter		
Instrument	**Principal Investigator (PI)**	**Scientific objective**
Optical remote-sensing instruments		
Composite Infrared Spectrometer (CIRS)	V. Kunde (PI), NASA Goddard Space Flight Center	Temperature and composition of surfaces, atmospheres, and rings within the Saturn system
Imaging Science Subsystem (ISS)	C. Porco (TL), University of Arizona	Multispectral imaging of Saturn, Titan, rings, and the icy satellites to observe their properties
Ultraviolet Imaging Spectrograph (UVIS)	L. Esposito (PI), University of Colorado	Spectra and low resolution imaging of atmospheres and rings for structure, chemistry, and composition
Visual and Infrared Mapping Spectrometer (VIMS)	R. Brown (TL), Jet Propulsion Laboratory	Spectral mapping to study composition and structure of surfaces, atmospheres, and rings
Radio remote-sensing instruments		
Radar Mapper (RADAR)	C. Elachi (TL), Jet Propulsion Laboratory	Radar imaging, altimetry, and passive radiometry of Titan's surface
Radio Science Subsystem (RSS)	A. Kliore (TL), Jet Propulsion Laboratory	Study of atmospheric and ring structure, gravity fields, and gravitational waves

[10] *A detailed description on the mission and spacecraft can be found at The Cassini-Huygens Mission, Orbiter In Situ Investigations. Edited by C.T. Russell, University of California, California, U.S.A. Reprinted from Space Science Reviews, volume 114, nos. 1-4, 2004.*

Particle remote-sensing instruments and in situ measurement instrument		
Magnetospheric Imaging Instrument (MIMI)	S. Krimigis (PI), Applied Physics Laboratory	Global magnetospheric imaging and in situ measurements of Saturn's magnetosphere and solar wind interactions
In situ measurement instruments		
Cassini Plasma Spectrometer (CAPS)	D. Young, Southwest Research Institute	In situ study of plasma within and near Saturn's magnetic field
Cosmic Dust Analyzer (CDA)	E. Grün (PI), Max Planck Institut für Kernphysik	In situ study of ice and dust grains in the Saturn system
Dual Technique Magnetometer (MAG)	D. Southwood (PI), Imperial College	Study of Saturn's magnetic field and interactions with the solar wind
Ion and Neutral Mass Spectrometer (INMS)	H. Waite (TL), Southwest Research Institute	In situ compositions of neutral and charged particles within the Saturn magnetosphere
Radio and Plasma Wave Science instrument (RPWS)	D. Gurnett (PI), University of Iowa	Measure the electric and magnetic fields and electron density and temperature in the interplanetary medium and within the Saturn magnetosphere
The Huygens Probe		
Instrument	**Principal Investigator (PI)**	**Scientific objective**
Doppler Wind Experiment (DWE)	M. Bird (PI), Universität Bonn	Study of winds from their effect on the Probe during the Titan descent
Huygens Atmospheric Structure Instrument (HASI)	M. Fulchignoni (PI), Observatoire de Paris-Meudon	In situ study of Titan atmospheric physical and electrical properties
Descent Imager/Spectral Radiometer (DISR)	M. Tomasko (PI), University of Arizona	Temperatures and images of Titan's atmospheric aerosols and surface
Gas Chromatograph Mass Spectrometer (GCMS)	H. Niemann (PI), NASA Goddard Space Flight Center	In situ measurement of chemical composition of gases and aerosols in Titan's atmosphere
Aerosol Collector and Pyrolyser (ACP)	G. Israel (PI), CNRS, Service d'Aeronomie	In situ study of clouds and aerosols in the Titan atmosphere
Surface Science Package (SSP)	J. Zarnecki (PI), University of Kent	Measurement of the physical properties of Titan's surface

The Cassini–Huygens spacecraft (5,650 kg) was launched successfully on October 15, 1997, from the Kennedy Space Center at Cape Canaveral at 4:43 a.m. EDT. The spacecraft used gravitational assists to gain the required energy to reach the Saturnian system. It first looped two times around the Sun, then around Venus (April 26, 1998, and June 24, 1999), Earth (August 18, 1999), and Jupiter (December 30, 2000) until reaching its target system on July 1st, 2004 (Fig. 1.10).

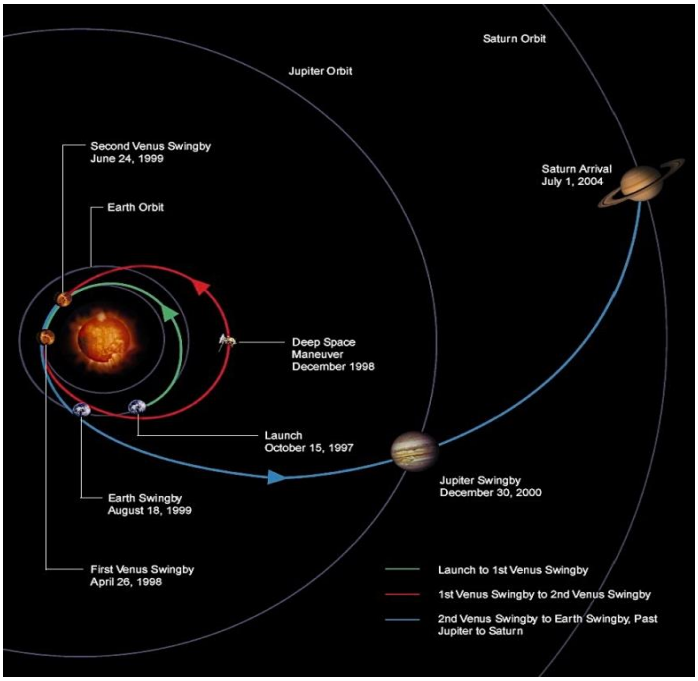

Fig. 1.10 - Gravitational assists of Cassini-Huygens on its way to the Saturnian system (Image credit: NASA/JPL).

Cassini then got into Saturn's orbit by achieving a flawless Saturn Orbit Insertion (SOI) (Fig. 1.11) on July 1st, 2004.

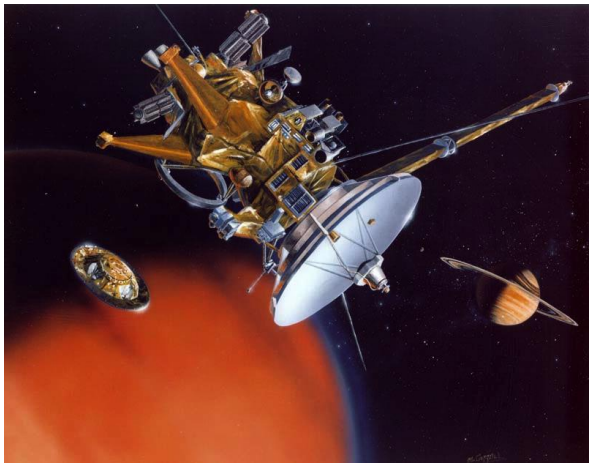

Fig. 1.11 - Artistic view of the Cassini Orbiter and Huygens Probe in the Saturnian system (Image credit: NASA/JPL).

Few months later, on December 25, 2004, the Huygens probe was separated from the orbiter at 02:00 UTC and reached Titan on January 14, 2005, where successfully returned data to Earth (Fig. 1.12). This landing was the first ever accomplished in the outer Solar system.

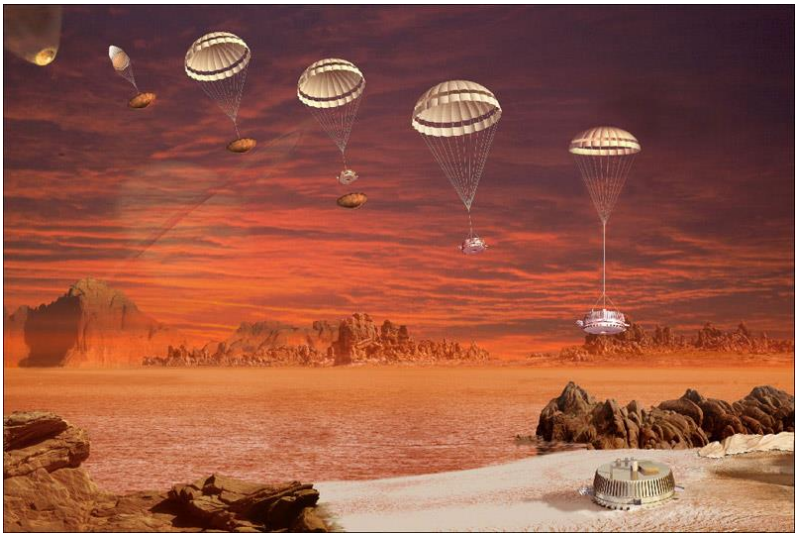

Fig. 1.12 - Artistic view of the descent of the Huygens probe in Titan's atmosphere and its landing (the real landing site is different from that depicted here). The three parachutes reduced the speed to about 5 m/s on the surface. The total descent lasted 2 h 28 mnm and the probe spent 1 h 12 mn on the surface. The signal from Huygens received on Earth also via radiotelescopes was during a total of 5 h 42 mn including 3 h 14 mn on the surface (Image credit: NASA/JPL/ESA).

As well as measuring the atmosphere and surface properties, the probe took samples of the haze and gases. These *in situ* measurements complement the remote-sensing data recorded from the orbiter. The Cassini instruments have since then returned a great amount of data concerning the Saturnian system. It will continue its operation until 2017. During its mission so far, the Cassini orbiter has made several flybys around the Saturnian icy moons and in particular more than 93 flybys of Titan (up to 2013), some as close as 54 km from the surface of Enceladus and 880 km from the surface of Titan (Voyager 1 flew by at 4,400 km).

Cassini performs direct measurements with the visible, infrared, and radar instruments designed to perform remote and *in situ* studies of elements of Saturn, its atmosphere, moons, rings, and magnetosphere. One set of instruments studies the temperatures in various locations, the plasma levels, the neutral and charged particles, the surface composition, the atmospheres and rings, the solar wind, and even the dust grains in the Saturn system, while another performs spectral mapping for high-quality images of the ringed planet, its moons, and its rings. A detailed description of the mission, spacecraft and instruments can be found in the following Chapter 2.

In general, the mission is divided into 4 phases, the Cruise Phase (including the Jupiter Flyby -December, 2000-January, 2001), the Prime Mission (including the Huygens Probe Landing -March, 2004-July, 2008), the Equinox Mission (July, 2008-October, 2010) and the Solstice Mission (October 2010-September 2017).

1.4 Brief overview of the major findings by the Cassini-Huygens mission about Titan and Enceladus

The Cassini-Huygens mission stands as one of the most successful and remarkable space missions in the history of the Space Age both for its technological achievements and its scientific findings. Some of the mission's technological breakthroughs are considered the following; (a) the large amount of planetary body flyby maneuvers (high-precision Cassini/Huygens separation maneuvers), which are the most a planetary mission has ever performed; (b) the successful entry, descent and landing on Titan of the Huygens probe, the first in an outer Solar system body that included a parachute deployment at supersonic speed; and (c) the sufficiently robust design to put up with unknown elements, especially atmospheric. In terms of scientific achievements, the mission's highlights can be summarized in; (a) the discovery of Saturnian new moons and rings; (b) the observation of Enceladus' water vapor and icy jets; (c) the observation of the evolution of a massive storm in Saturn's northern hemisphere; and (d) the revelation of unexpectedly new characteristics concerning Titan from *in situ* and remote sensing instrumentation that in addition to Enceladus' findings from Cassini I will discuss hereafter.

The Cassini-Huygens mission has provided a wealth of data and will continue until its foreseen termination in 2017, with a view to unveil in a larger depth the properties and nature of Titan and Enceladus' worlds. The current understanding of the nature of both satellites had largely and unexpectedly (for some issues) been enhanced by the discoveries of Cassini-Huygens that followed up the Voyager missions. An example of the development of the data in terms of resolution and information between Voyager 1 & 2 (1980-1981) and Cassini (2004) can be seen in Fig. 1.13 and 1.14.

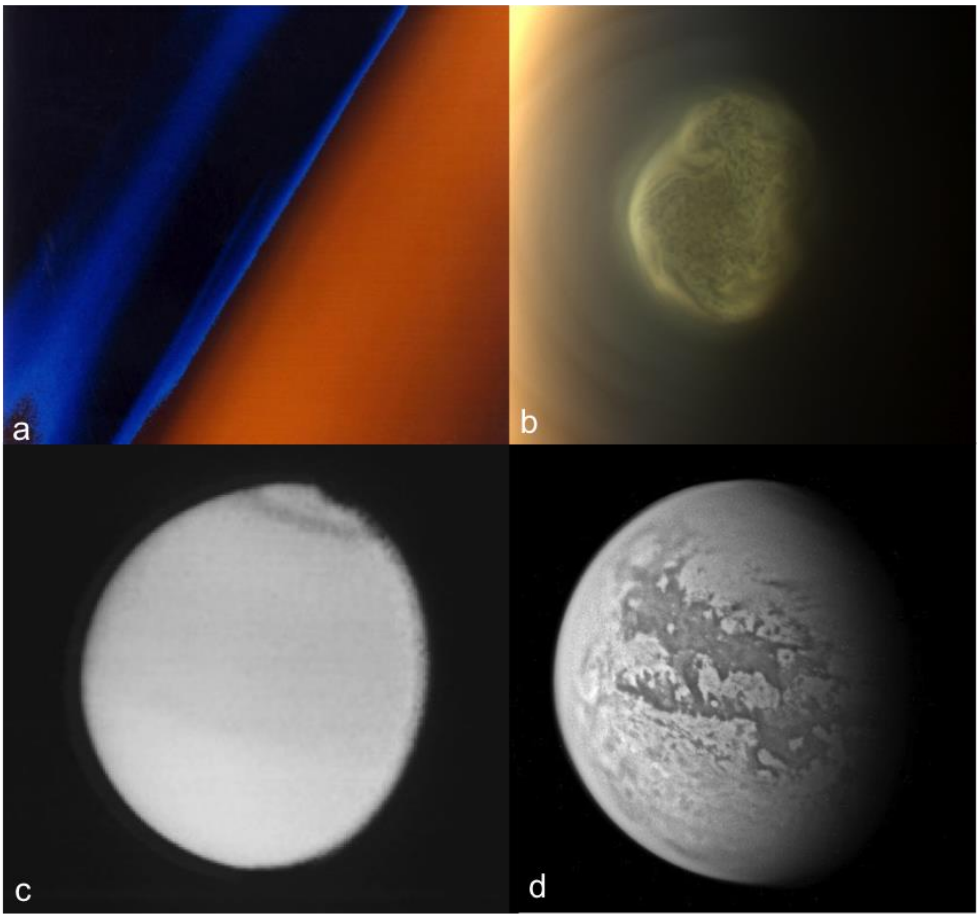

Fig. 1.13 - Atmosphere and surface observations from Voyager 1 (a;c) and Cassini (b;d). (a) The detached layers of haze hundreds of kilometers above the surface of Titan (Image credit: Voyager Project/JPL/NASA); (b) Swirling mass of gas around the south pole of Titan in the atmosphere (Image credit: NASA/JPL-Caltech/Space Science Institute, PIA06220); (c) Titan from Voyager 2 showing a hemispherical difference in brightness and some detail in the cloud system (Image credit: NASA/JPL); (d) Composite view of Cassini/ISS images showing the surface of Titan (Image credit: NASA/JPL).

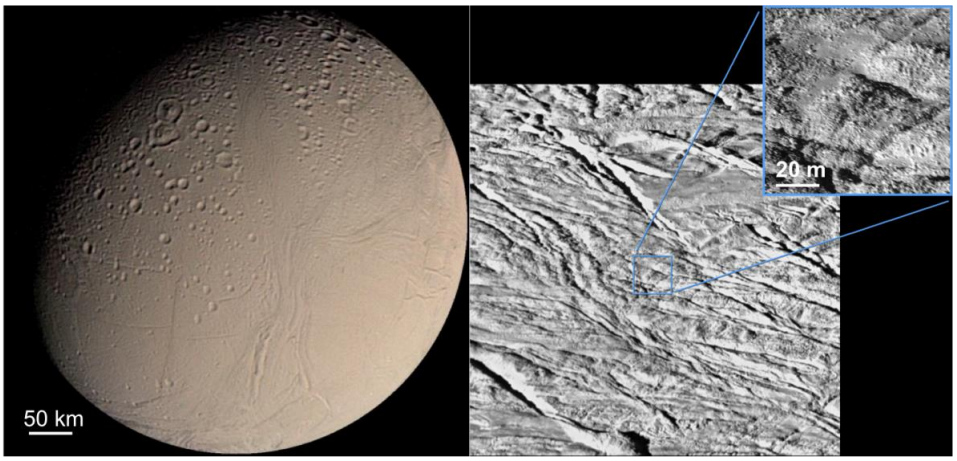

Fig. 1.14 - (left) Enceladus from the Voyager 2 cameras (Image credit: Voyager project/NASA); (right) a portion of the surface of the southern polar region of Enceladus from Cassini/ISS data (Image credit: NASA/JPL/Space Science Institute).

1.4.1 Titan

Undoubtedly, the Cassini-Huygens mission is what revealed Titan for the complex and intriguing world that it is. The data collection and the findings pertaining to all the aspects of this moon since 2004 surpass the expectations that the scientists had before the launch. Hereafter is a very brief reference to these findings, some of which will be presented in detail in later chapters according to their relevance to the subject of this thesis.

1.4.1.1 The atmosphere

The Cassini magnetometer measurements (Backes et al. 2005, Neubauer et al. 2006) showed that Titan is strongly influenced by the Saturnian dynamic magnetodisk (Arridge et al. 2008, Bertucci et al. 2008, Dandouras et al. 2009, Simon et al. 2010) and confirmed Voyager 1 observations (Ness et al. 1982) that Titan has no detectable large-scale global magnetic field. Indeed, Titan orbits at an average of 20.2 R_S (1 R_S = Saturnian radius = 60,330 km), while the Saturnian magnetopause standoff distance follows a bimodal distribution with means at 21 R_S and 27 R_S, mainly controlled by the solar wind (Achilleos et al. 2008). This means that Titan is mostly located inside the Saturnian magnetosphere, close to the Saturnian magnetopause. The Charge-Energy-Mass-Spectrometer (CHEMS/MIMI) measurements showed that although Titan can be considered as a source of the Saturnian magnetospheric plasma, the relative low concentration of N+ and N2+ in the outer magnetosphere suggests low nitrogen escape ratio of Titan (Krimigis et al. 2005), contrary to previous beliefs (Eviatar and Podolak 1983, Richardson, 1998). Additionally, Ion and Neutral Mass Spectrometer (INMS) measurements showed that high-energy photons (EUV and X-rays) and energetic particles from Saturn's magnetosphere are the main energy sources in Titan's upper atmosphere that create an extended ionosphere between 700 and 2700 km (e.g. Cravens et al. 2006).

Cassini unveiled many unknown characteristics of Titan's atmosphere. It started from the outer layer of the atmosphere called the exosphere, which interacts with the Saturnian magnetosphere (Dandouras et al. 2009). Since Titan lacks a protective intrinsic magnetic field, energetic particles originating from the Saturnian magnetosphere directly bombard its upper neutral atmosphere, undergoing charge-exchange collisions with cold neutral atoms and producing energetic neutral atoms (ENAs). The Ion and Neutral Camera (INCA) of the Cassini Magnetosphere Imaging Instrument (MIMI) measured the energetic neutral atoms ENAs flux and modeled Titan's exosphere to extend at an altitude of 50,000 km (Brandt et al.

2012) close to the Hill sphere radius, the limit of the gravitational influence.

The Huygens Atmospheric Structure instrument (HASI) measured Titan's temperature profile during the Huygens descent on January 14, 2005, from an altitude of 1,400 km until the surface, including the following thermal structure: a thermosphere (including exosphere and ionosphere), a mesosphere, a stratosphere and a troposphere (Fig. 1.15). The surface P,T conditions measured were 1467±1 mbar and 93.65±0.25 K respectively (Fulchignoni et al. 2005).

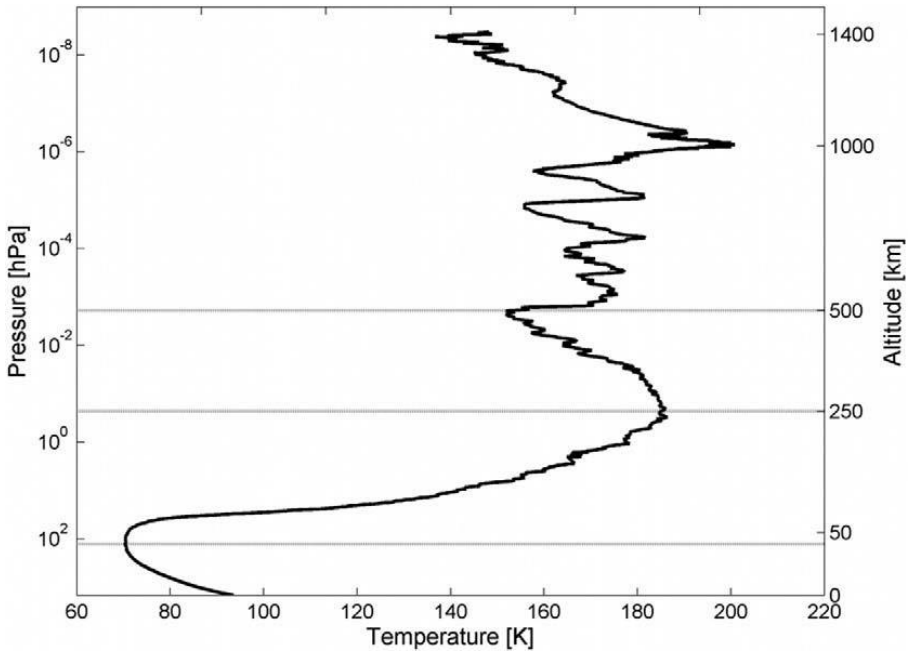

Fig. 1.15 - Titan's temperature profile from Huygens/HASI measurements. The several large inversion layers in the upper atmosphere correspond to gravity waves. The inflection at around 40 km marks the tropopause and the one at around 250 km the stratopause (Image credit: Fulchignoni et al. 2005).

Dynamical phenomena at higher levels (<500km), such as gravity waves of 10-20K recorded by HASI, create temperature fluctuations. In addition, HASI indicated the presence of a lower ionospheric layer at 40 to 140 km and Composite Infrared Spectrometer (CIRS) confirmed the presence of a stratopause around 310 km of altitude for a maximum temperature of 186 K and of a mesopause at 490 km for 152 K. However, HASI and CIRS measurements do not correlate with the altitude of the stratopause. CIRS data set it higher at 312 km (183 K) (Vinatier et al. 2007), while at this altitude HASI temperature is 185 K. Additionally, the calculation of the infrared radiance of HASI is inconsistent in relation to the observed CIRS radiance at methane 7.7 μm band (Lebreton et al. 2009).

CIRS has been mapping stratospheric temperatures over much of Titan's disk from the latter half of 2004, when it was early southern summer on Titan (solstice was in October 2002) to well after the northern spring equinox (in August 2009). In mid-2010 the epoch on Titan was the same as during the V1 encounter, almost 30 years before (1 Titan year) (see

Figure 1.17). Temperatures are found to have returned to their 1980 values, with the coldest ones in the north (by 10-20 K with respect to the equatorial ones below 300 km), where the season has been winter moving into spring after mid-2009.

Cassini-Huygens brought a wealth of data concerning the chemical composition of Titan. As mentioned above, INMS measurements showed that the upper atmosphere is composed of high-energy photons and energetic particles (e.g. Vuitton et al. 2007). The complex negative and positive ions have masses that range from few amu to thousands, while the detection of very heavy negatively charged particles (possibly aerosols), above the homopause level (800-850 km), suggest that the process of aerosol formation starts at more than 1000 km above the surface through complex ion and neutral chemical reactions in the atmosphere (Coates et al. 2007; Waite et al. 2007). These molecules are hydrocarbons and nitrogen, with variable sizes, containing species, which diffuse downwards. This was suggested by photochemical models, but confirmed with Cassini CIRS spectra from the thermal emission bands of the different molecules in the stratosphere, that shows the increase with altitude of the vertical distribution (Coustenis et al. 2007). Table 1.4 summarizes the chemical composition of the atmosphere of Titan from Cassini-Huygens results, up to date (unless otherwise indicated).

Table 1.4 - The Chemical composition of Titan's atmosphere (*[a]Increasing in the North, [b]From ground-based heterodyne microwave observations, [c]Only observed from the ground, [d]From ISO observations, [e]From Cassini/CIRS, [f]From Cassini and ground-based data, information adapted from* Encyclopedia of the Solar System 2e ©2007*).*

Constituent	**Mole Fraction (atm. altitude level)**
Major	
Molecular nitrogen, N2	0.98
Methane, CH4	4.9 × 10–2 (surface)
	1.4–1.6 × 10–2 (stratosphere)
Monodeuterated methane, CH3D	6 × 10–6 (in CH3D, in stratosphere.)
Argon, 36Ar	2.8 × 10–7
40Ar	4.3 × 10–5
Minor	
Hydrogen, H2	~0.0011
Ethane, C2H6	1.5 × 10–5 (around 130 km)
Propane, C3H8	5 × 10–7(around 125 km)
Acetylene, C2H2	4 × 10–6 (around 140 km)
Ethylene, C2H4	1.5 × 10–7 (around 130 km)
Methylacetylene,CH3C2H	6.5 × 10–9 (around 110 km)[a]
Diacetylene, C4H2	1.3 × 10–9 (around 110 km)[a]
Cyanogen, C2N2	5.5 × 10–9 (around 120 km)[a]
Hydrogen cyanide, HCN	1.0 × 10–7 (around 120 km)[a]
	5 × 10–7 (around 200 km)[b]
	5 × 10–6 (around 500 km)[b]
Cyanoacetylene, HC3N	1 × 10–9 (around 120 km)[a]
	1 × 10+ (around 500 km)[b]

Acetonitrile, CH3CN	1 × 10–8 (around 200 km)[c]
	1 × 10–7 (around 500 km)
Water, H2O	8× 10–9 (at 400 km)d and 10-10 (at 200 km)[e]
Carbon monoxide, CO	4 × 10–5(uniform profile)[f]
Carbon dioxide, CO2	1.5 × 10–8 (around 120 km)

Following the INMS organic chemistry detections, measurements in the stratosphere by the CIRS, (Coustenis et al. 2010), the chemistry inferences from the Gas Chromatograph Mass Spectrometer (GCMS) (Niemann et al. 2005) and density and temperature data retrieved by the HASI (Fulchignoni et al. 2005) during the descent to the surface provided in depth information on the chemical composition and the nature of the atmosphere. In addition, INMS detected highly complex organic species in the ionosphere that are considered to be the precursors of the hydrocarbons and nitriles found in the stratosphere (Waite et al. 2007). These forms aggregate and finally condense out on the surface (Niemann et al. 2005) (Fig. 1.16). Moreover, some of these chemical components are molecules of prebiotic interest such as hydrogen cyanide and HCN (Raulin et al. 2008). Thus, it appears that Titan is a chemical factory in which the formation of complex positive and negative ions is initiated in the high thermosphere as a consequence of magnetospheric-ionospheric-atmospheric interactions with the involvement of solar EUV, UV radiation, and energetic ions and electrons (Coustenis and Hirtzig, 2009).

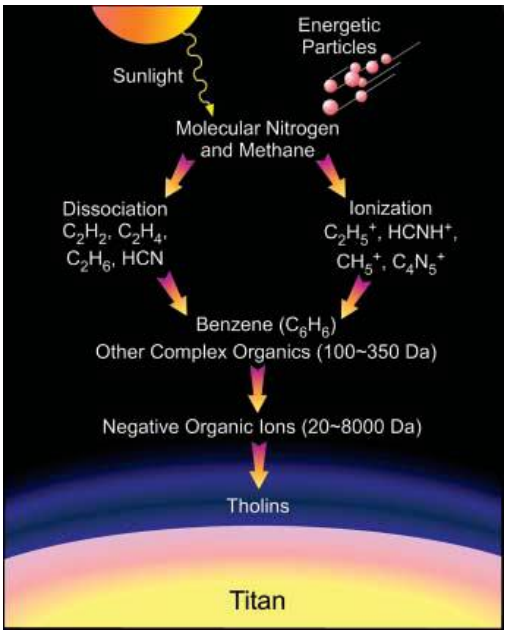

Figure 1.16 - Tholin formation in Titan's upper atmosphere according to INMS findings (Image credit: Waite et al. 2006).

The INMS data analysis showed that Titan possesses the most compositionally complex ionosphere in the Solar system. Modeling of INMS data (Vuitton et al. 2007)

detected polyynes (C_4H_2, C_6H_2, C_8H_2), cyanopolyynes (HC_3N, HC_5N) (Yung et al. 1984, Toublanc et al. 1995, Wilson and Atreya 2004), methylcyanopolyynes (CH_3C_3N, CH_3C_5N) and methylpolyynes (CH_3C_4H, CH_3C_6H) for the first time on Titan, as well as neutral mode of benzene (C_6H_6) in the ionosphere (Waite et al. 2007, Vuitton et al. 2008). Moreover, the model indicates the existence of ammonia (NH_3), methanimine (CH_2NH), other nitriles (C_2H_3CN, C_2H_5CN) and two unidentified N containing species (C_5H_5N, C_6H_7N). The aforementioned hydrocarbons and nitrile species form the tholins (a complex layering of organic aerosols) that diffuse through the atmosphere and accumulate on the surface (Coustenis et al. 2007, Tomasko et al. 2008) (Fig 1.9).

Titan atmospheric region from 500 to 950 km was observed by the Cassini Ultraviolet Imaging Spectrometer (UVIS), which monitored the occultation of two stars during the second Titan flyby (Shemansky et al. 2005). A mesopause was inferred at 615 km with a temperature minimum of 114 K. At altitude ranges from 450 to 1600 km, methane, acetylene, ethylene, ethane, diacetylene, and hydrogen cyanide were identified. The higher order hydrocarbons and hydrogen cyanide are undetectable below altitudes ranging from 600 to 750 km, leaving methane as the only identifiable carbonaceous molecule below 600 km in this experiment. Because Cassini instrumentation cannot probe down to this altitude, this region is called agnostosphere (Coustenis et al. 2010) or ignorosphere (Strobel et al. 2009).

Since the beginning of the mission, the CIRS instrument provides a complete pole-to-pole global coverage of Titan's stratosphere. It can operate in nadir and limb viewing modes and provide the most spatially resolved maps of constituent species to date. Nadir sequences provide global mapping of atmospheric temperature and composition, while the limb ones provide information on the vertical profiles. CIRS has detected organics, probing the atmosphere within the range of 150 and 450 km (Flasar et al. 2005, Coustenis et al. 2007, Vinatier et al. 2007, Teanby et al. 2008, Teanby et al. 2009, Coustenis et al. 2010, Vinatier et al. 2010) and confirmed the results of V1/IRIS and ISO and also confirmed latter's observations on the benzene detection at 674 cm^{-1} (Coustenis et al. 2003; 2007).

Cassini/CIRS also indicate that very strong zonal winds occur in the stratosphere of Titan in winter northern latitudes, while in the summer the stratospheric winds are weaker (Achterberg et al. 2008), supporting the presence of a North Polar vortex (Flasar et al. 2005).

Moreover, the Cassini-Huygens mission provided the opportunity to extensively study and monitor Titan's seasons during its long year (30 Earth years). As seen in Fig. 1.17, by the time the nominal Cassini-Huygens mission (in red), covers parts of one Titan season (northern winter), and the Cassini Equinox 2-year mission (in blue) and the Solstice mission (10

additional years, in orange) are taken into account, two seasons (winter and spring) will have been covered on Titan. These Cassini measurements in addition to Voyager's have acquired data over almost a full course of Titan's seasons.

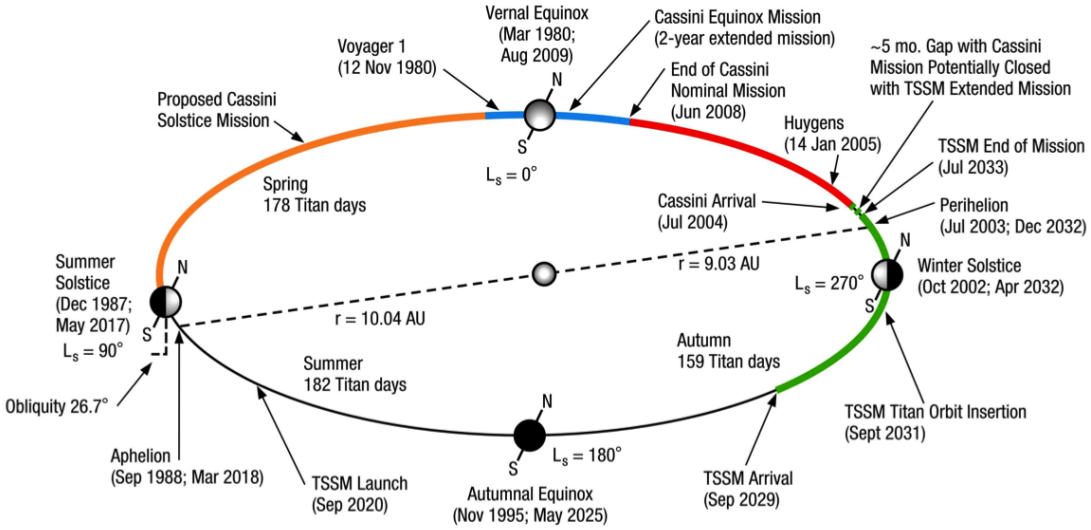

Fig. 1.17 - Monitoring of Titan over one year (30 terrestrial years) with different missions (Image credit: Ralph Lorenz).

1.4.1.2 The surface features and processes

One of the greatest discoveries of the Cassini-Huygens remote sensing and *in situ* instrumentation is that of the surface, including the features, the connection to each other and the processes that formed them. The orbiter offers detailed views of the surface through the radar, cameras and mapping spectrometer, instruments I discuss in detail in Chapter 2 and their data that I study, process and analyze in Chapters 4, 6 and 7. The Huygens probe returned the first surface *in situ* view from such a long distance object from Earth. Through the selection and analysis of such data a preliminary geological map including the topography, the morphology of the features and implications on their chemical composition is currently developed.

The first views of Titan's surface came from the orbiter, in particular from the cameras of the Cassini Imaging Science Subsystem (ISS) and the Visual and Infrared Mapping Spectrometer (VIMS) that penetrated the thick atmosphere (e.g. Barnes et al. 2005; 2006; Porco et al. 2005; Brown et al. 2006; Buratti et al. 2006; Jaumann et al. 2006; McCord et al. 2006). First, the observations by both ISS and VIMS confirmed previous HST observations (see § 1.2) concerning the presence of an extensive large region located at 10ºS, 100ºW officially named Xanadu (e.g. Barnes et al. 2005, Porco et al. 2005). This region is located in

the equator where the mid-latitude regions were found as uniformly dark with elevated topography. On the other hand, the poles were seen as bright filled with large dark patches characterized as hydrocarbon lakes, which were investigated more analytically by the Cassini/RADAR (e.g. Stofan et al. 2006). In terms of topography, Cassini found that Titan has an interesting topography with mountains ranging from 200 m to 2 km (e.g. Radebaugh et al. 2007) while the poles are topographically lower than the equator (e.g. Porco et al. 2005). The DISR data also led to such distinction concerning an average hypsometry (altitude) of the dark (lows) and bright regions (highs).

VIMS data provided the ability to classify different terrains depending on their spectral behavior (e.g. Soderblom et al. 2007a). The RADAR instrument gives information on their shape and morphology and in some cases on their hypsometry. The thorough interpretation of these surface terrains, in terms of chemical composition and morphology, is a difficult task due to instrumental and mission restrictions that I discuss in Chapter 3. Nevertheless, the Cassini-Huygens mission was the first to observe many features showing at least in terms of morphology an Earth-like pattern. Indeed, Cassini ISS images and RADAR echoes have recorded several different types of geological features such as mountains (Radebaugh et al. 2007; Lopes et al. 2010), ridges (Soderblom et al. 2007b), faults (Radebaugh et al. 2011), rectangular drainage patterns and cryovolcanic structures, which are controlled most likely, at least partially, by tectonic activity (Burr et al. 2009). Stable liquid lakes were spotted by both ISS and RADAR, located mainly at the polar regions (Mitri et al. 2007; Stofan et al. 2007; Hayes et al. 2008) and recently at the equatorial latitudes (Griffith et al. 2012). The major types of surface features that Cassini-Huygens discovered are summarized in Fig. 1.18. I discuss the Titan surface expressions in detail in Chapter 4.

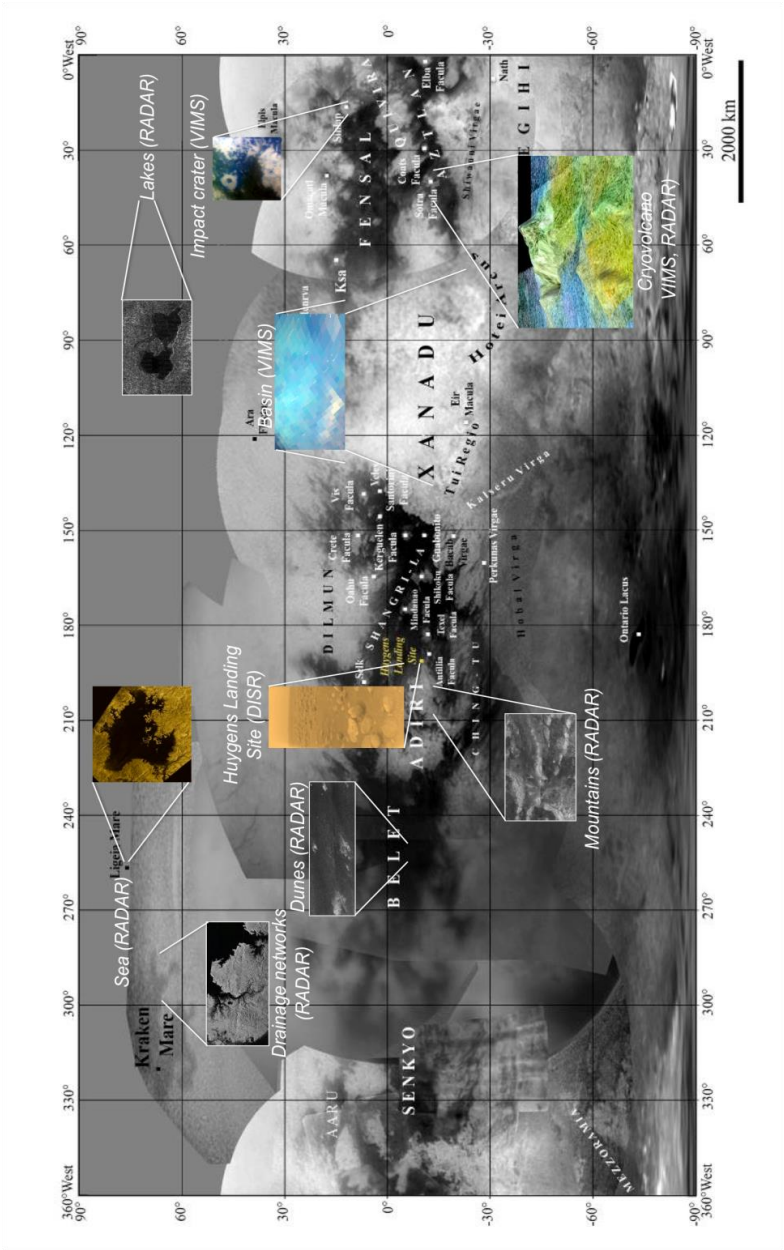

Figure 1.18 - Major types of surface expressions on Titan from VIMS, RADAR and DISR data characterized as fluvial, aeolian, tectonic-like, cryovolcanic etc. The background map is a mosaic of Cassini/VIMS data at 2.03 μm (Map credit: NASA/JPL/Space Science Institute).

A large number of studies have discussed the possible chemical composition of the materials that cover these surface features as well as the dynamic processes that form them. Indeed, among other, water ice, CO_2 ice and hydrocarbons have been implied from different observations (e.g. Sotin et al. 2005; Brown et al. 2008; Lorenz et al. 2008). The origin of such materials is attributed to various sources and triggered or deposited by various processes.

The first cryovolcanic implication on Titan was made for the Tortola Facula (8.5°N, 143°W) feature, a bright circular structure found in the VIMS images (Sotin et al. 2005). In addition, the Huygens probe with DISR imaged Titan drainage networks and the first *in situ*

images of hills (Tomasko et al. 2005; Soderblom et al. 2007). Later on, the RADAR swath unveiled the presence of large mountain chains and fault block mountains (Mitri et al. 2007; Radebaugh et al. 2007). Furthermore, The Cassini instruments have found no obvious evidence for a heavy craterization on the bright or the dark areas of Titan so far and only few features interpreted as impact craters have been announced to date. This may mean that the surface of Titan is young (less than a billion years) or highly eroded/modified (Lorenz et al. 2008; Wood et al. 2010; Neish and Lorenz, 2012).

Other surface terrains observed by the Cassini orbiter and the RADAR include areas covered with dunes similar to the terrestrial ones (e.g. Elachi et al. 2006) (Fig. 1.18). Additionally, and quite importantly for the hypothesized missing liquid methane or ethane surface reservoir, the RADAR instrument onboard Cassini has discovered lakes sprinkled over the high northern altitudes of Titan (e.g. Stofan et al. 2007). In addition, the first Titan *in situ* image showed a dark plain (darker than originally expected) covered in pebbles with the main constituents being water ice and hydrocarbon ice (Tomasko et al. 2005).

Titan is a dynamic system in which we find short or long-term variations of the surface caused by fluvial, aeolian, atmospheric and possibly endogenic (tectonic and/or volcanic) processes (Fig. 1.19). Moreover, Titan has an active methane cycle as illustrated in Fig. 1.19, similar to Earth's water cycle, causing precipitation phenomena, formation of channels and evaporation of lakes (e.g. Tokano et al. 2006). However, albeit methane's significant presence in Titan's thick nitrogenous atmosphere, as mentioned above, its preservation lasts 10-30 Myr as it is destroyed by photochemical processes and converted to heavier hydrocarbons (Atreya et al. 2006; Atreya, 2010). Therefore, a source that replenishes the methane present in the atmosphere is required.

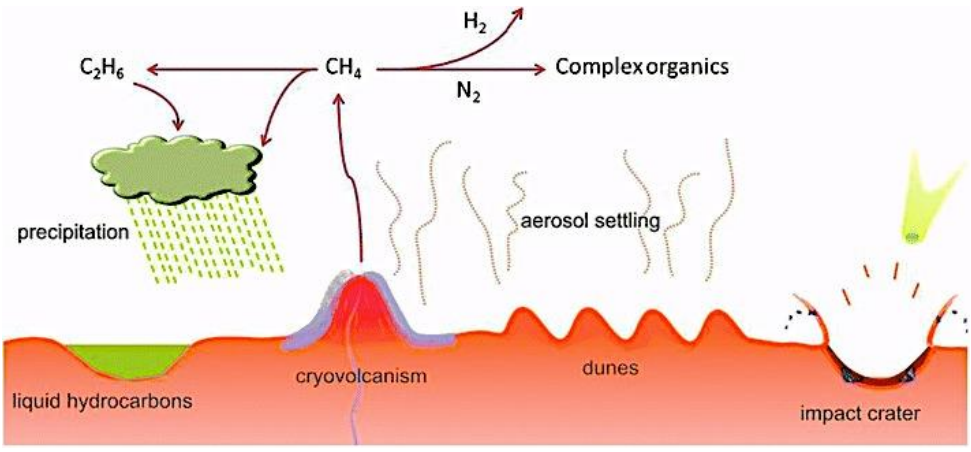

Fig. 1.19 – Schematic view of the dynamic internal-surface-atmospheric processes and the methane cycle of Titan from evidence of Cassini-Huygens data (Image credit: Raulin et al. 2012).

In the course of the Cassini mission we find examples of recent or past activity in the past lake-level changes (Barnes et al. 2009; Turtle et al. 2011a), in changes of fluvial deposits (Burr et al. 2012), in the dunes (Barnes et al. 2008) and possible on the cryovolcanic sites (Nelson et al. 2009a;b; Solomonidou et al. 2013c). In this thesis I focus on such type of surface changes and try to interpret some of the unknown aspects of the acquired Cassini-Huygens data.

As mentioned beforehand, Titan's surface features discovered by Cassini-Huygens indicate the presence of dynamic and complex Earth-like geological processes such as aeolian erosion, fluvial deposits, impact and possibly tectonic and cryovolcanic processes. The latter two processes, if indeed present on Titan, have endogenic origin. A number of tectonic patterns have been hypothesized for Titan, although much different than the terrestrial ones, and indicated by the presence of Cassini/RADAR bright elevated crustal features (Soderblom et al. 2007; Radebaugh et al. 2007; Mitri et al. 2010, Solomonidou et al. 2013a). These patterns include compressional and extensional tectonism (e.g. Mitri et al. 2010). Extensional tectonism is common and observed in almost all icy moons in the Solar system but this is not the case for contractional/compressional. Thus, if the formation of mountains on Titan is triggered due to crustal compressions then Titan is the only icy satellite where contractional tectonism occurs and is the predominant style (Mitri et al. 2010).

Cryovolcanism has also been suggested on Titan, although it has not been proven to day and is considered as a possible methane 'pathway'. Pre-Cassini models predicted the activity of cryovolcanism on Titan, but the discovery of the first cryovolcanic-like structure Tortola Facula (not a possible cryovolcanic candidate anymore –Lopes et al. 2013) and of more such as Tui Regio and Hotei Regio, from the extensive area of Xanadu, triggered again this hypothesis (Barnes et al. 2005; Soderblom et al. 2009). Moreover, I have studied these regions with the use of a radiative transfer code on Cassini/VIMS data from several flybys, and found albedo variations with time, suggesting possible fluctuating deposition of material with endogenic origin (i.e. cryovolcanism, Solomonidou et al. 2013c, see Chapter 7). Alternative hypotheses based on spectral similarities between Tui Regio and dry lakebeds at the poles, rank Tui Regio as evaporitic deposits with no interior connection (Barnes et al. 2011). Other studies, focusing on Tui Regio and Hotei Regio, describe the areas as paleolake clusters and fluvial or lacustrine deposits, indicating an exogenic origin (Moore and Howard; Moore and Pappalardo, 2011).

Nevertheless, correlation between Cassini/RADAR and VIMS data have indicated the best cryovolcanic candidate so far on Titan, namely Sotra Patera (area formerly known as

Sotra Facula), that includes a 1 km depression, lobate flows and two high mountains (Lopes et al. 2007; 2013). I study the temporal surface albedo variation of this region as well (Chapter 7).

1.4.1.3 The interior

In the previous section 1.4.1.2 I have discussed the possibility for tectonic and volcanic processes as indicated by the Cassini-Huygens remote sensing and *in situ* instrumentation, which I analyze in detail in Chapters 4 and 7. The triggering mechanism that leads to such dynamic processes and movements is possibly Saturn's tides. The maximum shear stresses are concentrated in the polar areas, while the maximum tensile stresses predominate in the near-equatorial, mid-latitude areas of the sub- and anti-saturnian hemispheres (e.g. Sohl et al. 2013). Most of the geophysical models that predict the activity of tectonism and cryovolcanism on Titan require the presence of a subsurface liquid water ocean (e.g. Stevenson, 1992; Tobie et al. 2005; 2012).

Cassini brought several indications pointing to the presence of an undersurface liquid water ocean on Titan. The Huygens Atmospheric Structure Instrument - Permittivity Wave and Altimetry (HASI-PWA) experiment, indicated the presence of a Schumann resonance between the ionosphere and an internal ocean that lies 50 km beneath the surface, through the extremely low-frequency electric signal recorded (Beghin et al. 2009, 2012). Furthermore, gravity measurements performed by the Cassini Radio Science experiment showed that the gravity field significantly varies along Titan's orbit, indicating that Titan is subjected to tides of about 10 m in height, instead of about 1m. Such strong tides confirm the deformability of the interior, while in addition to Titan's obliquity (Baland etal. 2011), confirm the presence of an internal liquid ocean roughly 100 km below the surface (Iess et al. 2012).

In addition, thermal evolution models testable with Cassini–Huygens measurements suggest that Titan may have an icy shell 50 to 150 km thick, lying atop a liquid water ocean a couple of hundred kilometers deep, with some amount (up to ~10%) of ammonia dissolved in it, acting as an antifreeze, in addition to a layer of high pressure ice that could exist underneath (e.g. Tobie et al. 2005; Fortes et al. 2007) (Fig. 1.20).

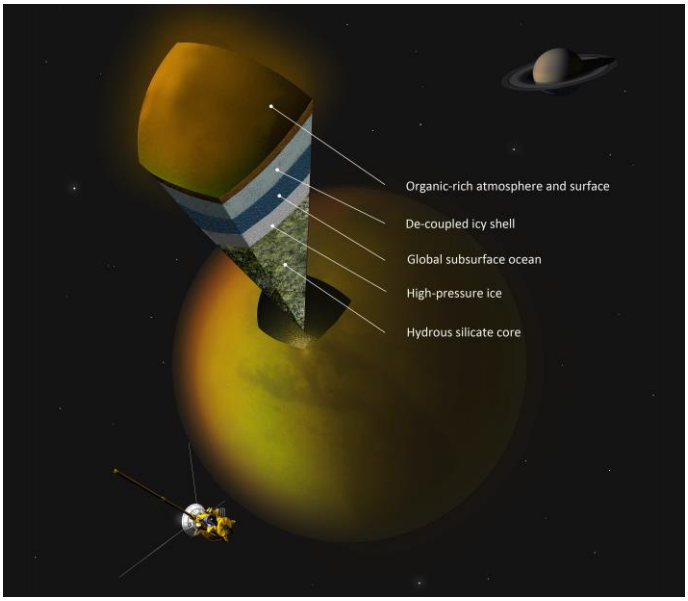

Fig. 1.20 - Artistic view of a possible internal layering in Titan as hypothesized by Cassini data (Image credit: A. Tavani/Iess et al. 2012).

Considering the presence of a subsurface liquid water body and of methane clathrates in the ice shell in Titan's interior, current models taking into account heat transfer, convection, tidal dissipation, clathrate dissociation and cooling of the subsurface ocean, suggest cryovolcanic and tectonic phenomena as a possible 'pathway' for methane to resupply the atmosphere through outgassing on the one hand and possibly for water and ammonia to be ejected covering patches of the surface around cryovolcanic sites on the other (Tobie et al. 2006; Fortes et al. 2007; Mitri and Showman, 2008; Choukroun et al. 2010; Sohl et al. 2013). According to these models, cryovolcanism and deposition of water and ammonia ice on the surface of Titan is plausible.

However, alternative theories for the methane ejection in the atmosphere exist. Among others, impacts (Howard et al. 2008) and surface lake sources for the methane replenishment that are currently less in favor since estimates show that only 1% of methane, can be provided by that source (Sotin et al. 2012).

Finally, Titan is a good candidate for habitability and astrobiological studies as its atmosphere exhibits more similarities with the Earth's today - and even more so in the past than any other Solar system body (e.g. Coustenis and Taylor, 2008). Recent Cassini-Huygens findings have revolutionized our understanding of Titan's system and its potential for harboring the "ingredients" necessary for life such as a rich organic budget and sufficient energy sources to drive chemical evolution (Coustenis and Taylor, 2008; Lorenz and Mitton, 2008).

The Cassini findings have also rank Enceladus as another fascinating planetary body of the Saturnian system.

1.4.2 Enceladus

Despite the fact that Enceladus has an icy bright surface that consists, to a large extend, of impact craters similarly to other airless moons, it also presents a strong contrast between rather old and cratered terrains and very young and tectonized terrains, which is unique in the Solar system. The first important discovery concerning Enceladus by Cassini was made even before SOI. UVIS instrument in 2004 detected neutral O emission concentrated near the orbit of Enceladus (Esposito et al. 2005). Follow up Cassini surface observations, as well as geophysical and geochemical measurements, proved the present activity of the satellite.

At the south pole of Enceladus the CIRS instrument detected anomalous thermal emission (Spencer et al. 2006). These emissions correlated well with four main faults, named 'Tiger Stripes', observed by ISS (Porco et al. 2006). Moreover, the presence of water vapor above the same region was detected during a stellar occultation by UVIS (Hansen et al. 2006), as well as dust grains by the Cosmic Dust Analyzer (CDA) (Spahn et al. 2006). Furthermore, high-resolution data from Cassini MAG showed a large perturbation of the magnetic field (Dougherty et al. 2006). The analysis and combination of these Cassini data confirmed the presence of erupting plumes and ranked Enceladus as active. After that, several ISS, INMS and CIRS observations have brought evidence regarding the nature of the plumes, the geology and the composition of the emanating area.

1.4.2.1 Geology and composition

Cassini observations of Enceladus, even from the very first close up view on February 17, 2005, begun to answer to many of those mysteries that Voyager observations presented and claimed Enceladus as an important target for Cassini to explore. A large number of flybys, with distances between the spacecraft and the surface ranging from 52 – 100,000 km was planned for the Cassini spacecraft which I present in Table 3.1 in Chapter 3.

The multiple flybys and instrument acquisition of data did reveal a distinct geological environment. The surface of Enceladus is covered by smooth and cratered terrains, ridges, grooves, escarpments and extensive linear fractures (Johnson, 2004). The most interesting and youthful terrain seen on this moon is the 'Tiger Stripes', that as Cassini observations and data

analysis showed, emanates jets of water vapor and simple organic compounds (Brown et al. 2006). The Tiger Stripes are tectonic structures consisting of four sub-parallel, linear depressions (faults), located in the south polar region (Porco et al. 2006) (Fig. 1.21).

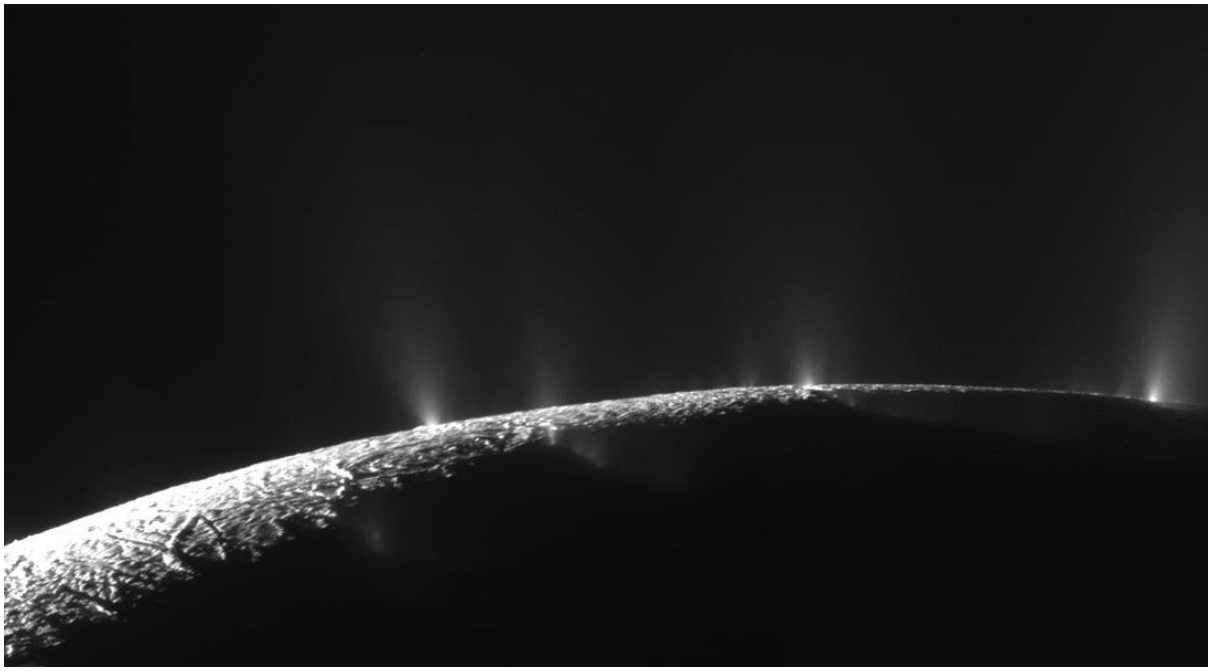

Fig. 1.21 - Mosaic of E8 flyby images of the emanating plumes from the Tiger Stripes in the southern polar region (Image credit: NASA/JPL/Space Science Institute).

1.4.2.2 Interior structure and jets

INMS and CDA measurements revealed that the jets of water vapour and ice from the fractures of Tiger Stripes contain many other compounds in addition to water, such as CO_2, NH_3 in the gas phase and Na, K salts in the solid phase (Waite et al. 2009; Postberg et al. 2009, 2011). These tectonic fractures discharge material by endogenic dynamic and most probably hydrothermal activity. The source of the jets is a controversial issue; as extensive internal stratification, as well as dynamic modeling, is required for the source to be identified. The CDA discovery of salts in Saturn's E-ring composition, which is fed from Enceladus' plumes (Postberg et al. 2009), suggest that the source of jets is possibly a "chamber" of liquid water that lies underneath the ice shell (Tobie et al. 2008). Alternatively, the material could derive from originally warm ice that is heated and explodes by the dissociation of clathrate hydrates (Kieffer et al. 2006). In addition, the VIMS instrument detected simple organic compounds in the Tiger Stripes. Such chemical composition which consists of liquid water, ammonia, carbon dioxide, benzene and other hydrocarbons (Waite et al. 2009), has not been

found in any other region on Enceladus (Brown et al. 2006). The presence of liquid water might also make it possible for Enceladus to support life (Lammer et al. 2009).

The idea of a subsurface sea becomes all the more compelling with Cassini data, since Enceladus's south polar region is actually a half-kilometer deep basin distinguishing from the surrounding expressions (Collins and Goodman, 2007; Schenk and McKinnon 2009; Nimmo et al. 2011).

The gravitational effects of Enceladus on Cassini and the calculation of its density of 1.61 g/cm³ indicate that the satellite contains a greater than expected percentage of silicates minerals and iron (Porco et al. 2006). Thus, models of the internal structure of Enceladus propose the presence of a rocky core, a liquid ocean or pockets of liquids decoupling the core from the ice shell and the icy crust (Collins and Goodman, 2007; Roberts and Nimmo, 2008; Tobie et al. 2008).

Finally, the Cassini data showed also that in terms of astrobiology and habitability studies Enceladus, like Titan, seems an ideal location for further investigation, as its astrobiological importance is obvious, because it proposes uniquely all the necessary ingredients for life emerging and evolution. Not surprisingly, scientists expect that their study will provide some important insights into the origin of life.

1.5 Looking ahead

The Cassini-Huygens mission has enormously advanced our knowledge of the Saturnian system and the satellites within. Future planetary investigations will use the Cassini-Huygens mission scientific findings and engineering developments as reference points. However, the key contribution to planetary science of Cassini may be the questions raised rather than those answered.

The Cassini data since 2004 show that seasonal variations are quite prominent in Titan's atmosphere attributing this to the summer-hemisphere heating of haze by absorption of solar radiation and winter-hemisphere cooling through infrared emission by haze and trace gases. After comparison with Voyager measurements and the completion of one Titanian year, it appears that the thermal and chemical structure of Titan's atmosphere is stable after one year, consistent with the solar input being the major energy source on Titan as on Earth; some interannual variations may exist for a few of the most complex molecules.

On Titan we are observing an active hydrologic cycle subjected to seasonal, and longer-term changes, as well as surface changes due to atmospheric, climate and possible internal phenomena, as on the Earth. The investigation of such a close Earth analogue in terms of processes, but with sufficient differences in working materials and timescales, we can rigorously test the depth of our understanding of planetary climate, atmosphere and geology.

Hence, Titan can be viewed as an analogue, albeit with different components, of a future state of the Earth when surface conditions, due to the increasing solar luminosity, shall preclude stable equatorial/mid-latitude oceans and the liquid water will be limited to the poles. Thus, by studying the evolution of Titan and how the various geologic and meteorological processes interact, we have a glimpse into the Earth's past and future "simulated" on a planetary scale by different materials.

These aspects of Titan, as well as the fragility and changeability of the climate with the interaction of the satellites' geology and atmosphere of our own world, are essential to be studied more thoroughly.

The purpose of this thesis is to contribute to the study of Titan's evolution by investigating its geology by, (a) searching for surface changes and investigating their nature, (b) studying the correlation of these changes or of geologically interesting features with the interior, (c) analyzing the differences in surface albedo between areas and make implications

on their formation, and (d) classifying observed surface features as per their possible origin and provide similar terrestrial mechanisms and feature analogues. The results of my PhD research are presented in Chapters 4, 6 and 7 as well as 8 and 10. In Chapter 2 I describe the Cassini-Huygens instruments dedicated to the surface research data of which I process and analyze in this thesis and the types of observations that are performed on Titan. I follow up with the description of the data I use in this work and the issues I encountered during that process in Chapter 3. Chapter 4 presents an overview of Titan's geology while it describes in particular the morphotectonic and possible cryovolcanic features on Titan, through a classification of current observations, correlation to terrestrial formation mechanisms and implications of their genesis and nature (Solomonidou et al. 2013a). Moreover, in the same chapter I describe the correlation of tidal responses with the aforementioned features based on a recent model that I contributed to its development (Sohl et al. 2013). During my PhD I have used several tools such as the Principal Component Analysis (PCA) and a Radiative Transfer (RT) code on VIMS data and a despeckle filtering technique for RADAR, which I describe in detail in Chapter 5. In Chapter 6, I study the spectral behavior and dynamical range of the surface albedos, that I retrieve through a radiative transfer code (Hirtzig et al. 2013), of the possibly cryovolcanic areas (Solomonidou et al. 2010; Solomonidou et al. 2013b). In Chapter 7, I present my work and results on the investigation of the temporal evolution of these same areas with implications on their origin (Solomonidou et al. 2013c) and I additionally present my work on the correlation with radar data studying morphological issues. In Chapter 8, I provide a thorough review on Enceladus' surface and interior and I present a model that I used in order to simulate the observed geyser eruptions (Solomonidou et al. 2010). I follow up with Chapter 9, where I discuss the astrobiological potential of Titan, Enceladus and other icy moons of the Solar System, since the recent results from the Cassini-Huygens missions showed that the habitability zone should be extended (Coustenis et al. 2012). In Chapter 10, I present my work focused mainly on the comparative planetology, providing terrestrial analogues in terms of surface structure and origin for Titan and Enceladus, as well as for Europa and Ganymede (Solomonidou et al. 2010; Solomonidou et al. 2013a). Chapter 11, describes my contribution to the design of experiments to be included in future missions (Bampasidis et al. 2011a;b). Then, in Chapter 12, since Cassini-Huygens results have raised the public interest for Saturn and its moon, I report the outreach activities I have organized/participated in bringing Cassini-Huygens mission's accomplishments closer to the layman public. In conclusion, in Chapter 13, I present the perspectives of my current work and my intentions concerning future researches.

Chapter 2

The Cassini-Huygens mission

Cassini-Huygens is one of the most ambitious and successful missions in the planetary space exploration. European and US scientists of NASA and ESA proposed a mission to the Saturnian system in 1982 and later on in 1989 the idea of the Cassini-Huygens was born. Later, the Italian Space Agency (ASI) got involved and thus the Cassini-Huygens is a Flagship NASA-ESA-ASI mission, composed of the Saturn robotic orbiter named 'Cassini' (American) and the Titan lander named 'Huygens' (European). Cassini-Huygens was launched in 1997 and reached Saturn in 2004 and has since then been exploring the Saturnian system, with an end of mission currently foreseen for 2017. The investigation has provided the first detailed survey of the Saturn, its rings, and the 62 currently known satellites, with a focus on Titan. The Cassini instruments have returned a great amount of data that have revolutionized our view of the Saturnian system. The trajectory, operations and an introduction to the payload of Cassini are presented in this Chapter, where I also describe the orbiter and probe's instruments that investigate the surface and lower atmosphere in more detail.

2.1 General facts about the mission

The Cassini-Huygens mission was launched on October 15th, 1997, on a Titan IV-Centaur rocket from Cape Canaveral and performed flybys of Venus, Earth, and Jupiter before entering into orbit around Saturn on July 1st, 2004, on a journey covering 3.5 billion kilometers. The Huygens probe executed its mission towards Titan in January 2005. More details on the mission were presented in section 1.3, on Chapter 1. After two extensions, the Cassini orbiter continues its exploration of the Saturnian system until 2017. Indeed, after the first mission extension (Equinox) that ended in October 2010, a second one has been approved (Solstice) that will last until 2017. Figure 2.1 summarizes the Cassini mission number of Saturn orbits and the flybys around its moons until the end of the mission.

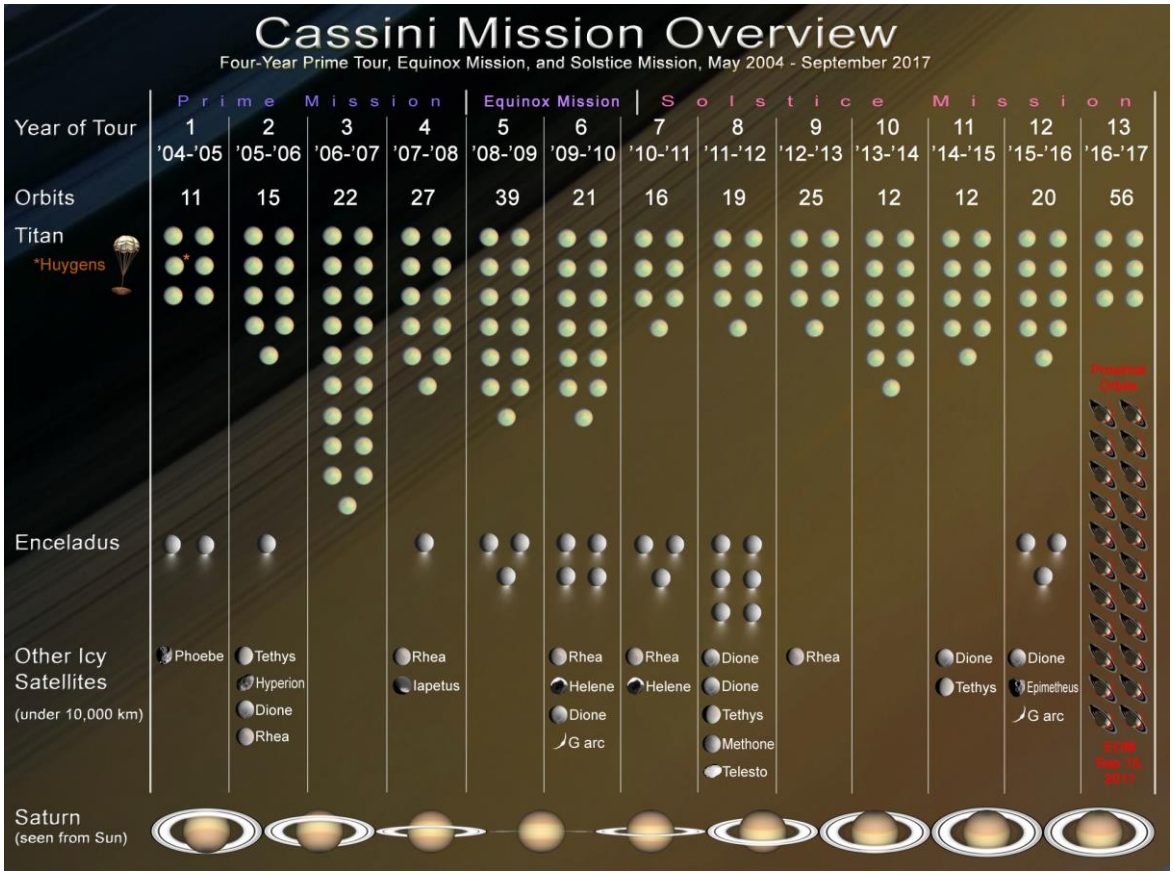

Fig. 2.1 - Overview of the tour of Cassini mission from the beginning until the end in 2017 (Image credit: David Seal/NASA/JPL-Caltech).

Cassini had performed its 93rd flyby around Titan up to July 2013 and its 19th around Enceladus. There are still about 34 flybys scheduled for Cassini to perform around Titan and 3 to Enceladus until the end of the mission in 2017.

The Cassini orbiter[11,12,13]

The Cassini orbiter has a mass of 2,150 kg and extends for 6.8 m in height and 4 m in width (Fig. 2.2). The 10 AU distance of Saturn from the Sun prohibited solar panels as power sources and hence the orbiter carries three Radioisotope Thermoelectric Generators (RTG), using the heat from the natural decay of plutonium to generate direct current electricity powers. Cassini is equipped with both remote sensing (the Remote Sensing Pallet) and *in situ* (the Fields and Particles Pallet) instrumentation.

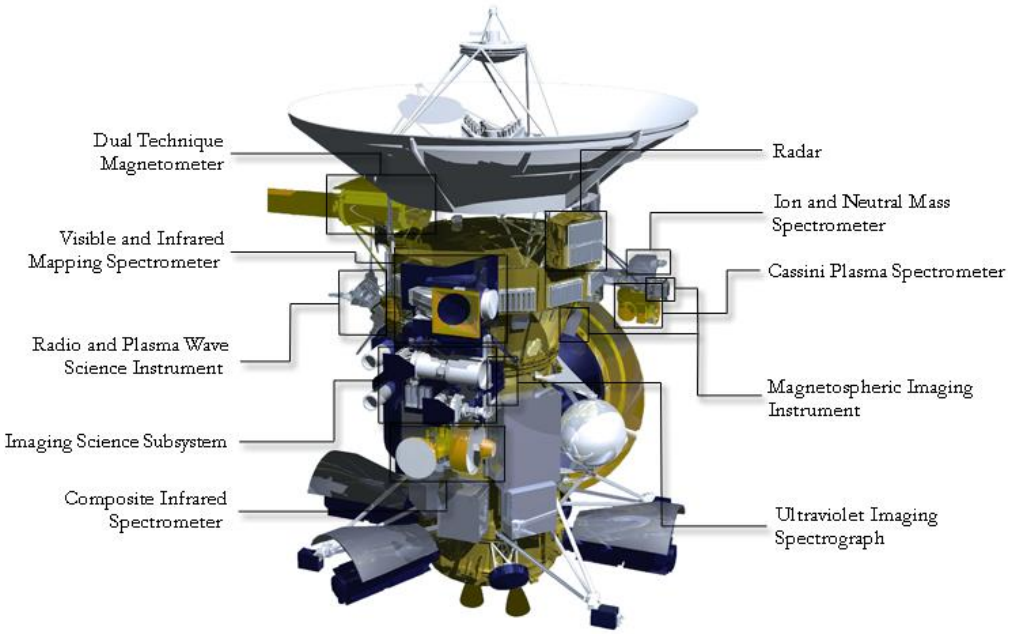

Fig. 2.2 - The Cassini spacecraft with the Huygens probe attached, its instruments and energy sources (Henry, 2002).

As seen in Figure 2.2 the Orbiter carries 12 instruments. These, gather data for 27 diverse science investigations, providing an enormous amount of information.

In situ instruments

Figure 2.3 indicates the locations of some of the fields and particles experiments on the Fields and Particles Pallet.

[11] *Information on both orbiter and probe's instruments adapted mainly from 'The Cassini-Huygens Mission' Editor: C.T. Russell, Springer, Volume 1,2,3 and*
[12] *Cassini-Huygens Saturn Arrival, NASA, Press Kit, June 2004 and*
[13] *Huygens. Science, Payload and Mission, ESA, SP-1177, August 1997*

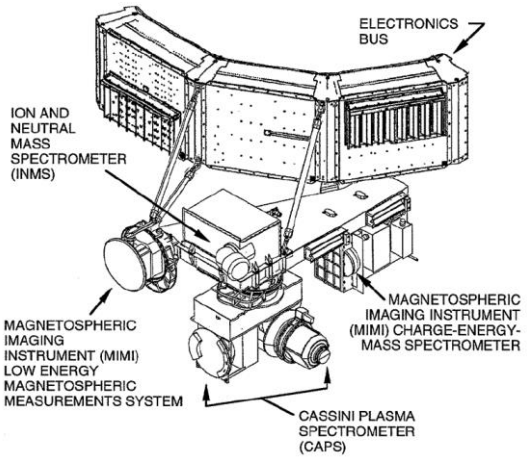

Fig. 2.3 - Cassini's Fields and Particles pallet and its instruments (Image credit: JPL).

The instruments for *in situ* investigations are the Cassini Plasma Spectrometer (CAPS), the Ion and Neutral Mass Spectrometer (INMS) and the Magnetosphere Imaging Instrument (MIMI) sensors, the Charge-Energy-Mass-Spectrometer (CHEMS) and the Low Energy Measurements System (LEMMS). The Dual Technique Magnetometer (MAG) is placed on the orbiter's boom 11 m antenna. The Radio and Plasma Wave Spectrometer (RPWS) and the Cosmic Dust Analyzer (CDA) are located in the main body of the orbiter as well as MIMI's Ion and Neutral Camera (INCA). Briefly:

The Cassini Plasma Spectrometer (CAPS) measures the energy and electrical charge of particles (electrons and protons) that the instrument encounters. Moreover it explores the nature of the Saturnian plasma within and near Saturn's magnetic field. CAPS sheds light to the complexity of the Saturnian magnetosphere and its interaction with its satellites, the rings and the solar wind. It is consisted of the Electron Spectrometer (ELS), the Ion Beam Spectrometer (IBS) and the Ion Mass Spectrometer (IMS). The ELS measures electron velocity distribution ranging from 0.6 eV to 28,250 eV, while the IBS records distributions of ion velocities within the range of .1 eV to 49,800 eV. IMS measures the composition of the hot, diffuse plasma from the Saturnian magnetosphere and low concentration ion species from 1 eV to 50,280 eV (Young et al. 2004).

The Ion and Neutral Mass Spectrometer (INMS) investigates the chemical, elemental and isotopic composition of the gaseous and volatile components of the neutral particles and the low energy ions in Saturn's magnetosphere and Titan's atmosphere. Thus, the instrument focuses on the upper part of Titan's atmosphere, between the altitudes of 900 and 1000 km, where the complex photochemistry of nitrogen and methane begin to build more complex organic molecules, which descend towards its surface. Moreover, INMS studies the

interaction of Titan's atmosphere with Saturn's magnetospheric plasma. It consists of two ion sources, one closed and one open. The former operates with the non-reactive neutrals, the nitrogen and methane, while the latter functions for reactive neutrals like the atomic nitrogen and for positive ions with energies less than 100 eV. The instrument is able to detect heavier hydrocarbon molecules such as benzene and determine their molecular mass (Waite et al. 2004).

The Magnetosphere Imaging Instrument (MIMI) measures the composition and the charge state and energy distribution of energetic ions and electrons. Moreover, it detects fast neutral particles and conducts remote imaging of Saturn's magnetosphere. MIMI also studies Saturn's magnetosphere dynamics and measures the interactions between the magnetosphere and the solar wind and the magnetosphere with Saturn's atmosphere, Titan and the other icy moons. It performs both *in situ* and remote measurements. Remotely it senses the magnetospheric ion plasma with energies greater than 7 keV through the detection of energetic neutrals produced through charge-exchange interactions of energetic ions with cold neutrals. It also measures in 3-dimensions the ion composition and charge states for ion energies between 3 keV/e and 220 keV/e. MIMI consists of 3 sensors the Ion and Neutral Camera (INCA), the Charge-Energy-Mass-Spectrometer (CHEMS) and the Low Energy Measurements System (LEMMS) which detects energetic electrons (>15 keV) and energetic ions with cold neutrals. During each Titan flyby, INCA studies the interaction of Titan's exosphere with the Saturnian magnetosphere every 90 s (Krimigis et al. 2004).

The Dual Technique Magnetometer (MAG) studies Saturn's internal magnetic field and its interactions with the solar wind, the rings and the moons of Saturn. MAG also maps the magnetic state of Titan and its atmosphere as well as Saturn's ring and dust interactions with the electromagnetic environment. MAG investigates the structure of the magnetotail and the dynamic processes therein. It consists of a fluxgate magnetometer and a vector/scalar helium magnetometer mounted both on the spacecraft's boom. Hence, MAG senses small changes in fields spanning four orders of magnitude with high sensitivity, recording the strength and direction of the magnetic fields (Dougherty et al. 2004).

The Radio and Plasma Wave Spectrometer (RPWS) studies radio emissions plasma waves, thermal plasma and dust. It consists of three orthogonal electric field antennas which focus on the detection of electric fields ranging from 1 Hz to 16 MHz, and three orthogonal search coil magnetic antennas to detect magnetic fields in the range within 1 Hz to 12 MHz. A Langmuir probe is used for measuring the electron density and temperature. The electric antennas, the search coils and the Langmuir probe are mounted on the orbiter's main

body. RPWS measures the electron density and temperature in Titan's ionosphere and study the escape thermal plasma from Titan's wake region (Gurnett et al. 2004).

The Cosmic Dust Analyzer (CDA) measures the ice and dust grains in and near the Saturn system with masses ranging from 10^{-19} and 10^{-9} kg. CDA studies the physical properties of the ice and dust grains and their chemical composition, as well as their interaction with the magnetosphere of Saturn, its rings and satellites (Srama et al. 2004).

Remote sensing instruments

Following the *in situ* instrumentation, Figure 2.4 indicates the locations of the imaging science instruments on the Remote Sensing Pallet which are the Composite Infrared Spectrometer (CIRS), the Ultraviolet Imaging Spectrograph (UVIS), the Radio Science Subsystem (RSS), the Imaging Science Subsystem (ISS), The Radar Mapper (RADAR) and the Visual and Infrared Mapping Spectrometer (VIMS). RADAR and RSS are parts of the Microwave Remote Sensing part.

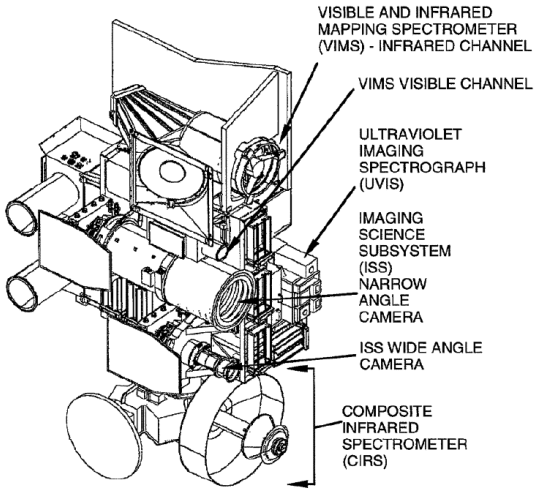

Fig. 2.4 - Cassini's Remore Sensing Pallet and its instruments (Image credit: JPL).

The Composite Infrared Spectrometer (CIRS) measures infrared radiation emitted from the surfaces, atmospheres and rings of Saturn and its moons to study their temperature and compositions (Flasar et al. 2004) by studying the thermal infrared range spectrum of Saturn and Titan. The information related to the surface is only derived from the 540 cm^{-1} brightness, which unfortunately suffers from large uncertainties because it sits close to the edge of the FP1 detector (Bampasidis et al. PhD Thesis) and cannot therefore provide secure information as to the surface, at least not as far as our studies here are concerned.

The Ultraviolet Imaging Spectrograph (UVIS) measures ultraviolet emission from atmospheres and rings to study their structure, chemistry and composition. UVIS determines the constituents' abundances in Titan's atmosphere, the aerosols in order to infer about the atmospheric circulation patterns. It also studies the UV emission from the upper atmosphere of Titan and its relation to the Saturnian magnetosphere as well. It hosts two moderate resolution telescope-spectrographs, providing images ranging from 56 to 118 nm (EUV) and from 110 to 190 nm (FUV) respectively (Esposito et al. 2004).

The Radio Science Subsystem (RSS) searches for gravitational waves in the Universe, studies the atmosphere, rings and gravity fields of Saturn and its moons by measuring telltale changes in radio waves sent from the spacecraft. It consists of a Ka-band traveling wave tube amplifier, a translator, an exciter, a S-band transmitter and various microwave components. It determines the temperature and composition profiles within Saturn's and Titan's atmospheres as well as the temperatures and electron densities within Saturn's and Titan's ionospheres (Kliore et al. 2004).

The Imaging Science Subsystem (ISS) is a high-resolution two-dimensional optical device, takes pictures in visible, near-ultraviolet and near-infrared light of the objects within the Saturnian system (Porco et al. 2004) (see § 2.2).

The Cassini Radar mapper (RADAR) probes the surface of Titan using RADAR imaging and measures its topography as well. The RADAR is a multimode Ku-band instrument (13.8 GHz, λ2.17 cm) having four operational modes: Synthetic Aperture RADAR (SAR) imaging, altimetry, scatterometry and radiometry (Elachi et al. 2004).

The Visible and Infrared Mapping Spectrometer (VIMS) searches for the chemical compositions of the surfaces, atmospheres and rings of Saturn and its moons by measuring colors of visible light and infrared energy emitted or reflected within the wavelength range 0.3 and 5.1 microns (Brown et al. 2004).

The latter three instruments provide the most relevant data to my research presented here and therefore more details on ISS, but especially on RADAR and VIMS can be found in the following sections. In addition to its instruments, the orbiter carried the Huygens probe, and successfully delivered it to Titan. It also operated as the link between the Huygens capsule, and the Earth providing telecommunications during the Huygens mission phase in 2005. On its orbit around Saturn, Cassini finds itself between 8.2 and 10.2 astronomical units (AU) from the Earth. I would like again to note here that Cassini is not an orbiter dedicated to Titan, but a spacecraft orbiting the whole Saturnian system.

2.2 The Cassini Imaging Science Subsystem (ISS)

2.2.1 Description of the ISS instrument

The Cassini Imaging Science Subsystem (ISS) is the highest-resolution two-dimensional imaging device on the Cassini Orbiter. It carries two framing cameras (i) a narrow angle, reflecting telescope with a 2 m focal length and a square field of view (FOV) 0.35º across, and (ii) a wide-angle refractor with a 0.2 m focal length and a FOV 3.5º across. Centered at each camera there is a charged coupled device (CCD) detector consisting of a 1,024 square array of pixels. Many options for data collection are offered from the data system including choices for on-chip summing, rapid imaging and data compression. The cameras are equipped with various spectral filters that cover the electromagnetic spectrum from 200 to 1100 nm. The ISS is also the optical navigation instrument for the Cassini mission. In Table 3.1 on Chapter 3 the Cassini flybys so far executed with ISS observations are presented (Porco et al. 2004).

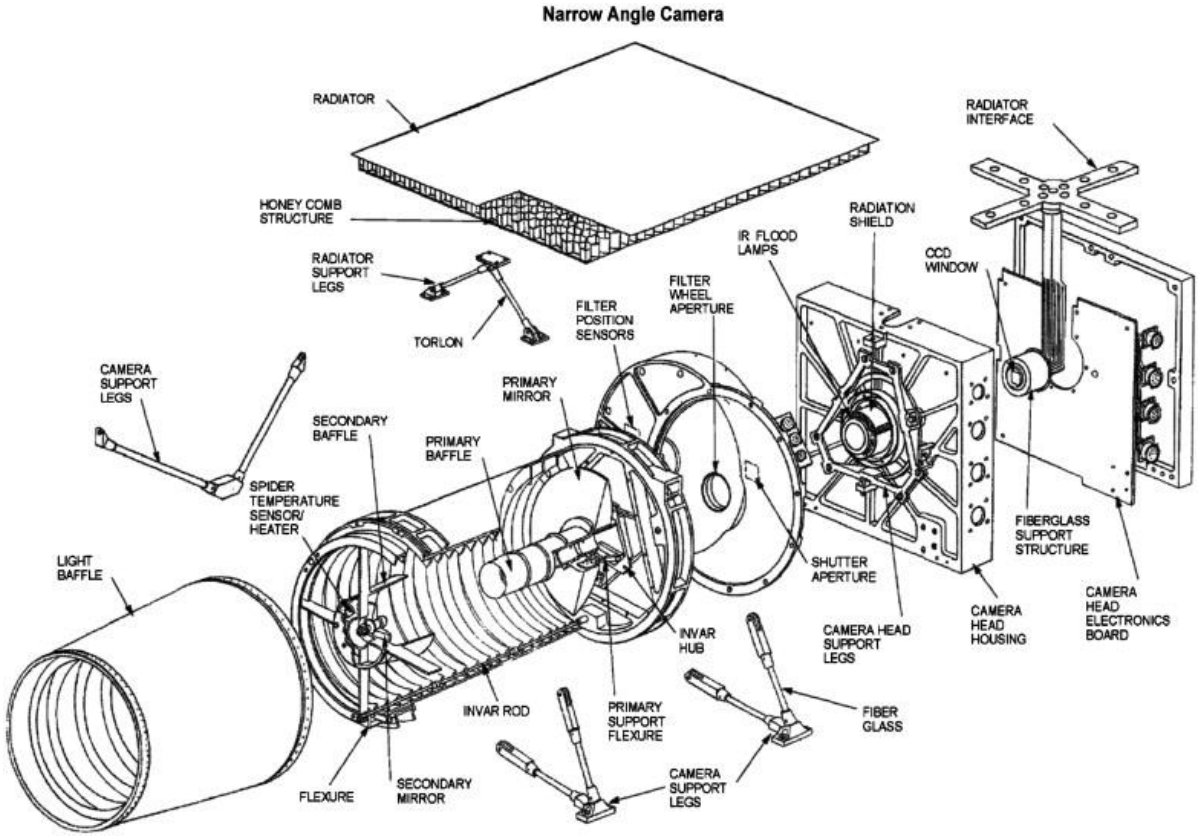

Fig. 2.5 – Schematic diagram of the Cassini ISS Narrow Angle camera (Porco et al. 2004).

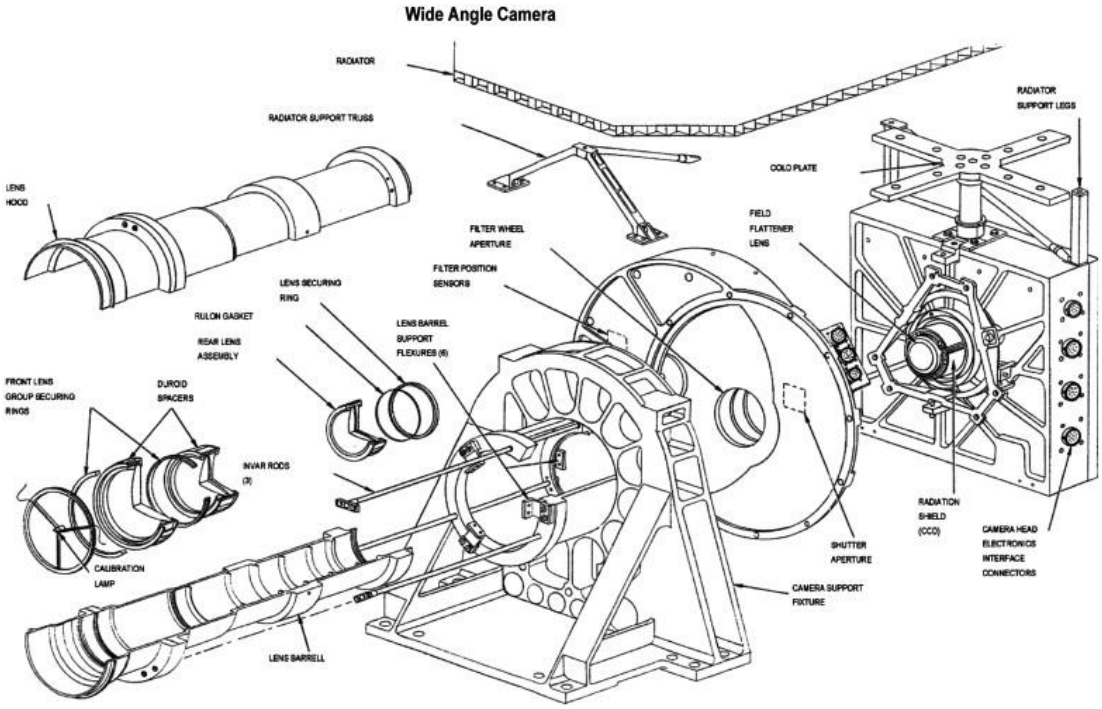

Fig. 2.6 – Schematic diagram of the Cassini ISS Wide Angle camera (Porco et al. 2004).

2.2.2 ISS observations of Titan's surface

The global map of Titan presented in Figure 2.6 shows a mosaic of ISS data collected from the beginning of the Cassini mission until April 2011. The images, acquired using a filter centered at 938 nm, provide information on variations in albedo. Due the scattering of light by Titan's dense atmosphere, no topographic shading is visible in these images.

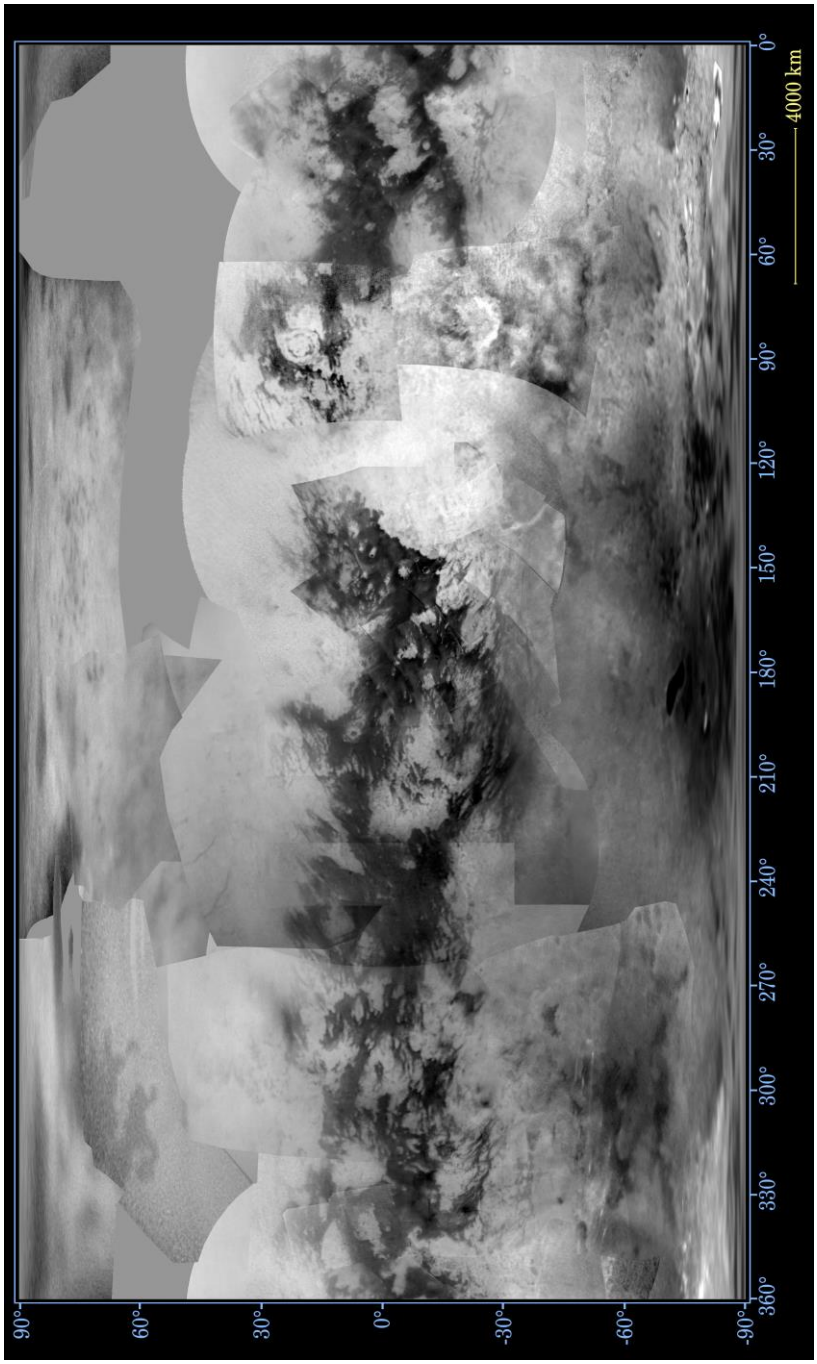

Fig. 2.6– Titan map from ISS data from the beginning of the Cassini mission in 2004 up to April 2011 (PIA14908) (Map credit: NASA/JPL-Caltech/Space Science Institute)

2.3 The Cassini Radar Mapper (RADAR)

2.3.1 Description of the RADAR instrument[14]

The Cassini Radar (RADAR) investigates the surface of Titan by taking four types of observations: imaging, altimetry, backscatter, and radiometry as mentioned earlier. The microwave radiation penetrates Titan's opaque atmosphere, maps the surface, and through the combination of RADAR data with the data other Cassini optical remote sensing instruments such as ISS and VIMS, obtain a more enhance understanding of the surface. Bounced pulses of microwave energy from different incidence angles, monitor the surface and the convertion to distances lead to the construnction of visual images in the imaging mode of the RADAR instrument (SAR data, see Chapter 3) (Fig. 2.7). Similar bouncing with the use of the altimetry mode of the instrument and measurements of the 'echo' return, helps on the recording of numerical data and the calculation of average altitudes of the surface areas (topography, see Chapter 3). In the backscatter operational mode, the RADAR acts as a scatterometer by measuring the intensity of the energy of the returning pulses. During imaging, altimetry, and backscatter operations, the RADAR instrument transmits linear frequency-modulated Ku-band pulsed signals in the direction of the surface of Titan using the high-gain antenna (HGA).

Moreover, the RADAR instrument with its multibeam nature allows the use of the SAR Monopulse Amplitude Comparison method (Chen and Hensley, 2005; Stiles et al. 2009), which estimates surface heights by comparing the calibration of overlapping SAR imagery obtained from different antenna beams) of the RADAR instrument. The results are the SARtopo data (Fig. 2.8) that can be used for the creation of Digital Terrain Models (DTM) and/or Digital Elevation Model (DEM) profiles.

[14] *Information adapted from Elachi et al. 2004 and http://saturn.jpl.nasa.gov/spacecraft/cassiniorbiterinstruments/instrumentscassiniradar/instcassiniradardetails/*

2.3.2 RADAR-SAR/SARtopo observations of Titan's surface

The most updated Titan global maps of RADAR-SAR swaths and SARtopo (with interpolation up to 90%) are shown in Fig. 2.7 and Fig. 2.8.

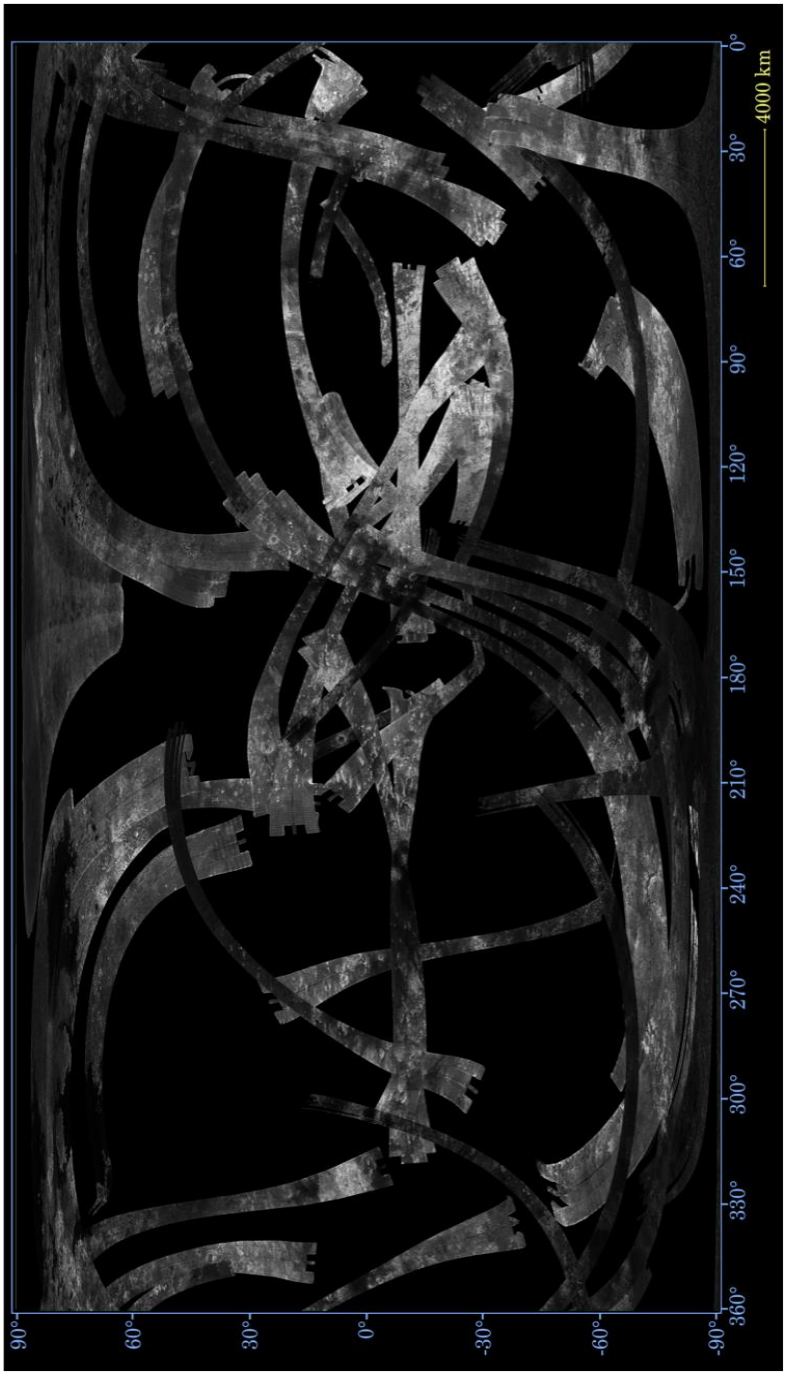

Fig. 2.7 – Titan map from RADAR SAR swaths up to July 2010 (Map credit: http://pirlwww.lpl.arizona.edu/~perry/RADAR/).

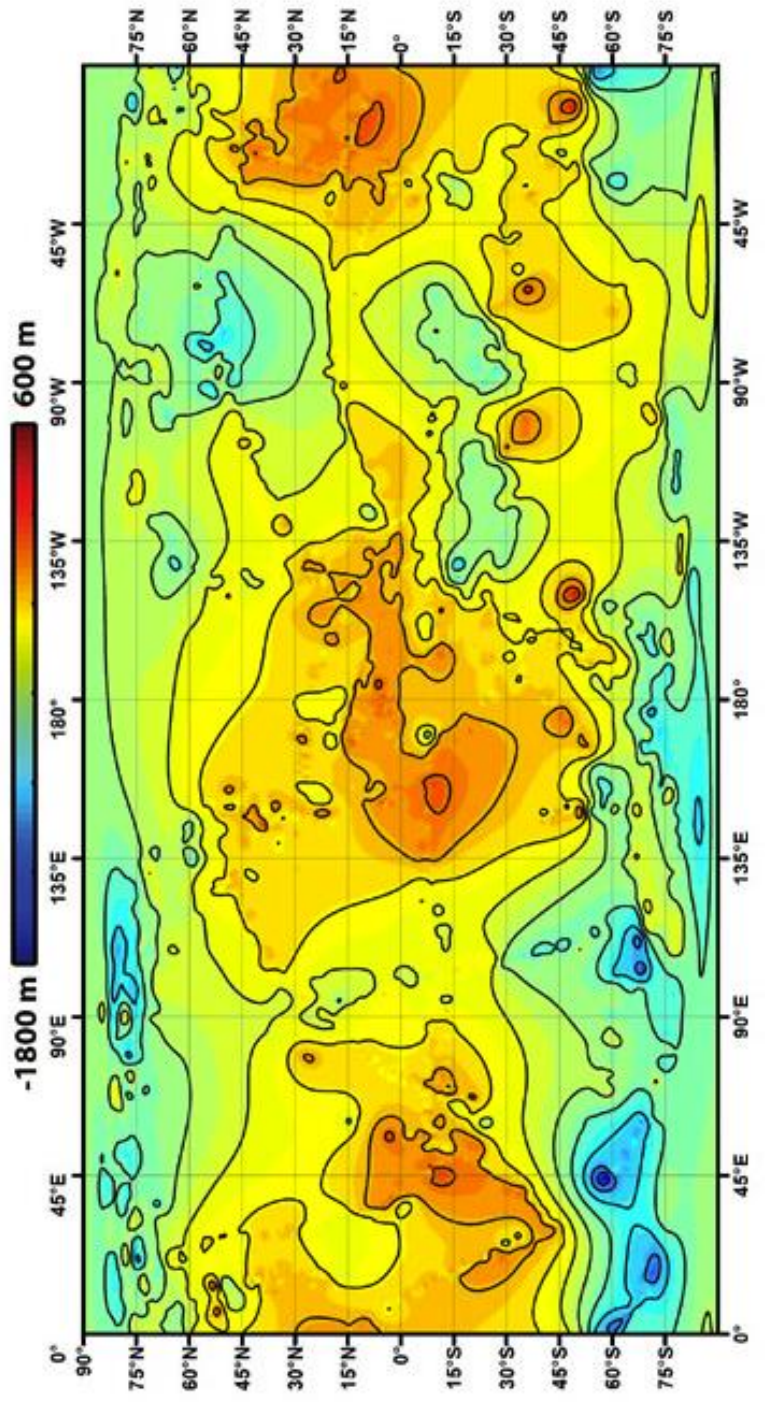

Fig. 2.8 – Titan map from SARtopo data in an interpolation scheme (Map credit: Lorenz et al. 2013).

2.4 The Cassini Visual and Infrared Mapping Spectrometer (VIMS)

Most of my work presented here was based on VIMS spectro-imaging data that I describe in detail hereafter and on Chapter 3.

2.4.1 Description of the VIMS Instrument[15]

VIMS is separated into two assemblies; the Optical Pallet Assembly (OPA) and the Main Electronics Assembly (ME) (Fig. 2.9). The ME, contains several electronic subassemblies and governs all OPA functions and serves as the only interface to the spacecraft. The OPA consist of two imaging spectometers, one infrared (VIMS-IR) and one Visible (VIMS-V). The latter contains two subassemblies, the Visible Channel Optical Head that is a visible imaging spectrometer and the Visible Channel Electronics (VCE) that is an electronic unit (Fig. 2.9). Additionally, VIMS-IR also contains the IR Channel, which is an infrared imaging spectrometer, and the Signal Processing Electronics (SPE) that transfer data from the IR and Visible channels to the ME.

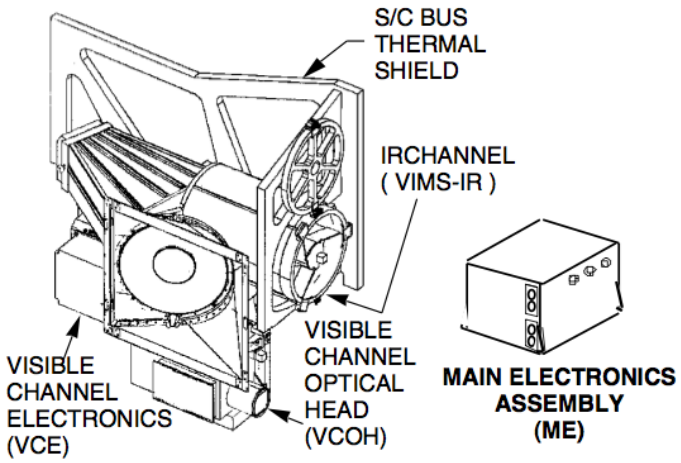

Fig. 2.9 – The Optical Pallet Assembly on VIMS (Scheme credit: Miller et al. 1996).

Table 2.1, presents the detailed design specifications of the instrument, while Figure 2.10 shows its functional block diagram.

[15] *Information on the instrument adapted from Miller et al. (1996) and Brown et al. (2004).*

Table 2.1 – VIMS detailed design specifications (Adapted from Miller et al. 1996).

	VISIBLE CHANNEL	IR CHANNEL	TOTAL SYSTEM
SPECTRAL			
Coverage	0.35 – 1.05 μm	0.85 – 5.1 μm	0.35 – 5.1 μm
Sampling	7.3 nm/spectel	16.6 nm/spectel	0.30 – 5.1 μm
Bands	96	256	
SPATIAL			
Inst. Field of View	0.17 x 0.17 mrad	0.25 x 0.50 mrad	0.5 x 0.5 mrad
Effective IFOV	(3x3 sum)	(1x2 sum)	
Field of View (FOV)	64 pixels X-Axis	64 pixels X-Axis	64 pixels X-Axis
	64 pixels Z-Axis	64 pixels Z-Axis	64 pixels Z-Axis
Swath width	576 IFOVs	128 IFOVs	
OPTICAL SYSTEM			
Effective Focal Length	143 mm	426 mm	
A-Omega	4.42 x 10-7 cm2 ster	4.37 x 10-5 cm2-ster	
Geometric throughput	100%	55%	
IN-FLIGHT CALIBRATION			
Spectral (internal)	2LEDs	1 Laser Diode	
Spectral (external)	Solar Calib. Port	Solar Calib. Port	
Radiometric	Stars	Stars	
Dark Signal	Space Background	Closed Shutter	
DETECTORS			
Active Area	24 x 24 μm/pixel	103 x 200 μm/pixel	
Pixel separation	24 μm	123 μm pixel-to-pixel	
ELECTRONICS			
Digitization	12 bits	12 bits	12 bits
Pixel Integration Times	80 msec to 130 sec	13 msec to 12 sec	
OPERATING TEMPERATURES			
Detector	-40ºC to -20ºC	-213ºC to -196ºC	
Optics	-10 to 20ºC	-143 to -113ºC	
Electronics	-20 to 50ºC	-20 to 50ºC	

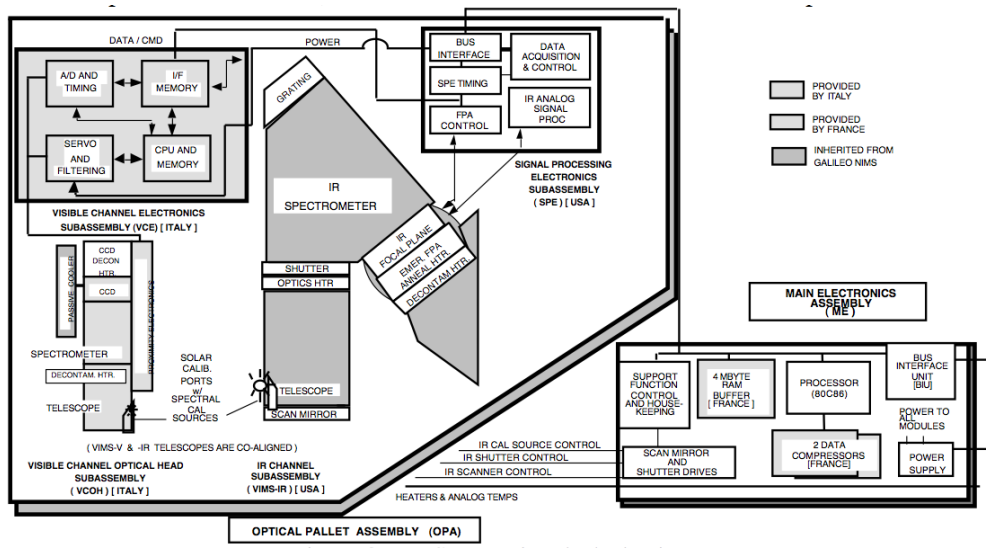

Fig. 2.10 – VIMS functional block diagram of the entire instrument with VIMS-VIS and VIMS-IR integrated on an Optical Pallet Assembly (OPA) (Diagram credit: Brown et al. 2004).

The VIMS-V and IR work together and simultaneously as a united device. However, synchronization of their mirror motion and data acquisition is not standard. The VIMS-VIS is

equipped with a frame transfer Charge-Coupled Device (CCD) matrix detector on which spectral and spatial information is stored at a time, in 'push-broom' mode (views one row of a square scene at a time). Moreover, the VIMS-IR is equipped with a linear array detector that collects the data in 'whisk-broom' mode (views only a single spatial pixel per exposure). In order to create 2-D images like the ones in use in this thesis, the VIS and IR channels start at the top of the scene and collect data row by row with excellent geometric alignment and synchronization.

2.4.2 Titan surface and lower atmosphere from VIMS

The acquired VIMS spectro-imaging data are dominated by scattering of solar radiation from particles in the atmosphere and strong absorptions that results on the lowering of the overall albedo level toward zero except in seven atmospheric windows (0.93, 1.08, 1.27, 1.59, 2.03, 2.69-2.79, and 5.0 μm). Hence, the Cassini/VIMS spectro-imaging data called datacubes (see Chapter 3), include information on the content of the lower atmosphere (0-200 km) as well as on the surface properties (Fig. 2.11). One of the major goals of this PhD thesis is the evaluation of the atmospheric content in the lower part of Titan's atmosphere and the consequent extraction of the true surface properties.

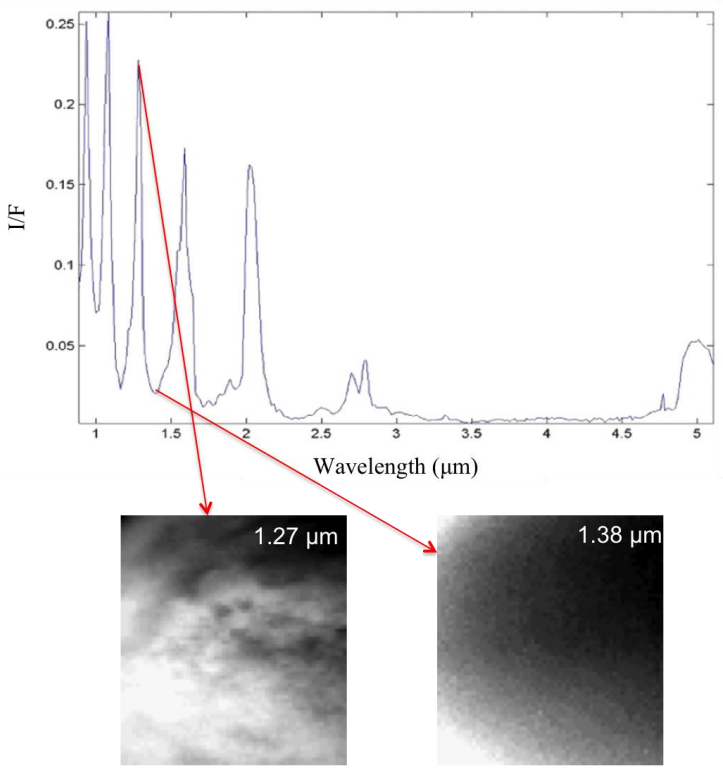

Fig. 2.11 – Transmission spectrum of gaseous methane, in the 1–5 μm wavelength range which spans the spectral range of the infrared channel of the VIMS instrument. The peaks in the spectrum define the 'methane windows' in Titan's atmosphere (lower right -1.38 μm) at which VIMS is able to penetrate the atmosphere and

image the surface (lower left -1.27 μm). However, the even in the 'methane windows' a portion of the atmospheric contribution is still present (Upper image credit: Nelson et al. 2006).

According to Table 3.1 (Chapter 3), up to this day, Titan has been observed many times by VIMS during a number of Cassini flybys acquiring low to high resolution VIMS data (section 3.3, Chapter 3) and from distances ranging from 5 km/pixel to 150 km/pixel. Figure 2.12, illustrates the global Titan map as synthesized by VIMS data at 2.03 μm up to 2010, while Figure 2.13 shows the mosaic from the same data in RGB mode (Le Mouelic et al. 2012).

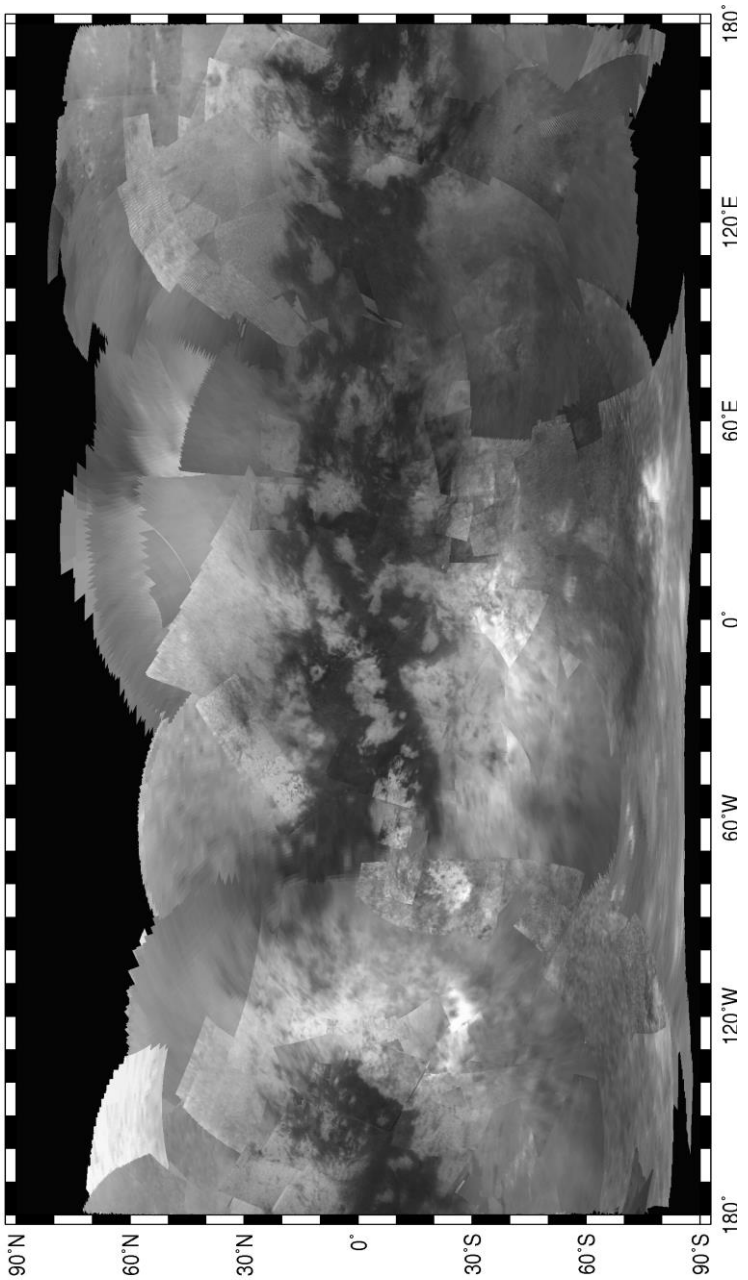

Fig. 2.11 – Titan map from VIMS data at 2.03 μm up to 2010 (Map credit: Le Mouelic et al. 2012).

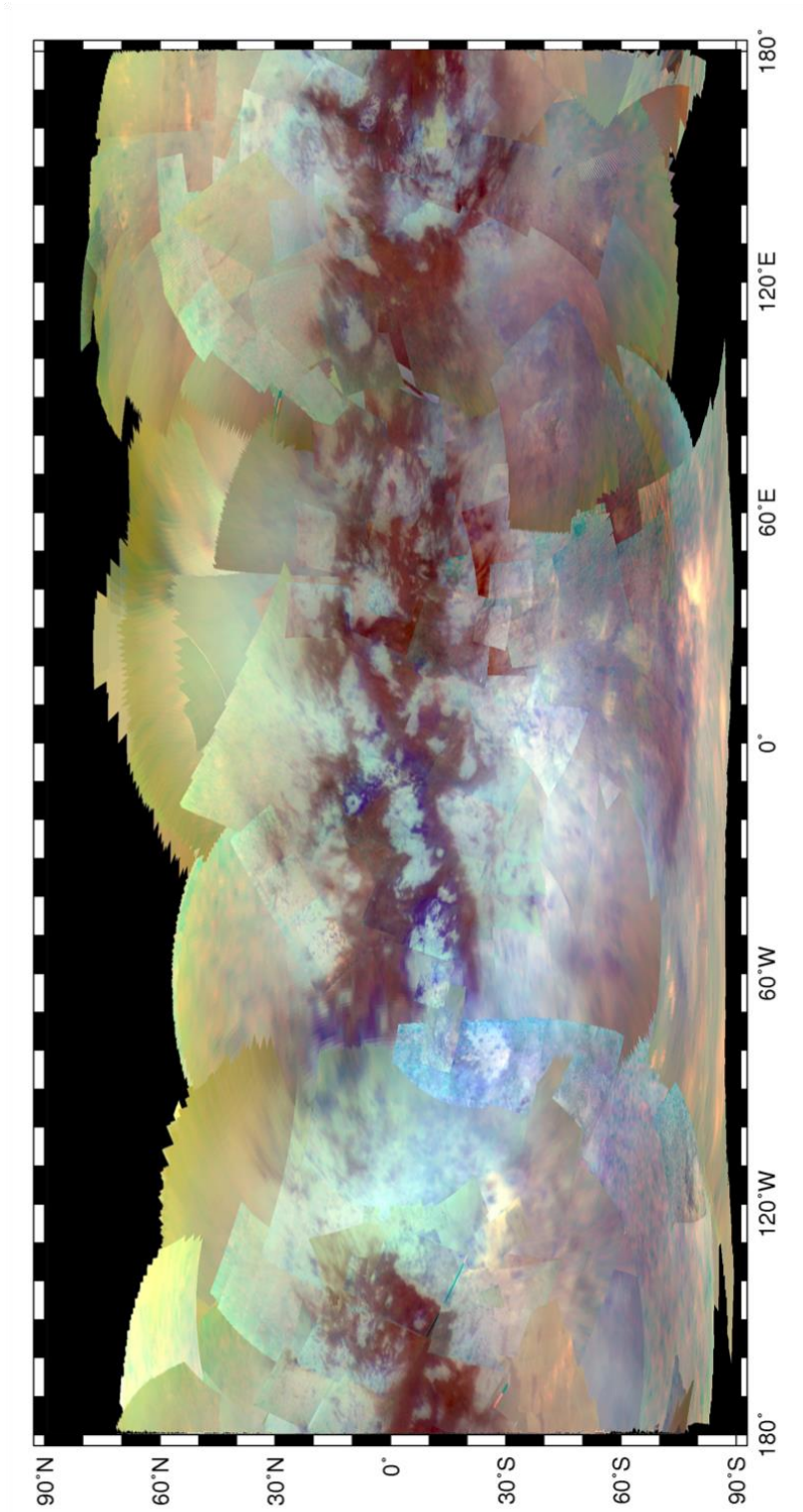

Fig. 2.12 – Titan map from VIMS data in RGB mode up to 2010 (R: 5μm, G: 2.03 μm, B: 1.27 μm) (Map credit: Le Mouelic et al. 2012).

2.5 The Huygens probe and instruments

The Huygens probe is a deep space probe that penetrated a planetary atmosphere and performed a successful landing farther away from Earth that any other man-made vehicle in the history. The probe released from the orbiter on a trajectory directed towards Titan on December 25th, 2004 and followed three phases, the Entry, the Descent and the Landing before landing on Titan on January 14th, 2005 after for 2 h 27 mins 50 s (Lebreton et al. 2009). The area where it landed is located in the equator (Adiri - 10.3° S, 192.3°W) (see also sections 1.3 and 4.1.1, Chapters 1 and 4 respectively).

The orbiter then passed below the probe's horizon, breaking the established link between Huygens and the Earth (Lebreton et al. 2005). However, the Very Long Baseline Interferometry (VLBI) network, consisting of 17 large radio telescopes, recovered the Huygens signal (Witasse et al. 2006) and thus Huygens continued to send back to Earth more measurements. Eventually, before Huygens' five batteries ran out of energy, it had already submitted the data from the 2.5 first hours of its descent and then 3 h and 14 min after its touchdown on the surface (Lebreton et al. 2009).

As in Figure 2.13 (right) the Huygens payload consists of six scientific instruments including a gas chromatograph and mass spectrometer, an aerosol collector, a descent imager and spectral radiometer, an atmosphere structure instrument, a Doppler wind experiment and a surface investigation package.

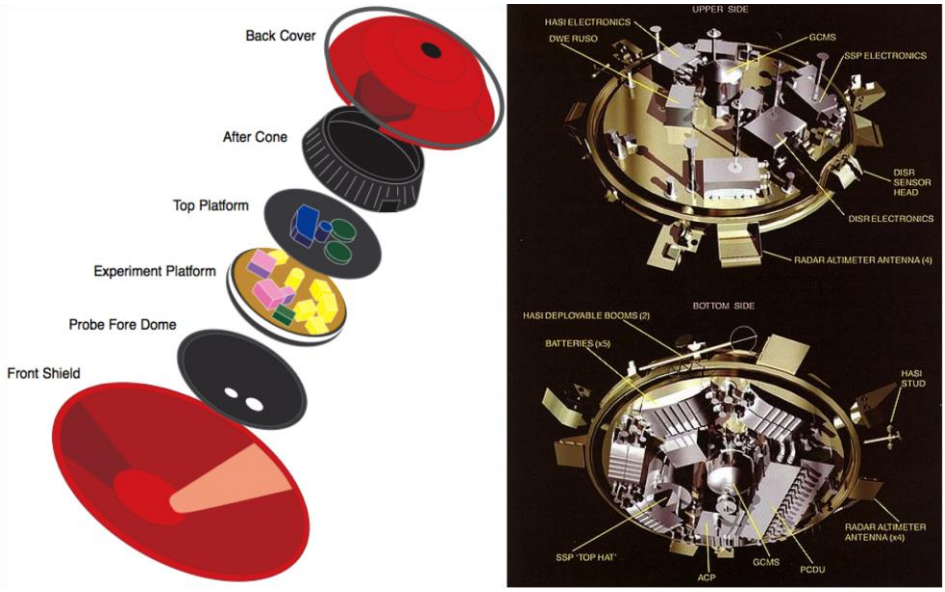

Fig. 2.13 - (left) Huygens' interior (right) Huygens probe instrumentation of the Experiment Platform, with the upper and the bottom side of the vehicle (Image credit: NASA Press Kit, June 2004).

2.5.1 Description of the probe's instruments

The Gas Chromatograph and Mass Spectrometer (GCMS) was a versatile gas chemical analyzer that identified the various atmospheric constituents and measured the composition of the atmosphere of Titan, isotopic ratios and trace species, from the parachute release time to the surface. It worked either in the direct mass spectrometer mode or by sampling gases that passed through gas chromatograph columns to distinguish components of similar mass prior to the mass spectrometer analysis. It began its operation after the protection shield release at the altitude of 160 km during the descent phase (Niemann et al. 1997; 2005).

The Aerosol Collector and Pyrolyzer (ACP) has sampled aerosols for GCMS to analyse their chemical composition. It operated during the descent in two stages: (a) from the top of the atmosphere to 40 km and from 23 km to 17 km altitude. When the sampling was accomplished the filter accumulated into an oven to conduct pyrolisis before sent it to GSMS (Israel et al. 2002; 2005).

The Doppler Wind Experiment (DWE) used one of the two redundant chains (Transmitter A) of the probe-orbiter radio link and it is mainly based on both probe and orbiter (Bird et al. 2002). The DWE data was transmitted to Cassini through Channel A, which due to a command error, was lost. Fortunately, the Earth-based large radio telescope network recorded the signal directly (Bird et al. 2005). DWE determined the direction and the magnitude of Titan's zonal winds and confirmed the super-rotation of Titan's atmosphere (Bird et al. 2005; Lebreton et al. 2009).

The Surface Science Package (SSP) is a nine sensors suite, which determined the properties of the lower atmosphere, the surface at the landing site and the subsurface. The sensors are accelerometers, internal and external, penetrometers, sonar-velocimeter and density, permittivity, refractive, thermal properties index sensors as well as a tiltmeter (Zarnecki et al. 2002). They showed a smooth surface but not flat, resembling wet clay, packed snow or sand (Zarnecki et al. 2005).

The Huygens Atmosphere Structure Instrument (HASI) consists of a 3-axis accelerometer, a set of a coarse and a fine temperature sensors, a multi-pressure sensor, a microphone and an electric field sensor array (Fulchignoni et al. 2002). HASI will be discussed in more detail in the following section.

The Descent Imager/Spectral Radiometer (DISR) is a multi-sensor optical remote sensing instrument with a wide spectral range capabilities (0.3 to 1.67 μm) (Tomasko et al. 2002).

In my research, I have had to compare with and use the "ground truth" obtained by the DISR and HASI instruments, so that I give some more details on their data in the following section.

2.5.2 Titan surface and lower atmosphere from the probe

HASI studied the atmospheric structure of Titan and gave a detailed temperature vertical profile and recorded the surface pressure and temperature (1,467 ± 1 mbar and 93.65 ± 0.25 K, respectively). HASI temperature and pressure sensors probed the atmosphere directly for the first time from an altitude of 1,400 km down to the surface. Indeed, the P, T sensors were deployed after the shield release and sampled the local atmosphere. These parameters help to calibrate measurements from other instruments both on the probe and from the orbiter. The derived HASI temperature vertical profile (Fig. 2.14) is used for instance as a reference when adopting inverse methods to retrieve the temperature and abundance from CIRS data. Following Voyager, HASI found Titan's atmosphere to be a terrestrial analogue in terms of thermal structure consisting of layers of: an exosphere, a mesosphere, a stratosphere and a troposphere, with two major temperature inversions at 40 and 250 km, corresponding to the tropopause (temperatures of 70 K –minimum) and stratopause (temperatures of 186 K - maximum) (Fulchignoni et al. 2005).

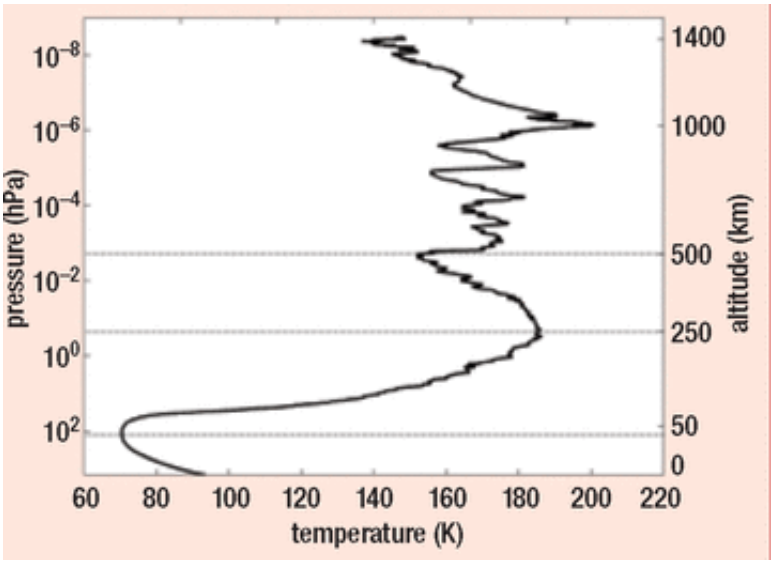

Fig. 2.14 - Titan's temperature profile as derived from Huygens/HASI measurements. The several inversions in the upper atmosphere may be due to gravity waves (Fulchignoni et al. 2005).

In addition, gravity waves signatures of 10–20 K in amplitude were recorded above 500 km around an average temperature of 170 K (Fig. 2.14). These temperatures are higher than predicted by the models. In the lower atmosphere, below about 200 km, all current

measurements on Titan agree with the Voyager 1 profile (Coustenis et al. 2007).

Another Huygens instrument that investigated the lower layer of the atmosphere but also the surface was the DISR. DISR acquired spectra and high-resolution images of Titan's atmosphere while also measuring the solar radiation in the atmosphere. Except for the imagers, a visible spectrometer, an IR spectrometer, a solar aureole camera, violet photometers, and a sun sensor are parts of the instrument. DISR also had a 20 W lamp (surface science lamp), which switched on during the last stages of the probe's descent (at 700 m altitude) in order to enlighten the surface beneath it. It also revealed traces of hydrocarbon liquids on its surface through complex drainage systems and sent back to the Earth the first images of Titan's surface (Tomasko et al. 1997; 2005).

During the descent of Huygens into Titan’s surface, DISR measured the haze properties of the lower atmosphere (Tomasko et al. 2005) finding the monomer radius to be 0.05 mm; similar to previous estimations. Although some measurements were not in agreement with previous assumptions, such as the haze optical depth that showed larger range from 2 at 935 nm to 4.5 at 531 nm (Tomasko et al. 2009).

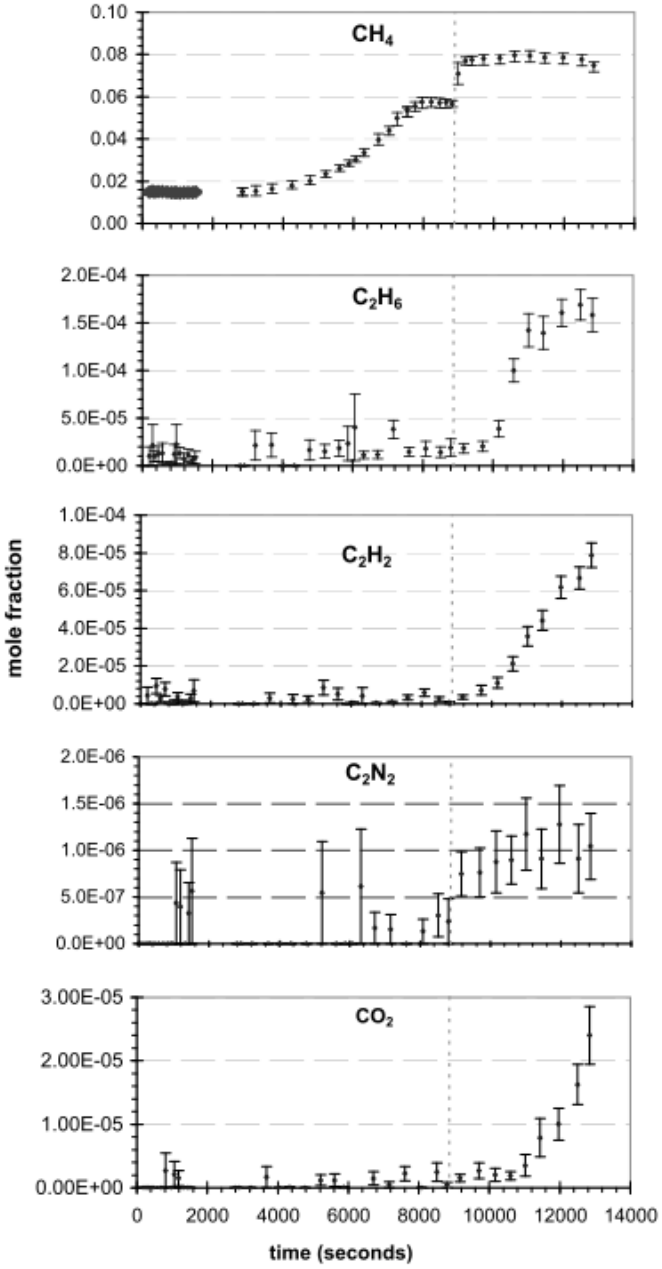

Fig. 2.15 - Mole fractions of CH_4, C_2H_6, C_2H_2, C_2N_2, and CO_2 with respect to the descent time. The time of surface impact is indicated by a vertical dashed red line (Image and information credit: Niemann et al. 2010).

In addition, the DISR spectral measurements of the methane mole fraction in the stratosphere were in agreement with CIRS and GCMS measurements of 1.4-1.6% while at altitudes close to 20 m DISR measured it at 5±1% (Tomasko et al. 2005; Lorenz et al. 2006b). Niemann et al. (2010) re-examined the GCMS data and suggested the methane mole fraction to be (1.48 ± 0.09) × 10−2 in the lower stratosphere (139.8–75.5 km) and (5.65 ± 0.18) × 10−2 near the surface (6.7 km to the surface). Additionally, the molecular hydrogen mole fraction was found to be (1.01 ± 0.16) × 10^{-3} in the atmosphere and (9.90 ± 0.17) × 10^{-4} on the surface. Isotope ratios were 167.7 ± 0.6 for $^{14}N/^{15}N$ in molecular nitrogen, 91.1 ± 1.4 for

$^{12}C/^{13}C$ in methane, and $(1.35 \pm 0.30) \times 10^{-4}$ for D/H in molecular hydrogen. The mole fractions of ^{36}Ar and radiogenic ^{40}Ar are found to be $(2.1 \pm 0.8) \times 10{-}7$ and $(3.39 \pm 0.12) \times 10^{-5}$, respectively. ^{22}Ne has been tentatively identified at a mole fraction of $(2.8 \pm 2.1) \times 10^{-7}$ (Fig. 2.15).

These results have significant implications for formation and evolution models of Titan, as discussed in later Chapters, but also demonstrate also from chromatography and spectral and mass spectroscopy the complexity of Titan's surface nature and composition.

As presented in Chapter 1, the Cassini-Huygens mission enhanced significantly our knowledge with respect to Titan's methane cycle and its role in the satellite's atmosphere. The DISR measurements suggested for the surface a relative humidity of methane at about 45% and in addition to GCMS evidence for evaporation (methane, ethane, acetylene, cyanogen and carbon dioxide) indicated the presence of fluid flows on the surface through rainfall of methane from the atmosphere. Moreover, the DISR observations unveil some surface characteristics, as I will discuss in detail in section 4.1.1, on Chapter 4 where we use it in our radiative transfer simulations.

Chapter 3

DATA description

This chapter introduces the data in use during my PhD researches. In particular, I have processed Cassini VIMS and RADAR data from several flybys while the Radiative transfer tool I apply for the VIMS data analysis (introduced in Chapter 5) makes use of parameters adapted from Huygens' DISR, HASI and GCMS, which I do not introduce here and the reader is referred to the paper by Hirtzig et al. (2013) for further details. Of course, I also take into account results from the Cassini cameras and other instruments (with access to the interior for instance) in trying to build a coherent picture of Titan's atmosphere-surface-interior exchanges.

3.1 Cassini Flybys and observations in relation to the surface

In the previous Chapter 2, I discussed the execution of flybys of Titan and Enceladus by Cassini while it tours the Saturnian system. Table 3.1 lists the so far completed (by July 2013) Cassini flybys of Titan and Enceladus and the operations by its various instruments (in color are the ones related to the surface) starting with the T0 flyby, which was executed right after the Saturn Orbit Insertion.

Table 3.1 - Cassini Titan flybys[16] over Titan and Enceladus. The list includes the coded name of the flyby ('T' for Titan and 'E' for Enceladus), the date of execution and the instrument(s) in operation. The flybys in color correspond to the ones dedicated mainly to the surface investigation.

Year	Flyby	Date	Target	Instrument in operation
2004	T0	03 July 2004	Titan	VIMS
	TA	26 October 2004	Titan	VIMS
	TB	13 December 2004	Titan	UVIS
	TC	14 January 2005	Titan	
2005	T3	15 February 2005	Titan	RSS
	E01	15 February 2005	Enceladus	
	E02	09 March 2005	Enceladus	
	T4	31 March 2005	Titan	ISS/CIRS
	-	31 March 2005	Enceladus	
	T5	16 April 2005	Titan	INMS/MAPS
	T6	22 August 2005	Titan	CIRS
	T7	07 September 2005	Titan	RADAR
	T8	28 October 2005	Titan	RADAR
	T9	26 December 2005	Titan	UVIS
2006	T10	15 January 2006	Titan	UVIS
	T11	27 February 2006	Titan	RSS
	T12	18 March 2006	Titan	RADAR
	T13	30 April 2006	Titan	UVIS/RADAR
	T14	20 May 2006	Titan	RSS
	T15	02 July 2006	Titan	MAPS
	T16	22 July 2006	Titan	RADAR/UVIS
	T17	07 September 2006	Titan	INMS/VIMS
	-	09 September 2006	Enceladus	
	T18	23 September 2006	Titan	INMS/RADAR
	T19	09 October 2006	Titan	RADAR
	T20	25 October 2006	Titan	VIMS
	-	09 November 2006	Enceladus	
	T21	12 December 2006	Titan	INMS/RADAR
	T22	28 December 2006	Titan	RSS
2007	T23	13 January 2007	Titan	RADAR
	T24	29 January 2007	Titan	VIMS

[16] *http://saturn.jpl.nasa.gov/mission/flybys/*

Year	Flyby	Date	Target	Instrument in operation
	T25	22 February 2007	Titan	RADAR
	T26	10 March 2007	Titan	INMS
	T27	26 March 2007	Titan	RSS
	T28	10 April 2007	Titan	RADAR
	T29	26 April 2007	Titan	RADAR
	T30	12 May 2007	Titan	RADAR
	T31	28 May 2007	Titan	RSS
	T32	13 June 2007	Titan	ISS
	T33	29 June 2007	Titan	RSS
	T34	19 July 2007	Titan	ISS
	T35	31 August 2007	Titan	VIMS
	T36	02 October 2007	Titan	INMS/RADAR
	T37	19 November 2007	Titan	INMS/VIMS
	T38	05 December 2007	Titan	RSS
	T39	20 December 2007	Titan	RADAR
2008	T40	05 January 2008	Titan	UVIS/VIMS
	T41	22 February 2008	Titan	RADAR
	E03	12 March 2008	Enceladus	
	T42	25 March 2008	Titan	INMS
	T43	12 May 2008	Titan	RADAR
	T44	28 May 2008	Titan	RADAR
	Cassini Equinox Mission			
	T45	31 July 2008	Titan	RSS
	E04	11 August 2008	Enceladus	
	E05	09 October 2008	Enceladus	
	E06	31 October 2008	Enceladus	
	T46	03 November 2008	Titan	RSS
	T47	19 November 2008	Titan	VIMS
	T48	05 December 2008	Titan	RADAR/INMS
	T49	21 December 2008	Titan	RADAR
2009	T50	07 February 2009	Titan	RADAR/INMS
	T51	27 March 2009	Titan	VIMS/ISS
	T52	04 April 2009	Titan	RSS/ISS
	T53	20 April 2009	Titan	CIRS
	T54	05 May 2009	Titan	ISS/VIMS
	T55	21 May 2009	Titan	RADAR
	T56	06 June 2009	Titan	INMS/RADAR
	T57	22 June 2009	Titan	RADAR/INMS
	T58	08 July 2009	Titan	UVIS/RADAR
	T59	24 July 2009	Titan	CAPS
	T60	09 August 2009	Titan	RADAR/ISS
	T61	25 August 2009	Titan	RADAR/MAPS
	T62	12 October 2009	Titan	VIMS/UVIS/CIRS
	E07	02 November 2000	Enceladus	
	E08	21 November 2009	Enceladus	
	T63	12 December 2009	Titan	CAPS

Year	Flyby	Date	Target	Instrument in operation
	T64	28 December 2009	Titan	RADAR
2010	T65	12 January 2010	Titan	RADAR/INMS
	T66	28 January 2010	Titan	VIMS/ISS
	T67	05 April 2010	Titan	CIRS
	E09	28 April 2010	Enceladus	RSS
	E10	18 May 2010	Enceladus	UVIS
	T68	20 May 2010	Titan	CIRS
	T69	05 June 2010	Titan	VIMS
	T70	21 June 2010	Titan	MAG
	T71	07 July 2010	Titan	INMS/RADAR/CAPS
	E11	13 August 2010	Enceladus	
	T72	24 September 2010	Titan	VIMS
	T73	11 November 2010	Titan	VIMS/CAPS
	E12	30 November 2010	Enceladus	RSS
	E13	21 December 2010	Enceladus	
2011	T74	18 February 2011	Titan	RSS/RADAR/CAPS
	T75	19 April 2011	Titan	RPWS/CAPS
	T76	8 May 2011	Titan	VIMS/UVIS/CIRS/MAG
	T77	20 June 2011	Titan	RADAR
	T78	12 September 2011	Titan	RSS/UVIS/CAPS
	E14	01 October 2011	Enceladus	
	E15	19 October 2011	Enceladus	
	E16	06 November 2011	Enceladus	RADAR/CIRS
	T79	13 December 2011	Titan	CAPS
2012	T80	2 January 2012	Titan	ISS/CIRS/VIMS/RPWS
	T81	30 January 2012	Titan	ISS/CIRS
	T82	19 February 2012	Titan	CIRS/VIMS
	E17	27 March 2012	Enceladus	INMS
	E18	14 April 2012	Enceladus	INMS
	E19	02 May 2012	Enceladus	RSS
	T83	22 May 2012	Titan	RADAR/MAG
	T84	7 June 2012	Titan	RADAR/ISS
	T85	24 July 2012	Titan	VIMS/MAG
	T86	26 September 2012	Titan	INMS/UVIS
	T87	13 November 2012	Titan	UVIS/INMS/VIMS/ISS
	T88	29 November 2012	Titan	CIRS/VIMS/ISS
2013	T89	17 February 2013	Titan	RSS
	T90	05 April 2013	Titan	CIRS/VIMS
	T91	23 May 2013	Titan	RADAR
	T92	10 June 2013	Titan	RADAR/ISS/CIRS
	T93	26 July 2013	Titan	VIMS/ISS

From Table 3.1 we can note the extensive use of the instruments dedicated to the surface research such as VIMS, RADAR and ISS, which operate during most of the flybys.

3.2 RADAR data

The RADAR instrument operates in three ways: imaging, altimetry and radiometry. Each mode allows for the collection of different types of data, from simple imaging to 3-D modeling, to passive collection of information, such as simply recording the energy emanating from Titan's surface (see also Chapter 2). As mentioned before, The RADAR sensing instruments include the SAR, the Altimeter and the Radiometer. During my PhD I have processed Cassini/SAR data with a filtering technique that I introduce in Chapter 5 and is also described in a paper that I co-authored by Bratsolis et al. (2012).

3.2.1 Swaths

The RADAR imaging mode provides low-to-high resolution synthetic aperture (SAR) images (Elachi et al. 2004) (Table 3.2).

Table 3.2 – Cassini SAR Data Characteristics (Adapted from Elachi et al. 2004).

Resolution	*Altitude (km)*	*Incidence angle (^{o})*	*Resolution*		*$NE\sigma_0$ (dB)*	*Number of looks*	*Surface coverage (%)*
			Azimuth (km)	Range (km)			
High	1,000-1,600	21-30	0.35-0.41	0.48-0.64	-28 to -21	2-3	≤1.1
Low	1,600-4,000	15-28	0.41-0.72	0.48-2.70	-25 to -15	2-7	≤1.1

As seen in Table 3.2, SAR can probe the surface with two resolutions: the High SAR Resolution (HiSAR) at 350-720 m per pixel and the low SAR resolution. The linear polarized electric field vector of the Cassini/RADAR is oriented to be approximately parallel to Titan's surface during SAR operation (Hayes et al. 2011). RADAR operates only during close flybys of Titan. Figure 3.1 illustrates the observational sequence during nominal Titan flybys, when the closest approach (C/A) is at an altitude of 1000 km or lower.

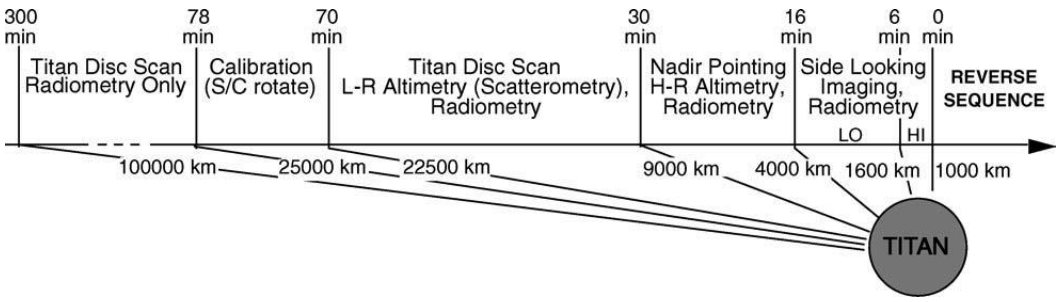

Fig. 3.1 - The sequence of the radar operational stages during a Titan flyby with closest approach at an altitude of 1000 km (Elachi et al. 2004).

The combination of the five individually illuminated sub-swaths results in the total width of RADAR swath and ranges from 120 to 450 km at the spacecraft altitudes from 1000 to 4000 km. Each nominal Titan flyby produces a SAR swath 5000 km long, which is about 1.1% of the satellite's surface. When the flyby has a C/A farther than 4000 km, no SAR images acquisition occurs (Elachi et al. 2004).

3.2.2 Usable data

The Cassini-Huygens data and in particular the SAR data are available in the data library of NASA Planetary Data System (PDS[17]) with the exception of newly acquired ones (last 6 months). Using the Integrated Software for Imagers and Spectrometers (ISIS)[18] that US Geological Survey has developed, Cassini/SAR images can be retrieved.

We have processed SAR data of Titan's lakes and cryovolcanic candidates using the filtering technique (TSPR) described in Chapters 5 and 7 (where I present my results). For a qualitative analysis using this tool a 32-bit version of SAR image is required. ISIS inputs the JPL Cassini RADAR science data products and extracts 32-bit images, which can be processed by GIS software applications and other numerical computing software.

At first, a 32-bit version of Cassini/SAR image PIA08630 was provided by Dr. A. Hayes (Cornell University) and then we were able to retrieve the required version of SAR images through the use of a simple routine in Matlab. Table 3.3 summarizes the characteristics of the 5 SAR data we have used during my PhD.

[17] *http://pds.nasa.gov/*
[18] *http://isis.astrogeology.usgs.gov/*

Table 3.3 – Characteristics of SAR swaths of the areas of interest (Information adapted from: Cassini RADAR User Guide –NASA).

Area of interest	*PIA (NASA)*	*Flyby*	*Longitude (º)*	*Latitude (º)*	*Incidence Angle (º)*	*Polarization Angle (º)*	*Azimuth Angle (º)*	*Range Resolution (km)*	*Azimuth Resolution (km)*
Lakes	PIA08630	T16	80N	92W	24	2.92	252.72	0.46	0.44
'Kissing lakes'	PIA08740	T18	73N	46W	29	0.027	123.35	0.37	0.31
Sotra Patera	PIA11831	T28	15S	40W	19	118.39	214.09	1.75	1.36
Hotei Regio	PIA13950	T41	26S	78W	14	191.29	220.24	0.95	0.57
Tui Regio	PIA9217	T48	20S	130W	31	134.17	213.12	No information	No information

3.3 VIMS data

As described in Chapter 2 VIMS consists of two imaging spectrometers on the Optical Pallet Assembly (OPA), which are the Infrared Channel (VIMS-IR) and the Visible Channel (VIMS- V). VIMS-V has two subassemblies: a visible imaging spectrometer called the Visible Channel Optical Head (VCOH) and an electronics unit called the Visible Channel Electronics (VCE). These imaging spectrometers and their subassemblies scan the target areas of Titan as seen in Fig. 3.2 and provide a pixel synthesis called ‘datacubes.

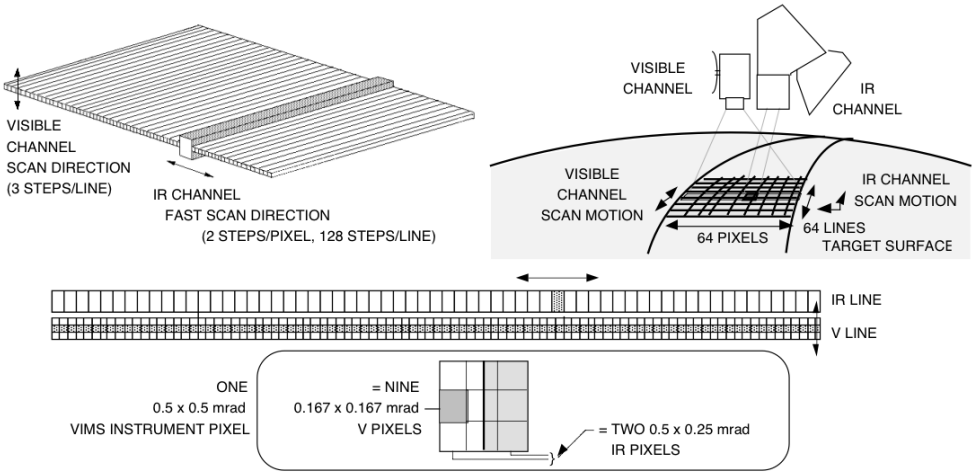

Fig. 3.2 – Operation of the VIMS instruments with its cameras and datacube synthesis (Image credit: Miller et al. 1996).

3.3.1 Datacubes

The VIMS is a dual imaging (pair of cameras) spectrometer that consists of two optical systems coordinated by a common electronics unit. This optical system generates 352 2-D images (64 x 64 pixels) in separate contiguous wavebands. These are combined by the electronics to produce "image datacubes" in which each image pixel represents a spectrum spanning 0.3 to 5.1 microns in 352 steps (Wellman et al. 1987; Miller et al. 1996; Brown et al. 2004).

So far, it appears that 13% of Titan’s surface has been mapped with VIMS at a resolution better than 10km/pixel, 56% with resolution ranging between 10-20 km/pixel and 24% between 20-50% km/pixel (Le Mouelic et al. 2012).

3.3.2 Usable data

One major part of my PhD thesis is the processing and analysis of VIMS data of geologically interesting areas, especially the ones that appear to be anomalously bright at 5

μm and are referred to as cryovolcanic candidates, such as Hotei Regio, Tui Regio and Sotra Patera. An extensive analysis of all these three regions, in addition to others like the Huygens Landing site, the Sinlap crater and some dune fields that have been used for calibration purposes and as test cases, is presented in Chapters 6 and 7. Hence, I have used several VIMS datacubes to complete this multi-data analysis from different flybys (dates), and very importantly with different parameters. Tables 3.4; 3.5; 3.6 and 3.7 summarize the characteristics of all these VIMS data. These are VIMS radiometrically calibrated images.

Table 3.4 summarizes the data in use during my first analysis of VIMS with the radiative transfer code (Hirtzig et al. 2013) that I describe in Chapter 5 and the derivation of the first results concerning the spectral behavior and the dynamical range of bright and dark regions from their actual surface albedos. This work was presented in Solomonidou et al. (2013b) and the data were provided by members of the VIMS team including Pierre Drossart from LESIA/Observatoire de Paris, that secured us direct access to the data, LPL's Bob H. Brown (Arizona-USA), JPL's Christophe Sotin (California-USA), LPG's Stephane LeMouelic (Nantes-France) and AIM's Sebastien Rodriguez (Paris-France), who also co-authored the aforementioned paper.

I followed up with the analysis of several VIMS datacubes from the beginning of the Cassini mission until 2010, but selected a number of them from 2005- 2009 for Hotei Regio and Tui Regio and 2005-2006 for Sotra Patera with the aim to monitor the surface albedo temporal variations of the areas. This work can be found in Solomonidou et al. (2013c). The data here, were provided by the same people I mentioned hereabove in addition to DLR's Ralf Jaumann and Katrin Stephan (Berlin-Germany).

For the processing of VIMS data I use two software systems. The ENvironment for Visualizing Images (ENVI[19]) software and the programming language Interactive Data Language (IDL[20]).

[19] *http://www.exelisvis.com/ProductsServices/ENVI/ENVI.aspx*
[20] *http:// www.exelisvis.com/ProductsServices/IDL.aspx*

Table 3.4 – Cassini/VIMS datacubes including dates, flyby and cube details such as spatial resolution, angles of incidence, emergence and phase, and exposure times of all areas investigated and presented in Chapters 5 and 6 (Solomonidou et al. 2013b). The numbers in the first column are used to facilitate the reader (see Chapter 6).

Observation					**Angles (deg)**		
Area / Coordinates	**Flyby/Date/ Datacube**	**Distance Cassini-Surface (km)**	**Spatial resolution (km/pixel)**	**Exposure time (sec)**	**Inc. (*i*)**	**Emer. (*e*)**	**Ph. (θ)**
#1 HLS/10°S, 192°W	TB/ Dec. 2004/ CM_1481624349	34,110	15	160	36	34	18
#2 Sinlap/11°N, 16°W	T13/ Apr. 2006/ CM_1525118253	27,180	14	68	42	12	40
#3a Hotei Regio/ 26°S, 78°W	T46/ Nov. 2008/ CM_1604411323	91,200	45	520	67	14	81
#**3b** Hotei Regio /26ºS, 78ºW	T47/ Nov. 2008/ CM_1605798513	26,800	13	500	75	11	80
#4 Tui Regio/20°S-130°W	T12/ Mar. 2006/ CM_1521406684	72,800	18	80	16	54	66
#5 Sotra Patera/15°S, 40°W	T09/ Dec. 2005/ CM_1514309549	36,400	18	160	5	14	29

Table 3.5 - Observations, including dates, spatial resolution, the angles of incidence (i), emission (e) of the cubes of the study areas, and the reference points that are located closely to the study area for Hotei Regio (in the same datacube of the actual area) (Solomonidou et al. 2013c).

Hotei Regio							
		Region of Interest (RoI)			**Test case**		
Date (Flyby)	**Cube**	**Res. (km)**	***i***	***e***	**Res. (km)**	***i***	***e***
03/2005 (T4)	CM_1490958010	80-100	10	65	80-100	5	63
04/2005 (T5)	CM_1492340963	40-50	15	70	40-50	10	69
09/2005 (T7)	CM_1504748185	80-100	21	73	80-100	23	70
10/2005 (T8)	CM_1509147231	50-60	47	71	50-60	58	80
12/2005 (T9)	CM_1514294223	60-80	45	69	60-80	36	62
01/2006 (T10)	CM_1515968621	80-100	34	75	80-100	30	72
03/2006 (T12)	CM_1521375965	100-150	19	84	100-150	24	80
12/2008 (T49)	CM_1608544208	30-40	65	15	30-40	70	23
02/2009 (T50)	CM_1612646996	110-120	61	22	110-120	63	18
03/2009 (T51)	CM_1616787365	90-100	60	28	90-100	64	20

Table 3.6 – Same as Table 3.4 but for Tui Regio (Solomonidou et al. 2013c).

Tui Regio									
Region of Interest (RoI)					**Test case A**				
Date (Flyby)	**Cube**	**Res. (km)**	***i***	***e***	**Date (Flyby)**	**Cube**	**Res. (km)**	***i***	***e***
10/2005 (T8)	CM_1509134841	75-85	9	32	10/2005 (T8)	CM_1509134411	86	47	40
03/2006 (T12)	CM_1521406684	15-25	15	50	01/2006 (T10)	CM_1515983150	96	48	23
05/2008 (T44)	CM_1590648938	20-30	45	48	05/2007 (T31)	CM_1559091379	58	34	47
11/2008 (T46)	CM_1604414186	30-40	36	47	02/2008 (T41)	CM_1582416832	65	21	47
02/2009 (T50)	CM_1612646996	110-125	31	39	12/2009 (T64)	CM_1640700264	129	58	33

Table 3.7 – Same as Table 3.4 but for Sotra Patera (Solomonidou et al. 2013c).

Sotra Patera									
Region of Interest (RoI)					**Test case B**				
Date (Flyby)	**Cube**	**Res. (km)**	***i***	***e***	**Date (Flyby)**	**Cube**	**Res. (km)**	***i***	***e***
03/2005 (T4)	CM_1490958010	85-95	26	31	02/2005 (T3)	CM_1487106401	103	22	13
12/2005 (T9)	CM_1514309549	75-85	09	27	10/2005 (T8)	CM_1509137850	76	22	12
02/2006 (T11)	CM_1519713017	20-30	28	29	03/2006 (T12)	CM_1521405451	37	46	23

Chapter 4

The surface and interior of Titan from Cassini-Huygens

Spectro-imaging and radar measurements by the Cassini-Huygens mission suggest that some of the Saturnian satellites may be geologically active and could support tectonic processes. In particular, Titan possesses a complex and dynamic geology, as witnessed by its varied surface morphology, resulting from aeolian, fluvial, and possibly tectonic and endogenous cryovolcanic processes. Indeed, the continuous presence of methane in the upper atmosphere, known to be vanishing by photochemical processes, suggests its replenishment, possibly through internal outgassing, contributing to an active methane cycle.

In this chapter I present a description of the geology of Titan, focusing on the surface features, the geological processes, the interior and the correlation between the atmosphere, the surface and the interior. This work, with an extension to a study on the geology of Enceladus, has been published in the *Hellenic Journal of Geosciences* (Solomonidou et al. 2010). First, I introduce a general view of the geological expressions that are present on Titan, following with up-to-date observations, in addition to comparisons between ice (e.g. Titan) and silicate (e.g. Earth) tectonism, showing the similarities and differences of their properties. I subsequently present the following part of the aforementioned work on Titan's morphotectonic features and their possible origin, which regards to a general classification of the tectonic-like and subject to erosion features and implications about their formation based mainly on terrestrial models. This work has been published in the *Planetary Space Science Journal* (Solomonidou et al. 2013a). Finally, I introduce my work, conducted in collaboration with German colleagues (Dr. Frank Sohl, Dr. Hauke Hussman, Frank Walter) from the Institute of Planetary Research (DLR, Berlin, Germany), which presents the geophysical dynamic potential of Titan's interior and the correlation with the observed geological features (Sohl et al. 2013).

4.1 Titan surface expressions

Data collected from the Cassini-Huygens space mission from the first Cassini flyby and the Huygens landing on Titan up to date, has completely changed our perception on the moon's geology, the processes that form the surface and the connection between the interior and the atmosphere. In relation to the observations, Titan offers a unique opportunity to study the geological processes of an outer Solar system satellite combining Earth-like geological features. Comparative Planetology (see also Chapter 10) studies similar planetary bodies, in terms of materials, such as Earth and Mars (silicates) or Titan and Enceladus (ices). In addition, it studies dissimilar ones in terms of composition, but also with many similarities in processes and features such as Earth's (silicates and tectonics) and Titan's (ices and tectonic-like trends) and provides important information about the formational mechanisms of the surface features and planetary terrains.

As described in detail in Chapter 2, the Cassini orbiter equipped with two spectro-imagers is capable of probing down to the surface via several of the near-infrared windows with the Visual and Infrared Mapping Spectrometer (VIMS -with a typical resolution of 10-20 km/pixel) (Brown et al. 2004) and the Imaging Science Subsystem (ISS -with a typical resolution of 1 km/pixel) (Porco et al. 2004), in addition to the Radar Mapper (RADAR) with a spatial resolution from 300 m to 1.5 km/pixel (Elachi et al. 2004). Furthermore, Huygens probe measurements and observations by the Descent Imager Spectral Radiometer (DISR- Tomasko et al. 2005), the Surface Science Package (SSP- Zarnecki et al. 2005) and the Gas Chromatograph Mass Spectrometer (GCMS- Niemann et al. 2005; 2010) provide additional information on Titan's geology.

These instruments revealed a large variety of surface features (e.g. Jaumann et al. 2009; Brown et al. 2011; Langhans et al. 2012; Lopes et al. 2010; 2013) for instance, among others, the morphotectonic features on Titan, something I examined in one of my recent publications (Solomonidou et al. 2013a). These features include mountains (e.g. Radebaugh et al. 2007; Lorenz et al. 2011; Tokano, 2012; Lopes et al. 2013), ridges (Soderblom et al. 2007), faults (e.g. Radebaugh et al. 2011), and canyons (e.g. Soderblom et al. 2007; Lopes et al. 2010). In addition, Titan exhibits fluvial features like river systems (e.g. Lorenz et al. 2008; Black et al. 2012; Langhans et al. 2012), lakes (e.g. Stofan et al. 2007; Cornet et al. 2012; Cordier et al. 2013; Hayes et al. 2013), and aeolian features such as vast dune fields (e.g. Radebaugh et al. 2009; Le Gall et al. 2012). Impact craters are present (e.g. Wood et al. 2010; Williams et al. 2011; Buratti et al. 2012) but no heavily cratered terrains are seen, indicating a relatively

young and dynamic surface. Several volcanic-like features have been identified, which are possible results of cryovolcanic activity (e.g. Lopes et al. 2007; Soderblom et al. 2009; Lopes et al. 2013), some of which I focus my study on, described on Chapters 6 and 7. One example for almost each surface feature type is illustrated in Figure 4.1. Current observations and modeling indicate both exogenic (aeolian, fluvial, etc.) and endogenic (tectonism, cryovolcanism) origin in the formation of Titan surface features and terrains. In addition, concsidering the composition of the different areas on Titan, Cassini/VIMS studies on the dark and bright regions of Titan resulted to the characterization of the VIMS dark blue and brown areas as dirty water ice and dark hydrocarbons respectively. The VIMS bright regions have been suggested to be air-fall accumulations of bright aerosol hydrocarbon dust (Soderblom et al. 2007; 2009).

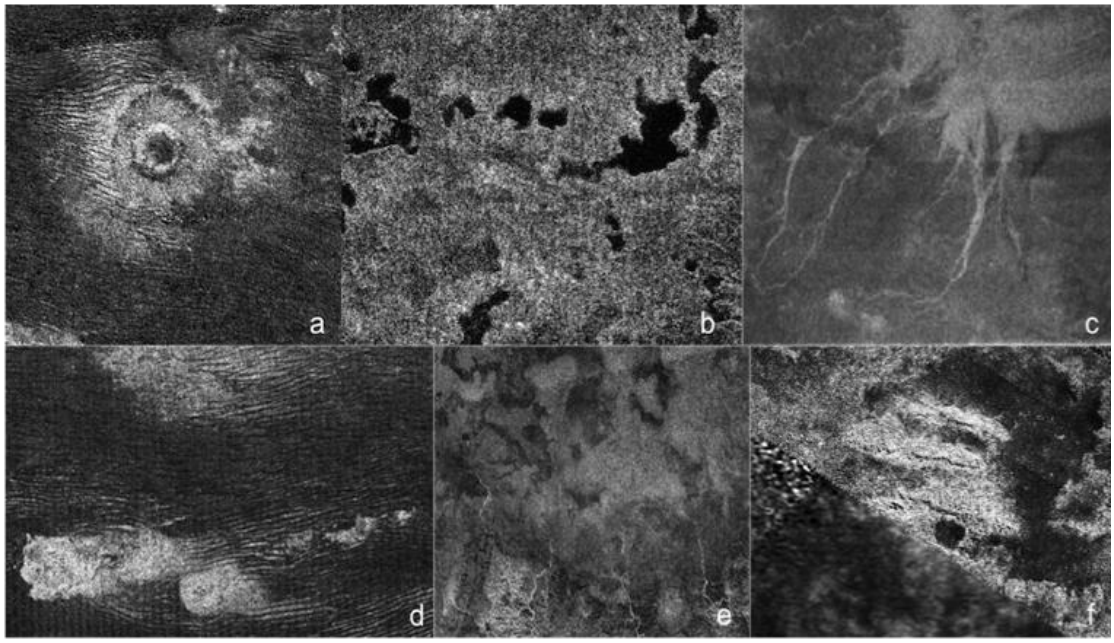

Fig. 4.1 - Surface features on Titan. (a) Impact crater surrounded by a radar-bright blanket of ejecta (NASA/JPL-Caltech); (b) Liquid lakes (radar-dark) (Image credit: NASA/JPL-Caltech/ASI). (c) Large fluvial deposit showing braided radar-bright channels. Deposits overlay radar-dark undifferentiated plains (Image credit: Lorenz et al. 2008). (d) Radar dark sand dunes formed by aeolian processes and radar-bright topographic obstacles (Image credit: NASA/JPL). (e) Lobate radar-bright feature and possible cryovolcanic deposits (Image credit: Soderblom et al. 2009). (f) Parallel radar-bright mountain chain (Image credit: NASA/JPL-Caltech).

4.1.1 The ground truth (Huygens Landing Site)

As mentioned in Chapter 1, Huygens provided the first *in situ* surface image of an outer Solar system body. During its descent into Titan's thick atmosphere, the Huygens/DISR captured a large number of images showing the general terrain of the area named 'Huygens Landing Site' (HLS from now on). Figure 4.2 is a 360° panoramic close up view from

synthesis of several DISR images from an 8 km altitude from the surface of Titan. Data acquired with DISR have shown that the topography close to the Huygens probe-landing site is roughly 150 m higher than the surrounding areas (Tomasko et al. 2005), suggesting that tectonic activity has shaped and uplifted the crust.

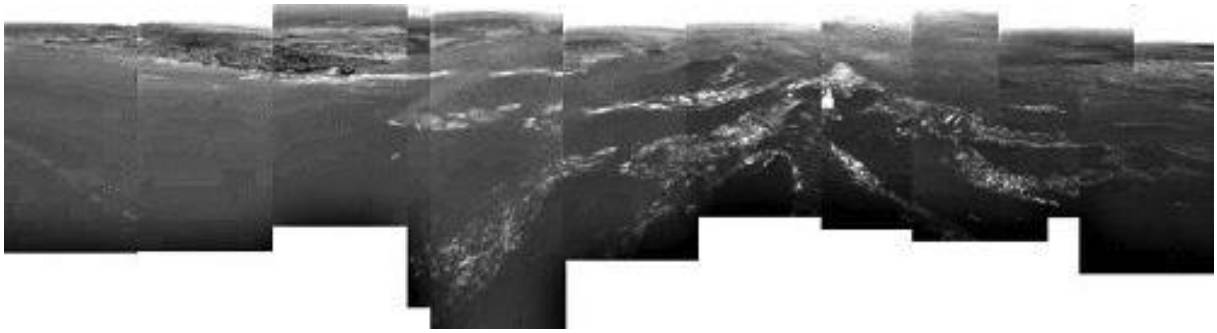

Fig. 4.2 - Panoramic view of Huygens Landind Site from DISR images. From left to right the mosaic shows an extensive boundary between dark and bright areas. The probe landed over a dark area that could be a drainage channel filled with liquid material (Image credit: ESA/NASA/JPL/University of Arizona; Information adapted from Tomasko et al. 2005).

The images of DISR indicated the presence of a dendritic network that is consistent with rainfall drainage and fluvial processes (Tomasko et al. 2005; Burr et al. 2013) (Fig. 4.3).

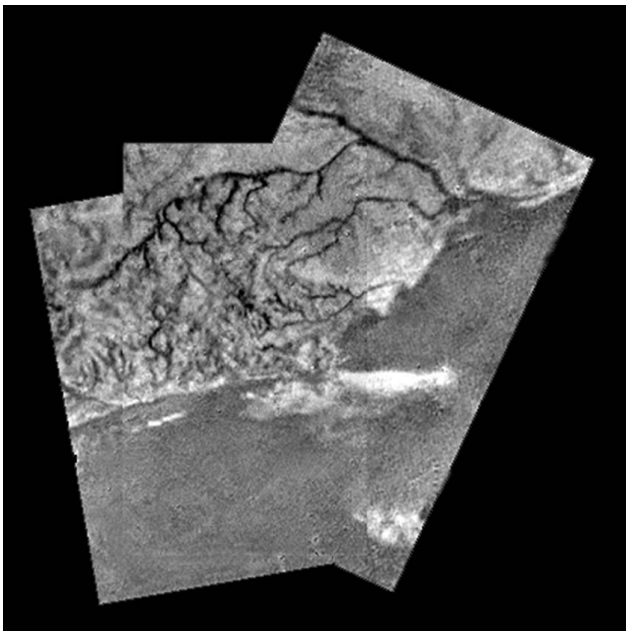

Fig. 4.3 - Complex network of narrow drainage channels on Titan from DISR at a 6.5 km latitude from the surface, running from brighter highlands to lower dark regions (Image credit: NASA/JPL).

In addition to fluvial processes, that seem to carve these drainage networks, preliminary tectonic influence in the observed patterns at HLS has been proposed by Soderblom et al. (2007) (Fig. 4.4). These linear structures (purple and green arrows in Fig. 4.4) can operate as the ideal path for the surface hydrocarbon liquids. The origin of these linear structures is still

under investigation. I discuss the possibility for transverse processes (fluvial-tectonic) on Titan in section 4.1.4.2.

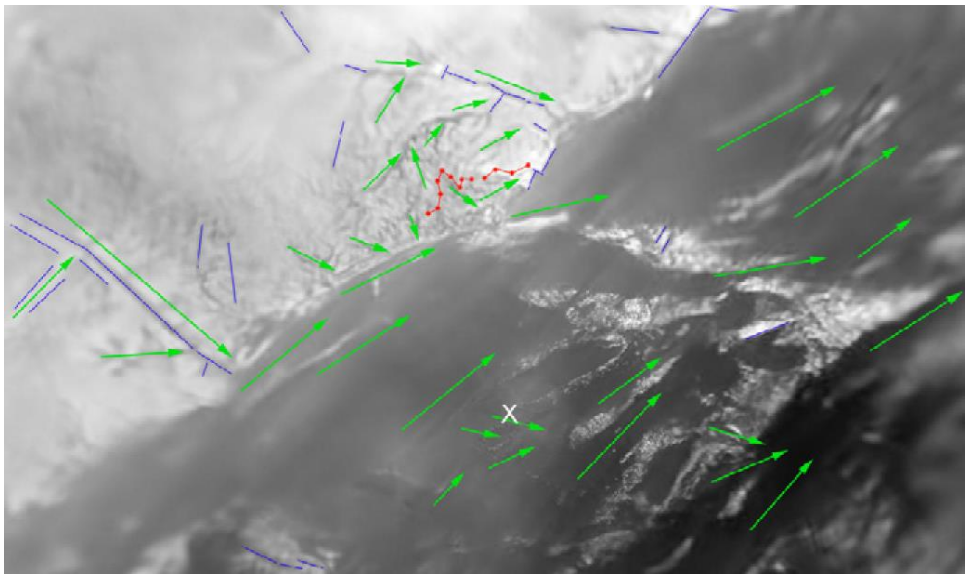

Fig. 4.4 - Fault (purple lines) and fluid-flow patterns (green arrows) at HLS (Image credit: Soderblom et al. 2007).

VIMS observations of the HLS terrain showed bright and dark diversity (e.g. Rodriguez et al. 2006). In addition, DISR data from the same area showed that the brighter regions correspond to icy upland areas, while the darker regions are lowlands that possess a higher proportion of the organic byproducts of Titan's atmospheric photochemistry (Soderblom et al. 2007). Huygens Surface Science Package (SSP) measurements (Zarnecki et al. 2002) showed that the site appears to be a relatively soft surface similar to tar or dry sand, tinted by methane ready to evaporate and provided ample evidence for fluvial and aeolian processes (Zarnecki et al. 2005). The visible ground "powder", in the image (Fig. 4.5), could possibly be the result of precipitation from the hydrocarbon haze above (Tomasko et al. 2005).

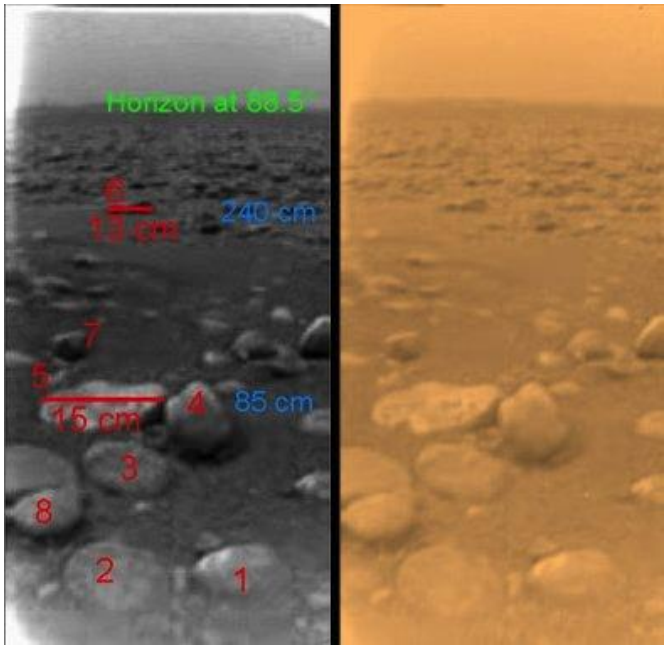

Fig. 4.5 - Titan's surface after the soft landing of the Huygens probe. The right panel shows, approximately, the true color of the scene (Image credit: Tomasko et al. 2005). The images are a synthesis of the Medium Resolution Imagers (MRI) and Side-Looking Imager (SLI) images. Solar illumination is obvious on the top left of the images while the brightening in the lower right side is lamp illumination from DISR (Image credit: ESA/NASA/JPL/University of Arizona).

As seen in Figure 4.5, most of the area is covered by pebbles, possibly made of water ice. The absence of rocks in an upper layer of the image is attributed to the presence of channel-like features (Tomasko et al. 2005). According to the scale the largest pebble of the scene extends for 15 cm (Zarnecki et al. 2005).

Hence, the close up *in situ* images from the HLS have been processed and analyzed by many studies, which suggest the activity of exogenous and endogenous mechanisms on the area such as aeolian, fluvial and tectonic processes.

The rest of Titan's surface exploration has been achieved from the orbiter's observations and I present the most important ones hereafter.

4.1.2 Surface expressions indicating impact cratering

Titan can be considered as a closed system if we take into account the interaction and exhanges between the atmosphere, the surface and the interior alone. Impact cratering on the other hand, is considered an exogenic process, therefore I classify it here as a phenomenon originating outside of the closed system.

The number of impact craters on the surface of a planetary body is an indicative index of the types of surface processes shaping the morphology as well as the resurfacing rating. When the surface of a planet or moon is heavily cratered, means that apparently has not suffered

significant resurfacing processes caused by geological or atmospheric phenomena. Indeed, Earth lacks a large number of impact structures, hosting an unscarred surface maintained by tectonic activity, volcanism and erosion. Similarly, the small number of impact craters that has been observed by the Cassini Radar on Titan during its flybys (Fig. 4.1a; 4.6) suggests that Titan's surface is relatively young and resurfaced (e.g. Wall et al. 2009; Neish and Lorenz, 2012). Pre-Cassini models suggested that Titan's lower impact velocities have allowed it to accommodate an atmosphere (Zahnle et al. 1992; Griffith et al. 1995), something that could, at least partially, prevent impact cratering from occuring. So far, six certain impact craters have been identified on Titanm namely Ksa, Sinlap, Menrva, Afekan, Selk and Senkyo (Wood et al. 2010; Buratti et al. 2012). Other 44 observed craters have been classified as Class 2 (nearly certain impact craters) and Class 3 (probable impact craters) (Wood et al. 2010). A comparative study with the terrestrial impacts is made in Chapter 10.

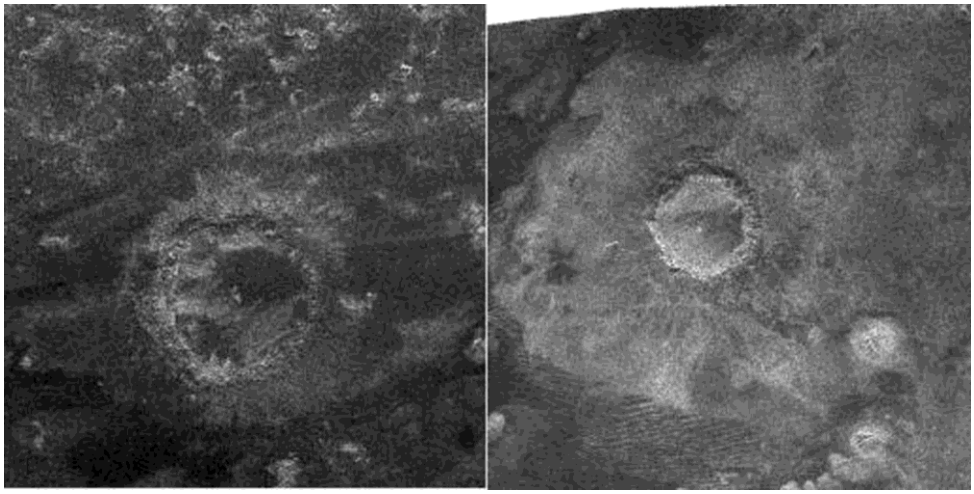

Fig. 4.6 - Impact craters discovered on Titan in 2008 (26°N, 200°W) (left) and in 2005 (11°N, 16°W) (right) (Image credit: NASA/JPL).

4.1.3 Surface expressions of exogenic origin: atmospheric methane, aeolian and fluvial features

In this Chapter, I focus on the interplay of the two main geological types of processes that develop the surface globe, which are the exogenous and endogenous processes. Both terms have been introduced basically for terrestrial geological processes but find equivalants on other planetary bodies as well. On Earth, as exogenic processes are considered the energy (heating) from the Sun, the force of gravity, the activity of organisms, weathering, the blowing wind, running water, underground - water, waves and currents in surface water bodies, glaciers and more. Critical products of such activities are the aggradation and

degradation[21]; the latter is mainly caused by weathering, mass wasting and erosion (e.g. Graniczny, 2006). Hence, precipitation, fluvial, aeolian and drain phenomena are included in the exogenic active processes of Titan. A short description of the general term of endogenic processes can be found in 4.1.4.

General

Since Titan harbors a thick nitrogen-dominated atmospheric envelope rich in organic substances, a dynamic coupling between the surface and the atmosphere is expected. Indeed, Titan's active cycle of methane appears to link the atmosphere with the surface and the interior (Fig. 4.7). As mentioned in the introduction, methane is the second most abundant compound in the atmosphere of Titan (Flasar et al. 2005; Waite et al., 2005; Niemann et al., 2010). The existence of a large number of hydrocarbons and nitriles found in Titan's atmosphere (Hanel et al., 1981; Coustenis et al., 1989), originates through methane and nitrogen photolysis essentially and recombination with nitrogen (Strobel, 1974).

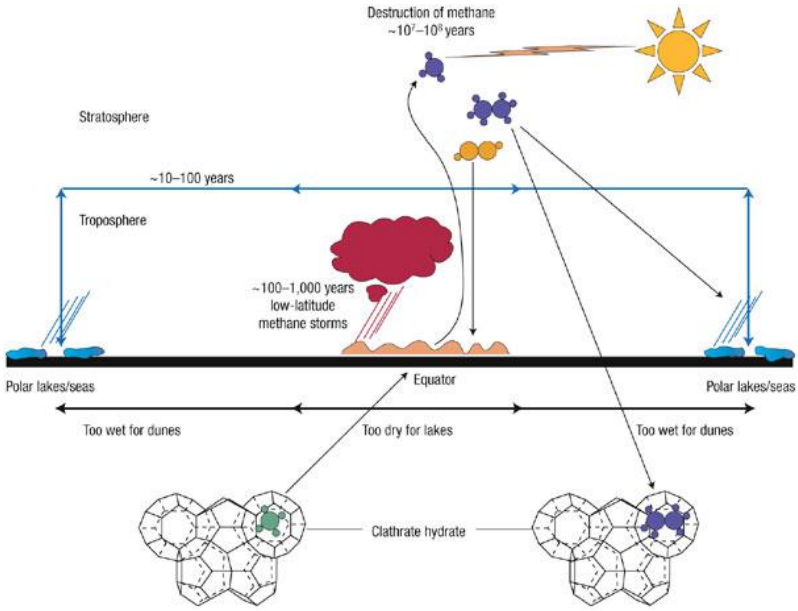

Fig. 4.7 - The methane cycle on Titan (Image credit: Atreya et al. 2006).

Short-lived radicals[22] of CH_n are the products of the photochemistry that occurs above the level of 700 km in the atmosphere and the reaction of CH_3 radicals produce ethane, which is a significant molecule during the process that methane follows (Choukroun & Sotin, 2012). Moreover, the methane photolysis produces various complex hydrocarbons, which form

[21] *Major categories of gradation: natural levelling of land as a result of the building up or wearing down of pre-existing formations*
[22] *A radical in chemistry is an atom, molecule, or ion that has unpaired valence electrons or an open electron shell*

Titan's haze layer. Some of the aerosols deposit on the surface and form lake-like features (precipitation-fluvial) with major significance in the process of the methane cycle and the habitability of Titan. When the deposition occurs on the equator, the climate turns the liquid hydrocarbons into hydrocarbon sand dunes (aeolian) (Lunine and Lorenz, 2009). In addition, photochemical reactions and hydrogen escape dissociate methane in the upper atmosphere (Strobel, 1974; Yung et al. 1984; Wilson and Atreya, 2004; Lavvas et al. 2008). Lack of any source that could replenish this loss means that methane should dissapear from Titan in the course of 10-30 Myr (Atreya, 2010).

Hence, this active process includes chemical reactions and climate and geological activity. This latter part, that appears to control major factors on Titan's evolution and current status, is a main part of my PhD researches.

Numerous models have proposed organic precipitation on Titan (Toon et al. 1988; Lorenz, 1993; Graves et al. 2008), either in the form of violent torrential storms (Hueso and Sanchez-Lavega, 2006), and smooth drizzle in the lower atmosphere (Tokano et al. 2006) or in the form of methane rainfalls from occasional short-lived clouds that have been modeled or observed (Griffith et al. 1998; Graves et al. 2008; Porco et al. 2005; Rannou et al. 2006). Methane rains can carve channels and fill lakes, while mass transport by winds causes erosion and creates extensive dune fields (Lancaster, 2006; Lorenz et al. 2006a; Radebaugh et al. 2008; Tokano, 2008; Lorenz and Radebaugh, 2009; Hayes et al. 2013). The fact that Titan is undergoing seasonal weather changes helps it maintain an active-dynamic climate, which forms complex surficial edifices.

Consequently, climate related processes, such as fluvial and aeolian, have created structures similar to those on Earth such as lakes, seas, riverbeds, sand dunes, shorelines and dendritic drainage networks. Moreover, seasonal climate variability, as illustrated among other, by the reduction of the southern lake shorelines (Turtle et al. 2008; Wye et al. 2009; Wall et al. 2010), is most probably present on Titan. I present hereafter the major types of non-tectonic in origin features on Titan, as presented in Solomonidou et al. (2010) and Solomonidou et al. (2013a) in addition to unpublished material.

4.1.3.1 Fluvial features

Lakes

As mentioned earlier in this Chapter, image and numerical data from Cassini-Huygens exhibited evidence for the presence of stable surface liquid extents, called "lakes", or "seas"

(e.g. Stofan et al. 2007; Aharonson et al. 2009; Hayes et al. 2010) instead of a global surface ocean or even large basins homogeneously distributed. This is one exceptional characteristic for an outer Solar system body since up-to-date, Titan, is the only object other than Earth for which clear evidence of stable bodies of surface liquid has been reported. The other important aspect is that the lakes are mostly concentrated in the North, with some exceptions. Currently, the Cassini/RADAR data confirmed the observations of hydrocarbon lakes on Titan's surface and their presence is now well established (Fig. 4.7) (Lopes et al. 2007). These lakes, observed on Titan, resemble terrestrial lakes (Cornet et al. 2012). Moreover, Titan, despite its small size in comparison with that of Earth's, exhibits massive lakes that compares to that of largest terrestrial lake (Lake Superior, USA).

More than ten currently identified Titan lakes have a mean diameter greater than 200 km. Most of the other lakes are quite smaller with diameters less than 100 km. Kraken Mare, Ligeia Mare (which reside in an endorheic basin dominated by seas –Wasiak et al. 2013) and Punga Mare located at the northern part of Titan have adequate sizes to be characterized as seas (according the IAU Committee on Planetary Nomenclature) (Fig. 4.8). Ontario Lacus is the largest lake located in the southern hemisphere. It has been suggested that a depression drains and refills from the undergroung, exposing liquid regions ringed by materials like saturated sand (Cornet et al. 2012).

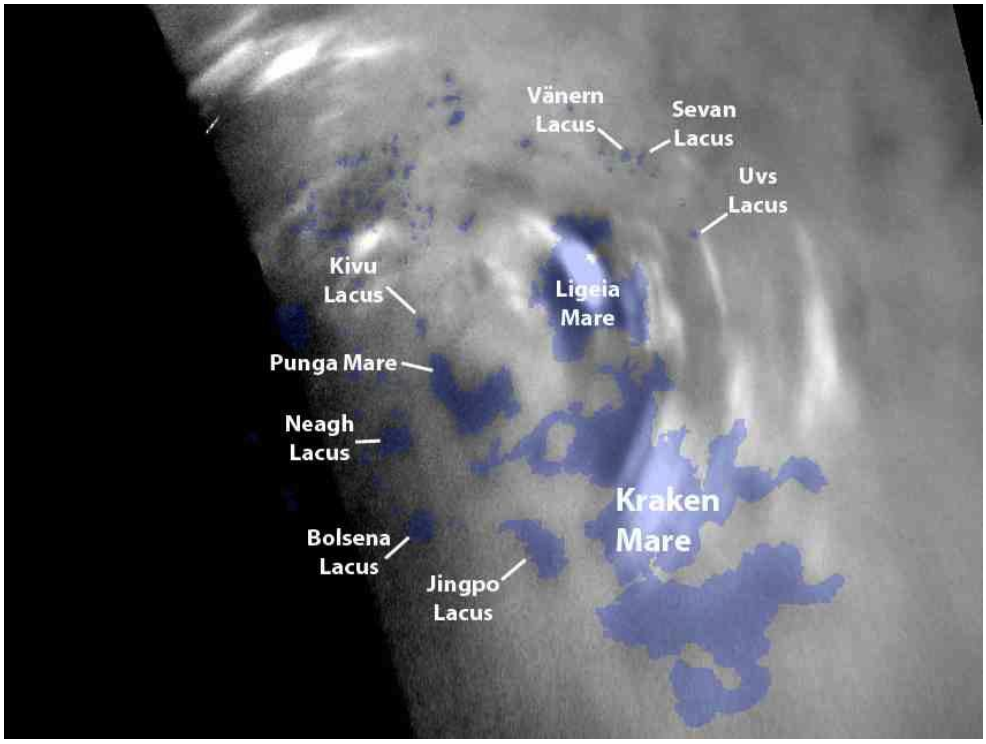

Figure 4.8 - The large seas of Titan greater than 200 km located in the satellite's North Pole from Cassini/ISS data (Image credit: NASA/JPL/SSI). For scale purposes, Kraken Mare extends for almost 400,000 km^2.

A major classification of Titan lakes has been made based on the RADAR obsevations: (a) the dark – liquid filled lakes that thoroughly absorb the incident RADAR beam, (b) the granular – partially filled lakes as recorded from SAR microwave penetrations and (c) the bright – empty lakes (Stofan et al. 2007) that appear brighter in SAR compared to their exteriors and have a depth of 200-300 m (Hayes et al. 2008) (Fig. 4.9).

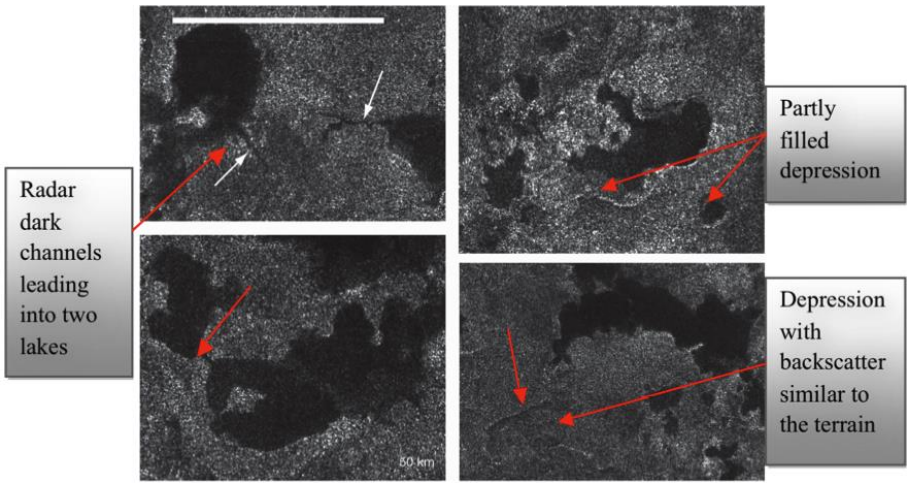

Fig. 4.9 - Lakes on Titan's surface as recorded from the Radar mapper during the Cassini T16 flyby on July 22, 2006 (Image adapted from Stofan et al. 2007).

In the course of the Cassini mission, examples of current or past fluvial activity have been found in the past lake-level changes of Ontario Lacus and changes in surface albedo of Arrakis Planitia, possibly due to evaporation (Barnes et al. 2009; Hayes et al. 2011; Turtle et al. 2009; 2011b).

Moreover, in spite of the detection of several lakes concentrated in the northern hemisphere (Stofan et al. 2007), the total amount of liquid methane on the surface remains too small (Sotin et al. 2012) for the required replenishment of methane in the atmosphere and in the absence of adequate hydrocarbon liquid exposed sources, several studies have suggested the existence of undersurface methanofers in various forms (Stevenson, 1992; Lunine et al. 1999).

Drainage networks

The Cassini SAR data presented evidence for the presence of fluvial networks on Titan's surface, interpreted as products of liquid alkane flow (Burr et al. 2009). The fluvial processes on Titan's surface, present a major geodynamic activity that contributes to the satellite's morphology.

Before SAR, the DISR observed branched lineations were interpreted as fluvial valley networks with inset streams formed by flowing methane (Tomasko et al. 2005; Perron et al. 2006). Data from RADAR and VIMS also confirmed the presence of network lineations interpreted as drainage networks (Elachi et al. 2005; Porco et al. 2005; Barnes et al. 2007b; Lorenz et al. 2008). Indeed, according to Burr et al. (2013) fluvial networks are present on SAR images covering ~40% of Titan from the RADAR up through T71 and on visible light images of the HLS collected by the DISR (see section 4.1.1).

Figure 4.3 shows a complex network of narrow drainage channels from Huygens/DISR, while Fig. 4.10 shows dendritic networks on Titan as seen with SAR and from morphological maps (Lorenz et al. 2008). The system in Fig. 4.10 is located at the western end of Xanadu close to an area that I discuss in detail here and from which data I analyze in Chapters 6 and 7, named Tui Regio. Possible changes in the fluvial deposits on Titan have been suggested by Burr et al. (2013).

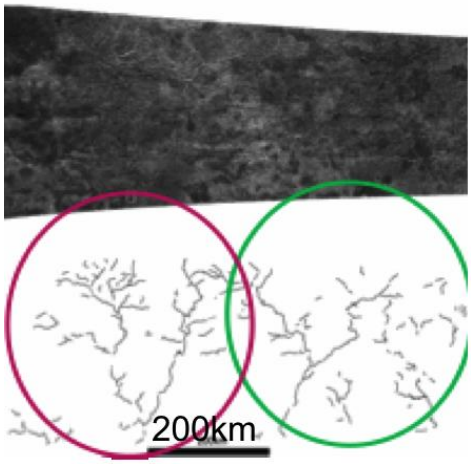

Fig. 4.10 - This fluvial network extends over 400km while it presents a dendritic morphology. The dendritic network drainage is the pattern formed by the streams, rivers and lakes in a particular 'watershed'. In this case incisions were not observed but a well-developed branching structure on both channels (red and green circle) is present (Image adapted from: Lorenz et al. 2008).

4.1.3.2 Aeolian features

Sand dunes

From several studies, it has been inferred that the surface age is about half a billion years old (Artemieva and Lunine, 2003; Lorenz et al. 2007), not too different from the average ages of Earth's and Venus'. In addition to the erosional and burial phenomena that may have eliminated most of the impact structures, tectonic disruption of the crust may also obliterate

craters. The consideration of Titan's young surficial age indicates the possible existence of active regions among the satellite. Contrary to impact craters surficial structures that are commonly seen on Titan are the dunes (Fig. 4.1d; 4.11). A sand dune is a semi-permanent accumulation of loose sand that forms in areas where the wind tends to blow in one direction, at velocities high enough to move sand, across a land surface that permits sand to amass in a regular and consistent form. Cassini/RADAR images have shown many dune formations at equatorial latitudes, mainly from 0°N to 30°N and in some isolated regions up to 55°N (Radebaugh et al. 2008). Due to their extent the equatorial dunes have been interpreted as sand seas (Lorenz et al. 2006a) and they are mainly concentrated in zonal east-west direction. The presence of these vast dune fields indicates the wind blow direction which is towards east, but they wrap around the topographically high features they meet like mountains and craters (Radebaugh et al. 2008).

Titan dunes are 1-2 km in width and are separated almost 1-4 km from one another, extending up to 150 km height and more than 100 km in length (Elachi et al. 2006). Cassini/ISS and VIMS observations have also captured many of the dunes fields (Porco et al. 2005; Soderblom et al. 2007b; Barnes et al. 2008).

The sand composition is possibly a mixture of organic materials and ice grains (Radebaugh et al. 2009). The dunes are generally smooth surfaces that diverge around topographic obstacles resembling terrestrial dunes (Radebaugh et al. 2009). Moderately variable winds that either follow one mean direction or alternate between two different directions have formed the observed longitudinal dunes (Lorenz et al. 2006) (Fig. 4.11).

Fig. 4.11 - Sand dunes from the Belet sand sea on Titan formed by aeolian processes from SAR data (Image credit: NASA/JPL).

Recent studies indicate the dunes as active features due to the presence of distinguishable interdunes in both RADAR and VIMS dune observations (Barnes et al. 2008). For the latter, as it happens on Earth the interdunes possibly represent the substrate surface layer that the displacement of dune material should blanket with time. Consequently, the presence of both dunes and interdunes on Titan probably indicate current surface activity in these areas (Barnes et al. 2008; Savage, 2011).

4.1.4 Surface expressions indicating endogenic origin

The 'endogenic processes' refer to activities that originate from the interior; such processes are governed by inherent in the planetary body forces and affected little (or more) by external influences. These include, earthquakes, emergence and development of continents, troughs, faults and mountain ridges, volcanic activity, deformation and movement of the Earth's crust both vertically and laterally etc (e.g. Vartanyan, 2006). Major categories are considered to be (a) Earthquakes; (b) Metamorphism; (c) Tectonic activity; and (d) Volcanism. The latter two could possibly occur on Titan as indicated by numerous models and observations (e.g. Tobie et al. 2006; Mitri and Showman, 2008; Mitri et al. 2010; Lopes et al. 2013).

Tectonic Geology (Tectonics)[23] or Structural Geology is the field of geological studies that focuses on the features of the crust of the Earth (or of other planets) as well as on the movements, processes and forces that shape these structures. Tectonics not only try to explain the forms of any tectonic-like structures observed on the surface and their spatial and temporal distribution, but also the causes that created these deformities. Furthermore, Planetary Tectonics considers inactive geological forms, edifices and structures as an expression of active planetary movements and the visible movements as a manifestation of invisible planetary forces (Cloos, 1936). The field of Tectonics is inextricably linked to Plate tectonics on Earth, concerning the Lithosphere, which consists of nine large plates and twelve smaller ones.

The study of Plate tectonics and Tectonics in general provides information on the orogenetic processes - how mountains are formed -, explanation about the continental drifts, the genesis and development of cratons. - which are old and stable parts of the continental lithosphere-, shields - stable areas that are being extracted from the interior due to tectonism-, terranes - parts of a tectonic plate that overlie another plate, and ridges - chains of elevated

[23] *A full description on Tectonics, its principals and applications can be found in: Tectonics, Moores, E., and Twiss, R., Publisher: W. H. Freeman; (November 15, 1995).*

crust-, the spreading of the sea floor and generally an holistic “view” on the activities that shape the Earth's geomorphology. Similarly to Earth’s, where very active plate tectonics dominate the geology, other rocky planets and moons in the Solar system may harbor tectonic activity in varying degrees. The processes of faulting, folding, or other deformation of the lithosphere of a planet or moon, often results from large-scale movements below the lithosphere. However, geology on Earth is dominated by active plate tectonics where rigid lithospheric plates float and move on a plastic asthenosphere. There is no other planetary body in our Solar system where plate tectonics have been firmly identified as that of Earth’s so far. Nevertheless, Titan and Enceladus in addition to more icy moons are under investigation as to whether any tectonic activity can exist (e.g. Radebaugh et al. 2007; Soderblom et al. 2007; Shubert et al. 2010; Spencer and Nimmo, 2013), albeit with completely different fashion than terrestrial tectonics.

Morphotectonics correlate landscape morphology to tectonism (Rosenau and Onchen, 2009; Scheidegger, 2004; Lidmar-Bergstrom, 1996) by studying landform evolution and degradation since tectonic features are subsequently subjected to exogenous processes. Major morphotectonic features on Earth are represented by mountains, ridges, faults and escarpments, as well as, significant types of linear features such as rifts, grabens and other linear terrestrial terrains that are subjected to erosion subsequently to deformational events (e.g. Scheidegger, 2004).

4.1.4.1 Mountains and ridges on Titan

Mountains on Titan are of several hundred meters high (Radebaugh et al. 2007) and provide a sign of the presence of tectonic-like activity. According to Lorenz et al. (2007), Titan has mountains that sometimes reach several hundred meters to more than 1 km in height, while other studies suggest that the height may exceed 2 km (Radebaugh et al. 2007; Lopes et al. 2010; 2013). Radar data showed that the mountains located close to equatorial regions have a mean height of about 900 m (Barth, 2010). Radarclinometry measurements determined that the height of the mountains on most of Titan's surface ranges between 200 m and 2 km (Radebaugh et al. 2008). The low height of mountains with respect to terrestrial mountains, is probably the result of erosional processes (similarly to the dependence of the height of terrestrial mountains on erosion), which operate on the mountainous terrains. However, there is also an alternative hypothesis that Titan's mountains are built with materials that hold properties that prevent their altitudinal growth (Radebaugh et al. 2008). RADAR,

VIMS as well as DISR data have provided some details on the characteristics of Titan's mountains and ridges. The term mountain describes large uplifted localized landforms while the term mountain ridges (in this manuscript I will refer to mountain ridges as ridges) chains of elevated (uplifted) ground that extend for some distance. The major mountains and ridges on Titan are listed along with their location and observational characteristics in Table 4.1.

Table 4.1 - Major mountain and ridge features on Titan (Solomonidou et al. 2013a).

Location	**Orientation**	**Heights**	**Characterization**	**Flyby/ Time**	**Instrument (Reference)**
10°N, 15°W 15°N, 45°W		380-570m	Blocks of mountains	T3/ February 2005	RADAR (Radebaugh et al. 2007)
20°N, 87°W	E-W	~300m	Ridges	T3/ February 2005	RADAR (Williams et al. 2011)
40°S, 340°W			Hills	T7/ September 2005	RADAR (Lunine et al. 2008)
5°-12.5°S, 63°-67°W	E-W	~860m to 2000m	Curvilinear mountains / Ridges	T8/ October 2005	RADAR (Radebaugh et al. 2007; Mitri et al. 2010; Lopes et al. 2010)
10°S,210°W		~400m	Mountainous region	T9/ December 2005 T13/ April 2006	VIMS/RADAR (Barnes et al. 2007b)
10°S,192°W	W-E	100m to 150m	Ridges	Huygens/January 2005	DISR (Tomasko et al. 2005; Soderblom et al. 2007b)
30°S,315°W	NW-SE	~1500m	Mountain ranges	T20/October 2006	VIMS (Sotin et al. 2007)
52°N, 347°W	E-W	~1400m	Mountain block	T30/May 2007	RADAR (Stiles et al. 2009; Mitri et al. 2010)
30°S, 107°W	S-W	~800m	Mountains	T43/May 2008	RADAR (Mitri et al. 2010)
2°S, 127°W	E-W	1930m	Ridges	T43/May 2008	RADAR (Mitri et al. 2010)

Two intriguing aspects are pointed out in Table 4.1. First, mountain-like edifices exist in almost all latitudes on Titan; however, they are concentrated in the equatorial region and in latitudes between 30°S and 30°N (Lopes et al. 2010). Second, their height is significantly lower than that of the terrestrial mountains ranging from 100 to 2000 m (Barnes et al. 2007b; Radebaugh et al. 2007; Soderblom et al. 2007b; Sotin et al. 2007; Mitri et al. 2010). This may

be partly due to erosional processes as suggested by the blanket-like materials that surround these structures (Radebaugh et al. 2007). Alternative hypotheses include the construction of Titan's mountains with materials that hold properties that prevent height growth (Radebaugh et al. 2008) and the effects of high temperature gradients on the ice shell according to calculations by Mitri et al. (2010), result in mountains from 100 m to 2,700 m. Similar to Earth, where terrain topography is defined by the interaction of tectonism and erosion (Montgomery and Brandon, 2002), I suggest here that there is a strong connection between slope morphology and erosional rates on Titan due to its extreme conditions of hydrocarbon rainfall and/or winds.

Figure 4.12 shows three portions of T8 and T43 SAR swaths that provide the most reliable evidence so far for the existence of mountains and ridges on Titan.

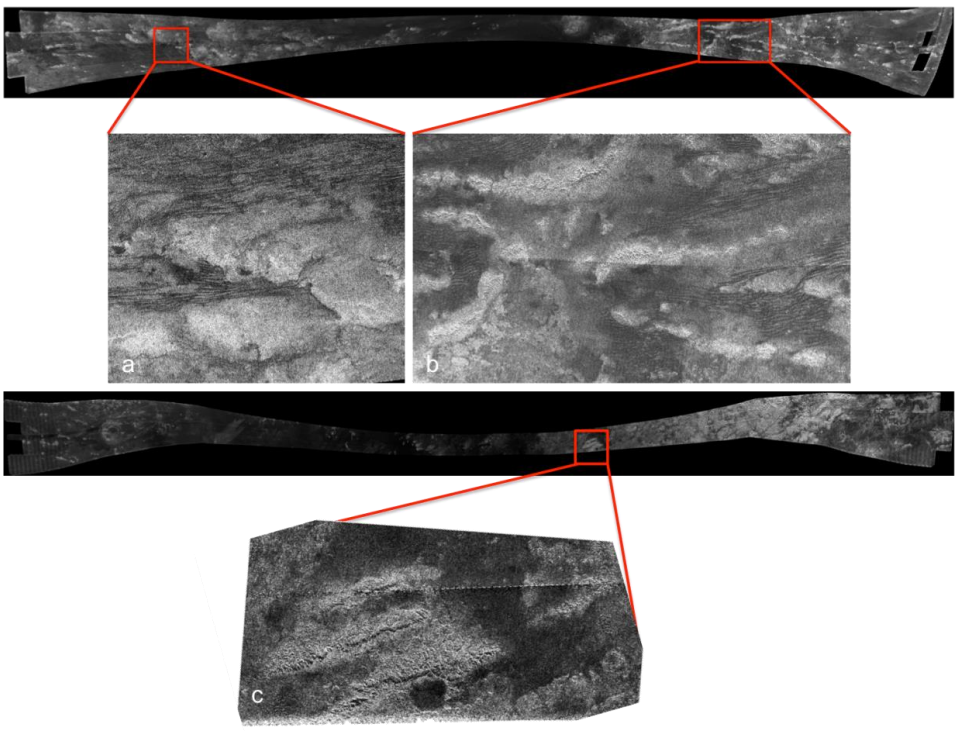

Fig. 4.12 - Major mountainous regions on Titan. (a) Mountain extends for almost 240 km (Image credit: NASA/JPL); (b) Long bright ridges with multiple mountain peaks were observed in T8 October 28, 2005 (Information credit: Radebaugh et al. 2007), extend over 480 km (Image credit: NASA/JPL); (c) Three radar bright parallel ridges within the mountainous area of Xanadu from T43 May 12, 2008, the length of the image is almost 400 km (Information credit: Mitri et al. 2010).

Cassini SAR instrument has been observing mountainous topography on Titan since 2005. Radebaugh et al. (2007) mentioned that the notably SAR bright features on Titan's surface most probably correspond to mountains and tectonic ridges (Fig. 4.13).

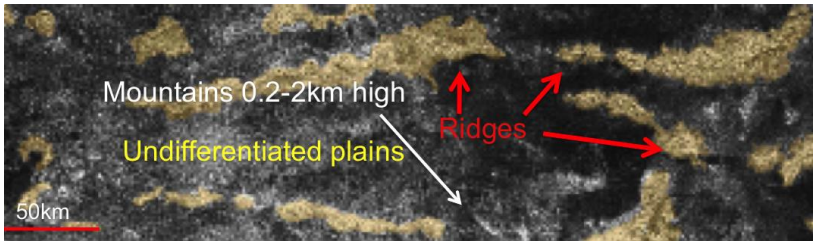

Fig. 4.13 - Titan's bright mountains (white) and tectonic ridges (yellow) from T8 swath (Lopes et al. 2010).

As mentioned, other than RADAR observations, both the DISR and the VIMS instrument brought evidence and details of the mountainous characteristics. Fig. 4.2 in section 4.1.1 shows a 150 m uplift topography close to the Huygens probe landing site, suggesting that tectonic activity has shaped the area (Tomasko et al. 2005). Additional observations of the area were obtained in 2006 during the T20 flyby by VIMS and RADAR. The combination of both types of data unveiled one of the highest mountains, which is a part of a chain of mountains (Fig. 4.14), ever observed on Titan, located southern of its equator. Near the center of the image (Fig. 4.14), the mountain range runs from S-E to N-W and is approximately 150-km long, 30-km wide and about 1.5-km high (Sotin et al. 2007).

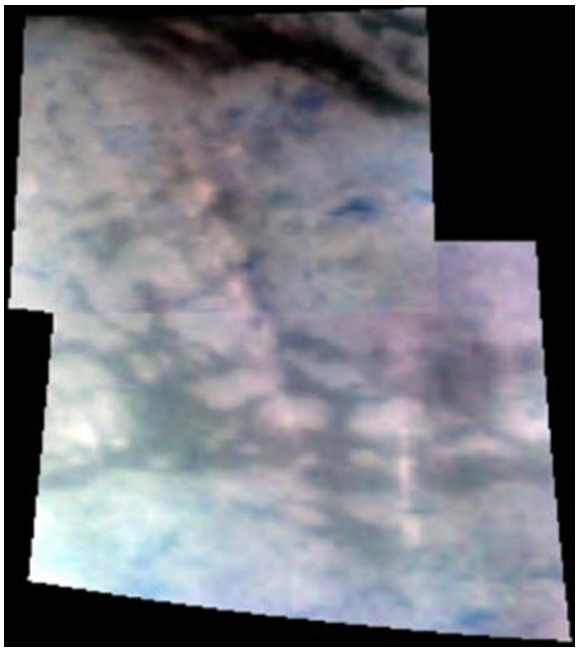
Fig. 4.14 - Titan's "Sierra" Mountains from VIMS (Image credit: NASA/JPL).

Figure 4.15 illustrates a mountainous terrain on Titan and its feature classifications. The area surrounded by the yellow circle, presents radar-bright and isolated peaks in high contrast to surrounding terrain that classifies it as smooth, as well as elongated, mountain ranges. The blue circle surrounds an extensive folded and pleated area that has possibly suffered fluvial

erosion. Finally, the red circle at the top of the image includes a plateau deformed by rounded drainages (Radebaugh et al. 2008).

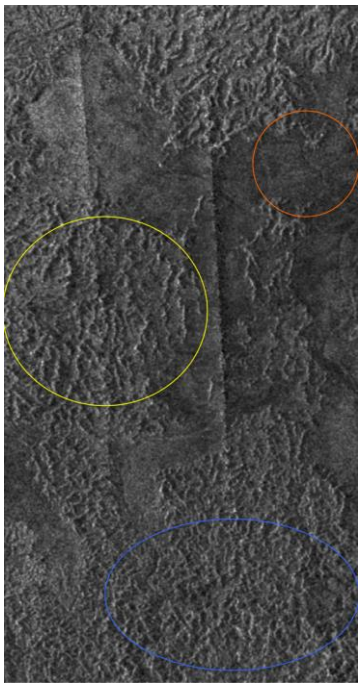

Fig. 4.15 - Types of mountains on Titan from T39 flyby (Image credit: NASA/JPL, Information: Radebaugh et al. 2008).

Ridges are another geological type of surface expressions seen on Titan featuring, most likely, the local uplift of the crust. One of the most interesting and unique types of ridges on Earth is the range of mountains formed by the shift of the solid crust, determining the fringes of the tectonic plates (Kious and Tilling, 1996). A major example is the Mid-Atlantic Ridge (MAR) (see also Chapter 10).

Several types of ridges have been observed on Titan's surface. The Cassini orbiter has recorded ridges around craters. Radebaugh et al. (2007) suggested that at least four ridge formations could be identified from the central crater to the edges of the Ganesa Macula (50ºN, 87ºW) area and it is plausible that these structures could bare crater ridges. Another type is the volcanic caldera ridge, placed around large volcano-like structures that are bordered by circular ridges. On Titan, this type of ridges could be identified within the cryovolcanic candidate areas like Hotei Regio, where a study by Soderblom et al. (2009) suggested two low dark parts of the structure as plausible calderas, and thus, as eruption centers (Fig. 4.16) (For Hotei Regio see also §4.1.4.3).

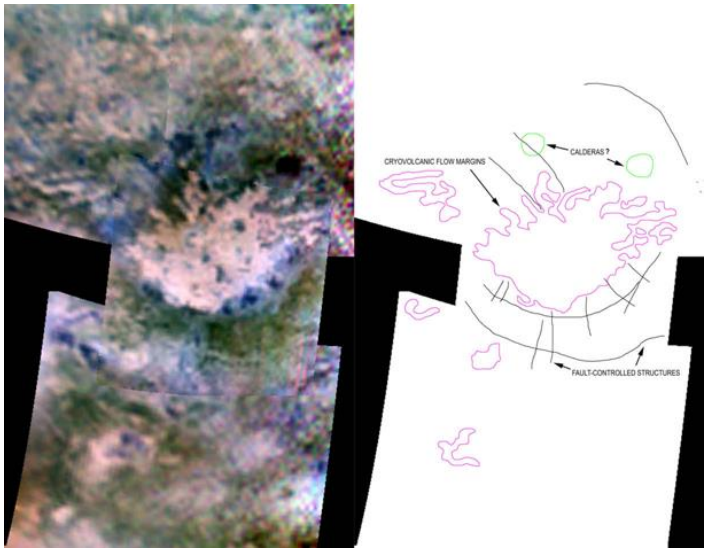

Fig. 4.16 - Caldera-like formations on Titan (Image adapted from Soderblom et al. 2009).

Furthermore, the SAR image acquired in 2005 (Fig. 4.17), displays bright high-standing ridges in an area centered at 8°S, 215°. The ridges could be tectonic in origin, formed by the deformation of parts of the crust. Other implications concerning their origin focus on aeolian and impact processes.


Fig. 4.17 - Tectonic ridges on Titan seen as bright in SAR images (Image credit: NASA/JPL).

4.1.4.2 Faults and transverse features (fractures, canyons and drainage networks)

Studies of the surface of Titan based on observations and mapping have suggested the presence of fault formations (see Fig. 4.4, section 4.1.1). The Cassini orbiter has recorded linear surface structures on Titan since its first flyby (T0) on July 2, 2004. Long and narrow lines extend up to 1000 km in length while only 10-20 km wide (Porco et al. 2005). Confirming the statement above, regarding the interaction of faults with other geological expressions, a collation of faults and river networks is being presented. Indeed, the DISR on

board the Huygens probe discovered a well-developed drainage network during its descent phase (Tomasko et al. 2005).

During the T3 encounter of the Cassini spacecraft a 200 km long fluvial network was also unveiled at 20°N latitude (Elachi et al. 2006). The T7 radar swath, discovered channel-like patterns close to the south polar region (Lunine et al. 2008). Cassini's SAR flyby T13 in 2006 provided evidence for the presence of rectangular river networks on Titan (Fig. 4.18); data analysis by Burr et al. (2009) suggested possible tectonic formation of the area. In particular, internal faults possibly control the methane flow direction and eventually the topography of the area (Burr et al. 2009).

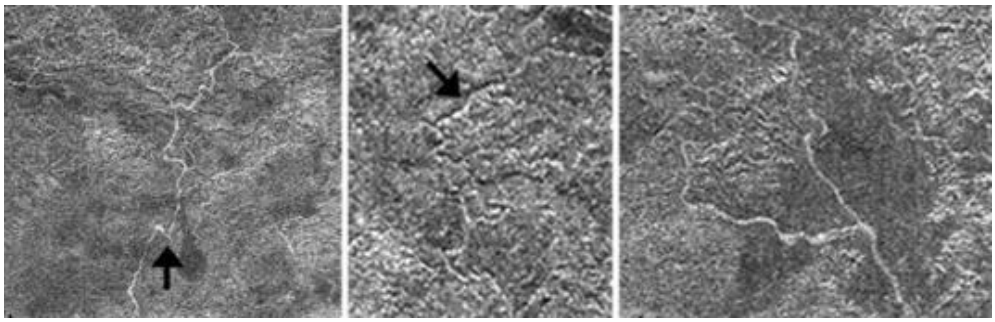

Fig. 4.18 - T3 RADAR images that indicate the influence by subsurface tectonic structures oriented predominantly east-west. (left) Radar bright boundary with the dark background terrain ; (middle) Illumination of a fluvial link; (right) fluvial morphology (Image and information adapted from Burr et al. 2009).

In addition, the Figure 4.4 of section 4.1.1 presents linear structures with possible tectonic infuence and Table 3 summarizes the major linear observations by Cassini.

Table 4.2 - Major fault, fracture and canyon formations on Titan (Solomonidou et al. 2013a).

Location	**Characterization**	**Flyby/Time**	**Instrument (Reference)**
15°S, 155°W	Conjugate-like faults	T0/July, 2004 TA/October 2004 TB/December 2004	ISS (Porco et al. 2005)
10°S, 145°W 0°N, 180°W	Joints and/or faults	T13/ April 2006 T44/May 2008	RADAR (Burr et al. 2009)
10°S-192°W	Linear fault patterns/canyon-like formations	Huygens DISR/January 2005	DISR (Soderblom et al. 2007b)
15°S, 100°W	Lithospheric fault-blocks	(model)	(Radebaugh et al. 2011)
26°S, 78°W	Radial fault system	T47/November 2008	VIMS (Soderblom et al. 2009)

Canyon formations

Cassini's SAR instrument captured a canyon-like morphotectonic feature on Titan on May 21, 2009 in the T58 swath as seen in Figure 4.19. This region is located at 71°S and 240°W. The dark structure depicted in the image is probably a complex canyon pattern lying

over old primary terrains. On radar images, the canyons are seen as black since they are filled by fine-grained material. The canyon-like structures reinforce the hypothesis that Titan displays recent or current active tectonic movements and surficial processes that shaped the prominent geological structures similar to that of Earth's (see Fig. 10.16 in Chapter 10).

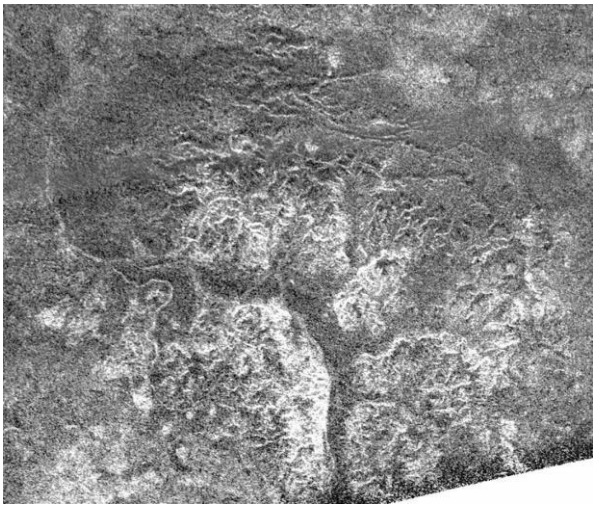

Fig. 4.19 - Radar image showing canyon systems, bedrocks, channels and high cliffs (Image credit: NASA/JPL). The orientation of the radar-bright rims at the lower part are suggested to be high cliffs and broken bedrock. The actual feature of the canyon appears as radar-dark indicating that fluids might ran from the highlands to the lowlands. This terrain resembles Earth's canyons controlled by tectonics like the Grand Canyon in USA.

4.1.4.3 Cryovolcanic candidates

A few topographic features appear to be likely candidates for large volcanic edifices (Fig. 4.20; 4.21). Lobate and fan-shaped features seen in radar images have been interpreted as cryovolcanic in origin like the lobate circular structure of Ganesa Macula (Paganelli et al. 2005; Lopes et al. 2007). The structure contains bright rounded features, interpreted as cryovolcanic flows, while the curved or linear shapes are lineaments that could be caused by the elevation of the underground due to volcanic activity (Lopes et al. 2007).

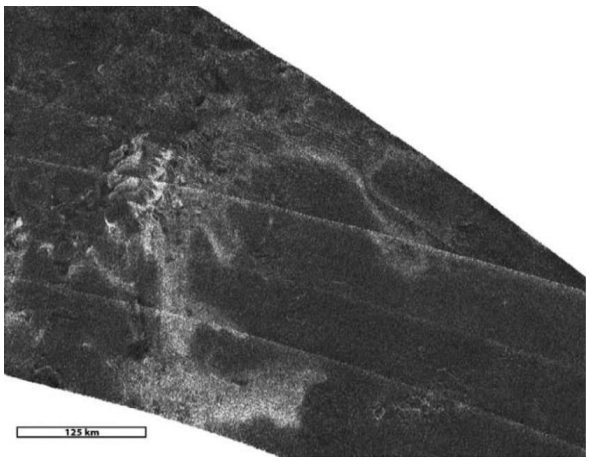

Fig. 4.20 - Cryovolcanic flow field, characterized based on its lobate nature, on Titan named Winia Fluctus (Image credit: Lopes et al. 2010).

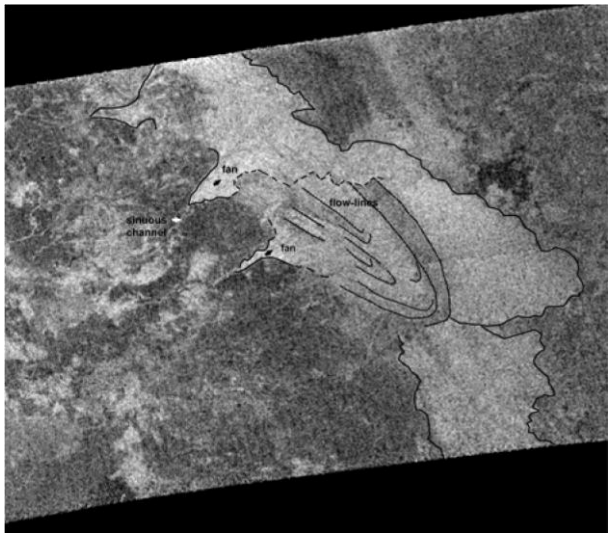

Fig. 4.21 - The Radar-bright fan-like deposits east of Ganesa Macula, observed on Titan and interpreted as either cryovolcanic or alluvial in origin (Image credit: Paganelli et al. 2005).

A number of areas and features, currently characterized as cryovolcanic candidates, and are summarized in Table 4.3.

Table 4.3 - Major candidates of cryovolcanic features on Titan and their association with volcanotectonic processes (Barnes et al. 2006; Lopes et al. 2007; 2013; Le Corre et al. 2009; Soderblom et al. 2009; Wall et al. 2009).

Location	**Name**	**Description**	**Possible tectonic features**
20°S, 130°W	Tui Regio	Flow-like region	Trending dark linear marks on VIMS data (Barnes et al. 2006)
26°S, 78°W	Hotei Regio	Volcanic-like terrain	Circular tectonic features (Soderblom et al. 2009)
14.5°S, 40.5°W	Doom Mons (Sotra Patera area)	Volcanic-like terrain	Topographic elevation, mountain-like structures (unidentified) (Lopes et al. 2010; 2013)
12°S, 38.5°W	Mohini Fluctus (Sotra Patera area)	Lobate flows	-
14.5°S, 40°W	Sotra Patera (crater)	Deep-pit	-
47°S, 39.5°W	Rohe Fluctus	Flow-like feature	-
40°N, 118°W	Ara Fluctus	Flow-like feature	-
10°S, 140°W	Western Xanadu flows	Flow-like feature	-
20°N, 70°W	T3 flow	Flow-like feature	-

Hotei Regio, Tui Regio and Sotra Patera (in this thesis by "Sotra Patera" I refer to the general area which includes the Sotra Patera, Mohini Fluctus, and Doom Mons regions, as defined in Lopes et al. (2013)) (Fig. 4.22) are such three geologically interesting and cryovolcanic candidate areas on Titan. All three are located in the 15°S-30°S latitudinal zone, implying that this close to the equator the area might be an extensive zone of crustal weakness (a tectonic fractured layer or feature (e.g. a fault) where the rock mass properties are significantly poorer than in the surrounding materials (Soderblom et al. 2009; Solomonidou et

al. 2013a). In addition, a map including all the current cryovolcanic candidate regions can be seen in Figure 4.34.

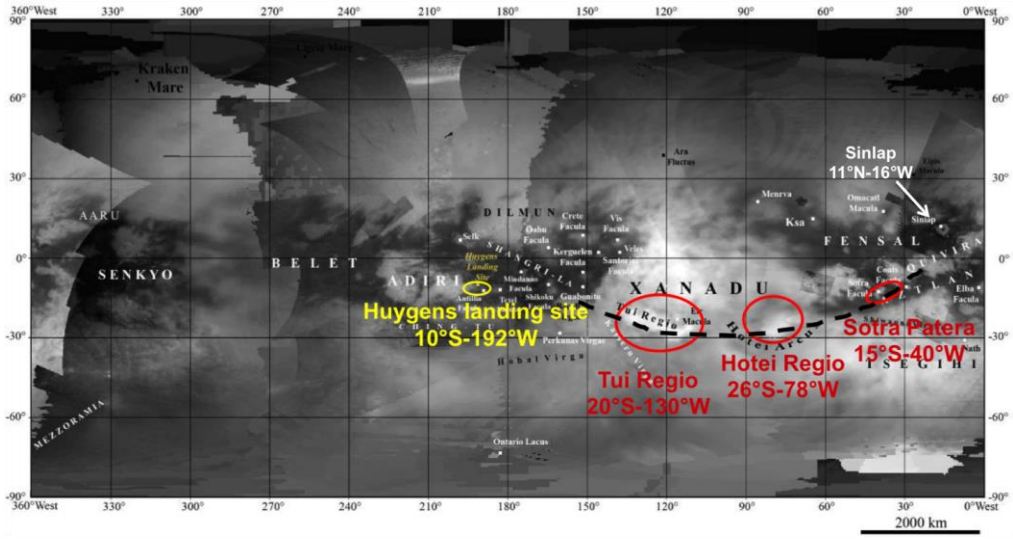

Fig. 4.22 - Map of Titan from VIMS data at 2 μm (background map credit: Stephan et al. 2009). From left to right the red circular shapes indicate some of the candidate cryovolcanic areas namely Tui Regio, Hotei Regio, and Sotra Patera, which are located within the major area of Xanadu and the southern part of Fensal. In yellow is the Huygens landing site. The black dashed line indicates the direction of a possible zone of weakness underlying the three candidate areas. Also visible is the Sinlap crater area (white arrow) (Solomonidou et al. 2013b).

I have analyzed in detail these three cryovolcanic candidates using specific tools for the retrieval of their nature in Solomonidou et al. (2013b) and Solomonidou et al. (2013c). I discuss in detail this work in Chapters 6 and 7.

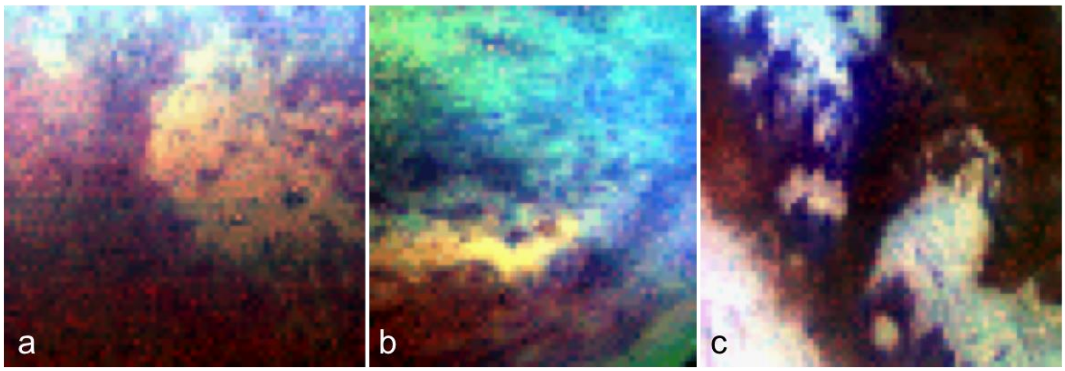

Fig. 4.23 - Hotei Regio (a), Tui Regio (b) and Sotra Patera (c) from VIMS T47, T12 and T09 respectively (VIMS data provided by Stephane Le Mouelic during personal communications from 2009).

Hotei Regio (26°S, 78°W, Fig. 4.23a) has been suggested to have a distinct surface composition by Barnes et al. (2005) and to be anomalously bright at 5 μm, connected perhaps to a geophysical phenomenon. Soderblom et al. (2007b, 2009) studied Hotei Regio's VIMS data color variations and correlation with morphological features seen in SAR images, and

suggested a possible influence of complex geological processes, like tectonism and cryovolcanism, that remained active until very recent geological times (possibly less that 10^4 years). Moreover, Nelson et al. (2009a) reported that Hotei Regio showed changes in the near-infrared reflectance from 2004 to 2006, which could be linked to cryovolcanism and ammonia deposits. I am testing this suggestion in the following Chapter 7. The Cassini SAR images indicate that the area is a low basin surrounded by higher terrains with possible calderas, fault features and extensive cryovolcanic flows. Soderblom et al. (2009) have studied the area and indicated significant geological features that resemble terrestrial volcanic features. These are viscous flow-like figures, a 1 km in height mountainous terrain (ridge-like) that surrounds the basin, as well as, dendritic channels, caldera-like features, dark blue patches (in VIMS RGB coloring) likely related with water ice-rich exposed terrains (Rodriguez et al. 2006) and possibly alluvial deposits (see Fig. 4.16, section 4.1.4.1).

An additional major structure located at the southern margin of Hotei Regio is the bright arc named Hotei Arcus, which Barnes et al. (2005) characterized as a possible heavily eroded crater. Geologically this leads to the assumption that different types of processes like cryovolcanism and/or aeolian/fluvial erosion may have acted upon and/or interplayed in the same feature. Moreover, Lopes et al. (2013) presented in this recent analysis topographic data obtained from the overlap between SAR swaths (T41 and T43) that enabled stereo determination of elevations (Kirk et al. 2008; 2009). The analysis provided results that revealed topographically high lobate areas, with heights of ~200 m above the base level at which the channels are found (Fig. 4.24).

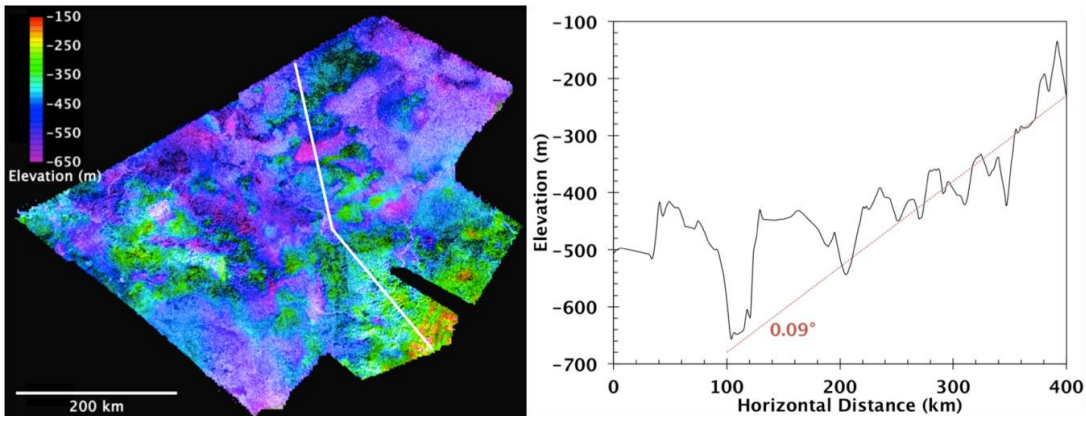

Fig. 4.24 - Hotei Regio's topography from DTM. The topographic analysis shows relief (~200 m) on the radar-dark flows, which are higher (at least 100 m) than the base level of channels. The area appears more consistent with a cryovolcanic than fluvial origin, as it implies a complex rheology, such as what might be expected for ammonia-water-methanol mixtures (Kargel et al. 1991; Lopes et al. 2007). (Image credit and information from Lopes et al. 2013).

The following Figure 4.25, is an attempt to understand the morphology of Hotei Regio and make implications on the possible present features from information I ammased from a number of studies that focus on Hotei Regio and its nature (e.g. Lopes et al. 2007; 2010; 2013; Soderblom et al. 2009; Wall et al. 2009).

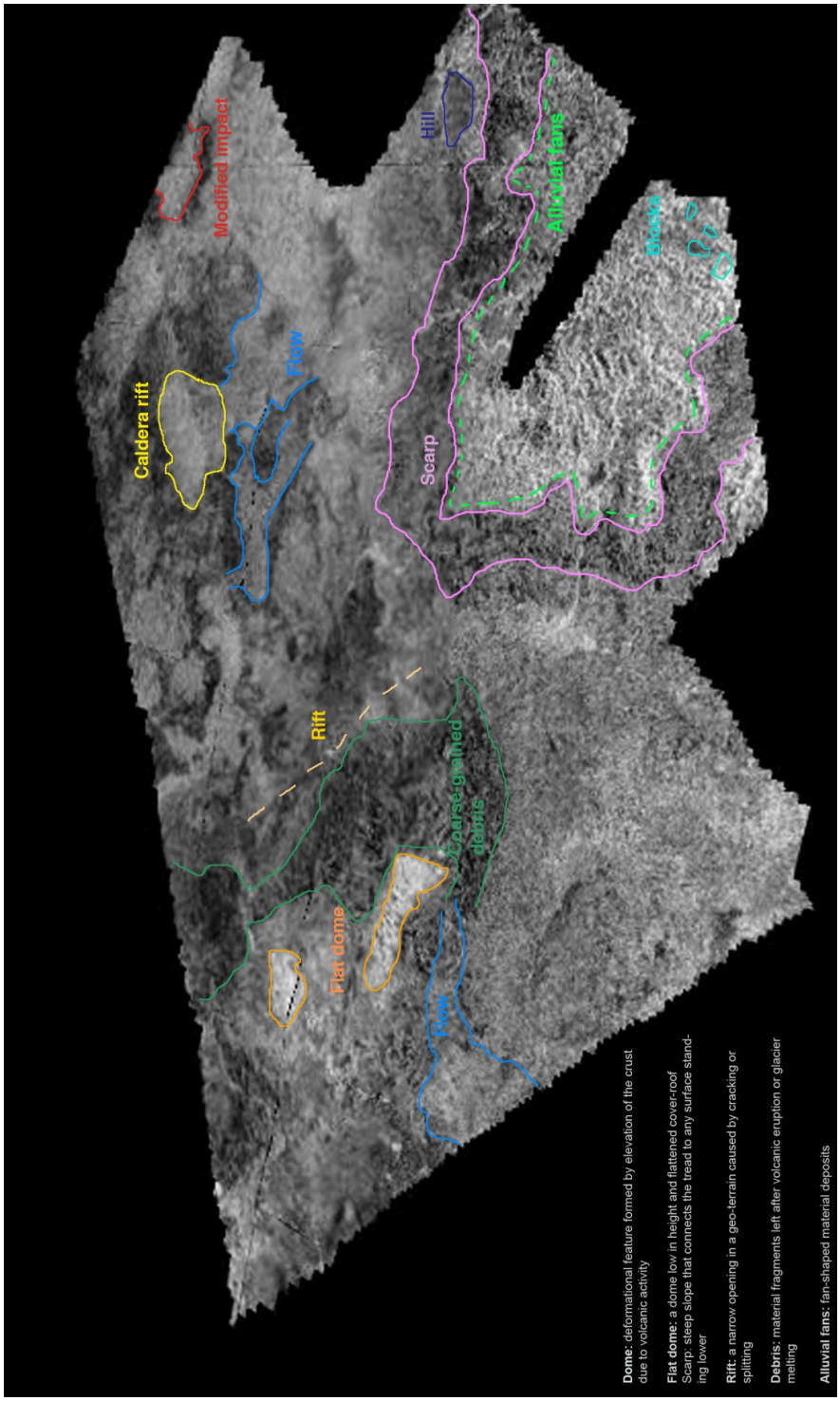

Fig. 4.25 - Schematic map of Hotei Regio's surface features possible present in the region (Background image adapted from DTMs of Randolf Kirk; NASA/JPL-Caltech/ASI/USGS, PIA11831).

Tui Regio (20°S-130°W, Fig. 4.23b) is a feature 150 km wide and extends for 1,500 km in an east-west direction (Barnes et al. 2005, 2006; Wall et al. 2009; Brown et al. 2011). The analysis of Cassini ISS and mainly VIMS data (Barnes et al. 2006, 2007a, b) suggested that the area is a massive flow field since at least three long lobate spectrally distinct tendrils (Barnes et al. 2006) have been observed and have possibly being effused from a main point like a caldera-like structure, fracture or fissure. McCord et al. (2008) also characterized it as a spectrally distinct unit in composition, especially because of its anomalous brightness at 5 μm, which has been confirmed using updated VIMS maps from Vixie et al. (2012). Barnes et al. (2006) suggested that a flow-like feature at the western part of Tui Regio could represent cryovolcanic activity, based on the study of its geometry, relative age and chemical composition. In fact, a number of studies suggest that the whole area may be geologically young and that the resembling lava flows could be deposits of cryovolcanic activity.

In Figure 4.26, the radar-bright mountains to the east (right-hand side) are topographically high as expected and seem to correlate with volcanic-filled depressions (middle) (Soderblom et al. 2009). However, SARTopo data showed that these depressions are possibly consistent with lakebeds (Mitchell and Malaska, 2011).

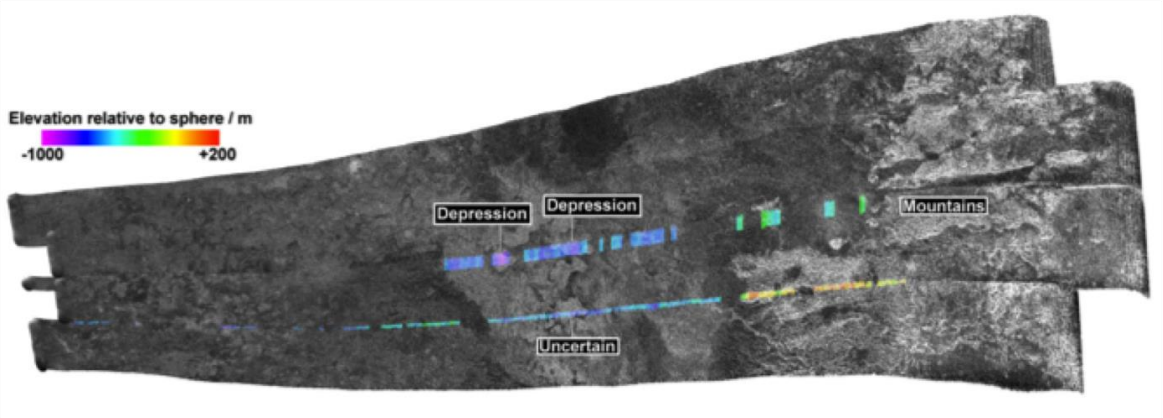

Fig. 4.26 - Tui Regio from T48 SARTopo data (Adapted from Lopes et al. 2013).

As mentioned hereabove, in the recent investigation with Cassini VIMS and RADAR data by Lopes et al. (2013) Tui Regio and Hotei Regio, along with another region, now called Sotra Patera (formerly Sotra Facula, 15°S, 40°W, Fig. 4.27), were also identified as geologically compelling areas, suggesting again the possibility of cryovolcanic activity. Sotra Patera, morphologically consists of two mountains, one of which is the highest known mountain on Titan, named Doom Mons (40°W, 15°S), while the other one is Erebor Mons (35°W, 5°S). Additionally, lobate flow deposits named Mohini Fluctus (12°S, 39°W), seem to emerge from Doom Mons while Sotra Patera is a deep non-circular depression that is

considered as the deepest local depression identified on Titan (Kirk et al. 2010; Lopes et al. 2010; 2013).

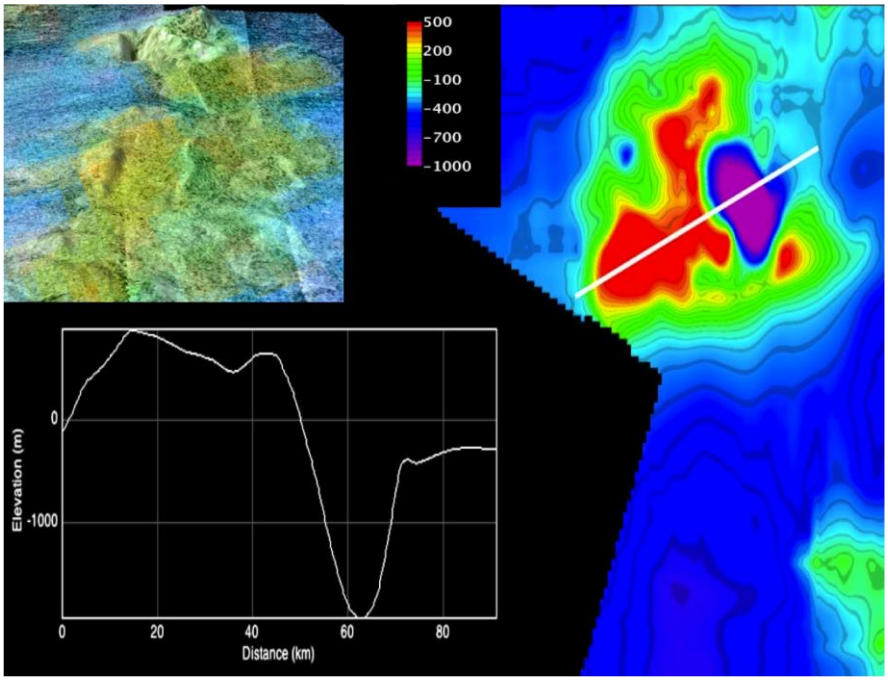

Fig. 4.27 - (upper left) Sotra Facula, a possible cryovolcano on Titan from VIMS and RADAR correlation. (right) Results of SAR stereo and DTM over the Sotra region. The peaks are more than 1 km high and the craters-caldera almost 1.5 km deep. Flow features about 100 meters thick are obvious following a radial pattern around the craters (NASA/JPL-Caltech/USGS/University of Arizona). (lower left) Topographic profile of the region (taken from the white line on the right). (Adapted from Lopes et al. 2013 and information therein).

Other studies based on estimations of Titan's topography for Tui Regio and Hotei Regio alternatively suggest that both areas could be sites of large low latitude paleolakes (Moore and Howard, 2010). In addition, Barnes et al. (2011) suggested the presence of dry lakebeds at Titan's north pole with spectral characteristics similar to Tui Regio and Hotei Regio, implying a common evaporitic origin (i.e., deposits due to dissolution of chemical solids that precipitate out of a mixture as their liquid solvent evaporates). Moore and Pappalardo (2011) also suggested that the areas are the result of exogenic deposits, either fluvial or lacustrine.

4.2 Mechanisms connected with the interior

As expected from the study of other icy satellites, the majority of formation mechanisms suggest extensional style tectonism. In the areas where fluvial networks seem to be controlled by tectonic patterns, the surface material appears to have the proper elasticity to create linear fractures. At HLS, as proposed by Soderblom et al. (2007b), the linear structures can function as the ideal path for the hydrocarbon liquids to escape towards the surface. Furthermore, the observed radial fault system around the possible calderas of Hotei Regio (Soderblom et al. 2009), argue in favor of cryovolcanism since the identification of radial faults around caldera formations (also on Earth), are indicators of crustal uplift due to volcanic activity.

Before I continue with the implications on the tectonic and cryovolcanic origin of these features, it is first essential, to present the current understanding of Titan's interior in terms of structure and composition.

4.2.1 Interior stratigraphic models

As presented earlier, there are regions on Titan's surface that show evidence of past volcanic and tectonic activity. It seems that Titan's crust is unstable (i.e. could be subject to deformation) and that tectonism is present by contractional processes rather than extensional processes (e.g. Radebaugh et al. 2007). That instability is most possibly related to the presence of a liquid layer underlying its icy crust (e.g. Grasset and Sotin, 1996). The indications about the presence of a subsurface liquid layer from Cassini data are presented in section 1.4.1.3 (Chapter 1).

There are studies that attempt to explain the cryovolcanic as well as the tectonic aspects on Titan by modeling the internal processes that lead to these dynamic activities. A major problem that regards the analysis of the moon's interior is the lack of data that could provide information about the internal structure of Titan. Rappaport et al. (1997; 2007) suggested that the Cassini Radio Science Subsystem (RSS) can gather such information by measuring the principal components of Titan (and even Enceladus) and studying its gravitational properties. The main goal in this case is to set some constraints about the ocean and the icy crust rather than try to acquire specific measurements regarding the thickness of the ocean and crust (Sohl et al. 2003), something that is not possible with the current instrumentation. Setting such constrains, it is important to determine Titan's interior history over time (e.g. Tobie et al. 2010a), as well as to understand the interactions and exchange of materials in between the system interior-surface-atmosphere.

Thermal evolution models suggest that Titan may have an icy crust between 50 and 150 km thick, lying on top of a liquid water ocean with some amount of ammonia dissolved in it, acting as an antifreeze material (e.g. Tobie et al. 2005; 2006). Indeed, Titan's internal structure consists of several layers, based on modeling. A rocky silicate core extends over 1,800 km, is overlaid by a high-pressure icy layer 400 km wide. On top of the latter layer, a 50 to 150 km liquid water layer exists, which is overlaid by Titan's ice-Ih crust and extends for few kilometers (Tobie et al. 2005; 2010; 2012; Fortes et al. 2007). In terms of chemical composition, Titan's interior can be broadly described, from the core to the crust, by the following structure: a serpentinite core, a high-pressure ice-VI mantle, a liquid layer of aqueous ammonium sulphate and an externally heterogeneous shell of methane clathrate with low-pressure ice-Ih and solid ammonium sulphate (Fortes et al. 2007). Tobie et al. (2005; 2010) suggest the presence of stored methane clathrates in the ice-Ih crustal layer (Fig. 4.28).

At this point it is essential to distinguish the phases of ice that potentially exist within and in the outermost of Titan. Ice-Ih is a phase of normal hexagonal crystalline ice, which is the most abundant solid phase of ice on Earth's surface. Water ice on Titan would be in the form of ice Ih up to a depth of 120-123 km, then it transforms to the polymorphs ice III, ice V, ice VI and ice VII. The high-pressure layer beneath the ocean is primarily composed of ice VII but depending on the thickness of the ocean an ice V layer may exist between the ocean and ice VI. Ice VII can exist only deep where P>2GPa, if some structure of rock-ice still exists in the core (Grasset et al. 2000; Tobie et al. 2006).

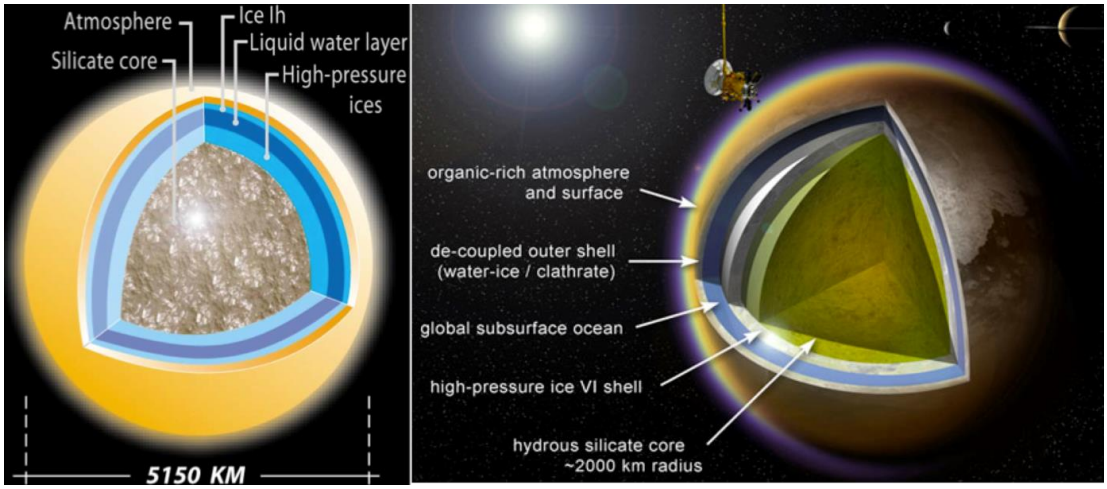

Fig. 4.28 - Two models of Titan's internal stratigraphy. (left) Model from Tobie et al. (2005); (right) Model from Fortes et al. (2012). Both models present the same structure, with some differences in the layers' thicknesses and composition.

I have contributed in a recent study by Sohl et al. (2013), where we worked on the correlation between the global tidal pontential of Titan and the observed geologically

interesting regions, in terms of internal interactions. Part of this study was the construction of a fiducial model of Titan's present interior structure. Briefly, based on Cassini gravity data, the model satisfies the 2σ (error margin of Moment of Inertia) observational data of the polar Moment of Inertia (MoI) factor and the degree-2 body tide Love number k2 (tidal potential). Furthermore, the radiogenic heat production rate ε is adjusted to meet Titan's surface temperature of 94 K and the viscosity of the silicate core is adjusted so that the central temperature will not exceed a critical threshold temperature of ~900 K for silicate dehydration (e.g. Perrillat et al. 2005; Castillo-Rogez and Lunine, 2010). The hydrated rock core is about 2,100 km in radius with an average density of 2,600 kgm^{-3}. While the central pressure is 4.9 GPa, the pressure at the core-mantle boundary is about 0.80 GPa.

The tidal gravity field of Titan is found to be consistent with a subsurface water-ammonia ocean of more than 180 km thickness with relatively low ocean ammonia contents of less than 5 wt.-% and ocean temperatures in excess of 255 K. The outer ice shell is fixed to 100 km, following previous studies (Nimmo and Bills, 2010).

Our model agrees with the structure of the previous presented models with some differences in the thickness of the layers (Fig. 4.29).

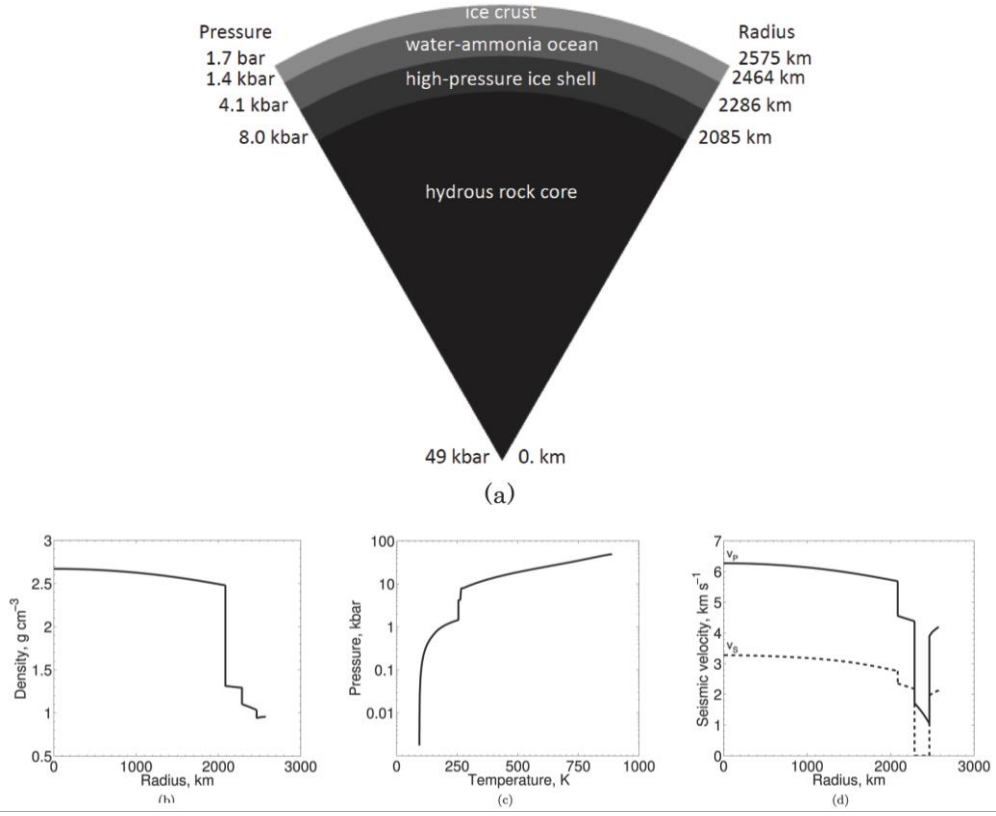

Fig. 4.29 - Titan's interior stucture. (a) Radial structure; (b) Density distribution; (c) Temperature-pressure diagram; (d) Seismic velocities (Adapted from Sohl et al. 2013).

To determine the sizes of Titan's bulk reservoirs such as the crust, ocean (isothermal) and core, we have adopted new laboratory data for the parameterization of the water-ammonia (H_2O-NH_3) phase diagram (Choukroun and Grasset, 2007; 2010). The P-T phase diagram of the H_2O-NH_3 system (ocean temprerature to a certain value) is an extremely important parameter and closely related to the thickness of the crust and the subsurface ocean. The model yields that lower ocean temperatures require thinner oceans and larger crusts. Nevertheless, the ammonia concentration (for NH_3 < 25 wt.-%) controls the ocean temperatures showing that smaller ammonia concentrations lead to warmer subsurface oceans and vice versa. Additionally, in the study by Sohl et al. (2013) we have studied the habitability potential of Titan based on the aforementioned internal layering concluding that a thinner crust could be more conducive to putative life since it would facilitate frequent cryovolcanism and upwelling and surface deposition of ammonia-water cryomagma.

4.2.2 Tectonic activity

In the previous sections I presented surface features on Titan that show a tectonic and cryovolcanic fashion as viewed and analyzed by several studies from Cassini VIMS, RADAR, ISS and Huygens DISR data. Moreover, the possible presence of a long-lived liquid layer underlying its crust reinforces the hypothesis of subsequent tectonism. Titan is of sufficient size, and with large enough silicate rock fraction (roughly 50%) to have undergone partialy to complete differentiation shortly after accretion. Thus, Titan might have undergone a later period of tectonism analogous to Europa or Ganymede (e.g. Grasset and Sotin, 1996).

4.2.2.1 Icy and silicate tectonism

The response of the crustal material to the applied stresses in addition to the atmospheric conditions at the moment of formation, define to a large extent the morphology and topography of a surface terrain. Importantly, the fashion under which the crust would deform depends on the nature of the material that composes it. Even though geological features such as mountains, faults and rifts on Titan present similar visual characteristics, the type of material (i.e. petrological properties) that builds the features plays an important role. Indeed, the properties of the source material such as viscosity, elasticity and density, in addition to the geological forces, control the structural characteristics of the feature such as height, expansion and gradient slope.

As mentioned earlier, the current understanding of Titan's interior and surface, indicates that the surface consists mainly of mixtures of water and other ices, organics-tholins, nitriles and the interior consists of rock and high-pressure ice (Tobie et al. 2005; Soderblom et al. 2007a). In our recent work, where we studied Titan's morphotectonic features and their possible origin in comparison to terrestrial systems (Solomonidou et al. 2013a), I found it essential to first assess the similarities and differences between water ices (Titan) and silicates (Earth), so that such a comparative study can be based on reasonable assumptions. It appears that the icy crust of the outer system satellites possibly reacts in a brittle fashion to the application of stresses, similarly to the Earth's rocky upper crust (Collins et al. 2009) while on both systems this reaction changes in proportion to depth. However, while water ice and silicate rock exhibit similar frictional strength when ductile yielding becomes important, ice is about ten times weaker than silicate rock (Beeman et al. 1988; Melosh and Nimmo, 2011). The major differences and similarities between water ice and silicates are included in Collins et al. (2009) and summarized in Table 4.4. As seen in the table, the silicate materials exhibit higher viscosity and Young modulus (elasticity) and higher density when compared to water ice. Thus, the homologous temperature (i.e. the temperature of a material as a fraction of its melting point temperature), on which rheology depends, is reached at greater depths in silicate environments while silicate magma eruptions are statistically more possible to occur than eruptions of ice (Collins et al. 2009). However, both icy and silicate systems seem to follow some similar general deformation principles and mimic each other's behavior. Also, since ice topography could viscously relax over geologic time (e.g. Dombard and McKinnon, 2006) and elastic, brittle and ductile deformation could occur in the icy crust, tectonic-like movements resembling the silicate plate behavior are plausible.

Table 4.4 - Comparison between silicate and ice properties (Solomonidou et al. 2013a).

Properties	**Water Ice**	**Silicate**	**Similarity**
Homologous temperature	0.4	0.4	Yes
Melting temperatures	273.15K	950-1500K	No
Density	Low (in solid state)	High	No
Young Modulus	~10 GPa	~100 GPa	No
Low stress and strain	Elastic deformation	Elastic deformation	Yes
High strain, low temperature	Brittle deformation	Brittle deformation	Yes
Low strain, high temperature	Ductile deformation	Ductile deformation	Yes

In this section (4.2.2), I describe Titan's morphotectonic features as a combination of a formation processes largely attributed to tectonism and one or more superimposed "transverse

processes" that occurred at the same time or subsequently, modifying the initial shape of the feature (Solomonidou et al. 2013a).

4.2.2.2 Mountain formation

In this subsection I present another part of the study on the mechanisms that possibly formed the aforementioned morphotectonic features and propose terrestrial analogues. Presentation of the images of the terrestrial analogues accompanied by analysis of the comparative study can be found in Chapter 10.

Many possible formation mechanisms have been proposed for the mountains identified on Titan (Radebaugh et al. 2007). Two scenarios suggest crustal compressional tectonism as the main tectonic process where upthrusting of blocks shapes the mountains, and extensional tectonism, where massive parts of the crust are being pulled away; in the same way as convergence and divergence tectonics occur on Earth (Fig. 4.30).

Horst-and-graben has also been proposed as the formation mechanism of tectonic edifices on Titan (Radebaugh et al. 2007). A horst is an uplifted elongated block of the crust placed between two faults and a graben is a depressed block of parts of the crust bordered by parallel faults (Fig. 4.31). Thus, it is possible for the crust to be separated due to extension and horst created next to grabens.

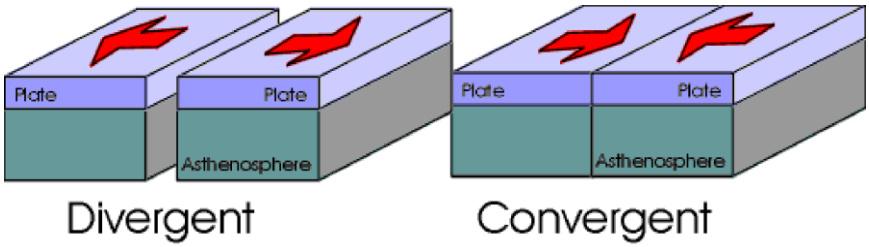

Fig. 4.30 - Two main movements of plate tectonics (Scheme credit: USGS).

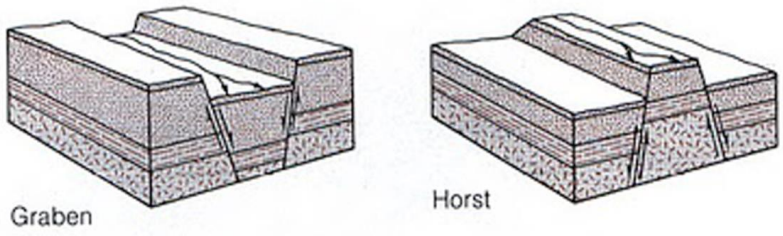

Fig. 4.31 - Graben and Horst tectonic formations (Scheme credit: USGS).

The third mechanism for the formation of mountains, as proposed by Radebaugh et al. (2007), is deposition as blocks of impact ejecta. The impact ejecta consist of material

discarded from an impact crater in its excavation stage and deposited around its margins. Finally, the last scenario regards mesas formations. Erosional and weathering processes of horizontally layered rocks form the geological landforms named mesas. These layers of rocks have been uplifted by tectonic activity (Easterbrook, 1999). It is important to note that the study regarding the orogenesis on Titan investigates mainly the possibility of compression crustal deformation to produce topography on Titan. This is of high priority in the research as extensional tectonism is observed on almost all icy moons of the outer Solar system and any evidence regarding compressional tectonism is limited (Mitri et al. 2008). Furthermore, if the mountainous figures seen on Titan are formed because of compressional tectonism, then Titan is the only icy active satellite on which compression features exist in the style of tectonism (Mitri et al. 2008).

Mitri and co-authors supported again this theory in a paper published in 2010. There, the authors studied the possible types of orogenesis on Titan focusing on compressional-contractional tectonism. Indeed, through modeling they showed that altered densities at the outermost layers of the crust could cause unusual surface behavior. Internal processes such as radioactive decay and temporal heat release lead to the moon's gradual cooling, thickening of the high-pressure layer which results in a global reduction of volume. Modeling and analysis of the Cassini SAR data showed that Titan's radius has shortened by about 7 km and its volume has decreased at about 1%. As mentioned earlier and in addition to the Mitri et al. (2010) modeling, Titan is the only icy satellite where the shortening and thickening are dominant.

In brief, the mechanisms for mountain formation on Titan, based on the so far analysis, are summarized in Table 4.7 (see § 4.4) and include pure extension (Sotin et al. 2007; Radebaugh et al. 2007-scenario 2), pure compression (Radebaugh et al. 2007-scenario 1; Mitri et al. 2010) and transitions between compressional and extensional stresses (Mitri and Showman, 2008).

On Earth, formation of mountains due to extension is represented by the classical example of the Basin and Range area and other examples that I present in Chapter 10. As a geological terrain, Basin and Range (Hawkesworth et al. 1995) consists of separate and semi-parallel mountain ranges as seen in Figure 10.12 in Chapter 10. Crustal extension appears to have been the main formational mechanism that developed large faults, along which mountains were elevated and valleys have submerged. Subsequently, fluvial deposits, aeolian erosion and other exogenous processes modified these features.

Nevertheless, convective stresses on silicate bodies tend to be larger and their rheological length scales are typically greater (Table 4.4). For Titan therefore it is essential to note that local/regional rather than global stress mechanisms are commonly suggested in the models for mountain building. Regional or local stress mechanisms invoked in these models include, (a) convection, which depends in the ice shell thickness, (b) local gravity, and (c) global convection > 1MPa (Mitri et al. 2010). Indeed, on large icy satellites, layers of high- and low-pressure ice may convect separately (McKinnon, 1998). One local stress mechanism is lateral pressure gradients that may have as a consequence the lateral flow of floating ice shells on their low viscosity base. Rigid ice floes rupturing and colliding are reminiscent of plate tectonics albeit in a random fashion. This could lead to the creation of blocks of high-standing topography that would subsequently be subjected to erosional processes. Such elevated morphotectonic features on Titan, such as mountains, ridges, hills and ranges, indicate a formation preference around the equatorial zone of the moon (Barnes et al. 2007a; Radebaugh et al. 2007; Mitri et al. 2010).

4.2.2.3 Linear feature formation

In geology, a fault is a rupture that separates a unit into two parts, moving one relatively to another, be it a rock in microscale studies or a whole field in macroscale studies. There is a variety of geological processes associated with faults and therefore their analysis is very important. Some examples that link faults and geological phenomena together on Earth are, amongst others, the direct relation of earthquakes and faults, the penetration of igneous rocks in the crust along faults, as well as the interaction of faults in the development of different formation phases in sedimentary basins.

In planetary studies, the identification of surface expressions of faults seems extremely important since their structure, size, shape and location hide information about the internal processes that formed them as well as the interactions of these faults with other geological structures within a significant region. A fault is usually a structure that is associated with other geological expressions by means of geomorphology. For example, as mentioned earlier, a graben if present on Titan, then it will form a valley bounded on both sides by normal faults. The movements along these faults would be vertical, with the central block moving downward. Thus, the identification of fault formations on Titan will help us develop the current state of understanding of the internal process, which led to geomorphologic changes,

as well as the interpretation of other geological structures. Table 4.5 presents a description for possible formation mechanisms for the currently observed linear feaures on Titan.

Table 4.5 - Proposed mechanisms with relation to tectonics for the formation of linear features on Titan.

Location	**Proposed mechanism**
15°S, 155°W	i. Large scale tectonic modification of bedrock material ii. Fluvial sapping of bedrock that enlarges tectonic zones of weakness (Porco et al. 2005)
10°S, 145°W 0°N, 180°W	Control by a subsurface tectonic structural fabric due to orbital processes (diurnal tides, non-synchronous rotation: tensional stresses) (Burr et al. 2009)
10°S-192°W	Preexisting faults reactivated from cryovolcanism and filled with deposited material and formed canyon-like systems (Soderblom et al. 2007b)
15°S, 100°W	Extensional crustal stresses (Radebaugh et al. 2011)
26°S, 78°W	i. Hot plume uplift and crust elevation-fault formation due to extension stresses ii. Large ancient impact crater (Soderblom et al. 2009)

In conclusion, on Titan the observed faults, fractures, canyons and ground lineaments are most likely the outcome of crustal movements due to tectonic-like (ice floes) and/or volcanic processes, as well as, structures associated with fluvial networks controlled by tectonism.

4.2.3 Cryovolcanism and association with tectonics

Cryovolcanism is thought to represent an important geological process in the history of several icy satellites of the outer Solar system (Kargel, 1994; Fagents, 2003; Lopes et al. 2007). This geological process is a form of ice-rich volcanism, and the material erupted is referred to as cryomagma, which appears in the form of ice (Kargel, 1994). The possibility of volcanic resurfacing on icy moons was first noted by Lewis (1971, 1972) and subsequently discussed by Consolmagno and Lewis (1978). The Voyager and Galileo missions to the Giant planets brought evidence for past and present tectonic and volcanic activity on moons such as Jupiter's Io, Europa and Ganymede, (e.g. Allison and Clifford, 1987; Morabito et al. 1979; Greenberg et al. 1998) and Neptune's Triton (Soderblom et al. 1990). Cryovolcanism in the Saturnian system was first suggested from Cassini data for Enceladus from the detection of the southern polar plume, and the enhanced thermal emission from the same region (e.g. Dougherty et al. 2006; Spencer et al. 2006; Hansen et al. 2006; Porco et al. 2006; Waite et al. 2006). The observed correlation between the brightness of the plume and Enceladus' mean anomaly (Hedman et al. 2013), confirms that the intensity of the jets are controlled by tidal forces (Hurford et al. 2007) and that volcanism is the end-result of geophysical and

geochemical processes triggered by the tides during Enceladus' elliptic orbit around Saturn. No such eruptions have been detected so far on Titan.

The mechanism of cryovolcanism resembles terrestrial type volcanism, where however the cryomagma differs from the terrestrial magma in composition, texture and of course temperature. Indeed, the cryomagma i.e. aqueous solutions of ammonia, methane, salts, etc, is cold, well below the freezing point of pure water and degassing replaces the traditional silicate volcanism. Cryovolcanic structures are openings, or ruptures -in a planetary surface or crust-, allowing various internal products like water, other chemical components, ash and gases to escape from the planetary body's interior.

Plate tectonics and volcanism are strongly associated on Earth (McDonald, 1982) and this could also be the case on Titan in the presence of tectonic features overlying a liquid water ocean. These can function as leading 'pathways' for the ammonia-water cryomagma to reach the surface and for the release of methane. As I discuss hereafter, liquid pockets with methane clathrates and with a high ammonia mass concentration in a water solution can dissociate in the ice shell and eventually exsolve on the surface and in the atmosphere (Tobie et al. 2006; Mitri et al. 2008; Choukroun et al. 2010). Hence, cryovolcanism can also act as the dynamic force that deforms tectonic features and bring methane in the atmosphere.

In addition to the theoretical modeling regarding cryovolcanism on Titan, the surficial evidence in the form of volcanic-like edifices and features is of great importance. Unfortunately, the identification of cryovolcanic features is rendered difficult mainly due to the observational restrictions that Titan's atmospheric veil causes and hampers the derivation of information on the composition; an issue that I am trying to resolve in Chapters 6 and 7. Other than that, the interaction of cryovolcanic features with features formed by other geological processes makes it difficult to unambiguously distinguish volcanic deposits from deposits formed by other fluvial processes (Lopes et al. 2010). One example of interaction between a cryovolcanic with a rather non-volcanic structure is located in Winia Fluctus area (45ºN, 30ºW, Fig. 4.20). There, aeolian processes form a dune field that subsequently and partially covered a cryovolcanic feature (Lopes et al. 2010). Another issue, concerns the two Cassini instruments in use for cryovolcanic investigation; the SAR which analyzes the morphological patterns and the VIMS that analyzes the chemical composition and the occurrence of some photometric variability (Nelson et al. 2009a; Nelson et al. 2009b). Both instruments provide data of different spatial resolution and cannot operate simultaneously and this renders the correlation of such data, that would extract thorough geological information, as very demanding if not problematic. However, theoretical modeling and the current Cassini

data offer the tools for a preliminary investigation suggesting cryovolcanic candidate features and triggering-formation mechanisms.

The source of heat that causes cryovolcanism is an intriguing issue. A number of heat sources have been proposed for Titan. First, radiogenic heating due to the decay of radiogenic elements such as ^{40}K, ^{232}Th, ^{215}U and ^{238}U is suggested. Most importantly, the presence of ^{40}K is determined by the present of the ^{40}Ar product (GCMS –Niemann et al. 2005), indicating the exhanges between the interior where ^{40}K is present and the surface (Dorofeeva and Ruskol, 2010). Moreover, for Titan during the early stage, impact heating seems to have been a source of energy contributing to the internal thermal budget (Jones and Lewis, 1987). In addition, during accretion triggering of the ice-rock layer separation, could have also contributed to the thermal budget (e.g. Ricard et al. 2009). However, these two sources of energy are negligible now. The significance of radiogenic heating to Titan's thermal history is limited to the materials of accretion that formed its inner part (Tobie et al. 2010a). Another source of importance with the outer ice shell is the tidal dissipation since Titan is subject to solid body tides exerted by Saturn on the time-scale of its orbital period. The tidal deformation is amplified with the ice shell due to the presence of the ocean, which can generate non-negligible heating (e.g. Tobie et al. 2005; Iess et al. 2012).

On Titan, internal heating due to radiogenic decay and tidal friction along with pressure alterations may trigger cryomagma eruptions and eventually cryolava deposition at temperatures much lower than the terrestrial ones (Davies et al. 2010). In general, the temperature of most terrestrial magma types ranges from 970 K to 1470 K while a plausible range of the Titan cryomagma temperature is between 177 K and 239 K (Mitri et al. 2008).

Tobie et al. (2006) suggested a cryovolcanic model that explains the methane replenishment since it is should vanish in 10-30 Myr (Atreya, 2010). These authors suggest that episodic methane outgassing events occurred through three distinct main episodes covering a chronological period from 2000 Myr ago until 500 Myr ago (Fig. 4.32): the first following the accretion and differentiation period; a second episode approximately 2000 Myr ago when convection initiated in the silicate core; and finally, a geologically recent period, circa 500 Myr ago, due to enhanced cooling of the moon by solid-state convection in the outer ice shell. The internal ocean provides the 'magma' chamber by means of material, while convective processes are the triggering mechanisms that initiate the dynamic activity. Apparently, the tectonic and cryovolcanic structures require a dynamic interaction as well as material exchange between the surface and the liquid ocean. A convective model of a stagnant lid is capable to explain such activities (Solomatov, 1995). The stagnant lid is a relatively cold

and stiff conductive layer on top of the warmer convective icy interior (Schubert et al. 2004). This layer of stagnant lid stops the upwelling of warm ice within the convective zone, and prevents cold near-surface icy material from submerging downwards to the ocean**.**

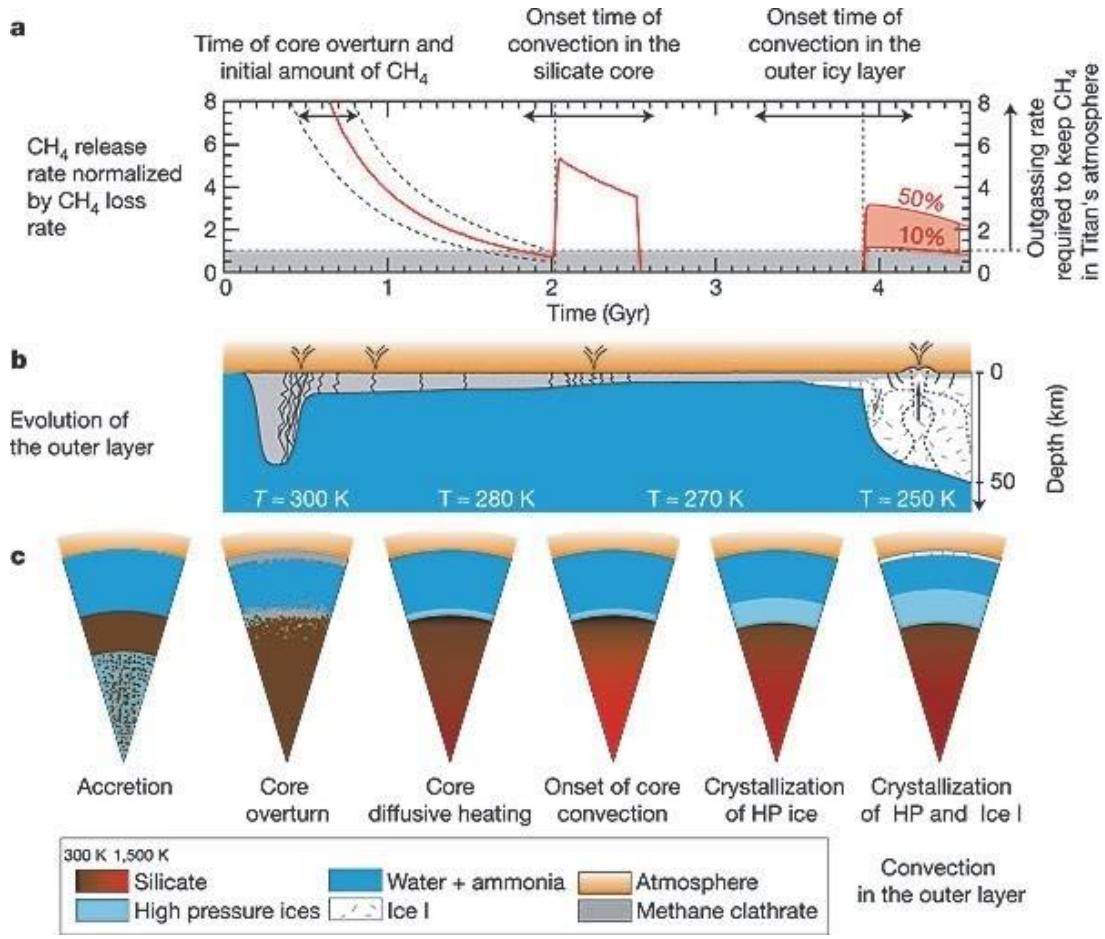

Fig. 4.32 - Possible cryovolcanic events during Titan's history emerging from its internal liquid ocean (Image credit: Tobie et al. 2006).

Since Titan's internal liquid ocean most probably range from 50 to 150 km (Tobie et al. 2005; Fortes et al. 2007; Mitri et al. 2010) and is thicker than that of Europa's, it is plausible for crust melting and/or cracking to occur. Thus, exchange of material and dynamic forces between the underground ocean and the icy surface are expected. Controvert to this hypothesis, several studies suggest that Titan is not currently convective (Mitri et al. 2010; Nimmo and Bills, 2010).

Indeed, a study by Mitri et al. (2010) proposes an internal thermal model, which favors the contractional deformation on Titan's surface. This study is focused on the changes in volume of a potential underground ocean caused by heat flux variations during melting or freezing. The authors suggest that the continuing cooling of the moon, as described in Tobie et al. (2005; 2006), can develop global volume contraction, while this is the most likely

source of stress in Titan's icy 'lithosphere'. Thus, contractional deformation triggering tectonic activity and fold formation is plausible to exist.

The subsurface instability due to the interactions within an interior liquid ocean could cause the modification of extended features on Titan's surface, whether they derive from cryovolcanic or morphotectonic dynamic processes. Currently, all the geophysical models that try to explain the geodynamics of Titan support the existence of an oceanic layer that decouples the mantle from the icy crust. Internal geodynamic activity can transport effusively the explosive material from the oceanic layer to the surface and form the cryovolcanic structures like the lobate flows (Mohini Fluctus) in Sotra Patera.

The existence of possible volcanic and tectonic features within a specific area seem to be manifestations of the most active region of Titan like the boundaries of tectonic plates on Earth. Although still under investigation in Titan's case, the definite identification and understanding of morphotectonic features in these regions is crucial in order to determine the presence and origin of zones of crustal weakness, which will in turn impose additional constraints on cryovolcanism on Titan.

4.3 Correlation with tides

In this section, I present amplitude patterns of diurnal tidal stresses on Titan and their correlation with the locations of morphotectonic and cryovolcanic candidates as presented in our recent paper by Sohl et al. (2013) following up the work by Solomonidou et al. (2013a) and the classification of morhotectonic and cryovolcanic features.

Gravitational field data acquired by the Cassini spacecraft suggest that Titan's state of internal differentiation is intermediate between partly separated Callisto and fully differentiated Ganymede (Iess et al. 2010). Titan is tidally locked with respect to Saturn, and thereby subject to solid body tides resulting in diurnal stresses at the satellite's surface. The tidal response depends on Titan's internal structure, its thermal state, the tidally effective rheology, and the frequency of tidal forcing. The existence of a shallow liquid-water ocean is the most probable interpretation of the Cassini measurements of the tidal contributions to the non-spherical part of Titan's gravity field (Iess et al. 2012). The occurence of dynamical processes such as cryovolcanism largely depend on the tide-induced internal redistribution of mass that results in variations of surface gravity, tilt, stress, and strain (Sohl et al. 2013). Here, I present the link between tidal deformation pattern and the candidate geodynamical surface features on Titan.

4.3.1 Modeling of Titan's tidal potential

We subdivide Titan's interior into four chemically homogeneous reservoirs and construct spherically symmetric structural models that are required to satisfy the satellite's mean density, polar factor MoI, and tidal potential Love number k2 as derived from Cassini gravity field data. Following the study of Hussman et al. (2011) in application to Europa, we first calculated the degree-2 body-tide Love numbers h2 and k2 and the Shida number l2 for our structural models of Titan's interior. The reference structural model was presented in Figure 4.29. Using corresponding linear combinations of the body tide Love-Shida numbers (e.g. Jara Orue and Vermeersen, 2011), we then calculated the expected amplitude patterns of tidal stresses at Titan's surface in response to the tidal forcing.

We have calculated the expected amplitude patterns of diurnal tidal stresses at Titan's surface and find peak-to-peak amplitudes. These are likely to accumulate over several tidal cycles up to larger values that even may exceed the tensile strength of ice. Hence, episodic stress release accompanied by localized tectonic quakes may occur where a certain threshold stress limit value is exceeded. It is distinguished between (a) the maximum areal stress

predominating in the equatorial and mid-latitude regions of the sub- and anti-saturnian hemispheres (Fig. 4.33a) and (b) the maximum shear stress concentrated in the polar regions (Fig. 4.33b). In addition, the superposition of the amplitude patterns of both areal and shear stresses (Fig. 4.33c) suggests that tidal flexure and stress accumulation are significantly enhanced in four adjacent, near-equatorial zones, approximately situated between the directions of the apex and anti-apex of Titan's orbital motion and that to the satellite's sub- and anti-saturnian point, respectively.

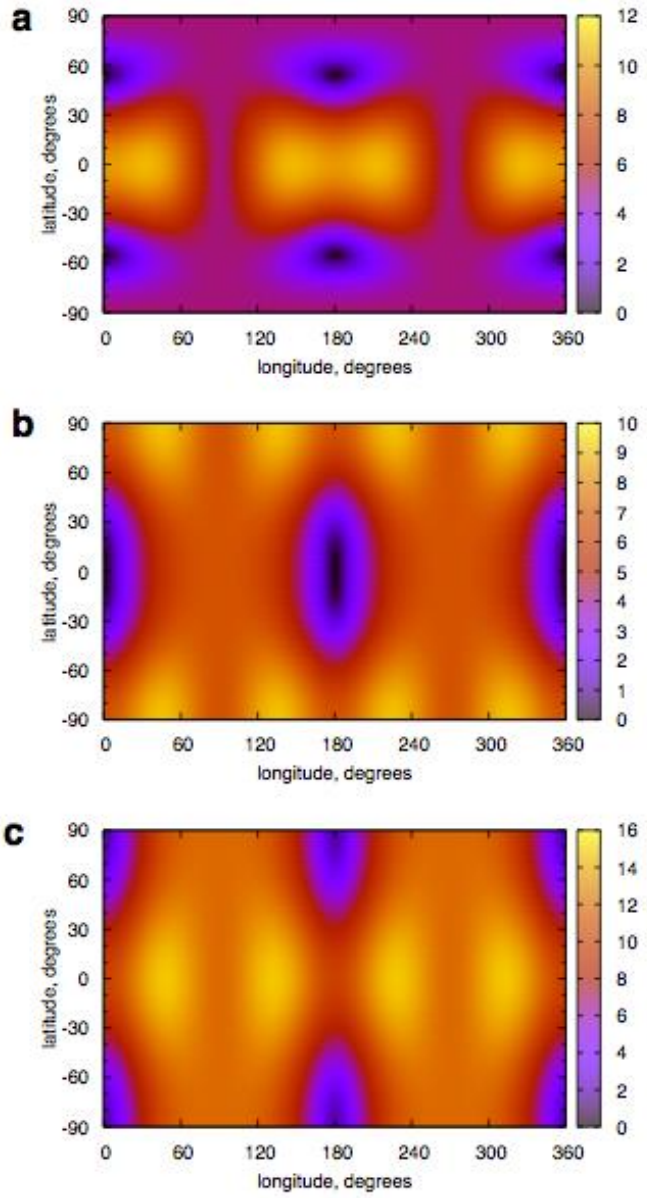

Fig. 4.33 - Global amplitude patterns of (a) maximum tensile stresses, (b) maximum shear stresses, and (c) the sum of maximum stresses color-coded in units of kPa (Sohl et al. 2013).

In the following sections, I examine the possibility for surface features, that shate tectonic-like and/or volcanic-like characteristics and/or anomalous spectral properties, to have a correlation with internal tides, and thus internal origin.

4.3.2 Correlation with geological features

As mentioned, the possible relation between tides on Titan and the observed features on the surface with indications of internal origin is the subject of this section and part of the work we conducted in Sohl et al. (2013). Indeed, tidal deformation of Titan's outer ice shell may have an effect on geologic processes retained in Titan's surface record. The concentration of morphotectonic structures around the equator and their young geological age suggests that the dynamic movements are connected to surficial stresses related to Titan's tidal environment. The global pattern of maximum tidal distortion is broadly consistent with the zonal distribution of cryovolcanic candidate areas and lakes at high latitudes that may provide possible pathways for the release of methane in the satellite's atmosphere.

In Table 4.6, I summarize all the morphotectonic and possible cryovolcanic features as described in section 4.1.4 with latitude.

Table 4.6 - Major geological features possibly related with endogenic processes on Titan. (Information from: [a]Cook et al. (2013), [b]Mitri et al. (2010), [c]Lopes et al. (2013), [d]Lopes et al. (2007), [e]Williams et al. (2011), [f]Le Corre et al. (2009), [g]Radebaugh et al. (2007), [h]Burr et al. (2009), [i]Lopes et al. (2010), [j]Barnes et al. (2007), [k]Wall et al. (2009), [l]Tomasko et al. (2005), [m] Soderblom et al. (2007), [n]Radebaugh et al. (2011), [o]Porco et al. (2005), [p]Barnes et al. (2006), [q]Soderblom et al. (2009), [r]Sotin et al. (2007), [s]Lunine et al. (2008).

Location	Name	Description	Tectonic-like features
57°N, 62°W	Misty Montes	[a]Mountain-chain	RADAR bright-dark pairing (T23/January 2007)
52°N, 347°W	-	[b]Mountain-block	1,400 m elevation from the surroundings (T30/May 2007)
47°N, 39.5°W	Rohe Fluctus	[c,d]Flow-like feature	Bright-rimmed, oval shaped caldera (TA/October 2004-T3/February 2005)
40°N, 118°W	Ara Fluctus	[c;d]Flow-like feature	Non-circular depression (T3/February 2005)
20°N, 87°W	-	[e]Ridges	Interplay with lineaments (T3/February 2005)
20°N, 70°W	T3 flows	[c,f]Flow-like feature	Flowing downhill (T3/February 2005)
10°N, 15°W 15°N, 45°W	-	[g]Blocks of mountains	Linear morphology (T3/February 2005)
0°N, 180°W 10°S, 145°W	-	[h]Joints and/or faults	Rectangular drainage classification (T13/ April 2006-T44/May 2008)
2°S, 127°W	-	[b]Ridges	Parallel formations (T43/May 2008)

5°-12.5°S, 63°-67°W	-	[b,g,i]Curvilinear mountains / Ridges	Linear-like traces (T8/October 2005)
10°S, 210°W	-	[j]Mountainous region	(T9/December 2005-T13/April 2006)
10°S, 140°W	Western Xanadu flows	[c,k] Flow-like feature	(T13/April 2006)
10°S-192°W	-	[m]Linear fault patterns/canyon-like formations	Linear faults (Huygens-DISR/January 2005)
10.4°S, 192.4°W	-	[l,m]Ridges	(Huygens-DISR/January 2005)
12°S, 38.5°W	Mohini Fluctus	[c]Lobate flows	(T25/February 2007-T28/March 2007)
14.5°S, 40.5°W	Doom Mons	[c]Volcanic-like peak	Topographic high, mountain-like structure (T25/February 2007-T28/March 2007)
14.5°S, 40°W	Sotra Patera	[c]Deep pit	Ovoid caldera/pit (T25/February 2007-T28/March 2007)
15°S, 100°W	-	[n]Lithospheric fault-blocks	(model)
15°S, 155°W	-	[o]Conjugate-like faults	Trending lineaments (T0/July 2004-TA/October 2004-TB/December 2004)
20°S, 130°W	Tui Regio	[c,p]Flow-like region	Trending dark linear marks on VIMS data (TA/October 2004-TB/December 2004)
26°S, 78°W	Hotei Regio	[c,q]Volcanic-like terrain Radial fault system	Circular tectonic features (T47/November 2008)
30°S, 107°W	-	[b]Mountains	(T43/May 2008)
30°S, 315°W	-	[r]Mountain ranges	Lineaments with tectonic control (T20/October 2006)
40°S, 340°W	-	[s]Hills	(T7/September 2005)

In Figure 4.34, I present a map that includes both the tide-induced deformational (Fig. 4.33) and surface geological information. On this map we see the morphotectonic and cryovolcanic candidate features of Titan, which are the current, identified major types of tectonic-like features and their distribution on the surface. These are the elevated features such as mountains (green), faults and fractures (blue), and the candidate cryovolcanic features (red). The map of morphotectonics in the updated version of the map presented in Figure 8 in Solomonidou et al. 2013a). On this updated map we overplotted the tidal stress pattern shown in Fig. 4.33c, which is the result of the superposition of the amplitude patterns of areal (Fig. 4.33a) and shear stresses (Fig. 4.33b). This map reveals the correlation features that are possible tectonic and/or volcanic in origin and zones of intense tide-induced surface deformation.

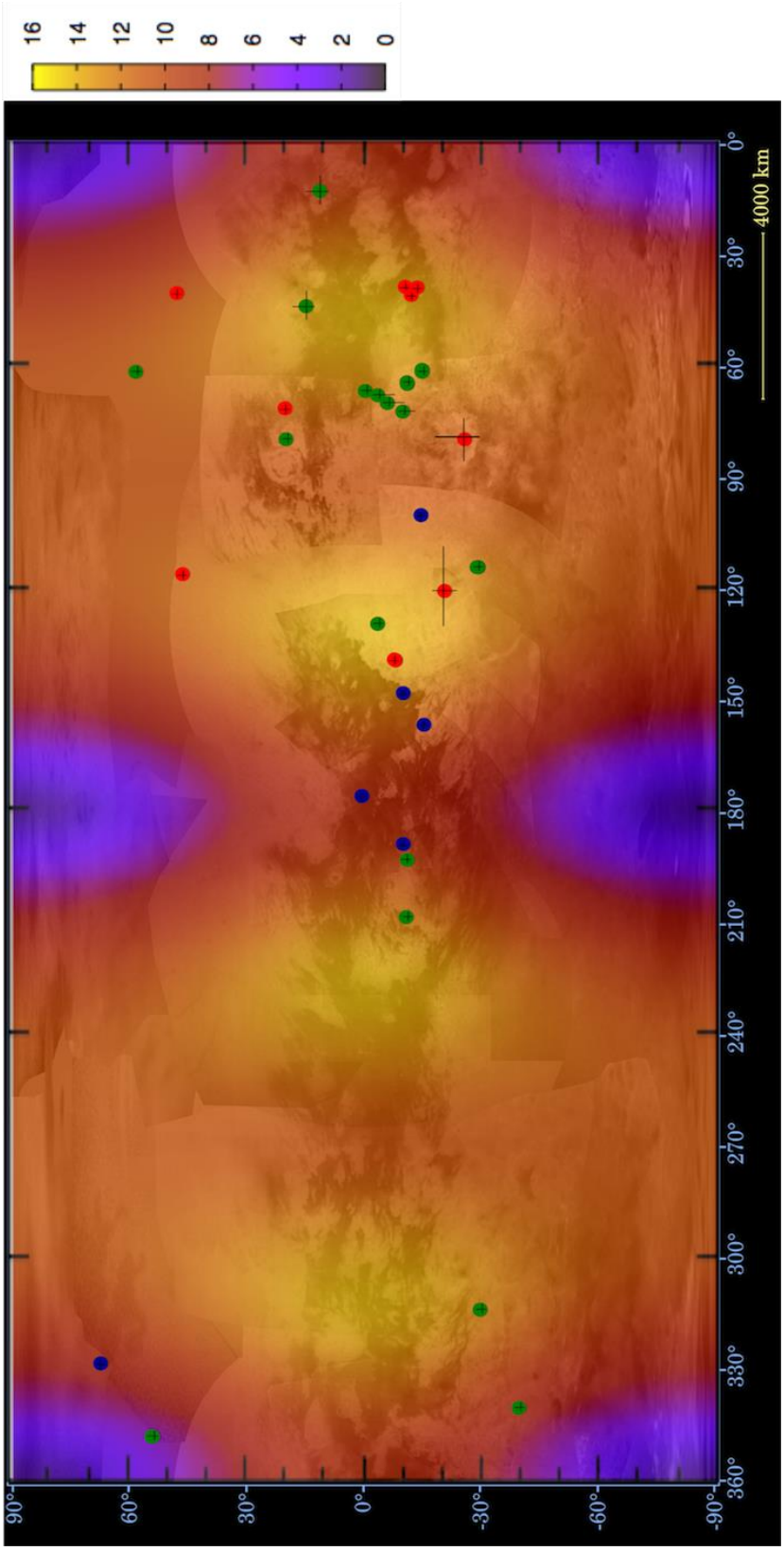

Fig. 4.34 - Global amplitude pattern of maximum tidal stress color-coded in units of kPa (from Fig. 4.33c), overplotted onto a base map (ISS mosaic –PIA14908 background map credit: NASA/JPL- Caltech/Space Science Institute) of Titan's surface with symbols indicating the current candidate cryovolcanic and morphotectonic features. Mountains and ridges (green), linear features such as faults and fractures (blue), candidate cryovolcanic features (red), the black crosses indicate roughly the extension of the features.

In conclusion, the model presented in Fig. 4.33c yield the most amplified zones in terms of tidal flexure stress accumulation, indicating zones of potentially high internal influence (Fig. 4.34). These are four mid-latitude zones (50ºS – 50ºN) centered at 40º, 120º, 230º and 310º west longitude. The map in Fig. 4.34 shows that most of the morphotectonic and cryovolcanic sites (Table 4.6) are located within the strongly tidally flexed zones. Indeed, the mountains (with some exceptions in the high northern latitudes around 60ºN) and the cryovolcanic candidates appear to be in the 'strong' zones, while exceptions mainly concern the faults. Notably, the cryovolcanic sites are concentrated in strongly tidally flexed zones as follows: Sotra Patera is located in the centre of the 1st zone (40º), reinforcing its status as the most favorable candidate cryovolcanic region (Lopes et al., 2013; Solomonidou et al. 2013c); Tui Regio is located within the limits of the 2nd zone (120º); and Hotei Regio is located on the border between these two zones of amplified tidal distortion.

It appears for Titan's leading hemisphere the two zones of maximum tidal stress are correlated with the distribution of possibly active regions (Solomonidou et al. 2013a). As mentioned in §4.1.2 Titan's should have a significant resurfacing rate and the apparent absence of cryovolcanic candidate features in the trailing hemisphere could be due to resurfacing processes that cover the areas (Langhans et al. 2012). Furthermore, such absence could be possible caused by the current observational bias toward the leading hemisphere, as indicated in the recent multispectral map of Cassini VIMS and RADAR/SARtopo and altimetry data (Lorenz et al. 2013) on extrapolation from the still relatively scarce data basis with several large gaps to be filled by future Cassini observa- tions. Additionally, a recent study on the possible stresses of Titan ice suggest that a porous ice crust soaked with liquids and combined with the low time rate of change of tide-induced surface deformation would help form zones of weakness near strongly tidally flexed areas that are conducive to episodic cryovolcanic activity (Litwin et al. 2012).

4.4 Geological Implications and connection to terrestrial mechanisms

In addition to two studies I previously conducted (one as principal author and one as co-author), I present, in this chapter, an overview of Titan's major surface features and interior models focusing on, (i) the tectonic and volcanic-like features and their possible origin, and (ii) their correlation with Titan's tidally flexed zones. I summarize in this section the results and try to address some implications regarding the genesis of these features in reference to terrestrial mechanisms.

As evidenced for instance by the recent albedo changes, observed in the Sotra Patera region and Tui Regio (see Chapter 7), and the extensive surface changes, that span more than 500,000 km^2 in the wake of a seasonal storm (Turtle et al. 2011b), Titan appears to be a dynamic satellite, in our present day.

We have argued that the morphotectonic and cryovolcanic candidate structures (concentrated in mid-latitudes between 30°S and 30°N), that are presented here, are related to surface stress fields, in analogy with terrestrial morphotectonic structures that originate through some form of compressional and extensional tectonic activity. Despite alternative theories that propose an exogenic origin (e.g. Moore and Pappalardo, 2011), the correlation between the tidal stress patterns illustrated in Fig. 4.34, with the morphotectonic features on Titan, may suggest an early endogenic origin of the latter. As aforementioned, two near-equatorial zones of strong tidal flexure and stress accumulation are present on the leading hemisphere, where the features of interest are present.

Therefore, Titan's rigid crust, the correlation of tidal distortion with the observed surface features and the probable existence of a subsurface ocean, create an analogy with terrestrial, at least surficial, plate tectonics. However, one should initially examine which factors control tectonism on a solar body before making such a comparison. Essential parameters are the stress mechanisms that may affect a Solar system body, which can be considered as global and/or local. Global stress mechanisms include tides, non-synchronous planetary rotation, polar wander, despinning, orbital recession and decay. The large density contrast between ice-I and water (Collins et al. 2009), is another array of mechanism that can cause volume change of a solar body. The crust of a Solar system body could react in a brittle, ductile or more rarely elastic fashion, producing corresponding landforms when are under the influence of global, regional or local stresses.

Another important factor is the mechanical properties of the material (icy or silicate) on which such stresses are applied (see Table 4.4, §4.2.2.1). It appears that ice and silicates

mainly share a similar crystal structure, with differences in melting temperature; when ice involves water and methane, an additional similarity with the silicates exists in the presence of the three physical stages of material.

Earth and Titan share all the global stress mechanisms and sources of internal heat such as radiogenic decay, heating by applied tidal forces and primordial heat. However, since Earth has preserved a capital of its primordial heat, we can assume that the analogy stops here. Earth's outer core, with a thickness of 2,890-5,150 km, has a temperature ranging between 4,400-6,100 °C, while the total heat flux from the interior ranges between 0.08-0.4 Wm^{-2} (Pollack et al. 1993; Davies and Davies, 2010). Moreover, thermal runaways escape from the core-mantle boundary in the form of hot spots, generating the phenomena of mantle convection and plate motion which follows the breaking of supercontinents (Pangea) or on a smaller scale, the breaking of continents (Africa).

On the other hand, Titan's primordial heat flux from the satellite's interior, ranges in the order of 0.02-0.06 Wm^{-2} and it is proposed by Mitri et al. (2010) that it can result in crustal fold processes and mountain building. Indeed, thermal stresses are responsible for updoming, weakening and subsequent fracturing the crust of a planetary body. On Earth, such a paradigm can be found in the continent of Africa, where hot spot activity has resulted in updoming, fracturing and volcanism (East African Rift, Ahaggar Mountains[24], Table 4. 7). On Titan, zones of tectonic weakness could form in an analogous manner, i.e. as a consequence of thermal stresses and weakening of the crust with subsequent formation of open fissures, which act as pathways for the ejection of material from the interior (cryovolcanism), something that has already been proposed for Enceladus and Europa (Manga and Wang, 2007). Moreover, there are two scenarios, focusing on the internal structure of Titan and the propagation of thermal convection (Mitri and Showman, 2008): (i) a thin ice with a low viscosity base and (ii) a thick ice with a high viscosity base; both are of significant importance since oscillations in the thermal state of the ice-I shell may cause repeated episodes of extensional and compressional tectonism and explain the presence of all aforementioned features. Similarly, on Earth, expansion and contraction processes are possibly due to internal thermal runaway cycles and can be important in controlling geotectonic mechanisms, as mentioned previously for Africa (Rice and Fairbridge, 1975; Fowler, 1986; Baumgardner,

[24]Most of the figures of terrestrial analogues mentioned in this Chapter in addition to many more can be found in Chapter 10 where I make the case for icy moons' comparative planetalogy.

1994; 2003; Benn et al. 2006), something suggested by a current widely accepted internal evolution model.

Following up the correlation between terrestrial formation mechanisms with the ones that possibly exist on Titan, Table 4.7 summarizes these implications and assigns observations to proposed mechanisms.

Table 4.7 - Proposed mechanisms for the formation of mountains and ridges of Titan.

Proposed mechanism	**Description**	**Observations**
Lithospheric shortening (Mitri et al. 2010)	Folding of the upper crust due to past high heat flux from the interior and high temperature gradients in the ice shell	Curvilinear mountains/Ridges T8, T30, T43
Tectonic stresses of the ice shell (Mitri and Showman, 2008)	Transitions of the ice shell over a liquid subsurface ocean, from a conductive state to a convective state, causes tectonic stresses and movements that influence the surface	(model)
Crustal compression/upthrust blocks (Radebaugh et al. 2007-scenario 1)	Localized compression due to thickening of the crust linked with the cooling of Titan at areas where fault structures exist	Linear mountains T8, T3 (15°N, 45°W)
Crustal stresses/upwelling of material (Sotin et al. 2007)	Generation of extensive stresses that penetrate the icy shell and create pathways for the internal material	High-standing mountain ranges T20
Crustal extension (Radebaugh et al. 2007-scenario 2)	Recent crustal thickening due to localized extension	Blocks and grabens T8
Blocks of impact ejecta (Radebaugh et al. 2007-scenario 3)	Deposition of ejecta blocks around craters in a radial manner	Blocks of mountains T3
Dissection and erosion (Radebaugh et al. 2007-scenario 4); Lunine et al. 2008)	Erosion and incision of terrains that form regional uplifted structures	Mountainous region T13

For example, for the linear mountains in T3 and T8 swath, which could have formed from localized compression and crustal thickening, the Laramide Orogeny is considered an analogue, since this mountain formation is attributed to compressive forces, conductive heating and crustal thickening (Dickinson and Snyder, 1978). In addition, for the T30 and T43 mountain observations, where folding of the upper crust, due to high heat flow from the interior, and high temperature gradients in the past is probably involved, the Rocky Mountains chain in Western-North America (see Fig. 10.10, Chapter 10) is considered an analogue, as it was formed over a high of mantle heat flow (Bird, 1998). Many more analogies can be found in Chapter 10.

In conclusion, identifying tectonism on Titan can provide significant insights on its internal structure. In reference to the terrestrial paradigm, where rigid lithospheric plates 'float' on a weaker asthenosphere, indirect evidence for the existence of a subsurface ocean on Titan can probably be provided. The importance of identifying morphotectonic and cryovolcanic features on Titan, which can be linked to tectonism and cryovolcanism respectively, can also be affective in decoding the methane cycle on Titan in analogy with the link between terrestrial tectonics and the global terrestrial carbon cycle (Bolin, 1981; Ruddiman, 1997). That is, Titan's tectonic and volcanic activity can probably be directly related to the replenishment of the atmosphere with methane (Sotin et al. 2005; Tobie et al. 2006; Coustenis and Taylor, 2008; Lunine and Atreya, 2008; Mitri et al. 2008). Finally, the origin of some morphological features can be attributed to exogenous processes (Porco et al. 2005; Stofan et al. 2006; Tomasko et al. 2005; Radebaugh et al. 2009; Moore and Pappalardo, 2011; Tokano, 2011). The amplitude pattern of diurnal tidal stresses though, correlates well with regions historically known as cryovolcanic (in addition to the outcome of my recent work that I present in Chapter 7), as well as features suggested by studies to be tectonic in origin.

Chapter 5

Analysis tools

This chapter introduces the fundamentals of the radiative transfer theory and the supplementary tools I used to retrieve the surface albedo of the Titan areas I am interested in. First, I present a statistical method, the Principal Component Analysis, which reduces the dimensionality of datasets with multiple variables, like the VIMS ones. Then, I introduce the 'atmospheric subtraction' method, which I used in a preliminary stage of my studies in order to obtain relatively clear surface images without the interference of the atmospheric contribution. The application and preliminary results of the PCA analysis and the 'atmospheric subtraction' are presented in the publication in the *Hellenic Journal of Geosciences* (Solomonidou et al. 2010) as well as in the proceedings of the *International Planetary Probe Workshop* in 2010. I should note that PCA has previously been applied to some planetary objects like Ganymede (Stephan et al. 2008) but never to Titan spectro-imaging data. I continue, with the description of a radiative transfer code, which was developed by my French colleague Mathieu Hirtzig (Hirtzig et al. 2013) and my supervisor Athena Coustenis. This code is the main tool I used for my studies, due to the necessity to evaluate the atmospheric contribution and to better constrain the real surface properties. In conclusion, I describe the properties and function of a filtering technique developed by my Greek colleague Emmanuel Bratsolis that we used in order to remove the speckle noise from RADAR data and infer some implications on the nature of the regions of interest (Bratsolis et al. 2012). In the course of my PhD studies, I have presented the applications of the aforementioned tools to Cassini VIMS and RADAR data for Titan in a number of international conferences as oral or poster presentations such as COSPAR, DPS, IAU, EGU and more.

5.1 The Principal Component Analysis (PCA)

The VIMS datacubes – as described in detail in Chapter 2 – are multivariable datasets consisting of 352 spectels (64x64x352 datapoints). In such cases, when large multivariate datasets are analyzed, usually the analysis is optimized by reducing the datasets' dimensionality. The Principal Component Analysis (PCA) is considered to be one such reduction technique. Briefly, it replaces the original variables with a smaller number of derived variables, called the principal components (PCs). These are linear combinations of the original variables and appear to retain most of the statistical variability present in the original variables. This technique can be functional for simple uses to very complex ones with many extensions (Jolliffe, 2005).

The PCA is well adapted to our study, as our primary concern is to determine the minimum number of factors that will account for the maximum variance of the data we use in this particular multivariate analysis. As mentioned, the main goal of PCA is to retain as much as possible of the variation present in the data set, highlighting the foremost information in all images. This is achieved by transforming the data into a new set of variables, the PCs which are uncorrelated, and which are ordered so that the first few retain most of the variation present in all of the original variables. On the resulting false-color image we produce from a selection of low-order PCs, we then isolate regions of different coloring, underlining different variabilities. The method is applied to VIMS radiometrically calibrated images. For the purpose of our research we use the ENvironment for Visualizing Images (ENVI[25]) software.

5.1.1 PCA background mathematics and application on Cassini/VIMS

The Principal component analysis (PCA) method is a mathematical/statistical procedure that uses an orthogonal transformation to convert a set of correlated observations into a new set of uncorrelated components. The number of PCs is less than or equal to the number of original variables. In the case of Cassini/VIMS analysis they are always equal. It is sorted so that the first principal component always includes the largest possible variance (Fig. 5.1). Furthermore, the PCs are guaranteed to be independent if the data set is normally distributed.

[25] *http://www.exelisvis.com/ProductsServices/ENVI/ENVI.aspx*

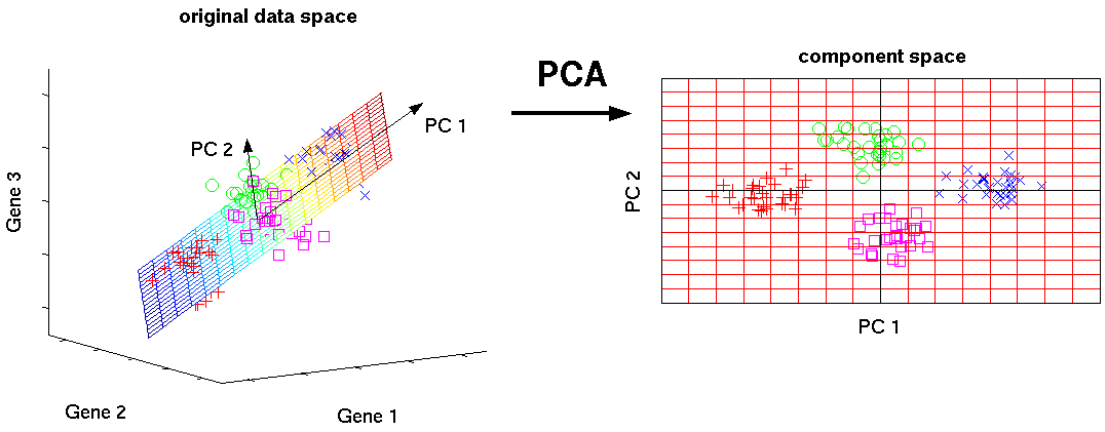

Fig. 5.1 – The Principal Component (PCs) transformation. The figure illustrates 3-D gene expression data located with 2-D subspace. With PCA the reduction of the dimensionality of the dataset occurs through the accumulation of the information hidden in the datasets into the first PCs. (left) PC#1 and PC#2 describe the highest variance of the data. (right) Representation of the 2-D component space (Image and information credit: Matthias Scholz).

5.1.1.1 Principal Components (PCs)

With the PCA a new coordinated system is obtained that maximizes the variance of data from the VIMS data containing a large number of spectral channels, (e.g. Richards, 1994). This can be achieved by concentrating in the PCs fewer spectral parameters from the relevant VIMS image information. The latter is concentrated in the first PC (PC#1). However, the content of the PC images strongly depends on the original information of the input data (Singh and Harrison, 1985; Gillespie, 1980). Thus, in a perspective analysis of VIMS data with PCA, the PC#1 contains the 'dominant' feature as seen in VIMS, by frequency of appearance from the 352 spectro-images (96 visible and 256 IR) or their selection depending on the kind of research (Jolliffe, 1986, 2002, 2005; Smith, 2002; Stephan et al. 2008; Abdi and Williams, 2010). Here, we use a series of VIMS infrared images (96 in total). Indeed, the VIMS datacube is made by VIMS-Visual and VIMS-IR channels that do not have coincident fields of view and viewing geometry; and the use of both could easily mislead the analysis. In order to avoid this, we are using only the VIMS-IR channels, as suggested by the reviewer, for all the datacubes in use in this analysis. Hence, we are using the bands 97 to 352 that correspond only to the infrared observations.

5.1.1.2 Selecting the appropriate PCs from the datacube

In order to extract and select in the final retransformed PCA image the PCs with significant spectro-imaging information the following issues should be taken into account: (a)

the significance of their eigenvalues (EV_j); (b) the spatial variations in the PC image itself as well as; (c) the content of spectral information in the corresponding eigenvectors (E_j) (Stephan et al. 2008).

Eigenvalues

The eigenvalues are a special set of scalars associated with a linear system of equations (i.e. a matrix equation) that are sometimes also known as characteristic roots, characteristic values (Hoffman and Kunze, 1971), proper values, or latent roots (Marcus and Minc, 1988). Eigenvalues are closely related to eigenvectors. Figure 5.2 shows a plot of eigenvalues from the Tui Regio datacube (No 4, Table 3.3). The slope presents a flattening that is often used as a criterion for the selection of PCs (e.g. Jöreskog et al. 1976; Stephan et al. 2008).

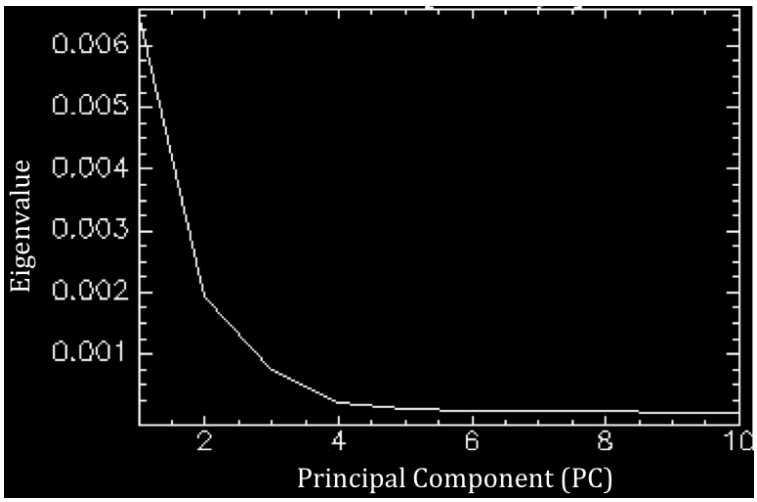

Fig. 5.2 - Eigenvalues plot for Tui Regio datacube NoX. The variability is accounted most for the 1st while PC2, 3, 4 are also significant statistically to our work. After that, the flatenning indicates the absence of variability in the PCs.

Eigenvectors and PC images

The eigenvectors (EV) are a special set of vectors associated with a linear system of equations that are sometimes also known as characteristic vectors, proper vectors, or latent vectors (Marcus and Minc, 1988). In this analysis the EV provide information on the spectral behavior of each PC. Thus, it enables us to distinguish between atmospheric and surface information and use the PCs that only or at least largely correspond to the surface. Figure 5.3 shows the eigenvectors extracted from Tui Regio's datacube. It appears that PC#1 does not reflect the spectrum of the surface since it misses any spectral response at 3 and 5 μm where the methane windows are centered. However, PCs #2,3,4 do, followed by PCs #5,6,7 where the spectrum is very noisy out of the windows. I should note here that the eigenvalues

hereabove have shown that the 1st PC contains significant information that is present in the datacube indicating that another parameter other than surface information is dominant in the datacube. The PC images should clarify the nature of PC#1. Moreover, PC#2 shows a distinct surface spectral behavior.

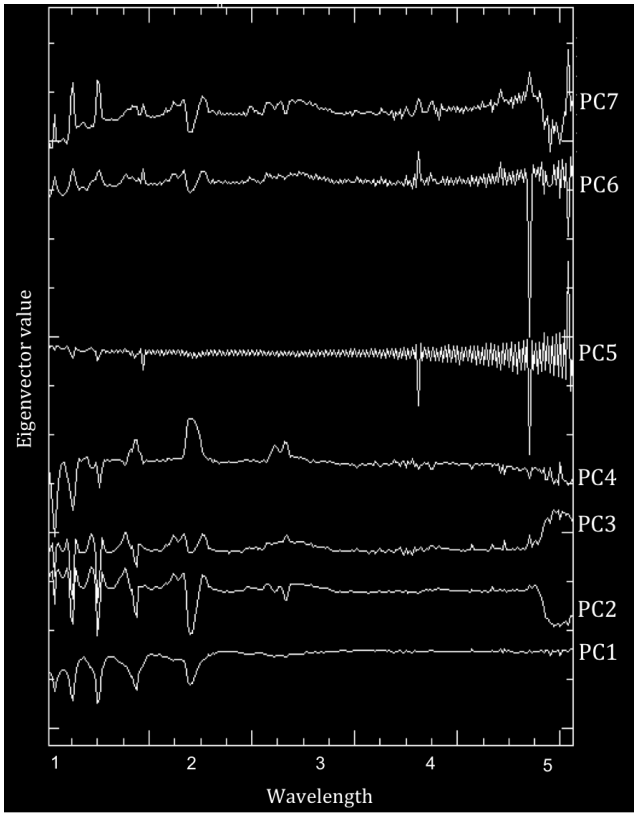

Fig. 5.3 - Calculated eigenvectors from the Tui Regio datacube. It appears that only PCs #2,3,4 are compatible with surface spectra.

Following the examination of the eigenvectors, I have used ENVI to retrieve the images of each PC and validate their nature. This step is very important since the correlation between EV and PC images shows if the PC images with a relative high EV shows spatial variations that are related to surface features or if PC images with a low EV are fully dominated by a distinct noise pattern (Stephan et al. 2008).

Figure 5.4 shows a series of the seven first PCs, where the first few, as mentioned earlier, retain most of the data variability present in all of the original variables.

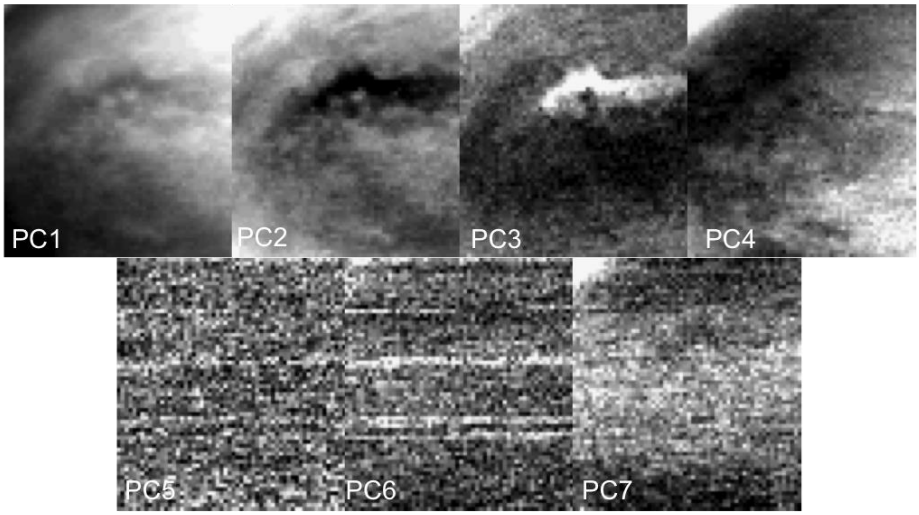

Figure 5.4 - The seven first 'Principal Components' (PCs) for the Tui Regio dataset. The first principal component (PC#1) presents the largest possible variance. At this datacube as seen in Fig. 5.2 the information concerning the variability of the dataset is present up to PC#4.

To describe what each PC represents, in the particular case of Tui Regio, we can say that PC #1 mainly reflects the atmosphere that lay over the area of Tui Regio and seem to be present more than any other feature. Nevertheless, such evidence enhance the need for a tool to evaluate and 'remove' the atmosphere (see sections hereafter). PC #2 indicates that frequently Titan shows dark surface features, while PC #3 shows that quite often, Titan's surface features are bright (for this dataset, PC #3 displays Tui Regio as particularly bright). PC #4 projection indicates that Titan's surface features are dark rather infrequently with a limb-darkening. Lastly, PC #5,6 and #7 show that the following PCs in this particular cube contain only noise. Thus, for Tui Regio, we will thereafter use only RGB composites of the three main principal components related only to the surface (which are here # 2,3,4, since PC#1 refers mainly to the atmosphere) (Fig. 6.13, Chapter 6).

Fig. 5.6 shows the images of the PCs for the Sotra Patera case, which is an example of a datacube where the 1st PC corresponds to the surface. This can be confirmed also by the eigenvectors as shown in Fig. 6.12 and the result PCA image in Fig. 6.13 in Chapter 6.

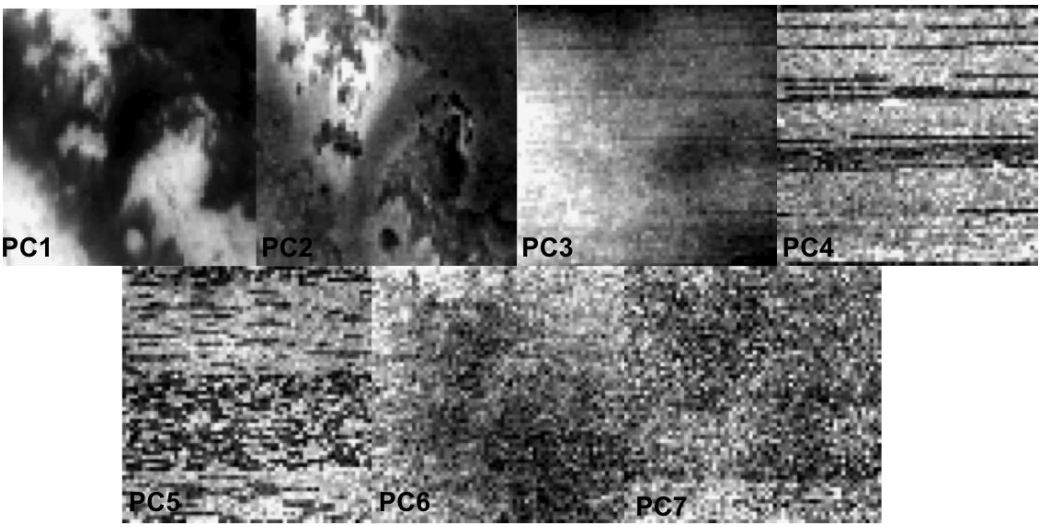

Fig. 5.5 - Same as for Fig. 5.4 but for Sotra Patera. PC#1,2,3 reflect the surface.

PCA images

For any given VIMS datacube there should be a specific selection of PCs based on their eigenvalues and images, as well as, on the information adapted from the eigenvalues. Hence, for Tui Regio's example by following this process we derive the PCA image seen in Fig. 5.6. We have used adequate colors for our type of analysis in order to illustrate the distinct spectral units, with the aim to color the actual Tui Regio, Hotei Regio and Sotra Patera features as red within the datacubes. Hence, knowing that the areas are particularly bright (anomalously at 5 μm) from previous studies (e.g. Barnes et al. 2006; McCord et al. 2008; Soderblom et al. 2009) we label the red spectral unit as 'brightest' and the green (at this particular datacube) as 'darkest'.

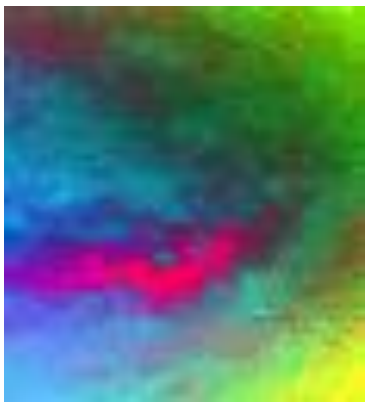
Fig. 5.6 – PCA image of Tui Regio using PCs#3,2,4 (Solomonidou et al. 2013b).

An additional advantage of PCA, other than identifying, and partially exploiting the atmospheric PCs (Fig. 5.4), is the ability to distinguish any clouds present in the data, which would appear in a separate RoI, distinct from surface features, due to their very specific spectral signatures.

5.1.1.3 Test case

By using the PCA method we aim at creating units of color heterogeneity that each correspond to units of diverse spectral response in all of our three study areas. Le Mouélic et al. (2008) studied the Sinlap crater on Titan –one of the few impact craters observed on Titan and through the use of band ratios they identified several units in the VIMS false color composites that indicate compositional heterogeneities. These units correspond to specific coloring as follows: the bright ring corresponds to the ejecta blanket, the blue and dark blue area is probably enriched with water ice (Rodriguez et al. 2006) compared to the surroundings, and the brownish area corresponds to dune fields (Soderblom et al. 2007a, 2007b; Barnes et al. 2008; Rodriguez et al. 2013) (Fig. 5.7). Such a classification led to three compositionally and geologically different types of surface regions. Applying the PCA technique in the exact same VIMS cube, we arrive at the same result of three distinct regions as seen in Figure 5.8 within the same regional boundaries. We thus have a confirmation that our principal component application works properly (Solomonidou et al. 2013b).

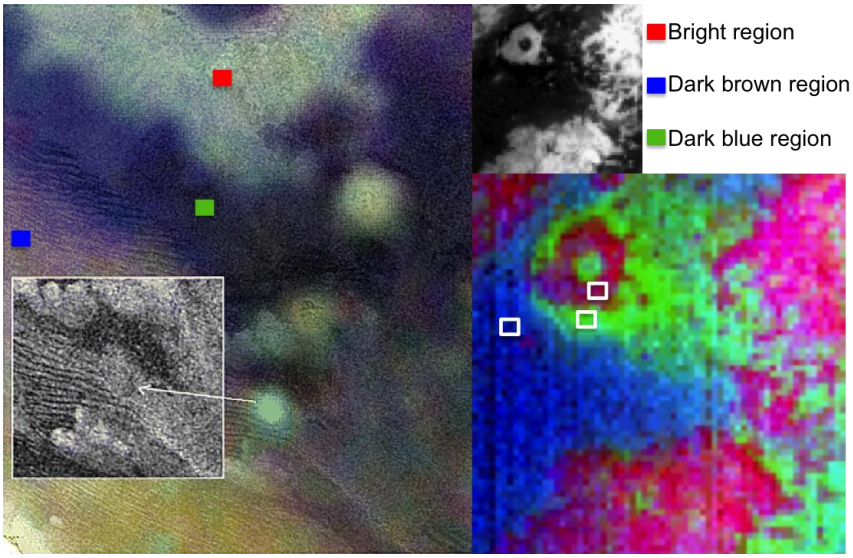

Fig. 5.7 - (left) On this RADAR/VIMS combined pan-sharpening image of the Sinlap crater region, from T3 SAR image and T13 VIMS cube CM_1525118253 taken at 2.03 μm (upper right), Le Mouélic et al. (2008) found spectral diversity between three regions. These authors used the band ratio technique in the VIMS RGB composites in this order: R=1.59/1.27 μm; G=2.03/1.27 μm; B=1.27/1.08 μm (left). Such a diversity is confirmed with our PCA which isolates 3 RoIs (lower right) that match the Le Mouélic et al. (2008) inferences. Following the coloring of this PCA image, the red rectangle in the left-sided image corresponds to bright region, blue to dark brown, and green to dark blue as characterized by Le Mouélic et al. (2008) (Image credit: Solomonidou et al. 2013b).

5.1.1.4 Application on icy moons data

The Principal Component analysis method has been applied another icy moon spectral study in the past by Stephan et al. 2008. In this study, the PCA was mainly used for the improvement of quality of the spectro-imaging data through the removal of noise and instrument artifact. This was also an outcome of our PCA analysis, since we were able to remove the noise (PCs#5,6 and 7) detect any present clouds. Stephan et al. (2008) studied Ganymede with the use of Galileo/NIMS data (0.7-5.2 μm). The PCA method was used in NIMS data in order to improve the signal-to-noise ratio (SNR), which accounts as an important parameters for mapping spectral properties as the wavelength position and band depth depends on that. The higher the SNR, the better the quality of the data. The improvement of SNR can be achieved by averaging the spectra, and PCA can be applied as to that matter without diminishing the amount of spectral information. The application of the method produced higher spectral data notably after the 3 μm. Such improvement is essential for mapping and spectral studies in terms of chemical composition analysis and surface properties.

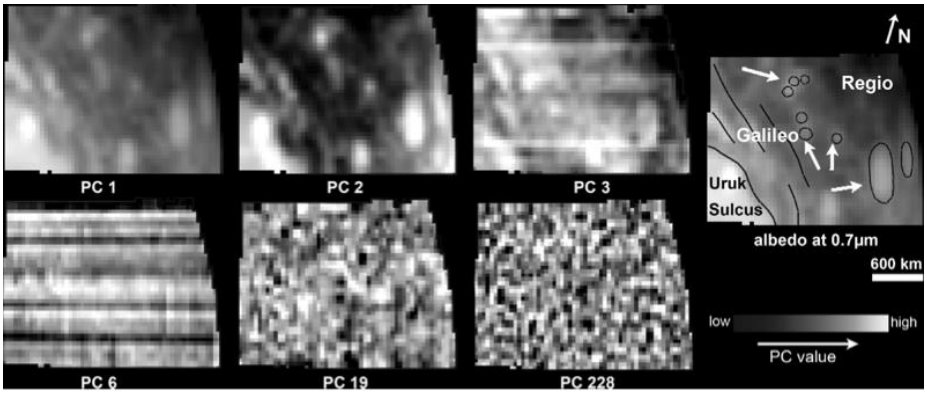

Fig. 5.8 – PC images from NIMS datacubes. On the right of the image an albedo map with the main geological features of the datacube area is shown (Image credit: Stephan et al. 2008).

5.2 The ‘atmospheric subtraction’ method

In order to understand Titan's geology and evolution, it is critical to investigate and identify the chemical composition of the areas of interest. As mentioned before in this manuscript, Cassini/VIMS acquire many spectral images from several flybys useful for chemical composition analysis and many of those images are taken within the so-called “methane windows” (centered at 0.93, 1.08, 1.27, 1.59, 2.03, 2.69-2.79 and 5.00 μm), where the methane absorption is weak, and therefore captured details of the surface. However, the fact that Titan possesses an extended, hazy, and dense atmosphere needs to be taken into account and its contribution (haze scattering, aerosol absorption, cloud opacity, etc) removed before accurate results on surface composition can be retrieved.

Our goal is to obtain relatively clear surface images without much of the interference of the atmospheric contribution. Thus, we have used an empirical method to correct the atmospheric effects and photometric analysis that decrease the constraint factor on the surface chemical composition.

The applied method of ‘atmospheric subtraction’ is based on simple mathematical models and has been tested in previous Titan studies (e.g. Coustenis et al. 2001; 2005). In detail, a VIMS spectrum of Titan is a measurement of I/F (Fig. 5.9), whose dependence on the surface true albedo A is roughly modulated by the atmospheric absorption a and aerosols’ diffusion d. It depends also on the wavelength λ, the latitude θ, the longitude φ, the incident angle i, the emergent angle e, the phase angle i_{ph}, and the time t (for seasonal/diurnal changes), as in Eq. 1.

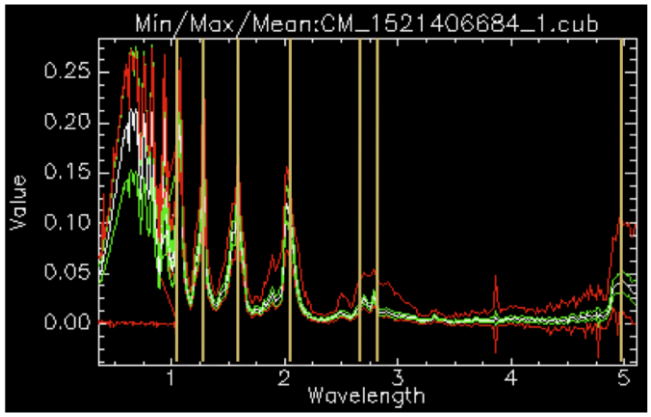

Fig. 5.9 – Titan’s Tui Regio full spectrum from VIMS (datacube #3, Table 3.4, Chapter 3). The vertical yellow lines indicate the seven methane windows.

Instead of the geometric albedo, the contrast analysis can reduce such dependencies, given a few sensible conditions: when two regions from the same hyperspectral image are close to each other (ideally within 60° of the nadir, and with observation parameters no more

different than 10-20°), the contrast can be simplified as in Eq. 2, dependent on 6 parameters instead of 12. The only model-dependent parameter to remain is the additive contribution by the aerosols *d*, which we have extracted from Khare et al. (1993):

$$(1) \qquad C_{1.2}(\lambda,t)=\frac{s_1(\lambda,\theta_1,\varphi_1,i_{i1},i_{e1},i_{ph1},t)}{s_2(\lambda,\theta_2,\varphi_2,i_{i2},i_{e2},i_{ph2},t)}\approx\frac{A_1(\lambda,\theta_1,\varphi_1)+\delta(\lambda,t)}{A_2(\lambda,\theta_2,\varphi_2)+\delta(\lambda,t)}$$

$$(2) \qquad s(\lambda,\theta,\varphi,i_i,i_e,i_{ph},t)=\alpha(\lambda,\theta,\varphi,i_i,i_e,i_{ph},t)\times\left[A(\lambda,\theta,\varphi)+\delta(\lambda,\theta,\varphi,i_i,i_e,i_{ph},t)\right]$$

Since the contrast analysis is still model-dependent (relying here on Khare's haze model), a different approach, simpler, focuses on subtractions instead of ratios. The underlying idea here is given by the simple equation

(surface + atmos) - surface = atmos

where *surface* (centre of spectral window) corresponds to the surface component, and *atmos* (wing of spectral window) to the atmospheric component (Fig. 5.10).

$$(3) \qquad \Delta I/F = (I/F)\lambda_1 - f \times (I/F)\lambda_2$$

$$= \int_{\lambda 1} (\mathrm{ATMOS} + \mathrm{surface}) - f \times \int_{\lambda 2} (\mathrm{atmos} + \mathrm{SURFACE})$$

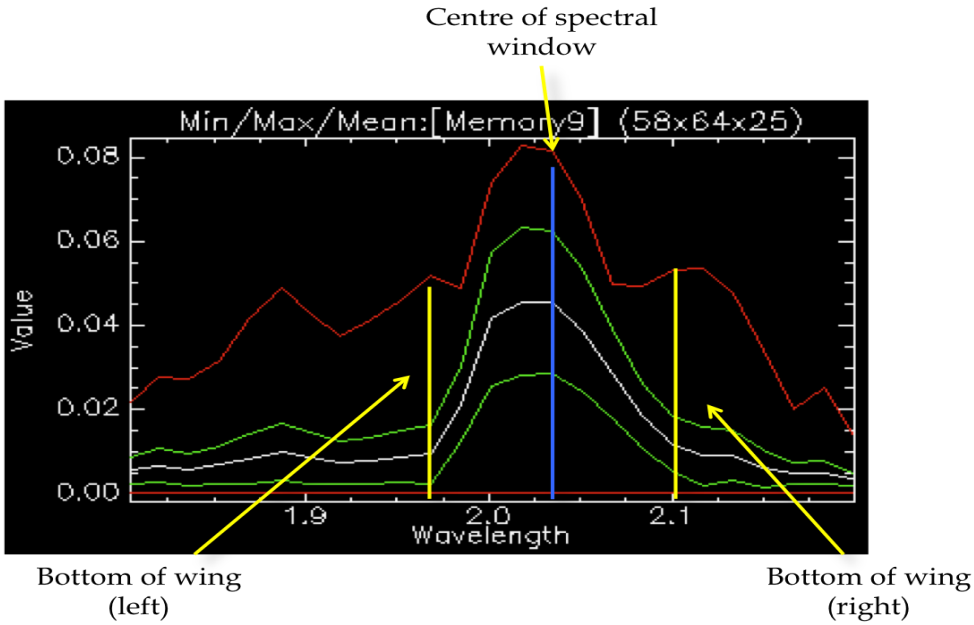

Fig. 5.10 – The centre and wing of the methane spectrum at 2.03 μm from the Tui Regio VIMS datacube.

In this specific case, we already assume that the surface and atmospheric components are independent with each other. This is false since there is a fraction of the atmospheric component that is related to photons backscattered by the surface and dispersed by the atmosphere. Here, we consider two different images, focusing either on a methane wing ($\lambda 1$, sensitive to the atmosphere) or on a methane window ($\lambda 2$, sensitive to the surface). The subtraction method aims at erasing one of the two components (surface or atmosphere) by a linear combination of the two images (our image at $\lambda 2$ is here modified by a multiplicative factor f). In the following Eq.3 and 4, for clarity, we wrote as uppercase the largest contribution at each wavelength. If we assume the integration over each bandwidth to be straightforward, we can continue the reasoning with monochromatic annotations.

$$\Delta I/F = (ATMOS_{\lambda 1} - f \times atmos_{\lambda 2}) \quad (4)$$

$$+ (surface_{\lambda 1} - f \times SURFACE_{\lambda 2})$$

The second term is assumed to be easily removed, and this is the main goal of this method. Nevertheless, from this simple formula we guess that this is not readily achievable, since, as was underlined in Kim et al. (2008), an overestimated f will lead to a negative image of the surface features. We want here to underline even more subtleties, because the behavior of the surface is probably not the same at one wavelength and at another. Indeed, the contrast is not constant. Furthermore, the limb-darkening of the surface of Titan is not proven to be the same at all wavelengths.

In conclusion, this method has managed to reduce the effect of the contribution of the atmosphere within the atmospheric methane windows (Fig. 5.11).

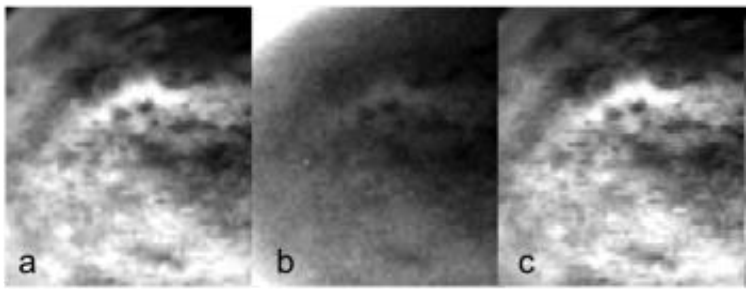

Fig. 5.11 - “Surface” (a) and “atmosphere” (b) references used to compute unaffected surface images (c).

The results from the application of this method can be found in Chapter 6 in addition to the issues and restrictions of this method and the necessity for radiative transfer simulation for the extraction of more qualitative Titan results from VIMS data.

5.3 The Radiative Transfer code

5.3.1 General

The physical phenomenon of radiative transfer concerns the energy transfer in the form of electromagnetic radiation, while the propagation of energy by radiative processes involves emission, absorption, and scattering of electromagnetic radiation (e.g. Hanel et al. 2003). The theory of radiative transfer provides the tool for determining the emergent spectrum of a planetary source either as a reflective or an emissive body, and also for describing the effects of media through which the radiation passes on its way to final detection (e.g. Gray, 1992; Mihalas, 1978). In other words, an atmospheric radiative transfer simulator estimates the processes of electromagnetic radiation through planetary atmospheres. Atmospheric emission, which at planetary temperatures occurs mainly in the thermal-infrared part of the spectrum, depends on the composition and thermal structure of the atmosphere, while reflection of the solar spectrum dominates the rest of the electromagnetic range. Absorption and scattering mainly occur at ultraviolet, visible and near-infrared wavelengths and depend on the prevailing molecular opacity and on aerosol and cloud properties.

Titan's spectrum is dominated by aerosol absorption and methane scattering in the visible and methane absorption and aerosol scattering in the near infrared (Fink and Larson, 1979), hampering the derivation of meaningful surface information. Nevertheless, the presence of the seven 'methane windows' (see more on the windows in Chapter 6) at 0.93, 1.08, 1.27, 1.59, 2.03, 2.79, and 5.00 μm in combination with a decreasing of the haze opacity with wavelength allows the penetration of the atmosphere and the probing of the lower atmosphere and of the surface. However, although the haze extinction in the whole infrared range decreases with wavelength, extracting information specifically from near-IR spectra requires a good understanding of the methane and haze contributions to the opacity.

Many attempts have been made so far to simulate Titan's atmosphere and/or retrieve the surface information through the use of radiative transfer codes (e.g. McKay et al. 1989; Griffith 1991; 2003; 2012; Thomas-Osip et al. 2005; Rannou et al. 2006; 2010; 2012). I present hereafter a new radiative transfer code (Hirtzig et al. 2013), developed by my colleague Mathieu Hirtzig from LESIA-Observatoire de Paris for which I am qualified as a user.

5.3.2 The Radiative transfer (RT) code

The code is based on the plane-parallel version of the Spherical Harmonic Discrete Ordinate Method solver (SHDOMPP; Evans, 2007). It divides the atmosphere of Titan into 70 layers, the vertical profiles of which combine pressure and temperature measurements from Huygens/HASI (Fulchignoni et al. 2005), the methane vertical profile from Huygens Gas Chromatograph Mass Spectrometer (GCMS) (Niemann et al. 2010), as well as a uniform CO mole fraction equal to 4.5×10-5 based on Cassini/CIRS measurements (de Kok et al. 2007), to reproduce the thermodynamic state and mixing ratios of the atmosphere. The opacity from methane and its isotopologues is simulated as described in Campargue et al. (2012) and Hirtzig et al. (2013) and references therein, using recent developments from laboratory measurements, theoretical calculations, and empirical models. We implemented these updated methane line lists in our modular radiative transfer model, as a set of correlated-k absorption coefficients, applied here to the P, T conditions on Titan.

Methane line parameters

Between 5854 and 7919 cm^{-1} (1.71-1.26 μm), we used the line list provided by Campargue et al. (2012) (isotopologues $^{12}CH_4$, $^{13}CH_4$ and CH_3D) from spectra recorded at 296 and 80 K using Differential Absorption Spectroscopy (DAS) in the center of the tetradecad and isocad and high-sensitivity Cavity Ring Down Spectroscopy (CRDS) in the 1.58- and 1.28-μm transparency windows.

For the region below 5854 cm^{-1} (above 1.71 μm), we calculated the line parameters for the pentad, octad and tetradecad, from a global analysis as described in Albert et al. (2009) and Boudon et al. (2006) obtaining a set of $^{12}CH_4$, $^{13}CH_4$ lines and CH_3D from modeling (Nikitin et al. 2013). These line parameters were used to calculate k-correlated coefficients for the VIMS infrared channels between 1.2797 and 5.1254 μm. No complete line list is available at wavenumbers above 7919 cm^{-1} (below 1.263 μm). For VIMS channels below 1.2797 μm, we used the methane absorption coefficients derived by Karkoschka & Tomasko (2010) from Huygens/DISR in situ measurements of methane absorption during the descent to Titan's surface.

Aerosol model

Analyzing a large set of Huygens/DISR data, Tomasko et al. (2008) proposed an aerosol model in terms of number density, extinction, phase function and single scattering albedo (w_0) as a function of altitude between 0.35 and 1.6 μm. De Bergh et al. (2012) showed that this aerosol model did not allow us to reproduce the VIMS observations near the Huygens site (10.3°S, 192.3°W) between 1.4 and 1.7 μm. A large fraction of the disagreement is due to the addition by Tomasko et al. (2008) of a backscattering peak in the phase function below 80 km, which they did not justify longward of 0.934 μm. De Bergh et al. then chose to use the same phase function below and above 80 km. We have done the same here, and used the values in Table 1a (phase function above 80 km) of Tomasko et al. (2008) to calculate the Legendre coefficients for the aerosols phase functions at all atmospheric levels from 0.8 to 5.2 μm. I have to mention here that the Legendre decomposition is a mathematical projection of the phase function of our aerosols.

As a nominal case, we used the optical depth profiles of Tomasko et al. (2008, their Table 3) both above 80 km ("haze" region) and below 80 km ("mist" region). As a free parameter, we only allowed for a single uniform multiplying factor to account for horizontal variations of aerosol opacity. Also, we determined the single scattering albedos by fitting the I/F reflectivity measured by VIMS in the core and the wings of the methane bands near the Huygens landing site ("HLS'' from now on). Up to 1.28 μm, we allowed for different values of w_0 in the haze and in the mist regions and actually used the values of Tomasko et al. (2008, their Table 2, Cols. 2-3). Beyond 1.28 μm, a single value of w_0 is used in both altitude regions. In conclusion, once w_0 is determined from VIMS data near the HLS, the only free parameter of the haze model is a uniform scaling factor for the number density, or accordingly the integrated haze optical depth.

Method and error estimation

To retrieve the surface albedo from the VIMS data at a given location, we first derived the haze optical depth from the I/F reflectivity in the methane bands (Fig. 5.12). This was done by minimizing the residuals between observations and calculations over spectral intervals that include the core and near wings of each methane band. This haze scaling factor, relative to the Tomasko et al. (2008) model, bears a typical uncertainty of ± 0.05.

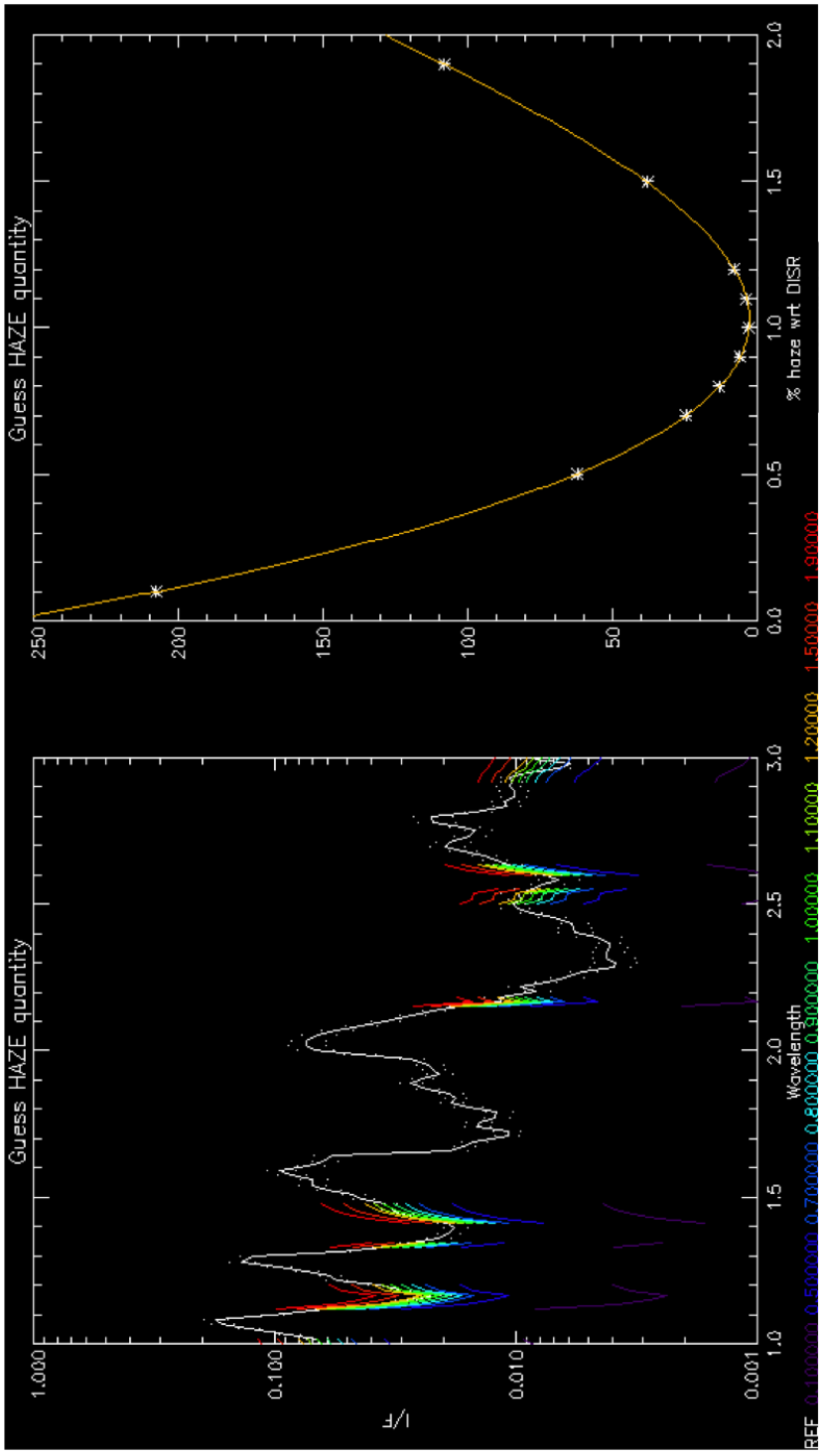

Fig. 5.12 - (left) Test simulations with various multiplicative factors (i.e. various haze populations –see colored values at the bottom of the figure). (right) Correlation between simulations (yellow line) and data (white points).

Hence, Using the aerosols model (single scattering albedo and phase function) derived from Tomasko et al. (2008) and adjusted as described in Hirtzig et al. (2013), their aerosol extinction is adjusted by shifting the DISR vertical profile used as a reference, so that we fit

the methane bands and windows deepest wings, almost completely insensitive to surface contribution.

With this best fit model, we produced three simulations with constant 0.05, 0.15, and 0.5 surface albedos, and assumed that the outgoing intensity varies linearly with surface albedo between these values (Fig. 5.13).

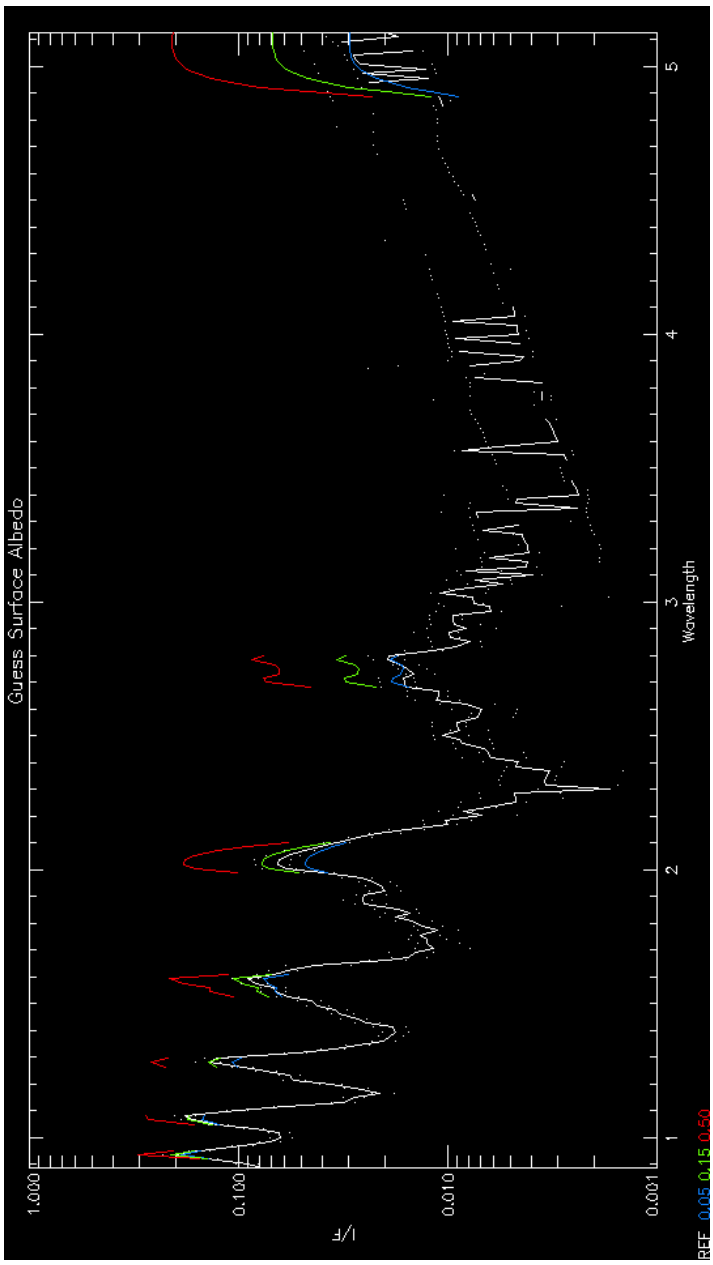

Fig. 5.13 – Three simulations with different surface albedos.

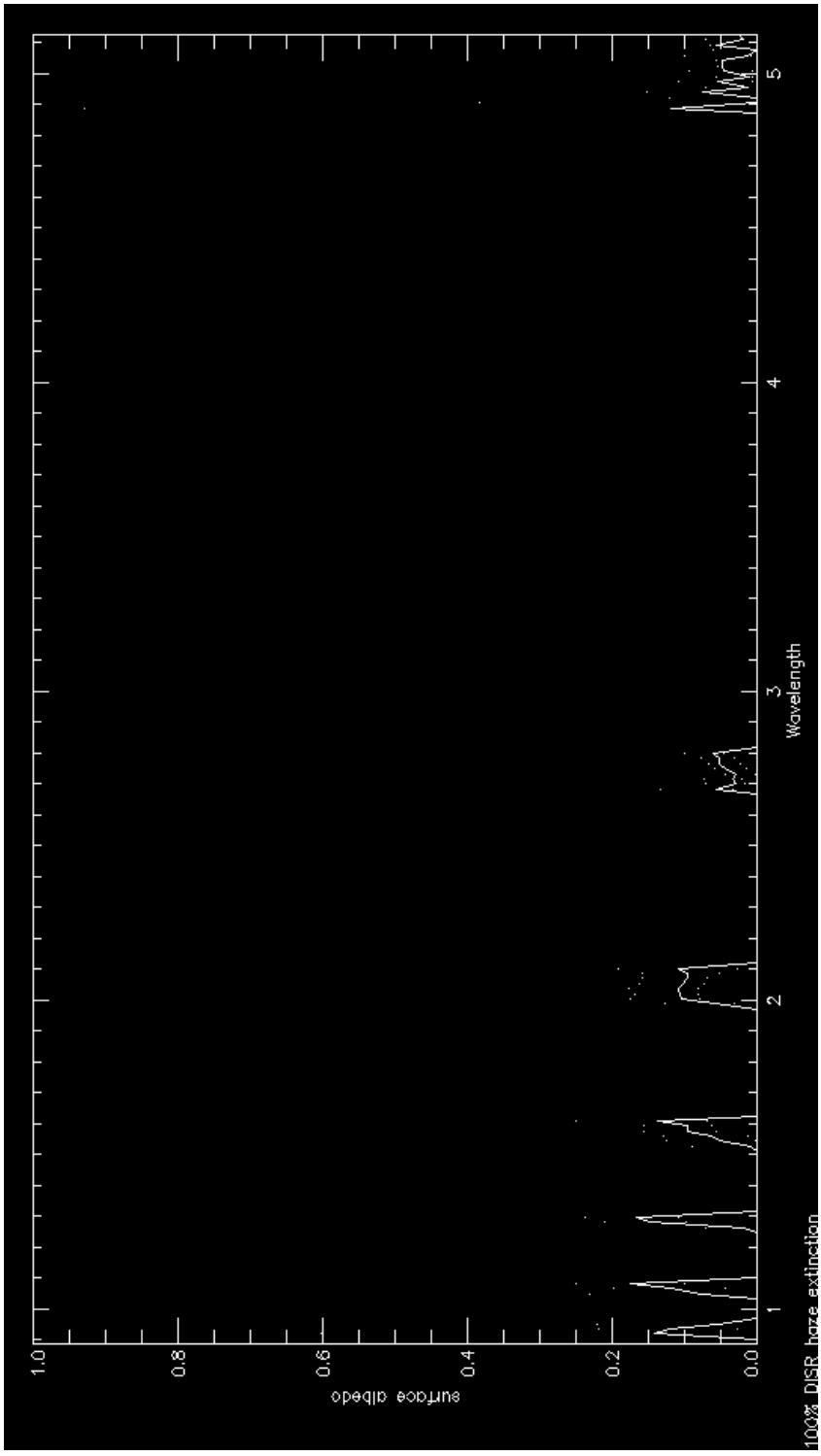

Fig. 5.14 – Retrieved surface albedo and an estimate of the total aerosol content, compared to the reference measurement by DISR, (shifted in the case of the HSL by a factor of 1).

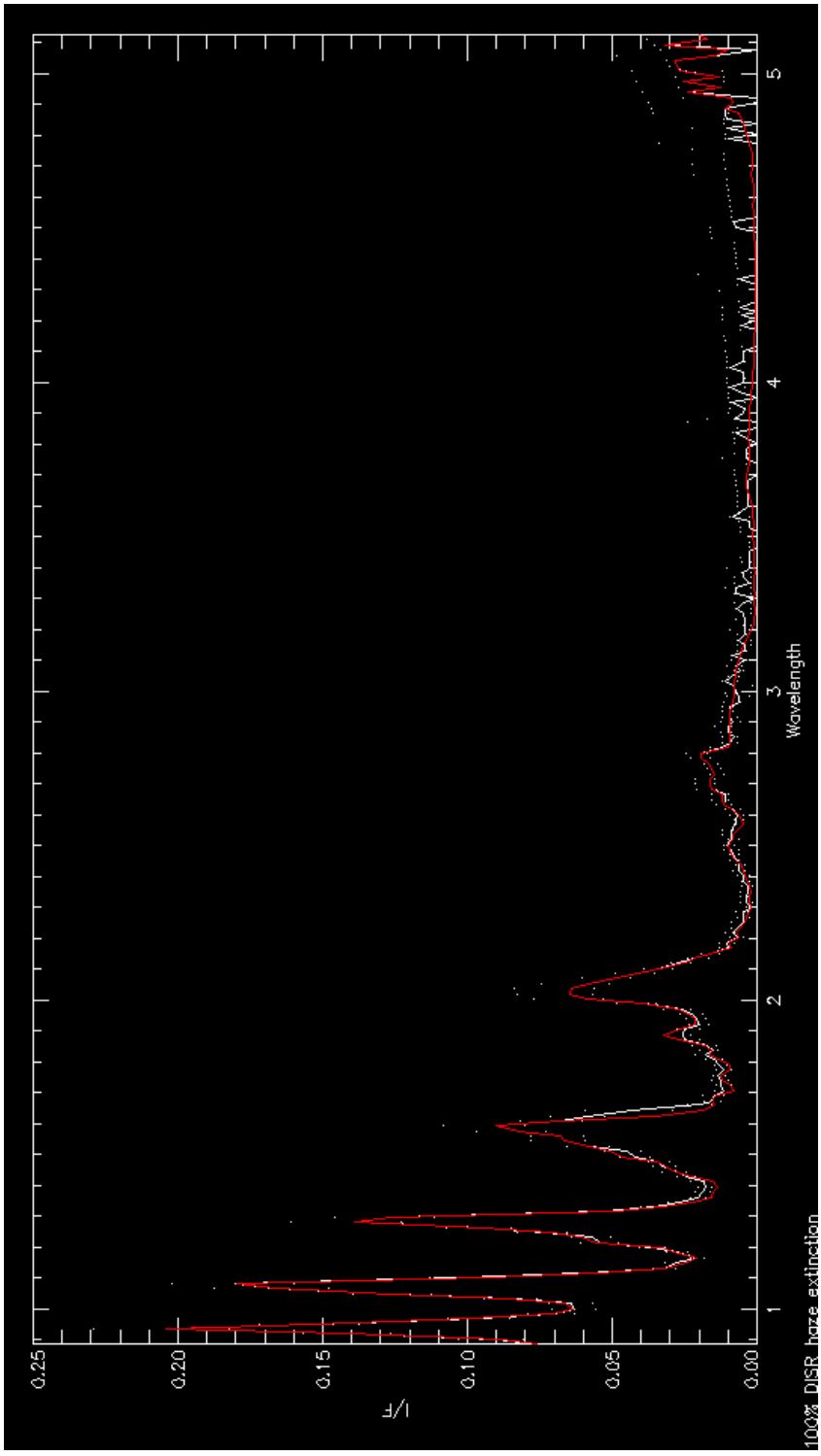

Fig. 5.15 – Best fit of data with simulation.

In Hirtzig et al. (2013) this assumption was checked for various test cases and found that the variation is almost exactly linear longward of 2.1 μm while this assumption induces an error of at most 3% on the retrieved surface albedo, near 0.9 μm. The code also takes into account the uncertainty on the surface albedo due to noise level. The signal-to-noise ratio (SNR) in an individual spectrum varies from ~100 in the short-wavelength windows to ~1

longward of 4 μm. The error induced is taken as the variation of the surface albedo that yields a relative 1/SNR variation of the I/F reflectivity. The uncertainty on the haze extinction introduces a significant uncertainty on the retrieved surface albedo. Table 3 in Hirtzig et al. (2013) shows the uncertainty on the retrieved surface albedo due to the 5% uncertainty on the haze extinction. As expected, the error bars are larger in the wings of the methane windows (e.g. at 1.54 μm) than in the centers (e.g. at 1.59 μm), as we lose sensitivity to the surface. We also note that the uncertainty varies from one window's center to another due to different transparencies (gas and aerosols). The 0.93- and 1.08-μm windows are the least transparent, while on the contrary the 2.03-μm window is so transparent that changing the aerosols has little impact on the retrieved surface albedo. In any event, the maximum total error on the retrieved albedos at the peak of the windows is ± 19%. These uncertainties, derived from a specific case, are considered as applicable to all of the VIMS spectra considered here. Calibration uncertainties of the VIMS datacubes, which are not very well documented, have not been taken into account. In the fitting procedure, we considered error bars due to random noise, to the aerosol model, as discussed above, and to systematic uncertainties in the representation of the model opacity (mainly due to unknowns in the far wing lineshape).

In summary, the aerosol model (Tomasko et al. 2008; Hirtzig et al. 2013) is fitted in the methane bands and deepest wings, completely insensitive to surface contribution. As said before, while the single scattering albedo of aerosols is fixed in the model, the vertical profile of the haze is adjusted by applying a multiplicative factor to the DISR measurements, once per simulation. Uncertainties at the 3σ level are also estimated by the code. The haze contribution is inverted with an absolute accuracy of +/-5%. The retrieved surface albedos in each methane window have a basic relative accuracy better than 11%, taking into account the uncertainties on the spectral lines profiles, the haze extinction fit, and the data intrinsic noise. Nevertheless, at shorter wavelengths where updated CH4 linelists were not available, error bars can reach 20%. In addition, when a methane window spans more than one VIMS channel (e.g. in the case of the 2.69-2.79 μm double window), we propose here only one datapoint computed through a weighted average of the surface albedos per channel, mitigated by the weakness of the methane absorption. This increases the error bars at 2.79 and 5.00 μm up to 40 and 33% respectively. In total we thus display computations at 0.94, 1.08, 1.27, 1.59, 2.03, 2.79, and 5.00 μm (and an additional point for the 1.54 μm wing), with error bars: 20%, 20%, 11%, 11%, 11%, 40%, 33% respectively.

5.3.3 RT on Cassini VIMS data of interest

We use the RT code to simulate the spectra, and retrieve the surface albedo of the Huygens Landing site (HLS). Figure 5.16 presents the best fit of data (black) with the simulation (red). We use HLS as a reference area as well as a calibration tool for the other areas. This specific area's observations are very useful as HLS provides the only ground truth for Titan's surface from Cassini. The HLS albedo retrieval from RT (Fig. 5.17) has been validated in Hirtzig et al. (2013) (Fig. 5.18), where it is shown that below 1.6 μm the retrieved surface albedos agree with those derived from Huygens/DISR (Jacquemart et al. 2008) and agrees also with the Griffith et al. (2012) results extended to longer wavelengths (see also Hirtzig et al. (2013) (Fig. 5.18 here) explanations on the discrepancies between models.

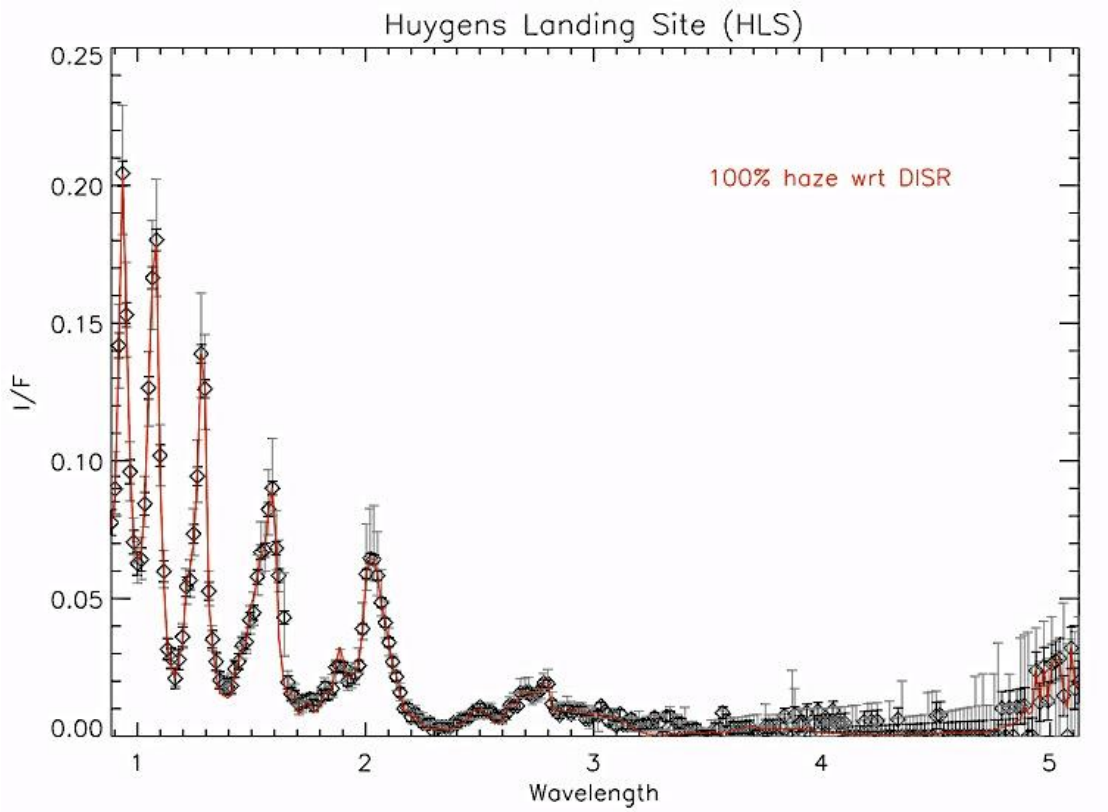

Fig. 5.16 - Best fit of the spectrum of the HLS showing all the methane windows (VIMS HLS data in black, and RT simulation in yellow; the DISR haze was adjusted by a factor of 1) (From Solomonidou et al. 2013b).

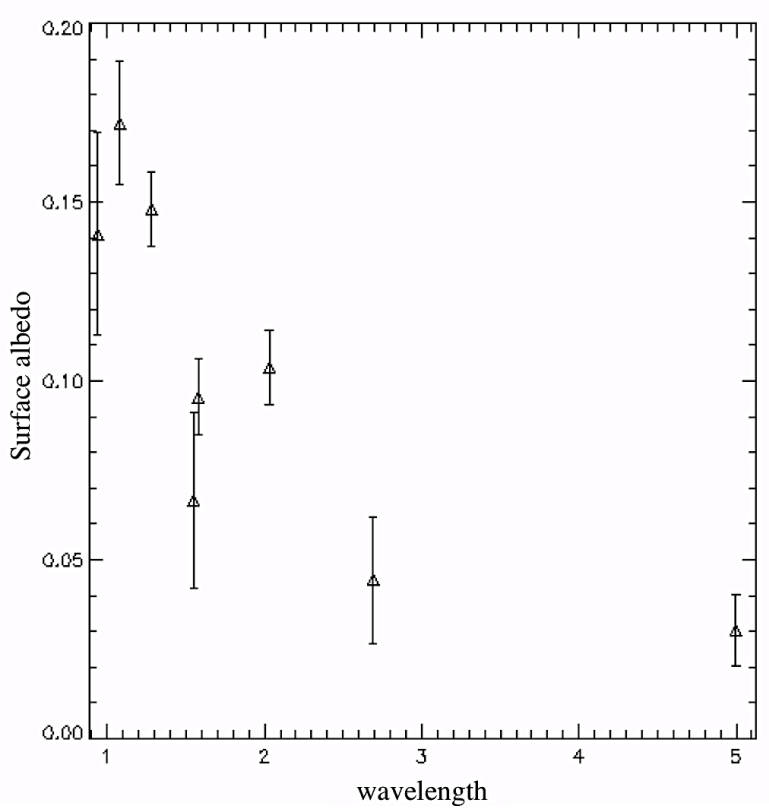

Fig. 5.17 - Surface albedo of the Huygens landing site in the methane window centers (From Solomonidou et al. 2013b).

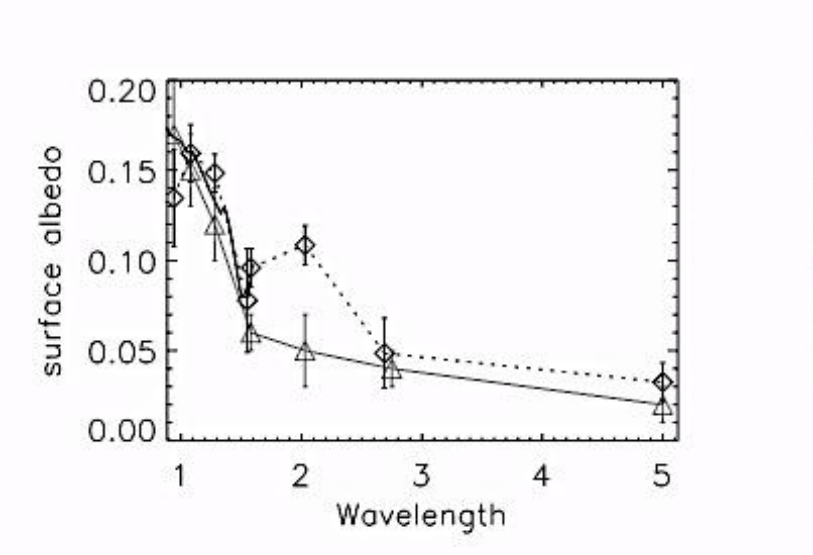

Fig. 5.18 - Albedos at the Huygens landing side (HLS) retrieved from the work by Hirtig et al. (2013) (black diamonds), compared to Jacquemart et al. (2008) (black curve) and Griffith et al. (2012) (gray triangles) (Image credit: Hirtzig et al. 2013).

5.4 Despeckle RADAR-SAR filter

As described in Chapter 2 the RADAR instrument consists of a Synthetic Aperture Radar (SAR) imager, an altimeter, and a radiometer. The RADAR imaging mode provides low-to-high resolution SAR images (Elachi et al. 2004). The basic textures present in SAR images, especially the high-resolution ones, are affected by multiplicative speckle noise. In order to acquire qualitative data and extract the real surface properties despeckling algorithms should preserve the data (Walessa, 2000).

5.4.1 Speckle noise and despeckle filtering

First, it should be noted that despite the fact that the RADAR observations are almost unaffected by the atmospheric conditions, the speckle noise exists in all types of coherent imaging systems. Its main cause is the coherent processing of backscattered signals from multiple distributed targets (Franceschetti and Lanari, 1999) while it affects the resolution of the images (reduction) and the detectability of the target (Goodman, 1976; Bratsolis et al. 2012). Indeed, speckle noise is not only signal dependent but it is reduces the effectiveness of image reduction and thus it is spatially correlated. However, the speckle noise affects SAR images even more largely than other types of imaging causing misleading interpretations. On SAR images, the speckle noise overlays real structures and causes grey value variations even in homogenous image parts, making automatic segmentation difficult.

Many methods are used to remove speckle noise and produce more qualitative SAR data for the surface researches such as multiple-look (single radar) processing that averages and removes the speckle noise (e.g. Tso and Mather, 2009). Other processes include adaptive optics and non adaptive despeckle filtering (Franceschetti and Lanari, 1999). Here, I present a despeckle filtering technique, called the Total Sum Preserving Regularization (TSPR) filter, developed by my colleague Emmanuel Bratsolis (Bratsolis and Segelle, 2003) and used on Titan studies by our LESIA and University of Athens Team and presented in a publication in the *Planetary and Space Science Journal* (Bratsolis et al. 2012), which I co-authored. Georgios Bampasidis and myself applied this filter on SAR data of lakes, impacts and cryovolcanic candidates. I present the results of the latter in Chapter 6.

5.4.2 The Total Sum Preserving Regularization (TSPR) filter and segmentation of different regions of interest - Application on Cassini SAR

As mentioned hereabove, the Cassini/SAR data (Fig. 5.19a; 5.20a) used in this study of their retrieval are discussed in detail in Chapter 3. The TSPR filter is based on a membrane model Markov random field approximation with a Gaussian (Chitroub et al. 2002) conditional probability density function optimized by a synchronous local iterative method which provides a sum-preserving regularization for the pixel values of the image (Bratsolis and Sigelle, 2003). Moreover, the method is based on probabilistic methods and regards an image as a random element drawn from a pre-specified set of possible images. Hence, it preserves the mean values of local homogeneous regions and decreases the standard deviation up to six times (Fig. 5.19b; 5.20b).

In addition to the despeckling capabilities, the TSPR filter can be used as a tool for the extraction of geologically meaningful structural units by dividing an image into specific regions with common characteristics and thus isolating regions of interest (Fig. 5.19d;e; 5.20c;d;e). We are using a segmentation method to classify these regions (Bratsolis et al. 2012). The supervised method of minimum Euclidean distance uses the mean values of each member and calculates the Euclidean distance from each classified object to the nearest class segmenting the image into different regions of interest or different labels (Fig. 5.19d;e). The Otsu's method (unsupervised segmentation) detects the optimum threshold of a histogram and separates the image into two (Fig. 5.20d) regions of interest.

Lakes

I present here the application of the filtering technique on two Cassini/SAR images that feature Titan lakes. The intended goal is to label regions in an image into three classes (dark lakes, granular lakes and the local background). First, a filtering technique is applied to obtain the restored image followed by a method of supervised segmentation, as explained hereabove.

Figure 5.19a shows the original Cassini/SAR image, 5.19b the filtering result and 5.19c the ratio between the initial and filtered one. We follow up with the segmented image on Fig. 5.19d where we have selected three classes: the dark lakes (black), the granular lakes (grey) and the background (light grey) that correspond to blue, green and red respectively in the color-coded version in 5.19e.

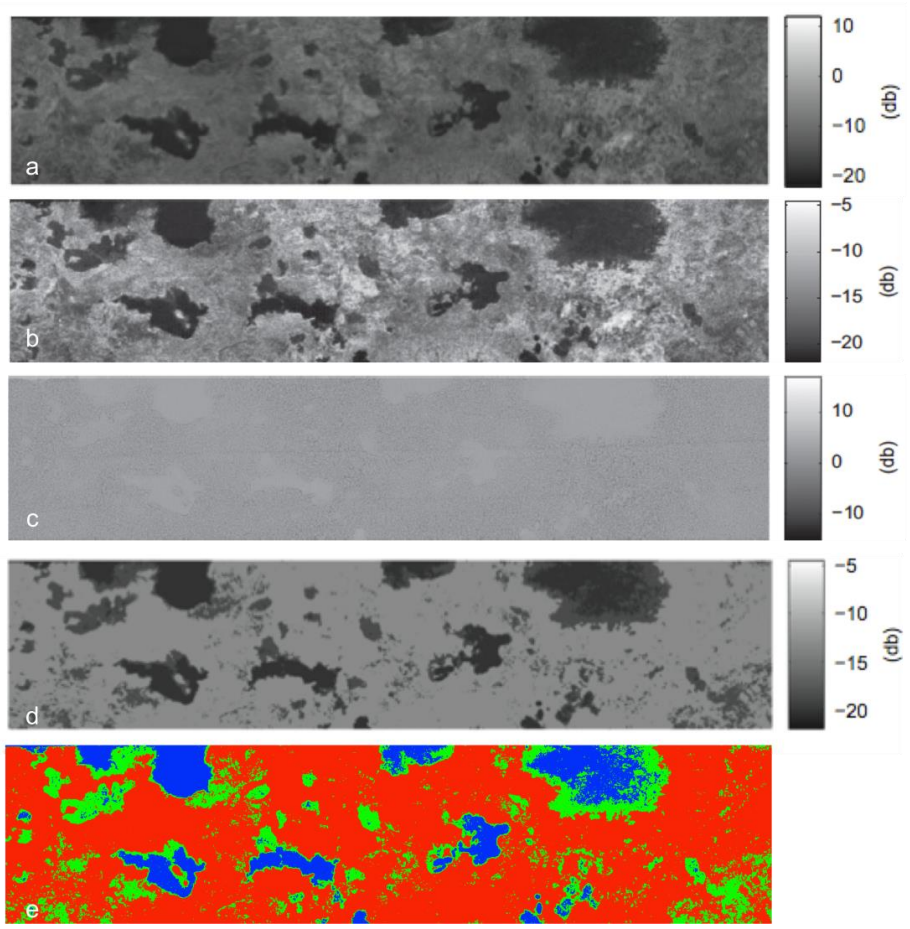

Fig. 5.19 – Filtering technique on Cassini/SAR original image PIA08630 showing several lakes. (a) The initial Cassini/SAR image (Image credit: NASA/JPL-CalTech/ASI); (b) The filtered Cassini/SAR using the TSPR filter (Bratsolis et al. 2012); (c) Image ratio between the initial (a) and the despeckled (b) image; (d) Segmented image after filtering; (e) Color-coded segmented image where the dark lake with low backscatter are illustrated with blue, the granular lakes with green and the local background is colored red.

I present hereafter another example of filtering and segmentation that we presented in the European Geosciences Union Congress in 2010. We use the Cassini SAR image of kissing lakes (PIA08740).

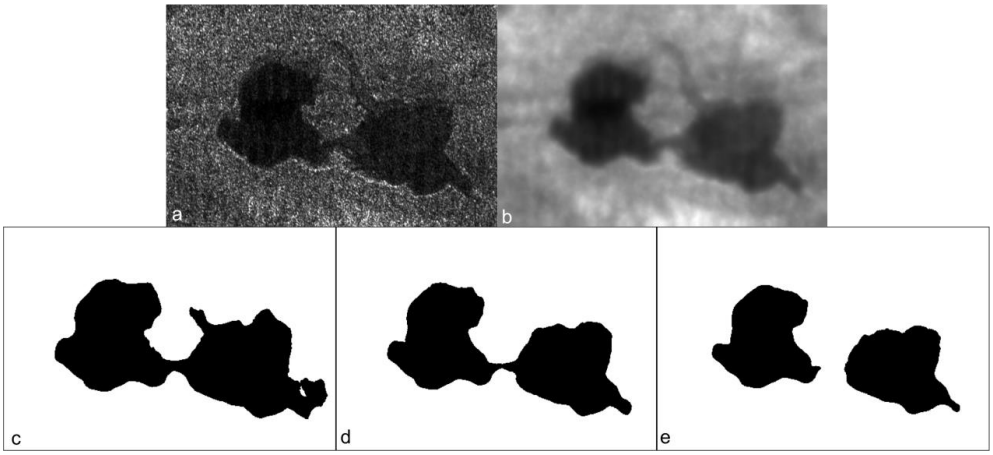

Fig. 5.20 – TSPR on the 'kissing lakes'. (a) Original Cassini/SAR image PIA08740 (Image credit: NASA/JPL); (b) TSPR filter image; (c) Segmented image after filtering and before the optimum threshold; (d) Segmented image after filtering with the optimum threshold; (e) Segmented image after filtering and after the optimum threshold. With black label we can see the lakes and with white the local background.

My original work using this technique concerns the processing of Cassini/SAR images of the candidate cryovolcanic regions from which I extract information regarding their surface texture. These applications and results are summarized in Chapter 6.

5.5 Summary and Future perspectives

As I have presented in this manuscript so far, the interpretations of surface features need a precise knowledge of the contribution by the dense intervening atmosphere, especially the troposphere. On that cause, I have gradually used three methods that treat the VIMS data aiming on the evaluation of the atmospheric contribution and the extraction of information on the nature of Titan's surface. Moreover, we can overcome the hampering of the Cassini/SAR data by speckle noise with the filtering and segmentation procedures described above. The outcome of these applications has been presented in three papers (Solomonidou et al. 2010; 2013b; 2013c) and one that I co-authored (Bratsolis et al. 2012) and many oral and poster contributions in International conferences (EGU, IAU, EPSC, DPS, IPPW, AOGS etc.).

One of my main and most ambitious perspectives for this work for the future is to superimpose VIMS images in which the atmospheric contribution is constrained by the RT code over the despeckled and segmented SAR images of the same region. The TSPR filter, in combination with the minimum Euclidean distance method of supervised segmentation, can be used to extract regions of interest, such as lakes, seas or volcanoes on the surface of Titan using Cassini SAR images. I have already been cooperating with Dr. Rosaly Lopes, a researcher of the Jet Propulsion Laboratory in Pasadena to this direction. My perspectives towards this work are also presented in more detail in Chapter 13.

In addition to the data correlation, updates and development of the codes and methods are some of my perspectives concerning the tools presented in this Chapter. In particular, for the RT code in collaboration with Mathieu Hirtzig, we intend to broaden our analysis to other geological areas on Titan and to update the code incorporating new laboratory measurements, for example, from published results (i.e. Boudon et al. 2010; Campargue et al. 2012). Also, since the code is incompatible with geometries of VIMS data that exceed 60º and many of Titan surface areas have been captured under these properties the use of a spherical radiative transfer code could be of necessary use.

Chapter 6

Surface properties of cryovolcanic candidate areas on Titan from VIMS data

In this Chapter I will introduce the work I performed analyzing the (favourable) cryovolcanic candidate areas that are spectrally and geologically interesting, as presented in Chapter 4, by applying a statistical, an empirical and a radiative transfer method on VIMS data. In the following sections I present the development of the analysis concerning both PCA and the surface albedo retrieval, where in a preliminary stage I use the empirical method of atmospheric subtraction. The results from PCA include the extraction of distinct spectral units within these areas (validated against a test case area; see Chapter 5, section 5.1.1.3). I also infer the associated spectral behaviour and dynamical range of the surface albedos using a radiative transfer code, aiming to achieve a better understanding of their nature. Furthermore, I present the comparison and calibration of the results from these three areas, with analogous inferences for the Huygens landing site compared with previous publications. First I use PCA as a single method, then proceed to the subtraction of the atmosphere method, again as a single method, and in conclusion I use both PCA and our radiative transfer code as follow up methods, that provide, amongst all, the most accurate results. The VIMS instrument and data and the possibilities they offer for investigating Titan's surface were presented in Chapters 2 and 3. In this Chapter, I will present a description of the surface characteristics of the specific areas, but I do not attempt a full interpretation, something that is presented in the following Chapter 7. The analysis tools in use here, such as the PCA, the atmospheric subtraction and the radiative transfer code (RT), were described in detail in the previous Chapter 5.

6.1 The necessity to evaluate Titan's surface albedo

The albedos of planetary bodies such as planets, asteroids and satellites can be used to infer much about their properties. The study of albedos, their dependence on wavelength, phase angle, and variation in time is the basis for a major part of studies regarding Titan's surface nature. Since Titan is a far away object and it cannot be thoroughly investigated by ground based data in terms of surface composition, much of what we know comes from the study of its albedo by Cassini, as in the work presented here, where we investigate the local surface albedo of Titan areas. For example, the absolute albedo can indicate the surface ice content of Titan, while the variation of albedo in time gives information regarding the process that can act on a specific surface field. In addition, contrary to other icy moons, where we see the surface, Titan is covered by an atmosphere hampering the surface investigation. Hence, knowledge of the true albedo of Titan's surface through the use of tools, such as radiative transfer models that resolve the problem of the atmosphere, is a crucial step on determining the composition of the surface. Moreover, the determination of Titan's surface composition is critical in order to unveil its geology and investigate the interactions between the interior, the surface and the atmosphere and hence enhance a complete image of the satellites' origin and evolution. One very crucial aspect of Titan's surface albedo and composition investigation concerns the identification of components with internal origin such as ammonia ice, something that would confirm Titan's dynamical and active geological history.

Table 6.1 summarizes the reported albedos of some icy moons including Titan during a three different methane windows (Adapted from Griffith et al. 1991).

Table 6.1. Surface albedo of the Jovian satellites and Titan (Table adapted from Griffith et al. 1991).

	2.0 μm	***1.6 μm***	***1.3 μm***
Europa (Clark and McCord, 1980)	0.09	0.25	0.45
Ganymede (Clark and McCord, 1980)	0.15	0.22	0.35
Callisto (Clark and McCord, 1980)	0.15	0.16	0.18
Titan's observed albedo (Fink and Larson, 1979)	0.11	0.14	0.22
Titan's corrected albedo	0.14	0.18	0.27

Ground-based telescope investigations of the integral disk of Titan attempted to retrieve the surface albedo in spectral windows between methane absorptions by calculating and removing the haze effects. Their results were reported to be consistent with water ice on the surface that is contaminated with a small amount of obscure material, perhaps organic matter

like tholin (e.g. Coustenis et al. 1995; Griffith et al. 2001; 2003). Figure 6.1 shows an example of Titan's surface albedo from its leading hemisphere with comparison to Gamymede's. Both albedos appear to be in analogy. The cyan dashed line represents laboratory synthesis of Titan tholins.

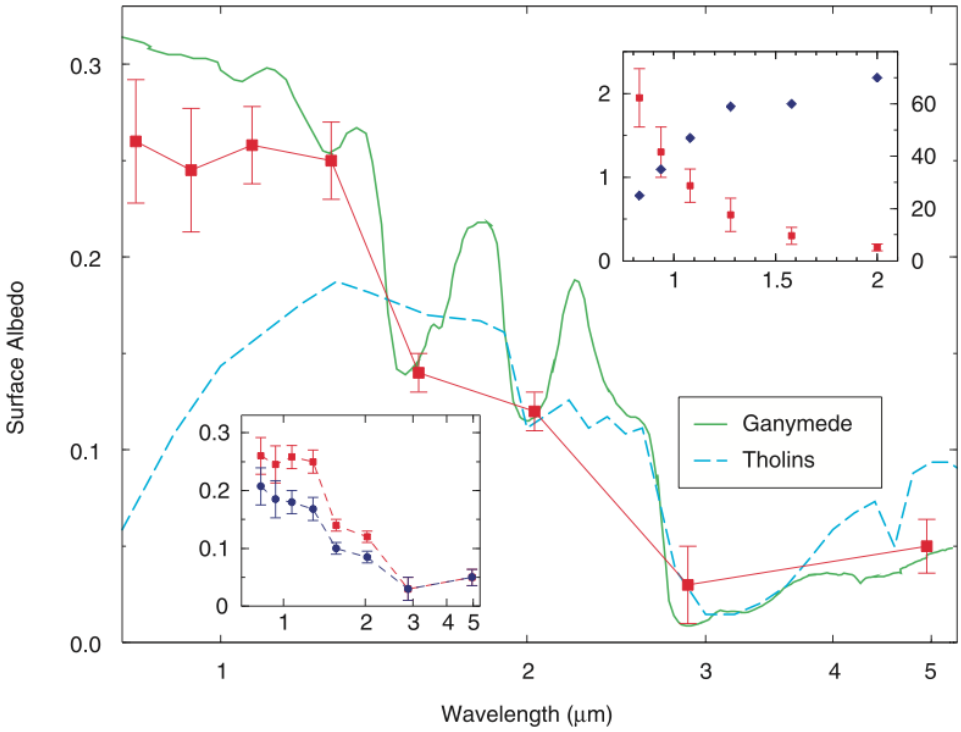

Fig. 6.1 - Surface albedo of Titan (red square), Titan tholins (cyan dashed line) and Ganymede (green line) (Figure from Griffith et al. 2003).

Prominently, the retrieved surface albedo depends not only on the compounds that synthesize a terrain but also on the state that these compounds depend on the temperature and pressure. Thus, water reflects different albedo values in its liquid or frozen state (Fig. 6.2).

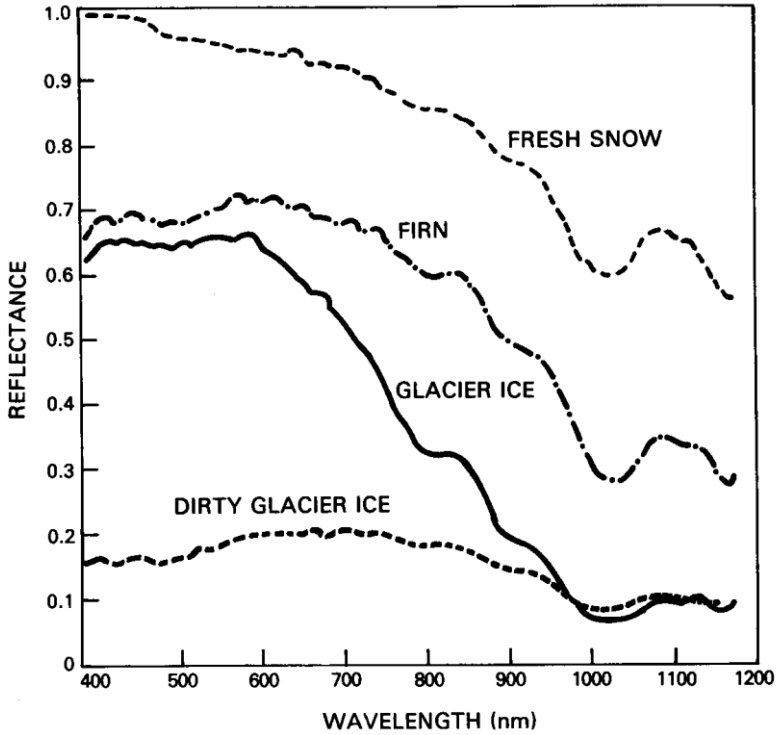

Fig. 6.2 - Graph of reflectance spectra for different snow and ice surfaces (Hall and Martinec, 1985).

The albedo of Titan's surface can only be determined through atmospheric windows that peer through Titan's thick atmosphere. The reflectance spectrum of the surface of Titan in the near-infrared, is difficult to derive, because of the absorbing and scattering effects of the methane and aerosol-rich atmosphere, but at wavelengths where methane absorption is minimum (0.93, 1.08, 1.27, 1.59, 2.03, 2.79, and 5.00 μm), radiative transfer models can remove most of the interference (e.g. Griffith et al. 2003; Hirtzig et al. 2013; Solomonidou et al. 2013b;c).

6.1.1 Past studies

Pre-Cassini investigations using ground-based and Voyager data have observed the variability of the satellite's geometric albedo, since the detection of Titan's surface from such data is possible, as in the near infrared, the extinction due to haze decreases (McKay et al. 1989; Griffith et al. 1991; Coustenis et al. 1995). Fig. 6.3 presents geometric albedo measurements recorded by various teams from the first conclusions of 'lightcurves'[26] giving the evolution of the geometric albedo of Titan, during its revolution, around Saturn (e.g. Griffith et al. 1991; Lemmon et al. 1993; 1995; Coustenis et al. 1995).

[26] *The lightcurve represents the periodic variation of the albedo variegation of the surface*

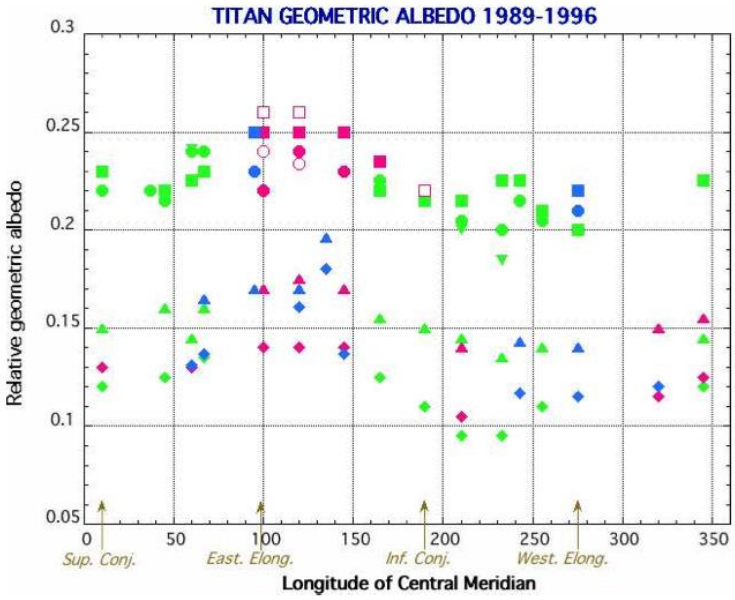

Fig. 6.3 - Lightcurves of Titan from the geometric albedo measurements recorded by various teams from 1989-1996: Coustenis et al. (1995; 2000; 2001) (green); Lemmon et al. (1993; 1995) (pink); and Griffith (1993), Griffith et al. (1998; 2003) (blue) (Adapted from Raynaud, 2000).

Fig. 6.4

In addition, Negrao et al. (2006) analyzed the geometric albedo in the 0.9–2.5 μm spectral region and provided the lightcurves of observations of Titan in a series of campaigns from 1991 to 1996 with the Fourier Transform Spectrometer on the CFH telescope. The authors retrieved surface albedo using various sets of methane coefficients from line-by-line calculations by Boudon et al. (2006) and band models by Irwin et al. (2006), Karkoschka (1998) and Moreno (updated from Coustenis et al. 1995) (Fig. 6.4). This stands as a good example in seeing how dramatically the retrieval of surface albedo depends on the available methane coefficients.

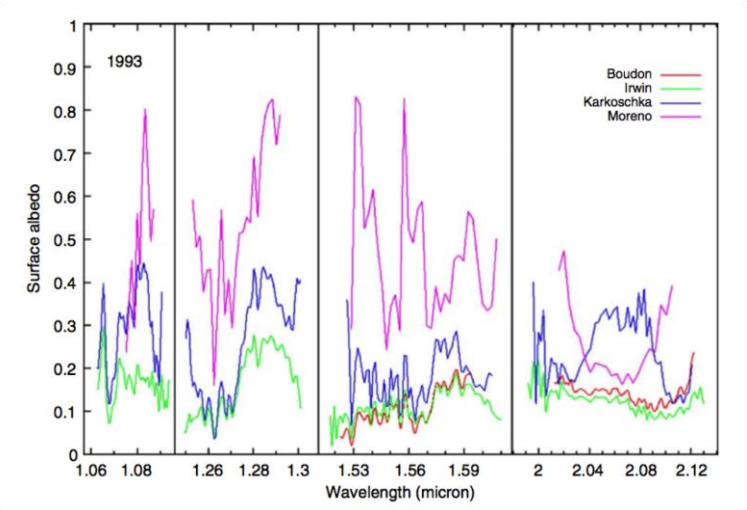

Fig. 6.5 - Retrieval of surface albedo from CFHT data (1993) using various sets of methane coefficients available in 2006 (Image credit: Negrao et al. (2006)).

The same authors compared the retrieved, the surface albedos of Titan dark and bright sides, using CFHT data of various dates (Fig. 6.5)

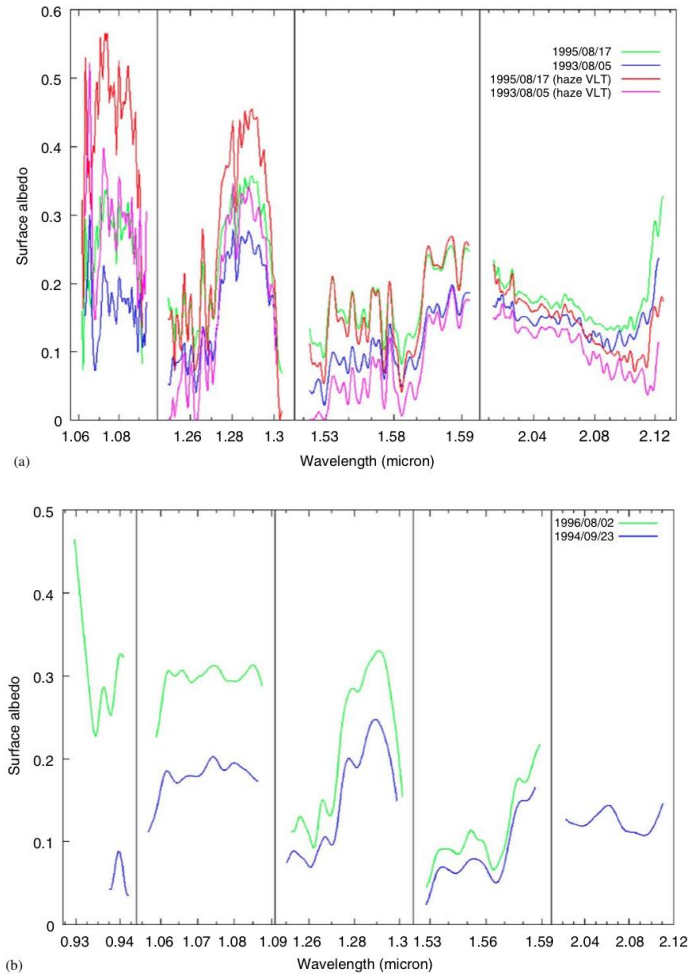

Fig. 6.6 - Retrieval and comparison of surface albedos. (a) Surface albedos of the bright and dark sides from 1993 and 1995 CFHT observations and the haze profile that fits VLT observations (b) Albedos of the bright and dark sides from 1994 and 1996 observations (Image credit: Negrao et al. 2006).

From the beginning of the Cassini investigation on Titan in 2004 many studies have been conducted concerning the surface albedo of this moon. Porco et al. (2005) studied ISS Titan surface images with limited spatial coverage and identified albedo patterns to vary with latitude, suggesting differences in the atmospheric processes that influence the surface. Furthermore, VIMS is able to see surface features and shows that there are spectral and therefore likely compositional units. From several methods, spectral albedo estimates within methane absorption windows between 0.75 and 5 μm were obtained for different surface units using VIMS image cubes. An analysis on Cassini/VIMS data of the equatorial area Hotei Regio by Barnes et al. (2005) showed the areas' anomalous brightness at 5 μm. The authors found an association between the area and a surface albedo feature, identified in images taken by the Cassini/ISS. An additional work on VIMS data, acquired from the first observation of the instrument on Titan, identified circular albedo features at 2.02 μm that indicated

characteristics of impact cratering (Brown et al. 2006), while based on albedo and textural variations, a geological interpretation of circular and volcanic-like features have been made by Sotin et al. (2005). In the latter study it is mentioned that morphological information from the VIMS data can be extracted by comparing images at different wavelengths. If ratio images do not correlate with albedo variations at a given wavelength, the I/F variations at each wavelength are not related to variations in surface composition. One possibility is that these brightness variations are due to illumination of local slopes.

Moreover, differences in the average normal reflectance using VIMS data have been found at 2.01 and 2.73 μm, distinguishing two albedo regimes on Titan's surface (Buratti et al. 2006). McCord et al. (2006), while investigating several spots on Titan, identified two compositional classes associated with the lower and higher albedo materials. The lower albedo is consistent with water ice contaminated with a darker material while the higher albedo presents a different and unknown composition. Nelson et al. (2006), in a photometric analysis of Titan areas, identified two albedo regimes similarly to McCord et al. (2006), where the normal reflectance of the darkest regions are about 0.06 and the brightest 0.19. I should note that the effect of absorption and scattering by the atmosphere and haze was not evaluated. Many issues hamper the accurate retrieval of surface albedo and thus surface composition, something I discuss in the following section.

6.1.2 The problem with observations

Studying Titan's surface requires very specific tools. Its atmosphere contains both methane (~1.5% in the stratosphere, Flasar et al. 2005; Niemann et al. 2010) and aerosols (e.g. Rannou et al. 2010). Methane scatters visible light and absorbs in the infrared, whereas aerosols are more absorbent in the visible and more scattering in the infrared. Fink and Larson (1979) showed that these atmospheric constituents dominate Titan's spectrum, with little possibilities to reach the surface through its opaque veil. McKay et al. (1989) and Griffith et al. (1991) showed that some windows of diminished absorption allow for surface observations in the near infrared. The Cassini VIMS makes extensive use of these 'methane windows' centred at 0.93, 1.08, 1.27, 1.59, 2.03, 2.79 and 5.00 μm. However, the haze extinction in the near-infrared decreases with wavelength, and methane absorption is not marginal, even at these wavelengths. Thus, extracting information on the lower atmosphere and the surface of Titan from near-IR spectra requires a good understanding of the methane and haze contributions to the opacity. Therefore, atmospheric scattering and absorption need to be

clearly evaluated before one can extract the surface properties (i.e. true surface albedo, interpretable in terms of chemical composition) from VIMS data.

The absorption due to the isotopologues of methane has been an intriguing issue for many studies. On that issue, three major approaches are applicable; direct laboratory measurements, theoretical calculations, and empirical models (de Bergh et al. 2012; Campargue et al. 2012). Indeed, theoretical (Boudon et al. 2006; Albert et al. 2009; Daumont et al. 2012; Nikitin et al. 2009; 2010; 2011; 2013) and experimental (Wang et al. 2010a;b; 2011; 2012; Campargue et al. 2012 and references therein) data were recently combined to cover the region longward of 1.19 μm with a complete line-by-line description. These data lists are used in a modular Radiative Transfer model capable of line-by-line as well as correlated-k calculations for planetary applications (see Chapter 5).

Even if the tools and methods are available to process VIMS data, limitations exist. Furthermore, VIMS collects data that is very limited in spatial coverage (a few km in resolution) or has large spatial coverage and low resolution (up to hundreds of km). An additional issue with the analysis of VIMS data is the incompatibility of a plethora of observations with the plane-parallel radiative transfer codes like the one I use and present (RT) on Chapter 5. As mentioned before, the RT code is based on the plane-parallel version of the Spherical Harmonic Discrete Ordinate Method solver (SHDOMPP; Evans, 2007), assumes plane-parallel conditions and divides the atmosphere of Titan into 70 layers. Many interesting areas on Titan, such as Hotei Regio, are very close either to the limb or to the terminator, with emergence or incidence angles over 60° (see Table 3.4 Chapter 3). This impeaches the proper use of a radiative transfer code (at least in the plane parallel approximation).

6.1.3 Further requirements

So far a large number of studies concentrated on the analysis of VIMS data is in our disposal, providing a deep view in the spectroscopic properties of Titan's system. However, many important parameters set boundaries to these studies, incommoding a holistic and thorough identification of the nature of the surface. First, an extensive knowledge and analysis of the far wing absorption properties of methane in Titan's P,T conditions is required. Such investigation should take into account the various band complexes that seem to control the opacity in the windows such as pentad, octad and more (Hirtzig et al. 2013). In addition, extension to short wavelengths below 1.3 μm line lists should be available in the

future. Moreover, CH_3D has important absorption coefficients (available only in the interval 1.26-1.71 μm and beyond 2.2 μm) and need expansion as well.

Other than the aforementioned proposed theoretical and laboratory developments, an important issue still remains on the capabilities of the current space mission with regard to the complexity of Titan's surface. The spectro-imaging sensors of Cassini and Huygens, VIMS and DISR respectively, have limitations on the acquisition of high-resolution data, as I have discussed on Chapter 2. This prevents a good detection of surface features as well as adequate information for the analysis of the chemical composition. However, since Earth-based observations, like the ones from CFHT, Keck and VLT, acquire, even partially, high quality (5-10 times better than Cassini) near-infrared Titan data, a reanalysis of these data with new methane coefficients in addition to Cassini data knowledge will develop new and interesting Titan spectral investigations. Nevertheless, the identification of the Titan's surface nature requires a future mission dedicated to this satellite, with enhance instruments for the surface studies. This should include a near-infrared spectro-imager with enhanced spectral capabilities.

In the following sections I present the results of my study concerning the retrieval of surface albedos of Titan geologically interesting areas (see Chapter 4) using specific applications (see Chapter 5).

6.2 Principal Component Analysis (PCA) applied to VIMS cubes

By using the PCA method we aim to isolate specific regions of interest (RoI) of distinct spectral behaviour (spectral units) within the aforementioned areas. I presented the method and its parameters in detail on Chapter 5. I have used the PCA method at many stages during my PhD thesis. First, I used it solely, trying to extract spectral information from the RoI isolation of the PCA results, and this work, which I present in the following 6.2.1 section, has been published in the *Hellenic Journal of Geosciences* (Solomonidou et al. 2010) and in the proceedings of the *International and Planetary Probe Workshop* (IPPW-7). Then, I used PCA with the follow up RT method, in a more sophisticated way and acquired updated PCA results, as presented in section 6.2.2. This work is now submitted for publication in the *Journal of Geophysical Research* (Solomonidou et al. 2013b). Finally, another set of PCA results, concerning the work that I present on Chapter 7 on the temporal variations, is now submitted for publication (Solomonidou et al. 2013c) and included and in this Chapter hereafter. Information on the datasets used in this Chapter can be found on Chapter 3.

6.2.1 Preliminary PCA results

I have presented the confirmation that our principal component application works properly in Chapter 5, section 5.1.1.3, where I thoroughly described the PCA technique.

I have used the PCA method on VIMS data in a preliminary stage of my study. In the following PCA results, presented in this section, I did not take into account the eigenvectors[27] and eigenvalues[28], the necessity of which was presented on Chapter 5. The Region of Interest (RoI) selection is different than the final one I use later on in this Chapter. Here, I use VIMS data for Hotei Regio, Tui Regio and Sotra Patera (see Table 3.4, Chapter 3).

By applying PCA on the VIMS data five distinct areas appear within Tui Regio (Fig. 6.6). Here, I used the entire VIMS spectrum, including the visual and the infrared observations. Depending on the order of PCs in use, each RoI takes a different color and that is why Figures 6.6c and d present different color composites. The Principal Component Analysis projections (Fig. 6.6c; d), show areas with different colors (spectral units) suggesting diversity in surface composition. As mentioned in Chapter 5, PCA is an independent

[27] *Eigenvectors are a special set of vectors associated with a linear system of equations that are sometimes also known as characteristic vectors, proper vectors, or latent vectors (Marcus and Minc, 1988)*
[28] *Eigenvalues are a special set of scalars associated with a linear system of equations that are sometimes also known as characteristic roots, characteristic values (Hoffman and Kunze, 1971)*

statistical method and independent of any a priori knowledge. Thus, by using the Regions of Interest (RoI) i.e. spectrally different units as derived from the PCA image, and the eigenvalues and eigenvectors (the latter two in the updated results, see section 6.2.2), we are sure that we select the correct VIMS pixels/spectra (i.e. pixels that correspond to a specific spectral unit) for our analysis. For that reason, we have used color composition in order to illustrate the distinct spectral units, with the aim to color the actual Hotei Regio, Tui Regio and Sotra Patera features as red, within the datacubes. Hence, knowing that the areas are particularly bright (anomalously at 5 μm) from previous studies (e.g. Barnes et al. 2006; McCord et al. 2008; Soderblom et al. 2009) we label the red spectral unit as 'brightest' and the green or blue (depending on the datacube) as 'darkest' owing to the fact that there are systematically associated with the lowest eigenvector norms. In a preliminary stage and before applying the RT method (see section 6.4), we have confirmed the 'red' spectral units as the brightest and the 'green' (Tui) and 'blue' (Hotei) as the darkest in the datacubes by simply comparing the I/F of each spectral unit extracted from the PCA analysis.

The brighter areas represent the highest I/F values and the darker areas the lowest, where 'I' stands for the intensity of reflected light measured by the instrument, and 'F' the plane-parallel flux of sunlight incident on the satellite normalized for Titan (Thekaekara, 1973; Barnes et al. 2007; Brown et al. 2004).

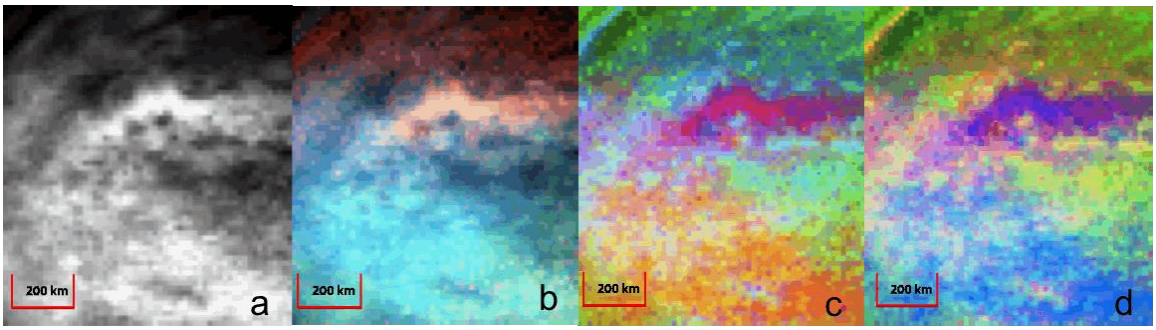

Fig. 6.7 - Reprojections of Tui Regio: (a) Gray scale 2.03-μm, (b) RGB false colors R: 5-μm, G: 2-μm, B: 1.08-μm, (c) PCA R: 1st , G: 2nd , B: 3rd components, (d) PCA R: PC3 , G: PC2, B: PC1.

I have isolated specific RoIs according to their distinction from the PCA method (Fig. 6.7) and plotted their I/F (Fig. 6.8). I use the application of the ENVI system (see Chapter 3) that provides the option of cutting/selecting specific regions within a cube and retrieving spectral information. Thus, I first isolate the areas as shown in the PCA image (Fig. 6.6c) and then I retrieve the I/F from the original VIMS datacube (Fig. 6.6).

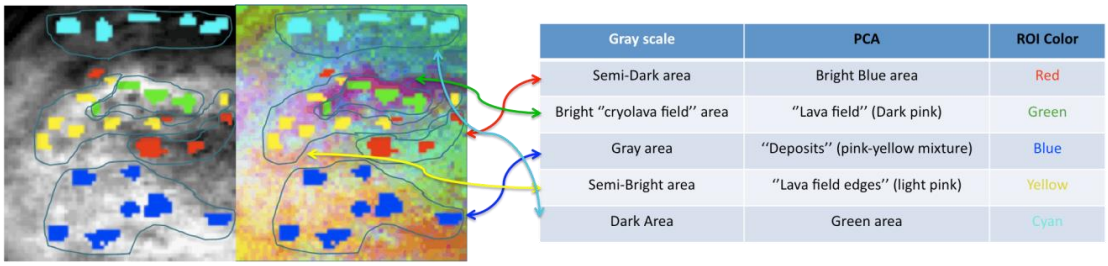

Gray scale	PCA	ROI Color
Semi-Dark area	Bright Blue area	Red
Bright "cryolava field" area	"Lava field" (Dark pink)	Green
Gray area	"Deposits" (pink-yellow mixture)	Blue
Semi-Bright area	"Lava field edges" (light pink)	Yellow
Dark Area	Green area	Cyan

Fig. 6.7 - Isolated areas with the use of visual colour alterations, which suggest areas of spectral difference.

The spectrum of "Bright cryolava field", in Figure 6.8, is different from the others, presenting higher I/F values at almost all wavelengths. This indicates that this RoI is extremely brighter with comparison to the rest regions. The wavelengths at which this area presents obvious alterations are the 2.8 μm and 5 μm (Solomonidou et al. 2010).

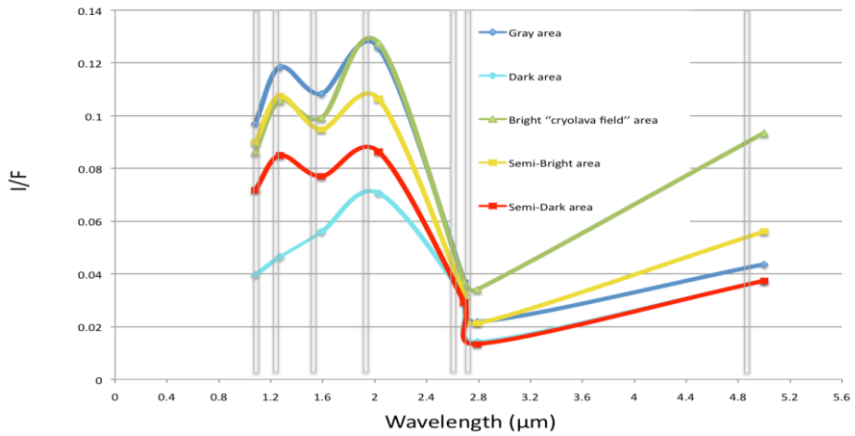

Fig. 6.8 - Spectral plot of five distinct areas at the seven atmospheric spectral windows.

I treated Hotei Regio similarly (Fig. 6.9). The PCA distinct five spectral units, within Hotei Regio's possible volcanic field (Fig. 6.10) and the PCA projections (Fig. 6.9c; d) show that the area, suggested to be cryovolcanic (red), is distinguished from the surroundings. The only compatible figures with the surrounding area are the caldera-like structures (pointed by green lines), which probably reveal the primal surface material, before resurfacing.

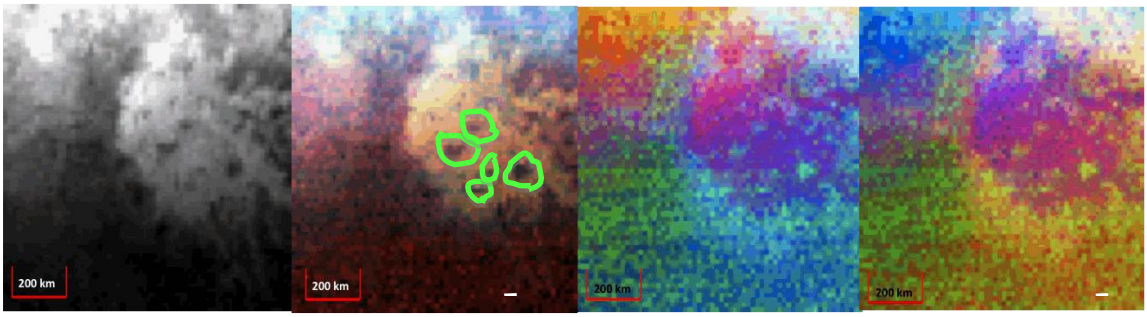

Fig. 6.9 - Reprojection of Hotei Regio: (a) Gray scale 2.03-μm, (b) RGB false colors R: 5-μm, G: 2-μm, B: 1.08-μm, (c) PCA R: 1st, G: 2nd, B: 3rd components, (d) PCA R: 3rd, G: 2nd , B: 1st components.

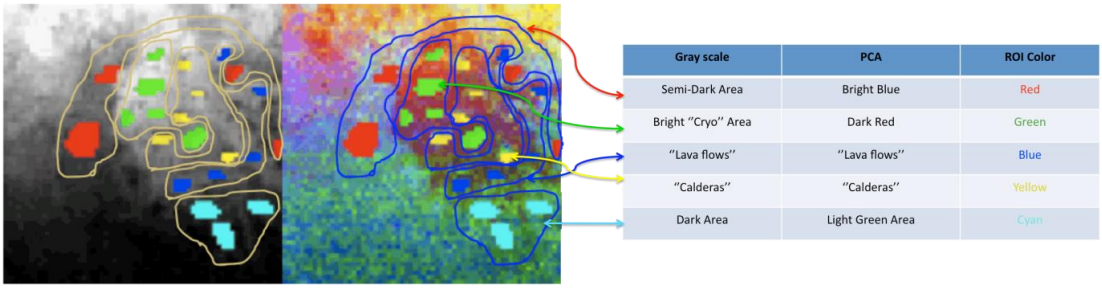

Fig. 6.10 - Isolated areas with the use of visual color alterations, which suggest areas of spectral difference.

Hotei Regio's spectral graph (Fig. 6.11) indicates that the "Bright Cryovolcanic area" has the highest I/F values and remains brighter with respect to the other areas at all wavelengths. In addition, the "Dark area" remains darker with low values of I/F at all wavelengths. Unexpectedly, the spectra from the caldera-like structures present medium I/F values, lying almost in the average between the brighter ("volcanic area") and the darker ("primal surface") at most wavelengths. This is compatible with terrestrial caldera structures that consist partially of primary surficial components on which the volcano is being built, as well as, new material coming from the interior.

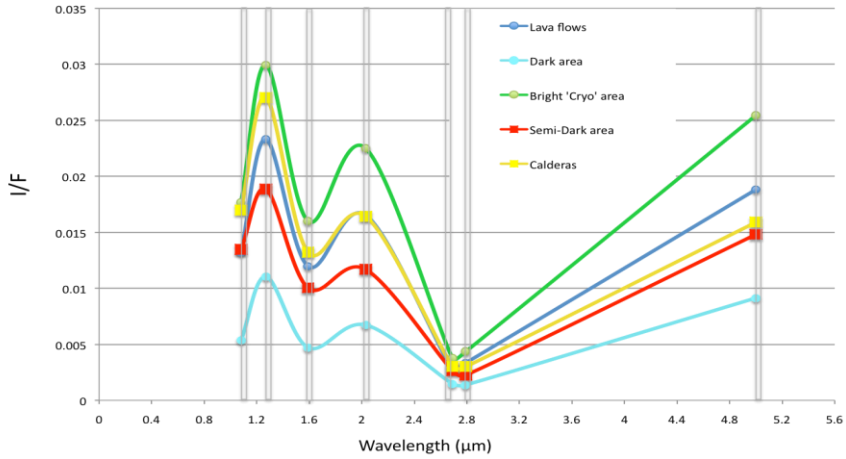

Fig. 6.11 - Spectral plot of five distinct areas at the seven atmospheric spectral windows.

This study's main purpose was to take a first look and perform a preliminary analysis of Titan original VIMS data with the Principal Component Analysis method, which has never been tried before. From the analysis it appears that Tui Regio's flow-like RoI, has the highest I/F value from its surroundings, especially in the 2.8 and 5-μm spectral windows (Fig. 6.8), suggesting compositional variability in the material between the dark and the bright spots. Furthermore, the dark area presents the lowest I/F values at all wavelengths of the seven spectral windows, while at some windows it has the same spectral values as the 'semi-dark' RoI. This suggests that if the area was ever active volcanically then the flow field has possibly been deposited over the initial (dark) material after single or multiple diachronic eruptions.

For Hotei Regio, the volcanic-like field has higher I/F values at all wavelengths with comparison to the semi-dark and dark areas that either surround the field or lie within it (Fig. 6.11). The dark areas present significantly lower I/F values. Even though the caldera-like structures are seeing as dark as the surrounding areas at VIMS images, they demonstrate medium I/F values suggesting altered chemical composition. The medium I/F values compared with the other areas, suggest that if the area was ever active, the calderas consist of the initial substrate (dark) material and the volcanic (bright) new material. Such a combination could result in the formation of rough surfaces with high textural variability. The VIMS analysis for the caldera-like structure of Hotei Regio reinforces the theory that assumes the volcanic origin of the area's pattern (Solomonidou et al. 2010).

However, even if some preliminary implications have been made using the results of PCA on VIMS original data, there is one significant problem remaining that hampers the quality of results (see Chapter 5). Atmospheric aerosols and gases are also measured in the signal by VIMS and depict in the datasets. Hence, de-convolution between atmospheric and surface signal is required. In the absence of tools, such as atmospheric subtraction and radiative transfer, that are capable of performing a de-convolution, the determination of surface spectral heterogeneities and the retrieval of spectral information, as present here above, is not trustful. Additionally, the PCA result images have been constructed here by taking into account random selections of the principal components (PCs), which are the basic elements of the end-image. More precisely, I have depended my selection only on the visual heterogeneities (i.e. image) and not the results on eigenvalues and eigenvectors (see Chapter 5.1).

In the following section all the appropriate parameters for the extraction of meaningful PCA results have been taken into account.

6.2.2 Updated PCA results on study cases

We have applied the PCA method, as did on Chapter 5, section 5.1.1, in a more explicit and sophisticated way than in the previous section. Hence, we applied the method to the three study areas; Hotei Regio, Tui Regio and Sotra Patera, but this time by taking into account the eigenvalues, eigenvectors and the visual results as seen in the PCA images. I have presented some examples of the steps taken during that method on Chapter 5. Moreover, we are using the bands 97 to 352 that correspond only to the infrared channel.

Hotei Regio

The eigenvalue information for the case of Hotei Regio (Fig. 6.12) indicates that the first PC contains most of the information present in the dataset but the second and third could be useful as well. For the datacube details see Chapter 3, Table 3.4, #3.

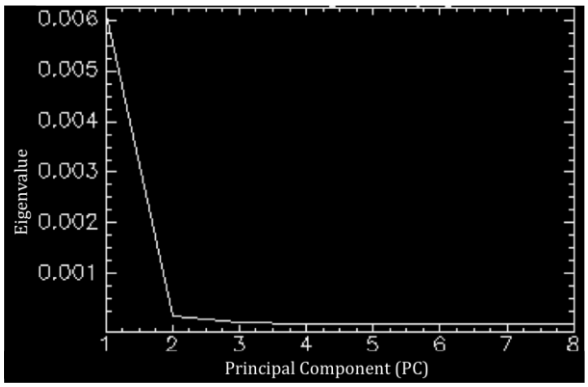

Fig. 6.12. Eigenvalues plot for Hotei Regio datacube #3 (Table 3.4, Chapter 3). The variability is accounted mostly for the 1st PC and 2nd PC, while PC3 is also of interest. After that, the flatenning indicates the absence of variability in the PCs.

Moreover, from the eigenvectors seen hereafter (Fig. 6.13), PC1 and PC2 seem to correspond to the surface, with signals in the short wavelengths, the 2.69-2.79 double window and the 5 μm one, while PC3 and PC4 present a light signal at 5 μm. However, at PC4, noise is also present. After that the PCs are dominated by noise.

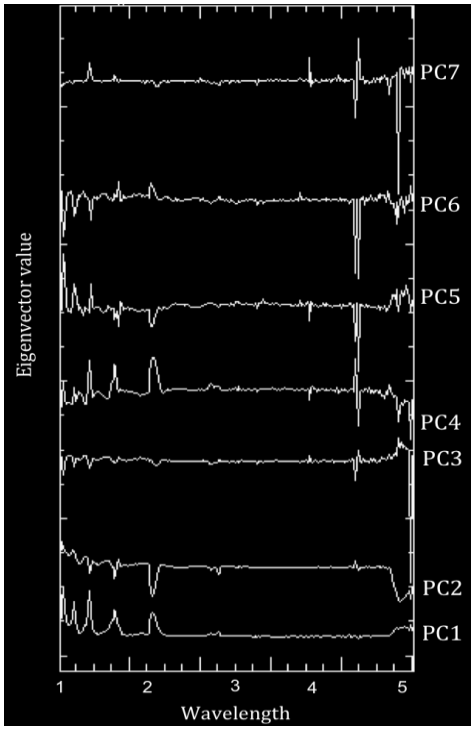

Fig. 6.13 - Calculated eigenvectors from the Hotei Regio datacube. It appears that only PCs #1,2,3 are compatible with surface spectra.

For the production of the PCA image we use PCs 1, 2 and 3 (R:PC1, G:PC2, B:PC3). We distinguish three major spectral units (red, green, yellow) (Fig. 6.16).

Tui Regio

All Tui Regio datacube's (see Chapter 3, Table 3.4, #4) results, regarding the eigenvalues, the eigenvectors and the PCs, can be found on Chapter 5, section 5.1.1.2.

Sotra Patera

In the case of Sotra Patera, the PCA eigenvalues yield that the 1st PC contains the largest information present in the dataset (Fig. 6.14). Nevertheless, the 2nd and 3rd are also of good use while after that only noise is present.

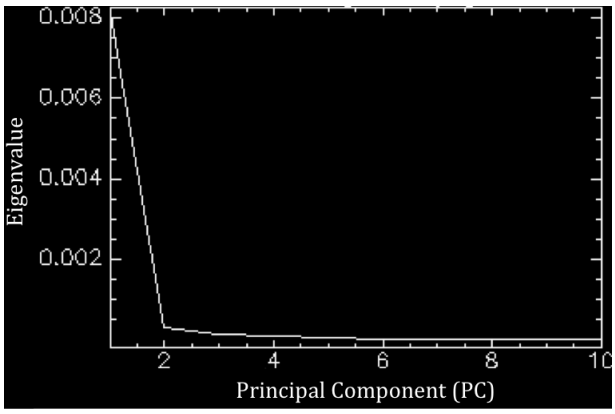

Fig. 6.14. Eigenvalues plot for Sotra Patera datacube #5 (Table 3.4, Chapter 3). The variability is accounted most for the 1st PC and 2nd PC, while PC3 is also of interest.

From the eigenvector investigation, it appears that PC1 and 2, and slightly 3, reflect the surface. The rest PCs are dominated by noise (Fig. 6.15).

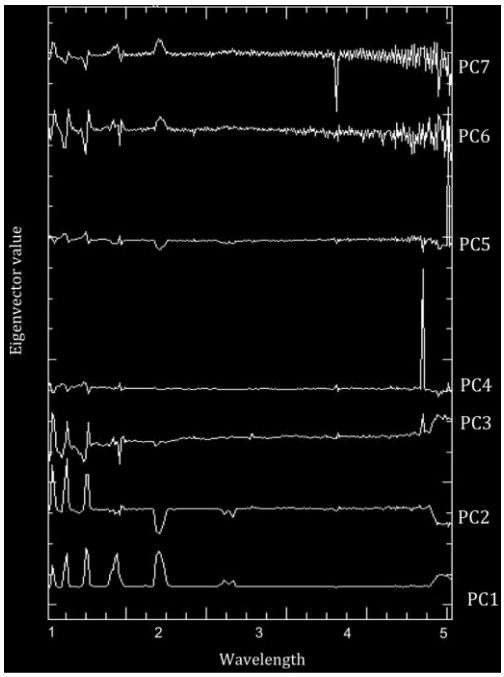

Fig. 6.15 - Calculated eigenvectors from the Sotra Patera datacube. It appears that only the first three PCs are compatible with surface spectra. Hence, we use PCs #1,2,3 to create the PCA image and extract the surface information concerning the heterogeneities of the regions.

Since PCA is not sensitive to brightness, we use certain color identification so that the brightest units appear in red and the darkest units in green or blue following the rationale described in section 5.1.1.2 of Chapter 5. With such a representation, it is easy to identify a number of RoIs that indicate the most diverse spectral response and possibly different chemical composition. We select two small RoIs, as close as possible to each other in the area, so that we can safely assume that, - although the RT code attempts to take this into account - the atmospheric contribution and the observational geometry is similar so that any changes in reflectivity are due mainly to the surface (Figs. 6.16c_1; c_2; c_3).

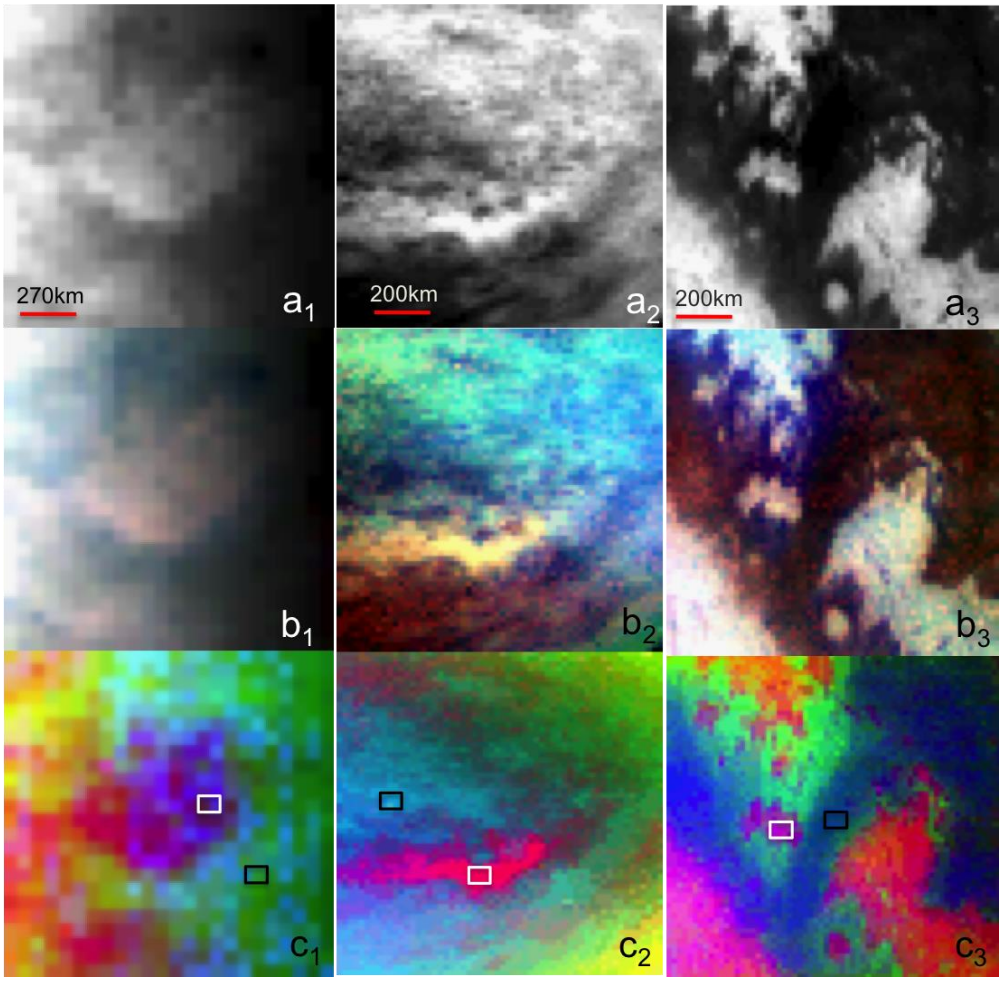

Fig. 6.16 - VIMS images for Hotei Regio (vertical left), Tui Regio (vertical middle) and Sotra Patera (vertical right) showing the spectral units of these areas. Upper panel: 2.03 μm band. Middle panel: RGB composite of the same spectro-images (with R: 5 μm; G: 2.03 μm; B: 1.08 μm). Lower panel: RGB composition of the PCs showing most of the surface contribution for the three areas. The white box includes the pixel selections of the 'bright' RoI and the black the 'dark'.

In conclusion, it appears that the combination of PCs, their eigenvectors and eigenvalues in the outcome image, and the RoI selection, is the best approximation and gives us confidence of the results. However, the selection of appropriate channels from the original

dataset is of significant importance as well. Before engaging the PCA method as an investigation, concentrated only to the infrared spectrum of the datasets, I have used it in an alternative way by using the seven narrow methane spectral windows centred at 0.93, 1.08, 1.27, 1.59, 2.03, 2.79, and 5.00 μm, wavelengths in which the methane absorption is weak, giving access to Titan's lower atmosphere and surface and in their adjacent bands. This caused error to our results since, for instance, in the Tui Regio case, the 0.93 channel and its two adjacent ones overlap between the visual spectrum of VIMS (Visual) and the infrared (IR), causing issues to the projection of the PCs and PCA image. Spotting and understanding the nature of this problem urged us to use only the IR spectrum, thus 256 channels from the original VIMS dataset. Figure 6.17 shows the PCA result images from the previous approximation in comparison to the new –more suitable one.

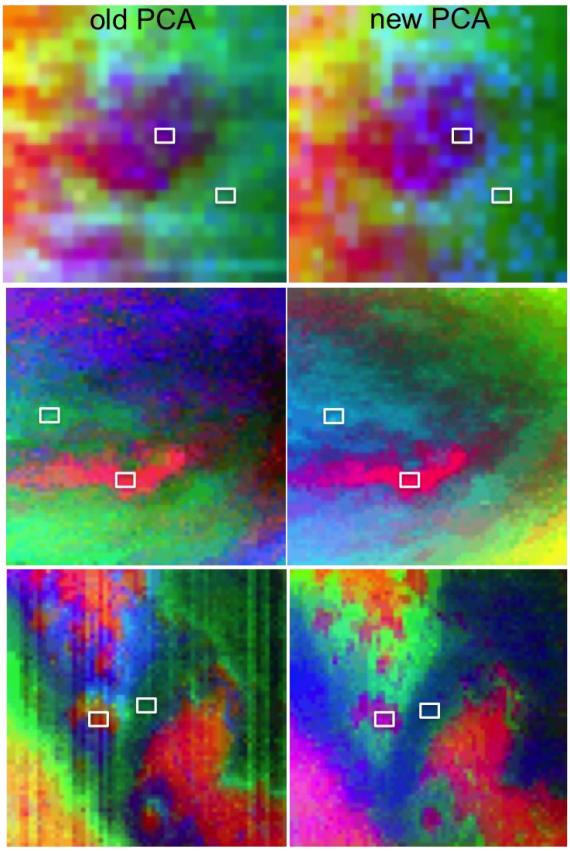

Fig. 6.17 – PCA images using 21 channels of both Visual and IR spectrum (left column) and 256 IR (right column).

It seems that, more or less, the method distinguishes the same spectral units among the datacubes as before, although with (at some cases) differences in their limits. For instance, at Hotei Regio the red spectral unit that corresponds to the actual Hotei feature is less extended to the west with respect to the old PCA image.

Additionally, for a follow up work that I present on Chapter 7, I have used the bright RoIs of each area (Hotei Regio, Tui Regio and Sotra Facula) for the study of the temporal variation of the areas. Figure 6.18 shows that the bright RoI is the same at all datacubes in the temporal investigation (2005-2009) of Tui Regio (Solomonidou et al. 2013c).

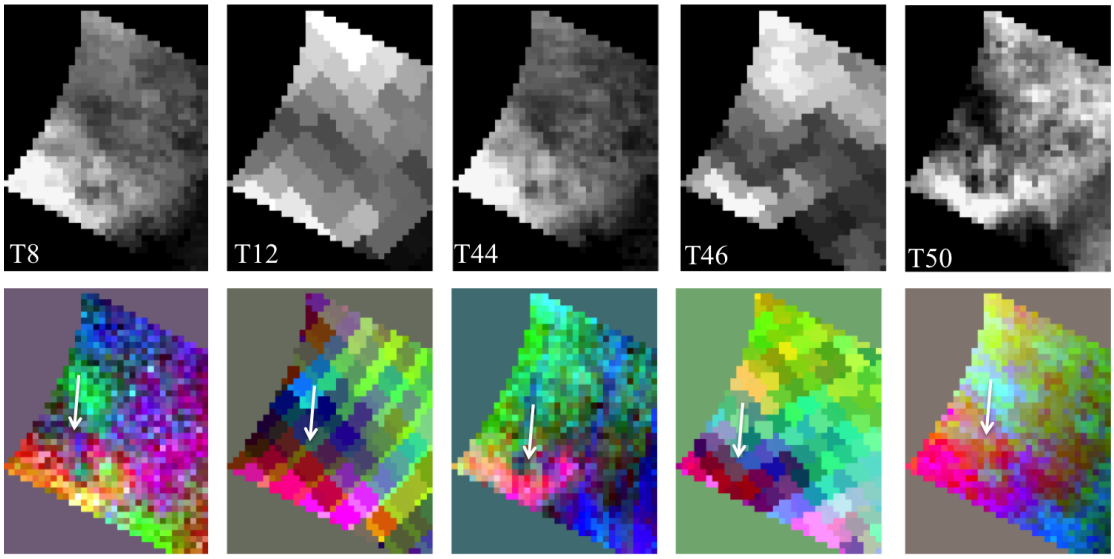

Fig. 6.18 - (upper row) Tui Regio from five VIMS datacubes (T8, T12, T44, T46, T50) at 2.03 μm using geometric projection (i.e. same projection parameters: spatial resolution, projection center, resampling method). (lower row) Same datacubes after PCA application. The PCA images distinguish 2-3 spectrally different areas (depending on the spatial resolution) identifying the bright region (RoI) in the Tui Regio area in red color as in Solomonidou et al. 2013b.

Finally, as mentioned earlier, I use the RoIs selections (Fig. 6.16) with RT code analysis to simulate the spectra and retrieve the surface albedo (see section 6.4).

6.3 Atmospheric Subtraction

On Chapter 5 and in the section 6.2.1 in this Chapter, I explained the necessity concerning the de-convolution of atmospheric and surface information in the VIMS data. My first attempt is presented here and published in the *International Planetary Probe Workshop proceedings (IPPW-7)*. I have used this method without the use of PCA.

I have used an empirical method of atmospheric effects correction and photometric analysis (see Chapter 5 for details on the method), that recreate the constraint factor on the surface chemical composition (e.g. Coustenis et al. 2001; Ádámkovics et al. 2009). With this method, the effect of the contribution of the atmosphere within the atmospheric methane windows is reduced, in order to better focus on the real alterations in surface composition, by comparing the spectral behaviours of these regions. We consider the centre of the methane window as the "surface" image, while the channel from the closest methane "wing" diagnoses best the "atmospheric" contribution.

I am using two original and calibrated Cassini/VIMS datacubes for Tui Regio and Hotei Regio (Chapter 3, Table 3.4, #4 and #5). I apply the method of the subtraction of the atmospheric component (Fig. 6.19b;f) from the images acquired from the centre of the atmospheric methane window (Fig. 6.19a;e) where we expect the surface contribution to be predominant, though nevertheless hampered by the atmospheric interference (Coustenis et al. 2005). This method has managed to reduce the effect of the contribution of the atmosphere within the atmospheric methane windows (Fig. 6.19c;g).

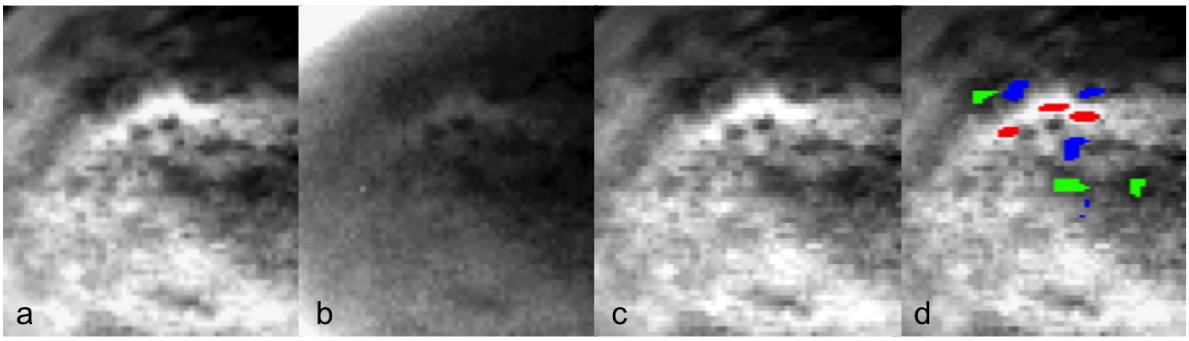

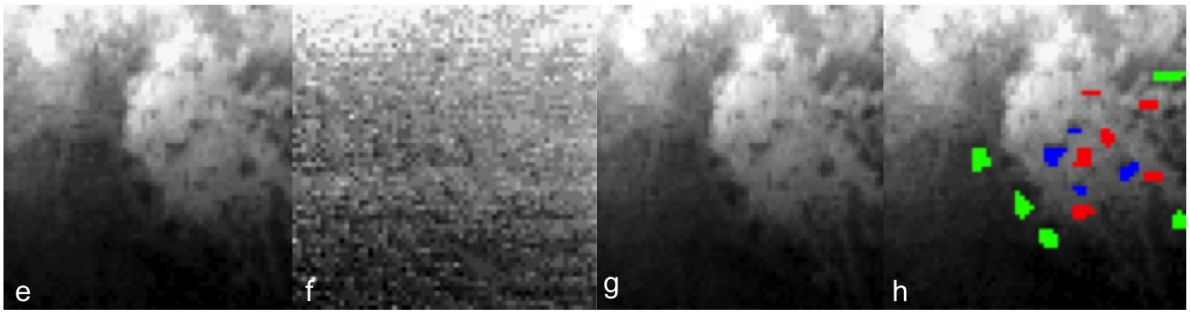

Fig. 6.19 - The "surface" at 2.03μm (a & e) and "atmosphere" at 1.96 μm (b & f) references used to compute unaffected surface images (c & g). (upper) Tui Regio and (lower) Hotei Regio. Figure 2d and 2h present the isolated areas using simple albedo evaluations. In (d) red corresponds to bright regions, blue to gray and green to dark. In (h) red corresponds to bright, yellow to gray and black to dark.

The Tui Regio images, after atmospheric subtraction at all wavelengths, are presented in Fig. 6.20 while Fig. 6.21 shows the I/F retrieval of the RoIs.

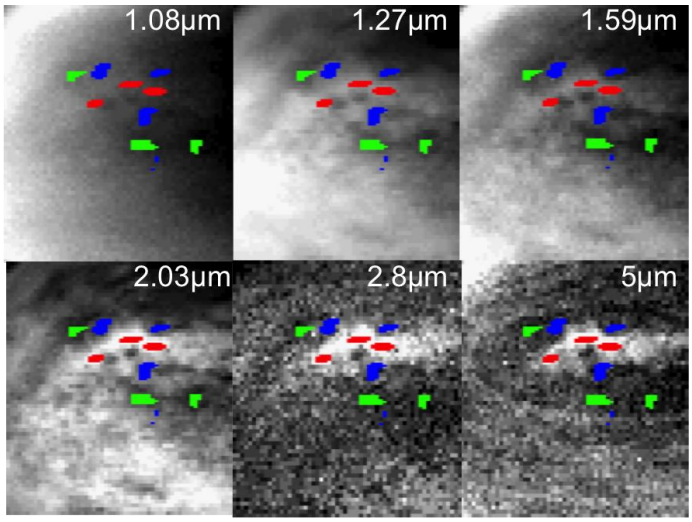

Fig. 6.20 - Subtractive images at six methane windows for Tui Regio and RoI selection. The 0.93 image subtraction returns a corruptive image and we did not took it into account in this research.

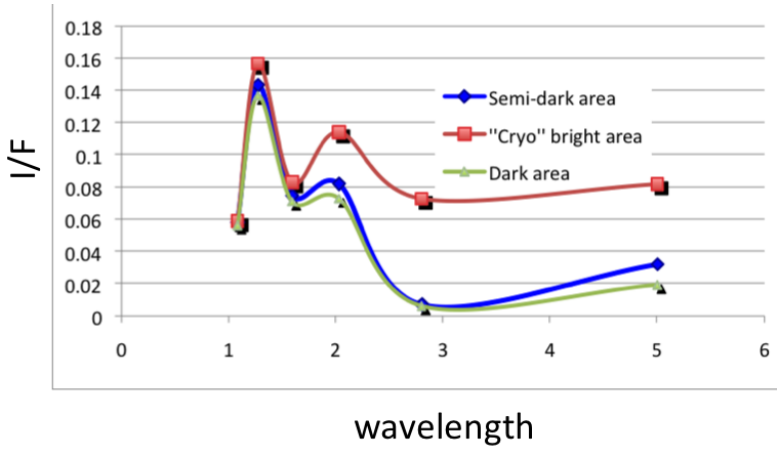

Fig. 6.21 - I/F of the major isolated areas as in Fig. 6.15 at all wavelengths for Tui Regio.

The plot of relative albedo after atmospheric subtraction, displays only six windows, as the atmospheric image at 0.93μm was corrupted. The 'Cryo' bright area (red) presents high I/F values, but is the very brightest only at longer wavelengths; obvious alterations are expected at 2.03μm, 2.79μm, and 5.00μm.

We treated Hotei Regio similarly (Fig. 6.22; 6.23).

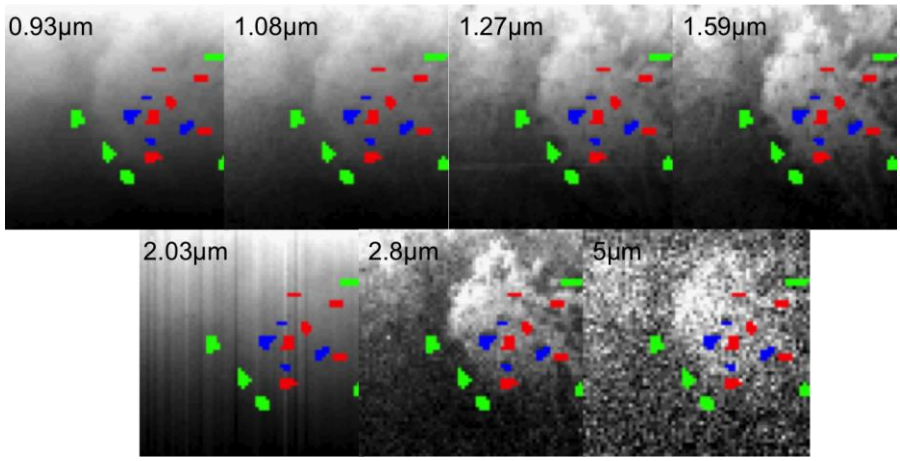

Fig. 6.22 - Subtractive images at the seven methane windows for Hotei Regio and RoI selection.

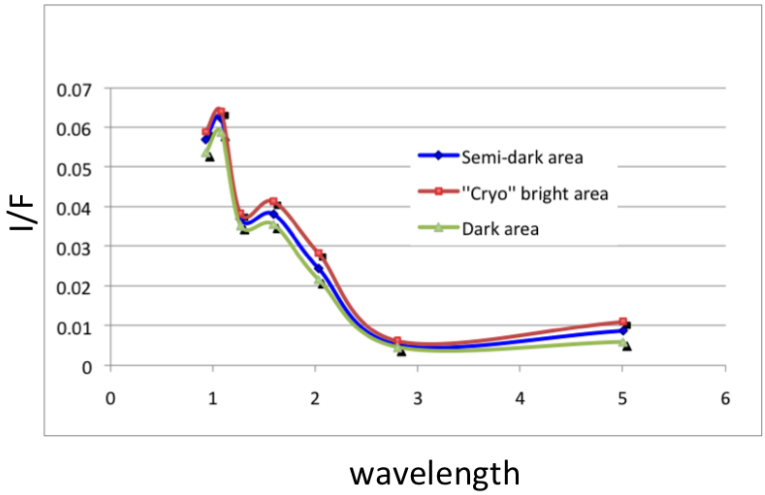

Fig. 6.23 - I/F of the major isolated areas as in Fig. 6.16 at all wavelengths for Hotei Regio.

The results, after applying the empirical method, showed that the effect and contribution of the atmosphere within the atmospheric methane windows could be reduced. We have isolated 3 distinct areas within Hotei Regio's possible volcanic field. We found that the areas seen as bright in the original data and suggested as cryovolcanic in origin, present high I/F values, especially at long wavelength. On the contrary, the surrounded dark areas present low I/F values at all wavelengths.

The diversity of I/F values suggests significant alterations in surface composition. Partially contrary to Tui Regio, Hotei Regio's spectral graph, indicates that the "Bright Cryo area" presents the highest I/F values and retains brighter than the other areas at all wavelengths. Impressively, the spectra from caldera-like structures present medium I/F values, lying almost in the average between the brighter ("volcanic area") and the darker ("primal surface") at most wavelengths. This is compatible with terrestrial caldera structures that consist partially of primal surface components in which the volcano is being built as well as new fresh material coming from the interior.

However, despite the attempt of separating the atmospheric contribution through subtraction, there are many artefacts in the method that are not constrained. Indeed, Kim et al. (2008) commented on the adequacy of the subtraction method, implying that artefacts are easily created and not enough precautions are taken to avoid over-interpreting them. While studying our subtraction results with the co-author Mathieu Hirtzig, there were many issues that made us question their quality. For instance, Fig. 6.19b shows that even though we are trying to subtract an 'atmospheric' image from a 'surface' image there is always a slight (or larger) contribution of the surface still present in the data, or there is a lot of noise hampering their quality (see Fig. 6.19f). Thus, the surface subtraction is not the optimum discovery tool for the surface investigation with VIMS data. Nevertheless some information on the surface properties can still be inferred.

A radiative transfer code could be efficiently used to monitor the haze population and retrieve the surface spectrum and that is the case I present hereafter and on which I base my most meaningful results.

6.4 Surface albedos from the Radiative Transfer (RT) code and results

The empirical method of atmospheric subtraction retrieve some surface information that according to the VIMS data properties and the complexity of atmosphere provide uncertainties and a radiative transfer code that clearly evaluates the atmospheric contribution and retrieves the true surface albedo is necessary. This is achieved through the extensive methane line lists that have recently been available and cover the infrared range longward of 1.263 μm (Hirtzig et al. 2013 and references therein). The combination of many line lists and the new methane absorption coefficients derived from the in situ Huygens/DISR measurements a complete Cassini/VIMS infrared spectra (0.8-5.2 μm) of Titan can now be fitted. A full description of the Radiative transfer code (RT) can be found in Chapter 5.

In this section I present the work that I currently submitted for publication in which I infer the associated spectral behavior and dynamical range of the surface albedos using a radiative transfer code, aiming to achieve a better understanding of the nature of the cryovolcanic candidates Tui Regio, Hotei Regio and Sotra Patera (Solomonidou et al. 2013b). Furthermore, I compare and calibrate the results from these three areas with analogous inferences for the Huygens landing site and compare them with previous publications.

In order to retrieve the surface properties from VIMS data of the areas of interest, I used, in combination, the procedures of PCA and RT that optimized results for these data and derived as much information as possible in terms of surface albedo and composition. On Chapter 5, I presented the procedure followed, in order to retrieve the surface albedo of the Huygens landing site, using the RT simulation.

I processed the RoIs that I selected, as seen in section 6.2.2, in Figure 6.16, of the three study areas, with our RT and retrieved the fit of the I/F spectrum for both bright and dark RoIs. As mentioned previously, our RT code allowed us to retrieve not only the surface albedo but also an estimate of the aerosols population, compared to the reference measurement by DISR, (shifted in the case of the HSL by a factor of 1, as shown in Fig. 5.16, section 5.3.2, Chapter 5). We then divided the 8 surface albedo points with those of HLS (Figs. 5.17, section 5.3.2, Chapter 5). In other words, I used the results from the HLS modeling to calibrate these regions. The following step comprises in producing the ratio of the bright RoI in each area with respect to the dark one.

6.4.1 Hotei Regio

We first used the RT code on the PCA RoIs of Hotei Regio data and obtained the best fits of the two RoIs as seen in Figure 6.24. The haze component in this case needs to be adjusted by 0.83 for the bright RoI and 0.78 for the dark RoI.

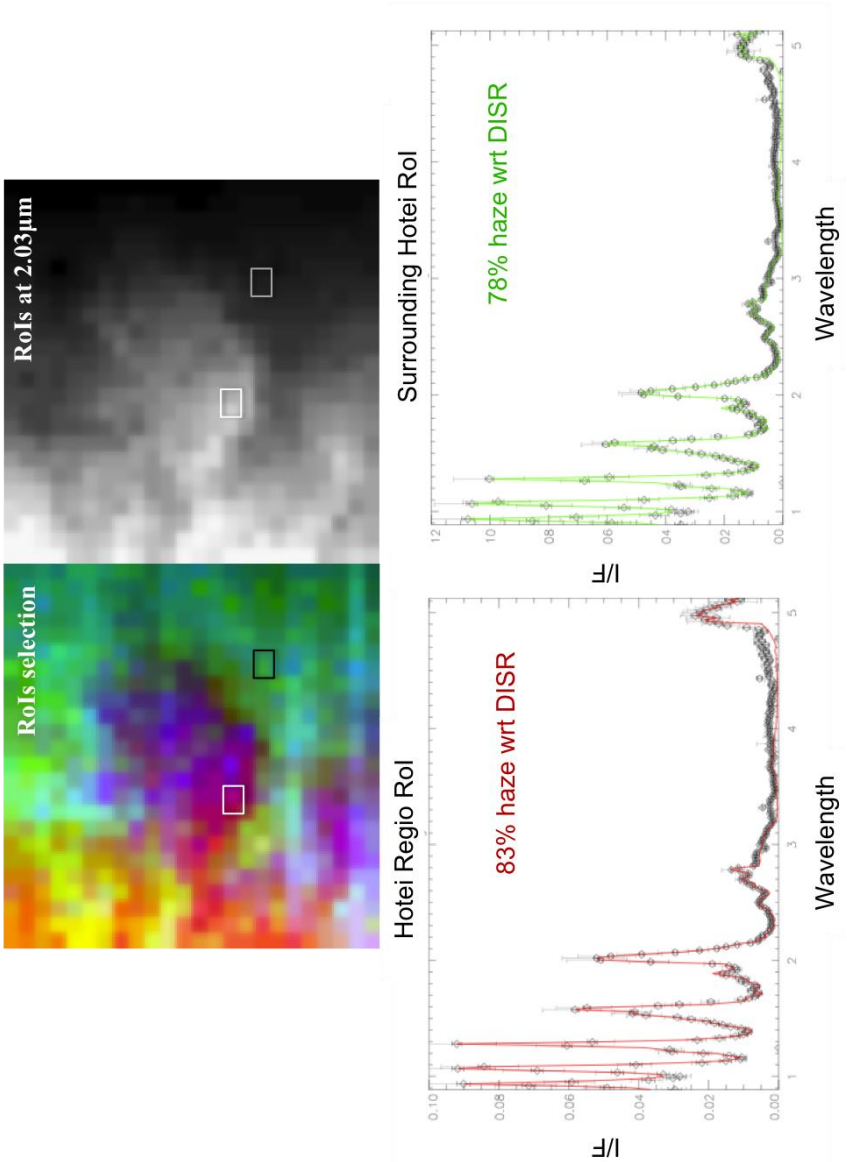

Fig. 6.24 - (upper panel) (left) Bright and dark RoIs from PCA (Hotei datacube #3a); (right) RoIs on gray scale; (lower panel) Best fit of the spectrum for Hotei Regio RoIs with the RT simulation in red for the bright region and in green for the dark surrounding region and VIMS data in black.

When the best fit is obtained we are able to retrieve the surface albedos of the RoIs as explained on Chapter 5 (Fig. 6.25).

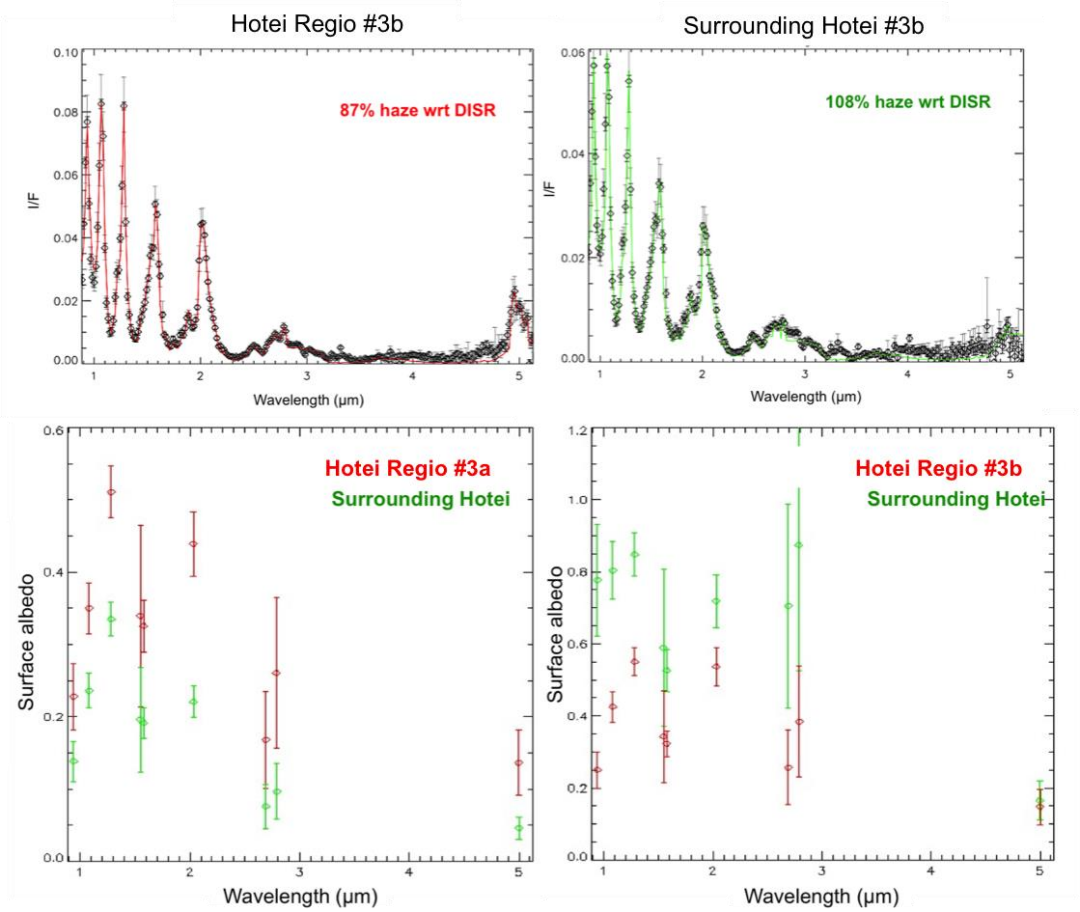

Fig. 6.25 - (upper panels) Best fits of the spectra for Hotei Regio RoIs from a datacubes that shows errors (#3b Table 3.4, Chapter 3). In Fig. 6.24 #3a returns sufficient results. (lower panel) RT simulations for both datacubes, in red for the Hotei Regio area and in green for the dark surrounding region as indicated by PCA. VIMS data are drawn in black. (lower) Surface albedo of Hotei Regio #3a (red) and the surrounding region (green) on the left and errors in surface albedo retrieval from datacube 'Hotei Regio #3b. Error bars from the data and the model parameters are also plotted for each wavelength.

We have been able to exploit only a subset of the currently available Hotei Regio data, which are in general not optimal in terms of geometry and thus not easy to analyse with the plane-parallel limitation of our RT code. We use the cube for Hotei Regio that we have found from the beginning of the mission until today, to have the best possible conditions (resolution 45km/pixel, incidence 67°, emergence 14°, and phase 81° degrees). That issue is also explained in Chapters 3 and 5. We obtained the best fits of the two RoIs from the RT model and then retrieved the surface albedos, as shown in Figure 6.25. The haze extinction profile reference in this case needs to be adjusted by a factor of 0.83 for the Hotei Regio RoI and 0.78 for the surrounding RoI.

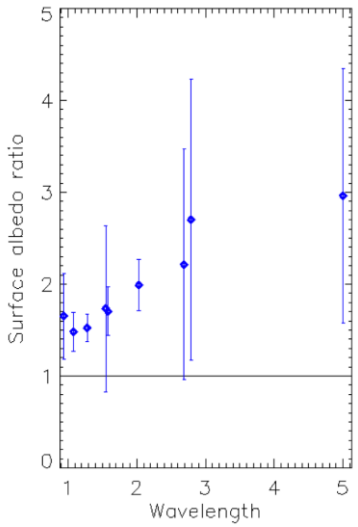

Fig. 6.26 - Surface albedo ratio of the bright region with respect to the dark region of Hotei Regio #3a. The line at 1 represents the surface albedo at the Huygens Landing site. Error bars from the data and the model parameters are also plotted at each wavelength (Solomonidou et al. 2013b).

The corresponding fits (shown in Fig. 6.25; 6.26) suffer from large uncertainty due to the fact that the observing geometry of the Hotei data reaches the limit of compatibility with our plane-parallel code (close to both the limb and the terminator, therefore with an incidence angle greater than 60 degrees) and lower spatial resolution than the other regions. Indeed, the code failed to work for some of the Hotei Regio datacubes processed with RT (returning a lower albedo for the bright areas compared to the dark ones, as shown in the lower right panel of Fig. 6) but produced a correct result for others. With all these caveats in mind, the retrieved surface albedo from the datacubes that work appears to be indeed higher for the Hotei Regio RoI than the surrounding one, especially at longer wavelengths (by a factor of 2 at 2.03 μm and up to a factor of 3 at both 2.69-2.79 μm and 5.00 μm). However, given the error bars we cannot firmly establish the difference in albedo between the two regions because even when the code works, our results for Hotei yield some times error bar larger than the ones for the other areas, which means that the VIMS data acquired for Hotei so far are not always adequate to be analyzed by simple methods (such as the Nelson et al. spectro-photometric analysis or our plane-parallel radiative transfer approximation). This could be remedied in the future with better quality observations of this area, or with a more sophisticated code.

6.4.2 Tui Regio

We treated Tui Regio similarly and obtained qualitative results since the geometric conditions and the spatial resolution are compatible to our code. Figure 6.27 shows the surface albedo of the RoIs.

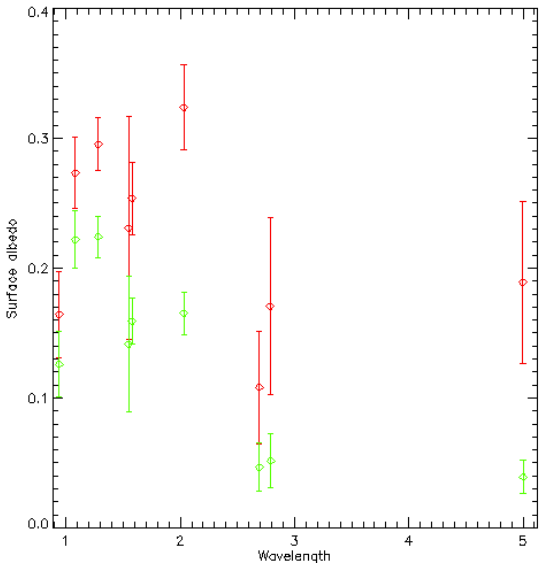

Fig. 6.27 - Surface albedo retrieval of the Tui Regio RoI (red) and its surrounding RoI (green).

For the Tui Regio RoIs, the RT code indicates that the aerosol population is 0.70 times the HLS one for the bright RoI and 0.75 for the dark. The differences in brightness between the two selected regions are large, especially at the longer wavelengths. In detail, there is a monotonic increase in difference of surface albedo, particularly at 2.03μm, 2.79 μm, and 5.00 μm by factors of 2, 3, and 5 respectively, with larger uncertainties for the latter two wavelengths (Fig. 6.28).

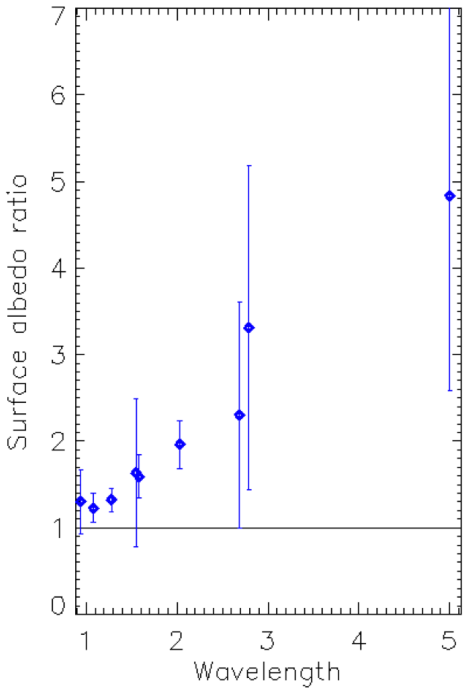

Fig. 6.28 - Same as Figure 6.26 but for Tui Regio.

6.4.3 Sotra Patera

From Figure 6.29 we can see that the red colored region that we considered as the bright RoI is constantly brighter than the green colored RoI up to a factor of 2-4, depending on the wavelength, with the largest differences around 5 μm, which is the spectral region; also identified as more sensitive to surface brightness (Barnes et al. 2005; Wall et al. 2009). The RT code indicates that the aerosol population for the bright and the dark RoI is 0.93 times the HLS one.

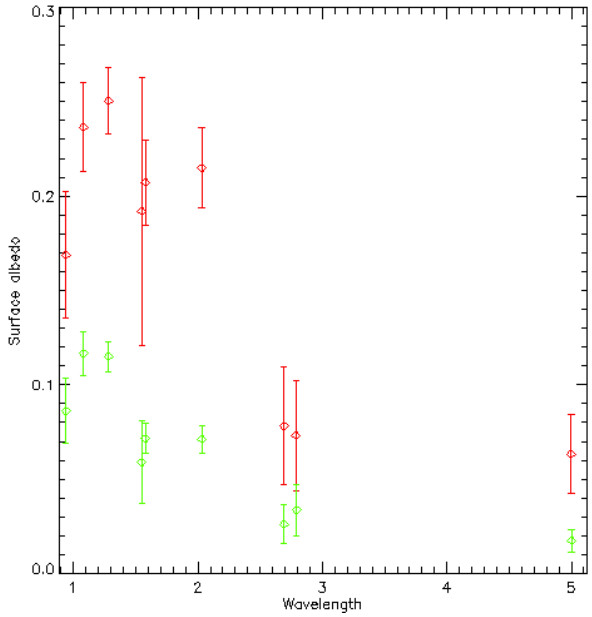

Fig. 6.29 - Same as Figure 6.25 but for Sotra Patera.

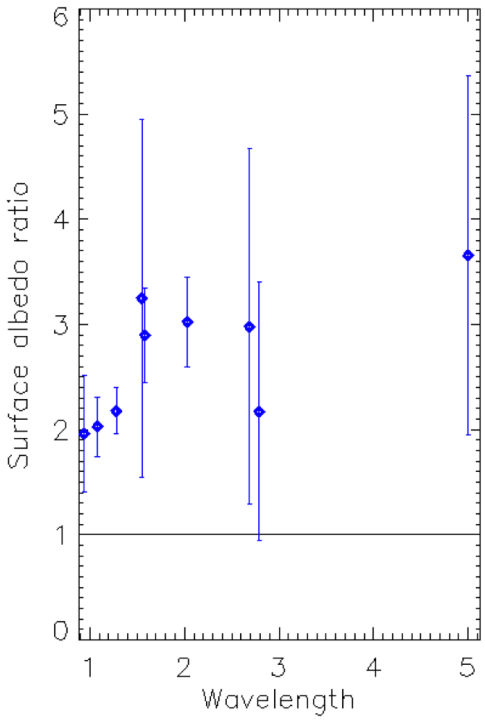

Fig. 6.30 - Same as Figure 6.26 but for Sotra Patera.

6.4.4 Comparison between Tui Regio and Sotra Patera

We have compared the surface albedo of Tui Regio and Sotra Patera from data acquired within a period of 3 months (for Tui Regio March 2006, for Sotra Patera December 2005), thus close in time. To do so we divided the surface albedo of the bright RoI of the Tui with the corresponding one for Sotra and we also performed the ratio for the dark regions. The results are shown in Fig. 6.31.

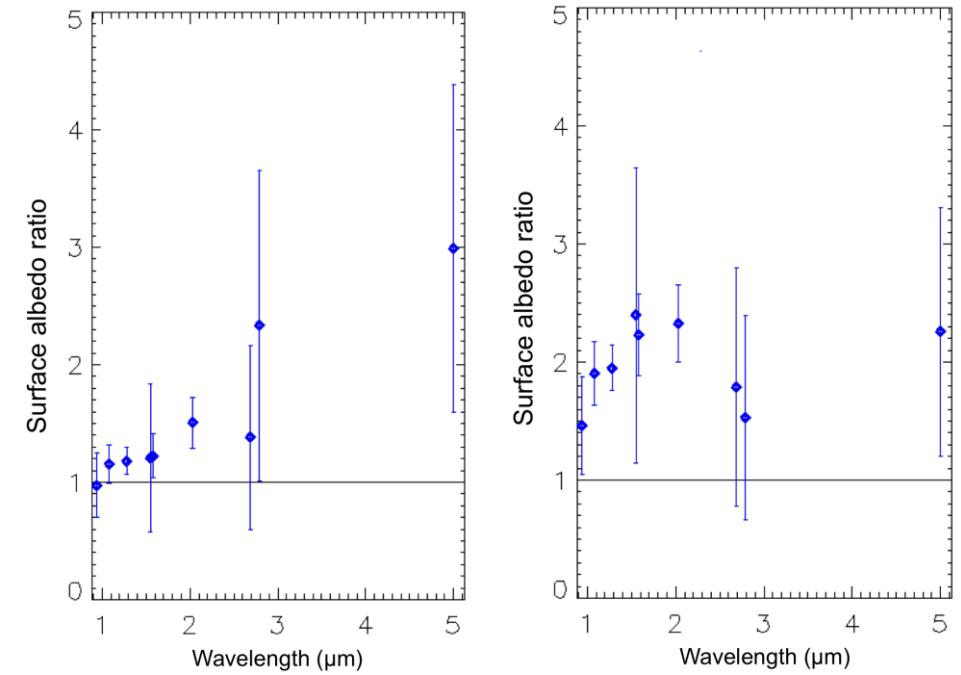

Fig. 6.31 - Surface albedo ratio of Tui Regio with respect to Sotra Patera for the bright regions (left) and the dark regions (right).

We discovered that Tui Regio is always brighter than Sotra Patera for the dark and for the bright regions. In the case of the dark regions, the ratio spectrum is rather flat with the Sotra Patera RoI being 1.5-2 times darker than the Tui Regio almost everywhere. For the bright RoIs, their brightness difference increases constantly with wavelength (Fig. 6.27) with factors higher than 2 at 2.79 μm as well as at 5.00 μm. While the permanent difference in brightness could be due to morphological variations, the distinct spectral behavior is probably a good indicator of differences in the components of each region. On the case of the rather flat dark ratio spectrum, a bright surface constituent with no particular spectral behavior (no strong bands) in the near-IR, present in the Tui Regio, is consistent with the data.

This in depth spectroscopic analysis, as presented gradually here (from subtraction to radiative transfer), provides important information concerning the nature of three favourable cryovolcanic candidates (Solomonidou et al. 2013b). However, the identification of the

regions as cryovolcanic, fluvial, etc., requires further analysis of these surface albedos, and more importantly, correlation with the areas' morphology. Such information comes from the Cassini RADAR data. A preliminary analysis of RADAR/SAR data (see Chapter 3) of the three aforementioned areas is presented in the following Chapter 7.

6.5 Implications on the surface composition

On Titan there have been suggestions for the presence of some simple ices, tholins and organics and even NH3 in relation to an internal liquid water ocean (Fig. 6.32).

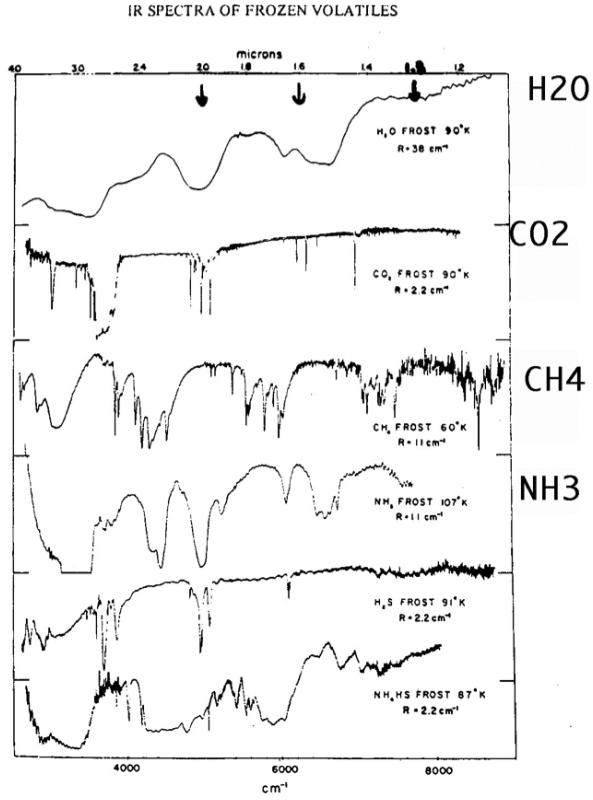

Fig. 6.32 - Suggestive composition of Titan areas.

H_2O, tholins, and CO_2 could have arrived on Titan's surface from comet impacts (Kress and McKay, 2004) and cryovolcanic deposition for CO_2 (Barnes et al. 2005) and NH_3 (Nelson et al. 2009). These compounds have been suggested from ground-based and VIMS spectroscopic evidence (Griffith et al. 2003; Coustenis et al. 2006; McCord et al. 2006; 2008; Negrao et al. 2006) (Fig. 6.32). In addition, higher order organics such as HC_3N, $C6H_6$, have also been suggested to be present on Titan (Clark et al. 2009). Moreover, some candidate 'antifreeze' substances include primitive and hydrothermal volatiles, such as NH_3, CH_4, CO, CO_2, and N_2; chondritic salts and acids, $MgSO_4$, Na_2SO_4, $(NH_4)_2SO_4$, H_2SO_4, and primitive and hydrothermal organics, CH_3OH, and $(CH_2O)_n$ (Lewis, 1971; 1972; Tobie et al. 2012).

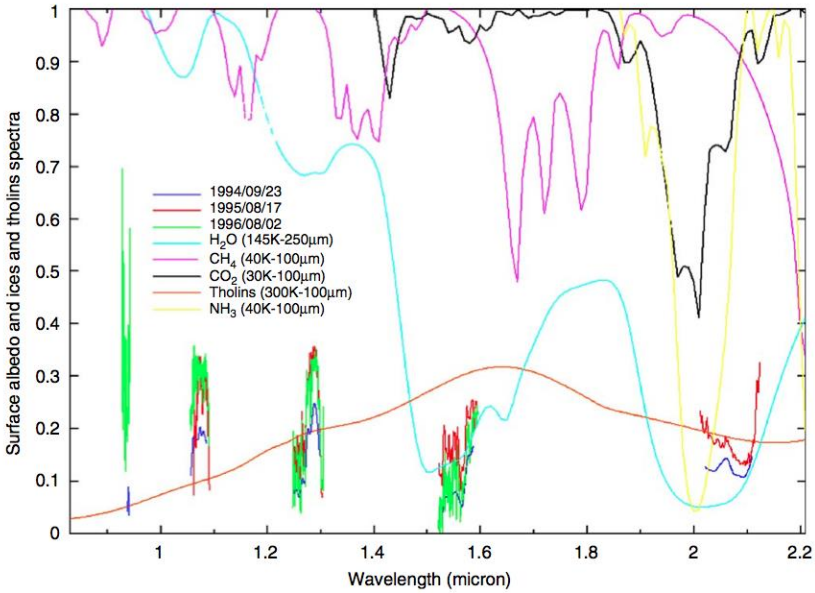

Fig. 6.33 - Surface albedo of Titan bright and dark areas at short wavelengths with comparison to candidate compounds (tholin in orange, H_2O ice in light blue, CH_4 ice in pink, CO_2 ice in black and NH3 ice in yellow) (Figure credit: Negrao et al. 2006).

Many suggestions have been made in regards to the chemical composition of the bright regions of Tui Regio and Hotei Regio (see Chapter 4), areas anomalously bright at 5 µm (Barnes et al. 2005). Tui Regio was analyzed in Hirtzig et al. (2013) (see Fig. 6.34 upper right panel) and Sotra Patera is currently under investigation (Lopes et al. 2013), while it seems that the identification of the bright material of the other two areas could also match or facilitate the investigation of Sotra Patera's bright region.

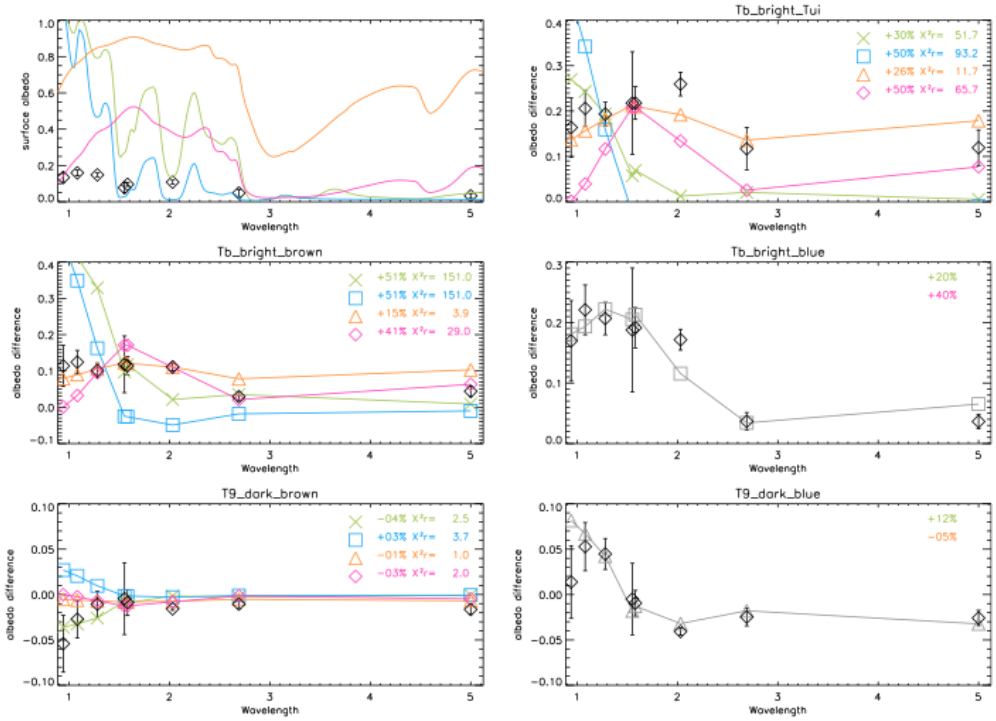

Fig. 6.34 - Interpretation of surface albedo variability of Titan areas. (upper left): HLS surface albedo spectrum compared to several forms of water ice (green: 100 µm grains; blue: 1000µm and tholins (orange:1 µm grains

and pink: 30 μm). In the other panels (one for each of the five RoIs: "Bright Tui", "Bright Brown", "Bright Blue", "Dark Brown", and "Dark Blue"), the black diamonds indicate the difference between the RoI and the HLS surface spectra, and the difference spectra are fit by adding/subtracting one of the four candidate material spectra at the expense of the HLS surface albedo. "Bright Brown", "Dark Brown" and "Bright Tui" can be reasonably fit by varying one component only. In contrast, "Dark Blue" and "Bright Blue" require combinations of surface components. In these cases (lower two right panels), the best fit is indicated by gray lines and symbols and the recipe is also indicated (Figure credit and information: Hirtzig et al. 2013).

Barnes et al. (2005) and McCord et al. (2006, 2008) proposed fine-grained recent deposits of CO_2 ice as a possible constituent for the bright regions of Tui Regio and Hotei regio. However, Soderblom et al. (2009) noted a shifting of the 5 μm feature from the laboratory CO_2 measurements that reduced the interest of this hypothesis. On the other hand, Fortes et al. (2007) suggested ammonium sulfate as a candidate material for the 5 μm regions and Nelson et al. (2009a) suggested depositions of ammonia as a possible explanation for Hotei Regio's reflectivity.

Additionally to general chemical composition indications, the analysis of the albedo can be used for the estimation of many important surface parameters, such as the mean dielectric constant and root-mean-square (rms) slope of the surface. Wye et al. (2007) estimated these parameters using data from the Cassini RADAR scatterometer at a wavelength of 2.18 cm. Furthermore, through Cassini RADAR reflectivity and emissivity measurements, Zebker et al. (2008) showed large-scale variations in radar brightness that are mainly diagnostic of composition and structure within Titan's near subsurface. A temporal study on VIMS data by Nelson et al. (2009) reported significant 2 μm albedo changes from 2004-2006 data of the Hotei Arcus (part of Hotei Regio area) feature, indicating cryovolcanic activity. This has been refuted by Soderblom et al. (2009), where they found a number of albedo markings in the area attributing them to a complex set of geological processes but with no changes in albedo with time.

For the areas of interest that I presented above, the surface albedo retrieval cannot alone identify the regions as cryovolcanic and further analysis of the albedos in terms of chemical composition is required. Additionally, for a holistic knowledge of the nature of the areas, the surface composition is not the only aspect that needs to be identified. Analysis of RADAR data and determination of the morphology of the different areas is necessary.

6.6 Conclusion remarks

This study, in which I have used the basic tools (i.e. PCA, Radiative Transfer) of my PhD, has focused on the investigation of Titan areas, namely Hotei Regio, Tui Regio and Sotra Patera, in order to analyse and interpret the data gathered from the VIMS instrument. Preliminary PCA results from VIMS data of the areas indicated that, spectral heterogeneities do exist among specific regions of interest (RoIs) (Solomonidou et al. 2010). Further and more explicit application of PCA on the same data confirmed the aforementioned indication and led us to the isolation of two RoIs, one bright (from the actual feature) and one dark (from the surroundings), from each area. Then, with the use of a radiative transfer code (RT), which I use, we retrieved the true surface albedos and their ratios (with respect to the HLS surface albedo –see Chapter 5) from the bright and dark RoIs. This enabled us to evaluate the dynamical range in surface albedo between them.

First, we found that the currently available Hotei Regio data are in general not optimal in terms of geometry and thus not easy to analyse with the plane-parallel limitation of our RT code. The surface albedo retrievals from all study areas showed that, the bright RoIs are brighter at all wavelengths than the corresponding dark RoIs, something that reassures us that the method works; and also tested in the test case (see Chapter 5). The distinctly lower albedo of the dark regions coincides rather closely with the HLS surface albedo, within a factor of 1.5 or so. This confirms that HLS is a rather dark region (e.g. Rodriguez et al. 2006).

The surface albedos inferred here for bright/dark ratios of all studied areas, display their largest variation long ward of 2 μm and mainly at 5 μm, with factors of 3 increase (for Sotra Patera) and up to a factor of 5 (for Tui Regio). Hence, all the bright regions of the candidate areas seem to be anomalously bright at 5 μm, again in agreement with previous studies (Barnes et al. 2005, 2006, 2007b; McCord et al., 2006, 2008; Soderblom et al., 2009). Moreover, comparing the retrieved surface albedos from Tui Regio and Sotra Patera, we can see, in addition, that Tui is always brighter than Sotra, with the largest surface albedo difference at 2.79 and 5 μm, up to a factor of 3. Tentative interpretation of Tui Regio's surface albedo variability with the use of the RT code has been performed in Hirtzig et al. (2013) (Fig. 6.34). There, the best fit of bright Tui Regio corresponds to an excess of 26% of small tholins.

The chemical diversity among the regions of interest here indicate that endogenic and/or exogenic processes acted in the area and resulted by depositing material of different chemical composition over the primary terrain (surrounding RoI). Settling of atmospheric aerosols over geological timescales suggest we should expect a global spectral homogeneity of the surface. Yet, one finds more and more localized heterogeneities, especially in the areas studied here. Such localized surface differences, with respect to the surrounding areas, are possibly due to the presence of secondary material and the result of recent (regarding the rate of re-homogenization by aerosol settling) material depositions and redistribution in surface composition (e.g. Soderblom et al. 2009). The three study areas analysed here have been considered as cryovolcanic candidates (Lopes et al. 2013 and references within). However, we cannot currently identify the type of process that formed these areas since cryovolcanism on Titan – even if the satellite seems to have the favourable conditions- is still an open issue and the so far acquired Cassini data does not provide conclusive evidence. However, the possibility for an exogenic origin of the areas is weakened by the absence of such surface heterogeneities in other locations where rain is present.

In the next Chapter, I extend the application of those methods to a more time-dependent VIMS data and try to extract information on the chemical composition of the regions and their nature, as well as on their evolution with time. I also introduce a preliminary RADAR data analysis.

In the future, I aim to combine chemical composition inferences, from these surface albedos, with morphological information from Cassini RADAR data that would help further constraining the origin and nature of these regions, as well as other surface regions on Titan.

Chapter 7

Possible surface activity on Titan from VIMS and RADAR data

Following up the investigation presented in the previous Chapter 6, I present here my work on the temporal surface albedo variations from VIMS data and a preliminary RADAR-based investigation of the same areas. This work has been presented in various international conferences such the *Division for Planetary Society* (DPS -2013), the *European Planetary Science Congress* (EPSC -2012; 2013) and more. In addition this work is now submitted for publication (Solomonidou et al. 2013c).

I investigate here the three potentially "active" areas on Titan's surface (Hotei Regio, Tui Regio and Sotra Patera, see Chapters 4 and 6), i.e. locations possibly subject to change over time (in brightness and/or in color etc) which, as showed in the previous Chapter, present significant surface albedo heterogeneities from their surroundings and anomalous brightness at 5 μm. In addition, claims of brightness changes with time from a previous study (Nelson et al. 2009a) also incited me to study these areas through their albedos evolution as a function of time, by use of our Radiative transfer code with the new methane absorption coefficients, to see if the claims were true and also to extend the previous analyses.

As mentioned before, we have already analyzed Cassini VIMS data of these three areas to identify distinct regions therein (through PCA techniques) and infer surface albedo information (See chapter 6 and Solomonidou et al. 2013b), albeit at a given period in time. Similarly but more extensively, we apply here our radiative transfer method to look for variations of the surface albedo with time, using the Huygens landing site region as 'ground truth' for calibration purposes.

Finally, I present a processing of RADAR data from the aforementioned regions (albeit partial coverage) with the TSPR filter and provide information concerning their texture

7.1 Reports on possible active regions on Titan

The presence of methane in significant quantities in the atmosphere of Titan and its preservation limit due to photodissociation in 10-30 Myr (Atreya, 2010), require a methane reservoir that resupplies the atmosphere with methane. The detected lakes concentrated in the Northern hemisphere (Stofan et al. 2007), appear to be very limited in total amount of liquid methane on the surface and not a valid reservoir (Sotin et al. 2012). Several studies have therefore suggested the existence of undersurface methanofers in various forms (the first such theories were by Stevenson 1992 and Lunine et al. 1999). The replenishment of Titan's atmosphere in methane coming from the interior may be the result of cryovolcanic activity (Tobie et al. 2005; Lopes et al. 2013).

7.1.1 The implications for surface active regions on Titan

Some of the areas monitored by the surface investigators of Cassini have been proposed as potentially "active" regions, meaning that they exhibit changes of their brightness, albedo, shape, size, level, or any other such characteristics as a function of time. The testimony of such changes can be found in t geological and/or spectral differences from the surrounding terrains. Indeed, Titan is a dynamic system in which we may find short or long-term variations of the surface caused by fluvial, aeolian, atmospheric and possibly endogenic processes. The Cassini mission since 2004 has found examples of current or past activity, such as:

- lake-level changes of Ontario Lacus and changes in the surface albedo of Arrakis Planitia, possibly due to evaporation (Barnes et al. 2009; Turtle et al. 2011a;b).
- possible changes in the fluvial deposits on Titan (Burr et al. 2012).
- the presence of distinguishable interdunes in both RADAR and VIMS dune observations (Barnes et al. 2008). Like on Earth the interdunes possibly represent the substrate surface layer that the displacement of dune material should blanket with time. The presence of both dunes and interdunes on Titan probably indicate current surface activity in these areas (Barnes et al. 2008).
- changes in the appearance of some surface areas as for instance in Hotei Regio in the leading hemisphere (Nelson et al. 2009a,b) and in the south of Belet in the trailing hemisphere (Turtle et al. 2011b). In the latter case darkening of an extensive surface area (500,000 km^2) was observed between 14-29 October 2010

and was attributed to wetting of the surface in the wake of a large rapid, low-latitude methane storm. It would also be compatible with aeolian modifications or effusive cryovolcanism although the timescales may be too short, the area too large and no cryovolcanic features have been observed in this area to date.

In what follows we investigate changes related to the appearance of some of the possible cryovolcanic candidate sites on Titan from VIMS data taken over the periods of time from 2005 to 2009.

7.1.2 Surface active regions on Titan with indications for endogenic origin

One of the mechanisms proposed as responsible for the changes mentioned in the previous subsection, is the possibility of existence of upwelling icy plumes i.e. cryovolcanism, as first suggested by Sotin et al. (2005) who analyzed a dome-like feature (Tortola Facula, 8.8°N, 143.1°W) from VIMS data. Such geologically interesting areas have since been suggested in other studies and from more extensive VIMS and RADAR data analyses. In particular, among others, Hotei Regio, Tui Regio and Sotra Patera have been proposed as cryovolcanic candidates by a number of studies using both VIMS (for spectral variability and possibly chemical composition variations) and RADAR (morphology, geology) data (e.g. Barnes et al. 2005; 2006; Lopes et al. 2010; 2013; Nelson et al. 2009a; Soderblom et al. 2009; Sotin et al. 2005; Wall et al. 2009). Studies that analyzed SAR and RADAR data including topographic, morphological, and stereogrammetric information suggest the presence of many volcanic-like features resembling terrestrial analogues (e.g. Kirk et al. 2009; Soderblom et al. 2009; Lopes et al. (2013) in these areas (see Chapter 10 for analogues). According to Lopes et al. (2013) additional strong possibilities for cryovolcanism are Ara Fluctus (40°N, 118°W), Western Xanadu flows (10°S, 140°W), Rohe Fluctus (47°N, 38°W), “T3” flows (20°N, 70°W), and Tui Regio (20°S, 130°W). A thorough description and discussion on the geology of Hotei Regio, Tui Regio and Sotra Patera can be found in Chapter 4, section 4.1.4.3.

The composition of the material referred to as cryomagma on Titan’s surface is still unknown, due to the lack of adequate measurements and in depth investigations, which may reveal its properties. However, the fact that all three candidate areas most probably contain cryolava flows is of particular importance due to the elevated temperatures they offer when they are active. In a research study, Davies et al. (2010), modeled the upper-surface heat removal for Titan's case. They concluded that the cooling of a lava flow was not caused by

radiative heat loss but from atmospheric convection. The statement of the cryolava flows from the time of deposition depends on the local climate as well as the flow thickness that controls the speed of solidification. Such a process resembles Earth's marine volcanic edifices named 'Pillow lavas' where slow extrusion provides enough time for a thick crust-shell to form on all sides of a pillow lobe, and prevents individual pillows from coalescing into a sheet. Internally, the pillows are fed via a distributary system of interconnected channels. Within a few hours to a few days, depending upon the particulars of the situation, the lava has all frozen and the opportunity of finding higher temperatures has passed.

An alternative hypothesis for the formation of these regions and their characteristics could be that the features observed at Tui Regio are evaporitic deposits with non-internal connection (Barnes et al. 2011). In addition, other studies focusing on Tui Regio and Hotei Regio describe the areas as paleolake clusters (Moore and Howard, 2010) or fluvial or lacustrine deposits (Moore and Pappalardo, 2011), indicating rather an exogenic origin.

Nevertheless, the identification or the refutation of the presence of cryovolcanic phenomena on Titan is of tremendous importance.

7.1.3 The importance of surface variations identification

Methane on Titan seems to follow the same pattern as water does on Earth, with a cycle of evaporation, condensation, and precipitation. Its destruction through various atmospheric processes should have led to its disappearance a long time ago. Recent geophysical studies (e.g. Iess et al. 2012; Sohl et al. 2013) and models (Tobie et al. 2006) seem to indicate/suggest an active interior on Titan, which if confirmed, will also have astrobiological implications. The replenishment of Titan’s atmosphere in methane may then be the result of cryovolcanic activity (Tobie et al., 2005; Lopes et al., 2013). In other words, material with internal origin and via cryovolcanic eruptions (e.g. Tobie et al. 2006; Fortes et al. 2007; Choukroun et al. 2010; Sohl et al. 2013) emanating from volcanic regions could potentially provide the observed amount of methane.

If cryovolcanism is at play, it could form surface expressions similar to terrestrial volcanic structures such as calderas (circular or elliptical structures formed by the fractureless elevation of the crust), domes (typical crustal elevation within a volcanic crater), lobate flows (resembling terrestrial pillow basalts), and ejecta. It could also manifest itself by changes in the appearance of these areas, which could be detected at different times. Moreover, it could lead to specific spectral characteristics due to composition related to the material ejected from

the interior, which would be possibly different from the immediate surroundings and can be identified through spectroscopic and imaging investigations.

Three of the aforementioned regions, Hotei Regio, Tui Regio and Sotra Patera, are the only ones among the possible cryovolcanic sites for which we have sufficient VIMS data adequate for testing this hypothesis by spanning long periods of time. All of the aforementioned areas are located in the 15°S-30°S latitudinal zone. Such concentration in an equatorial zone is a major characteristic of active regions on Earth that overlay a zone of crustal weakness. The Sumatran fault zone (10°N-7°S), a trench-parallel strike-slip system, presents a terrestrial example of such zone of weakness, which is located close to the Earth's equator (Sieh and Natawidjaja, 2000). Indeed, a zone of crustal weakness is associated with tectonic 'interruptions', such as an extensive fault, which can function as an open 'pathway' for internal material to rise to the surface. Both Tui Regio (1500x150 km) and Hotei Regio (700x700 km) have comparable sizes, as they are massive structures that resemble terrestrial supervolcanoes (e.g. Yellowstone, USA). Additionally, Hotei Regio, Tui Regio and Sotra Patera display higher 5-μm reflectivity than any other region on Titan suggesting that their chemical composition distinct from other regions and that they possibly consist of cryovolcanic deposits (e.g. Barnes et al. 2005; Solomonidou et al. 2013a). Indeed, the suggestive association with tectonics (e.g. Solomonidou et al. 2013b) and the presence of volcanic-like features such as lobate flows, calderas, domes, a deep crater and radial faults (e.g. Lopes et al. 2013) enhance this hypothesis since these are indications of typical volcanic surface expressions.

For a more explicit description of the areas' morphology please see Chapter 4.

Whatever the formation mechanism, it would be useful to know whether or not these geologically interesting areas are currently or were recently active and therefore had sustained some form of dynamical geological activity in the past. We follow with a brief description.

In brief, for Tui Regio, isolated lobate flows with no connection to a specific vent-source have been observed (Barnes et al. 2006; Stofan et al. 2009). Hotei Regio also presents a system of lobate flows (Nelson et al. 2009a; Soderblom et al. 2009) that seem to be cryovolcanic in origin (Wall et al. 2009). Additionally, an even more distinct than Hotei Regio's terrain of accumulated lobate flows (Mohini Fluctus) exists within the Sotra Patera area that Lopes et al. (2013) suggested as 'bright-edged lobate unit'. Other than lobate flows, the candidate areas consist of tectonic-like features such as radial fault systems and calderas in Hotei Regio (Soderblom et al. 2009), trending dark linear marks as seen on VIMS data at Tui Regio (Barnes et al. 2006), and a mountain structure that could be a volcanic shield or a

dome (Doom Mons), a deep crater (Sotra Patera) at the general area of Sotra Patera (Lopes et al. 2013).

In Solomonidou et al. (2013b) we selected bright (the actual features of Hotei, Tui and Sotra) and dark regions (surrounding areas) of interest (called RoIs) in each of these areas through PCA and then inferred by radiative transfer analysis their surface albedos. This method was applied to some of the strongest cryovolcanic candidates Sotra Patera, Hotei Regio and Tui Regio. In this work, we use the bright regions from the previous study (see Fig. 6.17 as an example) and look for any reflectance variations with time that might correspond to surface changes.

7.1.4 The first area ever suggested to change due to cryovolcanism on Titan and why the first report was wrong

Since the first observations of Titan's surface by Cassini, Hotei Regio was signaled out because it showed - with respect to other bright regions - a very high signal in the 5 μm window (Barnes et al. 2005) and because it was suggested to change brightness (Nelson et al. 2009a) with time. In addition to the appearance alteration report, a study dedicated to its morphology using T41 and T43 RADAR data, advocated the presence of cryovolcanic lava flows younger than the surrounding terrain (Wall et al. 2009). Thus, on the one hand, the analysis of VIMS data monitoring Hotei Regio from 2004 to 2006, as published by Nelson et al. (2009a), suggested a reflectance (I/F) variability of the area over that time period, which the authors interpreted as indicative of surface activity. Nelson et al. (2009a) used an empirical method consisting in retrieving the surface reflectance variation by differencing the brightness of Hotei Regio with that of the surrounding region. They suggested that between July 2nd, 2004 (T0) and March 31st, 2005 (T4), the 2 μm reflectance of the area was multiplied by 2, then at October 27th, 2005 (T8) it decreased significantly, to rise again at December 26th, 2005 (T9) and decrease again later (January 14th, 2006 and onwards). This temporal behavior was found to be different from one wavelength to the other, with small variations around 1 μm and larger ones around 2 and 5 μm, leading the authors to further propose the presence of punctual ammonia deposits. Conversely, Soderblom et al. (2009) suggested that VIMS observations to that date had not provided compelling evidence for actual ongoing volcanic activity in Hotei Regio since the brightening effect could be due to observing conditions such as large emission angles (Table 3.4, Chapter 3) and blurring of the surface contrast by aerosol scattering especially in wavelengths smaller than 3 μm (see Fig. 5 in Soderblom et al. 2009).

7.2 Study of albedo variations on specific Titan areas

We use the PCA and RT methods as in the previous Chapter and in Solomonidou et al. (2013b). In that study, we had extracted one distinct bright and one distinct dark sirrounding region within #3, #4 and #5 VIMS datacubes from Table 3.4 (Chapter 3), applying the PCA method. Here, we use the same method and the same 'Bright' RoIs that correspond to the brightest portion of each area/datacube under investigation in the right conditions (Table 3.5; 3.6; 3.7, Chapter 3).

7.2.1 Observation and data

We use a selection of VIMS data that include our areas of interest and a datacube for the Huygens landing site (HLS) (see Solomonidou et al. 2013c), as well as an additional selection of datacubes for the two test case areas (Fig. 7.1). Tables 3.5; 3.6 and 3.7 in Chapter 3 presents the details for each datacube.

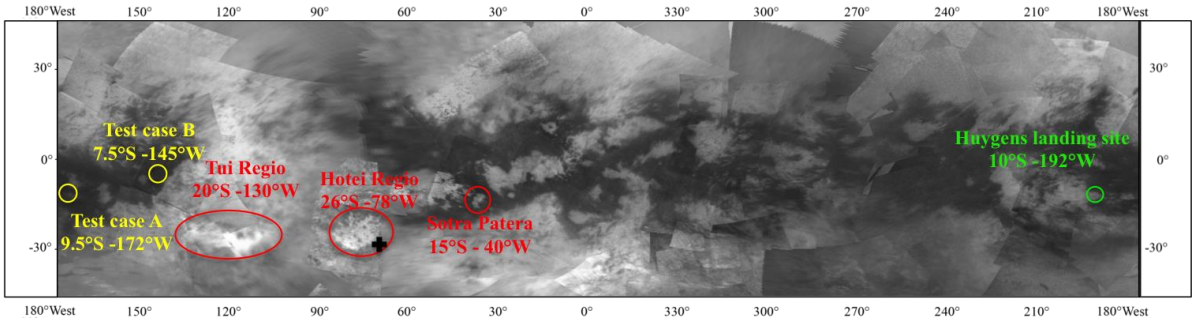

Fig. 7.2 - Areas of interest identified on a VIMS mosaic at 2.03 μm. The red circles and ellipses surround the candidate cryovolcanic areas namely Tui Regio, Hotei Regio, and Sotra Patera. The green circle indicates the Huygens landing site (HLS) area. The yellow circles indicate the test case areas 'Test case A' and 'Test case B' that provide reference to Tui Regio and Sotra Patera respectively and the black cross corresponds to one out of eight reference points that Nelson et al. (2009a) used in their analysis (Background map credit: Le Mouelic et al. 2012).

We process the same RoIs of all cubes of the three study areas with our RT and retrieve the fit of the I/F spectrum. As mentioned previously, our RT code allows us to retrieve not only the surface albedo, but also an estimate of the aerosols population, compared to the reference measurement by DISR. We then divided the 8 surface albedo points with those of HLS (Figs. 5.17, section 5.3.2, Chapter 5) that is used for calibration purposes.

In order to validate our code and confirm that the areas under study changed with time as isolated areas and not due to changes that affected the whole globe or massively a large part of it, we applied our code for approximately the same period of time on two test case areas far

away from Tui Regio and Sotra Patera. These correspond to dunes fields (expected to be homogeneously dark unless subjected to endogenic or exogenic processes) and located at 9.5°S, 172°W named 'Test case A' (for Tui Regio), and 145°S, 7.5°W named 'Test case B' (for Sotra Patera) (Fig. 7.1; Tables 3.6; 3.7 in Chapter 3). For Hotei Regio we use one of the eight reference points for each datacube as in Nelson et al. (2009a, Fig. 1(b)).

7.2.2 Analysis of Hotei Regio data (2004-2009)

In this section, we use our radiative transfer plane parallel code to assess the spectral and look for any temporal variations of these regions over the course of the Cassini 2004 – 2006 observations (reanalysis of the data used by Nelson et al. 2009a), and also with an extension to 2009 observations.

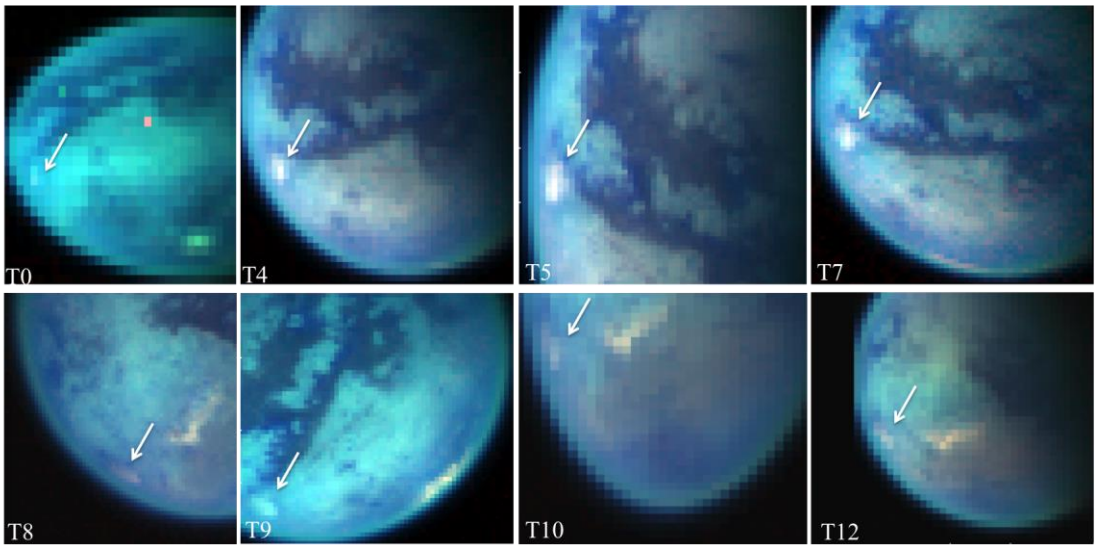

Fig. 7.2 - Images extracted from the datacubes used to suggest brightness variability with time of Hotei Regio by Nelson et al. (2009a). For each datacube a false color composite is shown focusing on the surface spectral variability (R=5.00 μm, G=2.03 μm, B=1.59 μm). Datacube properties are summarized in Table 1.

As seen in Table 3.5 in Chapter 3, and the images in Figure 7.2, we first of all identify some problematic issues with all the Hotei Regio datacubes from 2004-2009 that would impede the proper use of a radiative transfer code (at least in the plane parallel approximation which is our case) and even more so the application of a simple contrast method to the data. Indeed, the datacubes correspond to emergence angles and (until 2009) to incidence angles, larger than 60°. In particular, the cubes selected by Nelson and co-authors always present limb observations (Fig. 7.2), which are difficult to analyze with a plane parallel RT code. This was demonstrated in our analysis where we selected two regions, one in the middle of Hotei (RoI) and one South-East thereof (for the reference "neutral gray" area) (Fig. 7.1), as Nelson et al. did, extracting the spectra shown in Figure 7.3 (right). Additionally, the T0 VIMS

datacube that Nelson et al. 2009a used, was voluntarily rejected as it exploits only few out of the 352 channels and hence a radiative transfer analysis is not possible.

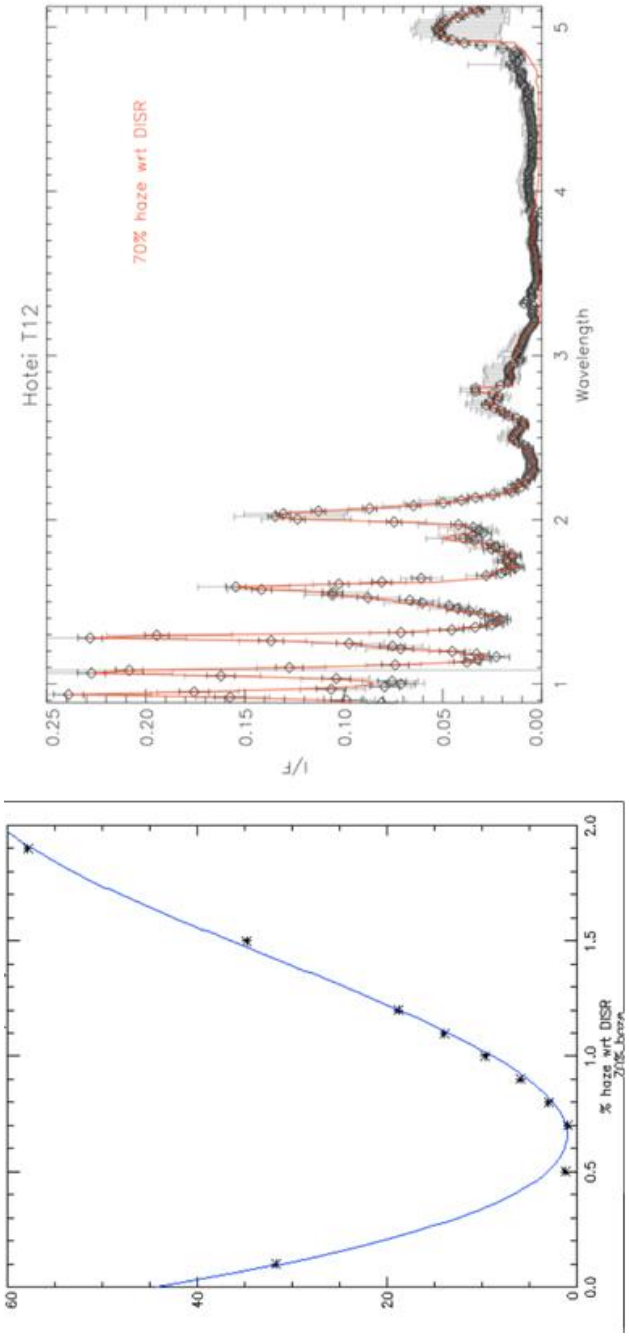

Fig. 7.3 - (left) Correlation between simulation (colored line) and VIMS data (black points) for the T12 datacube of Hotei Regio. (right) Best fit of Hotei Regio T4 showing all the methane windows (VIMS Hotei Regio data in black, and RT simulation in red).

Hotei Regio is very close either to the limb (high emergence angle, T4-T12) or to the terminator (high incidence angle, T49-T51), so that when we apply our RT code, we get at best large error bars difficult to evaluate. Figure 7.3 shows that even for the haze simulation we are not getting a good fit between the simulation and the data. Using the method described in Hirtzig et al. (2013), we inverted the surface albedos for both Hotei Regio and the reference

area (Fig. 7.4). In addition, Figure 7.5 shows the ratios of the Hotei Regio RoI and the reference area with the surface albedo of HLS.

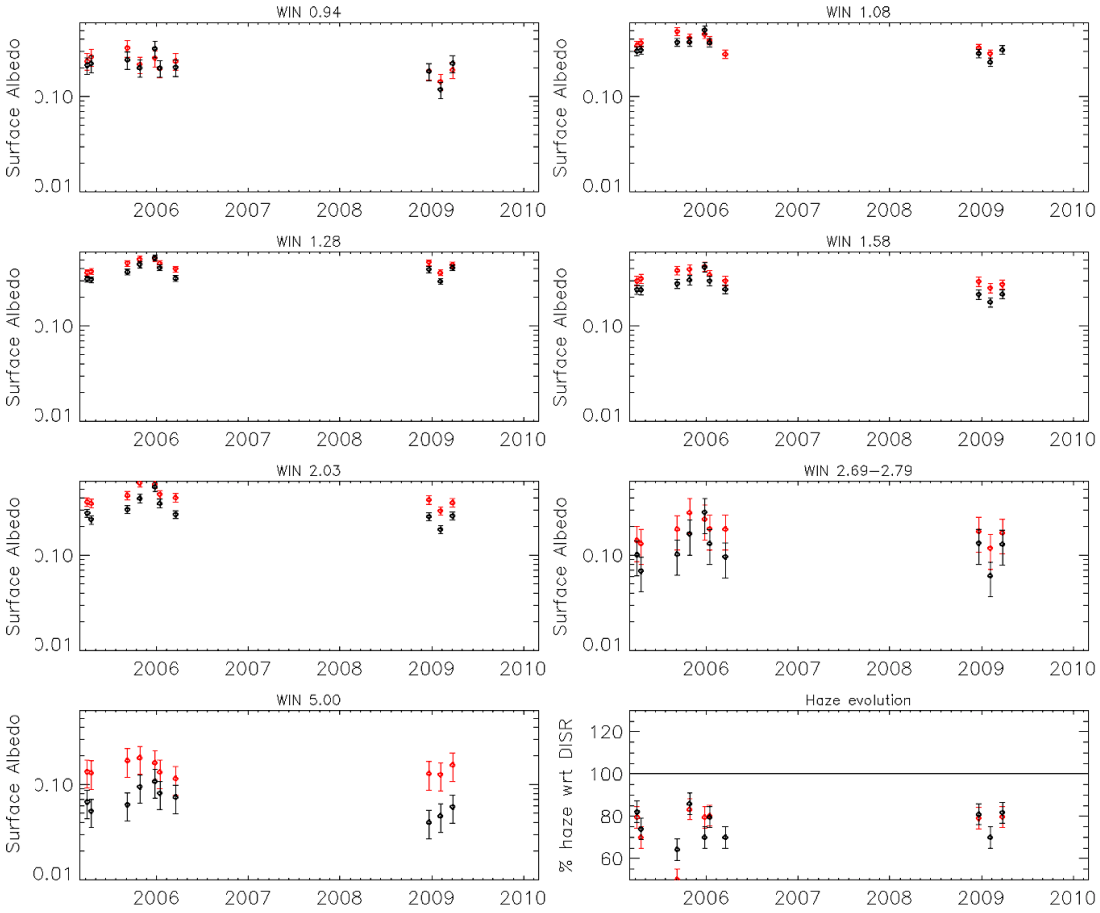

Fig. 7.4 - Time variation of the surface albedo obtained within each methane window and haze evolution with time. The red and black points correspond to bright Hotei Regio RoI and our test case (one of the eight points characterized as 'gray reference' in Nelson et al. 2009a, whose analysis stopped in 2006) respectively, and they coincide in time because we have used the same datacubes. Lower right is the haze content evolution over both areas for the same time period (with green is the haze evolution of HLS) (Solomonidou et al. 2013c).

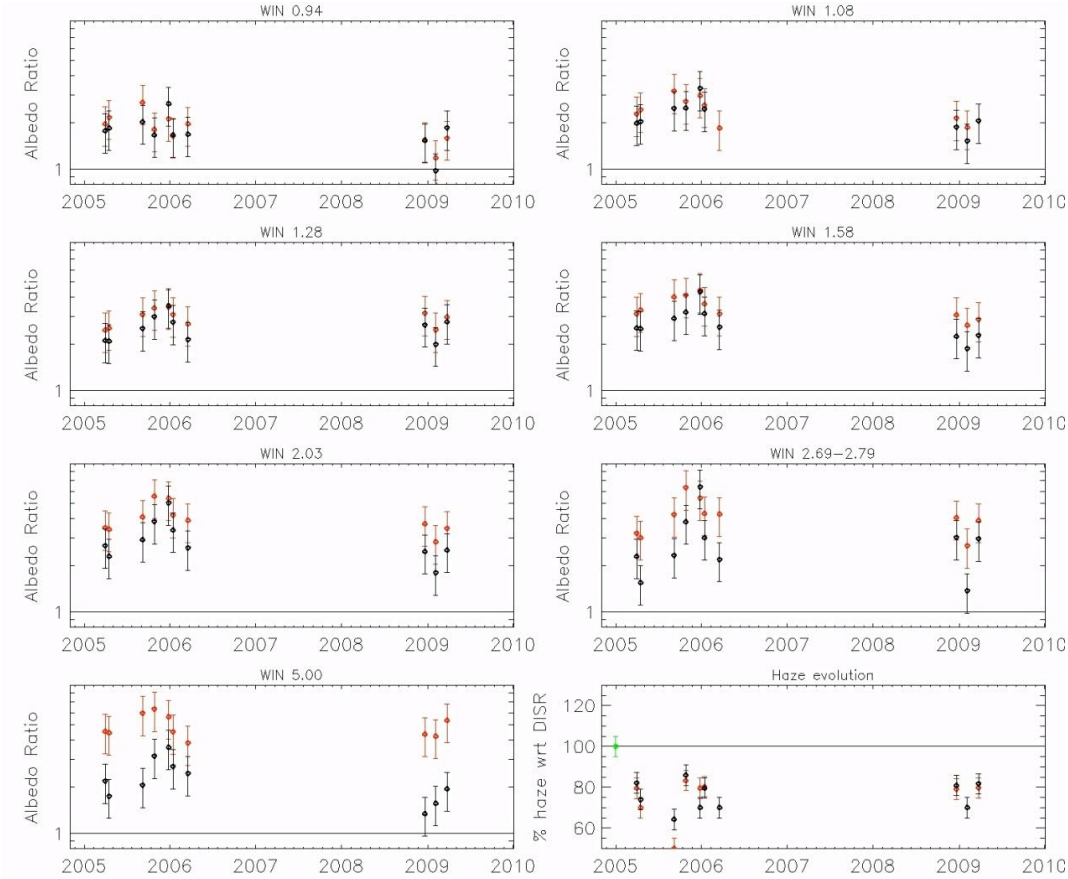

Fig. 7.5 - Time variation of the surface albedo obtained within each methane window with respect to HLS surface albedo from 2005 to 2009. The colored points correspond to the same as in Figure 7.5. The black line and green point correspond to HLS.

At first sight, the surface albedos seem to be varying intrinsically as a function of time for all the datacubes. This cannot be due to the atmosphere because the haze population is similar in all cases. All the surface albedos considered here including the reference area are higher than HLS. This difference is more pronounced at longer wavelengths (>1.6μm) with almost doubled values. Nevertheless, the two regions show a similar behavior (with the exception of the T9 reference area –more obvious in Fig. 7.5) versus time in each and every window. This trend may be a simulation artifact and/or a spatial resolution bias, since we use our plane-parallel code in very unorthodox conditions (i.e. large values of angles). The black spectrum of the reference point at T9 (12/2005) is brighter than at other dates because of the spatial resolution that forced us to encompass brighter regions in our selection of pixels. Hence, it seems that there is no significant spectral variation over time of Hotei with respect to the reference area. However, as noted in Solomonidou et al. (2013a) and earlier in this section, with the so far retrieved Cassini/VIMS data we cannot accurately test Hotei Regio temporally due to inadequate geometry properties with respect to our code.

As we shall demonstrate hereafter, there are other clues as to a possible activity in Hotei Regio (and in the other cryovolcanic candidates), like morphology and composition.

7.2.3 Analysis of Tui Regio (2005-2009)

We processed similarly Tui Regio data from October 2005 to February 2009 (see Table 3.6, Chapter 3). In order to validate our code and confirm that the area of Tui Regio changed with time as an isolated area and not due to changes that affected the whole globe or massively a large part of it, we applied our code to a test case area ('Test case A'), far away from Tui Regio that corresponds to a dune field at 145°W, 9.5°S, for approximately the same time period.

For that period of time, the analysis of the datacubes shows again a haze content lower than the DISR HLS results by ~25% (as for Hotei) for the bright RoI whereas the test case has a higher content until early 2008 (T41), joining the bright RoI haze by 2010. The Tui Regio RoI has 10% more haze at T8 than at any other date (see Table 3.6) (Fig. 7.6, lower right).

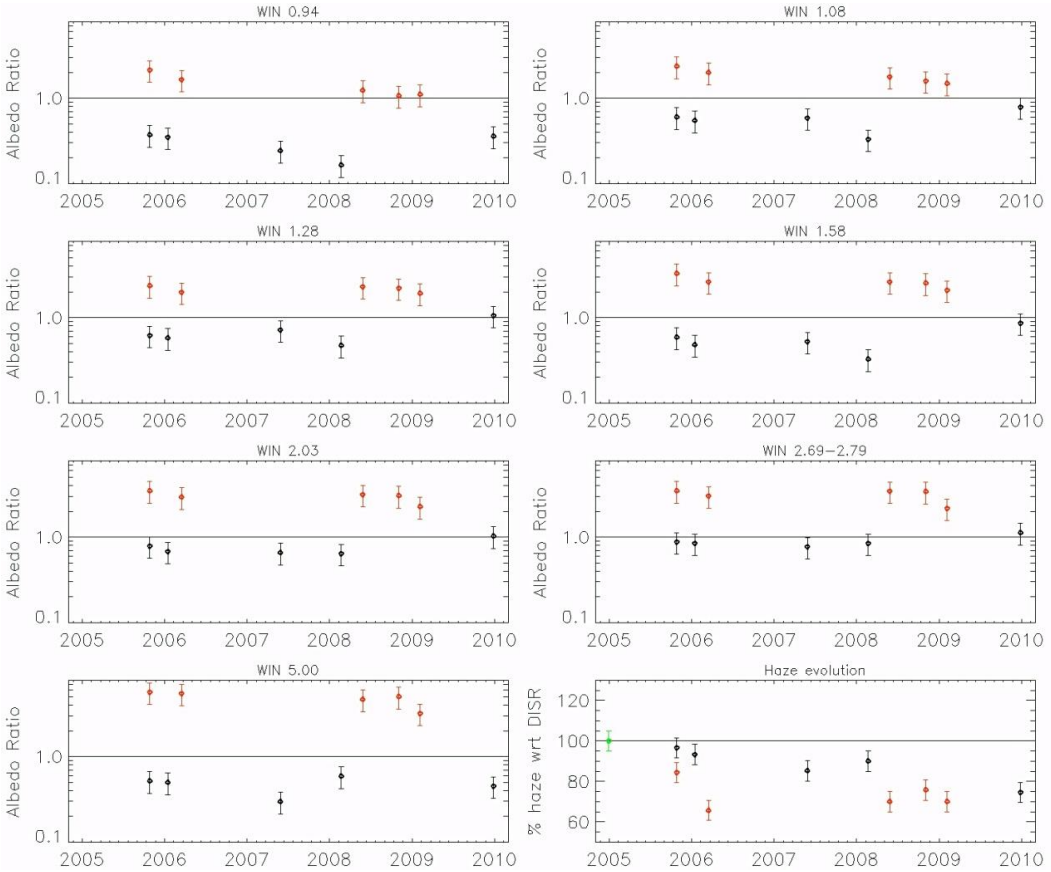

Fig. 7.6 - Evolution with time from 2005 until 2009 for Tui Regio area (in red) and test case A (in black) at all wavelengths. Lower right is the haze evolution over both areas for the same time period (with green is the haze evolution of HLS).

Furthermore, for the same period of time the analysis of the surface albedos show that Tui Regio appears darker by about 20-50% (Fig. 7.7).

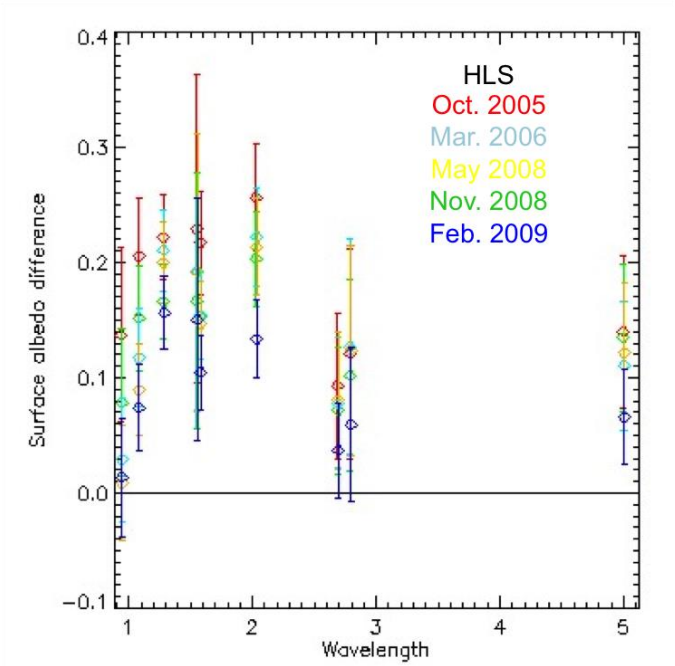

Fig. 7.7 - Tui Regio surface albedo differences with time from RT application on VIMS data with respect to HLS. The surface albedo starting from 2005 (red points) becomes constantly darker until 2009 (blue points).

During three years from 10/2005-11/2008 the evolution of surface albedo of bright Tui Regio is flat with consistently higher values than HLS by factors of 2-5 depending on the wavelength. The surface albedo is highest at 5 μm and lowest at 0.94 μm. Then during the T50 observations in February 2009 the bright Tui Regio appears persistently darker by 20-50% with respect to October 2005 date. The decrease is most significant at 1.08 μm and 5 μm by about 50%[29] where at these particular wavelengths the errors are 20% and 33%. The decrease is smaller but still significant in other wavelengths. The test case is always flat and there is no change with time while Tui Regio becomes darker with time by about 20-50%.

7.2.4 Analysis of Sotra Patera (2005-2006)

Similarly to Tui Regio, we processed Sotra Patera data from 2005 to 2006. We applied our RT code to the Sotra Patera area and to a reference area ('Test case B'), located far away from Sotra at 172°W-7.5°S, and corresponding again to a dune field. The surface albedo of Test case B does not change with time, presenting a homogenously dark dunes field, while Sotra Patera becomes brighter with time, up to a factor of 2 (Fig. 7.8). The results show that

[29] *A full description of the error bars can be found in section 5.3.2, Chapter 5*

the surface albedo appears to have increased within a year (2005-2006) by a factor of 2 (Fig. 7.9).

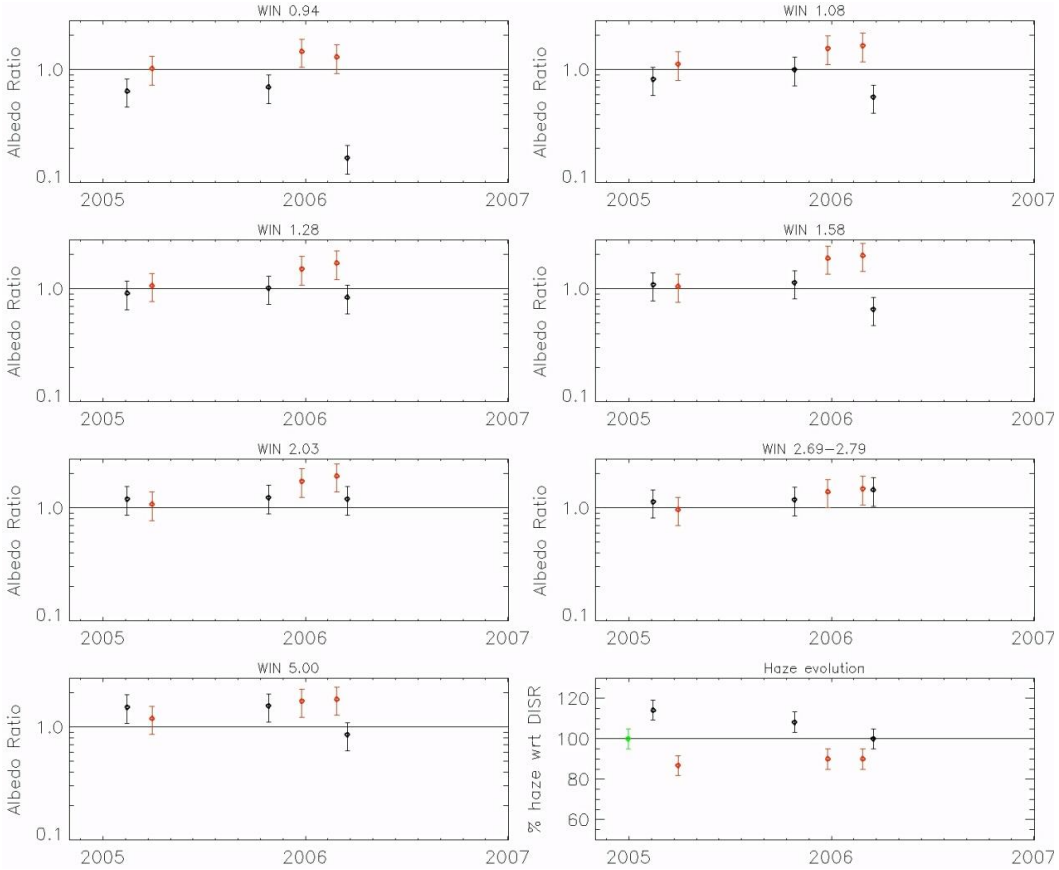

Fig. 7.8 - Evolution with time from 2005 until 2006 for Sotra Patera area (in red) and test case B (in black) at all wavelengths. Lower right is the haze evolution over both areas for the same time period (with green is the haze evolution of HLS).

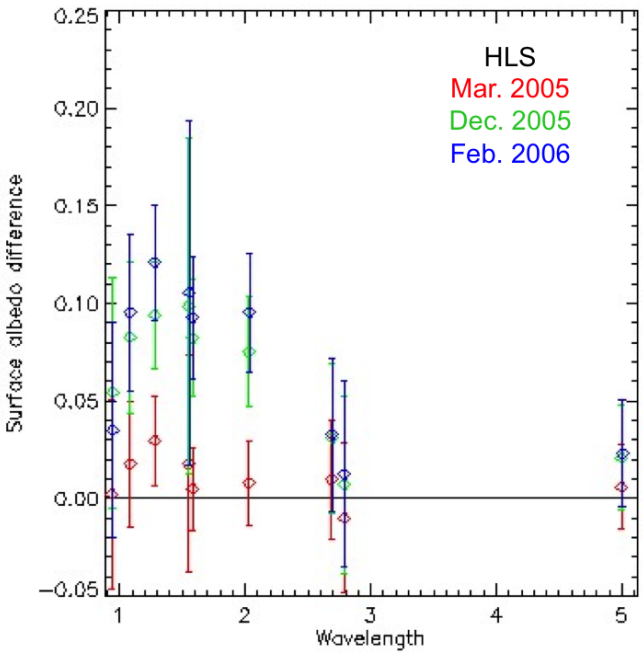

Fig. 7.9 - Sotra Patera surface albedo differences (with respect to HLS) with time from RT application on VIMS data from 2005 (red points) to 2006 (blue points).

Figure 7.8 (lower right) shows that the haze evolution of the test case presents a decrease by 14% within a year bringing it down to the DISR value. The bright RoI on the other hand, shows a flat haze evolution remaining lower by 10-14 % with respect to DISR.

For the bright Sotra Patera RoI, the general trend is an increase from March 2005 (with the same surface albedo as HLS) until December 2012 up to a factor of two for certain wavelengths (outside error bars) and then no change until February 2006. This brightening is not observed in the test case where in the contrary we seem to have a darkening (except for at 3 μm where the test case and the bright RoI seem to display similarly no albedo evolution) and so this adds some confidence to the result.

In conclusion, for both Tui and Sotra our results indicate possible surface albedo fluctuations, while the dune fields test cases did not show the same changes. This may be indicateive of surface activity with either exogenic or endogenic origin. However, our surface albedo retrieval cannot alone validate or refute the case for these regions to be cryovolcanic in origin. But, as noted in the previous Chapters 4 and 6, the morphology of the area itself is compatible with a volcanic association with the interior. This is even more the case for Sotra Patera, as pointed out by Lopes et al. (2013).

For the purposes of exploring this possibility and looking for morphological signs of volcanic activity in that region, to further support the theory of possible cryovolcanism, I thus conducted a study using RADAR data on which I applied the TSPR filter (see Chapter 5) and extracting information concerning the texture of the materials present in these areas. Nevertheless, combination of VIMS and RADAR (SAR and SARtopo) data that provide both compositional and morphological information from the same targeted areas are very important, while it consists one of the best analysis approaches for geological interpretations, according to the capabilities that the Cassini instrumentation provide.

7.3 The TSPR filter on RADAR/SAR data and results

I have processed Cassini/SAR images (Chapter 3) using the despeckle filter technique described in Chapter 5 in order to characterize in terms of texture the areas of interest and provide implications on the morphology. I have presented this work in oral and poster presentations in the *European Geosciences Union Annual General Assembly* in 2011, as well as in *the 14th Panhellenic Conference of the Greek Physicists Union* in 2012. The method in use here is published in a paper to which I contributed and appeared in the *Planetary Space Science Journal* (Bratsolis et al. 2012).

The RADAR data observations, as seen in Fig. 7.10, cover only a part of the area that is covered in VIMS data.

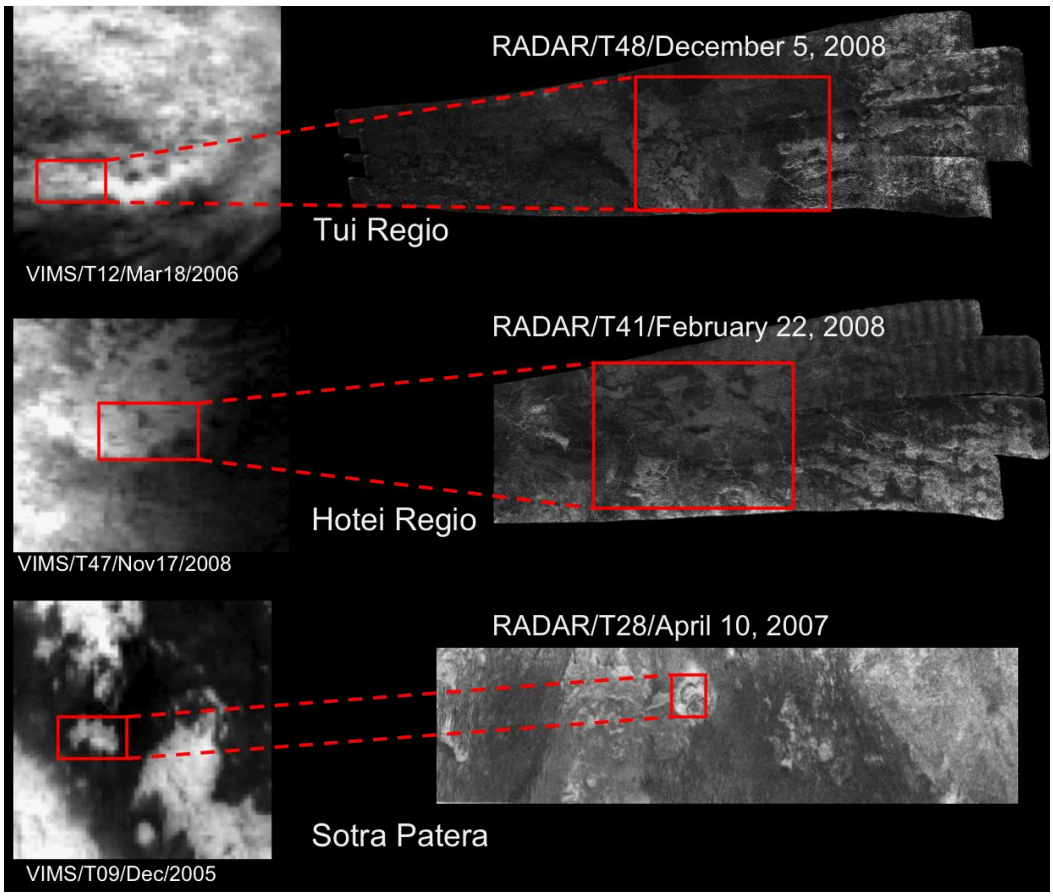

Fig. 7.10 - VIMS data (left) and the respective RADAR/SAR coverage data (right).

Texture, in geology, refers to the relationship between the materials of which a rock is composed. In this study we are looking at a specific parameter, the surface roughness. The surface texture depends on the cooling history of a surface terrain, the weathering conditions, the size of the grains of the present material and the relationship between that material and any background/primary material (e.g. Means and Park, 1994). We benefit here from a

method put together by Emmanuel Bratsolis used in Bratsolis et al. (2012), in which it was applied it to lakes. In this work, we use the TSPR filter in order to remove the speckle noise and optimize the data. Then, I select regions of interest (RoIs) based on radar brightness heterogeneities. The proportion of standard deviation and mean value as extracted from these RoIs provides the texture variability of each region (Bratsolis and Sigelle, 2003).

Fig. 7.11 shows a part of T41 RADAR swath illustrating a portion of Hotei Regio on the left and the same image after the application of the TSPR filter on the right that removes the speckle noise.

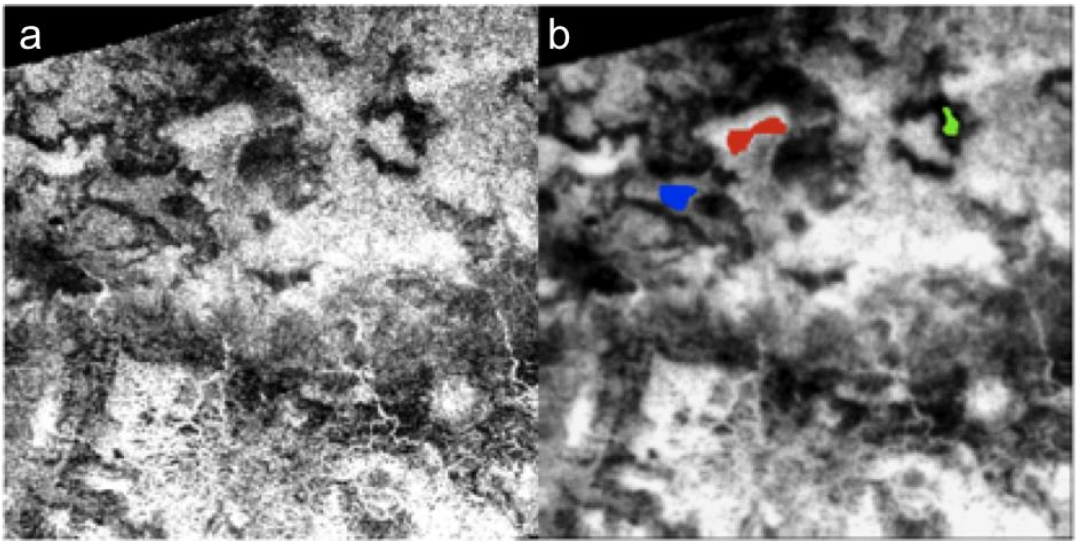

Fig. 7.11 - RADAR image of Hotei Regio (portion) adapted from the T41 swath. (a) Original RADAR/SAR image; (b) TSPR filtered image and isolation of areas with distinct brightness (Red: bright; Blue: intermediate; Green: dark).

From the values of standard deviation and mean, the type of a region's texture is inferred as in Table 7.1, 7.2 and 7.3 for Hotei Regio, Tui Regio and Sotra Patera respectively.

Table 7.1 - Texture variability from the selective regions (RoIs) of Hotei Regio. Green corresponds to dark radar region, Blue to intermediate and Red to bright.

Area	***Mean***	***Standard deviation***	***St. deviation/Mean***
Blue	167	10.16	0.060
Green	37	16.36	0.435
Red	219	11.24	0.052

In terms of texture variability, the red RoI (Table 7.1) presents low texture variability (smoothest), the blue RoI medium texture variability (mild) and the green RoI high (roughest). This means that the radar bright region is the smoothest in terms of texture and the radar dark region is the roughest.

Fig. 7.12 shows a portion of the RADAR/SAR T48 swath that covers a part of Tui Regio (rectangle). The western part of the field consists of relatively bright deposits that

appear to originate from radar-bright floored channels. On the southern part, the flows form figures that resemble dome-like structures, more likely coming from within the field rather from the channels. In addition, the lowest part resembles the flow region at Hotei Regio supporting the suggestion of cryovolcanic deposition within the areas of Tui Regio and Hotei Regio (Barnes et al. 2005).

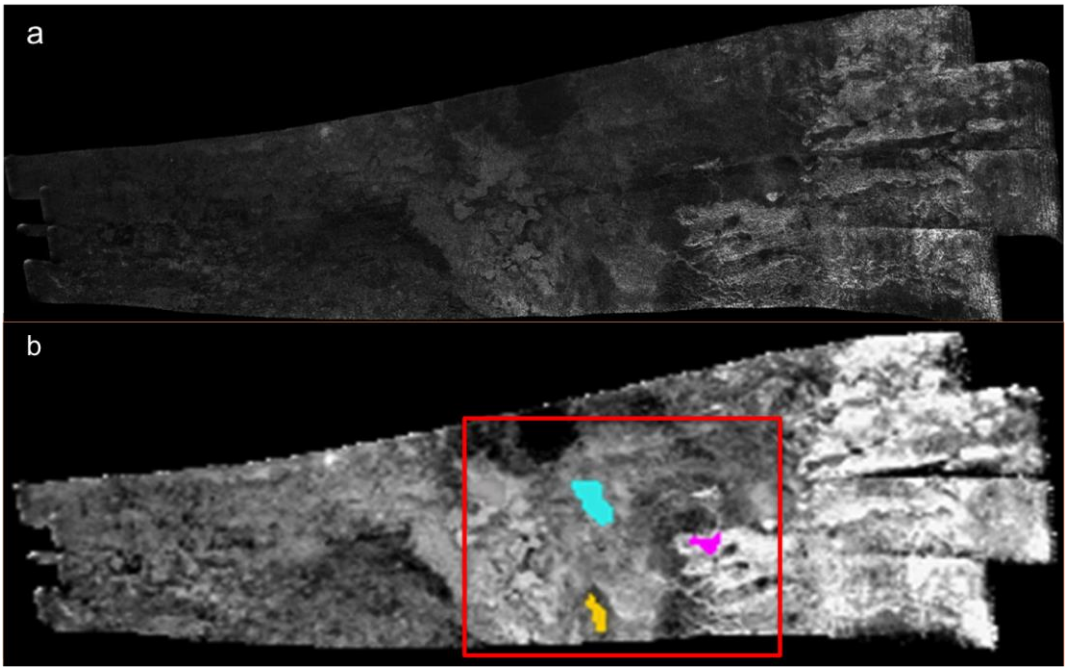

Fig. 7.12 - RADAR image of Tui Regio (portion) adapted from the T48 swath. (a) Original RADAR/SAR image; (b) TSPR filtered image and isolation of areas with distinct brightness (Magenta: bright; Cyan: intermediate; Yellow: dark).

For Tui's case, again three different RoIs were selected, and sorted by increasing texture variability from Cyan (smoothest), Magenta (mild), to Yellow (roughest) in Table 7.2.

Table 7.2 - Same as Table 7.1 but for Tui Regio. Yellow corresponds to dark radar region, Cyan to intermediate and Magenta to bright.

Area	***Mean***	***Standard deviation***	***St. deviation/Mean***
Cyan	175	4.63	0.026
Magenta	203	6.78	0.033
Yellow	158	6.62	0.042

From the table it seems that the radar dark region has the roughest terrain while the bright radar regions has an intermediate texture.

Lastly, Fig. 7.13 presents a portion of the RADAR/SAR T28 swath that covers the whole area of Sotra Patera.

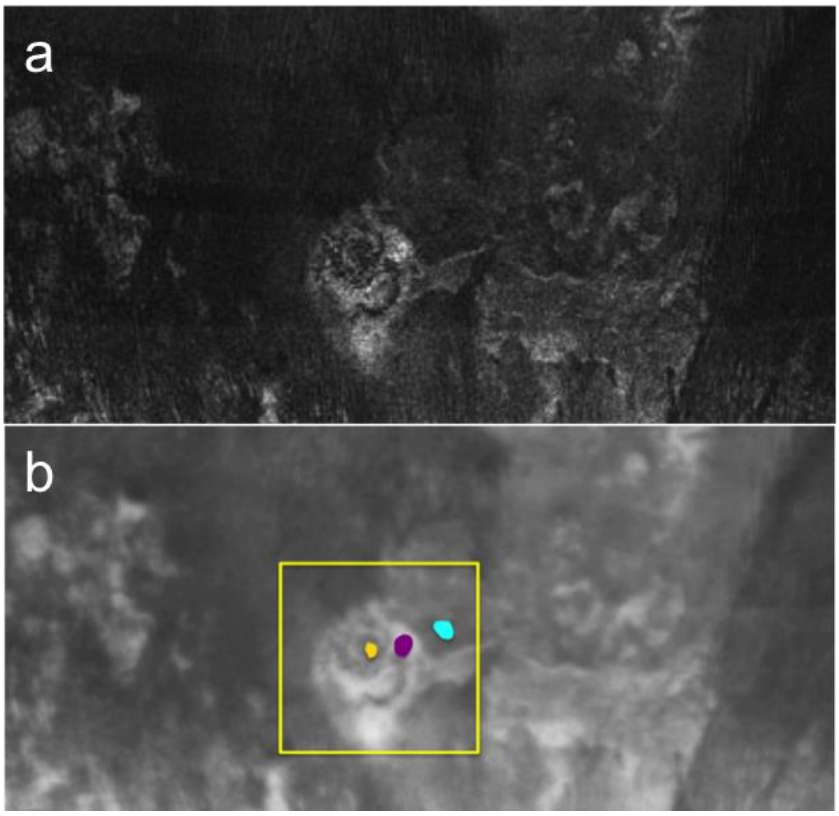

Fig. 7.13 - Same as figure 6.26 but for Sotra Patera from T25 swath. (Magenta: bright; Cyan: intermediate; Yellow: dark).

Table 7.3 - Same as Table 7.2 but for Sotra Patera. Yellow corresponds to dark radar region, Cyan to intermediate and Magenta to bright.

Area	***Mean***	***Standard deviation***	***St. deviation/Mean***
Yellow	106	17.41	0.163
Cyan	223	17.92	0.080
Magenta	116	11.74	0.101

This RADAR investigation provides some information on the surface nature of the areas of interest. However, further investigation is required aiming to the unveiling of topography and morphology and the correlation with the chemical composition (see Chapter 13).

7.4 Conclusions and Implications on cryovolcanism

Our findings indicate that even if Hotei Regio has been previously suggested to present brightness variations over a two-year period (2004-2006) (Nelson et al. 2009a), to-date available observations of that region present issues (e.g. geometry) and prevent an accurate application of our or any plane-parallel RT model to infer surface information with the desired accuracy. All the more so, simpler methods, as previously used, cannot be applied to Hotei Regio current data. Having said that, the shape of the region itself, with lobate flows and possible calderas, is not incompatible with cryovolcanism. In particular, Soderblom et al. (2009) notably reported that there are two features that are possibly caldera formations (see Section 7.1.3), which is a typical volcanic feature in addition to volcanic-like flows. We only demonstrated here that its activity, if any, must spans periods of time far longer than a few months or a few years.

On the other hand, we found significant changes with time in Tui Regio and Sotra Patera that indicate possible surface albedo fluctuations. A darkening for Tui Regio from 2005-2009 and a brightening for Sotra Patera is observed during a year in 2005-2006. On the contrary, the dunes fields test cases do not change with time. Tui Regio's surface albedo spectrum indicates a similar behaviour with time and it is always brightest in October 2005 and darkest in February 2009 (Fig. 7.6; 7.7). Hence it shows a significant darkening with time, which is more pronounced after 2008. The darkening we observe in February 2009 could be due to the same phenomenon as the large rapid methane rainfalls reported by Turtle et al. (2011b) in October 2010. This appears more probable than atmospheric organic deposition, which would be constant with time and would also show up in the test case, except on the case where the test case is a dune field already covered by organic sand of the same nature than the atmospheric aerosols (e.g. Barnes et al. 2008, Rodriguez et al. 2013).

Sotra's surface albedo spectrum does show a similar behavior with time on December 2005 and February 2006. In general, Sotra becomes brighter from March 2005 until February 2006 (Fig. 7.8; 7.9). This brightening could be due to a change in the surface composition through exposed ice or deposition of bright ejecta. An alternative explanation is that the lower albedo of the March 2005 data could be caused a sudden precipitation deposition before the area returned to its bright appearance.

Many different physical processes could explain these variations while we cannot exclude atmospheric phenomena, such as precipitation or organic deposition or erosional and fluvial processes. A possibility could be a change in the surface composition. In that case, we could

be looking at a flat dark component in the case of Tui Regio and a brighter at $\lambda \leq 2$ μm constituent for Sotra Patera. Several such constituents have been proposed to alter Titan's surface (see Section 6.5, Chapter 6), the most common suggestions being water ice, tholin-organic material but also ammonia, CO_2 and other ices, although a definite identification has not been made today. We note that water ice has absorption bands at 3 and 5 μm and that tholin material is rather homogeneously dark in the near infrared (see Fig. 6.32 in Chapter 6). The spectral resolution of the VIMS data does not easily allow for the identification of narrow spectral features due to other ices or species, such as CO_2, NH_3 and more.

Our surface albedo retrieval cannot alone identify the regions as cryovolcanic and I intend to analyze these albedos in terms of chemical composition in the future. Nevertheless, the morphology of the areas with differences in surface texture between the different areas of interest (implying different materials or grain sizes) suggests a cryovolcanic origin and implies a volcanic association with all three cryovolcanic candidate regions.

Cryovolcanic features on Titan's surface are believed to be a significant source of the methane present in the atmosphere (Lorenz and Mitton, 2008; Lopes et al. 2013). It is important, before addressing any implications on cryovolcanism for the study areas to briefly mention some models with regard to the presence of an internal ocean, the stratigraphy of Titan and the potentials for outgassing (more details can be found in Chapter 4).

There are several indications pointing to the presence of an undersurface liquid water ocean on Titan. Modeling of Titan's rotation has shown a decoupling between the interior and the crust from spin rate measurements suggesting the presence of a liquid layer in the interior (Lorenz et al. 2008; Stiles et al. 2008; Sotin et al. 2009). The Huygens Atmospheric Structure Instrument-Permittivity Wave and Altimetry (HASI-PWA) experiment indicated the presence of a Schumann resonance between the ionosphere and an internal ocean that lies 50 km beneath the surface through the extremely low-frequency electric signal recorded (Beghin et al. 2009, 2012). Furthermore, Cassini acceleration measurements showed that tides in Titan are about 10 m in height, instead of about 1m. Such strong tides confirm the deformability of the interior indicating again the presence of an internal liquid ocean roughly 100 km below the surface (Iess et al. 2012). The presence of methane and liquid water layer has also been predicted in several Titan interior models. One hypothesis for methane is its formation in the interior of Titan through serpentinization if the liquid water ocean is in contact with the rocky core (Atreya et al. 2009; Mousis et al. 2009). Other models however, have the liquid water layer sandwiched between two ice layers. Tobie et al. (2005, 2010, 2012) divided Titan's interior in their stratigraphic model as follows starting from the surface: an ice Ih crustal layer

with stored methane clathrates, an ammonia-rich water liquid layer, a high-pressure ice layer, and a rocky core. Fortes et al. (2007) in their model presented the same structure, with some differences in the layers' thicknesses and composition, such as the addition of solid ammonium sulphate in the Ih layer and in the liquid layer.

Considering the presence of a subsurface liquid water body and of methane clathrates in the ice shell in Titan's interior, current models taking into account heat transfer, convection, tidal dissipation, clathrate dissociation and cooling of the subsurface ocean suggest cryovolcanic and tectonic phenomena as a possible 'pathway' for methane to resupply the atmosphere through outgassing on the one hand and possibly for water and ammonia to be ejected covering patches of the surface around cryovolcanic sites on the other hand (Tobie et al. 2006; Fortes et al. 2007; Mitri and Showman, 2008; Choukroun et al. 2010; Sohl et al. 2013). In the model by Tobie et al. (2006) three major cryovolcanic episodes are evoked: (i) during Titan's accretion, where methane accumulated in the ice shell and raised the oceanic temperature leading to the release of methane in the atmosphere, (ii) due to convection and methane accumulation at the base of the ice shell and methane exsolution through buoyancy-driven crustal discontinuities and (iii) due to the thickness of the ice shell that becomes thick enough for convection processes to initiate. The latter episode seems to explain the current presence of methane and 40Ar in Titan's atmosphere (Waite et al. 2005; Tobie et al. 2006; Jaumann et al. 2009; Niemman et al. 2010). Moreover, Fortes et al. (2007) suggested the formation of plumes in the ice shell due to cooling of the subsurface aqueous ammonium sulphate ocean and accumulation of partial melts (melt pockets) at the base of the shell, and subsequent advection of the melt pockets enriched with methane clathrates up to the surface through cracks. Thus, according to these models, cryovolcanism and deposition of water and ammonia ice on the surface of Titan is plausible.

In addition a recent study by Sohl et al. (2013 –see section, Chapter 4) presents the global pattern of maximum tidal distortion of Titan to be consistent with the location of the cryovolcanic candidate areas, which is in the 15°S-30°S latitudinal zone, a possible characteristic of active regions that overlay a zone of crustal weakness (e.g. Head et al. 2002).

In conclusion, the surface albedo variations together with the presence of volcanic-like morphological features suggests that the cryovolcanic candidate features are connected to the satellite's deep interior, which could have important implications for the satellite's astrobiological potential. Further investigation of the surface albedos' retrieved in this study, in terms of chemical composition, will shed light on the origin of these changes and the possible processes that possibly acted or are still acting at these regions.

Chapter 8

Enceladus

In this Chapter I will describe the geological environment and the internal dynamics of Enceladus. As mentioned previously on Chapter 1, Enceladus is an unambiguous example of cryovolcanically active icy satellite that is identified in the outer Solar system. Here, I present my studies, included in two publications, one in the *Hellenic Journal in Geosciences* (Solomonidou et al. 2010) and one in the *Journal of Cosmology* (Solomonidou et al. 2011), where I suggest, among other things, a general classification of the different types of surface features on Enceladus, as seen from the current observations and derive implications concerning their connection to the interior, with the so far developed models. Furthermore, I am describing a simple simulation of an eruption of a potential cryovolcanic jet on Enceladus. This work has been presented at the *European Geosciences Union Annual Meeting* in Vienna, Austria in 2010.

I will begin with an overview of our current understanding of the satellite's properties.

8.1 General facts

Enceladus is a satellite of major geological interest in the Kronian system. Located at almost 5 Saturn radii from the primary planet, it is the sixth largest moon, with a mean radius of 252 km; that is, 1/25 Earth's size. On the case of the geological activity in the satellites of the Saturnian system, the Cassini-Huygens mission made a discovery of tremendous importance; large plumes are ejected from Enceladus' South Pole (Dougherty et al. 2006; Hansen et al. 2006; Porco et al. 2006). This jet volcanically-driven activity, together with possible secluded tectonic movements, shape the satellite creating Earth-like features, thus a geologically interesting planetary body. On Earth, a geyser is a hot spring characterized by intermittent discharge of water ejected turbulently and accompanied by a vapour phase.

The plume source region displays a warm, chemically rich environment that may facilitate complex organic chemistry and biological processes (Hurford et al. 2009). Indeed, the combined observations during dedicated flybys by the Cassini Plasma Spectrometer (CAPS), the Ion-Neutral Mass Spectrometer (INMS) and the Cassini Ultraviolet Spectrometer (UVIS) instruments, detected water vapor in the geysers along with molecular nitrogen (N_2), carbon dioxide (CO_2), methane (CH_4), propane (C_3H_8), acetylene (C_2H_2), ammonia (NH_3), and a number of other components, together with all of the decomposition products of water (Waite et al. 2009). Similarly to the case of Europa (Jupiter's satellite), with a potential water liquid ocean underneath the surface, the presence of these plumes and the detection of the aforementioned simple and complex hydrocarbons, suggests an underground liquid water ocean either global or regional in Enceladus and increases the astrobiological potential, raising the question for the existence of simple life forms beneath the surface in the underground existing fluids. It is considered that the geyser eruptions on Enceladus follow a quite similar model to the one found on Earth although the temperatures do differ, as Earth's reservoir that is much warmer, reaching 370 K while the pressurized subsurface reservoirs of liquid water in Enceladus should not be above 273 K.

Other than the plumes, that seem to be associated with tectonism, Enceladus appears to have suffered from multiple and distinct episodes of severe tectonic activity in the past. Cassini's investigation brought to light evidence that show this tectonic activity in the form of specific features on Enceladus surface; smooth and cratered terrains, ridges, grooves, scarps, shields and extensive linear fractures indeed shape its crust (Johnson, 2004).

Schubert et al. (2007) suggested an approximate 60:40 rock-ice mixture by mass based on the measurements of bulk density being 1,609 ± 5 kg m^{-3} (Thomas, 2010). Preliminary

measurements have shown that Enceladus exhibits rotational librations forced by Dione (Giese et al. 2011) and its obliquity is expected to be ~0.001º (Chen & Nimmo, 2011).

Other than Titan, which consists of a substantial atmosphere, Enceladus is considered a Saturnian moon with significant atmosphere despite its regional presence only in the south, possibly due to the influence of the gasses that are exsolved from the geyser forms (e.g. Hansen et al. 2006).

8.2 Surface Geological evidences

Currently, tectonics on Enceladus is a field of active research, comprising this Kronian satellite among the most promising bodies for tectonic investigation. Several observations on Enceladus performed by Voyager 2 -during summer at the northern hemisphere- (Squyres et al. 1983; Kargel and Pozio, 1996) and Cassini -during summer at the southern pole- (Porco et al. 2006) revealed distinct geological features that suggest the action of tectonic processes on Enceladus. Since Cassini images are still being acquired and several scientific teams worldwide are trying to interpret them, tectonics on Enceladus is likely to remain a field of active scientific research for some time, awaiting new data and analysis. Therefore, the studies presented here are still on-going. A geological map, including the so far identified terrain on Enceladus, is seen in Fig. 8.1. In addition, I present a detailed description as well as the current interpretations of the global geology in the section that follows.

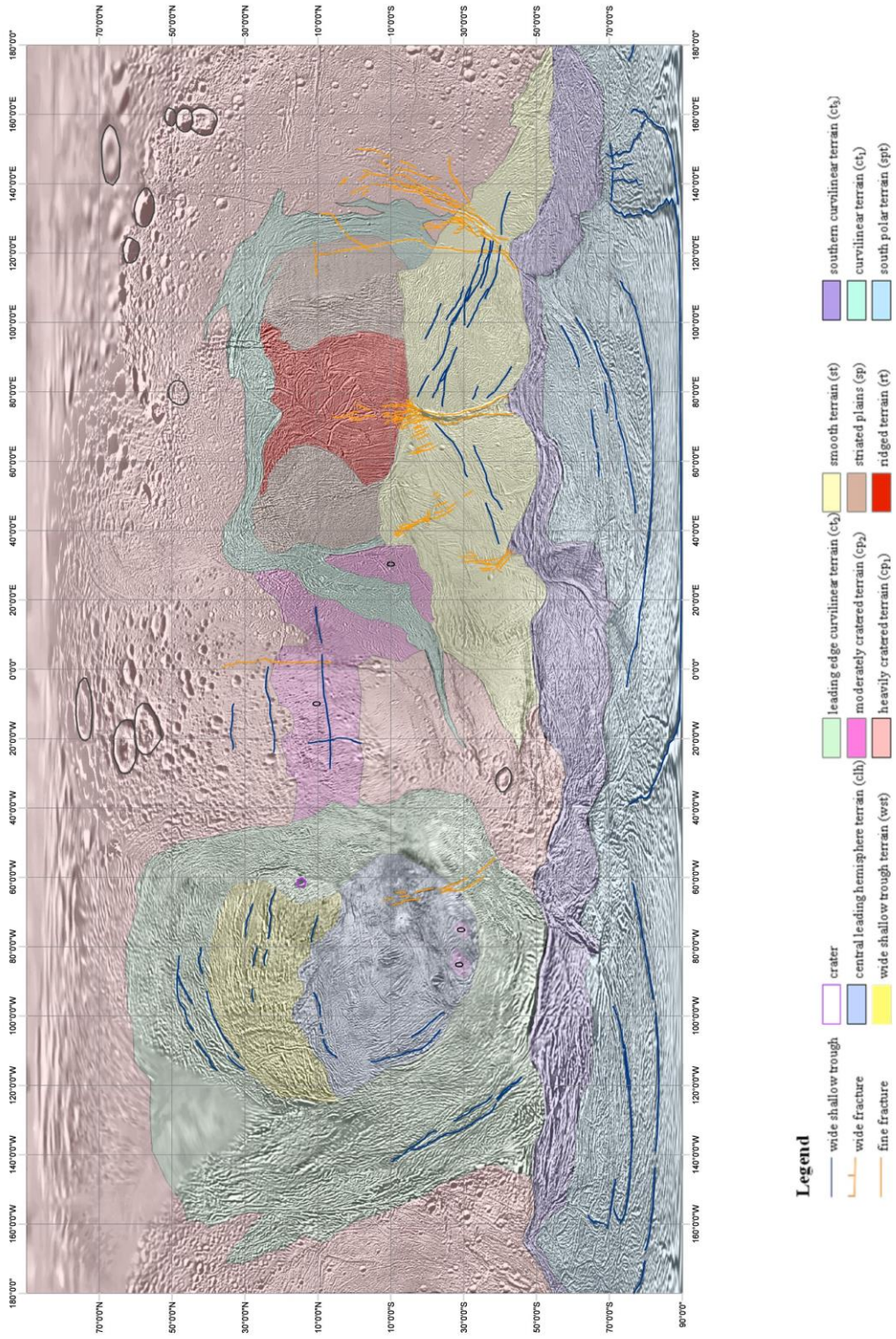

Fig. 8.1 - Global geological sketch map of Enceladus showing the major of geological terrains formations and structures such as cratered, smooth and curvilinear (Map credit: Crow-Willard and Pappalardo, 2010).

8.2.1 Grouping of Tectonic features: two main terrains

The uncratered south polar region of Enceladus is subject to highly active tectonism. The central region is modified by tectonism, while the North Polar Region is the less influenced

one by active tectonic forces. Following is a description of our current understanding of geological processes on Enceladus starting with the observations of the surface.

Thus, we suggest the categories of, i) northern polar terrain; ii) central and iii) southern polar terrain based on the influence and effect of tectonism in each area. The correlation between tectonic surface expressions and the observed impact craters suggests that tectonism has been active during most of the geological history of Enceladus (Barnash et al. 2006).

8.2.2 Northern Polar terrain

Cratered landforms

Craters that present various surface manifestations as well as different values of densities, broadly cover Enceladus' landscape (Fig. 8.1, pink color). Based on the various densities, which were identified by Voyager 2 observations, the craters have been grouped into three categories, in which the first two include the 10 to 20 km wide craters and the third one the lightly cratered plains (Smith et al. 1982). The moon's most heavily cratered terrains lie along the 0° and 180° longitude lines, over the northern polar region. Massive areas of the northern hemisphere, that were imaged by Cassini, with even six times greater resolution of that of Voyager 2, exhibited the presence of craters in this area (Fig. 8.2), suggesting that the northern is rather older than the south polar region that hosts an active uncratered geological formations.

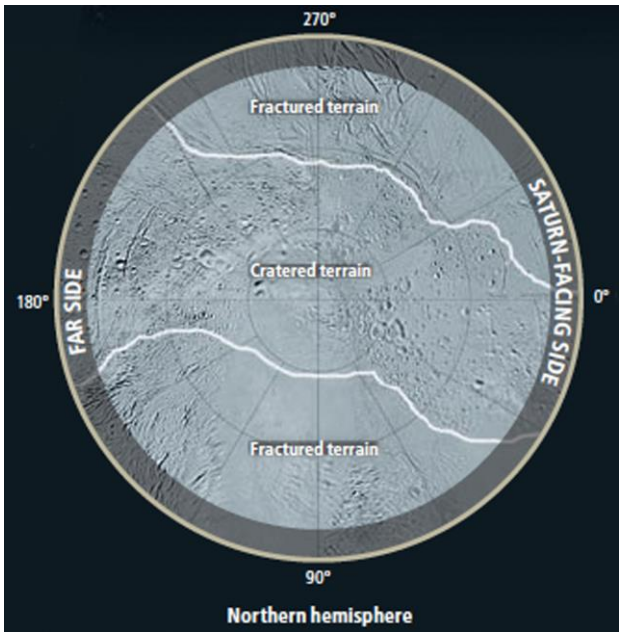

Fig. 8.2 – Evidences of cratered terrain at the northern hemisphere of Enceladus suggesting older surface age than the southern uncratered one (Porco, 2008).

In addition, the craters' density and structural variability indicate age differentiation among the craters, thus resurfacing processes occurred or possibly still occurring on the satellite (Helfenstein et al. 2006). Many of them are unusually shallow due to resurface processes; i.e. modifications by tectonic fracturing after their formation from relaxation and material redeposition (Bland et al. 2012). Moreover, these cratered terrains have possible surface ages between 1-4 Byr (Kirchoff & Schenk 2009).

The area Samarkand Sulci, indicated in Figure 8.3, is a highly tectonized grooved terrain that consists of ridges. It displays an intermediate area between the smooth terrains and the more dense cratered regions (Rothery, 1999).

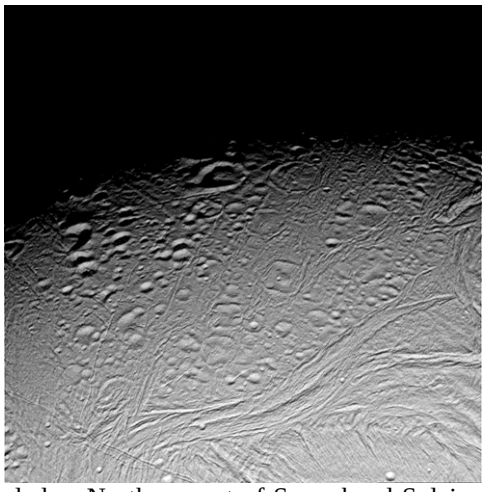

Fig. 8.3 - Cratered terrain on Enceladus. Northern part of Samarkand Sulci as captured by Cassini-ISS (Image credit: NASA/JPL/Space Science Institute).

The Cassini ISS high-resolution images have indicated young fractures overlying the old craters. Additional studies suggest that these young fractures are pit chains (Wyrick et al. 2010). In terms of tectonic geology, the pit chains are linear expressions of craters of circular or elliptical depressions. They are distinguished from impact craters as they lack the ejecta deposits and the elevated rims. In planetary geology, the pit chains are commonly associated with extensional fault systems regime and is consider that are formed by collapse into a subsurface cavity (Wyrick et al. 2010); also, they are usually formed within tectonic grabens (see Chapter 4, section 4.2.2.2) by subsidence of two parallel blocks. On the case of Enceladus, the pit crater chains (Michaud et al. 2008), it is believed to have been formed by the drainage of unconsolidated surface material into dilational-fault-induced voids with the contribution of extensional forces (Wyrick et al. 2010). They are placed within the cratered plains, while adjacent to that area is a greatly tectonized terrain with craters that possess low

densities and correspond to surface ages of almost 1 to 10 Myr (Porco et al. 2006). Cratered terrains are also, limited, present in the equatorial and southern regions.

8.2.3 Central terrain

Central - tectonic molded terrain

The presence of accumulated diverse and density-varied craters at the North Polar Region is the evidence of Enceladus' tectonically active geology that ranges from its past to this day (Porco et al. 2006). The regions that lie in the centre of the trailing and leading hemispheres are younger than the northern region and are significantly uncratered (Collins et al. 2009), with ages that range from 2 Byr to 10 Myr (Spencer and Nimmo, 2013). In addition, analysis of equatorial rifts, in terms of elastic thickness and heat flux (Giese et al. 2008; Bland et al. 2012), provided results similar to the current output of the south polar region, suggesting similar dynamics at the time of their formation or post formational processes (Spencer and Nimmo, 2013).

The general geological environment of that central region consists of topographic features that are also present in the southern polar region but lack the major fractures of Tiger Stripes (Spencer et al. 2009). The tectonic features seen within this area are sub-parallel ridges (Fig. 8.1, red color) and troughs (Fig. 8.1, gray color) that were formed under the process of intense faulting (Collins et al. 2009). Curvilinear terrains are also present (Fig. 8.1, green color). Due to the lack of craters with size greater than 1 km in diameter, the suggestive age of the surface that covers the central region is approximately 1 Myr (Porco et al. 2006).

Additionally, as mentioned before for the northern polar region, the depth of those craters is shallow, which is supposedly the result of stresses that caused relaxation and elevation in the crater interior (Schenk and Moore, 1995). This observation provided evidence of viscous relaxation that influenced the craters due to high heat flux that has occurred for long periods (Schenk and Moore, 2007; Smith et al. 2007). Tectonic surface expressions such as low ridges and troughs have also been observed in Sarandib Planitia (Fig. 8.3), which is located at the centre of the trailing hemisphere at 4.4°N, 298°W, with a fault-terrain traversing the middle of the area from northwest to southeast direction.

8.2.4 Southern region

Cassini investigations added significant knowledge about tectonism on Enceladus, most importantly regarding the smooth terrain (Fig. 8.4) that is found extensively tectonized

(Rathbun et al. 2005). The South Polar Region displays extensive tectonic features and cryovolcanism (see also Chapter 1, section 1.4.2). This region distinguishes itself from the northern part of Enceladus due to both the complete lack of craters and the complexity of its terrain. Thus, according to Porco et al. (2006), the surface age should be less than a few Myr.

The most interesting tectonic surface expressions of the South Polar Region are the four sub-parallel linear depressions called the Tiger Stripes. The depressions are almost half-km deep, 2 km wide and 130 km long and they distance about 35 km (Porco et al. 2006). These four features, which are almost evenly spaced to each other, are, Alexandria Sulcus, Cairo Sulcus, Baghdad Sulcus, and Damascus Sulcus. The Tiger Stripes faults are surrounded by margins enclosing a central trough approximately 2 km wide and 0.5 km deep (Fig. 8.5). These faults are considered the interior-surface 'pathway' for the jet to exsolve in a geyser fashion. There, is located the source of the thermal emission (Spencer et al. 2006; 2009), which is estimated to be 180 K by CIRS data (Spencer et al. 2009, 2011; Waite et al. 2009), as well as the main 'vent' of the plume jets (Spitale & Porco 2007). Moreover, Howett et al. (2011), estimated the total endogenic power from the Tiger Stripes to be 15.8°±3.1 GW. In addition, this uncratered portion of the surface is getting resurfaced by ice-rich particles from the plumes (Kempf et al. 2010), as observed by the Cassini cameras (Schenk et al. 2011).

Damascus Sulcus (Fig. 8.5) is 5 km in length, consisting of two almost 150-m high parallel ridges, separated by a deep V-shaped medial trough. This trench is approximately 250 m deep and may have been formed from crustal movements, possibly shearing, under the influence of tidal forces (Spencer and Grinspoon, 2007). The most cryovolcanically active among the Tiger Stripes, Damascus Sulcus, is also tectonically deformed. Small parts of the crust have slid into the sides of the medial trough, creating blocks that are observed as small ridges. In addition, the folded area is being interrupted by sets of parallel ridges, which arise for a few tens of meters.

Similarly to Damascus Sulcus, Cairo Sulcus (Fig. 8.5) is surrounded by two ridges that extend over 2 km, flanking a V-shaped trough. A scarp and a number of troughs (ridges) that rise up to 50 m high are some of the geological expressions of the area. In addition, as aforementioned, these can be the surface expressions that act as "pathways" to numerous jets that in accumulation form the massive geyser plume observed by Cassini.

Alexandria Sulcus is the least active of the Tiger Stripes. This ridge-flanked trough is a clear evidence of the complex deformation that the southern region has faced and is a subject to tides, as the structure has been overlaid by an older part of its length, due to tectonic movements (Kattenhorn and Patthoff, 2009).

Baghdad Sulcus (Fig. 8.6) is a very interesting southern tectonic structure. A combination of high-resolution data of Cassini ISS and CIRS showed that this area displays anomalously warm temperatures along its youthful geological structures (uncratered and smooth surface).

Concentrating on the entire area, the major tectonic surface expressions are illustrated in Figure 8.4. Moreover, Figure 8.6 shows more, in detail, of the structures within Bagdad Sulcus; on the left part of the image, sets of fractures appear, initiating from the central ridges of Baghdad Sulcus. Rope-like ridges that extend for almost one kilometre and rise up to hundreds of meters surround these fractures. On the right, tectonic stresses have created a complex tectonic pattern of subdivided fractures and ridges.

After geological mapping and crater analysis, Schenck and Seddio (2006) suggested that, at least four to six resurfacing episodes have occurred during Enceladus' history. Cryovolcanism is the major resurfacing process on Enceladus. Such events erase any past tectonic expression from the surface, leaving gaps in the understanding of the moon's tectonic past. The whole Tiger Stripes' area is surrounded by sets of scarps, something that is expected in an area that is under the influence of compressional forces. The area has also, most possibly, suffered extensional forces as shown by fractures that extend from Y-shaped discontinuities noted as 'cracks' in Figure 8.4 (Porco et al. 2006).

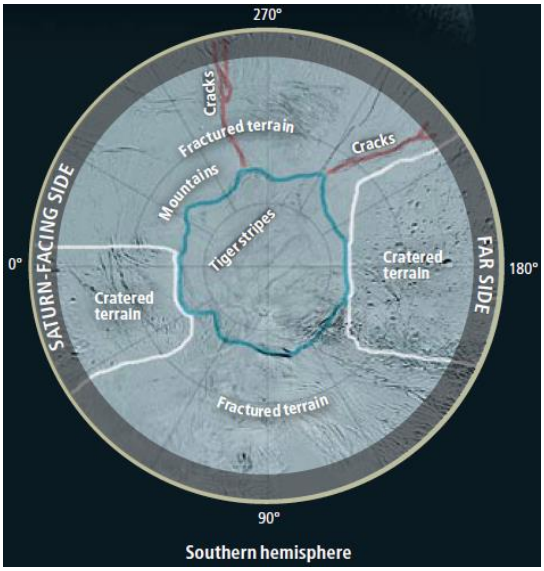

Fig. 8.4 - Tiger Stripes and tectonic surface expressions in the Southern hemisphere of Enceladus (Image credit: Porco, 2008).

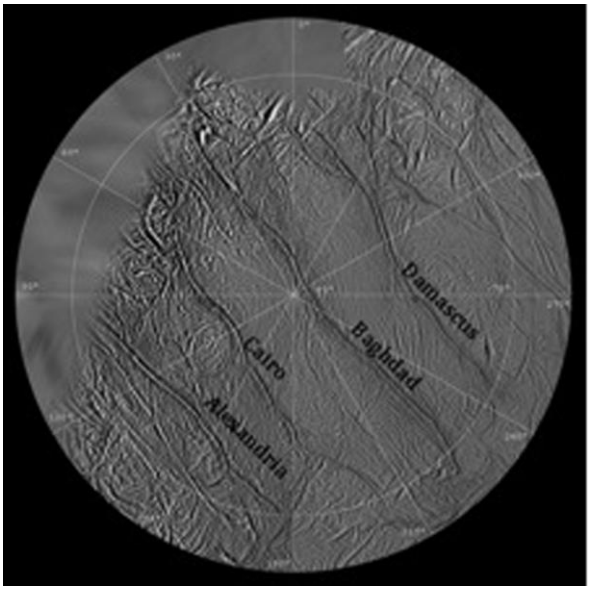

Fig. 8.5 – The Tiger Stripes sub-parallel depressions (Image credit: NASA/JPL). This mosaic presents evidence of tectonic deformation in the fractured South Polar Region of Enceladus.

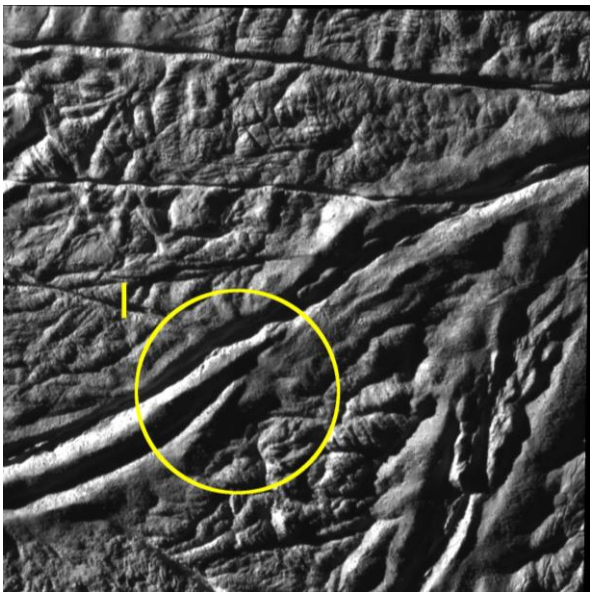
Fig. 8.6 - Baghdad Sulcus on Enceladus as seen by Cassini/ISS (NASA/JPL/Space Science Institute – PIA11114).

As mentioned in Chapter 1, Enceladus has the highest average albedo of any known Solar system object and according to Howett et al. 2010, it reflects almost 80% of the sunlight.

The surface composition has been constrained by near-infrared spectroscopy to be, pure water ice (most abundant), ammonia, carbon dioxide, H_2O_2, Na and K salts, benzene and other hydrocarbons (Emery et al. 2005; Brown et al. 2006; Porco et al. 2006; Newman et al. 2007; 2008; Waite et al. 2009). The surface composition is similar to the plume composition as I will discuss later on. Moreover, such chemical composition has not been found in any other region on Enceladus yet (Brown et al. 2006).

The southern polar region will be thoroughly discussed in the following sections.

8.3 Cryovolcanism and the Southern Polar region of Enceladus

The sub-parallel linear 'Tiger Stripes' depressions are tectonic structures that have been suggested, as the passage for the cryovolcanic material to exsolve from the interior to the icy surface. The evidence came in 2005 from several of Cassini's instruments, beginning with the magnetometer (MAG) (Dougherty et al. 2006) and continuing with the ISS instrument (Porco et al. 2006), that collected data that proved the existence of active cryovolcanism, that initiated from a series of jets located within the Tiger Stripes. The evidence of active plumes of water vapor and ice crystals emanating from localized thermal anomalies (Spencer et al. 2006), rank Enceladus as one out of only three outer Solar system bodies, along with the satellites of Jupiter and Neptune, Io and Triton respectively, that is volcanically active (Fig. 8.7).

The jets produce a plume of gas and particles, as mentioned above, containing NH_3 and Na, K salts in the icy grains (Waite et al. 2009; Postberg et al. 2011). These tectonic fractures discharge material by endo-dynamic and most probably hydrothermal activity. The source of the jets is a controversial issue, because the internal stratification is not yet well determined and further modeling is required. A large pocket of liquid water that lies underneath the ice shell (Tobie et al. 2008) is suggested as a possible source. Alternatively, the material can derive from originally warm ice that is heated and periodically explodes by the dissociation of clathrate hydrates (Kieffer et al. 2006). The clathrate hydrates are crystalline water-based ices, where the host molecule is water and the trapped-guest molecule is typically a gas (Ripmeester et al. 1987). Moreover, I discuss in detail, the interior models in the section that follows.

Data indicating pockets of heat appear in Cassini data, along a fracture called Baghdad Sulcus, one of the Tiger Stripes, that erupt jets of water vapor and ice particles (Hurford et al, 2009). The temperature along Baghdad Sulcus exceeds 180 K (Spencer et al. 2006; Waite et al. 2009) as indicated by CIRS. Baghdad Sulcus could possibly represent a tectonic zone of weakness from which the internal materials find their way to the surface. The idea of a subsurface sea becomes all the more compelling, since Enceladus' South Polar Region is actually a half-kilometre deep basin, distinguished from the surrounding expressions (Collins and Goodman, 2007). Such a feature, like the deep basin in the Tiger Stripes, resembles Titan's Hotei Regio (see section 4.1.4.3, Chapter 4), a basin located 1 km deeper than the surrounding area (Soderblom et al. 2009), reinforcing the theory of Hotei Regio being cryovolcanic in origin.

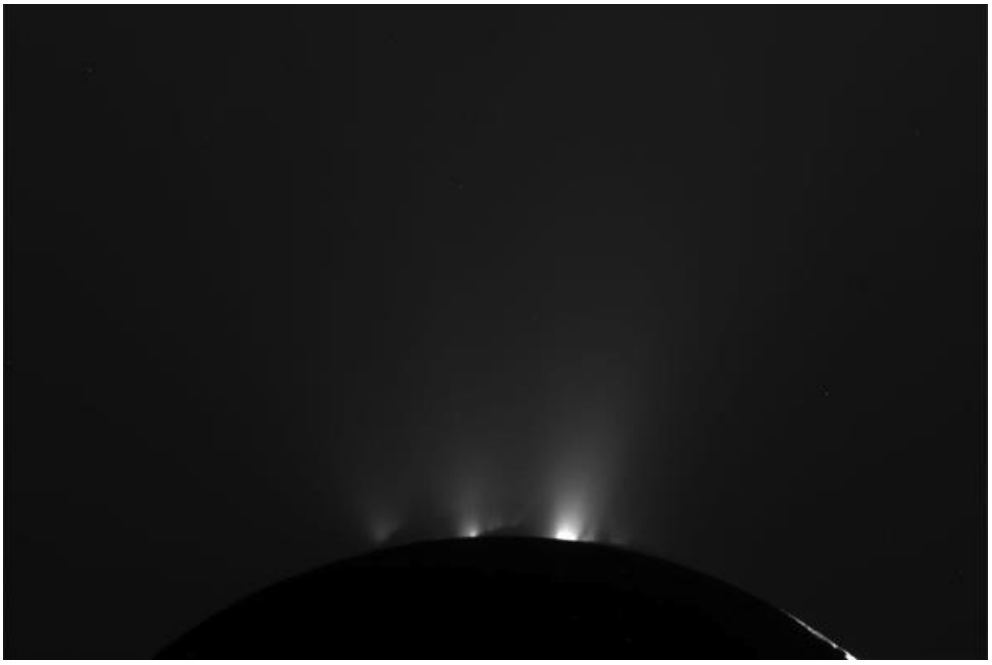

Fig 8.7 - Jets of water vapor and ice on Enceladus as seen from Cassini's high resolution cameras on October 1st, 2011 flyby (NASA, JPL-Caltech).

8.4 Interpretation and models for the interior

8.4.1 Internal structure models

The major and most valuable evidence of Enceladus' cryovolcanic activity, that supports the ocean existence as well, is the geyser formation or geyser jet accumulation that forms a fountain of more than 400 km in height, as observed by Cassini UVIS (Hansen et al. 2006).

Despite the fact that Enceladus is a considerably small satellite (mean diameter of 505 km), it is an active body that has undergone massive geodynamic processes. Since this Saturnian moon is not in hydrostatic equilibrium (Schubert et al. 2007), its internal structure is not thoroughly identified. However, the observed high heat output suggests a fully differentiated body and thus several models have been proposed for Enceladus, based on a simple two-layer internal structure (Fig. 8.8) with a 169 km rocky core overlaid by an icy 82 km mantle (Barr and McKinnon, 2007; Fortes, 2007; Schubert et al. 2007).

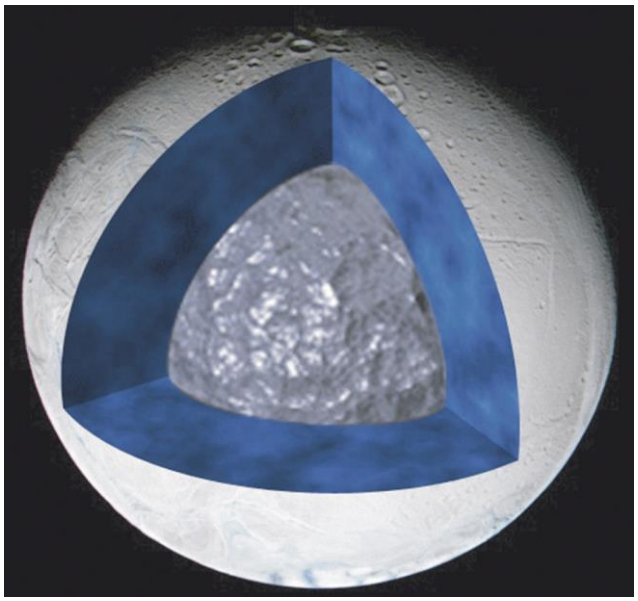

Fig. 8.8 - Possible internal structure of rocky core material and liquid water of Enceladus (Image credit: Schubert et al. 2007).

Between the two major layers of the interior, a subsurface ocean has been suggested to be present (e.g. Collins and Goodman, 2007; Postberg et al. 2009). Postberg et al. (2009) reported the detection of Na in the jets, based on Cassini Cosmic Dust Analyzer (CDA) measurements that indicated possible past interaction of the silicates with the liquid water (Zolotov, 2007). This liquid layer probably decouples the ice shell from the silicate interior and increases the tidal deformation, which may be one of the causes of tectonic activity on Enceladus. Cooper et al. (2009) (Fig. 8.9), proposed that liquid water from Enceladus'

subsurface has been driven upwards due to radiolytic gas-driven cryovolcanism. Essentially, most models regarding the internal processes on the case of Enceladus, support the moon's tidal dissipation as the cause of complex internal and surficial phenomena such as material upwelling, convection-conduction and expansion-contraction, that lead to surface deformation (Sotin et al. 2002; Mitri and Showman, 2008; Tobie et al. 2008; Mitri et al. 2010).

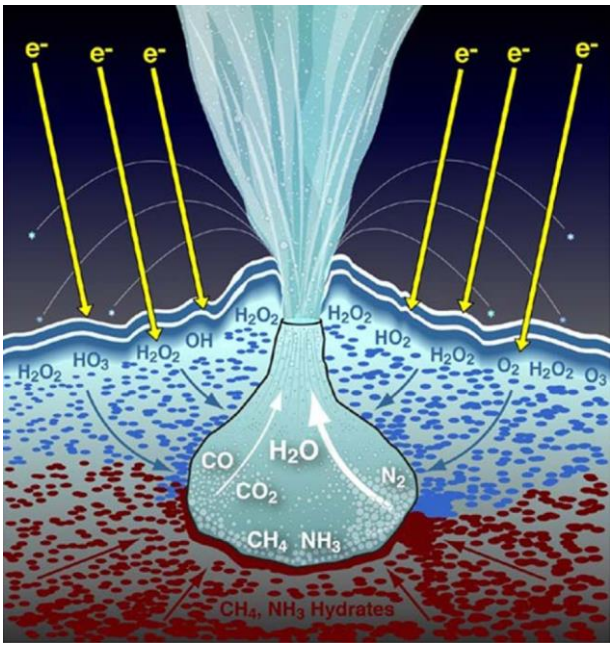

Fig. 8.9 – Model that represents the sequence of continuous rain of energetic electrons (yellow arrows) that drives radiolysis (exposed water ices can become oxidized from radiolytic chemical reaction of near-surface water ice by space environment irradiation) and saturates the upper ice surface with oxidants (blue), mostly H_2O_2 but mixed with other species. Plumes that act periodically, eject ice grains falling back to the surface (white ballistic curves) (Image credit: Cooper et al. 2009).

The sustainability of a global water ocean through geological times is very dependent on the constituents. Waite et al. 2009 (Fig. 8.10) reported the presence of ammonia in the plumes after Ion and Neutral Mass Spectrometer (INMS) data analysis at almost 1% concentration. Ammonia stands as efficient antifreeze and if present in larger percentages it will postpone the entire freezing of the ocean. Conversely, if tidal heating and liquid water are both confined to the southern polar region, then steady-state situations, permitting a regional sea and matching the observed heat output, can be constructed (e.g. Tobie et al. 2008).

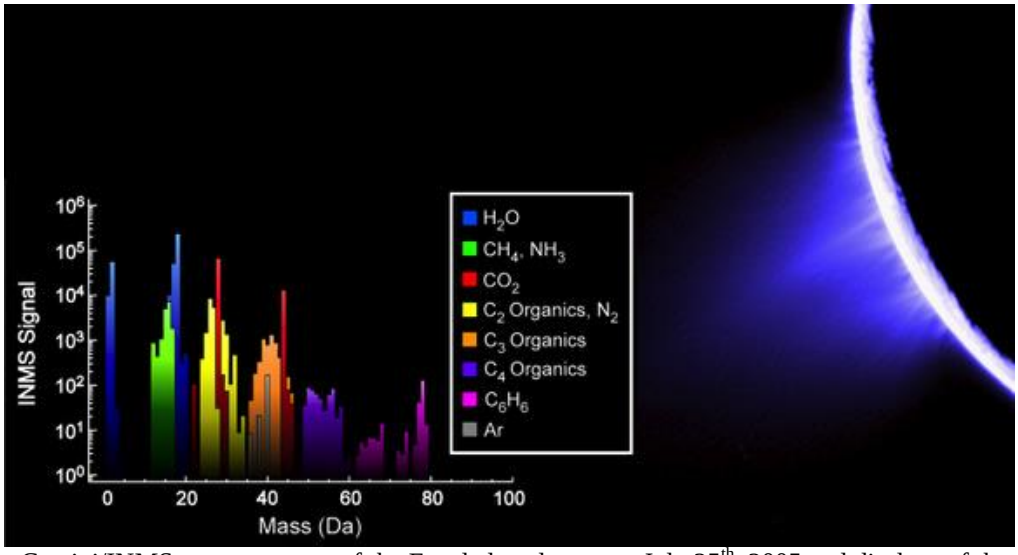

Fig. 8.10 - Cassini/INMS measurements of the Enceladus plumes on July 25th, 2005 and disclose of the chemical composition (Image credit: Waite et al. 2009).

Recently, Spencer and Nimmo (2013) suggested another possible interior structure for Enceladus' (Fig. 8.11). They propose the existence of a regional salty sea between the silicate core and the ice shell.

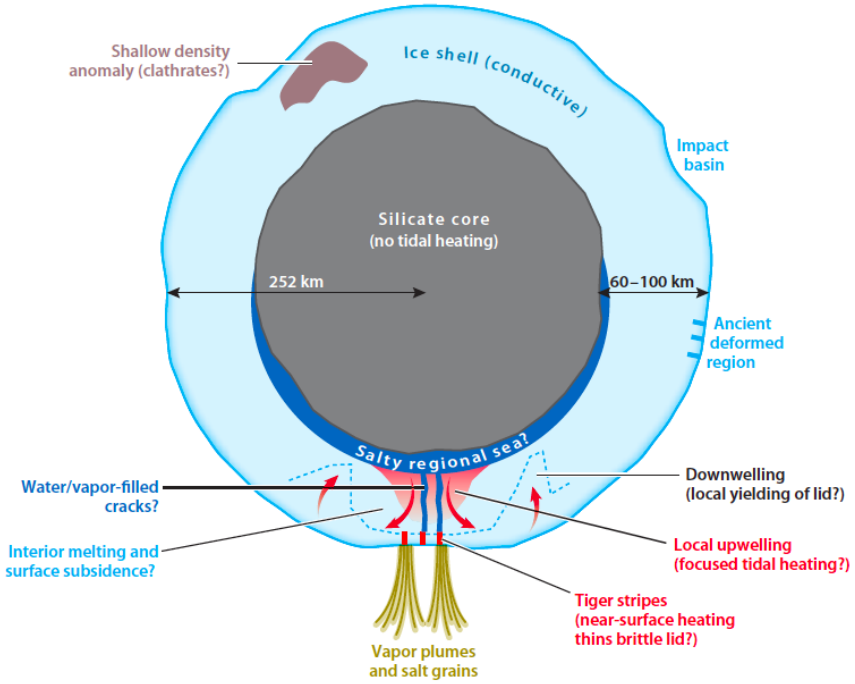

Fig. 8.11 – Model of Enceladus' interior. The structure of this model shows the differences in topography, the possible regional salty sea and the rigid silicate core (Image credit: Spencer and Nimmo, 2013).

8.4.2 Convection, tides and heat source

For Enceladus, localized solid-state convection underneath the fractured Tiger Stripes area seems more possible than global convection due to the thin ice shell and low gravity

(Barr, 2008; O'Neil and Nimmo, 2010; Han et al. 2012). According to current data, the observed topography presents variability that cannot be explained from thermal convection alone (Roberts and Nimmo, 2008). Nimmo and Pappalardo (2006) suggested that, the existence of ice shell lateral density variations can also been invoked to explain the polar location of the hot spot.

The heat flux from Enceladus south polar region is 5.8 ± 1.9 GW, based on Cassini Composite Infrared Spectrometer (CIRS) data (Spencer et al. 2006). Since radiogenic heating within Enceladus' rock component supplies only ~0.3 GW (Schubert et al. 2007), tidal dissipation is likely the source of the rest of the heat (Hurford et al. 2007). The amount of tidal heating, that consequently controls the tidal flexing and dissipation, depends on whether Enceladus' interior is warm and/or liquid. Furthermore, data analysis provided evidence of viscous relaxation within impact craters on Enceladus, suggesting great values of heat flux acting for ages (Passey, 1983; Schenk and Moore, 2007; Smith et al. 2007). Figure 8.12 shows, from CIRS data, the heat radiation at the Tiger Stripes and Baghdad Sulcus in particular.

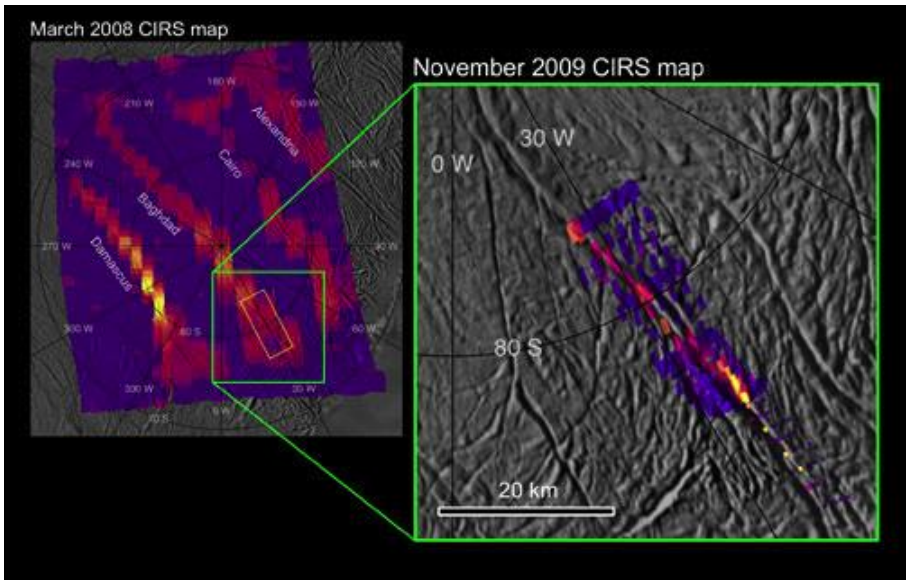

Fig. 8.12 - Heat radiation from CIRS data from the March, 2008 flyby (left) and November, 2009 flyby (right) of the warm cracks of Enceladus' South Pole. The latter data showed that the area of heat is limited to less than 1 km in width. It also shows the variability along the fissure of thermal distribution (Image credit: NASA/JPL/GSFC/SWRI/SSI).

Dynamic processes within Enceladus' interior produce warm pockets of material, called the plumes. These plumes form the jet structures that arise from the warm surface of the Tiger Stripes fractures. Many studies have suggested alternative plume generation mechanisms, such as decomposition of clathrates within the potential ocean (Kieffer et al. 2006),

outgassing caused by warm surface ice (Spencer et al. 2006), boiling of liquid water hidden beneath the surface (Porco et al. 2006) and sublimation at depth due to frictional heating (Nimmo et al. 2007). The plume latent heat carries away another ~1 GW in addition to the surface fractures which radiate almost 6 GW (Spencer et al. 2006). This internal energy, probably, exsolves the material to the surface through the fountain-geyser structure and the ejecta.

The gas grains present in the plumes are rich in sodium salts while the vapour is poor (Schneider et al. 2009; Postberg et al. 2011), suggesting that both are not generated from the same source (Spencer and Nimmo, 2013) (Fig. 8.13). One problem initiating here is that water would freeze in the source as it boils into a vacuum (Postberg et al. 2009). To overcome this problem, the same authors proposed the presence of gas bubbles at the water surface, to introduce the flash-frozen salty water droplets into the plume. The gases could be released from the dissolved gases and return back to the interior (Matson et al. 2012).

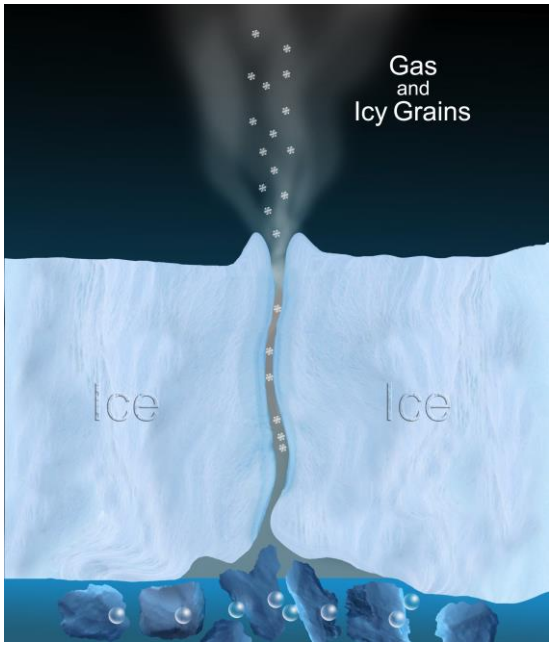

Fig. 8.13 - Ice particles and water vapour exsolve from the Tiger Stripes of Enceladus (Image credit: NASA/JPL).

The plume particle size and distribution are critical factors that control the cryovolcanic process and deposition (e.g. Spahn et al. 2006). The current knowledge on both factors is limited, thus the ice particle production, and the escape rates of the material that are significantly related to particle size, and distribution, is only described by simulations. Even though the mass production rate of the plume gas is 120–180 kg/s approximately, as measured from UVIS stellar occultation data (Tian et al. 2007), it seems that this value is high enough

to remove a significant fraction (~20%) of the satellite's mass over the age of the Solar system (Kargel, 2006).

The Cassini Plasma Spectrometer (CAPS), during the E3 encounter (March 12, 2008), reported fluxes of negative ions detected within the plumes spewing from the Tiger Stripes (Coates et al. 2010). The same authors suggest that according to the ions' restricted lifetime, the production occurs in or near the plume or within the extended source, which is the column of the plume. Nevertheless, negative ions have also been observed on Earth, Comet Halley and Titan (Coates et al. 2010), providing an additional parameter in comparative studies among Earth, Titan and Enceladus. Besides, negative water ions appear on Earth's surface only where ocean waves or waterfalls keep liquid water in motion, suggesting that this might be the case for Enceladus also.

Another suggestion came from a model by Tobie et al. (2008) based on the instability of low viscous regions beneath Enceladus' crust. The low viscous region of the south polar area is considered to be a localized liquid zone that permits the tidal dissipation to occur. In addition, negative gravity anomaly is being created (Collins and Goodman, 2007) resulting to the establishment of an active region (Fig. 8.14).

Given the aforementioned observations and analysis, it is now known that Enceladus contains enough heat to drive complex and dynamic geologic activity, while several different tectonic processes seem to be at work.

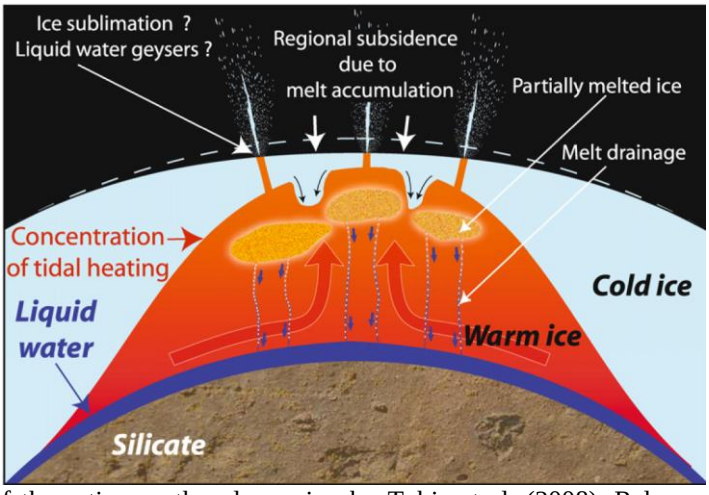

Fig. 8.14 - Modeling of the active south polar region by Tobie et al. (2008). Release of internal heat occurs through the Tiger Stripes, is attributed to the convergence of warm material heated over a relatively broad dissipative region. The warm material rises through the tectonic fractures and promotes sublimation of the ice lying in the crust. Furthermore, destabilization of clathrates within the reservoir or water ice melting will result to the exsolution of the geyser-jets and the formation of the cryomagma fountain.

The global view of Enceladus' geology unveils its palaeogeography, suggesting that tectonic activity operated at different regions and different times in the satellite's history. An

amount of 1.1 GW heating can sustain a regional sea for a great period of time; energy that is not adequate for a global ocean (e.g. Tobie et al. 2008). Hence, a regional ocean at the South Polar Region is more consistent with the current geological state of Enceladus. However, the same could apply for other locations, different than the southern polar region, during past times (Spencer and Nimmo, 2013).

8.4.3 Interaction with Saturn's E-ring

The interaction between Enceladus and Saturn's E-ring was speculated from the early days of the outer Solar system exploration, in the 1980's, from Voyager data (Smith et al. 1982; Haff et al. 1983). However, Cassini's far away and close up flybys (Fig. 8.15; 8.16) brought the evidence with image data, showing the moon with its active plumes in the actual E-ring (e.g. Kempf et al. 2010). As I will present in the following section, a number of particles escape from the Hill Sphere[30] and move towards the E-ring (Fig. 8.17; 8.18). These particles are the smaller and salt-poor ones that reach the highest speed (Postberg et al. 2009). When they arrive at the E-ring they decay by sputtering in a decadal time frame (Ingersoll and Ewald, 2011).

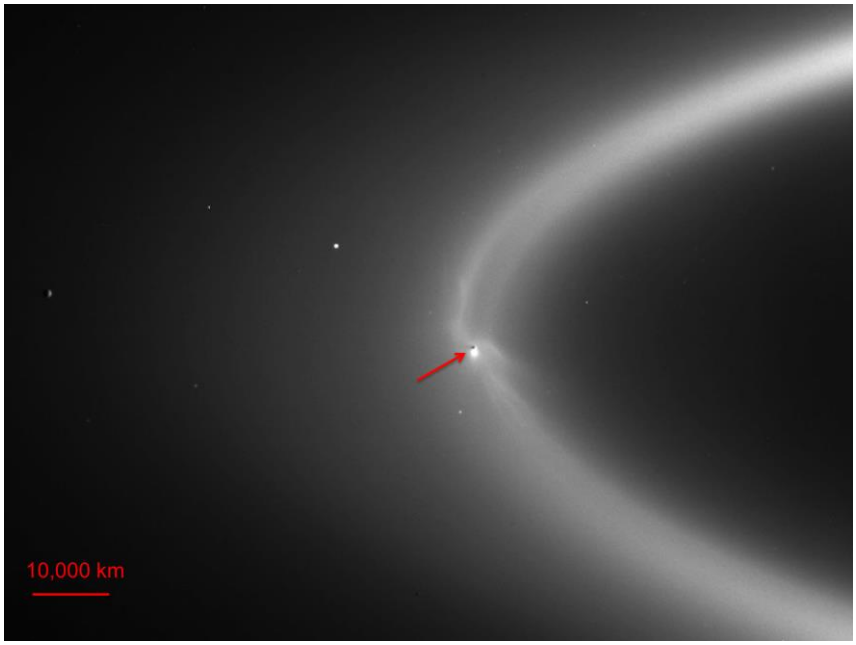

Fig. 8.15 – Enceladus (red arrow) orbits and interacts within Saturn's E-ring. Cassini/ISS (September, 2006) captures this image showing the jets of plumes emanating from the South Polar Region and feeding the E-ring with small particles (Image credit: NASA/JPL/Space Science Institute).

[30] *The region around a planet, within which the planet's gravity dominates that of the star it orbits, is called, the Hill sphere, whose radius is called the Hill radius.*

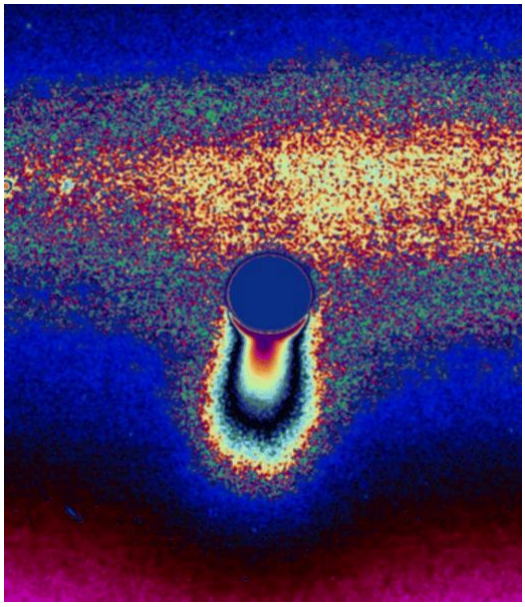

Fig. 8.16 Color-coded image from Cassini/ISS showing the location of Enceladus within Saturn's E-ring (bright areas above and below the moon (Image credit: NASA/JPL/Space Science Institute).

Other than resupplying the E-ring, material coming from the plumes of Enceladus possibly interact with Saturn and Titan's atmospheres (Cassidy and Johnson, 2010), making the exploration of the mechanism and nature of the plumes even more interesting and important.

8.4.4 A simple simulation for the jets

8.4.4.1 The simulation

I present here a simple simulation of the conditions of Enceladus' cryovolcanic activity based on the moon's properties. The main prospect of the simulation is the analysis of the surface distribution of cryovolcanic material, in addition to a general understanding of the dynamics of the particles after the escape of Enceladus' gravitational influence.

The simulation has been designed with a three dimensional representation of particle projectile motion that has been ejected from Enceladus' Tiger Stripes. At first, the initial position of the particles can be predefined to be ejected from any Tiger Stripe chosen. A random position function adjusts the initial distribution of particles at the ejection area. Also the conditions of the ejection, such as the number of particles, the initial velocity and the ejection angle, can be preconfigured.

A hydrothermal type eruption is simulated with an initial velocity at 215 m/s (deviation ~30m/s)[31], the number of particles exsoluted is 500, while Enceladus' Hill sphere is approximately 1,000 km from the surface (Kempf et al. 2010). Table 8.1 describes all the model properties and parameters.

Table 8.1 – Parameters and calculations of the simulation

Enceladus icy plumes simulation (software: MATLAB)	
Graphic environment	
Internal circle	Planetary surface
External circle	Hill Sphere (~1000km)
Time indicator	Real time counter in second
Parameters	
Number of particles	500
Start position	North Pole
Gravity	0.111 m/s^2
Initial velocity Vo	215 m/s^2
Velocity V	± 50 m/s^2
Vent opening	85°-95°
Calculations	
How gravity ''g'' affects each particle, depends on the distance from the surface	
We are taking into account the gravity from Enceladus that affect each particle	
We are taking into account Enceladus' spin	

We have also used Earth volcanic eruptions as a test case; a planetary body where volcanoes have been monitored and analysed and is thus a physical laboratory that provides material samples and real time observations with measurements. We used the same simulation adapting Earth's parameters. For that case, the gravity is 9.78 m/s^2, the initial velocity Vo: 200 m/s^2 and the Hill sphere is 1,500,000 km. Earth's simulation returned images of a possible volcanic eruption that correlate with analogous terrestrial observations. Almost all the particles return as deposits on the surface, while only a small number is distributed to the atmosphere. However, there are many more parameters on which this mechanism depends on, such as wind direction and speed, the type of lava, the type of explosion, magma composition, viscosity and many others. Generally, the simulation shows a typical eruption on Earth and how it looks is based on a global view. Since we were able to return an averagely consistent simulation to Earth's standards, for the purpose of a rough modelling of volcanic eruptions, we continued with the simulation of Enceladus' possible hydrothermal eruption.

[31] *Mean initial velocity of terrestrial volcanic eruptions*

Taking into account the characteristics of Enceladus and setting specific requirements, such as the initial velocity, we calculate the amount of particles that deposit on the surface and the amount of the ones that escapes.

8.4.4.2 Test case and results

For Enceladus, the number of particles exsoluted is 500 from which 275 are deposited on the surface, as seen in the images (Fig. 8.17). The rest of the particles manage to surpass the gravitational influence of Enceladus and their fate is unknown. As discussed in the previous section, Enceladus' plumes are strongly suggested as a possible source of Saturn's E-ring (e.g. Postberg et al. 2009; 2011). Based on that, it is hypothesized that not all particles will hit back the surface after eruption and that a number of them will diffuse to space near Saturn's E-ring.

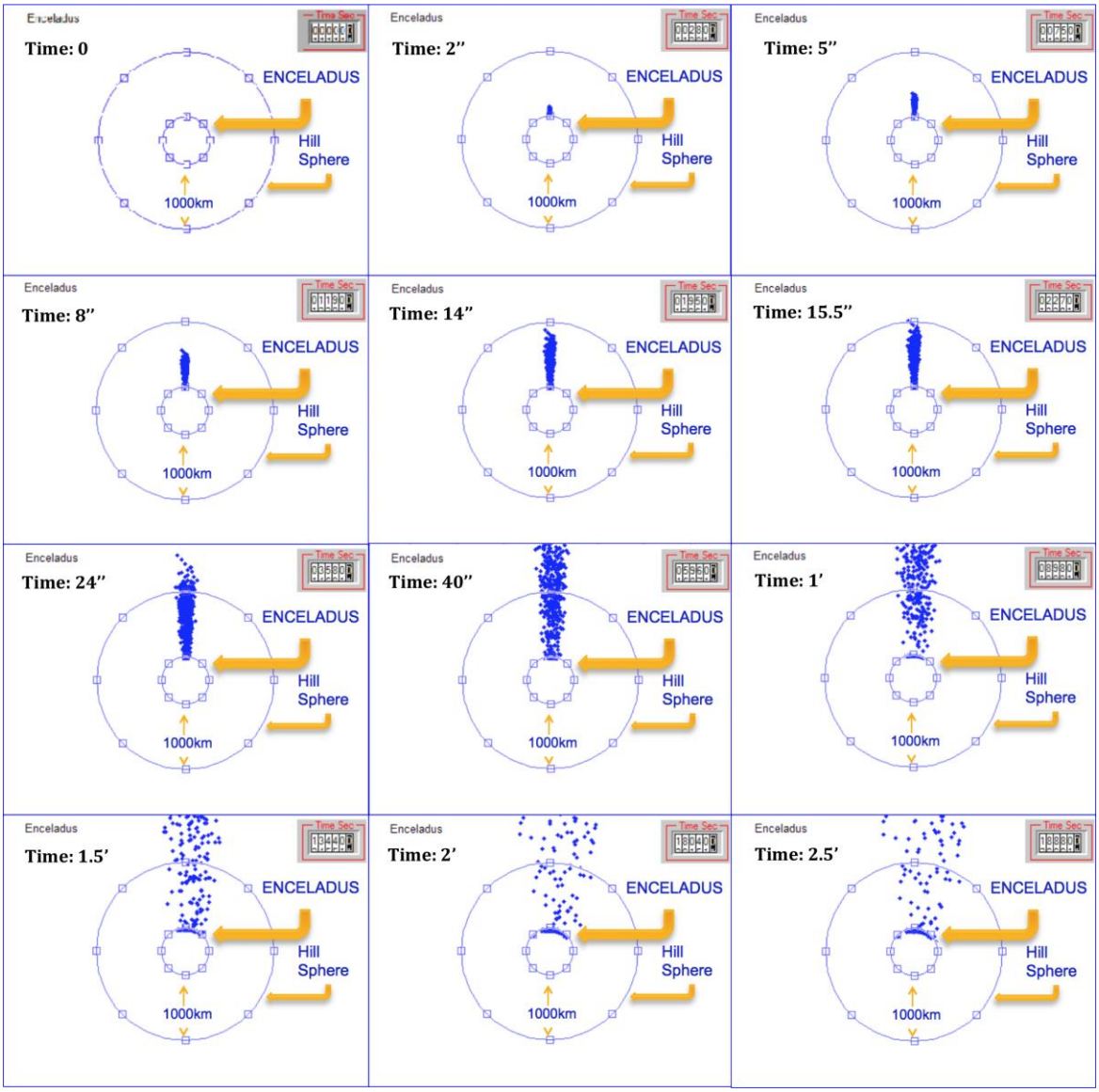

Fig. 8.17 - Compilation of images derived from the simulation of a volcanic eruption on Enceladus. The images are captured at different times as the code is running for up to 2.5 min.

Figure 8.18 presents a global view of the simulation showing the hydrothermal eruption from its start, (a) until the final material deposition on the surface, (i) and the intermediate stages (b-h) from different observational angles and distances. In order to facilitate the reader we have used 1,000 particles in this simulation while the results remain statistically the same as before.

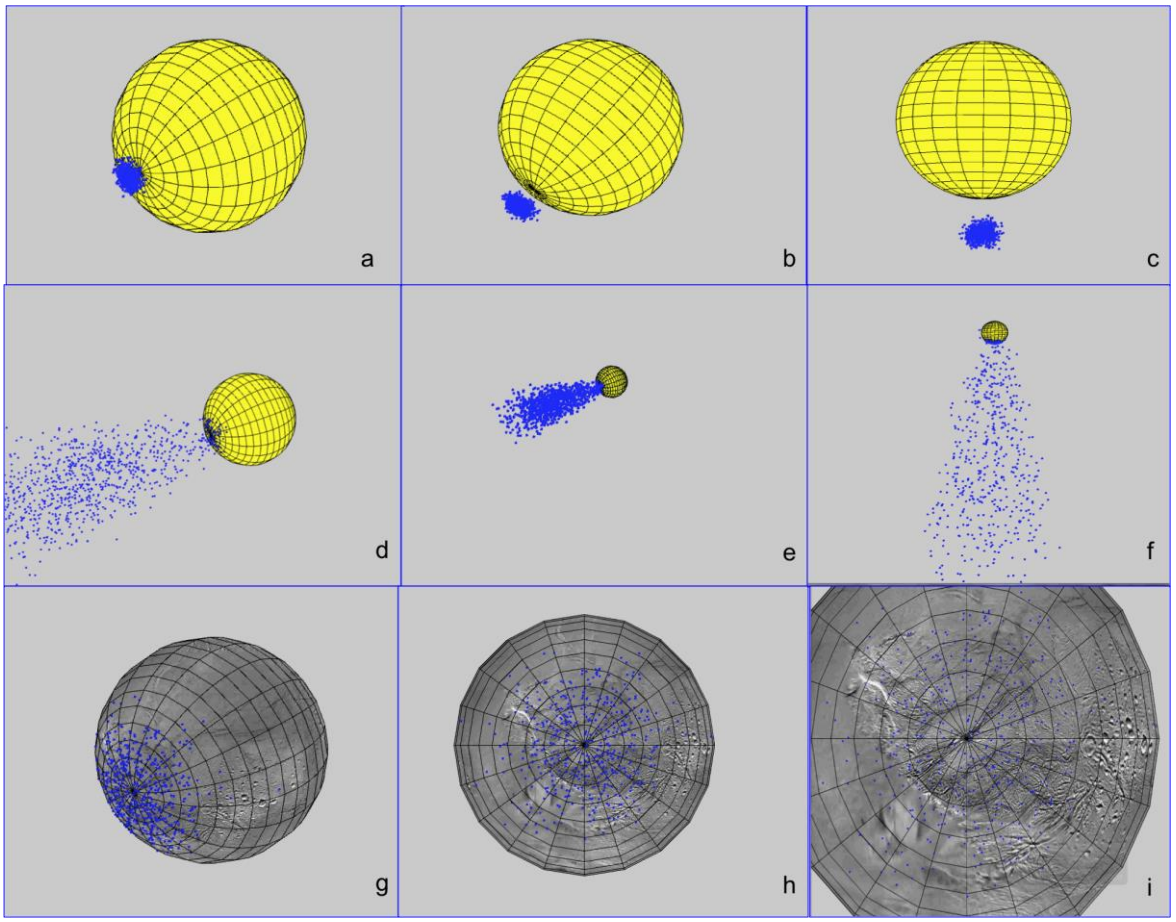

Fig. 8.18 - The global view of a prospective hydrothermal eruption on Enceladus, the same as in Fig. 8.17 with doubled the amount of particles. From (a) to (i) the process of the eruption is captured in different angles and distances.

8.4.4.3 Simulation prospects

In order to advance the simulation and produce developed simulations of Enceladus' volcanic eruption by taking into account more parameters, such as Saturn's gravity and magnetic field. I also consider working with the Graphic User Interface (GUI)[32] for this

[32] *The Graphical User Interface is a type of user interface (field of human-machine interaction) that allows users to interact with the graphical icons and visual indicators (Martinez, 2011).*

multitasking analysis. In addition, I look forward to make simulations and detailed studies based on similar models for other icy moons.

The development and addition of new parameters suggests a thorough analysis of material surface distribution after the end of the volcanic eruption for Enceladus. In comparison with RADAR images of the South Polar Region that could indicate areas of eruptive material contribution, we will isolate areas of interest. Following this, significant suggestions for the composition of the pre-geyser phase into the Tiger Stripes can be made (indications of the initial velocity), that will take into account the surface material distribution and the maximum height of the particles, as seen with Cassini. Finally, we intend to investigate the particle dynamics after the escape from the gravitational influence of Enceladus and a partial illustration of the formation of E-ring.

Chapter 9

Habitable worlds around Giant planets: Icy moons

In the recent years great progress has been made in physical and biological research regarding living organisms. However, the exact conditions for life emergence on Earth remain largely unknown. Our planet is submitted to erosional and tectonic activity causing the destruction of most traces of the geological record and therefore we have to turn to extraterrestrial environments for the missing link, exploring the possibility of life emergence, sustainability and development on other planetary (or exoplanetary bodies) in order to extrapolate to our planet. Such an investigation can also help us characterize the Earth as a habitat.

Current missions and data analysis revealed that among the main candidates for finding signs of past and/or current life within our Solar system, besides Mars, are the icy moons of the giant planets Europa, Ganymede, Callisto, Titan and Enceladus. The reason is that it has been demonstrated recently that liquid water could be present at distances considerably further from the Sun than previous models of the Habitable Zone defined. At the same time, observational evidence, first for Europa from Galileo and then more recently for Titan and Enceladus by Cassini, point to the possibility of having liquid water extents in the interior. Under the name of "waterworlds", these moons could harbor undersurface oceans of liquid water mixed in some cases with ammonia (as I have described in section 4.2 in Chapter 4). Under this assumption, Ganymede, Europa and Callisto on the one hand and Titan and Enceladus on the other, are unique environments and may host conditions for the emergence and/or support of biological building blocks, something that gives these moons a high astrobiological potential.

Comparative planetology among the satellites of the outer planets affords us a glimpse into the nature, origin and evolution of these bodies and permits us to better constrain their habitability aspects (Coustenis and Encrenaz, 2013). To investigate this subject, my colleagues and I have written an overview paper published in the *Journal of Cosmology*

(Solomonidou et al. 2011). Another study, with my colleagues and astrobiology specialist F. Raulin, entitled "Life in the Saturnian Neighborhood" was published as a chapter in Cellular Origin, Life in Extreme Habitats and Astrobiology book series of Springer Editions, J. Seckbach, Ed. [33] (Coustenis et al. 2012). Hereafter I give a brief account of these studies.

[33] *http://www.springer.com/series/5775*

9.1 The habitability concept

As explained in Coustenis and Encrenaz (2013), planetary habitability is the ability of a planetary environment to support and sustain life forms. The habitability potential of a planet or a satellite depends on a combination of factors, which are considered to be essential for life appearance, evolution and maintenance. Crucial factors are, among other, the orbital properties of the planetary body, its stability, its bulk composition, the existence of an atmosphere, a magnetic field and a surface, as well as the proper chemical ingredients. According to what we know from our own planet, habitability and life require at least four raw ingredients: (a) the existence of liquid water, (b) a stable environment (c) carbonaceous matter as nutrients and (d) energy. The fulfillment of these conditions over a long period of time can be considered as an indicator of suitable environments for hosting the proper biological building blocks, which may lead to the formation of primitive life forms.

Astrobiology (or bioastronomy or exobiology) investigates the conditions under which life may originate and evolve on Earth or elsewhere in the past, present and future (Des Marais et al. 2002; Raulin, 2007). The question then rises of where in the Solar system outside the Earth one might look for life or at least habitable environments. In that case we primarily consider the areas around a star or a planet favourable for life in any form and called habitable zones (HZ). Within the habitable zone, a planetary environment can have the right temperature, pressure and luminosity conditions to allow for water to remain in a stable liquid state on its surface. In such a zone, living organisms may arise and evolve or at least survive if transported there (Huang, 1959).

As we discussed also in Coustenis et al. 2012, the boundaries of our own habitable zone in the solar system, according to this basic definition requiring the existence of liquid water on the surface, then extend from 0.95 AU to 1.2 AU (Figure 9.1). However, these boundaries are flexible (Lammer et al. 2009). According to the latter authors classification, besides Class I and II planets like the Earth, Venus and Mars, planetary bodies where the internal ocean interacts directly with silicates, like Jupiter's Europa, belong to the Class III potential habitats. In this structure, the silicates provide various chemicals and energy through hydrothermal or volcanic activity, mimicking some processes we find on Earth. Finally, Class IV habitats are planets or satellites that have water underground deposits without interacting with silicate material. These subsurface oceans of the icy satellites of the gas giants may be in direct contact with heat sources below their icy crust or encapsulated between two ice layers, or liquids above ice. This is the case for Jupiter's Ganymede and Callisto and Saturn's Titan.

In this context, the habitable zone limits can be expanded to beyond the surfaces of Earth-like planets: a subsurface ocean within a planet or a satellite of a gas giant may be habitable for living organism that could be very different from terrestrial life. Indeed, icy surfaces may cover liquid oceans, move and fracture like plate tectonics and exsolute the internal material and energy through a related system. These underground water deposits might be able to support some kind of life forms.

But beyond liquid water, life requires other essential elements such as nutrients, and sources of energy present in a stable environment for long enough times to allow the reactions to take place. Looking for habitable conditions in the outer Solar system brings us closer to the natural satellites than the planets themselves (Figure 9.1). In the paper Solomonidou et al. (2011), I reviewed the surface features of Ganymede, Europa, Titan and Enceladus, their internal structure and their astrobiological potential, also exchanges between the different milieus.

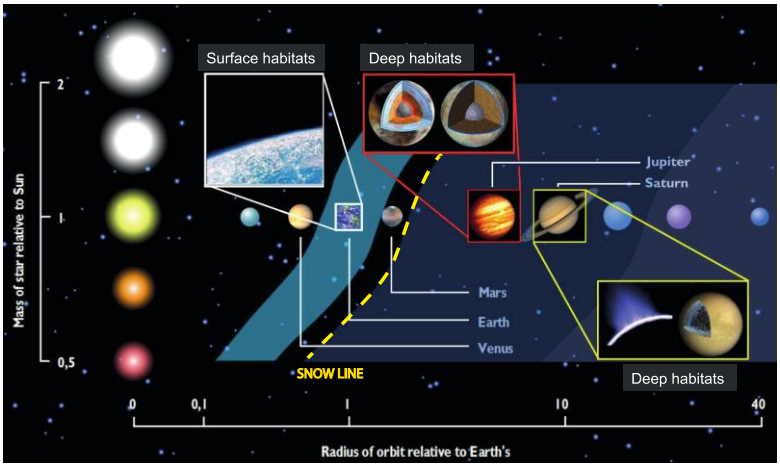

Fig. 9.1 – Illustration of the habitable zone of our galaxy, where habitability appears not to be limited to planetary bodies, where surface liquid water may exist but also to the ones where subsurface water is possibly present (Image credit: Grasset et al. 2013; Neal Powell - Imperial College – London).

All in all, and contrary to what was thought before when habitable conditions were only explored on the surface, Class III and Class IV waterworlds appear to have a large astrobiological potential and could be possible habitats found in icy moons if some conditions are united. Besides the right pressure and temperature conditions to have liquid water, the moon should have energy sources to support metabolic reactions, chemical elements to provide nutrients for the synthesis of bio-molecules. So that another very important aspect to consider when looking at outer moon's habitability is the tidal effect. While the effect of tidal acceleration is relatively modest on planets, it can be a significant source of energy on natural satellites and an alternative energy source for sustaining life.

Hereafter we look at some of the icy moons with a view to habitability.

9.2 Titan as a possible habitat

Large satellites of gas giants at orbits beyond the ice-line (also called snow line), like Jupiter or Saturn, are known to include a large amount of water. But in our quest for extraterrestrial habitats, we also have to consider places where carbon is present and could be involved in the formation of complex molecules. Among Saturn's moons, Titan and Enceladus, show evidence of a subsurface water ocean from measurements performed essentially by the Cassini-Huygens mission since 2004, but not only. Titan, the Earth-like moon and its rich organic chemistry and Enceladus and its potential cryovolcanism and liquid subsurface water reservoir, are essential discoveries brought to us by space exploration and which have recently revolutionized our perception of habitability in the solar system.

Titan is a good candidate for astrobiological studies as its environment exhibits many similarities with the Earth's. Current investigations have shown that Titan fulfills many of life's prerequisites as it is rich in organics from high atmospheric levels down to the surface, most probably contains a vast subsurface ocean, and has sufficient energy sources to drive chemical evolution.

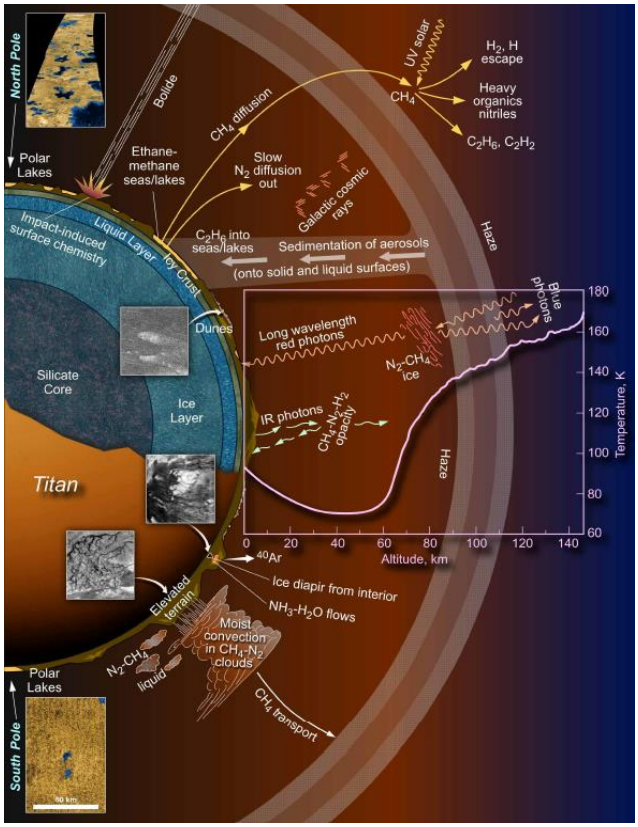

Fig. 9.2 – Schematic illustration of the subsurface, surface and atmosphere of Titan. Demonstrating the relevant chemistry in each region and how all three are correlated (adapted from the TSSM Final Report).

As the Earth, Titan is indeed a very complex world (Fig. 9.2). Measurements throughout the atmosphere have indicated the presence of numerous hydrocarbon and nitrile gases, as well as a complex layering of organic haze that persists all the way down to the surface. Several of the organic processes which are occurring today on Titan form some of the organic compounds which are considered as key molecules in terrestrial prebiotic chemistry, such as hydrogen cyanide (HCN), cyanoacetylene (HC_3N) and cyanogen (C_2N_2). In fact, with several percent of methane in dinitrogen, the atmosphere of Titan is one of the most favourable atmospheres for prebiotic synthesis. Hence, on Titan, the upper thermosphere is linked intimately with the surface and the intervening atmosphere (Fig. 9.3).

Besides its rich organic budget, we also find a geologically active surface including lake-like features filled with organic liquid (Stofan et al. 2007). Additionally, recent discoveries reveal that Titan probably contains a vast subsurface liquid water ocean (Lorenz et al. 2008; Beghin et al. 2009; Iess et al. 2012) Moreover, Titan lacks liquid water surface deposits and therefore is an ideal environment to study the processes of chemical evolution under anhydrous conditions (Raulin and Owen, 2002).

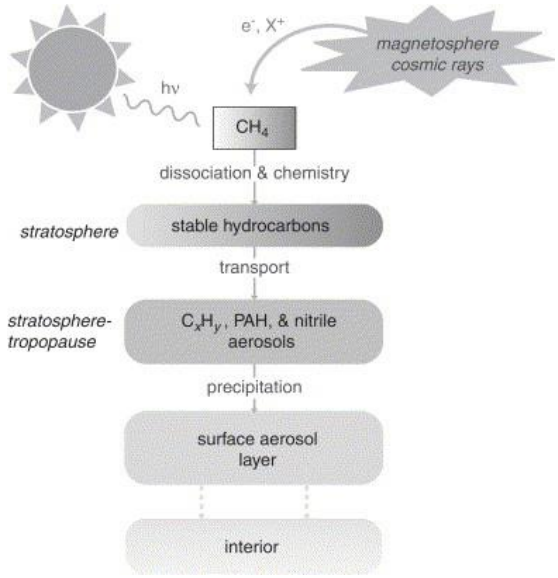

Fig. 9.3 - Illustration of methane sink in Titan (Atreya et al. 2006).

Titan's active organic-icy surface and implications for the interior

The Gas Chromatograph and Mass Spectrometer (GCMS) on board the Huygens probe, which successfully landed on Titan's surface on January 14, 2005, did not detect a large variety of organic compounds in the low atmosphere. But Titan is an evolving planetary body with several terrestrial shaped surface features distributed globally. The Cassini-

Huygens mission has observed a small number of impact craters (Wood et al. 2010), which implies an active surface environment that erased almost all traces of past activity and records. Indeed, as on Earth, sedimentological and meteorological processes, mark the surface of Titan. Erosional processes have been reported on Titan's surface (Jaumann et al. 2008; Lopes et al. 2010). Huygens/DISR recorded well developed rivers, like dedritic networks, close to the probe's landing site at 10°S and 192°W (Tomasko et al. 2005), see Section 4.1.1, Chapter 4. Cassini/RADAR unveiled large liquid deposits (Fig. 9.4) on Titan's surface distributed at polar regions (Stofan et al. 2007; Hayes et al. 2008; 2010) and the equator (Griffith et al. 2012). With its lakes and seas, Titan is the only body in the Solar system hosting large liquid bodies on its surface except for the Earth. These very dark radar spots were finally proved to be filled with liquid, most probably with ethane rich mixtures (Brown et al. 2008). The features range in size from less than 10 km^2 to at least 100,000 km^2 (see also Solomonidou et al. 2011).

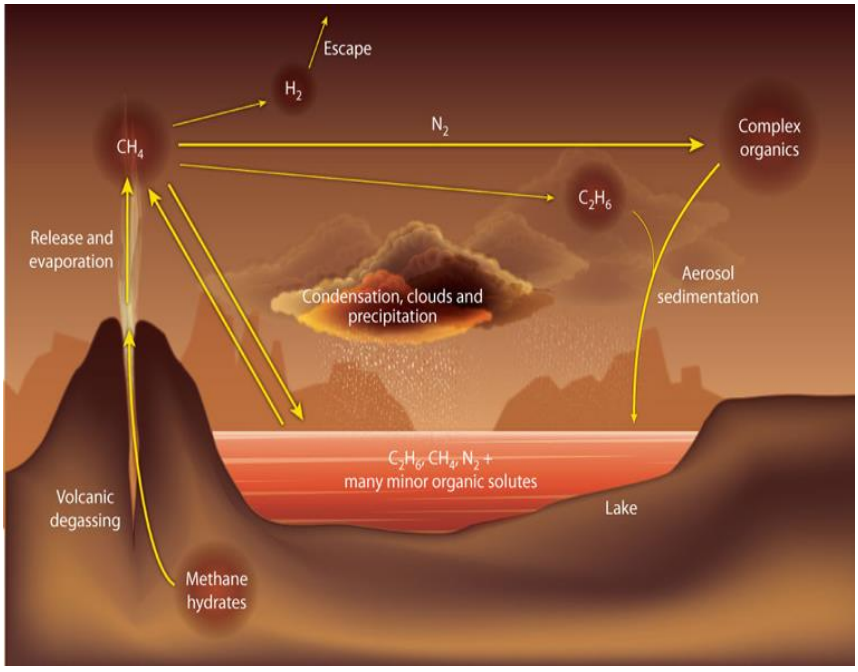

Fig. 9.4 – Illustration of the methane cycle and the chemical reactions. Methane (CH_4) is released into the atmosphere from Titan's interior sources through cryovolcanic activity, and evaporates from the lakes of methane and ethane (C_2H_6). Chemical reactions in the atmosphere convert it to ethane; complex organic aerosols consisting of carbon, hydrogen and nitrogen; and hydrogen gas (H_2), which escapes into space. Ethane and methane partly condense, forming clouds and hazes that precipitate, replenishing the lakes and bearing many organic species in solution (Scheme credit: Raulin, 2008).

The reaction rate in the upper layers of the surface liquid on Titan, in combination with the low temperature, remains very low since the cosmic rays that reach the surface have a quite low flux (Raulin et al. 1992). The surface liquid deposits can then offer the proper

stable environmental conditions for prebiotic chemistry. The stability depends on the long duration, the freezing degree, the dissolved organics and the sedimentary deposition to the bottom of the lakes (Tokano, 2009). Pure methane lakes develop and freeze in short geological periods of time, and, therefore, such lakes have no prebiotic significance. Instead, lakes deeper than a few hundred meters, consisting of a mixture of ethane, methane and nitrogen (Cordier et al. 2009; 2012), can favor stable composition at the bottom with accumulation of acetylene, as the latter sinks being denser than the liquid. The deeper layers do not show any significant movement and create an isolated environment with the proper constituents for prebiotic chemistry.

In addition, Cassini images have allowed for the compilation of a nearly global surface map and the monitoring of both the surface and atmosphere for activity have revealed changes in time consistent with ponding of hydrocarbon liquids on the surface due to precipitation from a large storm (Turtle et al. 2011).

Titan possesses a complex and dynamic geology as witnessed by its varied surface morphology resulting from aeolian, fluvial, and possibly tectonic and endogenous cryovolcanic processes (Solomonidou et al. 2011; Solomonidou et al. 2013a). Linear features and possible cryovolcanic spots are located close to the equator. In particular, elevated as well as fractured crustal features are observed, and the fact that these features are locally regrouped indicates a morphotectonic pattern. Their shapes, sizes, and morphologies suggest that they are tectonic in origin, although it may be a different form of tectonism than the terrestrial one, originating from internal compressional and/or extensional activities. The triggering mechanism that leads to such dynamic movements is possibly Saturn's tide, whose effects concentrate around the equator. These and other features, such as dunes are believed to be composed of rain, ice and organics falling as rain onto the surface into producing the liquid extents and in turn, as a result of Titan's methane cycle. The lakes could supplement in turn the methane at least partly from the hydrocarbon liquid at the high latitude lakes and seas (Lorenz et al. 2006b; Radebaugh et al. 2008). The source of the methane replenishment may lie beneath the lakes in an underground "aquifer" (or "methanofer") system hinted at strongly by Cassini data. According to Lammer et al. 2009, due to this encapsulated water layer, Titan can be considered as Class IV habitat. The existence of an ocean layer below the surface is crucial in determining the habitability potential of the moon.

The presence of an internal liquid water ocean for Titan is supported by internal models, radar and gravity Cassini measurements and the HASI experiment. The extremely low-frequency electric signal recorded by HASI was recently interpreted as a Schumann resonance

between the ionosphere and a modestly conducting ocean roughly 50 km below the surface. Thermal evolution models of Titan (e.g. Tobie et al. 2006; Sohl et al. 2013) suggest it may have an ice crust between 50 and 150 km thick, lying atop a liquid water ocean a couple of hundred kilometers deep, with some amount (a few to 30 percent, most likely ~10 percent) of ammonia dissolved in it, acting as an antifreeze. Beneath lies a layer of high-pressure ice. The presence of ammonia distinguishes Titan's thermal evolution from that of Ganymede and Callisto. Cassini's measurement of a small but significant asynchronicity in Titan's rotation is most straightforwardly interpreted as a result of decoupling the crust from the deeper interior by a liquid layer. In Iess et al. (2012), the authors suggested the existence of a globe-encircling, shallow liquid-water ocean as the most probable interpretation of the Cassini measurements of the tidal contributions to the nonspherical part of Titan's gravity field. Indeed, the determination of the tidal potential Love number k2 from Cassini gravity indicates a fluid response on a tidal timescale. If a liquid body exists in Titan's interior it could be an efficient medium for converting simple organics to complex molecules and to reprocess chondritic organic material deposited through meteoritic impacts into prebiotic compounds.

Taking into account all the characteristics described above, the astrobiological potential of Titan is significant. Titan seems to be a real good candidate as a habitat. Also, it is an ideal planet-size laboratory for increasing our knowledge of the evolution of the Earth's atmosphere, the formation of complex organics, the possible sources of energy and the viability of an undersurface ocean as a habitable medium,. However, the full extent of current geologic activity is still under investigation.

As we have mentioned in the Book Chapter by Coustenis, Raulin, Bampasidis and Solomonidou (2012), although it presents many similarities with the primitive Earth, Titan should not be considered as a frozen analogue. It is an evolving planetary body with an active complex organic chemistry occurring from the upper atmosphere to its surface and should be studied as such.

9.3 Enceladus, liquid water jets at 10 AU

The Cassini-Huygens mission has revealed to us the small moon Enceladus (Dougherty et al. 2006; Porco et al. 2006). Enceladus posed a major challenge to traditional models of the Habitable Zone, since liquid water is now demonstrated to be existing a long way away from the Sun (10 AU), albeit underneath the surface.

By studying Enceladus, an example of active cryovolcanism in icy satellites at distances of 10 AU, we can understand the processes that shape the surfaces of other icy moons. These processes include tidal heating, possible internal convection, cryovolcanism, and ice tectonics. Moreover, the plume source region on Enceladus samples a warm, chemically rich environment that may facilitate complex organic chemistry and biological processes. If we follow the water, then the discovery of water vapour plumes, the sources of which are fractures in the southern hemisphere of Enceladus, suggests the presence of a liquid water ocean (or pockets) in the interior, at distances from the Sun defying all previous notions of habitable zone in the solar system.

Cassini/INMS data identified H2O vapor as the predominant component of Enceladus' plumes, CO2 as the second most abundant, in addition to methane and trace quantities of acetylene and propane and other organics. Whereas the surface of Enceladus is mostly water ice, the composition measurements of the geyser by the INMS experiment aboard the Cassini orbiter showed a more complex composition of the endogenous reservoir, which includes mixtures of organics, salts and ammoni (Waite et al. 2009). Thus, all requirements for habitability are probably present at Enceladus but most likely not the stable environment..

This chemical composition of the jets and thermal inferences on the surface suggests the presence of a very hot interior, for such a frozen satellite, implying internal temperatures on the order of 500-800 K. Such hot interior decomposes ammonia into N2 and drives reactions with hydrocarbons (Matson et al. 2007).

Enceladus' extremely high temperatures at the south polar region are probably generated by the hydrodynamic processes that form the fountain, as previously described, and thus enhance the potential for habitability. The most convincing theory, after Cassini data analysis, suggests that a liquid ocean exists beneath the Tiger Stripes (Schmidt et al. 2008; Tobie et al. 2008; Postberg et al. 2009; Behounkova et al. 2012; Matson et al. 2012) (see Figure 9.5). As explained in Solomonidou et al. (2011), there are standards for life that Enceladus' possible ocean is not consistent with: the sunlight, the oxygen compounds, and the organics produced on a surficial-crust environment. However, terrestrial regions like the deep

oceans that do no satisfy the aforementioned prerequisites for life, still function as active ecosystems (McKay et al. 2008; Muyzer and Stams, 2008). There, sulfur-reducing bacteria consume hydrogen and sulfate, produced by radioactive decay. Notably, the comparison with the terrestrial ecosystems suggests that plume's methane may be biological in origin (McKay et al. 2008). Hence, Enceladus displays an internal warm and chemically rich ocean that may facilitate complex organic chemistry and biological processes (Coustenis et al. 2011).

Since Enceladus is not in hydrostatic equilibrium (Schubert et al. 2007; 2010) a simple and very general stratigraphic interior is being suggested which consists of a 169 km rocky core overlain by an icy 82 km mantle (Barr and McKinnon, 2007; Fortes et al. 2007; Schubert et al. 2007).

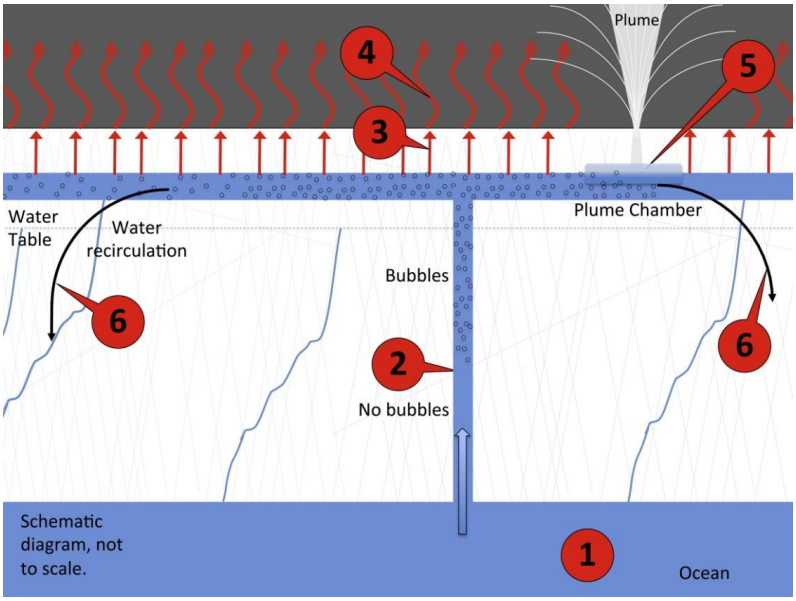

Fig. 9.5 – Schematic model of the interior mechanism occurring in Enceladus' south polar region: No1 indicates the internal water ocean, No2 shows the fracture from where the water ocean exsoluted gases rises towards the surface. No3 indicates thermal anomalies where heat from the water is being conducted through ices to the surface and radiated to space (No4). The label 5 marks the plume chamber which feeds the geysers. The label 6 indicates the return of the water back to the ocean after the ejection of the volatiles (adapted from Matson et al. 2012).

Thus, Enceladus fulfills most of the habitability prerequisites, but may not prove to be a stable environment. For that reason, we need to continue monitoring the evolution of its plumes, which seem to present differences in recent studies (e.g. Solomonidou et al. (2011); Spencer and Nimmo (2013) and references therein).

9.4 Habitability conditions in Jupiter's satellites Europa, Ganymede, and Callisto

In our paper, Solomonidou et al. (2011), we investigated and compared the surface aspects of Jupiter's Ganymede and Europa with those of Saturn's Titan and Enceladus and try to find ties with the habitability conditions. In this section, I look at possible considerations regarding the astrobiological potential of Jupiter's Ganymede and Europa, as we did before for Saturn's moons. Ganymede and Europa in the Jovian system are currently major exploration candidates for finding an internal liquid water ocean among the giant planets satellites and to explore the theme of emergence of habitats in the Solar system, as identified by the Jupiter Icy Moons Explorer (JUICE) mission that we discuss in Chapter 11.

Voyager and Galileo data indicate that Europa and Ganymede, and possibly Callisto, possess important prerequisites to be considered habitable. Galileo's detection of induced magnetic fields combined with imaged surface characteristics and thermal modelling of the moons' evolution, advocate the presence of liquid water oceans below the icy crusts of Ganymede, Europa, and Callisto.

Ganymede

Ganymede is the largest moon of the Solar system and a Class IV potential habitat. It is thought to be the most common "waterworld" in the Universe. Gravity data point to a fully differentiated structure. It possesses a very tenuous atmosphere, a hydrosphere, which may be at least 500 km thick (meaning 50% wt), a silicate mantle and an iron core (Fig. 9.6). A liquid layer up to 100 km thick is trapped between the icy crust on top and a layer composed of high-pressure ices, which do not exist in natural environments on the Earth. It is one of three solid bodies which possess an intrinsic or dynamo magnetic field (along with Mercury and the Earth) and this Ganymede magnetic field is in turn embedded in the Jovian magnetic field. Moreover, it has an induced magnetic field, generated by currents flowing in a conducting liquid, the best proof of the existence of the deep ocean.

Reinforcing Ganymede's possibility for life to exist, Barr et al. (2001) imply that magmatic events could form pockets of liquid, which would then ascent buoyantly carrying nutrients to the internal ocean. Based on their calculations, a water plume could reach Ganymede's ocean and carry nutrient-rich material with an eruption time of 3 hours to 16 days. Additionally, Ganymede's system could provide the necessary tools to concentrate biological building block ingredients (Trinks et al. 2005; Solomonidou et al. 2011) especially

since it possesses a magnetic field that is able to protect life from harmful radiation and lies in a relatively quiet radio zone.

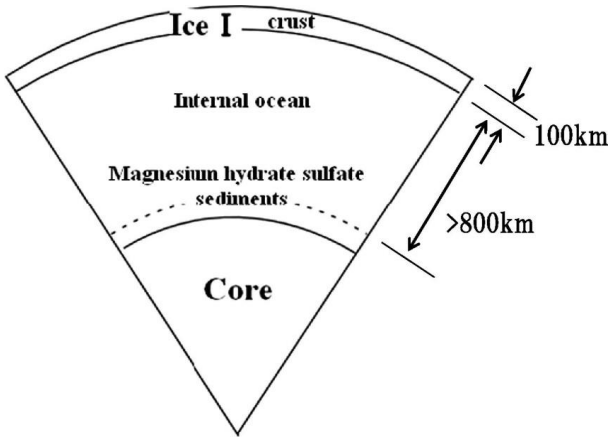

Fig. 9.6 - The interior structure of Ganymede (adapted by Nakamura & Ohtani, 2011).

Models predict that a liquid ocean possibly exists 200 km below the surface, between layers of ice (McCord et al. 2001). Reflectance spectra from Galileo/NIMS discovered hydrated minerals on Ganymede's surface, similar to Europa's (McCord et al. 1998), derived from the encapsulated internal ocean.

Europa

Europa is layered in a same way. We think that it possesses a similar metallic core and a silicate layer, about the same size as Ganymede's, but a thinner hydrosphere no more than 100 km thick. The big difference here is that the liquid layer is almost certainly in direct contact with the silicates, making it a Class III habitat. As shown by the Galileo mission, the lack of many impact craters on its surface (Pappalardo et al. 1998) indicates that it is relatively young and active,. It is mainly composed of water ice (Dalton, 2010; Dalton et al. 2010) and the most typical surface structures are linear chains, the lineae (e.g. Figueredo & Greeley 2004). Reflectance spectra from Galileo's Near Infrared Mapping Spectrometer (NIMS) showed that the surface of Europa also contains hydrated salt minerals such as magnesium sulfates and sodium carbonates (McCord et al. 1998).

Hubble Space Telescope observations showed that Europa possesses a tenuous exosphere mainly consisting of molecular oxygen (Hall et al. 1995) which has not a biological origin. However, it may interact with the possible internal liquid ocean and thus it may have biological significance.

As indicated in Galileo gravitational data (Anderson et al. 1997), the interior of Europa is differentiated and primarily composed of silicate rock (Sohl et al. 2010) and an iron-rich core (Anderson et al. 1998). Galileo's magnetometer data showed that Europa has an induced magnetic field, which suggests the presence of a subsurface conductive layer (Kivelson et al. 2000). The layer is likely a salty liquid water ocean decoupled from the icy crust no more than 100 km thick (Fig. 10.22, Chapter 10) (Schenk and McKinnon, 1989; Zimmer et al. 2000; Schenk and Pappalardo, 2004). The big difference compared to Ganymede, the large satellite, is that the liquid layer is almost certainly in direct contact with the silicates (Class IV).

As described in Solomonidou et al. (2011) in detail, the assumed internal processes that trigger the geodynamic phenomena are the tidal stresses, which produce considerably less energy than radioenergetic decay. Europa is being compressed and stretched when affected by the gravitational forces of Jupiter and the other Galilean satellites and thus, the resulting tidal friction provides enough energy, as well as temperature, for an extensive ocean to exist underneath the crust. The provision of large amounts of energy at the bottom layer of an ocean can conceivably form hydrothermal vents like the ones seen on Earth. Notably, life could emerge around hydrothermal vents, which are important geological forms in terms of life propagation. Greenberg (2010) suggests that even ecology including complex organisms could exist on Europa. The author provided evidence of oxygen concentration within the ocean greater than that of the Earth's, which is suggested as an indicator for aerobic organisms. Nevertheless in the case where the concentration of salts is large, only extremophile organisms (like halophiles) could survive (Cooper et al. 2001; Marion et al. 2003).

Recent analyses of Galileo images suggest that ice-water dynamics are active. Surface features may be formed from exchanges between the ice shell and shallow subsurface water deposits. This mechanism provides transfer of energy and nutrients between the surface and the interior, increasing the associated habitability potential (Schmidt et al. 2011).

Callisto

Callisto is the third largest moon in the Solar system after Ganymede and Titan with a diameter of 4,821 km, while its mass is at 107.6×10^{21} kg and its density at 1830 kg/m^3. Its surface has a mean temperature of about 134 K (Fig. 9.7). Of the four Galilean moons, Callisto orbits farthest from the giant planet at 1883×10^3 km (Anderson et al. 2001). Due to its orbital distance, Callisto is less affected by the magnetosphere of Jupiter compared to the

other Galilean satellites (Cooper et al. 2001) and it has a tenuous carbon dioxide exosphere (Carlson, 1999).

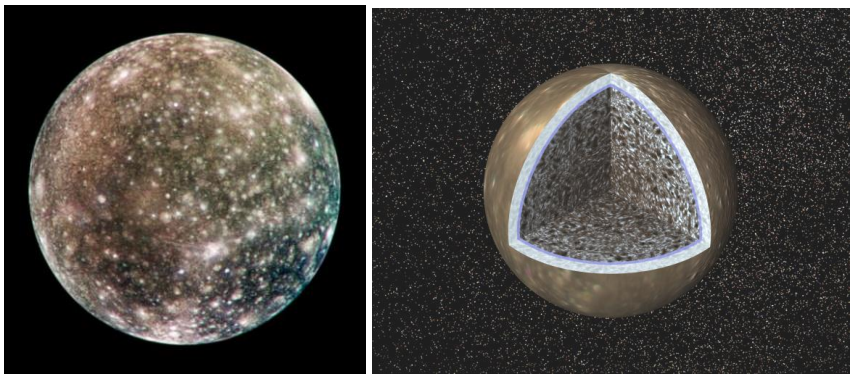

Fig. 9.7 – (left) The only complete global color image of Callisto obtained by the Galileo orbiter. Callisto is uniformly cratered (the bright scars on the darker surface) (credits: Galileo/SSI/PIA03456 NASA/JPL/DLR). (right)The interior of Callisto from Galileo data. An internal ocean lies probably beneath the 200 km icy crust (credit: NASA/JPL/PIA01478).

Callisto is very similar to Ganymede, apart from the fact that it is not fully differentiated (Spohn & Schubert, 2003) and that it does not have an intrinsic field. This lack of differentiation, rather surprising for a body of this size, may be due to the fact that Callisto is decoupled from the Laplace resonance, one of the most striking pieces of evidence of the complexity of the coupling processes occurring in the jovian system. Its surface is very old and heavily cratered, and finally, it is thought to possess a deep ocean similar to Ganymede. The surface of Callisto is heavily cratered which means that it is probably very ancient and inactive (Greeley et al. 2000).

Models suggest that the thickness of Callisto's icy lithosphere is between 80 and 150 km (Fig. 9.7). It possesses a deep water-ammonia ocean similar to Ganymede with a thickness between 70-90 km beneath the crust indicated by Galileo magnetometer and gravity data (Khurana et al. 1998; Zimmer et al. 2000; Spohn and Schubert, 2003; Kuskov and Kronrod, 2005). Beneath the ocean the interior is composed by rock and ice and the rock percentage increasing by the depth without having a core (Nagel et al. 2004).

Implications

These icy Galilean satellites Callisto, Ganymede and Europa, then show a tremendous diversity of surface features and differ significantly in their specific evolutionary paths. Each of these moons exhibits its own fascinating geologic history – formed by the competition of external and internal processes. Their origins and evolutions are influenced by factors such as density, temperature, composition (volatile compounds), stage of

differentiation, volcanism, tectonism, the rheological reaction of ice and salts to stress, tidal effects, and interactions with the Jovian magnetosphere and space. These interactions are still recorded in the present surface geology. The record of geological processes spans from possible cryovolcanism through widespread tectonism to surface degradation and impact cratering. The surface features can be manifestations of current or past activity.

Indeed, the Galilean satellites show signs for an increase in geologic activity with decreasing distance to Jupiter. Io, nearest to Jupiter, is obviously volcanically active. Europa could still be tectonically and volcanically active today, while Callisto, the outermost Galilean satellite, may be geologically "dead". Understanding the gravitational interactions between Jupiter and the Galilean satellites is essential to understand habitability. In particular, the Laplace resonance and its evolution may be important in terms of the differentiation processes in the interior of the satellites involved and for the subsurface oceans of Europa and Ganymede and for the future of volcanism on Io. Indeed, as tidal dissipation can be an important heat source for the satellites, while gravitational interactions can also drive the internal dynamics and the evolution of a satellite's interior and surface.

In addition, organic matter and other surface compounds will experience a different radiation environment at Europa than at Ganymede (due to the difference in radial distance from Jupiter) and thus may suffer different alteration processes, influencing their detection on the surface. Deep aqueous environments are protected by the icy crusts from the strong radiation that dominates the surfaces of the icy satellites. Since radiation is more intense closer to Jupiter, at Europa's surface, radiation is a handicap for habitability, and it produces alteration of the materials once they are exposed (Fig. 9.8). The effect of radiation on the stability of surface organics and minerals at Europa is poorly understood but it should be noted that radiation can cause the generation of oxidants and thus raise the potential for habitability and astrobiology. Surface oxidants could be diffused into the interior, and provide another type of chemical energy.

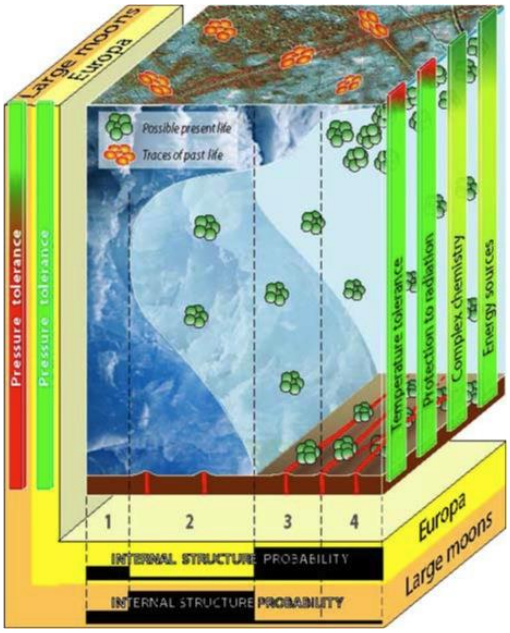

Fig. 9.8 - Possible schematic location of oceans in the icy moons of Jupiter as a function of depth. Europa probably agrees with internal structures 3 (thick upper icy layer <10 km and a thick ocean) or 4 (very thin upper icy layer 3-4 km). Ganymede is closer to 1 (completely frozen) or 2 (three-layered structures impeding any contact between the liquid layer and the silicate floor) (Lammer et al. 2009). The color scales on the right side indicate the physical and chemical constraints on which habitability depends on (Scheme credit: Blanc et al. 2009).

Ganymede lays between structures 1 and 2 in the scheme shown on Fig. 9.8 indicating that it is much colder than Europa, a factor that lowers its habitability potential.

9.5 Thoughts for future habitability exploration

The intriguing discoveries of geological activity, excess warmth and outgassing on many of the icy moons (due probably to the presence of water and organics in subsurface pockets bathed in heat, or some other mechanism), mandate a follow-up investigation of these waterworlds with a high astrobiological potential that can only be achieved with high resolution remote observations, and detailed in situ investigations in the future.

Many internal processes play crucial roles in the evolution of these moons and are intimately linked to the satellites' interior structure and dynamics. Open issues that need to be explored in the future include for instance:

- what is the organic inventory of the satellites ?
- what are their present-day structure and levels of activity ?
- did the satellites undergo significant tidal deformation, and do they possess intrinsic or induced magnetic fields and significant seismicity ?
- do they have heat sources, internal reservoirs of volatiles (in particular methane and ammonia) and eruptive processes ?
- are there prebiotic compounds on the surfaces or near subsurface. Long-term chemical evolution is impossible to be studied in the laboratory: in situ measurement for example of Titan's surface thus, offers a unique opportunity to study some of the many processes which could have been involved in prebiotic chemistry, including isotopic and enantiomeric fractionation.

Future exploration of the Jovian and Kronian systems will be discussed in Chapter 11. We can mention that although the Cassini-Huygens mission is a remarkable success, answering many outstanding questions about the Saturnian system and Titan in particular, it has also raised perhaps more interrogations. It is clear that Titan's organic chemistry and the presence of a subsurface ocean remain to be investigated. In particular, joint measurements of large-scale and mesoscale topography and gravitational field anomalies on Titan from both an orbiter and an aerial platform would impose important constraints on the thickness of the lithosphere, the presence of mass anomalies at depth and any lateral variation of the ice mantle thickness. It is astrobiologically essential to confirm the presence of such an internal ocean, on Titan and elsewhere, in particular on Europe and Ganymede, which will be explored in the future by the mission JUICE. However, the detection of a potential biological activity in the putative liquid mantle seems very challenging.

Chapter 10

Comparative Planetology

One very informative field in planetological studies and astronomy in general, is Comparative Planetology. Comparative Planetology, by definition, is the systematic study of the similarities and differences among the planets, aiming to shed light in the formation of our solar system and its evolution with time (Young, 1973). In that manner, this field focuses on the study of understanding the evolution of the Earth and the basis of life, as well as on the investigation of other planetary bodies and the discovery of extraterrestrial life. Hence, through the comparison of atmospheres, surfaces and other aspects of different planetary bodies, we unveil information about Earth and vice versa.

Mercury, Mars and the Moon in their craters, lava flows and other surface features retain a part of the history of our Solar system (e.g. Gault et al. 1975; Pike et al. 1987; Oberbeck et al. 1977). Moreover, Venus presents an atmospheric aspect that might be viewed as the future of Earth, in the case of an increase of the greenhouse effect (Ringwood and Anderson, 1977; Kasting, 1988). For the outer Solar system the best candidate for comparative studies with planet Earth are some of the icy moons of the giant planets.

Titan has nowadays been acknowledged as an Earth-like world in many aspects, ranging from its atmospheric environment to its surface morphology (e.g. Coustenis and Taylor, 2008). Indeed, its surface morphological structures resemble that of Earth's, even though they are made from materials and under surface conditions very different than those of our own planet. In addition, Enceladus' volcanically-driven geysers, as presented on Chapter 8, together with possible secluded tectonic movements, shape the satellite, creating Earth-like geological structures with multivariable geology.

In this chapter, I compare features of endogenic and/or exogenic origin, observed on Titan and Enceladus, and on some of Jupiter's satellites, with terrestrial ones, in order to discover visual and constructional similarities. Also, I provide a comparative study on the correlation of the surface features with current internal models, as well as with formation

processes found on Earth. This work has been presented in several international conferences, like the European Geosciences Union and the European Planetary Science Congress. It is also part of papers published in the *Planetary and Space Science Journal* (Solomonidou et al. 2013a), the *Hellenic Journal of Geosciences* (Solomonidou et al. 2010) and the *Journal of Cosmology* (Solomonidou et al. 2011).

10.1 Comparative study: Titan and Enceladus Vs Earth

Titan is considered as an Earth-like world because it possesses a thick N_2 atmosphere laden with organic chemistry and it has several terrestrial-like features on its surface (Coustenis and Taylor, 2008). Titan revolves far enough from Saturn (about 20 Saturnian radii), thus avoiding any critical interactions with the rings or the magnetosphere, although sometimes Titan moves close enough to Saturn to allow its atmosphere to interact with the energetic particles of the Saturnian magnetosphere. Together with the solar photons, these interactions play a key role in Titan's chemical evolution. Indeed, Titan possesses an extensive atmosphere with a column density 10 times more that of Earth's (Fig. 10.1).

Fig. 10.1 - (left) Titan's thick, orange and smoggy atmosphere (Image credit: NASA); (right) Earth's atmosphere as seen from space (Image credit: NASA); the cloudy nature of both atmospheric envelopes and also commonalities. Both Titan and Earth experience a greenhouse effect and complex photochemical reactions in their upper atmospheric layers.

Titan's surface environment has been discussed in detail in Chapters 4, 6 and 7. Comparing Titan's landscape with what we see on our own planet, we suggest that contractional tectonism, followed by atmospheric modifications, has resulted in the observed morphotectonic features (see Chapter 4). To test the possibility of morphotectonics on Titan, we provide in this work a comparative study between Cassini observations of the satellite versus terrestrial tectonic systems and infer suggestions for possible formation mechanisms (Solomonidou et al. 2010; 2013a). It is very important to state here, like on Chapter 4, that on Titan's low surface temperature of 94 K ice behaves much as silicate rocks do on Earth (Radebaugh et al. 2007).

In addition, in this chapter I discuss the resemblances of Titan with Earth's surface features of exogenic origin such as dunes, lakes, river systems and more.

Furthermore, as discussed in detail on Chapter 8, Enceladus is an active cryovolcanic world presenting the spectacular volcanic phenomenon of hydrothermal volcanic eruption known also as 'Geysers' on Earth. In addition, tectonic terrains, with many similarities to terrestrial ones, are also presented in this Chapter. Table 1 summarizes the major characteristics of each body, in order to facilitate the comparative investigation.

Table 10.1 - List of orbital, physical and compositional characteristics of Earth, Titan and Enceladus[34].

	EARTH	**TITAN**	**ENCELADUS**
Mass	5.972×10^{24} kg	1.345×10^{23} kg (0.022 Earth's)	1.080×10^{20} kg (1.8×10^{-5} Earth's)
Mean density	5.515 g/cm^3	1.880 g/cm^3	1.61 g/cm^3
Equatorial surface gravity	9.780 m/sec^2	1.352 m/sec^2	0.114 m/sec^2
Atmospheric pressure	1.013 bars	1.5 bars	low
Surface pressure	1.013 bars	1.467 bars	trace, significant spatial variability
Mean surface temperature	288 K	93.6 K	75 K
Rotational period	1 day	15.945 days	1.370 days
Orbital period	365.256 days	15.945 days	1.370 days
Mean orbital velocity	29.8 km/sec	5.58 km/sec	12.64 km/sec
Mean distance from the Sun	$1.496x10^8$ km	1,429,400,000 km	1,429,400,000 km
Mean distance from the Sun (Earth = 1 AU)	1 AU	9.539 AU	9.539 AU
Semi-major axis	149,598,261 km	1,221,850 km In Saturnian radii	238,020 km In Saturnian radii
Surface area	510,072,000 km^2	8.3×107 km^2	799,916 km^2
Composition (Atmospheric)	78.08% nitrogen (N_2) 20.95% oxygen (O_2) 0.93% argon 0.039% carbon dioxide 1% water vapor	98.4% nitrogen (N_2) 1.4% methane (CH_4) ~0.2% hydrogen (H_2)	91% Water vapour 4% Nitrogen 3.2% Carbon dioxide 1.7% Methane
Mean radius	6,371 km	2,575 km (0.404 Earth's)	252 km (0.039 Earth's)
Equatorial radius	6,278 km	2,575 km (0.404 Earth's)	252 km (0.039 Earth's)
Polar radius	6,356 km	2,575 km (0.404 Earth's)	252 km (0.039 Earth's)

[34]*Information adapted from JPL HORIZONS solar system data and ephemeris computation service: http://ssd.jpl.nasa.gov/horizons.cgi#top.*

10.1.1 Craters/Impacts

The number of impact craters on the surface of a planetary body is a secure index of the existence of surface processes shaping the morphology. When the surface of a planet or moon is heavily cratered, suggests that, apparently, has not suffered significant resurfacing processes caused by geological or atmospheric phenomena. Indeed, Earth lacks a large number of impact structures (187 according to the Earth Impact Database (EID[35])), hosting an unscarred surface maintained by tectonic activity, ice ages, volcanism or erosion. Similarly, the small number of impact craters that has been observed by the Cassini RADAR on Titan, during its flybys (Fig. 10.2) (6 certain and 44 under investigation –see section 4.1.2, Chapter 4), suggests that Titan's surface is relatively young and resurfaced (Wall et al. 2009). Such similarity suggest that erosional processes, in the same pattern as sediments erode Earth's surface, could occur on Titan as well, covering the craters that have probably formed by impacts in the past. In Figure 10.2, a structural resemblance between Titan's and Earth's impacts appear to exist. Indeed, in both cases some major impact crater parts as present such as, (a) the floor (white arrow), which is the bottom of the crater that is usually formed below the lever of the surrounding area; (b) the central peak (red arrow) that is an elevated formation at the center of the structure; (c) the rim (yellow arrow) that is the edge that surrounds the crater and (d) the rays (blue arrow) that are bright or dark streaks (depending on the material) composed of ejecta material.

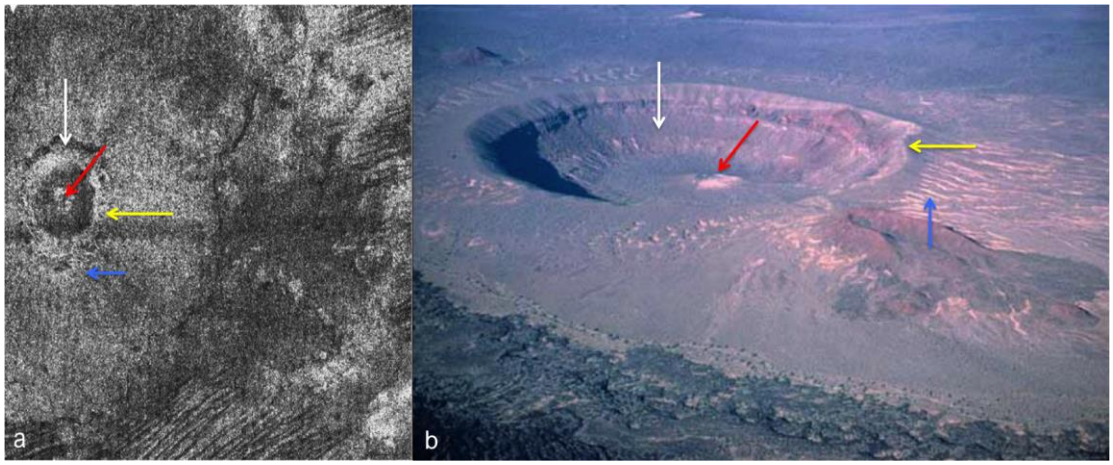

Fig. 10.2 – Comparison of analogous phenomena on Titan and Earth: (a) Impact crater on Titan-one of the few (Image credit: NASA/JPL). (b) El Elegante Crater, part of the Pinacate Biosphere Reserve in northwestern Sonora, Mexico, (Image courtesy: Jim Gutmann).

[35] *http://www.passc.net/EarthImpactDatabase/*

10.1.2 Aeolian and fluvial processes

Titan displays a 'methanological' weather cycle of clouds, rainfall and evaporation that parallels the 'hydrological' cycle of Earth, as well as its complex morphology, and that makes Titan an extremely important astrobiological place. Climatic related processes, such as aeolian and fluvial processes (see also section 4.1.3, Chapter 4), have created structures similar to those on Earth, such as dunes, lakes, seas, riverbeds, shorelines and dendritic drainage networks. Moreover, an active global hydrological circulation system based on methane (e.g. Atreya et al. 2006; Mingalev et al. 2006) is certainly occurring on Titan, as well as seasonal climate variability, as illustrated among other by the reduction of the southern lake shorelines (Turtle et al. 2008; Wye et al. 2009; Wall et al. 2010).

Dunes

The surface age of Titan is probably about half a billion years old, not too different from the average age of Earth (Artemieva and Lunine, 2005; Lorenz et al. 2007). In Chapter 4 I presented a set of the different types of surface features and a categorization of endogenic and exogenic in origin. In this comparative study hereafter, I will present the terrestrial analogues of these features based on their physical characteristics and, for some, on the formational mechanisms.

The Cassini Radar has found many dune fields in the equatorial regions of Titan (Fig. 10.3). They resemble the linear terrestrial sand dunes seen in Thar dessert, Kalahari desert, Namibia and many more (Fig. 10.4b and 10.5b). Dunes form from the interactions between the drifting sand and the blowing wind. Their existence, by itself, means that meteorology plays an important role in shaping the surface of Titan. Comparisons between the structure and the behavior of sand dunes on Earth and Titan, provide a better understanding of the global wind directions, the sand properties and the processes that form the surface. A sand dune is a semi-permanent accumulation of loose sand that forms in areas where the wind tends to blow in one direction, at velocities high enough to move sand. Dunes also form under the action of water flow (alluvial processes), on sand or beds of rivers or sea-beds. Dunes with relatively long and parallel formation are classified as linear or longitudinal dunes, a type of dunes very common on Titan. On Earth, they form in at least two environmental settings, (a) where winds of bimodal direction blow across loose sand, and (b) where single-direction winds blow over sediment that is locally stabilized, be it through vegetation, sediment cohesion or topographic shelter from the winds (Rubin and Hesp, 2009).

Once it's in motion, sand continues to move until a natural obstacle causes it to stop. The heaviest grains settle against the obstacle and a small ridge forms. Since the obstacle breaks the force of the wind, the lighter grains deposit on the other side of the obstacle. After it cumulates around an obstacle, the dune itself becomes the obstacle, and it continues to grow. Depending on the speed and direction of the wind and the weight of the local sand, dunes will develop into different shapes and sizes. Stronger winds tend to make taller dunes; gentler winds tend to spread them out. If the direction of the wind is generally the same over the years, dunes gradually shift in that same direction causing the movement of the dune (Pye and Tsoar, 2009). Graphically, this model is illustrated in Fig. 10.3c and such mechanism could form the dunes on Titan as well, despite the complete different nature of the surface material.

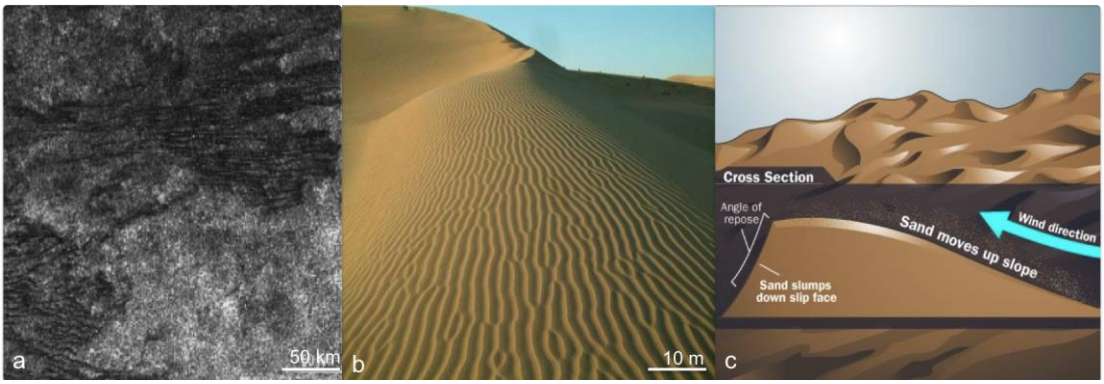

Fig. 10.3 - Dunes on Titan and Earth. (a) Dunes in the western T3 swath, which are discrete, fine and wide dunes (Image credit: NASA/JPL). (b) Sand dunes in Thar dessert that covers a part of the Indian subcontinent and runs along the border between India and Pakistan (Image credit: USGS). (c) Graphic view of a model that describes the sand dune origin mechanism and the relation with the wind (Image credit: USGS).

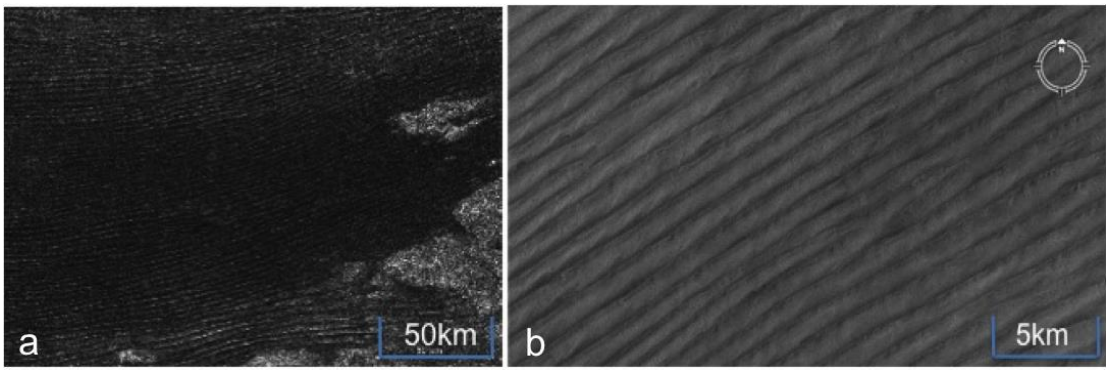

Fig. 10.4 - (a) Longitudinal sand dunes in Saudi Arabia on the edge of the Rub' al-Khali or Empty Quarter. The Rub' al-Khali is a vast desert in southern Arabian Peninsula covering about 402,000 km^2 of Saudi Arabia, Yemen, Oman, and the United Arab Emirates (Image credit: NASA/UCSD/JSC). (b) Longitudinal equatorial dunes on Titan (Image credit: Radebaugh et al. 2009).

According to Radebaugh et al. (2009), dunes on Titan are similar in size, radar reflectivity, and morphology, to dunes imaged on Earth (Fig. 10.5), and they provide a key to understanding Titan's surface evolutionary history, active and past global atmospheric processes.

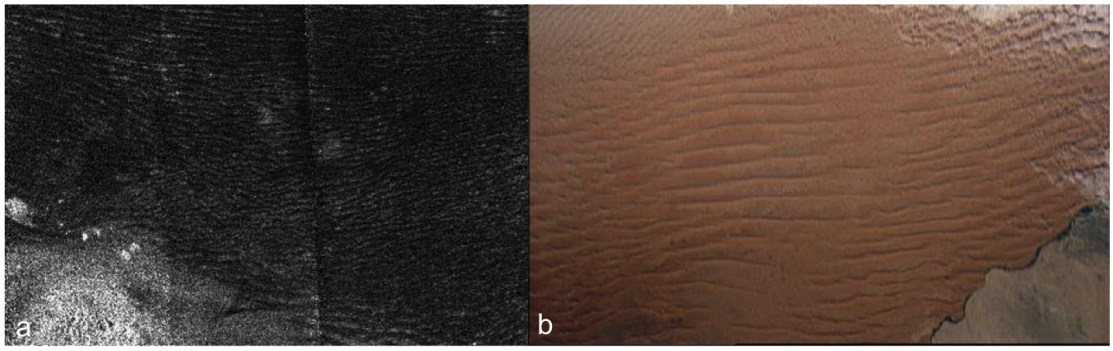

Fig. 10.5 - (a) Sand dunes on Titan (Image credit: NASA/JPL). (b) Namibian sand dunes-terrestrial analogue (Image credit: NASA/JPL).

As mentioned in section 4.1.3, recent studies (Barnes et al. 2008; Savage, 2011) report Titan dunes as 'active' through a comparative study with terrestrial dunes. They suggest possible activity attributed to the presence of both dunes and interdunes; structures that indicate recent interplay.

Lakes

The lakes and seas observed on Titan in the Polar Regions (Mitri et al. 2007; Stofan et al. 2007) make Titan the only body in the solar system that has large liquid bodies on its surface, other than Earth. These very dark features, at the high northern latitudes of Titan, were finally shown to be liquid-filled (most probably with ethane rich mixtures, (Brown et al. 2008)) basins—"lakes". Titan is thus the only planetary body, other than Earth, with long-standing bodies of liquid on its surface (although direct observational evidence and estimation of the longevity of Titan's surface liquids remains to be obtained) (Fig. 10.6); more information about the lakes on Titan can be found in section 4.1.3.1, Chapter 4. More important, the Cassini mission has brought indications of fluvial-type activity (erosion re-deposition, meanders gradually migrate downstream etc.), either past or present, for example, through the changes of level in lake Ontario Lacus (Barnes et al. 2009; Hayes et al. 2011).

One of the largest lakes on Earth is Lake Michigan (Fig. 10.6) which covers a surface area of 58,000 km^2; on the other hand Titan's largest lake is Kraken Mare that extends for almost 400,000 km^2, meaning that it is seven times larger than Michigan lake. However, the

lake systems of lake Michigan and Titan's north polar lakes, appear to have similarities in lake distribution (Fig. 10.6).

All of this suggests that Titan maybe even more similar to the primitive Earth than we thought. However, the degree of complexity, which can be reached from such an organic chemistry, in absence of permanent liquid water bodies on Titan's surface, is still unknown, although it could be quite high.

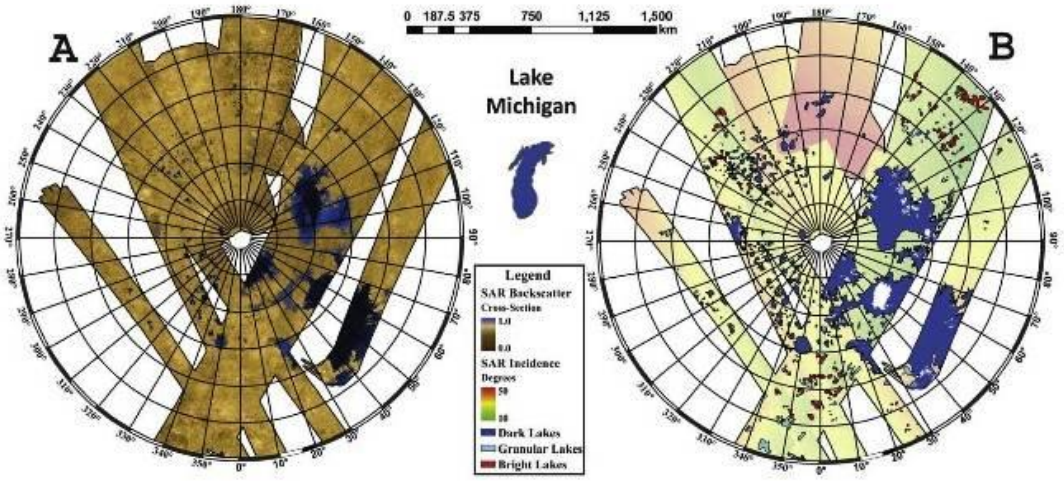

Fig. 10.6 - Map of almost 655 lakes and sea features by the Cassini radar system in azimuthal projection at the North Pole of Titan. Map A (left), shows the radar swath mosaic up to May 2007 flybys. Map B represents the spatial distribution of mapping units. Lake Michigan is illustrated for scale purposes. (Image credit: Hayes et al. 2008).

Channels

The drainage networks on Titan, first observed by Huygens/DISR during its descent, are another major Earth-like feature with fluvial origin (Fig. 10.7). As seen on the left of the figure, Titan's drainage networks appear dark, sharp and angular with junctions between fairly linear segments (Jaumann et al. 2009). Similar shapes are present on terrestrial drainage valleys (Fig. 10.7). Indeed, Fig. 10.7 presents two drainage networks, one on Titan and one on Earth that show similar patterns with branches and streams, where evidence of past or current liquid are present.

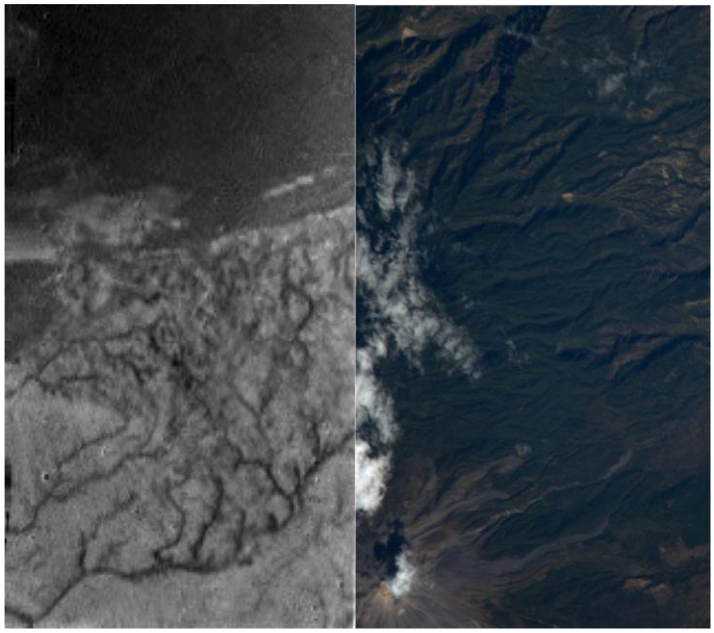

Fig. 10.7 - (left) Short, stubby drainage channels on Titan leading to a 'shoreline' or boundary of some sort from Cassini/DISR (Image credit: ESA/NASA/JPL/University of Arizona). (right) Volcan de Colima drainage network in Mexico (Image credit: NASA).

Fig. 10.8 shows again one channel system on Titan, from Cassini/RADAR T13 observations, on top, and on the bottom a sketch map by Lorenz et al. (2008), that illustrates the network. This network is very similar to the one of Borrego Valley on Earth shown in Fig. 10.8b.

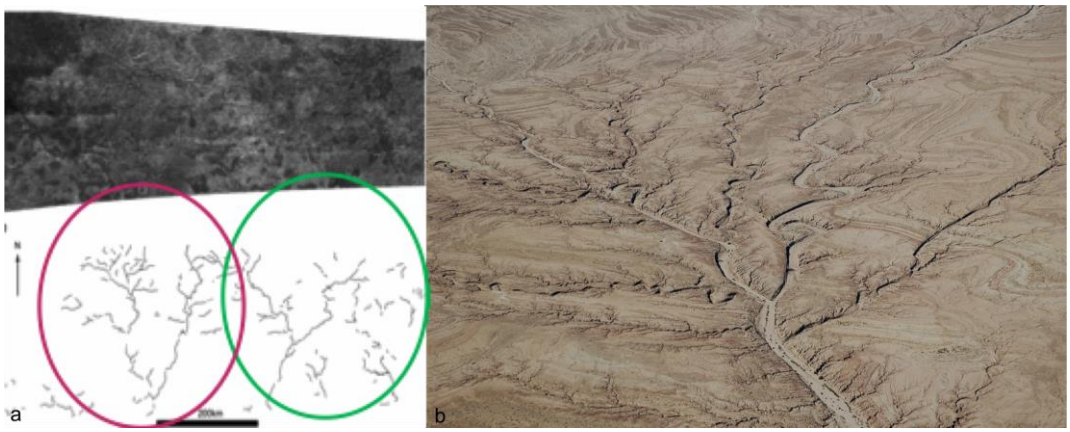

Fig. 10.8 - Two similar channel systems; (a) Titan radar T13 drainage networks (Image adapted from: Lorenz et al. 2008) and (b) Borrego valley channels in California, USA (Image credit: USGS).

10.1.3 Mountains, ridges, canyons, faults

Many possible formation mechanisms have been proposed for the mountains identified on Titan (Radebaugh et al. 2007). Two scenarios suggest crustal compressional tectonism as the main tectonic process, where upthrusting of blocks shapes the mountains, and extensional tectonism where massive parts of the crust are being pulled away, in the same way as

convergence and divergence tectonics occur on Earth. Solomonidou et al. (2013a) paper presented the case of terrestrial analogues for a number of Titan surface expressions presenting physical similarities and making implications for their formation mechanisms. In Table 10.2, I make a correlation between Titan observations of mountains and ridges and terrestrial features.

The mechanisms for mountain formation on Titan are summarized in Table 4.7 on Chapter 4 and include pure extension, pure compression and transitions between compressional and extensional stresses (Tobie et al. 2006; Sotin et al. 2007; Radebaugh et al. 2007; Mitri and Showman, 2008; Mitri et al. 2010). In Table 10.1, I present the terrestrial analogues of the Titan mountain observations previously presented in Table 4.1 of Chapter 4.

Table 10.2 - Major observations of mountains and ridges on Titan and their terrestrial analogues based on the proposed origin mechanisms.

Observations	**Terrestrial analogue**
Curvilinear mountains/Ridges T8, T30, T43	Folded mountains: Rocky Mountains, North America.
(model)	Rocky Mountains, North America.
Linear mountains T8, T3 (15°N, 45°W)	Eroded mountains: Acadian Mountains, USA. Mountain-building due to Sevier/Laramide Orogeny.
High-standing mountain ranges T20	Tectonic and magmatic aspects on geological terrains: Mid Atlantic Ridge, Atlantic Ocean. Ahaggar Mountains, North-cental Sahara Desert.
Blocks and grabens T8	Mountains due to extension: Basin and Range Province (Harcuvar Mountains, Gila Mountains, Maricopa Mountains) (Radebaugh et al. 2007).
Blocks of mountains T3	Ejecta patterns: Meteor crater, Arizona.
Mountainous region T13	Erosional geomorphological structures: Colorado Plateau, USA (Lorenz and Lunine, 2005; Radebaugh et al. 2007). It is dissected by a number of long north-south trending normal faults while deep entrenchment of streams and differential erosion have formed high standing crustal blocks.

On Earth, orogenesis is predominantly a compressional event due to the motion of the lithospheric plates (plate tectonics movement) on the plastic asthenosphere. The phenomenon is attributed to global convection, initiated from the liquid external core and may not be random, but with peaks related to the orbit of our Solar system around the galactic center (Watters and Schultz, 2012). The structural results of orogenesis are the faults and mountains, including all their forms. Significant terrestrial examples are considered to be, the Rocky Mountains, the Andes and the Himalayas chain (71 Myr). Figure 10.10 shows the Rocky Mountains, an almost 5,000 km long mountain chain, extending from Canada to the western United States. This region was formed by subduction of the Pacific plate beneath the North

American plate (Bird, 1988), when two tectonic plates of different densities sank one beneath the other inducing internal compressive forces within the plates. Mitri et al. (2010), argued, in the case of Titan, that ice floes of altered densities, moving on a liquid layer, could reproduce structures and simulate phenomena similar to subduction processes. If this hypothesis is confirmed in the near future, by geophysical measurements from a future mission and modeling, and under the assumption that ice floes would react like silicate plates to the stresses simulating subduction, something not unmanageable as seen in Table 4.4 (Chapter 4), then it would be suffice to say that what we see on Titan is an Earth-like mountainous terrain with peaks and extensive ranges.

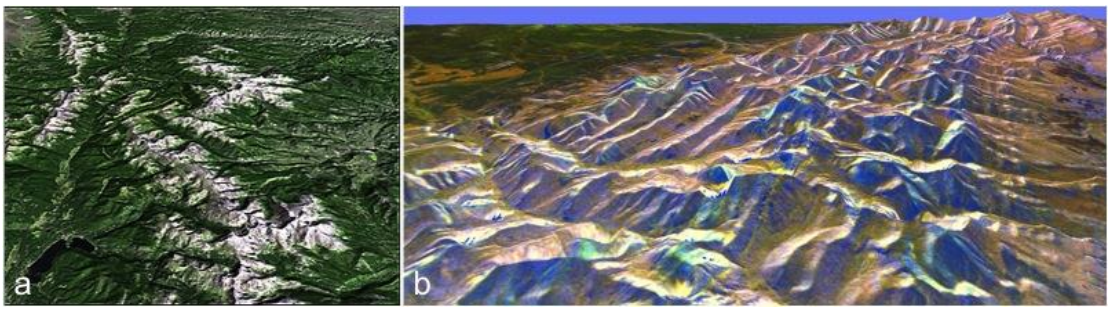

Fig. 10.10 - Rocky Mountains, USA (a) in Landsat TM scene with DEM data (Image credit: Federation American Scientists FAS); (b) 3-D perspective view by combining two spaceborne radar images (PIA01840, Image credit: NASA/JPL).

On Earth, the Himalayas formed due to the collision of the Eurasian and Indian plates. The formation by plate collision, which corresponds to compressional mechanisms, finds resemblance in Titan's mountain formation, where compression may have first led to blocks of high-standing topography that would subsequently be subjected to continuous erosional processes (Fig. 10.11). Furthermore, if the mountainous features seen on Titan are formed due to compressional tectonism, then Titan is the only other planetary body, along with Earth, on which compression features exist in the style of tectonism (Radebaugh et al. 2007; Mitri et al. 2008; 2010).

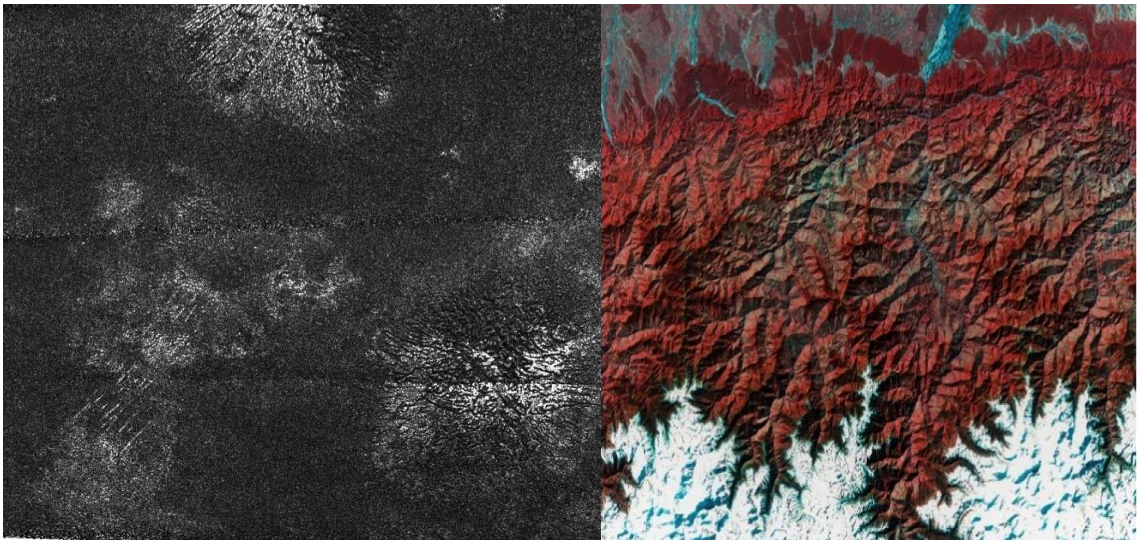

Fig. 10.11 - Mountains on Titan (left) (Image credit: NASA/JPL). The Himalaya mountain range on the Tibet-Nepal border (right) (Image credit: NASA/JSC). The bright radar regions on the left image correspond to the highland features of Titan.

One terrestrial example of mountain formation attributed to extensional stresses is the Basin and Range features (Fig. 10.12 –right). The area includes separate and semi-parallel mountain ranges (Hawkesworth et al. 1995). These morphotectonic features formed due to crustal extension and subsequent modification by erosional processes. As discussed on Chapter 4, this could apply to Titan as well. Indeed, at least structurally, Fig. 10.12 represents the similarities of both features such as parallel ranges with extensive distances from one another (Solomonidou et al. 2013a).

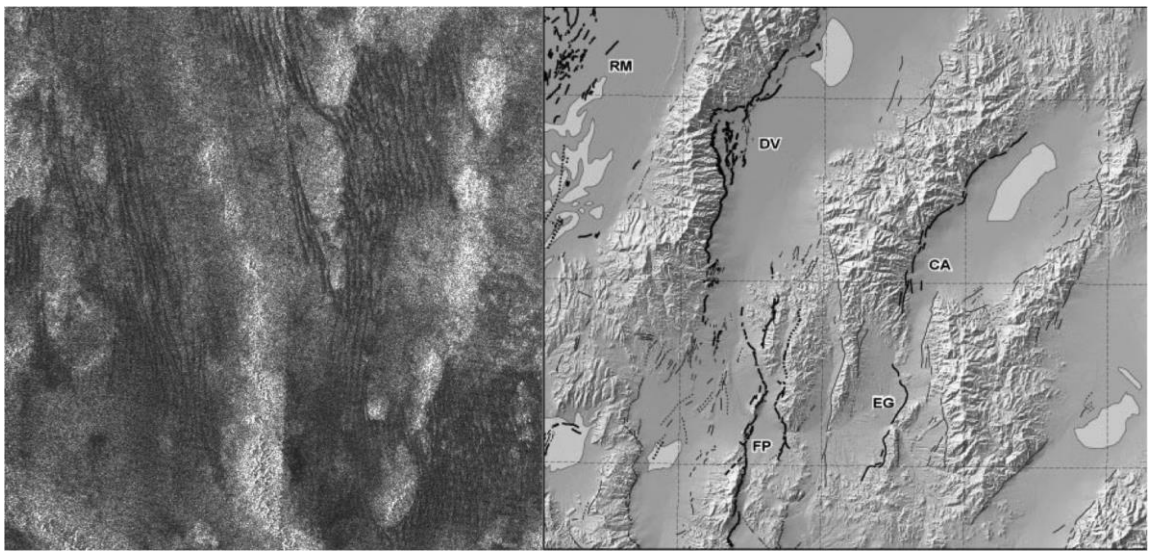

Fig. 10.12 - (left) Fault-block mountains on Titan (portion of figure 2b) (PIA03566, Image credit: NASA/JPL) formed possibly due to crustal extension (Radebaugh et al. 2007). (right) Relief map of the Basin and Range province in west-central Nevada (Image credit: USGS) displaying the parallel ranges and valleys created by both crustal thinning and fracturing by extensive stresses.

A ridge is an elevated feature and more details on ridges on Titan can be found in section 4.1.4.1, Chapter 4. One of the most interesting and unique types of ridges on Earth is the range of mountains formed by the shift of the solid crust, determining the fringes of the tectonic plates (Kious and Tilling, 1996). A major example is the Mid-Atlantic Ridge (MAR).

On Earth, the upwelling magma generates the forces that stress the sea floor apart at the mid-oceanic ridges. Eventually, as the ocean floor is spread apart, cracks appear in the middle of the ridges, allowing molten magma to reach the surface through the cracks and to form the newest ocean floor (Hess, 1965). Similar mechanisms, despite the absence of lava material, could have formed ridges on Titan and Enceladus, allowing for internal -possibly oceanic- material to reach the surface (Fig. 10.13).

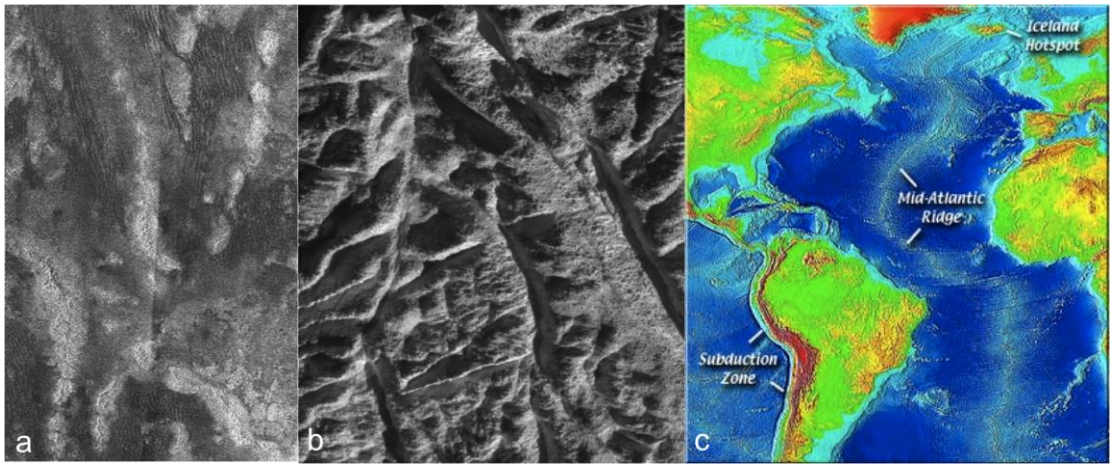

Fig. 10.13 - (a) Tectonic ridges on Titan from SAR imagery (left) (Image credit: NASA/JPL). (b) Perspective view of Damascus Sulcus ridges on Enceladus (Image credit: NASA). (c) Mid-Atlantic Ridge (MAR), a divergent tectonic plate boundary located along the floor of the Atlantic Ocean on Earth (Image credit: USGS).

For Enceladus, the feature of Damascus Sulcus (Fig. 10.14) is presented in section 8.2.4, on Chapter 8. Briefly, Damascus Sulcus is formed by two parallel ridges and it is considered to be a trough (linear structural depression). Damascus Sulcus formation is hypothesized to have occurred due to shearing, triggered by tidal forces. A similar phenomenon has also been observed on terrestrial terrains that suffer tectonic compression, like the Waterpocket Fold area in the U.S.A. (Fig. 10.14). There, uplift and shearing of the crust acted on a buried fault that created the monoclical fold. In addition, the Gabilan Mesa in California is a block formation with evenly spaced ridges and valleys that at least visually resembles Damascus Sulcus.

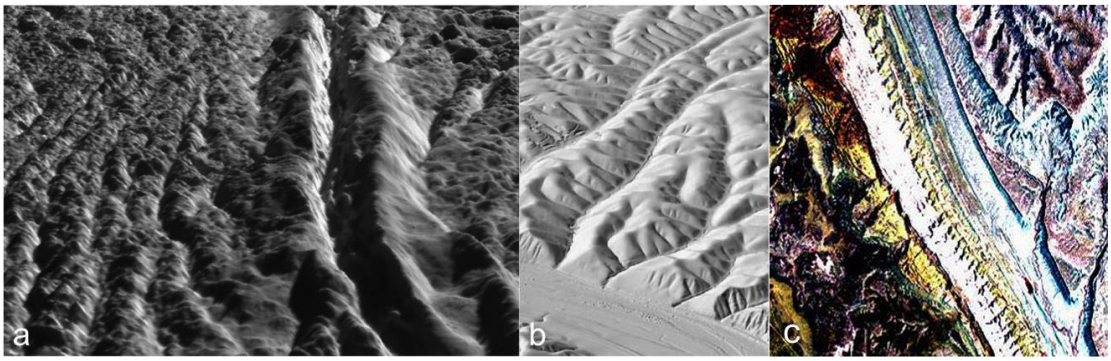

Fig. 10.14 - (a) Tectonic ridges on Enceladus 'Damascus Sulcus' one of the 'Tiger Stripes' (Image credit: NASA/JPL/Space Science Institute/Universities Space Research Association/Lunar and Planetary Institute). (b) Perspective view of the Gabilan Mesa of central California (USGS) (Image credit: Perron et al. 2009). (c) The Waterpocket Fold at Capitol Reef National Park, presents a similarity to Damascus Sulcus crumpled rock pattern (Image credit: USGS).

Figure 10.15 exhibits another resemblance of terrestrial parallel ridges. In this case the distance between the ridges is significantly smaller (few hundreds of meters) than the distance of Titan's ridges that reaches almost 50 km.

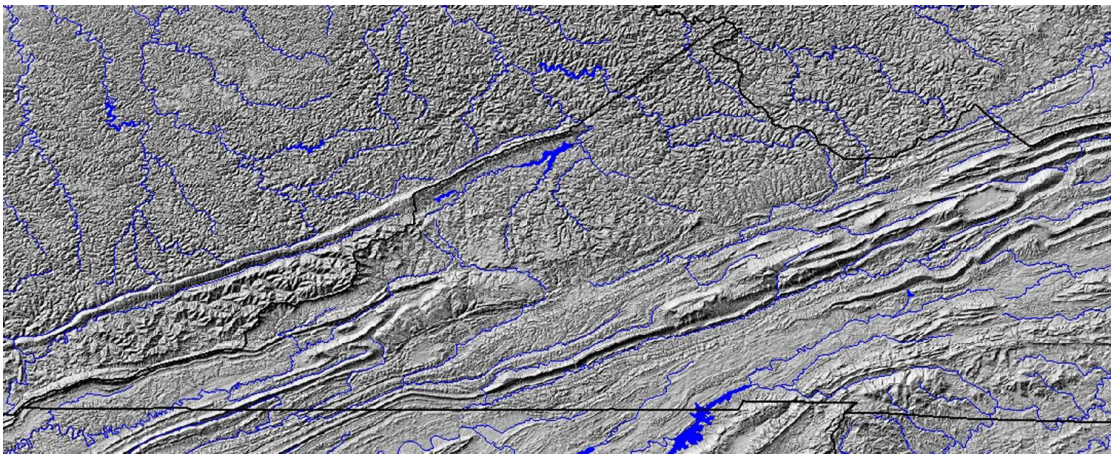
Fig. 10.15 - Parallel ridges at the Valley and Ridge provinces in Virginia, USA (USGS).

Canyons are rare fluvial-tectonic features on Earth (see section 4.2, Chapter 4). As mentioned before, their formation can be related to a specific behavior of rivers that are trying to reach a base line elevation (Huntoon, 1990). Figure 10.16 displays a complex feature on Titan (71°S, 240°W), that –even if it is not confirmed by radar data processing yet– appears to be a canyon-like morphotectonic feature, since it consists of a sinuous dark, rather narrow feature, with tributary-like off shoots and it is limited on all sides by high albedo, i.e. elevated terrains (e.g. Radebaugh et al. 2007). The morphology of the bright and dark areas of this region resembles the Grand Canyon in the United States. This terrestrial feature is adjacent to the Basin and Range Province that was mentioned earlier. The formation of the Grand Canyon on Earth, is the end result of the active extensional tectonics, that formed the Basin

and Range Province and continuous rifting and erosion (Sears, 1990). This terrestrial feature is adjacent to the Basin and Range Province that was mentioned earlier.

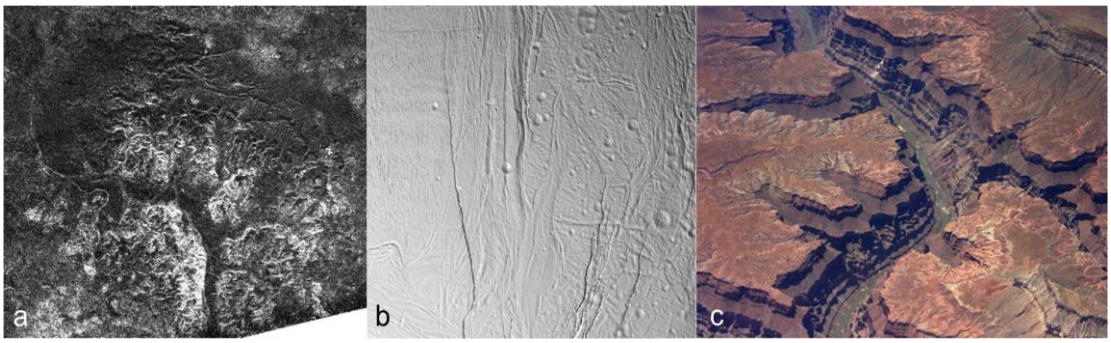

Fig. 10.16 - (a) Radar image showing canyon-like systems on Titan (PIA12036 NASA/JPL). (b) Broad canyon formation on Enceladus from Cassini/ISS (PIA08355 NASA/JPL/Space Science Institute). (c) Massive canyon formation on Earth, Grand Canyon, USA (USGS).

10.1.4 Volcanic-like features and jets

In Chapters 4, 6 and 7, I presented my analysis on some of Titan's current cryovolcanic candidate features and indicated the aspects in favour to this suggestion. Tui Regio, Hotei Regio and Sotra Patera are all located in the 15°S-30°S latitudinal zone which is close to the southern margin of Xanadu (Soderblom et al. 2009), implying that the region might be an extensive zone of crustal weakness. The existence of possible volcanic and tectonic features within a specific area seem to be manifestations of the most active region of Titan, like the boundaries of tectonic plates on Earth. Although, still under investigation on Titan's case, the definite identification and understanding of morphotectonic features in these regions is crucial in order to determine the presence and origin of zones of crustal weakness, which will in turn impose additional constraints on cryovolcanism on Titan. Indeed, on Earth, as well as on other planetary bodies, the interplay of volcanism and tectonism causes the formation of extensive and distinct geological terrains.

A terrestrial region that appears to reproduce the evolution of Hotei Regio is Harrat Khaybar, located north of Medina in Saudi Arabia (Solomonidou et al. 2010; 2013a). It is a 14,000 km^2 volcanic field that was formed by eruptions along a 100 km N-S linear vent system. The area contains multiple volcanic rock types, lava flows, and volcanic structures such as calderas and domes (e.g. Baker et al. 1973). The internal mechanism, that most likely formed the terrain, is a mantle plume, causing diffused lithospheric extension (Chang and Van der Lee, 2011). The association of the volcanic centers, that lie over a linear zone of weakness with the Red Sea, transform fault, i.e. conservative plate boundary, where plates slide past

each other along transform faults, characterizes them as geological structures that are presently active. This suggests that local movements of parts of the crust probably affect areas of great extent like Hotei Regio and Harrat Khaybar, even if they are not located precisely in the center of the active area. In the case of Harrat Khaybar, the adjacent Red Sea fault continues to propagate; its rifting causes seafloor spreading, triggering the volcanic centers of the region (Camp et al. 1991). Such process illustrates the relation between the terrestrial volcanic terrains and tectonism, a relation that seems possible for Titan and Enceladus' cases as well. In Figure 10.17, I present a comparison between Earth's, Titan's and Enceladus' possible volcanic terrains and tectonic zones of weakness, that constitute the passage of internal material to be deposited on the surfaces.

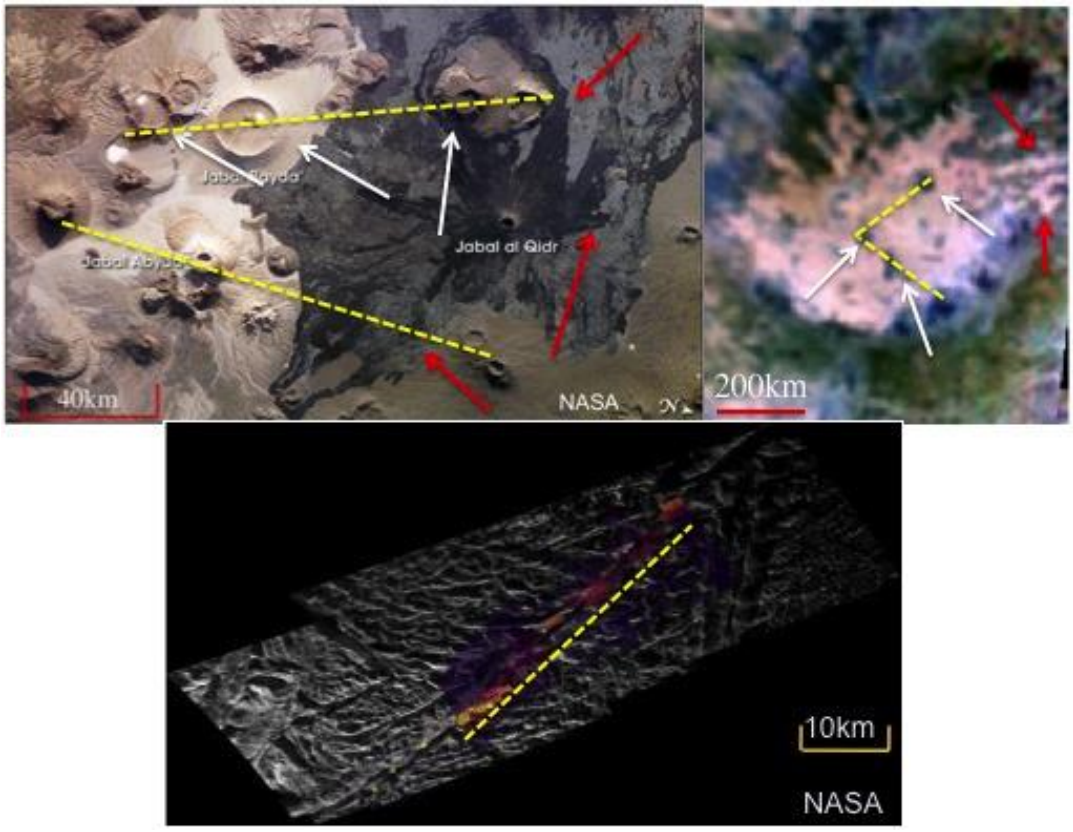

Fig. 10.17 - Volcanic fields on Earth, Enceladus and a cryovolcanic candidate on Titan. (a) Harrat Khaybar volcanic terrains, North of Medina, Saudi Arabia (Image credit: NASA). (b) Possible cryovolcanic terrain on Titan, Hotei Regio (Soderblom et al., 2009; Solomonidou et al. 2013b;c). (c) Baghdad Sulcus, volcanic fracture on the south pole of Enceladus, Tiger Stripes where pockets of heat have appeared along the fracture (Image credit: NASA). The white arrows indicate structures of tuffs, domes and calderas for Harrat Khaybar and possible dome and caldera formations for Hotei Regio. Additionally, the red arrows indicate lava flows and possible cryovolcanic flows within the volcanic landform. The yellow dashed lines indicate areas that are possibly tectonic zones of weakness from which internal material may pass through (Solomonidou et al. 2010).

Figure 10.18 shows the current, best cryovolcanic candidate region for Titan (Lopes et al. 2013; Solomonidou et al. 2013c). In the image, volcanic-like structures are seen; such as a

crater as deep as 1.5-km and two peaks more than 1 km high that surround the crater. Similar structure presents the Kirishima volcano in Japan, which consists of highland surroundings and a deep volcanic –caldera formed- crater (Imura, 1992).

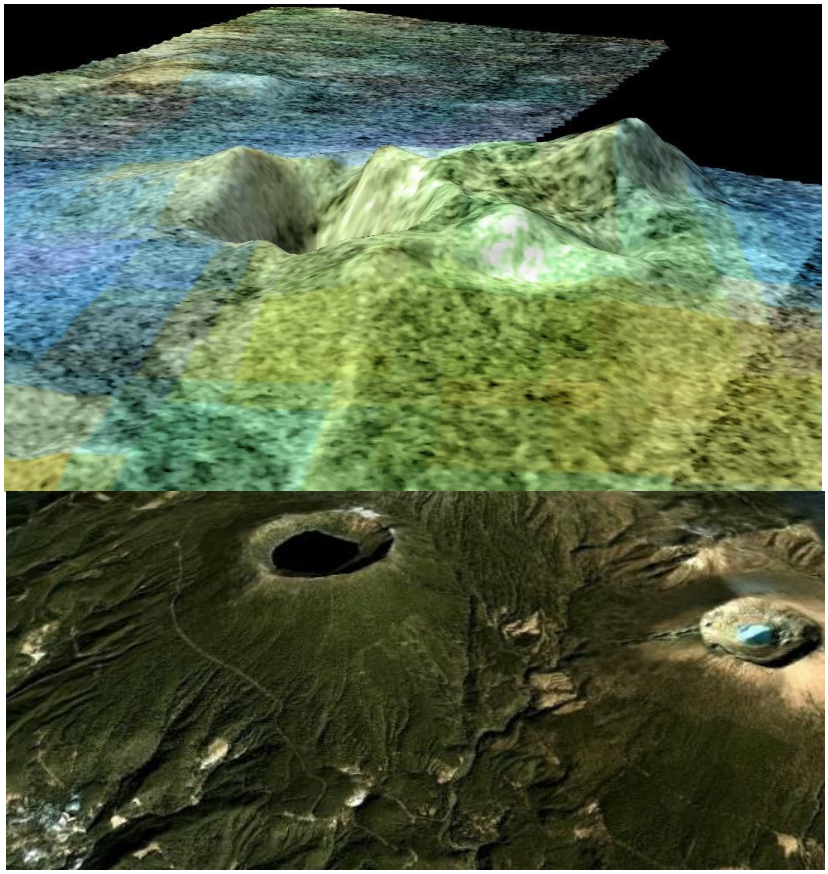

Fig. 10.18 - Cryovolcanic candidate 'Sotra Patera' on Titan (upper) (Image credit: NASA/JPL Caltech/USGS/University of Arizona). The Kirishima volcano in Japan (Image credit: USGS).

As discussed in detail in Chapters 4, 6 and 7, Tui Regio is a massive (1,500 km) flow field-like figure that could have possibly formed after accumulation of cryolava flows erupted at different times, following the area's topography. On Earth, a massive edifice resembling Tui Regio, emerges in the Tularosa Basin in south-central New Mexico, USA (Fig. 10.19). Carrizozo flow field is 75 km long and covers 328 km^2. The volume of eruptive material was about 4.3 km^3 (Bleacher et al. 2008). The field was probably formed from periodic deposition of eruptive material, spewing from a source located 27 m high, named Little Black Peak. The peak consists of three nested cinder cones and a solidified lava pond.

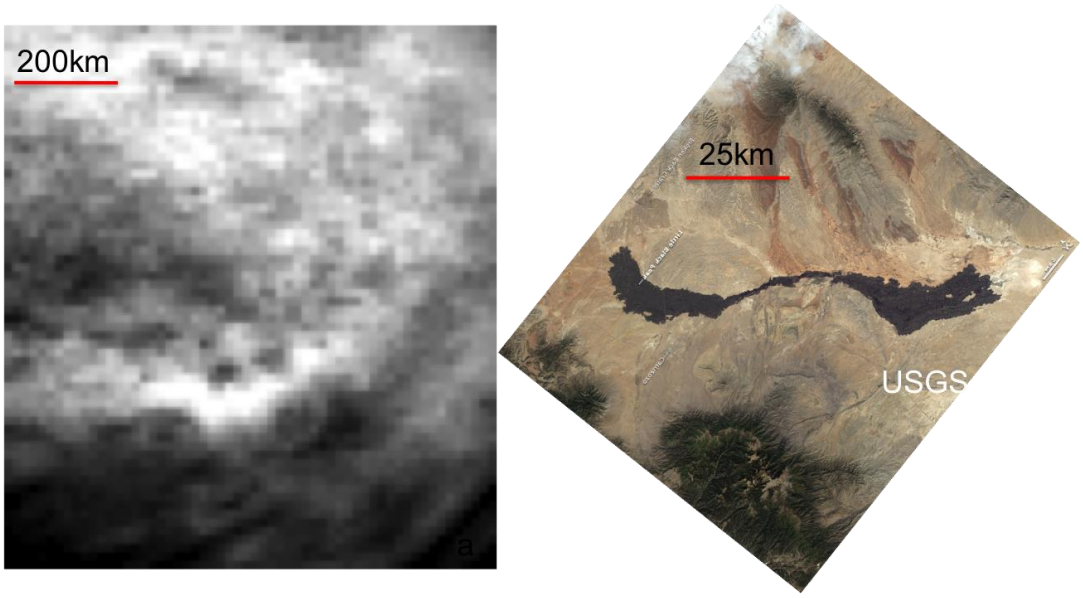

Fig. 10.19 - (left) Cryovolcanic candidate flows on Titan, Tui Regio (Image credit: Solomonidou et al. 2013b). (right) Carrizozo flow field, New Mexico, USA (Image credit: USGS).

On Earth, a geyser is a hot spring characterized by intermittent discharge of water ejected turbulently, and accompanied by a vapour phase. As thoroughly discussed on Chapter 8, it is believed that underneath Enceladus' surface lies a liquid water ocean acting as a source that supplies geysers in the same way as particular hydrological conditions trigger geysers on Earth (e.g. Spencer and Nimmo, 2013). Ice particles mixed with liquid water are expelled from at least one part of Enceladus's surface out to distances of 400 km or more. I will try to describe the interior dynamics of Enceladus and other icy moons hereafter.

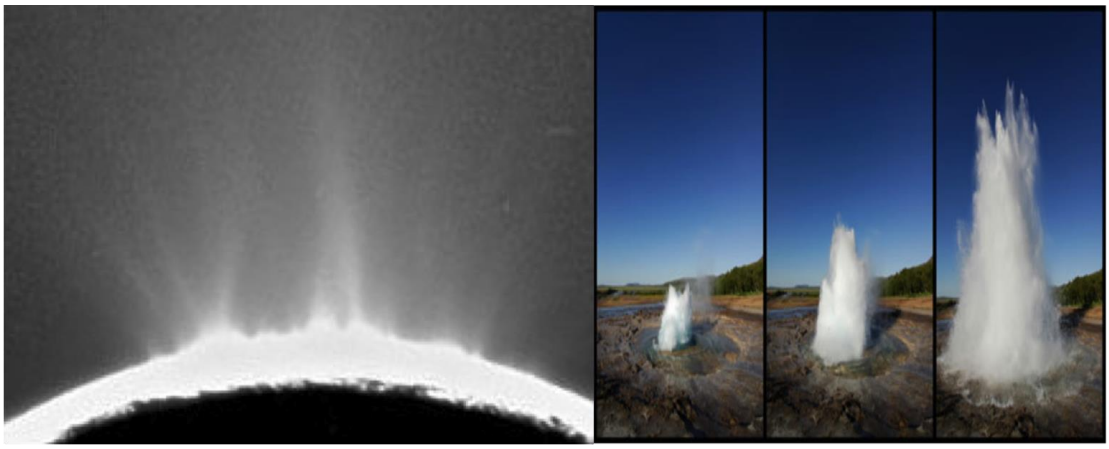

Fig. 10.20 - (left) Massive geyser-like formations on Enceladus (NASA/JPL/ISS). (right) Three stage eruption of Geyser Strokkur in Iceland (Courtesy of Christoph Achenbach).

10.2 Comparative study: Interior models and mechanisms for Titan, Enceladus and Jupiter's satellites

In terrestrial geology, convection plays an important role, significantly related to plate tectonics. Convection currents beneath the plates move the crustal plates in different directions. Similarly to the hypotheses for Titan and Enceladus oceans, underneath Earth's crust there is a malleable layer of rocks, deep within the mantle known as "asthenosphere", heated by K, Th, and U radioactive decay. The layer of fluid asthenosphere circulates as convection currents that are located underneath the solid lithosphere. This layer is the source that feeds the geyser formations, like the ones seen in Iceland, as well as volcanoes worldwide. Moreover, it is also the source of raw material that causes the elevation of mid-oceanic ridges and forms a new ocean floor. The upwelling magma generates the forces that stress the sea floor apart at the mid-oceanic ridges. Eventually, as the ocean floor is spread apart, cracks appear in the middle of the ridges, allowing molten magma to surface through the cracks to form the newest ocean floor. The creation of magma plumes, due to convection, also cause the continental crust to deform, producing mountains, ridges and other surficial morphotectonic expressions.

Such a pattern resembles the tectonic processes occurring on Titan and Enceladus, even though the conditions and materials are different. Local stress mechanisms include, (a) convection, the occurrence of which depends on the ice shell thickness, (b) local gravity and most importantly, (c) the viscosity of the ice, that dependents on the temperature and even more on the grain-size (Barr and Pappalardo, 2005; Collins et al. 2009). For large, icy satellites, layers of high- and low-pressure, ice may convect separately (McKinnon, 1998). However, convective stresses on silicate bodies tend to be larger, and their rheological length scales are typically greater. The kilometer-high uplifts with long wavelengths typical of Earth and of silicate convection, does not characterize the icy satellites (Collins et al. 2009).

Figure 10.21 presents the interior stratigraphy of major layers of Earth (Image credit: USGS), Titan (Image credit: Fortes et al. 2007) and Enceladus (self creation).

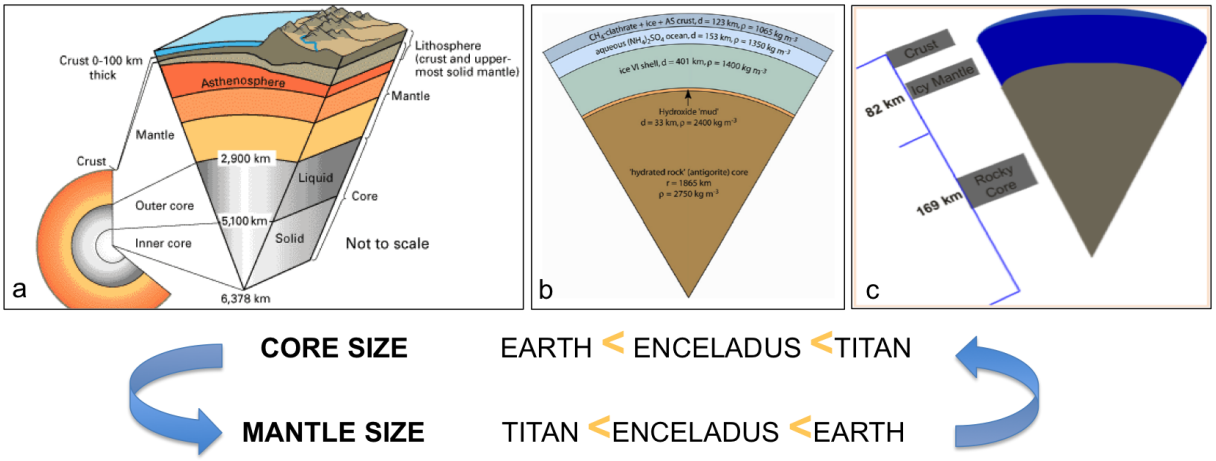

Fig. 10.21 - Sketches showing the interior strata of Earth (Image credit: USGS), Titan (Image credit: Fortes et al. 2007) and Enceladus. All three differentiated bodies consist of a core, mantle and crust in various sizes and with different materials. The difference in size of each layer, in analogy to their mean radius of the body, is shown in a sketch below the models.

According to the models and as seen in Figure 10.21, Titan has the largest core, always in analogy to its mean radius, while Earth's mantle extends more in its rocky body than Titan and Enceladus' mantles do. A detailed analysis of their interiors is discussed in Chapters 4 and 8.

The possible existence of subsurface liquid oceans underneath the crusts of the icy moons of Jupiter (Europa and Ganymede) and Saturn (Titan and Enceladus), makes them part of a potential group of planetary bodies where life could emerge and evolve, something that holds another resemblance with Earth (Fig. 10.22). Even if an ocean is not currently hidden within the interior, it is suggested that a liquid layer was present in the past but cooled to ice over time. An example of such case is Neptune's moon Triton. Our current knowledge of the internal stratification and composition of Europa, Ganymede, Titan and Enceladus is built on a combination of spacecraft data, laboratory experiments, and theoretical geophysical modeling. Resembling Earth's moon in terms of structure, these icy moons consist of a core, a mantle, and a crust, with the specificity of the existence of a liquid ocean lying within the icy mantle (e.g. Sohl et al. 2010; Schubert et al. 2010 and references therein).

For instance, focusing on Titan, there are indeed studies suggesting the presence of an internal ammonia-water ocean (Grasset and Sotin, 1996; Grasset et al. 2000; Tobie et al. 2005; Mitri et al. 2007), while another study has modeled and suggested an ocean filled with methane clathrate pockets that lead to explosive cryovolcanism (Fortes et al. 2007).

The theory of trapped methane clathrates in the potential liquid ocean is of a major astrobiological interest. The presence of methane clathrates in an aqueous environment is attached to the "clathrate gun" hypothesis, and concerns the rises in temperature at seabeds

and permafrost on Earth. Adapted to Titan's conditions, this hypothesis suggests that potential movement and rise of the temperature in an underground liquid reservoir could trigger the sudden release of methane from methane clathrate compounds buried in permafrost or seabeds (Kennett et al. 2003) or an ocean like on Titan's case. The initiation of such process, leads to further temperature rise and further methane clathrate destabilization that could easily cause and trigger cryovolcanic eruptions (Kennett et al. 2003). For Titan, a dynamic process like the one suggested by the clathrate gun hypothesis, could result to the increase of temperature values, creating an environment more favorable for life to exist.

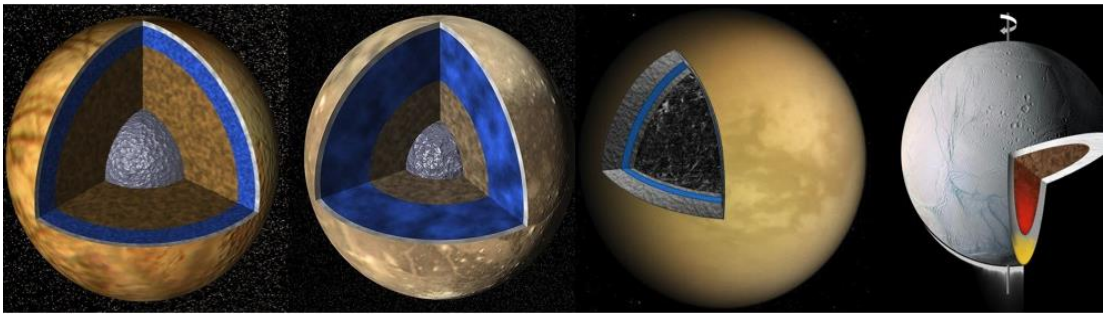

Fig. 10.22 - From left to right: Europa, Ganymede, Titan and Enceladus' internal stratigraphic models (Image credit: NASA/JPL).

Other than data processing that provides evidence and information about the internal liquid layers, the surficial expressions that are related to the hydrothermal and dynamic processes occurring within these layers, are the surface evidence that could lead to their identification. Specifically, the cryovolcanic and morphotectonic structures seen on the aforementioned satellites (see Chapters 4 and 8), are the surface expressions of the internal activity as they are formed by modification of the crustal layer and deposition of material coming from the subsurface ocean. Therefore, investigating these surface exposures and associating them with terrestrial features, where water is involved, could shed some light in the investigation of internal liquid water oceans in the icy moons. Trying to model what triggers the internal active phenomena, basic geophysical models usually propose liquid water reservoirs, while the geodynamic models point at both radioactive decay and tidal stresses, caused by the giant planets Jupiter and Saturn. I shall herein try and reconcile both views.

First, I provide a brief introduction to the major geological expressions of both Europa and Ganymede. The most significant structures on Europa's surface in terms of internal correlation are the bunch lineae (e.g. Prockter et al. 2010). Morphological and spectral evidence have shown that they change through time (Geissler et al. 1998; Dalton, 2010), suggesting diachronic activity related to the interior. Such activity seems to be different types

of cryovolcanism, in which multiple eruptions of ice (warmer than crustal ice) emerge through ‘tectonic’ crustal weaknesses (Figueredo & Greeley, 2004).

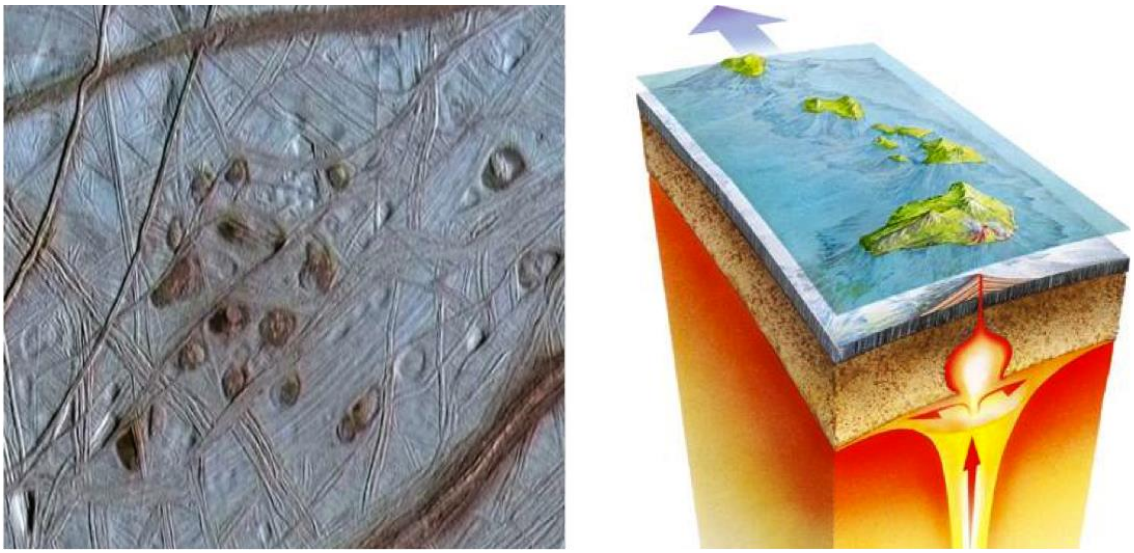

Fig. 10.23 - (left) Lenticulae on Europa (reddish semi-circular spots in the middle of the image. (right) Schematic view of the formation of the islands of Hawaii from hot spot volcanism.

This tectonic formation resembles the terrestrial mid-ocean ridges basalts (MORB), which are the extensive opening seafloor terrains, and considered to be a global rather than a local phenomenon. MORB are dynamic and volcanically active structures that constantly provide and deposit new material from the mantle to create new oceanic crust. As seen in Figure 10.23, the red streaks, as well as the red spots called lenticulae, are most possibly evidence of upwelling warmer material emerging from the liquid layer while colder ice near the surface sinks downwards. A similar type of volcanism, albeit with different materials, appears to have occurred during the formation of Hawaii, where stationary plumes of magma rised from Earth’s deep interior to the surface. In a resembling fashion to the case of Europa, thermal diapirism most likely formed the lenticulae and streak features. Such activity suggests that convective upwelling thermal plumes could have originated in the lower boundary of the convective system and came in contact with the cold stagnant lid, and partially melted the crustal ice as in Figure 10.23 -left (Showman and Han, 2004).

Unlike Europa’s conflicting oceanic hydrothermal system that originates in a rocky sea layer, Ganymede’s ocean lays between two icy layers that decouple it from the mantle. Barr et al. (2001; 2004), suggested that large magmatic events due to convective plumes could occur at Ganymede’s rock – ice boundary. The surface expressions that are most possibly connected to tectonism are the deep fault structures, like the horst-and-graben (resembling terrestrial continental rifts), as well as many cracks that are observed on Ganymede’s bright terrain

(Showman and Malhotra, 1999). Tidal heating events, either past or current, could cause dynamic forces that modify the icy lithosphere. The main mechanism that deforms tectonically the lithosphere is most likely warm liquid plumes that rise from the upper mantle to the surface, following a pattern similar to the plume-lithosphere interactions at the Hawaiian Swell, that cause thinning and instabilities at the crust layer (Moore et al. 1998). Even though the plume theory indicates cryovolcanic processes, little evidence of such activity has been detected on Ganymede. Notably, the extreme morphological difference between the bright and the dark terrains, as described in a previous section, suggests a massive geological event or set of events that have caused such large-scale geo-terrain alteration. Hence, it is possible that the extensive tectonic forces that fractured the dark terrain, partially affected the bright terrain as well. Such tectonic weaknesses could display pathways to small cryovolcanic events that lead to resurface processes. However, tilt-block faulting and shears (Head et al. 2002), are some of the structures that appear bright within the dark terrain, suggesting that tectonic cracks functioned as path for warm internal oceanic material to pass through, similar to what occurred in the bright terrain. In terms of tectonics, and similarly to the other icy moons, there is no evidence of compressional deformation (Showman and Malhorta, 1997). Since the deformational pattern is extensional, the question is whether it is a global or a local phenomenon. Collins et al. (1998), studied observations of grooved terrains of specific stratigraphic ages that have consistent directions over hundreds of kilometers, something that indicates global stressing phenomena. On Earth, stressing phenomena could occur, where severe forces cause convective currents in the ocean. In a similar way, the plume convection within Ganymede's oceanic layer could create enough turbulence and temperature-pressure instabilities to cause global stressing phenomena with an impact on tectonism. Nevertheless, Ganymede presents styles of tectonism different from Europa's.

For the case of Enceladus' its internal dynamics have been discussed in detail in Chapter 8. The jets initiate from four sub-parallel linear depressions that are tectonic in origin. Other surface expressions are scarps, ridges, and shields (e.g. Collins et al. 2009). On the other hand, Titan's surface structures related to its dynamic interior, that also support the existence of a subsurface ocean, are the three cryovolcanic candidate regions, Tui Regio, Hotei Regio and Sotra Patera, and many morphotectonic structures like mountains, ridges and canyons (e.g. Solomonidou et al. 2010; 2013a;b;c and references therein).

However, on Titan, fluid water mobilized and made buoyant by ammonia and possibly other materials, could replace terrestrial melted silicates. Cryovolcanism suggests a dynamic

process than involves the interior, the surface and the atmosphere as well (see Chapters 1 and 4). It is a multi-complex activity that resembles terrestrial volcanic processes as it follows a similar pattern, although in extremely altered conditions and different initial and depositional products. Cryovolcanism on Titan is believed to be a significant source of methane in the atmosphere (Tobie et al. 2006). An underground liquid ocean, several hundred kilometers deep at the surface of Titan, is suggested to be the source of cryomagma, hence outgassing methane into the atmosphere and thus replenishing the destroyed amounts.

Generally, for the cases of both Titan and Enceladus, it is thought that their ice shells transit from a conductive to a convective currents state; since they probably overlay a pure liquid ocean (Tobie et al. 2005), this can have major effects on surface morphotectonics (Mitri and Showman, 2008). Thermodynamic oscillations within the ice shells may trigger repeated extensional and compressional events. In the presence of a subsurface ocean underneath Titan, and as a consequence of local stress mechanisms, parts of the icy crust could behave like rigid ice floes due to lateral pressure gradients. If such floating occurs, many morphotectonic features like faults and canyons can relate their formation to this event. Furthermore, radial contraction of the internal high-pressure ice polymorphs could possibly amend the radial expansion caused during the cooling stage of the moon (Mitri and Showman, 2008), in which the existence of a liquid layer plays a significant role. As a result, the overall global contraction could form mountainous chains (Radebaugh et al. 2007).

10.3 Conclusions

All the aforementioned aspects, which mainly are the nitrogenous atmosphere, the liquid lakes, as well as the Earth-like geological structures, suggest that Titan resembles Earth more than any other body in the Solar system, despite the huge differences in temperature and other environmental conditions. Thus, a holistic understanding of Titan and Enceladus' environments will allows us to better understand Earth's evolution, starting with its primordial phase, since early Earth probably looked a lot like Titan looks today (Owen, 2005).

Vice-versa, further investigation and comparison of similar features from the three bodies, Titan-Enceladus-Earth, could provide information regarding their formation and future development on the icy moons. Titan, as described in detail hereabove, is perhaps one of the most intriguing objects in our Solar system. The combination of Titan's nitrogenous atmosphere and the geologically complex and dynamic surface, ranks the satellite as an Earth-like body (Coustenis and Taylor, 2008). The existence of liquid bodies identified as lakes, exposed on the surface (Stofan et al. 2007), the equatorial dunes, dendritic flows, potential tectonics and volcanism, enhance Titan's resemblance to our own planet. Prior to this discovery, such combination of surface features and dense nitrogen atmosphere has only been identified on Earth. Even though a future mission will bring to light more detailed data referring to tectonic features, it should be noted that alternative tectonic formation styles should be expected, other than the ones seen on Earth or even in our entire Solar system.

Chapter 11

Future exploration of the satellites of the gas giants

The planetary environment of Jupiter has been studied by the Pioneer 10 and 11, Voyager 1 and 2, Ulysses, Galileo, Cassini-Huygens and New Horizons missions. The Saturnian system has been explored by the Pioneer 11, Voyager 1 and 2 spacecraft and more recently by the Cassini-Huygens mission, which is still ongoing. My involvement and work on data from the latter mission was described in the previous chapters.

Looking into the future of outer planets exploration, a new long-term mission, focusing on the Jovian satellites, is being developed, the "Jupiter Icy Moons Explorer" mission (JUICE) (ESA L-class mission). This mission will scrutinize the nature and dynamics of Jupiter's extensive magnetosphere and the icy satellite Ganymede; and to a lesser extent, explore Callisto and Europa. Such a mission should consist of advanced instrumentation that will certainly enhance our perspectives. Our presentation of the major scientific evidence that require further exploration for these satellites' surfaces, can be found at the *Journal of Cosmology* (Solomonidou et al. 2011) and the mission's goals relative to my research are further described hereafter.

The Cassini-Huygens mission, the current on-going outer Solar system mission, has significantly advanced our understanding of the Saturnian system, especially that of Titan's, and the coupling of its atmosphere and surface. In addition, Cassini significantly has contributed to the investigation of the surface complexity of Enceladus. Since 2004, Titan and Enceladus have been under investigation during many Cassini orbiter encounters; however only a limited surface coverage will be accomplished with a high spatial resolution. Therefore, the composition, fracture and evolution of their diverse features, still remains unlocked. Even though the Cassini spacecraft will extend its investigations until 2017, a variety of issues demand further extensive exploration. Without a doubt, a new mission focusing on the seasonal, astrobiological and geological aspects of several of the satellites of

Saturn is needed in order to improve our understanding of these unique planetary bodies. On that scope, I have proposed some promising candidate locations for future landing on Titan; a work that has been published in the proceedings of the *International Planetary Probe Workshop* in 2013 (Solomonidou et al. 2013d).

In addition, on the scope of the Saturnian and Jovian icy moons' geological exploration, I will briefly discuss hereafter my contribution to a work concerning the proposal for a seismic experiment and a surface science package on the icy moons as a payload of future missions' landers (Bampasidis et al. 2011a; 2011b). Furthermore, I describe my involvements in a recently developed White Paper submitted to ESA for the definition of L2 and L3 class missions in ESA science program, concerning the future exploration of Titan and Enceladus (Tobie et al. 2013).

11.1 Missions to Jupiter: From EJSM to JUICE

Titan and Europa were identified, among others, as main targets for future exploration by NASA, in their 2003 and 2011 Decadal Surveys. ESA in collaboration with NASA has performed extended studies for the outer planets satellites exploration (TandEM, TSSM, EJSM) and finally selected JUICE, as the first large mission to be launched within the Cosmic Vision 2015-2025 Program[36].

Jupiter, with its 63 natural satellites, and its imminent position as the largest planet with the most impressive magnetosphere in the Solar System, is considered a major target for exploration. A NASA mission, called the Juno mission[37] is on its way to the Jovian System. This is the first mission dedicated to Jupiter's system since the Galileo spacecraft observations from December 1995 until September 2003. Galileo made significant geological discoveries regarding Ganymede, Europa and Callisto. The most important was the reinforcing of the theory concerning the presence of an underground liquid ocean in these satellites, retrieved from magnetic data and surface evidence (Showman and Malhotra, 1999). The spacecraft obtained high-resolution, near-infrared and UV spectra from Ganymede's surface that revealed various non-water materials, such as carbon dioxide, sulfur dioxide and, possibly, cyanogen, hydrogen sulfate and various organic compounds (e.g. McCord et al. 1998). The Juno spacecraft was launched in August 2011 and it will enter orbit insertion in 2016. The eight instruments of Juno will study Jupiter's gravitational potential and magnetic field, as well as its composition, with a focus on the planet and not so much its satellites.

11.1.1 The Europa Jupiter System Mission (EJSM)[38]

The EJSM (Europa Jupiter System Mission) was a joint NASA/ESA mission study, that would focus on the exploration of Jupiter and its moons. It was a L-scale (large) mission, consisting of two orbiters, the Jupiter Ganymede Orbiter (JGO) and the Jupiter Europa Orbiter (JEO) (Fig. 11.1). JGO would be developed by ESA and it was a continuation of the LAPLACE proposal (Blanc et al. 2009), submitted in response to ESA's Cosmic Vision 2015-2025 Call[3]. It was proposed to focus, mainly on Ganymede and Callisto, and the Jupiter system. JEO, on the other hand, would be developed by NASA and would focus mainly on Europa, exploring its habitability potential. Both orbiters' model payloads were designed to

[36] *http://sci.esa.int/cosmic-vision/*
[37] *http://juno.wisc.edu/juno-mission.html; http://missionjuno.swri.edu/*
[38] *EJSM, NASA/ESA Final Report, 30 January 2009*

study the moons' surfaces, interiors, their gravitational fields and magnetospheres as well as their atmospheric environments.

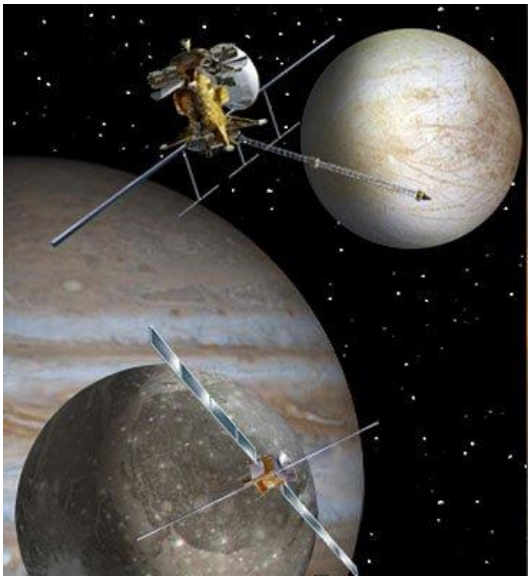

Fig. 11.1 – Jupiter Europa (upper) and Jupiter Ganymede (lower) Orbiters (Image credit: NASA/ESA).

EJSM was in competition with a mission concept for the exploration of the Kronian system that focused on Titan (the Titan Saturn System Mission-TSSM), for a slot among the L-class Cosmic Vision Program missions. After the initial studies, the Europa Jupiter System Mission (EJSM) mission was prioritized by NASA and ESA to be launched first, in order to explore the Jupiter system. The TSSM mission for the Saturnian system, which I will describe later in this Chapter, was to be developed and launched later. However, due to budgetary cuts, NASA could not support, for the immediate future, the development of such a large-scale mission as JEO, and terminated that study. ESA decided to continue with the same objectives as for JGO and some enhancement where Europa science is concerned, with a unique spacecraft dedicated to the studying of Jupiter and its main Galilean moons. In this context, the ESA Jupiter Icy Moons Explorer mission (JUICE), was proposed as a reformulation of JGO. The mission has won the competition for the first L-class mission of ESA's Cosmic Vision 2015-2025 Program. It was selected for the L1 slot of the program, on May 2nd, 2012. Two other proposals were competing, the Advanced Telescope for High ENergy Astrophysics (ATHENA)[39], a big X-Ray telescope, and the Gravitational wave Observatory (NGO)[40], a concept of three satellites that could detect gravity waves. The complete instrument payloads, as well as the instrument contractors, are currently in the finalizing stage. The participation of NASA will be limited to a few instruments perhaps and to co-investigators.

[39] *http://www.the-athena-x-ray-observatory.eu/*
[40] *http://sci.esa.int/ngo/*

11.1.2 The Jupiter Icy Moons Explorer mission (JUICE)

The Jupiter Icy Moons Explorer mission (JUICE) will visit the Jupiter system, focus on the investigation of Ganymede mainly, but also of Callisto, and to a lesser extent of Europa, as potential habitats, and on the coupling processes involving Jupiter, the moons and the magnetosphere (Fig. 11.2). JUICE will study the conditions that may have led to the emergence of habitable environments among these icy satellites and their internal oceans. The mission will also focus on characterizing the diversity of processes in the Jupiter system, including gravitational coupling between the Galilean satellites and their long term tidal influence on the system as a whole (Grasset et al. 2013). With regards to the icy moons exploration, the mission will focus on the following,

- Ganymede, as a planetary body and possible habitat.
- Europa, as a dynamic body with recent active zones.
- Callisto, as a remnant of the early Jovian system.

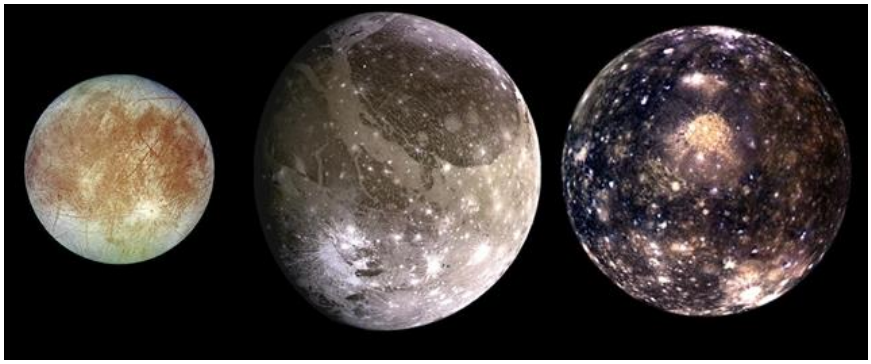

Fig. 11.2 – The targets of JUICE from left to right, Europa, Gamymede, Callisto (Image credit: ESA).

The schedule

As summarized in Table 11.1, the mission[41] will be launched in June 2022 on an Ariane 5 rocket carrier and will perform a 7.3-year cruise towards Jupiter, based on an Earth-Venus-Earth-Earth gravitational assist. The Jupiter orbit insertion will take place in January 2030, and will be followed by a tour around the Jupiter system (Fig. 11.3). It will comprise a transfer to Ganymede (11 months), a phase studying of Europa (with 2 flybys) and Callisto (with 3 flybys), lasting one month all together. Then, a "Jupiter high-latitude phase" will begin, that includes 9 Callisto flybys (lasting 9 months) and the transfer to Ganymede, that will last 11 months. In September 2032, the spacecraft will enter into orbit around Ganymede,

[41] http://sci2.esa.int/cosmic-vision/JUICE_Yellow_Book_Issue1.pdf

starting with elliptical and high altitude circular orbits (for 5 months), followed by a phase at a medium altitude (500 km) circular orbit (of 3 months), and by a final phase at a low altitude (200 km) circular orbit (for 1 month). The end of the nominal mission is planned to be in June 2033.

Table 11.1 - Schedule of the baseline mission for JUICE (Adapted from Grasset et al. 2013).

Phase	**Start**	**End**	**Duration**	**Science priorites**
Cruise	06/2022	01/2013	7.6 yrs	
Jupiter Tour				
Jupiter equatorial phase no 1/Transfer to Callisto	01/2030	01/2031	12 mon	Jovian atmosphere structure, composition, and dynamics.
				Jovian magnetosphere as a fast magnetic rotator and giant accelerator.
				Remote observations of the inner Jovian system.
Europa flybys	02/2031	03/2031	36 days	Composition of selected targets with emphasis on non-ice components
				Geology and subsurface of the most active areas
				Local plasma environment
Jupiter high latitude phase with Callisto	04/2031	10/2031	6 mon	Jupiter atmosphere at high latitudes
				Plasma and fields out off equatorial plane
				Callisto internal structure, surface and exosphere.
				Remote observations of Ganymede, Europa, Io, and small moons.
Jupiter equatorial phase no 2/Transfer to Ganymede	11/2031	08/2032	9 mon	Interactions of the Ganymede magnetic field with that of Jupiter.
				Jovian atmosphere and magnetosphere as in phase #2
Ganymede Tour				
Elliptic no 1	09/2032	10/2032	30 days	Global geological mapping
				Search for past and present activity
High altitude (5000 km) circular	10/2032	01/2033	90 days	Global compositional mapping
Elliptic no 2	01/2033	02/2033	30 days	Local plasma environment and its interactions with Jovian magnetosphere
Medium altitude (500 km) circular orbit	02/2033	06/2033	102 days	Extent of the ocean and its relation to the deep interior
				Ice shell structure including distribution of subsurface water
Low altitude (200 km) circular orbit	06/2033	07/2033	30 days	Geology, composition and evolution of selected targets with very high resolution
				Global topography
				Local plasma environment
				Sinks and sources of the ionosphere and exosphere
				Deep interior

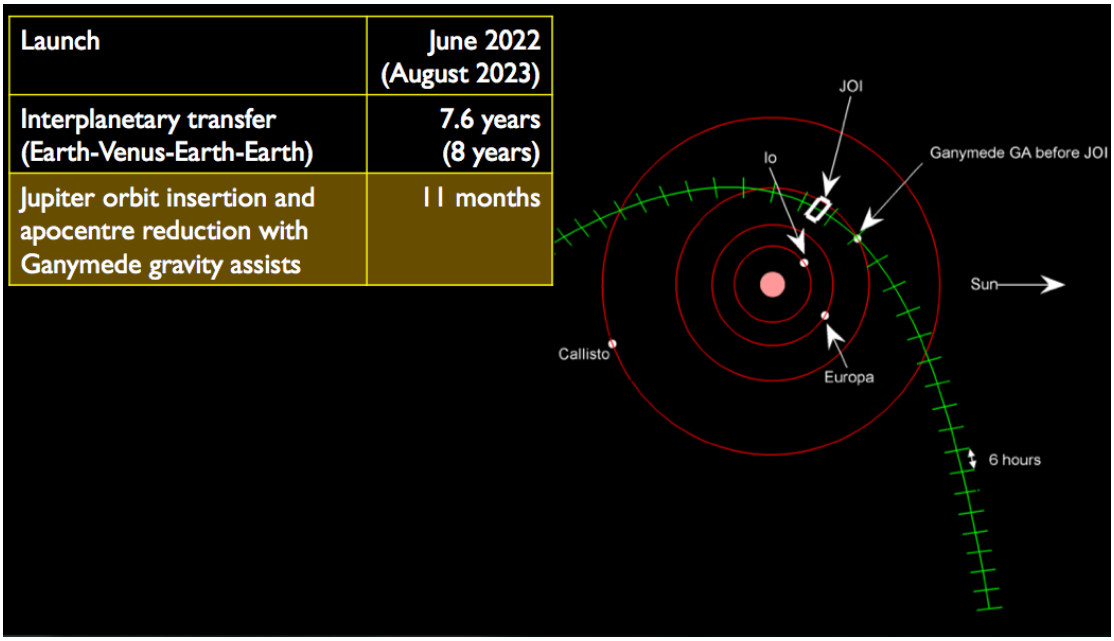

Fig. 11.3 – Orbits of JUICE within Jupiter's system (Image credit: ESA).

The spacecraft

The spacecraft is three-axis stabilized and powered by solar panels, providing around 650 W at end of mission (Fig. 11.4). Communication with Earth is provided by a fixed 3.2 m in diameter high-gain antenna, in X and Ka bands, with a downlink capacity of at least 1.4 Gbit/day.

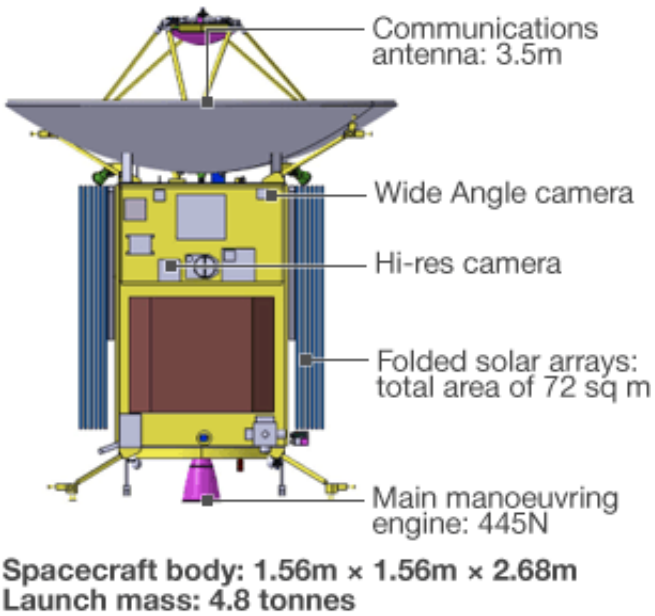

Fig. 11.4 - The JUICE spacecraft design (Scheme credit: ESA)

The spacecraft's dry mass at launch, will be approximately 1.8 tons. The selected payload is a suite of 11 instruments weighting about 110 kg,

- **Camera system (JANUS).** JANUS will provide high-resolution images of Jupiter and its moons. This will include global imaging from the high orbit around Ganymede and imaging of selected targets, few meters per pixel from the low altitude at Ganymede in resolution. Hence, the global, regional and local morphology and processes of Ganymede, and the other moons, will be studied in addition to mapping of Jupiter's clouds (PI: P. Palumbo, Università degli Studi di Napoli "Parthenope", Italy).
- **Moons and Jupiter Imaging Spectrometer (MAJIS).** MAJIS will study the composition of the moons' surfaces and the composition, dynamics, structure and morphology of the Jupiter atmosphere (PI: Y. Langevin, Institut d'Astrophysique Spatiale, France.
- **Ultraviolet Imaging Spectrograph (UVS).** UVS will acquire images that will help us explore the surfaces and atmospheres of Jupiter's icy moons and allow us to see how they interact with the Jupiter environment. In addition, the instrument will determine the interactions between Jupiter's upper atmosphere with its lower atmosphere, and the ionosphere and magnetosphere above. The instrument will perform both nadir observations and solar and stellar occultation sounding (PI: R. Gladstone, Southwest Research Institute, USA).
- **Submillimeter Wave Instrument (SWI).** SWI will investigate the structure, composition and dynamics of the middle atmosphere of Jupiter, and exospheres of its moons, as well as the thermophysical properties of the satellites surfaces (PI: Hartogh, Max-Planck-Institut für Sonnensystemforschung, Germany).
- **GAnymede Laser Altimeter (GALA).** GALA will study the tidal deformation of Ganymede and the morphology and topography of the surfaces of the icy moons (PI: H. Hussmann, DLR, Institut für Planetenforschung).
- **Radar for Icy Moons Exploration (RIME).** RIME is an ice – penetrating radar that will study the subsurface structure of the icy moons. It can penetrate the ice up to 9 km in depth, with vertical resolution of up to 30 m (L. Bruzzone, Università degli Studi di Trento, Italy).
- **Magnetometer for JUICE (J-MAG).** J-MAG will characterize the Jovian magnetic field. In addition, it will establish and characterize magnetic induction signatures in possible subsurface oceans at Ganymede, Europa and Callisto (PI: M. Dougherty, Imperial College London, United Kingdom).
- **Particle Environment Package (PEP).** PEP will measure the neutral material and

plasma that accelerates and heats to extreme levels in Jupiter's fierce and complex magnetic environment. It will also measure the composition of the moons' exospheres, with a resolving power of more than 1000. (PI: S. Barabash, Swedish Institute of Space Physics (Institutet för rymdfysik, IRF), Kiruna, Sweden).

- **Radio and Plasma Wave instrument (RPWI)**. The RPWI is a radio plasma wave instrument that will characterize the radio emission and plasma environment of Jupiter and its icy moons. It is based on four experiments, GANDALF, MIME, FRODO, and JENRAGE. Moreover, it consists of a set of sensors that measures the DC electric field (two E-field dipole sensors), the electric component of plasma waves (E-field sensors and use of the radar antenna), magnetic field component of electromagnetic waves (Search Coil Magnetometer), radio emissions (triad of radio antennae) and some detailed characteristics of the thermal plasma (Langmuir Probes), including electric conductivity (J-E. Wahlund, Swedish Institute of Space Physics (Institutet för rymdfysik, IRF), Uppsala, Sweden).
- **Gravity & Geophysics of Jupiter and Galilean Moons (3GM).** The 3GM is a radio science package comprising a Ka transponder and an ultrastable oscillator. It will study the gravity field - up to degree 10 - at Ganymede and the extent of internal oceans on the icy moons, and will also investigate the structure of the neutral atmospheres and ionospheres of Jupiter and its moons (PI: L. Iess, Università di Roma "La Sapienza", Italy).
- **Planetary Radio Interferometer & Doppler Experiment (PRIDE).** PRIDE will perform precise measurements of the spacecraft position and velocity in order to investigate the gravity fields of Jupiter and the icy moons. Note that this, does not include spacecraft hardware, but will exploit VLBI – Very Large Base Interferometry – to conduct radio science.

The scientific goals

JUICE will provide a thorough investigation of the Jovian System in general, including the investigation of Jupiter's extensive magnetosphere and especially will focus on the potential habitats Ganymede, Callisto and Europa, searching to determine if they satisfy the habitability prerequisites, the existence of water, the energy supply, the organic chemistry and the stability over time. I have presented the intriguing geological aspects, of these planetary bodies, in a paper published in the *Journal of Cosmology* (Solomonidou et al.

2011). In addition, detailed discussion on their astrobiological potential can be found on Chapter 9.

The JUICE mission will perform extensive geological investigations through topographical, geological and compositional mapping, as well as analysis of the physical properties of the icy crusts. Moreover, the interiors will by analyzed in detail, through the detection of putative subsurface water reservoirs, the characterization of the ocean layers and the internal mass distribution; in addition to the study of the dynamics and evolution of the interiors. Finally, Ganymede's intrinsic magnetic field, and detailed studies of the moons' exospheres/ionospheres, will be performed.

My PhD Thesis supervisor, Dr. A. Coustenis, was the European Science co-Lead of the JUICE Science Study Team and defined all the steps of the mission during its study by ESA and NASA and then by ESA alone (JUICE). In cooperation with the Space Physics Team of the University of Athens, we focused on a twofold contribution in the JUICE mission, (a) instrument calibration and (b) outreach activities (Chapter 12). I am collaborating with investigators involved in the JANUS camera of JUICE (R. Lopes and R. Jaumann) and hope to have the opportunity in the future to become involved in this and in other instruments of the mission.

For instance, as presented in detail in previous Chapters, with Dr. Mathieu Hirtzig we developed, and are currently exploiting, a multi-stream radiative transfer code (Hirtzig et al. 2013; Solomonidou et al. 2013b;c) with which we can process spectro – imaging data. In particular, after correcting the atmospheric contribution in Cassini Visual and Infrared Mapping Spectrometer (VIMS) observations (Brown et al. 2004), we can deduce Titan's surface spectrum, by inverting the I/F reflectivity. But this code can be further applied to the in-flight data of the foreseen JUICE/MAJIS instrument, included in the model payload of the JUICE mission, in which LESIA is implicated. The RT code I have could be used to yield spectral calibration constraints for the instrument and of course to exploit the data when they arrive in 2030...

The JUICE mission will be the next mission to the outer Solar system, after the completion of the Cassini mission. Hence, the exploration of the icy moons will continue for the next decades. However and in addition, the unexpected findings of the Cassini mission, concerning Titan and Enceladus, exhibit the need for a future mission to the Saturnian system, with these satellites as main targets. I hereafter discuss current plans for missions to the second largest satellite of the Solar system.

11.2 Mission studies for a return to Saturn, Titan and Enceladus: TSSM, TAE, AVIATR, TiME, JET

Undoubtedly, the Cassini-Huygens mission has provided us with valuable data, data that has magnified our knowledge. However, there are still aspects, especially regarding the surface and the seasonal effects on the whole environment, that are not yet covered, along with several unanswered questions. The revelation of Titan's surface will be a key point in unveiling the atmosphere and the interior but also a major contribution to icy moons' understanding. After having evaluated Cassini-Huygens mission's data, it is now clear how important it is to acquire direct sampling of the surface and have mobility in the near-surface environment. Thus, we should have the opportunity to map Titan on a global scale, from orbit, and visit other targets in the Saturnian system. The geological objectives request landing site measurements of the *in situ* geological context, chemical composition by several types of spectroscopy, mineralogy provided by infrared data and petrological properties such as porosity, grain size, permeability and more (Jaumann et al. 2009). This could be achieved with measurements taken from close range, at scientifically interesting areas, with a montgolfière that could explore the surface in a close-up range and also, perhaps, crash onto the surface and get measurements[42]; and/or a lander that will descend in an equatorial or polar region and take measurements of solid ground or a liquid.

11.2.1 From the Titan and Enceladus mission (TandEM[43]) to the Titan-Saturn System Mission (TSSM)[44]

TandEM mission concept

The Titan and Enceladus mission (TandEM), was a large International collaborative effort, in which 155 expert scientists and engineers participated (Coustenis et al. 2009). The Proposal Lead was my supervisor, Athena Coustenis.

The TandEM mission was planned to be launched around 2018, or later, and wanted to address several of the Cosmic Vision 2015-2025 themes; with the help of an orbiter, a balloon, and several landers/penetrators to be delivered to the satellite around 2030. Its design was based on the Cassini-Huygens architecture and it was expected to surpass the latter's

[43] http://www.lesia.obspm.fr/cosmicvision/tandem/
[44] *TSSM NASA/ESA Joint Summary Report, ESA-SRE(2008)3, JPL D-48442, NASA Task Order NMO710851, 2009.*

legacy by exploring Titan and Enceladus in full close-up and *in situ* coverage over long periods of time, something that is not currently possible.

The mission concept of TandEM (Fig. 11.5) consisted of two moderate-size spacecraft's, the Titan-Enceladus Orbiter, with the Enceladus penetrators, and the Carrier for the Titan *in situ* investigation elements that consisted of the Titan Montgolfier-hot air balloon and the three lander/mini-probes (Coustenis et al. 2009).

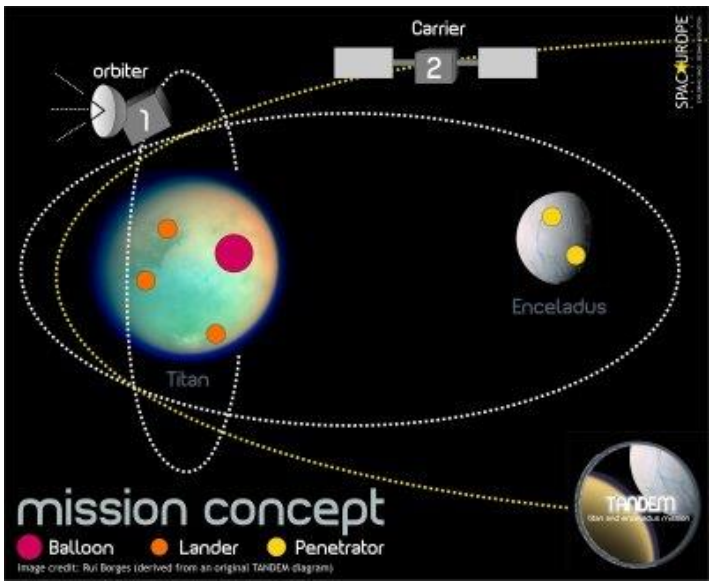

Fig. 11.5 - TandEM mission concept (Coustenis et al. 2009) (Image credit: Mathieu Hirtzig).

After its arrival, the orbiter would perform several flybys of Titan and Enceladus and carry the Enceladus landers/penetrators. The carrier spacecraft would release the Titan hot air balloon as well as up to three entry probes. To facilitate the telecommunication with the *in situ* vehicles, the carrier could be converted into an orbiter and perform science measurements, like occultations, using the telecom link between the two orbiting spacecraft's. The telecom relay between the Titan *in situ* elements and the Earth orbiter would be provided by the orbiter.

The Montgolfière consisted of a balloon and a gondola. The balloon would be filled by Titan's gas, heated by the energy from the two Multi-Mission Radioisotope Thermoelectric Generators (MMRTGs) that would be located in the gondola with the scientific equipment. Titan's dense nitrogen atmosphere, with temperatures less than 100 K at the first 70 km above the surface, is favorable for a hot air balloon flight. The average operation altitude of the Montgolfière is 10 km above the surface.

The Titan mini-probes design would follow mainly the Huygens probe experience as well as the GEP-ExoMars (Geophysics Package). The parachute system would have been similar to the one used for the Huygens Entry Descent and Landing (EDL) sequence. These penetrators could be released by the Montgolfière or the carrier. They could include seismometers as payload and thus construct a seismic network on the surface of Titan. Two penetrators would be delivered to Enceladus surface from the Titan-Enceladus orbiter.

The TandEM proposal, along with the LAPLACE mission to Jupiter (Blanc et al. 2009) proposal, were the two finalists selected by ESA in October 2007 for further study in the framework of the 2015-2025 Cosmic Vision Plan as L-class missions in collaboration with NASA. Both studies were accepted as fully responsive to the Cosmic Vision Goals.

An international team of 16 US and 15 European scientists and engineers, the Joint Science Definition Team (JSDT), was formed, in order to develop a mission to Titan that would address the key questions left unanswered by the Cassini-Huygens mission. The JSDT merged, the NASA Titan Explorer study –for a mission to Titan (Leary et al. 2008)– and the TandEM study, into the "Titan and Saturn System Mission" (TSSM)[45]. The JSDT also examined the Decadal Survey of 2003 documents of the US National Academy of Sciences, documents that regarded Titan and Europa as the highest priority targets for future missions.

The TSSM mission concept

The TSSM mission was a merge of the Titan explorer (Leary et al. 2008), and the Titan and Enceladus Mission (Coustenis et al. 2009) concepts, that had been selected respectively by NASA and ESA for studies. TSSM was studied in 2008. TSSM has to do with an in-depth long-term exploration of Titan's atmospheric and surface environment. Also with *in situ* measurements in one of Titan's lakes, aiming to explore Titan as an Earth-like System, examine Titan's organic inventory and explore also Enceladus and Saturn's magnetosphere. To achieve these goals, a dedicated orbiter would carry two *in situ* elements, the Titan montgolfière (hot air balloon) and the Titan Lake Lander, that would combine in order to provide data and analyses directly in the atmosphere, on the surface and sound the interior of Titan. The mission would launch in the 2023-2025 timeframe on a trajectory, using Solar Electric Propulsion (SEP), as well as gravity assists, to arrive ~9 years later for a 4-year

[45] *http://www.lesia.obspm.fr/cosmicvision/tssm/tssm-public/*
http://sci.esa.int/science-e/www/area/index.cfm?fareaid=106
http://opfm.jpl.nasa.gov/titanriskreduction/

mission in the Saturn system. Soon after arrival on Saturn, the montgolfière would be delivered to Titan. The TSSM three elements would operate as follows,

a) The orbiter, using nuclear power, would perform 7 close-up Enceladus' flybys and then enter into orbit around Titan, for an estimated time of 2 years of dedicated observations (Fig. 11.6).

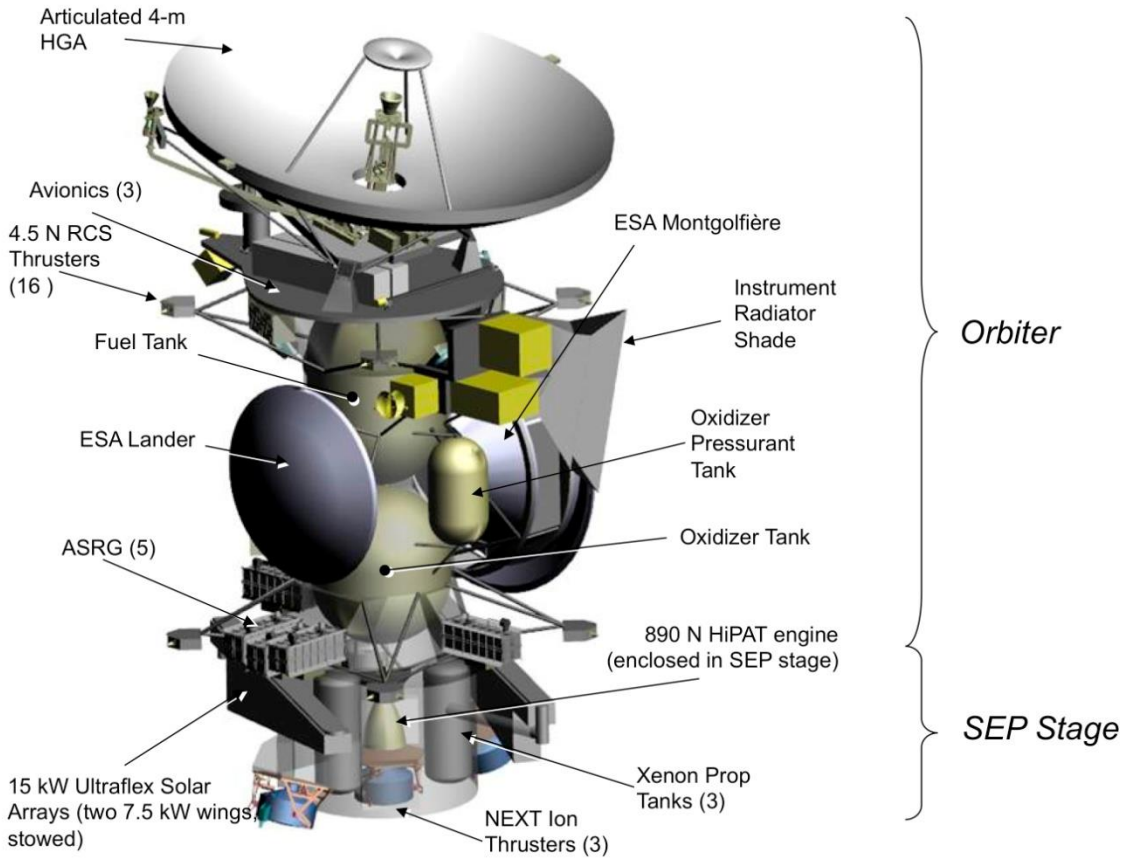

Fig. 11.6 - The TSSM orbiter (Image credit: TSSM Final Report. JPL D-48148 NASA Task Order NMO710851).

b) The hot air balloon would probe both Titan's atmosphere and surface, from above the equator, and at a low altitude orbit of 10 km, for at least six months, using MMRTGs (Fig. 11.7).

c) The Lake Lander would perform the first extraterrestrial oceanographic experiment by landing in one of the Titan's lakes, the Kraken Mare, at approximately 75° N.

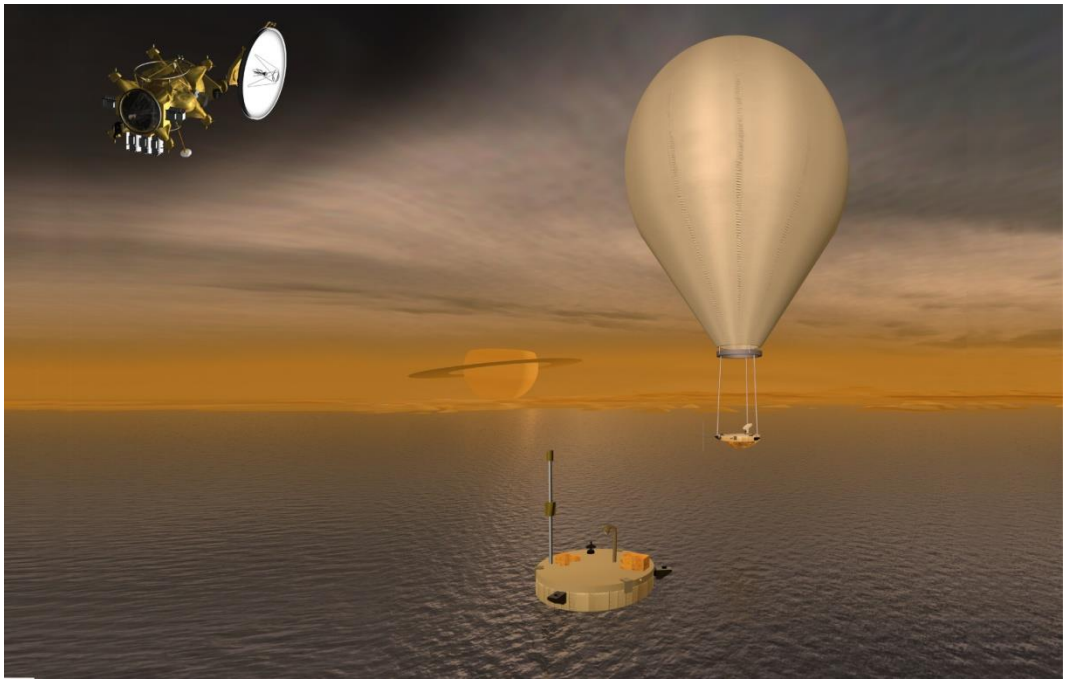

Fig. 11.7 - The TSSM basic concept: the orbiter, the balloon and the lake lander (Image credit: TSSM Final Report. JPL D-48148 NASA Task Order NMO710851).

The TSSM concept was designed to carry the adapted instrumentation in order to study the atmosphere, the surface, as well as the subsurface (Table 11.2). Considering that the current resolution from images acquired from Cassini/VIMS observations of Tui Regio, Hotei Regio and Sotra Patera, range between 12-150 km/pixel, the surface exploration payload will greatly improve the spectral data to an extremely high extend. Including specific instruments on-board the orbiter, such as a high-resolution imager and spectrometer, it is capable to acquire spectra at 1–6 μm and perform global mapping at 50 m/pixel in three colors. Another important part of the payload is going to be the Penetrating Radar and Altimeter instrument that could obtain global mapping of subsurface reflectors with 10m altitude resolution in altimetry mode and more than 10m in depth resolution, with roughly 1km x 10km spatial resolution. Furthermore, a montgolfière, travelling over 10,000 km in linear distance, could image and map Titan's diverse landscapes at a close range. The TSSM montgolfière will be equipped with the following instrumentation; a Balloon Imaging Spectrometer, a Visual Imaging System and a Titan Radar Sounder (>150 MHz). In addition to topography, the radars on both the orbiter and the montgolfière will provide information on the tectonics and stratigraphy of the crust, with different and complementary resolution. TSSM is expected, according to plan, to acquire the ability to examine in detail the lakes and their surrounding environment, through the probe entry, the descent and landing of a lake lander that could also include efficient electronic equipment focusing on the study of the liquid itself, like MEMS

(Micro-Electro-Mechanical Systems) instrumentation. The proposal of MEMS as part of the science surface properties package, on board of a future Lake Lander on Titan, reinforces such kind of research (Bampasidis et al. 2011b). MEMS devices offer a low cost and reduced size of instrumentation, in order to accomplish the 3D sounding of the liquid deposit, and detect the presence of any biomarkers in a broader area. By dramatically reducing the production cost without decreasing the efficacy, these micro devices can execute scientific investigations in places, and micro scales like never imagined before.

Table 11.2 - The orbiter's payload (TSSM Final Report. JPL D-48148 NASA Task Order NMO710851).

	Orbiter planning Payload	**Instrument Capabilities**
HiRIS	High-Resolution Imager and Spectrometer (near IR)	1–6 μm global mapping at 50 m/pixel in three colors. Adjustable spectral editing for surface/atmosphere studies.
TiPRA	Titan Penetrating Radar and Altimeter	>20 MHz global mapping of subsurface reflectors with 10 m altitude resolution in altimetry mode & >10 m depth resolution. Lower data rate sounding mode with ~100 m depth resolution ~1 km x 10 km spatial resolution.
PMS	Polymer Mass Spectrometer	TOF MS with M /ΔM ~10,000 for masses up to 10,000 Da. From 600 km to upper atmospheric in situ analysis of gases and aerosol precursors.
SMS	Sub-Millimeter Spectrometer	Heterodyne spectrometer with scanning mirror. Direct winds from Doppler and temperature mapping from ~200-1000 km altitude; carbon dioxide and nitrile profiles.
TIRS	Thermal Infrared Spectrometer	Passively cooled Fourier spectrometer, 7–333 μm. Organic gas abundance, aerosol opacity and temperature mapping 30–500 km.
MAPP	Magnetometer	Tri-axial fluxgate sensors. Noise level ~11pT$_{rms}$. Interaction of field with ionosphere: internal and induced field.
	Energetic Particle Spectrometer	TOF Analyzer w/ss detectors to measure magnetospheric particle fluxes, ~10 keV to >MeV with 150° x 15° FOV.
	Langmuir Probe	Swept voltage/current probe. In situ electron density and temperature, ion speed constraint, including during aerosampling.
	Plasma Spectrometer	Electrostatic analyzer with Linear electric field TOF MS. Measures ion and electron fluxes at ~5 eV to ~5 keV. M/ΔM~10.
RSA	Radio Science and RSA Accelerometer	All components part of spacecraft telecom system. Lower stratosphere and troposphere T profile. Gravity field.

This mission came second in decision by the agencies, and was abandoned. However, it inspired several other proposed concepts for smaller size missions, like the Titan Aerial Explorer (TAE) (Hall et al. 2011), the Aerial Vehicle for In-situ and Airborne Titan Reconnaissance (AVIATR) (Barnes et al. 2011) and the Titan Mare Explorer (TiME) (Stofan et al. 2011).

11.2.2 Aerial explorers: The Titan Aerial Explorer (TAE) and the Aerial Vehicle for In-Situ and Airborne Titan Reconnaissance (AVIATR)

The Titan Aerial Explorer (TAE)[46,47]

[46] *http://www.lesia.obspm.fr/cosmicvision/tssm/tssm-public/*

Titan Aerial Explorer (TAE) was an M3 candidate for ESA's Cosmic Vision call (Fig. 11.8) (Hall et al. 2011). TAE was a balloon, and it was planned to fly in the lower atmosphere of Titan at an altitude of 8 km, for 3 to 6 months on Titan's equatorial latitudes, with Direct to Earth transmission without the need of an orbiter. The TAE scientific goals were organized around two themes, (i) the presence of an atmosphere and liquid volatile "hydrologic" cycle on Titan that implies climate evolution through time, and (ii) the Organic chemistry, pervasive through its atmosphere, surface, and probably interior.

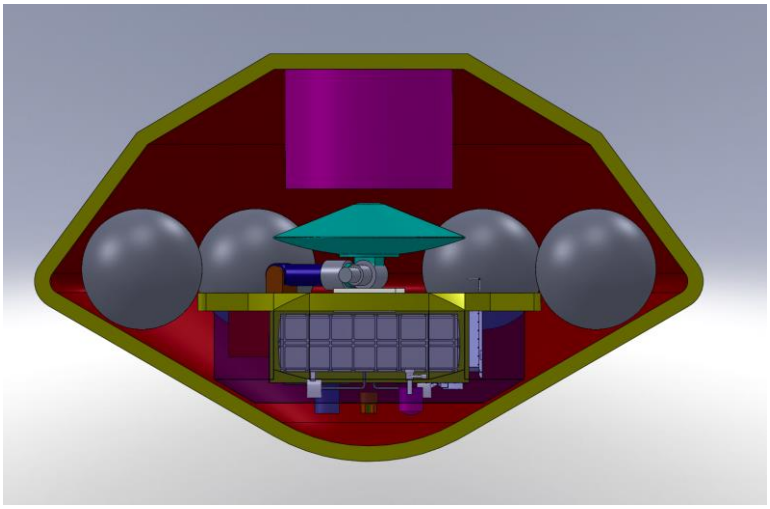

Fig. 11.8 - The gondola of TAE (Scheme credits: Hall et al. 2011).

The Aerial Vehicle for In-Situ and Airborne Titan Reconnaissance (AVIATR)

The AVIATR was a proposal suggesting alternative concept to the Titan balloon mission (Fig. 11.9) that was not selected among the Discovery mission studies. Since Titan experiences low gravity and a dense atmosphere, a nuclear powered airplane could fly easier, more than 20 times than on Earth. It could sample directly the atmosphere and cover huge swaths of Titan's landscape (Barnes et al. 2012).

[47] http://users.sch.gr//gbabasides/joomla/

Fig. 11.9 - AVIATR air vehicle exterior blueprint (Barnes et al. 2012).

11.2.3 Lake lander: The Titan Mare Explorer (TiME)

The Titan Mare Explorer (TiME), a Discovery candidate, is a probe, focusing on exploring Titan's lakes and especially the Ligeia mare (Fig. 11.10). This lake lander could study the chemical composition and the geological characteristics of the hydrocarbon lakes (Stofan et al. 2011).

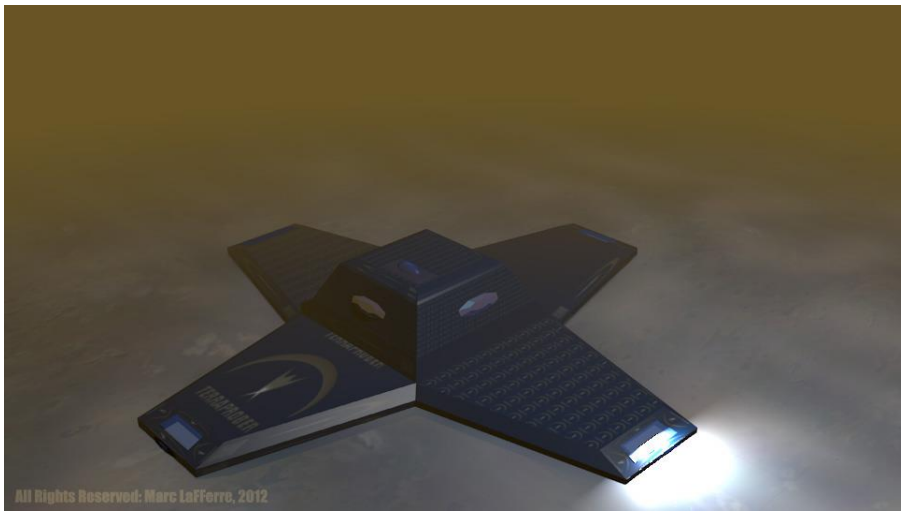

Fig. 11.10 - Artist's view of the TiME sailing Leigia Mare on Titan (Stofan et al. 2011).

The TiME concept was studied until 2012 but was not selected among the 3 Discovery mission proposals, so in August 2012, the study was terminated. InSight (Interior exploration using Seismic Investigations, Geodesy and Heat Transport), a mission to Mars, was selected. InSight would study the interior of Mars by performing a seismic experiment and probing the rate of heat that escapes from the interior. However, in a proposed spending bill for 2014, the

Senate Appropriations Committee directed NASA to resume design work on one of the Discovery finalists, a lander that would hop on and off a comet racing toward the sun; and TiME.

Adjacent to the mission concept of TiME was the Titan Lake Probe; it included a submarine (Fig. 11.11) (Waite et al. 2010).

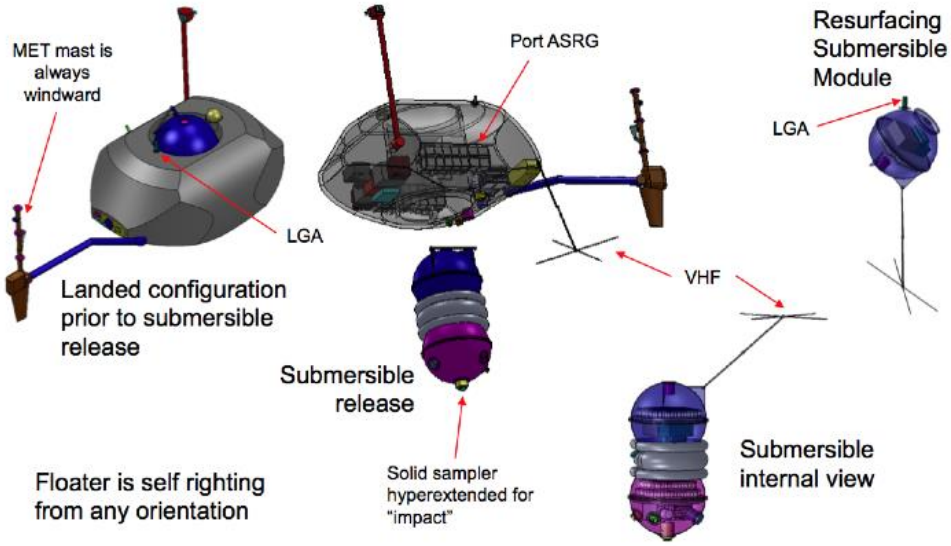

Fig. 11.11 – Titan Lake Probe (Scheme credit: Waite et al. 2010).

Another Discovery candidate was the Journey to Enceladus and Titan (JET); a simple orbiter with two instruments only and radio science that would explore the plumes of Enceladus and the atmosphere and surface of Titan (Sotin et al. 2011).

In the following section, I have focused on the investigation of areas that appear as good candidate sites for landing, for a perspective future mission to the Saturnian system with the main target being Titan. The findings of the Cassini mission have indicated these areas and their scientific importance that yields further investigation. This work has been presented and published in the proceedings of the *10th International Planetary Probe Workshop (IPPW-10).*

11.3 Experiment proposals for future mission to the icy moons

11.3.1 Micro-Electro-Mechanical-Systems (MEMS) for Titan Lakes

As described on Chapters 4 and 7, during the Cassini-Huygens mission, the lakes have shown variations through time. Hence, the connections among the lakes, the atmosphere and the interior, as well as the lakes' astrobiological potential, are in the forefront of investigation and modeling. In addition, the surface liquids are also of astrobiological interest. The understanding of the interior layering will definitely benefit by the potential unveiling of the composition of the lakes, through the use of specific *in situ* instrumentation of a future landing mission (like the ones proposed in the beginning of this Chapter e.g. TiME).

We have proposed Micro-Electro-Mechanical-Systems (MEMS) devices as part of the science surface properties package of a future probe to Titan, like the TSSM Lake Lander (Bampasidis et al. 2009; 2011b). My Greek colleague, Georgios Bampasidis, leads the proposal. I have co-authored this work and presented it at the *9th International Planetary Probe Workshop* in 2012. This proposal has been published in the IEEE proceedings of the *International Conference of Space Technology (ICST)* in 2011.

MEMS micro probes (e.g. Stark and Bernstein, 1999) (Fig. 11.12) as part of the payload of a future mission could help scrutinize the composition and the physical parameters of the liquid and its surroundings. MEMS devices seem ideal for such an experiment for two reasons, in addition to their technological and scientific importance, (i) they are of low budget instrumentation and (ii) they are significantly reduced in size. These micro sensors will function as reconstruction tools of the temperature and the pressure vertical profile within the liquid deposit, while also operate as internal sources of radiation giving the opportunity to the lake lander to analyze the composition and the structure of the lake (Bampasidis et al. 2011b). Full description of the proposed experiment can be found in the Appendix.

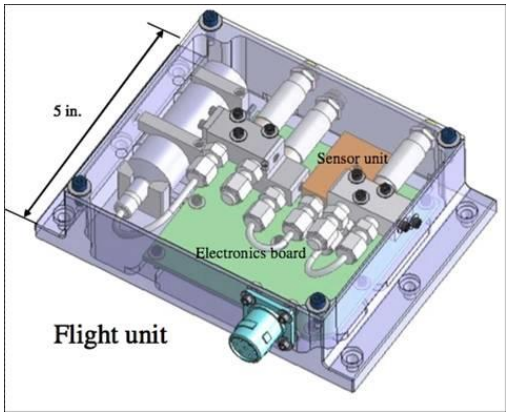

Fig. 11.12 - A pattern of the MEMS 5-inces package (Scheme and information source: NASA, Nano ChemSensor Unit (NCSU) Experiment http://128.102.216.35/factsheets/view.php?id=118).

I have to note that even though this proposal concerns Titan, as well as a future landing mission to Titan, the proposed instrumentation can be incorporated in the payload of any future space mission to other planetary bodies that consist of liquid layers, like Europa and even Enceladus. Briefly, as Titan resembles Earth more than any other planetary body in the Solar system, any results from Titan can be used for studying the terrestrial environments and help scientists to test and evaluate their models for Earth.

11.3.2 Seismometers on icy moons

Titan and Enceladus, and Jupiter's Ganymede and Europa, preserve evidence about the genesis and evolution of their systems (Kronian and Jovian), but also of the entire planetary system. Thus, through the studying of their internal structure and the processes occurring within these planetary bodies, many researches and experiments are dedicated to the decoding of the geological processes that govern the Solar system.

Here, I present briefly the proposal for a seismic experiment for the icy moons, as a payload of future missions' landers, from a study that I co-authored (Bampasidis et al. 2011a). More information on the experiment can be found in the Appendix. This proposal has been published in the IEEE proceedings of the *International Conference of Space Technology (ICST) in 2011* (Bampasidis et al. 2011a) and presented by our German collaborator, Martin Knapmeyer (DLR), at the annual conference of the European Geosciences Union in 2012, as part of an overview for planetary seismometers (Knapmeyer et al. 2012).

The internal geological structure of each planet or moon can only be determined by *in situ* measurements. The local or global tectonic field, meteoroid impacts and the moon's tidal deformations induced by Jupiter or Saturn's gravity field, as well as temperature and pressure fluctuations, may originate ground vibrations within the icy moons. These ground vibrations provide information about the nature of the subsurface material, its fracture and its chemical composition.

In the proposed experiment hereafter, we also suggest pre-target areas with internal dynamic potential and multivariable surface expressions (see next section). Through these experiments, it will be possible to identify active regions along the satellites that will provide important information regarding the fluid transfer processes towards the surface, as well as determine the presence of a subsurface liquid deposit (Bampasidis et al. 2011b). Hence, the scientific goals of this seismic experiment are concentrated on the unveiling of the internal

structure of the aforementioned icy moons, the detection of any tectonic activity and the confirmation of the presence of an internal liquid ocean.

A seismograph is the basic instrument for measuring the ground vibration (Fig. 11.13). It mainly consists of the seismometer and the unit that records the signal. The seismometer consists of three sensors placed in the same sealed case and each sensor is a pendulum that when it is triggered, by the ground movement, it moves from its equilibrium position. This movement is the record of the instrument. The sensors can measure any ground motion within a frequency range usually of 0.001 Hz to 100 Hz, at the north/south, east/west and vertical component in orthogonal system. Both low and high frequencies can be recorded by broadband seismometers used on Earth. Newer seismographs measure ground movements smaller than 1 nm.

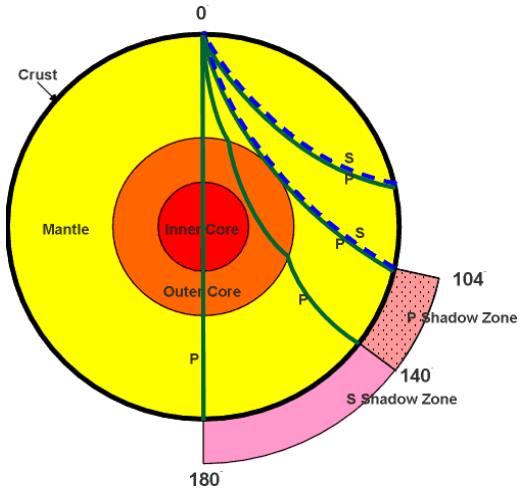

Fig. 11.13 - Seismic waves propagation through Earth. Earth is a differentiate medium. The two types of body waves, initiated by earthquakes or by explosions, travel through the interior and provide crucial information about the internal structure. The primary waves (P) compress the material and can travel either through solid or fluid media. On the other hand, the secondary waves (S) shear the medium and can only travel through solids. Hence, the recordings of P and S waves on the surface can give us clues about the nature of the interior of a planetary body (credit: JL Ahern, 2009).

Seismic waves refract when they pass from the fringes of layers with different densities or changes in temperature, since the local seismic velocities are different. These boundaries are tracers of changes in rock types of the interior. The waves can be detected through a network of sensors providing constraints for the modeling of the internal structure. Seismic waves from distant events travel deeper into the interior of a planetary body than waves from nearby events. Hence, measuring events at various distances, with seismometers, can provide the variance in depth of seismic velocities within icy moons.

A seismic network has been proposed (see Fig. 11.14) to be part of the geophysical payload of forthcoming missions (Lorenz et al. 2009; Lange et al. 2011). A seismic network

can consist of an array of sensors based on the promising MEMS technology, as well as several piezoelectric transducers and new developments based on laser-interferometric sensing or convection in electrolytic liquids.

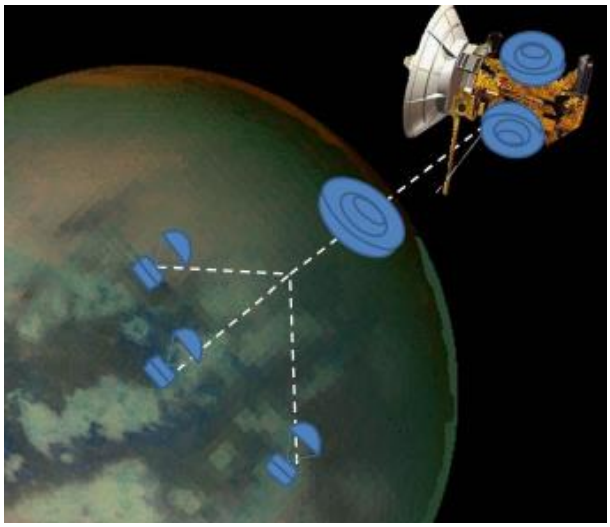

Fig. 11.14 - Titan network mission scenario. Detailed long-term surface studies require data collection trhough out a geophysical network (Lange et al. 2011). Seismic equipment can be included as payload of such a mission. As in other planetary bodies, except Earth (Moon, Mars, Venus), Saturn's icy moons seem ideal targets for seismic experiments since they possibly possess active interior.

11.4 Candidate Regions on Titan as promising landing sites for future *in situ* missions and ground-based experiments

In Chapters 4, 6 and 7, I presented information gathered from the Visual and Infrared Mapping Spectrometer (VIMS) (Brown et al. 2004), the Synthetic Aperture Radar (SAR) and RADAR (Elachi et al. 2004) and some Huygens' instruments, regarding Titan's atmosphere, surface composition and morphology. It appears that, a combination with unique geological surface expressions (Lopes et al. 2013; Solomonidou et al. 2013a) makes Titan a prime candidate for geological, internal and surface *in situ* investigation. Moreover, many of those surface expressions have counterparts in Earth geology, but the materials in play are different (see also Chapters 4 and 10). The diversity of surface formational mechanisms include potential cryovolcanism on a number of areas, such as Tui Regio, Hotei Regio and Sotra Patera (Solomonidou et al. 2013b;c). Results processing data acquired from these areas, with specific tools, as presented on Chapter 5, showed possible endogenic or exogenic processes that occur in two of these areas that affect their brightness with time, implying changes in composition (Tui Regio and Sotra Patera).

In the work I present in this section, we focused in those areas and Hotei Regio as well, since it provides very interesting geology, from VIMS and RADAR data. I also present the suggested pre-target areas with internal dynamic potential and multivariable surface expressions, as proposed by Bampasidis et al. (2011a) for the seismograph experiment (previous section).

Promising landing sites on Titan for in situ investigation

The two cameras of Cassini/VIMS observed the surface of the candidate areas at visible and infrared wavelengths, and have given insights about their composition. Furthermore, the Cassini/RADAR with SAR, acquired topographic pictures using microwaves, penetrating Titan's hazy thick atmosphere. Combined investigations, specifically of Hotei Regio and Sotra Patera, suggested that both instruments are in agreement with results pointing towards a variety of geological processes, having occurred in the past or recently, possibly indicating cryovolcanism. Indeed, data correlation and analysis from VIMS and RADAR provided us with images and mosaics, combining both spectral and morphological information. The evidence presented on Chapters 6 and 7 rank these areas as geologically interesting, enhancing the significance of a future mission to Titan with *in situ* capabilities (Reh et al. 2008; Coustenis et al. 2009) that would focus on these or similar areas.

The question rising is why the geological terrains Tui Regio, Hotei Regio and Sotra Patera have multivariable geomorphology and qualify as candidates for future landing sites. The answer comes from the wealth of data acquired from VIMS and RADAR on board Cassini spacecraft. Not only has the data revealed the uniqueness of those areas, by means of morphological aspects, but also has depicted the variability in composite component. Moreover, candidate regions for *in situ* investigations should combine atmospheric, surficial, near sub-surficial and deep internal investigations. If the cryovolcanic origin of the areas is identified, they will stand as case study areas for all the aforementioned investigations.

A crucial point for the selection of a landing site is the determination of investigation, and sampling after landing (Fig. 11.15). A potential lander, like the Huygens probe, should be capable to land on a solid surface and carry a fully instrumented robotic laboratory down to the surface. The lander's principal function is to sample and analyze grains attributed from regions of the surface within the areas of interest that lie at the margins of alternative structures (i.e. the area where two geological edifices/plains conjunct). Since all three areas, Tui Regio, Hotei Regio and Sotra Patera, are suggested to be cryovolcanic in origin, the sampling process should be treated similarly as on terrestrial volcanic terrains. Tui Regio is possibly an accumulation of, cryolava flows forming a massive flow. Ideal *in situ*, and remote imaging of the Tui Regio area, should comprise sampling from diverse regions by means of chemical composition and morphology. Such regions could be the main part of the flow, the marginal areas, and the surrounding terrain, considered as the primary material on which possible cryovolcanic material is deposited. Since *in situ* imaging of multiple areas that are considerably distant between them, is impossible, then the selection of a landing area is restricted to an area that presents spectral scientific interest. Such area could be the margin between the flow-like feature and the "old" spectrally dark terrain.

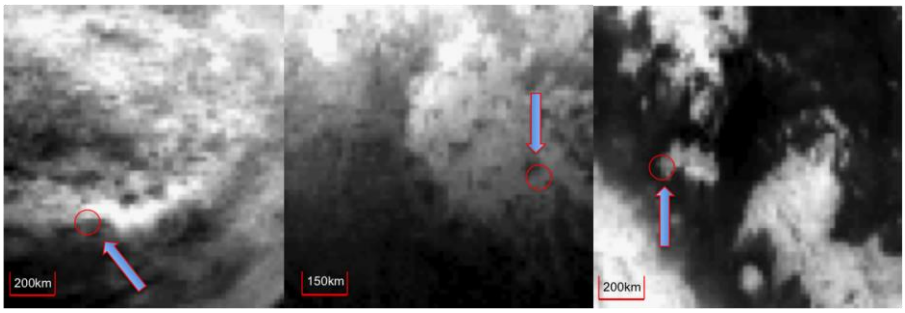

Fig. 11.15 - Areas of potential landing on Tui Regio (left), Hotei Regio (middle) and Sotra Patera (right).

As presented on Chapter 4, Hotei Regio exhibits a more complex geological terrain than Tui Regio in terms of morphology, as seen from the current data. As mentioned before,

central Hotei Regio is a low basin, consisting of caldera-like figure, flows, channels, and faults, while mountains surround it. Data processing showed that the area suggested being cryovolcanic is different from its surroundings, in terms of surface albedo (Solomonidou et al. 2013b). This is compatible with terrestrial caldera structures that consist partially of primal surficial components on which the volcano is being built, as well as the rise of newly fresh material coming from the interior. Potential sampling and identification of the chemical composition, of both the surrounding dark area and the material from the caldera-like feature, could bring into light significant information regarding internal processing on Titan. Thus, the landing region proposed, is, the margin area lying between the largest caldera within Hotei Regio's terrain and the bright component that surrounds the caldera.

Sotra Patera consists of a topographically diverse terrain with a 1-km crater (Sotra Patera), two mountains (Doom and Erebor Monters) and a lobate flow region (Mohini Fluctus); a potential landing site option should be carefully selected having in mind the safety of the landing. Thus, it seems that the lobate flow region is a safe and scientifically interesting option, since the in situ identification of the material covering such feature, will provide insights regarding the unknown material of the 5 μm anomalously bright regions.

In conclusion, Titan's spectacular surface terrain requires further and deeper investigation. The identification of ongoing processes on the surface will reveal the internal, sub-surficial and atmospheric processes as well, giving a holistic view on Titan's evolution. Tui Regio, Sotra Patera and Hotei Regio are some of Titan's cryovolcanic candidates, with the first two probably subject to changes in surface albedo with time. The indications of multivariable processes occurring in all three areas, identifies them as desirable candidate landing sites, for a lander that could measure the chemical composition as well as detect the geological properties of each area. Future *in situ* explorations with landers and close-up *in situ* elements is the most thorough and profound way to move forward concerning such investigations.

Discussions on future missions on Titan, after the Cassini mission comes to an end in 2017, have been presented earlier on this Chapter.

Candidate locations for ground-based experiments

The ideal setting for the location of seismic equipment will have to ensure that its recordings will represent accurately and separately every ground vibration. For this purpose, the seismic instruments on Earth should be placed in a hole of approximately 0.5 m depth.

Thus, less ground noise will be recorded. Noise on an icy surface can be originated by the atmosphere due to its seasonal and diurnal effects as reviewed in Hirtzig et al. (2009), on Titan's case. Noise can be produced also from the local wind and meteor impacts.

In the case of Titan, its dense atmosphere protects the surface from meteoroid impacts and few craters have been observed so far (Elachi et al. 2005; Wood et al. 2010). Therefore, the seismometers will record merely interior events. On the other hand, the same instrumentation will also measure vibrations caused by impacts on Enceladus, Ganymede and Europa.

The proper contact between the feet of the seismograph and the local surface at the landing area is another issue to be confronted. Any particles and dust can easily perturb the seismic sensors during their function and cause random errors in the sensor's record. This type of surface features has already been found on Titan. The Huygens probe landed on a relatively soft solid surface, analogous to wet clay, lightly packed snow and wet or dry sand (Zarnecki et al. 2005). Moreover, the Descent Imager and Spectral Radiometer's (DISR) surface images showed rounded stones, approximately 15 cm in diameter, to lie on top of a finer-grained surface in variable spatial distribution (Tomasko et al. 2005). If the icy pebbles, lying over the instrument's feet move or/and melt, the equilibrium position of the seismic equipment will be disturbed and the sensors will misplace their initial orientation. The measurements should be corrected if such a micro-movement of the probe is noticed.

11.5 Proposals for future missions in the 'L2', 'L3' Cosmic Vision 2015-2025 plan[48]

The 'Cosmic Vision' is the European space exploration plan into the advancement in space science in a contemporary context. On this scope, ESA calls proposals for the next Small (S-class), Medium (M-class) and Large (L-class, L2, L3) class missions (the criteria for the S, M and L-class proposals can be found here: http://sci.esa.int/cosmic-vision/46510-cosmic-vision/?fbodylongid=2153).

Based on the outstanding Cassini-Huygens discoveries, several missions to Titan and Enceladus have been identified as highest priority targets in the *National Research Council* (NRC) Planetary Decadal Survey for 2013–2022. Additionally, the Titan and Enceladus Mission (TandEM, Coustenis et al. 2008) was proposed in 2007 as an L-class (see §11.2.1) in response to the first ESA's Cosmic Vision 2015–2025 Call, and accepted for further studies, while it merged in 2008 with NASA's Titan Explorer concept, to become the joint large (Flagship) Titan and Saturn System Mission (TSSM). In 2013, ESA's Director of Science and Robotic Exploration announced a Call to define the science themes and associated questions for the next L2 and L3 Large missions in the Cosmic Vision 2015-2025 plan, that are planned for launch in 2028 (L2) and 2034 (L3). The JUICE mission to the Jupiter system (§11.1.2) is already accepted and prioritized as an L1 mission.

The procedure started with a consultation of the broad scientific community, in the form of the current Call, soliciting White Papers to propose science themes and associated questions that the L2 and L3 missions should address. Following that, many White Papers were submitted to ESA for the definition of the L2 and L3 missions in the ESA Science Program. I have contributed to one proposal concerning the future exploration of Titan and Enceladus (Tobie et al. 2013) that I describe in this section.

Mission concept: Future exploration of Titan and Enceladus[49]

The Cassini heritage

As already mentioned many times in this manuscript, the Cassini orbiter and the Huygens probe has revealed Titan and Enceladus as extremely fascinating bodies in terms of general planetology, geology, astrobiology, organic chemistry and more. Many findings throughout the Space Age exploration concerning Titan enhance this interest, including the

[48] *http://sci.esa.int/cosmic-vision/51454-call-for-white-papers-for-definition-of-l2-and-l3-missions/*
[49] *http://www.sciences.univ-nantes.fr/lpgnantes/lpg/fichiers/tobie-g/ESA_WP_Titan-Enceladus-final.pdf*

extensive N_2 atmosphere, the methane that develops the rich organic chemistry, the cloud activity, the Earth-like geology etc. Furthermore, Enceladus discovery of the water wapour jets emanating from its south pole ranks the satellite as one of the most promising targets for future exploration, since it is the only icy moon that presents endogenic activity with proofs. In addition, the plumes' composition, including water vapour, organics and salt-dominated ice grains indicate the connection of this geyser-like phenomenon with the interior and the presence of a subsurface liquid ocean.

Hence, the Cassini findings present the need for further, more sophisticated and detailed exploration of Titan and Enceladus. For Titan, a future mission will study an Earthly environments with a methane cycle equivalent to terrestrial water cycle and analyse complex chemical processes that may have dominated on the early Earth. Furthermore, for Enceladus' case, the jets discovery request further analysis of the internal in origin materials that possibly contain prebiotic compounds. Also, such investigation will shed light to other icy worlds that are hypothesized to have a subsurface oceanic layer in their interiors.

The proposal

As mentioned earlier in this section, the unexpected and very intriguing discoveries raised many mission proposals since 2007 to the space agencies with main targets being Titan and Enceladus. The White Paper I discuss here is being authored and supported by many scientists from all over the world. The spokesperson is Gabriel Tobie from the University of Nantes, France. I have contributed in the composition of the geological part of this proposal where we describe the current understanding of Titan and Enceladus' geology (interior and surface) and summarize on the scientific hey questions that are currently present.

This proposal, is built on the heritage of TSSM, and presents science goals that could be achieved from the combination of a Saturn-Titan orbiter and a Titan balloon.

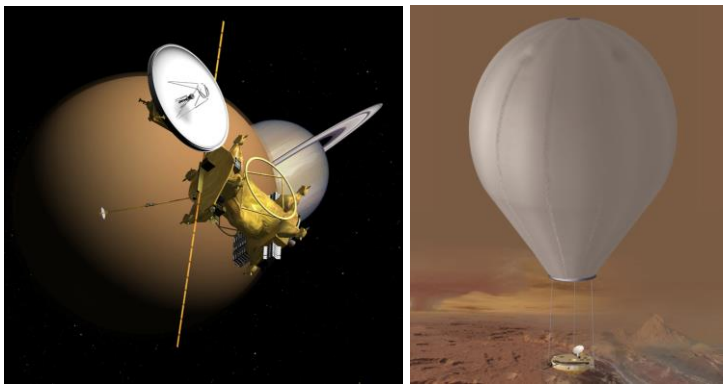

Fig. 11.16 - Concepts of orbiter (left) and hot air balloon (right) as illustrated for the TSSM proposal (Tobie et al. 2013).

The main science goals of this mission are three, as described in the proposal:

i. Understand how Titan functions as a world, in the same way that one would ask this question about Venus, Mars, and the Earth,

ii. Further characterize the present-day activity of Enceladus, to understand what processes power it and how it affects the Saturnian environment,

iii. Determine the degree of chemical complexity on the two moons, to analyse complex chemical processes that may have prevailed on the early Earth, and to detect compounds of prebiotic interest.

Tables 11.3 and 11.4 summarize the tentative instrumentation for both the Orbiter and the balloon designed to achieve the aforementioned science goals.

Table 11.3 - Tentative instrument Orbiter payload to address the three mission goals i, ii and iii (Adapted from Tobie et al. (2013).

Saturn-Titan Orbiter (Science goals i, ii and iii)
1. High-resolution Imager (2, 2.7, 5–6 μm) and Spectrometer (0.85–2.4/ 4.8–5.8 μm)
2. Penetrating Radar and Altimeter (> 20 MHz)
3. Thermal Infrared Spectrometer (7-333 μm)
4. High Resolution Mass spectrometer (up to 10000 amu)
5. Icy grain and organic Dust analyser
6. Plasma suite
7. Magnetometer
8. Radio Science Experiment
9. Sub-Millimetre Heterodyne
10. UV Spectrometer

Table 11.4 - Tentative instrument Balloon payload to address the two mission goals i and iii (Adapted from Tobie et al. (2013).

Titan Balloon
1. Visual Imaging System (two wide angle stereo cameras and one narrow angle camera)
2. Imaging Spectrometer (1–5.6 μm)
3. Atmospheric Structure Instrument and Meteorological Package (science goal i)
4. Electric Environment Package
5. Radar sounder (> 150 MHz)
6. Gas Chromatograph Mass Spectrometer (1-600 amu)
7. Radio science using spacecraft telecom system
8. Magnetometer

In terms of geology that is of significance interest for me, the understanding of the interplay of various geological processes on Titan and Enceladus as well as the distinctions between the geology, hydrology, meteorology etc of Titan and other planetary bodies in the Solar system is very important in order to comprehend the past and the possibilities for the future in our Solar system. Although the Cassini-Huygens mission provided major insights for understanding the geological on Enceladus, as well as the atmospheric processes that are present on Titan, many questions remain unanswered—requiring future missions enhanced with developed and adjusted to these worlds instrumentation.

11.6 Conclusions

Future missions on icy moons of the outer planets will be a great opportunity in studying them comparatively and also give proof for active planetary systems. Jupiter's Ganymede, Callisto and Europa will be the main targets of a future ESA mission at the outer planets, to study the emergence of habitable worlds and the Jovian system as a whole. The Jupiter Icy moons Explorer (JUICE) mission will study in depth the icy satellites of Jupiter. It will focus on detailed investigations on Ganymede, Europa and Callisto in order to understand their surface geology, detect the presence of a liquid ocean in their interior and study their habitability potential.

Saturn's Titan and Enceladus can also be studied in the future, in order to improve our understanding of their atmospheric circulation, the surface geological processes and tectonics and their internal oceans, among others. The icy moons of the gas giants can also provide hints regarding the emergence of life and the climate of Earth.

To study Titan as a system, the Titan Saturn System Mission (TSSM) or smaller more focused concepts have been proposed, based on interdisciplinary scientific interest, in order to understand the nature of the geological playground, surface formation and its interaction with the atmosphere, meteorology and aeronomy. They could determine the present-day structure and levels of activity of Titan and Enceladus. Such a mission could also identify heat sources, internal reservoirs of volatiles (in particular methane and ammonia) and eruptive processes and astrobiological processes that possibly occur in its organic environment. The mission will also investigate the relation and interaction between Titan and Saturn and between Enceladus and Saturn.

The utilization of Micro-Electro-Mechanical Systems (MEMS) technology will give to future missions, the opportunity to improve the exploration. By exploiting their small shape, these prospective devices can reach distant areas where traditional instrumentation is unable to visit. MEMS are some of the most innovative technologies available today. The MEMS experiment we proposed for the lake lander, will monitor extensively the ground beneath the liquid, and quantitatively define precisely its chemical composition. As a consequence, a MEMS experiment on Titan’s lakes will appreciably enlighten our view of the largest Saturnian moon, unraveling a crucial link for understanding atmospheric dynamics and geological processes on it. This conceptual project, after surviving a rigorous testing procedure, can be part of any planetary mission, establishing a path for forthcoming surveys.

The seismic experiment, which we also proposed as part of a future landing mission, can identify the existence of liquid internal deposits, with a great astrobiological potential. Isolated environments that consist of water and organics, components that have already been identified on most icy satellites, provide ideal conditions for the survival of biological building blocks.

We strongly suggest the aforementioned geological and geophysical experiments as part of the framework of a future mission to the icy moons of the outer Solar system. The White Papers submitted to ESA for a future mission to Titan and Enceladus carrying the TSSM heritage is a good opportunity to re-visit and investigation the fascinating Saturnian system.

Chapter 12

Outreach activities related to the Cassini mission and astronomy

People always have been fascinated by the beauty of the starry sky, the Sun, the Moon, the planets, the Solar system and the mystery of birth and evolution of the Cosmos. As deep space is believed to be the only territory unexplored by mankind, humanity, always, has been looking forward to the discoveries of Space Science. However, due to the perception of complexity of modern Science and Technology, people usually are alienated from scientific issues. Dealing with this situation, the Space Physics Team (Scientific Team of the Physics Department organized by Prof. Moussas) of the National and Kapodistrian University of Athens, in collaboration with LESIA of the Observatoire de Paris-Meudon, have been performing several campaigns to raise the public awareness of Science and Astronomy with emphasis on the Solar system exploration.

Outreach, is an essential endeavour for a researcher, and for me in particular who likes to communicate my findings with the public in return of their investment in our research and also because it is an excellent way to attract the attention of children, pupils and students towards space studies, including aeronautics, planetology and theory.

During my PhD studies, I got profoundly involved and invested in many outreach activities. The Space Physics Team has been selected as the organizer for NASA's 'Cassini scientist for a day' student competition in Greece and I was the official coordinator over the course of the past three years (2010-2013) (Solomonidou et al. 2012). Throughout the years of organizing the Greek edition of the competition, I had a close and direct communication with members of the Cassini Outreach Team of NASA/JPL, while in 2013 we were part of an integral European group, under the guidance of the European Space Agency (ESA) Outreach team, led by Dr. Nicholas Altobelli. A website dedicated to our Space Physics Group, of the Sector of Astronomy, Astrophysics and Mechanics, can be found at http://www.space.phys.uoa.gr/outreach.html. In addition, in order to attract the general public's attention towards Astronomy, Physics and Technology, at my Institute, as co-investigators, we

presented the Antikythera Mechanism, the oldest known complex scientific calculator, in many exhibitions around the world. I have given several lectures, at different academic levels, on these and other subjects, and have presented the 'Cassini Scientist for a day –Greek edition' and the Antikythera Mechanism at international scientific conferences, such as, the *European Geosciences Union-EGU* (2010-2013), the *European Planetary Space Congress -EPSC* (2010-2013) and the *International Astronomical Union -IAU* (2012). I discuss all these activities, in detail, in the following sections.

12.1 Cassini Scientist for a day

The international contest '*Cassini Scientist for a Day'*, organized by the Cassini Outreach at NASA's Jet Propulsion Laboratory, provides students all around the world with the opportunity to get involved in astronomy, astrophysics and planetary sciences. It gives excellent opportunity for outreach and publicity for the Cassini mission, ESA and NASA activities in Greece. Between the years 2010-2013, as well as during the ongoing Academic year, 2013-2014, the Space Physics Team of the Astronomy, Astrophysics and Mechanics section of the University of Athens, in association with external colleagues, has been selected as the coordinator of NASA for the competition in Greece.

Cassini Scientist for a Day is an excellent initiative that attracts pupils of all kinds of backgrounds and all ages to a very constructive activity, through which they are, for the first time in their lives, in direct contact with real science, with research, with scientific bibliography, and they learn how to perform searches in accordance with a scientific subject. They try to write an essay; learn that they are not allowed to copy, plagiarize, but that they are instead obliged to use and rely on their abilities, their knowledge and reason in order to write a proposition for research. It has been very moving to see children from very isolated villages, distant from urban areas or from small islands and places with no internet access, to participate successfully and with great satisfaction.

12.1.1 Introduction

Under the guidance of the JPL's and ESA's Cassini Outreach teams, the members of the Space Physics Team, informed, explained and spread the rules of the competition at primary, secondary education and high schools, all over Greece. Our members kept open communication for questions and guidance, with students, teachers and parents throughout the competition.

12.1.2 Rules and Awards

In general, the students, aged between 10-18 years old, researched three possible targets that the Cassini spacecraft could image during a given time; images set aside for educational purpose. They had to choose the one observation they thought would yield the best science results and explain their reasons by writing an essay. Their arguments should be summarized in

an essay of 500 words or less. They also had the option to do team work through groups of a maximum of three students. Each year, the targets change, giving the opportunity to former participants to contribute again.

Fig. 12.1 – Advertising flyer of the 'Cassini Scientist for a day' (Greek version) school contest posted in every school in Greece, for the Academic years 2010-2011 (left), 2011-2012 (middle) and 2012-2013 (right), showing also a preview of the contest's 'essay targets' in the Saturnian system for each year.

CASSINI SCIENTIST FOR A DAY

TSIADIS ELEFTHERIOS

TARGET NUMBER 3 – A DAY ON SATURN

ESSAY

Upon trying to analyze the so called "Saturnian System", meaning Saturn, its rings and its natural satellites, information are to be gathered by Saturn itself. After all, the effects of Saturn on the system are greater than the effects of any other astronomical object of it. Specifically, Saturn's rotational period has not been assigned a standard fixed value yet. That is mainly because of different measurements made by Voyager and Cassini. Nevertheless, it is known that Saturn's period is to be smaller than 10 hours, 39 minutes and 22 seconds. As a result, using the wide angle camera Cassini spacecraft is equipped with, a direct calculation of Saturn's period becomes feasible, since the camera will capture images of Saturn for 12 hours. The greatest discrepancy between the two measurements was the period of the interior latitude of the planet, giving rise to several theories trying to explain the cause of change in value. Furthermore, the period of a planet has a great effect on several other constant physical quantities regarding that planet, some of which are related to and directly affect the Saturnian system as a whole, eg the gravitational field strength of the planet.

To start with, by learning the period of the planet, Saturn's gravitational field strength can be found.
Let's consider the gravitational field strength on the surface of Saturn, expressed as the centripetal acceleration (g) experienced by an object with tangential velocity v at the surface of Saturn (at a radius (R)).

$$\vec{g} = \frac{\vec{v}^2}{R} = \vec{v}\frac{\vec{v}}{R} = \vec{v}\vec{\omega} = \vec{v}\frac{2\pi}{T}$$

Where T is the period and ω the rotational velocity.
Providing that the object is on the equator of Saturn, it covers a distance of 2πR, where is the radius of the equator at time T. Thus:

$$\vec{g} = \frac{4\pi^2 R}{T^2}$$

However, the real important issue is not the calculation of the period and field strenght. Instead, the outmost important issue is the calculation of the interior rotation period. The two main theories suggested regarding Saturn's interior rotation period, were that solar winds affected the magnetic field of Saturn, which emitted radio waves in different periods, and, secondly, that the geysers of Enceladus affected the magnetic field of Saturn causing the same result. The key point of Cassini's current mission is to take advantage of the optical means, the spacecraft carries. Using the wide angle camera enables us to create a video from which the rotational period can be measured in different latitudes, without being altered by either solar winds or Enceladus' effects. Further by acknowledging the rate of rotation of Saturn, the velocities of Saturn winds can be calculated using the already existing evidence, in addition to the new ones. For the time being, it is known that their velocity will be smaller if a smaller period is recorded. However, only through the expected video from Cassini, it will be feasible to calculate their value.

Ultimately, I firmly believe that Cassini Solstice Mission is to emphasize in determining the period of different latitudes of Saturn, having as major result to the calculation of the interior rotational period and the velocities of Saturn winds.

Fig. 12.2 – A winning essay from the 1st contest of the Cassini Scientist for a day. The students had the option to write the essay in Greek or English.

Figure 12.1 shows the flyers distributed to every Greek school (private and public). An example of a winning essay can be found in Figure 12.2.

12.1.3 Outcome and participation

This kind of school competition in Greece, is particularly important, since Astronomy, Astrophysics and Space Sciences, although very popular, are not included in the school curricula and thus students rarely have the opportunity to experience and participate actively in these subjects. The participation in the contest for the year 2010 (first year) was unexpectedly high and thoroughly satisfied. The winners were awarded at a ceremony, held in the largest amphitheatre in the central building at the University of Athens (Fig. 12.3). We awarded 9 winners, three from each grade, and praised all participants (Fig. 12.4).

Fig. 12.3 - Award ceremony 'Cassini Scientist for a day' school contest in the central building at the University of Athens, room 'Ioannis Drakopoulos' on June, 17, 2011.

Fig. 12.4 – The moment of awarding the winner and the reading of the winning essays.

The following year, 2011, the participation increased up to 300%, while a large number of the 2010 contest participants were either participating in the new contest of 2011-2012 or – since some of them have graduated- were still in touch with the members of our group for reasons of study guidance.

The Academic year 2012-2013 the participation increased up to 150% from the previous year and 900% from the 1st year of the contest (see Table 12.1).

Table 12.1 – Participation in the contest 'Cassini scientist for a day –Greek edition' for the years 2010-2013.

Participation (2010-2013)		
Academic Year	**Number of participants**	**Increase (%)**
2010-2011	50	
2011-2012	200	300% from the 1st year
2012-2013	500	900% from the 1st year 150% from the 2nd year

For the 2013 award ceremony, with funding from ESA, we needed a larger room due to the acute increase of participants. The ceremony was held on the 29th of April, 2013, in the Main Room at the University of Athens, with a guest lecture from Dr. Athena Coustenis, who is a specialist on the Saturnian system and the Cassini mission (Fig. 12.5). The awards where given away by Professor Stamatis Krimigis and Professor Xenophon Moussas (Fig. 12.6).

Fig. 12.5 – Guest lecture by Dr. Athena Coustenis, in the '3rd edition of the Cassini Scientist for a day contest' on the Saturnian system and the Cassini mission.

Fig. 12.6 – Awarding by Prof. Stamatis Krimigis (left) and Prof. Xenophon Moussas (right).

In conclusion, one very important aspect of the activity is, that schools and pupil feel very close to the University and Science and the Cassini Scientist for a day acts as a good attractor of children's interest towards science.

12.2 The Antikythera Mechanism as an Outreach attractor

The Space Physics Team at the University of Athens has a scientific impact on both the Space Physics field and the public outreach of Astronomy throughout Europe, Northern Africa and the United States of America. Using the Antikythera Mechanism as central object and as a great attractor of children's attention, and the general public to astronomy and even philosophy, we have performed numerous outreach activities focusing on the general audience, in order to conceptualize astronomical phenomena and change their prior, usually not very clear, knowledge and intuitions. These Solar system events, conducted by our Team, help young people develop their critical thinking, self-expression and creative talents, an interest towards the planetary bodies and eventually to love astronomy in general. Their introduction to the space field seems essential for the cultivation of these skills.

12.2.1 What is the Antikythera Mechanism?

The Antikythera Mechanism is the oldest known, complex, scientific instrument, the oldest (analogue – scales - and digital – gears with teeth) computer and the first known Mechanical Universe, i.e. the first planetarium. Made, somewhere in Greece, around 150 to 100 BC, the Antikythera Mechanism was salvaged, from a 1st century B.C. shipwreck, in 1900-2, during sponge diving operations, near the small Greek island of Antikythera (Fig. 12.7) (Moussas et al. 2010; 2012). Although the device was well- oxidized, its fragments present many things for exploration. The extensive investigation of the mechanism's remnants recently revealed its complicated functions and astronomical knowledge that it embedded. The instrument is now exhibited at the National Archaeological Museum of Athens.

Fig. 12.7 – The Antikythera Mechanism. Beyond its tremendous scientific importance, the Antikythera Mechanism could be readily used as an attractor of public's attention towards Science, Mathematics and technology.

The Mechanism uses mathematical theories developed by the Greeks; theories that are the first exact models of the Cosmos. Consequently, the Mechanism, is ideal, in order to teach children what “law of nature” means, what is “causality” and what is “modelling”, how we predict natural phenomena like the position of the Sun, the Moon, the phase of the Moon, how to predict eclipses, both solar and lunar, and possibly the position of the planets.

The instrument works with appropriately designed bronze gears. The sequence of gears is designed to perform the appropriate mathematical operations in order to model the Cosmos. The very word Cosmos appears in the manual of this old computer. The trains of the gears, as they move, change the position of pointers that represent the Sun and the Moon, the phase during the month, predict eclipses and possibly the planets, based on ancient Greek texts that describe similar instruments called either Planetarium or Pinax (Table in Greek).

The instrument maintains several calendars that the Greeks, and other nations, used at the time, or even use today, for example, for the Greek Easter. One of the calendars is based on the Meton’s period (19 years) and another on its multiple Callippus period (76 years). The instrument determines the dates of the Olympic and other important Greek Games, namely the Pythian, Isthmian, Naa, and Nemean as we read in one circular dial. It predicts the solar and lunar eclipses based on a long tradition of previous observations and on two lunisolar cycles, the Saros and its multiple, the Exeligmos (3 Saroi cycles), in combination with Meton's and Callippus cycles. The Saros gives the date and the Meton and Callippus cycles give the exact position in the sky, with respect to the stars, something essential for an exact prediction of the longitude of Earth, when will a solar or a lunar eclipse occur and the position where it will be visible.

12.2.2 General Description of the Antikythera Mechanism Exhibition

The exhibitions we have presented, the History of Science, and especially the history of the study of the Solar system, were addressed to the general public and pupils. Usually the exhibitions were centered on the Antikythera Mechanism and are addressed to pupils, students, scholars and the general public to their benefit and to the benefit of Science, Astronomy, Physics and Philosophy. I have contributed to a number of the exhibitions that are summarized in table 12.2 and others to Greek schools, where we present the antikythera mechanism in the way that is described hereafter and provide guidance to students that want to proceed with studies in Astronomy, Astrophysics and/or Geology.

Our Team, had several exhibitions or contributed to exhibitions; New York (Children Museum of Manhattan), the NASA Kennedy Space Center, during the Juno spacecraft launch, at UNESCO (Paris, beginning of the International Year of Astronomy 2009, Upsala Gustavianum Museum for the International Year of Astronomy 2009 (the exhibition doubled the number of visitors in the year and remains at this level since then), the Library of Alexandria, Institute of Astronomy of the Slovac Academy, Olsztyn Planetarium (Copernicus observatory in Poland), Crakow University, Budapest, the Greek School of Cairo, the Greek School of Alexandria (Egypt), Constantine (7eme salon' astronomie, Algeria), Instituto Veneto per Science, Lettere ed Arte during the International Year of Astronomy and various others in Greece. At the Ionian Center, The University of Athens, University of Patras, at the Stadium Erinis and Philias, and at numerous schools and summer schools.

Without a doubt, having the Antikythera Mechanism as en educational tool, both scientists and teachers could easily capture the interest of their audiences and improve the impact of their lectures. The outreach performances, related to the Mechanism, contain a cluster of interactive and hands-on activities.

Table 12.2 - Table of Exhibitions on the Antikythera Mechanism and the History of Greek Astronomy.

Event	Location	Date	Visitors
AMERICA			
Gods, Myths and Mortals: Discover Ancient Greece Children's Museum of Manhattan	New York, USA	From 2007 to 2010	500,000
Juno spacecraft launch	NASA, J F Kennedy Space Center, Florida, USA	August 2011	5,000
EUROPE			
Inauguration of the International Astronomy Year, IAU Symposium 260 and Art Exhibition	UNESCO Headquarters, Paris, France	15–23 Jan. 2009	3,000
Hellenic Physical Union, Technopolis, Gazi, Athens,	Technopolis, Gazi, Athens, Greece	1-5 Nov. 2010	1,000
Maritime Museum of Crete	Chania, Greece	Oct., Nov. 2010	2,000
European Planetary Science Conference	Angelicum Centre – Pontifical University of Saint Thomas Aquinas Rome, Italy	19 – 24 Sep. 2010,	1,000
Delphi Cultural Center	Delphi, Greece	27-31 Jul 2010	200
High School of Kythera,	Kythera, Greece	Jun. 2010	200
European Geophysical Union (EGU) 35th General Assembly	Austria Center Vienna, Austria	2-7 May 2010	2,000
High School of Skiathos	Skiathos, Greece	Feb. 2010	300
CosmoCaija/ Huygens Workshop	Barcelona, Spain	12-15 Feb. 2010	500
Museum of Science and Technology of the University of Patras	Patras, Greece	2010	1,000
Secondary Education,	Kallithea, Athens, Greece	Jan. 2010	100
Conference and Cultural Center of the University of Patras	Patras, Greece	05-08 Apr. 2009 and 2010	3,000

Secondary Education,	Kallithea, Athens, Greece	2009	400
Municipality of Salamis	Salamis, Greece	2009	300
High School of Chios, Center for Natural Studies (EKFE)	Chios, Greece	Dec. 2009	700
School *Hellenic Education*	Rhodes, Greece	Nov. 2009	600
Astronomical Institute SAS, (AISAS) Exhibition of the Antikythera Mechanism	Tatranska Lomnica, Slovakia	01 Oct.-07 Nov. 2009	351
34th Convention of Polish Astronomical Society, Institute of Physics of the Jagielonian University, Exhibition of the Antikythera Mechanism	Krakow, Poland	15 Sep.-30 Oct. 2009	350
Festival International des Sciences, Les Rencontres de la Terre	Athens, Greece	12-15 Oct. 2009	2,200
3rd Scientific Symposium: Science and Art, Hellenic Physical Society and Harokopion University	Athens, Greece	09-11 Oct. 2009	300
6th Hellenic Conference on Amateur Astronomy	Alexandroupolis, Greece	25-27 Sep. 2009	400
7th General Conference of the Balkan Physical Union	Alexandroupolis, Greece	09-13 Sep. 2009	300
Olsztyn Planetarium	Olsztyn, Poland	06 May–20 Sep. 2009	10,000
International Exhibition Thessaloniki	Thessaloniki, Greece	Sep. 2009	5,000
The 13th Science Picnic of Polish Radio and the Copernicus Science Centre – The largest outdoor event in Europe promoting Science	Warsaw, Poland	30 Sep. 2009	4,000
Skiathos Cultural Center, and School of Skiathos, Greece	Skiathos, Greece	Sep. 2009	300
Museum Gustavianum Uppsala University	Uppsala, Sweden	31 Jan.–26 Apr. 2009	10,000
Culture Center City of Rethymnon	Rethymnon, Greece	27–30 Mar. 2009	300
Istituto Veneto di Scienze, Lettere ed Arti	Venice, Italy	2009	200
High School of Kranidi	Argolida, Greece	Since Mar. 2009	700
Communication with the ISS, 1st Lyceum of Alexandroupolis - Amateur Astronomic Club of Thrace	Alexandroupolis, Greece	11 Feb. 2009	530
Ionic Center, Athens	Athens, Greece	Dec. 2008 - Jan. 2009	4,000
Exhibition of Research and Innovation, Zappeion	Athens, Greece	Nov. 2008	5,000
International Exhibition Thessaloniki	Thessaloniki, Greece	Sep. 2008	5,000
Nursery School Ermioni	Ermioni, Greece	21 Feb.2008	60
High School, Kassos	Kassos, Greece	2008	200
Theognis Cultural Center	Megara, Greece	2010	200
Exhibition of Research and Innovation, Zappeion	Athens, Greece	Nov. 2007	5,000
	AFRICA		
Averofian Greek School in Alexandria	Alexandria, Egypt	Permanent exhibition 2009	200
Planetarium Science Center Bibliotheca Alexandrina Alexploratorium	Alexandria, Egypt	Since 1 Nov. 2008	2,000

Greek Cultural Center	Alexandria, Egypt	2011	1,000
Exhibition at CRAAG, Centre de Recherche en Astronomie Astrophysique et Géophysique	Algiers Observatory, Algeria	2 Nov. 2008	50
Abet Greek School in Cairo	Cairo, Egypt	Permanent exhibition inaugurated on 29 Nov 2008	300
Exhibition in Constantine 7em Salon d'Astronomie	Constantine, Algeria	30 Oct.–1 Nov. 2008	6,000

The exhibition usually consists of:

- Some 20 panels describing the Mechanism and the history of science in Greece,
- Two interactive programs with simulations of the Mechanism (by Professor Manos Roumeliotis of the University of Macedonia and Ms. Amalia Porligi),
- A short movie (by Mr. Nick Giannopoulos) and
- Several interactive 3D photographs of the Mechanism (by Dr. Tom Malzbender of HP - Palo Alto California).

When possible, we normally use, for the interactive programs and film:

- 4 to 7 computers and a DVD player with large plasma display for the film.

Any old computer can run the computer applications. They run on MS Windows (either old or new).

Description of the computer usage of the:

- 1st computer or DVD player and a large plasma display; at first we have a little movie showing about how the Mechanism is made. The model is based on graphics made by Mr Nikos Giannopoulos, digital artist. It plays well in a DVD player or PC.
- 2nd computer that shows a 3D interactive model of the Mechanism (based on mathematics and programming in C), made by Prof. Manos Roumeliotis of the University of Macedonia at Thessaloniki. A visitor can play with the model, it can turn it, enter into the mechanism and see how it works. It sufficiently displays the four gear train of the lunar motion that simulates, to a good approximation, Kepler's second law.
- 3rd computer that shows a 3D interactive model (based on graphics), made by Mrs Amalia Porligki-Giannopoulou, digital artist. A visitor can play with the model, it can turn it around.
- 4th-8th computers have an interactive program that displays three-dimensional interactive photos made by Dr. Tom Malzbender. It illuminates the object (with mathematics) from any point the user wants it to. It allows to take off the rust of the ancient object (using mathematics) and to see clearly the surface detail, e.g. the writings on the computer

manual that is embedded on the Mechanism. These 3D interactive photos are very educational. Amongst several functions, they display the unit vectors, perpendicular to the surface, with colors, "take off the rust" using mathematics, and all that to the surprise of the visitors, that play with this interactive program by Dr. Malzbender.

We have many 3D interactive photos that are displayed in this way, like:

a) Part of the text of the manual of the Mechanism that is written on bronze sheets

b) The wheel of the Sun that runs the Mechanism

c) The display (pointer and cycle) of the Moon

d) The concentric circular scales of the ecliptic and the zodiac, together with the year scale

e) The spiral scale of Meton's 19 year period

In conclusion, the interdisciplinarity of the Antikythera Mechanism makes it a great educational tool, as it permits its usage for outreach purposes in Philosophy, Language, History, Geography, Technology, Physics, Mathematics and Astronomy.

Chapter 13

Future research/Prospects

So far, in the previous Chapters, I presented the work I conducted during my PhD studies. I have started this PhD focusing on Titan's and Enceladus' surface investigations, with tools and data that my supervisors, colleagues and collaborators provided me with at that time and developments that emerged in this 4-year research. Recent Cassini data and new studies unveil more regions of interest on Titan's surface that require further investigation. Such regions include tectonic and cryovolcanic candidate regions that have been captured either in VIMS or RADAR data or both. Our recent study (Sohl et al. 2013) in addition to the one by Lopes et al. (2013) present the evidence and the need for an in depth investigation of these regions, that I describe in section 13.1. In addition to the current methods in use such as PCA, RT and despeckle filter (Chapter 5), new methods are necessary for application with these regions' data, that combine the VIMS (chemical composition) with the RADAR (morphology/topography) data. In section 13.1, I present a general new methodology on that matter, which I intend to use in the future, as my intention is to continue and develop my work on Titan's surface investigation.

Furthermore, in this manuscript surface features analogues between the Saturnian satellites Titan and Enceladus and Jupiter's Ganymede and Europa with Earth are presented in addition to their astrobiological significance. Moreover the next mission to the outer Solar system, the JUpiter ICy moons Explorer (JUICE), is dedicated to the exploration of the Jovian icy satellites suggesting them as a scientific focus for the next years. All these, as described in section 13.2, present the need for further exploration of especially Ganymede and Europa, in terms of individual geological bodies, but also as possible analogues to Titan, Enceladus and Earth. This is a study that really interests me and I intend to concentrate on, in the future.

13.1 More in-depth study of cryovolcanic candidate areas on Titan and correlation between VIMS, RADAR and topographic data

As presented in the previous Chapters of this thesis, the Cassini-Huygens instruments revealed that Titan, Saturn's largest moon, has a complex, dynamic and -in some aspects- Earth-like atmosphere and surface. Data from the remote sensing instruments, particularly the RADAR, have shown the presence of diverse terrains on Titan's surface, suggesting exogenic and endogenic processes. However, interpretations of surface features need a precise knowledge of the contribution by the dense intervening atmosphere, especially the troposphere. Indeed, Cassini's Visual and Infrared Mapping Spectrometer (VIMS) collects spectra and images within the so-called "methane windows" where the methane atmospheric absorption is weak, but non-negligible, permitting however a good perception of the surface. I propose to shed light on the origin of some of the most interesting Titan's terrains by (i) using RADAR data, including despeckled SAR images, to identify geomorphologic units and to investigate spatial and temporal geological relationships; (ii) using state-of-the-art Principal Component Analysis (PCA) to specify regions of distinct spectral behavior (iii) applying a radiative transfer code to retrieve the surface composition of different units from VIMS data, following on from my recent efforts to derive an improved methane opacity description in these spectral regions by using the most recent methane parameters derived in recent work of the Project ANR CH4@Titan (see Hirtzig et al. 2013 and references therein) and (iv) by combining RADAR and VIMS data, including SAR imaging, aided by radiometry and topographic data with compositional information from VIMS. The combination of such data will lead to new insights into the chemical composition and the geology of the surface, and on how geological processes have combined to form the complex surface we see today. If endogenic processes (tectonism and/or cryovolcanism) are found to have been present on Titan, these would have important implications on the evolution of Titan's interior and atmosphere, as well as for the satellite's potential as an exobiological habitable environment. I have begun this work during my thesis but there are certainly ways of advancing, improving and completing in the near and longer future, which I expose hereafter.

13.1.1 Statement of problem/Scientific rationale

Studying Titan's surface requires very specific tools as presented in Chapters 5, 6 and 7. Hereafter, I present a brief summary of the issues that the remote sensing Cassini data have

and can be overruled with sophisticated methods as the ones presented in Chapter 5 and more that I intend to use in the future more extensively.

Among other, Titan's atmosphere contains both and aerosols (see Chapters 1,4,5 and 6). Methane scatters visible light and absorbs in the infrared, whereas aerosols are more absorbent in the visible and more scattering in the infrared. Therefore, atmospheric scattering and absorption need to be clearly evaluated before one can extract the surface properties (i.e. true surface albedo, interpretable in terms of chemical composition) from VIMS data (see Chapter 5,6 and 7), with the use of specific tools adapted to Titan's properties.

In order to thoroughly investigate processes involved in the formation of a geological terrain, in addition to the chemical composition, one must also study the terrain morphology. The Cassini RADAR instrument (a multicode Ku-band 13.78 GHz, $\lambda = 2.17$ cm) with its four operating modes in Synthetic Aperture Radar (SAR), altimetry, radiometry and scatterometry (Elachi et al. 2004), provides an excellent set of data for the study of Titan's surface morphology and topography, from which valuable geological interpretations can be obtained (e.g. Lopes et al. 2010; 2013). The SAR mode is used at altitudes lower than 4,000 km above the surface, resulting in a spatial resolution ranging from about 350 m to more than 1 km. However, one of the major problems hampering the derivation of meaningful texture information from SAR imagery is speckle noise. Hence, a filtering technique is required to make the SAR images more easily interpreted in terms of surface morphology (see Chapters 5 and 7).

Even if the tools and methods are available to process VIMS and SAR data, limitations exist. The RADAR and VIMS instruments cannot observe a target area at the same time because of spacecraft operational considerations. Furthermore, the RADAR collects low-resolution (up to tens of km) radiometry and scatterometry data, as well as high-resolution (~350 m to 1 km) SAR images, while VIMS collects data that are very limited in spatial coverage (a few km in resolution) or have large spatial coverage and low resolution (up to hundreds of km). Thus, a correlation between such datasets, even though ideal in terms of information, is challenging in application. Additional techniques are required for the correlation of altimetry data since they generally do not overlap with SAR imagery. To conduct a thorough and efficient investigation of the surface of Titan from existing Cassini data, one needs to take into account these observational constraints and use adequate methods to obtain the maximum information from VIMS and RADAR data. This is what I intend to do in the future.

13.1.2 Cryovolcanic candidate areas require further investigation

In Table 4.3 on Chapter 4, I have summarized the currently major cryovolcanic candidate features as suggested by Lopes et al. (2013) and other studies. During my PhD, I have focused on the investigation of three of them, Hotei Regio, Tui Regio and Sotra Patera. However, Ara Fluctus (40°N, 118°W), Western Xanadu flows (10°S, 140°W), Rohe Fluctus (47°N, 38°W), "T3" flows (20°N, 70°W) are possible candidates as well, presenting many interesting geological volcanic- like features that require further analysis. More potential cryovolcanic sites will be recognized possibly in the future.

13.1.3 General methodology and new procedure

The main tasks of the proposed future procedure would be:

- To use RADAR data for the identification of geomorphological units and study their spatial and temporal changes;
- to retrieve the surface composition of different units from VIMS data and investigate their evolution with time, following on from my recent work on the methane opacity in these spectral regions (Solomonidou et al. 2013b;c) and by using state-of-the-art Principal Component Analysis (PCA) and radiative transfer (RT from now on) methods;
- to combine RADAR and VIMS data, including specifically SAR imaging, radiometry and topographic data obtained from the RADAR and compositional information from VIMS.

The methodology will consist of:

- First select and process the data and import them into ArcGIS (Geographic Information System (GIS) that is used as a tool for mapping and compiling geographic information);
- apply PCA to VIMS data;
- apply radiative transfer to VIMS data based on PCA selections;
- match with spectral signatures and make appropriate compositional interpretations;
- perform filtering of SAR data;
- obtain processed topographic information (altimetry, SARTopo, and radar stereogrammetry, available in the PDS, the literature, or from collaborators
- finally combine all the data into a map using ArcGIS and interpret the geology and make implications on the geological history of Titan.

The correlation of VIMS data with SAR images and topography can be achieved for areas that both instruments have (even partially) observed. Preliminary analysis of the topographic information shows that topography (from the SARTopo technique, Stiles et al. 2009) can greatly help in mapping and interpreting features, and has already led to a revision of some interpretations e.g. of Ganesa Macula as the result of tectonic and fluvial processes rather than cryovolcanism. For Titan, topography has been derived in areas with overlapping SAR swaths using stereo photogrammetric methods, but coverage is limited. Radarclinometric methods provide reasonable coverage, co-located with SAR imagery, but they are model dependent and uncertainties can be substantial without additional constraints from overlapping altimetry. To overcome this, Stiles et al. (2009) devised a technique, based on Amplitude Monopulse Comparison (Chen and Hensley, 2005), enabling the extraction of additional model-independent topography, not reliant on overlap between SAR scenes. Mitchell et al. (2011) have also derived higher along-track resolution (sometimes better than 1 km, with vertical resolutions of <100 m) products more suited to local studies. All available topographic data will be incorporated into this proposed study.

In addition, initial results using a combination of SAR and high-resolution radiometry were obtained by Paganelli et al. (2007), in which normalized radar cross-section versus brightness temperature plots revealed a range of signatures that characterize various terrains and surface features. Janssen et al. (2009) reported radiometry results from 69 separate observational segments in Titan passes from Ta (October 2004) through T30 (May 2007) and included emission from 94% of Titan's surface. These radiometry maps, as available, will also be incorporated into the proposed study. Hence, to understand the surface of Titan by combining and analyzing multiple datasets from Cassini, I will use:

- RADAR including despeckled SAR images;
- topography;
- radiometry & scatterometry maps;
- VIMS maps processed by PCA/RT.

All the data will be assembled into a multi-layer Geographic Information System within ArcGIS.

13.1.4 Expected results and their significance and application

The aim of this future work would be to understand the surface properties of Titan by combining and analyzing multiple datasets from Cassini-Huygens. I plan to work on the

processing of Cassini VIMS and RADAR data and investigate correlations between composition, morphology, topography and backscatter properties to understand Titan's geology. I expect to obtain insights into local regions of interest having different types of geological features such as dunes, plains, mountains, and candidate cryovolcanic features. The processed VIMS and SAR images, after the application of PCA and RT methods for VIMS and the despeckle filtering technique for SAR, will provide valuable information regarding the chemical composition and morphology of Titan's surface. The radiative transfer code is an updated version of a previous one well-adapted to Titan but with new methane coefficients from new laboratory and theoretical measurements (Hirtzig et al. 2013), while the combined procedure of PCA and RT has never, to my knowledge, been previously applied to Titan's geological expressions. Both methods have been tested and verified as part of this PhD thesis, which examined a number of the candidate cryovolcanic areas as defined in Lopes et al. (2013). The same applies to the updated version of the TSPR technique with regard to a number of SAR swaths for the lakes.

One crucial goal from the treatment of VIMS datacubes is to provide the dynamical range of each target area, retrieve the surface albedo, and eventually match with spectral signatures of candidate materials. So far, the major spectral units identified from the methane windows and VIMS color composites are the so-called "white" units that correspond to mountains and elevated areas; the "blue" units at marginal (dark-bright) areas; and the "brown" ones that correspond to dune material (Soderblom et al. 2007; Jaumann et al. 2009). These units are distinct but their chemical composition is not yet identified. The process mentioned above aims at providing more information on the constituents of these regions of interest and should permit the analysis of these units in greater depth, and give insights as to any inter-unit spectral distinctions. Thus, this procedure allows for (i) different units to be distinguished (first using PCA and subsequently with the retrieval of true surface albedo) from a single VIMS cube, and also (ii) the identification of the physical limitations from the retrieval of their chemical composition, which would indicate different processes and origins such as precipitation (organic compounds), endogenic formation (NH_3), etc. The application of these methods to distinctly different surface features and areas, is expected to lead to a classification of RoIs between different cubes, which will add valuable information to the global geological map of Titan. Another significant goal of RT processing will be the investigation of the temporal variation of surface albedo of specific geological terrains. This analysis can be done for regions of interest that have been observed by VIMS more than twice with sufficient resolution and adequate geometry (incidence and emergence angle

>60°). Particular emphasis will be given to the candidate cryovolcanic areas due to their potential variation with time, which if confirmed, and if traced back to material from the interior, would be the first conclusive evidence of Titan's internal activity. However, this code can be applied to all VIMS data for every Titan surface unit in order to retrieve spectrographic information and test the evolution with time. Hence, the search for surface temporal variation will be applied to other Titan regions, such as the dunes, in order to investigate surface changes due to exogenous processes (e.g. related to wind) with time. For the morphological studies of the regions of interest, the filtering technique will provide an enhanced SAR dataset, which will also be useful to other researchers. Particular attention will be paid to the areas that have been monitored by both RADAR and VIMS with appropriate observational geometries. Moreover, the correlation of VIMS, SAR and, where available, topographic data (Lopes et al. 2013) of the areas that have been analyzed with methods such as radarclinometry, radar stereogrammetry (Kirk et al. 2005; 2008) and monopulse 'SARTopo' (Stiles et al. 2009), will be of great value for geological interpretations. An example of such data combination can be seen in Figure 6 in which the VIMS data processing is obtained using the standard VIMS pipeline (Barnes et al. 2007) and therefore lacks an effective atmospheric correction. Additional processing with PCA/RT will result in the evaluation of the atmosphere and will eventually indicate the different constituents of the local features, suggested as volcanic crater, peaks and flows.

The analysis proposed here, using multiple datasets, is expected to provide new information and shed light on many aspects of Titan's surface environment, on any correlation between the surface, on the interior and the atmosphere structure, and on Titan's potential as an internally active satellite. For example, if the processed overlapping VIMS and SAR data, combined with topographic information, show a region that is a highland (i.e. a peak, such as Doom Mons) with distinct composition and an adjacent topographically low region (such as Sotra Patera crater) with the same distinct composition, this will imply that they are linked in origin. If the compositional results differ, it would indicate different formation mechanisms and material probably originating from different sources.

The presence of seasonal effects, unique geomorphological features and a probable internal liquid water ocean make Titan one of the astrobiologically most interesting bodies in the Solar system. Titan is a dynamic moon, as shown by the relatively young surface (e.g. Elachi et al. 2004), by recent albedo changes observed in the Sotra Patera region and Tui Regio (Solomonidou et al. 2013c), and by the extensive surface changes spanning more than 500,000 km^2 in the wake of a seasonal storm (Turtle et al. 2011b). Dynamic activity is clearly

a prerequisite of a habitable planetary body as it allows the recycling of minerals and potential nutrients. This is especially relevant for Titan, because the moon has in principle several, if not all, of the ingredients needed for life including polymeric chemistry, an energy source, and a liquid solvent being present in appreciable quantities (Schulze-Makuch and Irwin, 2008). When addressing Titan's habitability, understanding its surface environment and its interior structure is therefore of key importance. The study of the relationship between the interior and the surface from morphological and compositional studies will hence lead to valuable geological and geophysical interpretations. For instance, evidence for cryovolcanic phenomena and upwelling of ammonia water pulses onto the surface (i.e. cryovolcanic candidate sites or at the bottom of a hydrocarbon lake) will lead to the assumption of a thin crust (based on a model of 17-111 km crust thickness; Sohl et al. 2013); a geodynamical setting that is conducive to putative life.

Understanding the distribution and interplay of geologic processes on Titan, this Earth-like world, is important for constraining models of its interior, surface-atmospheric interactions, and climate evolution. The variety of geologic processes on Titan and their relationship to the methane cycle make it particularly significant in Solar system studies. In addition the interior-surface correlation is an important issue for both Titan and Enceladus and extensive study of the tidal potential of their interior is required. The Cassini-Huygens mission has demonstrated the complexity of Titan's environment and further investigation is necessary in order to better understand this satellite, and in extension the rest of the Saturnian system. Discussions on future missions to Titan, beyond the end of the Cassini mission in 2017, are already underway with proposals for aerial explorers, such as airplanes or balloons, and dune and lake landers that will more thoroughly investigate this complex world. My studies will contribute to better prepare such missions.

13.2 Expansion of the studies of comparative planetology

Future data and evidences are awaited and further in depth analysis has already been in the way, concerning the case of possible existence of subsurface liquid oceans underneath the crusts of Jupiter's icy moons, Europa, Ganymede and Titan and Enceladus of Saturn. That possibility places these icy moons potential planetary bodies where life can exist and thrive. Concerning evidence and information of the internal liquid layers, besides some preliminary data process, we can dwell on the surface evidence, surficial expressions that are related to hydrothermal as well as the dynamic processes that occur within these layers. More specific, the surface expressions of the internal activity are the cryovolcanic and morphotectonic structures - that can bee seen on the aforementioned satellites - while formed due to modifications of the crustal layer and deposition of material, deriving from the subsurface ocean. Based on that, if we associate these surface exposures to terrestrial features where water is involved, we can possibly shed some light on the case of investigating internal liquid water oceans on these icy moons. Also, concerning the question of what triggers the internal active phenomena, we can see that basic geophysical models propose liquid water reservoirs, while the geodynamics model points at both radioactive decay as well as tidal stresses that are caused by Jupiter and Saturn.

I intend to extend my study on these moons in terms of comparative geological processes that would link to or refute their internal origin. Thus, extensive investigation of the surface features, comprehensive modelling of the interiors and good knowledge of terrestrial geology are required for such complex investigation.

In conclusion, with the use of comparative studies, as well as data analysis and the development of analysis tools, I aim and intend to work, should I be given the opportunity, on the future preparation of possible observations with JUICE, by looking at Europa and Ganymede from the geological point of view.

Conclusions

During my Thesis study, I have investigated different aspects of the geology of Titan and Enceladus environments with a focus on the surface features and their connection with the interior and the atmosphere in addition to their resemblance with terrestrial features and processes. My thesis research and the findings can then be divided into four major parts.

The first part deals with the overview of Titan's geology, focusing on the surface features, the geological processes, the interior and the correlation between the atmosphere, the surface and the interior (Solomonidou et al. 2010; 2013a). These are the morphotectonic features present on Titan, that I have managed to classify into specific types of surface features and provided implications based on terrestrial models. The outcome of this investigation is the creation of a map pointing out the so far discovered major features with possibly an internal origin. Moreover the comparative study between Cassini observations and terrestrial tectonic systems provided some possible formation mechanisms for the morphotectonic features and indicated the possibility for ice floes of altered densities, moving on a liquid layer and reproduce structures and simulate phenomena similar to subduction processes. Such movements could explain the formation of mountains, faults and crustal pathways to facilitate cryovolcanic phenomena for areas like Hotei Regio, Tui Regio and Sotra Patera, which are an intriguing and interesting morphotectonic type.

A second part deals with the investigation of these aforementioned specific Titan regions (Hotei Regio, Tui Regio and Sotra Patera), which have been recognized as geologically interesting, although their exact nature and formation processes have not been firmly identified (Solomonidou et al. 2013b). I have applied a statistical Principal Component Analysis (PCA) and a radiative transfer (RT) method (Hirtzig et al. 2013) on Cassini VIMS Titan data of these areas, including both the surface and the atmospheric contribution, and re-analyzed the spectral characteristics of the Huygens Landing Site (HLS). By using PCA I managed to isolate specific "regions of interest'' (RoIs) as distinct spectral units within these areas. With the follow-up RT calculations I managed the retrieval of the surface albedos for these RoIs taking into account the contribution of the lower atmosphere. I have used as inputs the latest inferences of the atmospheric parameters for Titan, including new methane absorption coefficients, essential in properly evaluating the atmospheric content and thereafter extracting the real surface contribution.

I have been able to exploit only a subset of the currently available Hotei Regio data, which are in general not optimal in terms of geometry and thus not easy to analyse with the plane-parallel limitation of our RT code. Our results (calibrated by the HLS spectrum) show that the surface albedos inferred for dark RoIs do not display any particular spectral features. The surrounding Regions of Interest of the studied areas display their largest variations longward of 2 μm and mainly at 5 μm, with factors of 3 increase for Sotra Patera up to 5 for Tui Regio. The increase, and in general the spectral behavior, is different for these two areas, indicative of probable diverse chemical composition and origin.

Moreover, I have analysed the SAR data that include the areas of interest and are affected by multiplicative speckle noise. In order to acquire qualitative data and extract the real surface properties I got involved on the application of a despeckle filtering technique for obtaining restored Cassini/SAR images (Bratsolis et al. 2013). The outcome shows that the areas of interest have differences in surface texture implying the presence different materials or altered grain sizes. The spectral variability, in addition to the morphological interest of these regions, led me to investigate the surface albedo temporal variations of the areas (Solomonidou et al. 2013c). This investigation showed indications for temporal change for two of them in their surface albedo in the course of 1-3.5 years implying dynamic exogenic-endogenic processes that affect the surface and compatible with cryovolcanism in the case of Sotra Patera. These two areas, Tui Regio and Sotra Patera, identified as possibly correlated to internal processes, were tested against a geophysical model of tidal distortion and found to be consistent in terms of location and internal dynamics (Sohl et al. 2013). This investigation has great potential for future exploration and I am looking forward to new data from the areas and data from other instruments (RADAR) that will show the current state of their surfaces. Moreover, I propose these areas as promising landing sites for future missions to the Saturnian system and justify the reasons (Solomonidou et al. 2013d) and provide my contribution to the planning of future mission payload and experiments (Bampasidis et al. 2011a;b).

A third part deals with the processes that shape Enceladus' surface and a simulation that I constructed is presented that enhances the understanding of the satellite's violent eruptions.

The final major part of this thesis focuses on the analogues of terrestrial surface features and internal processes that are pointing the intriguing similarities and informative differences between the silicate Earth and the icy satellites of Saturn (Titan and Enceladus) and Jupiter (Ganymede and Europa). This investigation addresses the observational

similarities, in the structural parts of the geological expressions and the similarities in modeling for the origin of such multivariable surface terrains (Solomonidou et al. 2013a).

In addition, the astrobiological implications of this work are discussed as part of a work that I have been involved in (Coustenis et al. 2012) showing great potential of both Titan and Enceladus, but also Ganymede and Europa, that seem to have most of not all of the appropriate prerequisites for the development and sustainability of life.

Finally, the outreach activities that I have been involved such as the organization of the ‘Cassini Scientist for a Day’ school competition presented a growth in participation up to 900%, ranking it as a great tool for the motivation of childer and the general public towards science and astronomy-planetology in particular.

Appendices

Appendix A1

Imaging of potentially active geological regions on Saturn's moons Titan and Enceladus, using Cassini-Huygens data: With emphasis on cryovolcanism*

Journal article published in *Hellenic Journal of Geosciences* (2010),
Volume 45, pp. 257-268.

Imaging of potentially active geological regions on Saturn's moons Titan and Enceladus, using Cassini-Huygens data: With emphasis on cryovolcanism*

Anezina Solomonidou[1,2], Georgios Bampasidis[2,3], Konstantinos Kyriakopoulos[1], Emmanuel Bratsolis[3], Mathieu Hirtzig[4], Athena Coustenis[2] & Xenophon Moussas[3]

[1]Faculty of Geology and Geoenvironment, National & Kapodistrial University of Athens, Panepistimiopolis, 157 84 Athens, Greece
[2]LESIA, Observatoire de Paris – Meudon, 92190 Meudon Cedex, France
[3]Faculty of Physics, National & Kapodistrial University of Athens, Panepistimiopolis, 157 84 Athens, Greece
[4]LMD – IPSL, Paris, France
email: asolomonidou@geol.uoa.gr

ABSTRACT: Since 2004, investigations, measurements and data analysis by the Cassini-Huygens mission showed that Titan, Saturn's largest satellite, presents complex, dynamic and Earth-like geology. Endogenous, as well, as exogenous dynamic processes, have created diverse terrains with extensive ridges and grooves, impact units, caldera-like structures, layered plains and liquid hydrocarbon lakes. Observations by the Cassini Visual Infrared Spectrometer instrument (VIMS) have indicated possible cryovolcanic terrains in the areas called Tui Regio (20°S, 130°W) and Hotei Regio (26°S, 78°W). In addition, Cassini's investigation over another icy moon of Saturn, Enceladus, identified its cryovolcanic activity and partially revealed its unique topography indicating several types of surface expressions. We present a comparative study of volcanic analogues from Earth and Enceladus that derive insight on the origin of some of these features. In this work, we focus on the analysis of VIMS data using the Principal Component Analysis technique in order to identify regions of altered chemical composition on Titan. The analysis of VIMS data suggests that possible cryovolcanic activity formed both the Tui Regio and the Hotei Regio.
Key-words: *Planetary geology, icy satellites, Titan, Enceladus, cryovolcanism, spectroscopy.*

ΠΕΡΙΛΗΨΗ: Μακροχρόνιες έρευνες, μετρήσεις και αναλύσεις δεδομένων από την αποστολή Cassini-Huygens από το 2004, έδειξαν ότι ο Τιτάνας, ο μεγαλύτερος δορυφόρος του Κρόνου, παρουσιάζει περίπλοκη, δυναμική και παρόμοια με τη Γη γεωλογία. Ενδογενείς, όσο και εξωγενείς δυναμικές διεργασίες, έχουν δημιουργήσει ποικίλα γεωλογικά πεδία με εκτεταμένες ράχες και αύλακες, κρατήρες πρόσκρουσης, δομές καλδέρας, πεδιάδες με στρωμάτωση καθώς και λίμνες υδρογονανθράκων. Παρατηρήσεις από το Cassini Visual Infrared Mapping Spectrometer (VIMS) όργανο, έχουν δείξει πιθανές κρυοηφαιστειακές εκτάσεις στις περιοχές Tui Regio (20 ° N, 130 ° Δ) και Hotei Regio (26°N, 78°Δ). Επιπλέον, η έρευνα του Cassini στον παγωμένο δορυφόρο του Κρόνου, Εγκέλαδο, επιβεβαίωσε την κρυοηφαιστειακή του δραστηριότητα και αποκάλυψε μερικώς τη μοναδική του τοπογραφία, παρουσιάζοντας ποικίλους τύπους επιφανειακών εμφανίσεων. Παρουσιάζουμε μια συγκριτική μελέτη, δείχνοντας ηφαιστειακά ανάλογα της Γης και του Εγκέλαδου, που παρέχουν πληροφορίες για τη δημιουργία κάποιων σχηματισμών. Σε αυτή τη μελέτη, επικεντρωνόμαστε στην ανάλυση δεδομένων VIMS, χρησιμοποιώντας τη μέθοδο Ανάλυσης Κύριων Συνιστωσών σε περιοχές με διαφορετική χημική σύσταση. Οι αναλύσεις των VIMS δεδομένων των προαναφερθέντων εκτάσεων δείχνουν ότι τόσο η περιοχή Tui Regio όσο και η περιοχή Hotei Regio πιθανά σχηματίστηκαν από κρυοηφαιστειακή δραστηριότητα.
Λέξεις-κλειδιά: *Πλανητική Γεωλογία, Παγωμένοι δορυφόροι, Τιτάνας, Εγκέλαδος, κρυοηφαιστειότητα, φασματοσκοπία.*

INTRODUCTION

Icy moons are small celestial bodies whose surfaces are partially, if not principally, covered by ice, mostly water ice (Johnson, 2004). The most remarkable icy moons around the giant planets are Jupiter's Ganymede, Neptune's Triton, Uranus's Miranda and Saturn's Titan and Enceladus in a variety of sizes, composition and temperatures. It was thought that due to the abundance of water ice, the large distance from the Sun, the absence of internal energy sources and of an atmosphere in most cases, the geology of these bodies would be simple, or rather simpler than the geology of Earth; however, subsequent images have shown complex surfaces with several notable morphological formations. Furthermore, the composition, as well as, the structure of the surfaces of the icy moons depends on geological and geophysical factors (Johnson, 2004).

Titan is the second largest moon in the Solar system after Jupiter's Ganymede, with a radius of 2,575 km (Lindal *et al*., 1983) and spherical geometry. Titan has a unique atmosphere, in that it is dense and consists mainly of N_2 (98.4%), as on Earth. CH_4 (1.4%), H_2 (0.1%) and traces of argon, ethane, acetylene, propane and more complex hydrocarbons and nitriles, as well as condensates and organic aerosols (Coustenis & Taylor, 2008) constitute the rest of the atmosphere. The identification of such atmospheric compo-

* Απεικόνιση των πιθανών ενεργών γεωλογικών περιοχών στους δορυφόρους του Κρόνου Τιτάνα και Εγκέλαδο: Μελέτη για την κρυοηφαιστειότητα με τη χρήση υπέρυθρων φασματικών δεδομένων

nents endorse theories suggesting that even though Titan is far out of the habitable zone, it is one of the most likely worlds in our solar system of astrobiological interest (RAULIN, 2008). Except for the new atmospheric discoveries such as the organic chemistry in the ionosphere, new components in the neutral atmosphere and the properties of the troposphere, Cassini-Huygens' most surprising discovery was Titan's complex and Earth-like geology (COUSTENIS & TAYLOR, 2008). As far as the surface is concerned, one of the moon's exceptional characteristics is the existence of surface liquid bodies that resemble terrestrial lakes (STOFAN *et al*., 2007). Other surface formations, were captured both by the Cassini orbiter's *remote sensing* instrumentation such as the Synthetic Aperture Radar (SAR) (ELACHI *et al*., 2005); the Visual and Infrared Mapping Spectrometer (VIMS) (BROWN *et al*., 2004) and the Imaging Science System (ISS) (PORCO *et al*., 2004; MCCORD *et al*., 2006), as well as by the Huygens probe's *in situ* instruments i.e.: the Surface Science Package (SSP) (ZARNECKI *et al*., 2005), the Descent Imager and Spectral Radiometer (DISR) (TOMASKO *et al*., 2005) and the Gas Chromatograph Mass Spectrometer (GCMS) (FULCHIGNONI *et al*., 2005). The surface discoveries include extensive mountains, ridges, dendritic networks, dunes, lakes, channels, canyons and riverbeds. Of even higher importance is the possible existence of active zones on the satellite due to past or recent cryovolcanic and tectonic activity (e.g. SODERBLOM *et al*., 2007; LORENZ *et al*., 2008; SOLOMONIDOU *et al*., 2010). Caldera-like edifices characterized by radial faults, features resembling lava flows and other possible volcanic structures and deposits, within large areas of volcanic-like terrains, in addition to spectral data indications, suggest that Titan is a world that once suffered cryovolcanic activity which could possibly still be active. The suggestion of an active cryovolcanic interior that supplies the atmosphere with methane is compatible with the current level of methane in Titan's atmosphere. According to calculations, the lifetime of atmospheric methane is limited to 10-100 Myrs (WILSON *et al*., 2004). If we assume that methane in the atmosphere should be replenished, then Titan needs a reservoir that would supply the atmosphere with enough methane to maintain the atmospheric abundance. The requirement of sufficient supplies of methane in combination with the volcanic-like expressions did trigger the theory of active cryovolcanism on Titan (TOBIE *et al*., 2006).

Other than Titan, the Cassini mission unveiled another unique world among Saturn's icy moons. Enceladus is a significantly smaller satellite than Titan (500 km in diameter), it presents however, extremely interesting surface features including cratered as well as smooth terrains, extensive linear cracks, scarps, troughs, belts of grooves in addition to the spectacular phenomenon of volcanic geysers that Cassini instrumentation captured in 2005 in the south pole (PORCO *et al*., 2006). High-resolution data from Cassini magnetometer (MAG) (DOUGHERTY *et al*., 2006), ISS (PORCO *et al*., 2006) and the Ultraviolet Imaging Spectrograph (UVIS) (HANSEN *et al*., 2006), reported cryovolcanic activity in the form of jets in the southern Polar region, at the geological surface expressions called "Tiger stripes". The accumulation of multiple jets resulted in the formation of a massive fountain that reached over 435 km in height (PORCO *et al*., 2006).

Our work provides: i/ an overview of the geology of Titan and Enceladus, ii/ terrestrial analogues and iii/ the results of our data analysis regarding Titan's potentially active regions. This study implicates the presence of cryovolcanism on Titan's surface.

GEOLOGY AND CRYOVOLCANISM ON TITAN & ENCELADUS

Cryovolcanism

Cryovolcanism is considered to be one of the principal geological processes that have shaped several of the icy moons' surfaces. This activity can be described as ice-rich volcanism, while the cryovolcanic ejecta are referred to as cryomagma. The cryomagma appears in the form of icy cold liquid and, in some cases, as partially crystallised slurry (KARGEL, 1994). The possibility of volcanic resurfacing on icy moons was first noted by LEWIS (1971, 1972) and subsequently addressed by CONSOLMAGNO & LEWIS (1978), but it was not until after the Voyager flybys of Jupiter and Saturn that evidence for past and present tectonic and volcanic activity on moons such as Europa, Ganymede, and Enceladus was brought to light. In our Solar system the only observed recent eruptions are limited to Earth and three other locations: 1) Io, moon of Jupiter; 2) Triton, moon of Neptune; and, 3) Enceladus, moon of Saturn. Titan is also major candidate for past and/or present cryovolcanic activity awaiting for a definitive evidence.

Subsequent to the Cassini-Huygens findings, the term 'cryovolcanism' has been associated with Titan more than any other Saturnian moon (SODERBLOM *et al*., 2009). Even though, for the case of Enceladus the cryovolcanic origin of the plume is now confirmed (PORCO *et al*., 2006), the cryovolcanic activity on Titan presents a controversial scientific issue within the scientific community. However, some facts are in favor of such processes like the theory of cryomagma being relevant to the formation of prebiotic compounds (e.g. FORTES, 2000).

The composition of the material called cryomagma on Titan's surface is still unknown, due to the lack of *in situ* measurements and in depth investigations, which may reveal its properties. Cryovolcanic features on Titan's surface are believed to be a significant source of the methane present in the atmosphere (LORENZ & MITTON, 2008). Considering this, a model has been suggested regarding the evolution of Titan, indicating that the methane supply may be trapped in a methane-rich ice and episodically released by cryovolcanic phenomena (TOBIE *et al*., 2006). However, the definite answer of the composition of Titan's cryomagma is still a subject of research.

According to TOBIE *et al*. (2006) the methane could have

originated through three distinct episodes: the first following the silicate core formation, accretion and differentiation period; a second episode approximately 2000 million years ago when convection commenced in the silicate core; and finally, a geologically recent period, circa 500 million years ago, where subsequent cooling and crystallization of the outer layer occurred. FORTES *et al*. (2007) suggested that ammonium sulphate is the possible origin of cryovolcanism. Titan's interior is broadly described by these authors, from the core to the crust, in distinct layers: a serpentinite core, a high-pressure ice VI mantle, where ice VI has a differentiated crystalline structure ordering and density than typical water ice, a liquid layer of aqueous ammonium sulphate and an externally heterogeneous shell of methane clathrate with low-pressure ice Ih (similarly as ice VI) and solid ammonium sulphate (FORTES *et al*., 2007).

The geological map below (Fig. 1) has been derived from albedo and texture variations and indicates that the circular feature shows signs of several series of flows, as shown by the black lines (SOTIN *et al*., 2005). The black circle indicates a caldera, similar to vents that appear above reservoirs of molten material associated with volcanoes on Earth. The colours of the map are representative of the brightness of the features where yellow-green to light brown are the bright patches; blue are the dark patches, red the mottled material and finally the yellow area marks the location of the volcano (SOTIN *et al*., 2005).

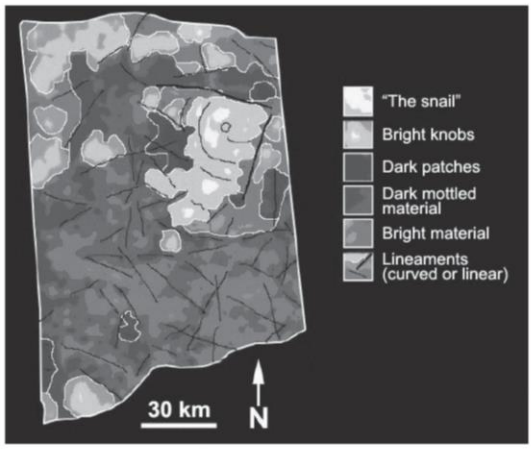

Fig. 1. Geological map of Titan possible volcano (SOTIN *et al*., 2005).

Enceladus

Cassini's observations on Enceladus did reveal distinct geological features. The surface of Enceladus is covered by smooth and cratered terrains, ridges, grooves, escarpments and extensive linear fractures (JOHNSON, 2004). The most interesting and youthful terrain seen on this moon called "Tiger Stripes" and presents a very complex structure and evolution. The Tiger Stripes (Fig. 2) are tectonic structures consisting of four sub-parallel, linear depressions located in the south polar region (PORCO *et al*., 2006). In 2005 Cassini's instrumentation and especially the ISS experiment provided evidence of active cryovolcanism (Fig. 3), emanating from a series of jets located within the Tiger Stripes (PORCO *et al*., 2006).

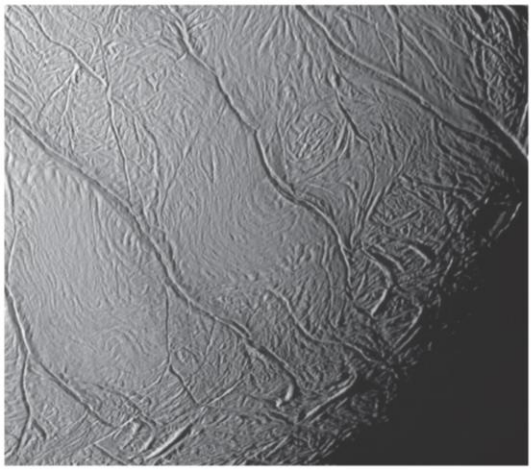

Fig. 2. Tiger Stripes on Enceladus (NASA).

The jets of water ice from the fractures of Tiger Stripes produce a plume of gas and particles like NH_3, Na, K salts (WAITE *et al*., 2009). These tectonic fractures, discharge material by endogenic dynamic and most probably hydrothermal activity. The source of the jets is a controversial issue as extensive internal stratification as well as dynamic modeling, is required for the source to be identified. The recent discovery of salts in Saturn's E-ring composition, which is fed from Enceladus' plumes (POSTBERG *et al*., 2009), suggests that the source of jets is possibly a "chamber" of liquid water that lies underneath the ice shell (TOBIE *et al*., 2008). Alternatively, the material could derive from originally warm ice that is heated and explodes by the dissociation of clathrate hy-

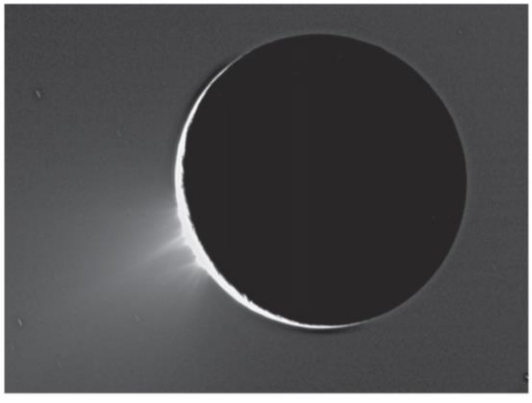

Fig. 3. Enceladus' Plume from Cassini/ISS (PORCO *et al*., 2006).

drates (KIEFFER *et al*., 2006). The clathrate hydrates are crystalline water-based ices where the host molecule is water and the trapped-guest molecule is typically a gas. The VIMS instrument detected simple organic compounds in the Tiger Stripes. Such chemical composition which consists of liquid water, ammonia, carbon dioxide, Na and K salts, benzene and other hydrocarbons (WAITE *et al*., 2009), has not been found in any other region on Enceladus (BROWN *et al*., 2006). The presence of liquid water might also make it possible for Enceladus to support life (LAMMER *et al*., 2009).

Recent data from Cassini reported pockets of heat that appear along a fracture named Baghdad Sulcus (Fig. 15), one of the Tiger Stripes that erupt with jets of water vapor and ice particles (HURFORD *et al*, 2009). The temperature along Baghdad Sulcus exceeds 180 Kelvin (WAITE *et al*., 2009). As is the case for Titan's Hotei Regio, Tiger Stripes on Enceladus and in particular Baghdad Sulcus represent tectonic zones of weakness from which the internal materials find their way to the surface. The idea of a subsurface sea becomes all the more compelling since Enceladus' south polar region (Tiger Stripes area) is actually a half-kilometer deep basin distinguishing from the surrounding expressions (COLLINS & GOODMAN, 2007). Such figure, like the deep basin in Tiger stripes, resembles Titan's Hotei Regio which is a basin lying one kilometer deeper than the surrounding area (SODERBLOM *et al*., 2009). This basin could be the surface expression of a subsurface sea (COLLINS & GOODMAN, 2007).

Titan

Titan's geology has been extensively studied using Cassini image data. In this research, we investigate and process data acquired from VIMS in order to identify areas of cryovolcanic deposition.

The most intriguing problem in regard to the decoding of Titan's surface is the atmospheric veil that covers the surface. This veil prevents any direct observation from Earth and space-based telescopes. However, VIMS on board Cassini has the ability to acquire partial surface images, taken within the so-called "methane windows" centered at 0.93, 1.08, 1.27, 1.59, 2.03, 2.8 and 5 μm, where the methane atmospheric absorption is weak (MCCORD *et al*., 2008; COUSTENIS

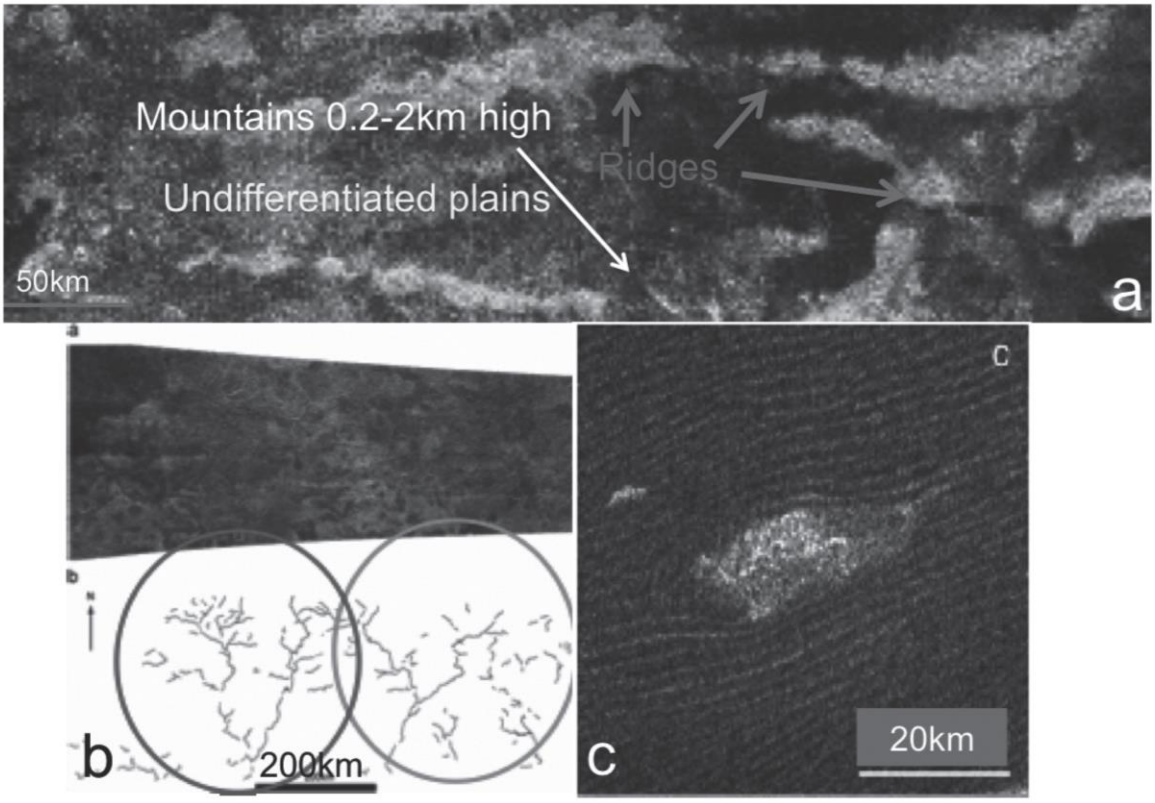

Fig. 4. (a) Ridges and mountains on Titan's surface. The radar bright features are part of the undifferentiated plains (LOPES *et al*., 2010). The proposed processes that formed this terrain have possibly tectonic origin. (b) Dendritic networks as seen with SAR and morphological map (LORENZ *et al*., 2008). The system is located at the western end of Xanadu close to our area of interest, Tui Regio. (c) Sand dunes around the Belet sand sea on Titan. The dunes are formed due to Aeolian processes. The bright figures are topographic obstacles that advance the formation of the dunes (RADEBAUGH *et al*., 2009).

et al., 2005). In general, Titan's surface appears to have smooth and rough areas of various altitudes which include extensive mountains and ridges (Fig. 4a) (LOPES *et al*., 2010), longitudinal dunes (Fig. 4c) (RADEBAUGH *et al*., 2009), dendritic networks (Fig. 4b) (LORENZ *et al*., 2008), liquid lakes (Fig. 6) (STOFAN *et al*., 2007) and impact craters that are intermittently filled by atmospheric precipitations (ELACHI *et al*., 2005). RADEBAUGH *et al*. (2008) suggests that mountains on Titan range from 200 m to 2000 m in height (Fig. 4a). Erosional processes that operate at the area where mountains lie, are probably the reason of the significant short height of the mountains. However, there is also the assumption that the mountains are built by material with properties that prevent the altitudinal growth (RADEBAUGH *et al*., 2008). RADEBAUGH *et al*. (2007) mentioned that the notably SAR bright features on Titan's surface most probably correspond to mountains and tectonic ridges which represent mountain chains (Fig. 4a). In particular, the tectonic ridges could have suffered atmospheric precipitation (i.e. hydrocarbon rain) acquiring a rough and fractured surface (SODERBLOM *et al*., 2007). Rivers are common on Titan, while in some cases a few craters are traversed by them (WOOD *et al*., 2009). The observation of river systems with dendritic patterns (Fig. 4b) (LORENZ *et al*., 2008), in addition to the observation of storm clouds (PORCO *et al*., 2005), suggest that rainfall may be a continuing erosional force erasing impact craters. Other surficial structures observed on Titan are impact craters. Of particular importance is the small number of impact craters which has been observed by the Cassini/Radar which suggests that the surface of Titan is relatively young (i.e. WALL *et al*., 2009).

The consideration of Titan's young surficial age indicates the possible existence of active regions among the satellite. Contrary to impact craters, surficial structures that are seen commonly on Titan are the dunes (Fig. 4c). The dunes are generally smooth surfaces that diverge around topographic obstacles resembling terrestrial dunes (RADEBAUGH *et al*., 2009). Moderately variable winds that either follow one mean direction or alternate between two different directions have formed the observed longitudinal dunes (LORENZ *et al*., 2006).

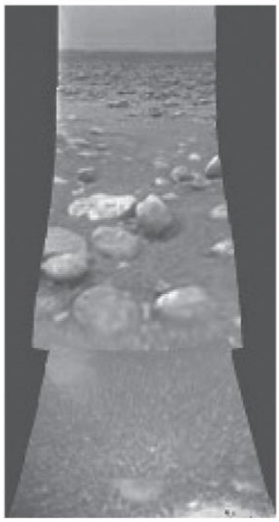

Fig. 5. Titan's surface from the Huygens probe (TOMASKO *et al*., 2005).

Our knowledge regarding Titan's surface deposits is limited to the data acquired from Huygens' landing site. The Huygens captured image was that of a dark plain covered in pebbles mainly composed of water ice (Fig. 5) (TOMASKO *et al*., 2005). The size of pebbles is estimated to be roughly 10-15 cm. There is evidence of erosion at the base of the icy rocks, indicating possible fluvial activity (TOMASKO *et al*., 2005). The surface is darker than originally expected, consisting of a mixture of water and hydrocarbon ice. It is believed that

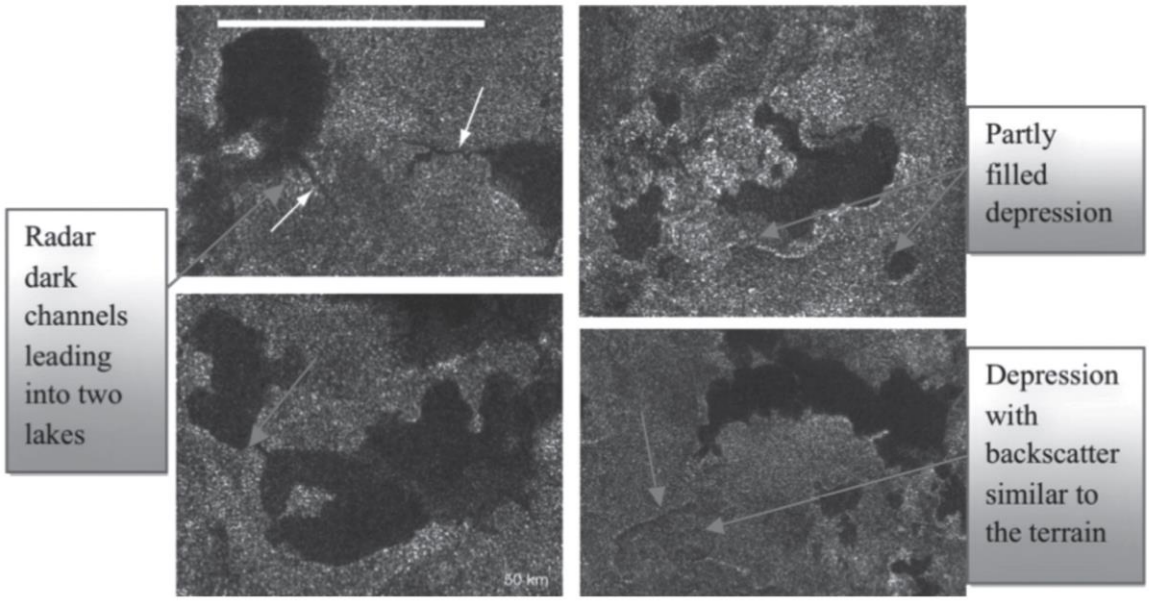

Fig. 6. Lakes on Titan's surface as recorded during the Cassini's T16 flyby on July 22, 2006 (STOFAN *et al*., 2007a).

the visible ground "powder" in the image is possibly precipitation from the hydrocarbon haze above (TOMASKO *et al*., 2005).

One of the moon's exceptional characteristics is the existence of large liquid bodies described as lakes of surface liquids (Fig. 6) (STOFAN *et al*., 2007). These features resemble terrestrial lakes consitute a unique characteristic displayed by the icy moons. Based on data provided by the Cassini/Radar, the presence of hydrocarbon lakes on Titan's surface is now well established (Fig. 6) (LOPES *et al*., 2007a).

Candidates of cryovolcanic areas on Titan

Our study involves two major areas on Titan that are the most significant, as well as, interesting cryovolcanic candidates. These areas are Tui Regio and Hotei Regio (Fig. 7) lying within the bright region of Xanadu (100°N, 15°S). Tui Regio is centered at 130°W, 20°S and presents relatively high 5 μm reflectivity. Its size is 1,500 km long and 150 km wide. This bright area has been identified as a surface feature and not as the image capture of fog, due to the area's spectral behavior at 2.7 mm (MCCORD *et al*., 2006). Tui Regio is a massive flow-like terrain, which resembles flow field volcanic areas on Earth. Another area whose spectrum matches that of Tui Regio is Xanadu's Hotei Regio. Hotei Regio is centered at 78°W, 26°S and comprises a 700 km wide field that is probably volcanic in origin. VIMS images confirm the interpretation that the area is a low basin surrounded by higher terrains with possible calderas, fault structures and extensive cryovolcanic flows (SODERBLOM *et al*., 2009).

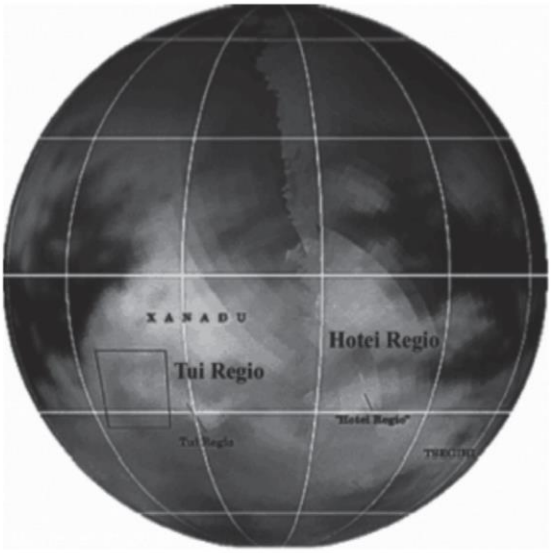

Fig. 7. The location of Tui Regio and Hotei Regio on Titan's globe (BARNES *et al*., 2006).

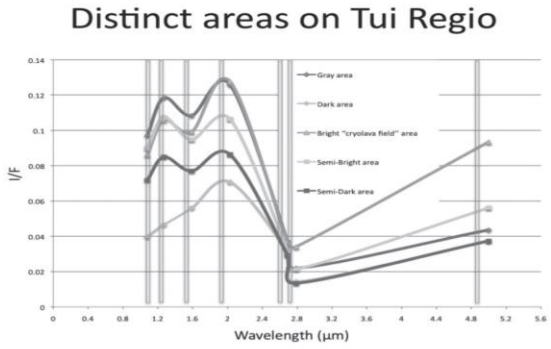

Plot 1. Spectral plot of five distinct areas at the seven atmospheric spectral windows.

Method and Data analysis

Both Tui Regio and Hotei Regio are suggested to be geologically young due to the fact that both present anomalously bright and spectrally distinct areas that have not changed from seasonal precipitation (BARNES *et al*., 2006).

In order to investigate geologically the regions of interest, it is essential to study their chemical composition that lead to the aforementioned brightness as well as their morphology in order to derive the geological factors that led to their formation.

We have processed spectral images acquired from VIMS, for both areas in the seven narrow spectral windows centered at 0.93, 1.08, 1.27, 1.59, 2.03, 2.8 and 5 μm for which absorption by atmospheric methane is minimal.

The main goal is to identify the composition as well as the alterations of the components that compose the possible cryovolcanic structures. We have used the principal components (PCs) of the Principal Component Analysis (PCA) method. The PCA method involves a mathematical procedure that transforms a number of possibly correlated variables into a smaller number of uncorrelated ones called principal components (JOLLIFFE, 2002). The PCA is well adapted to our study, as our primary concern is to determine the minimum number of factors that will account for the maximum variance of the data we use in this particular multivariate analysis. The main goal of PCA is to reduce the dimensionality of a data set consisting of a large number of interrelated variables, while retaining as much as possible of the variation present in the data set. This is achieved by transforming, the principal components (PCs) into a new set of variables, which are uncorrelated, and which are ordered so that the first few retain most of the variation present in all of the original variables (JOLLIFFE, 2002).

PCA images for both Tui Regio and Hotei Regio allowed us to isolate areas with distinct and diverse false coloring, which imply areas of distinct and diverse spectral and chemical composition (Fig, 9; 11). Such chemical diversity suggests that endogenic and/or exogenic geodynamic processes have formed these regions.

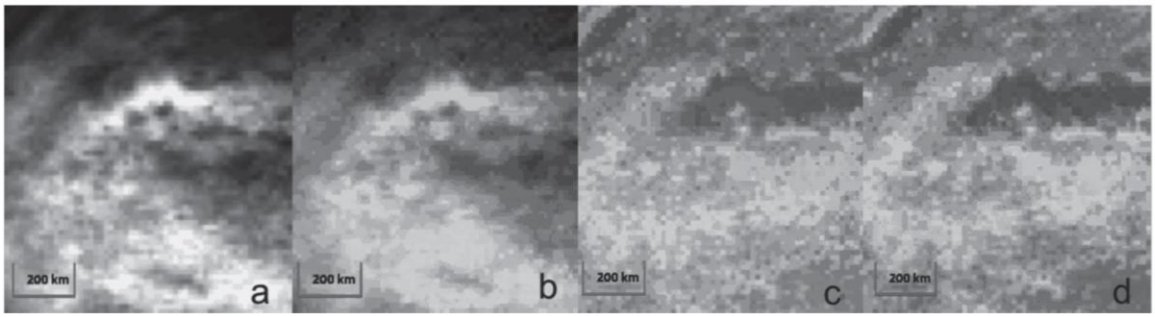

Fig. 8. Reprojection of Tui Regio: (a) Gray scale 2.03 μm, (b) RGB false colors R: 5 μm, G: 2 μm, B: 1.08 μm, (c) PCA R: 1st , G: 2nd , B: 3rd components, (d) PCA R: 3rd , G: 2nd , B: 1st components.

RESULTS

Tui Regio

We have isolated five distinct areas (Fig. 9) within Tui Regio. The Principal Component Analysis projections (Fig. 8c, d) showed areas of different colors and brightness suggesting diversity in surface composition. The PCA method is compatible to gray scale (a) and RGB (b) projections of Tui Regio. The visually brighter areas represent the highest I/F values and the darker areas the lowest, where I stands for the intensity of reflected light measured by the instrument and F the plane-parallel flux of sunlight incident on the satellite normalized for Titan (Thekaekara, 1973; Barnes *et al*., 2007; Brown *et al*., 2004).

The plot (Plot 1) of "Bright cryolava field" terrain is different from the other plots, presenting higher I/F values. This suggests that, additionally, this area is extremely brighter than the rest of the region. The wavelengths at which this area presents obvious alterations are the 2 μm, 2.8 μm and 5 μm.

Hotei Regio

We have also isolated five distinct areas within Hotei Regio's probable volcanic field (Fig. 11). The PCA projections (Fig. 10c, d) are presented in false colors areas of different spec-

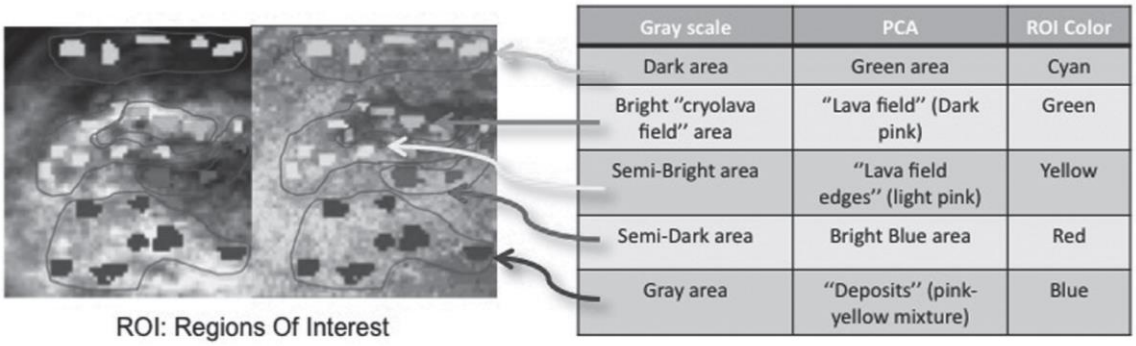

Gray scale	PCA	ROI Color
Dark area	Green area	Cyan
Bright "cryolava field" area	"Lava field" (Dark pink)	Green
Semi-Bright area	"Lava field edges" (light pink)	Yellow
Semi-Dark area	Bright Blue area	Red
Gray area	"Deposits" (pink-yellow mixture)	Blue

Fig. 9. Isolated areas with the use of visual colour alterations, which suggest areas of spectral difference.

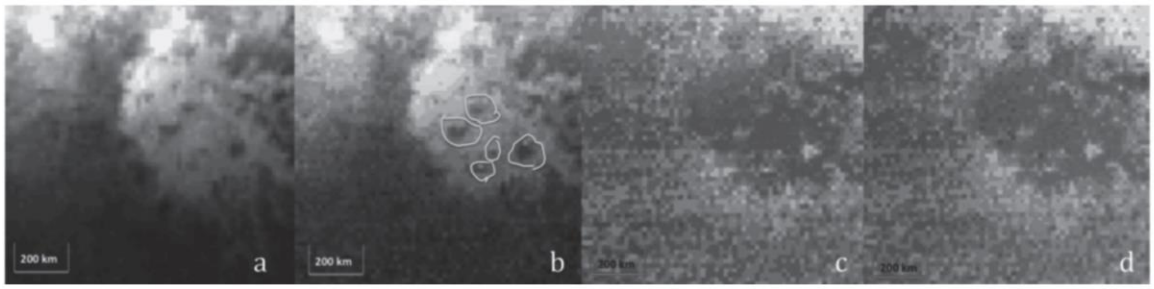

Fig. 10. Reprojection of Hotei Regio: (a) Gray scale 2.03 μm, (b) RGB false colors R: 5 μm, G: 2 μm, B: 1.08 μm, (c) PCA R: 1st , G: 2nd , B: 3rd components, (d) PCA R: 3rd , G: 2nd , B: 1st components.

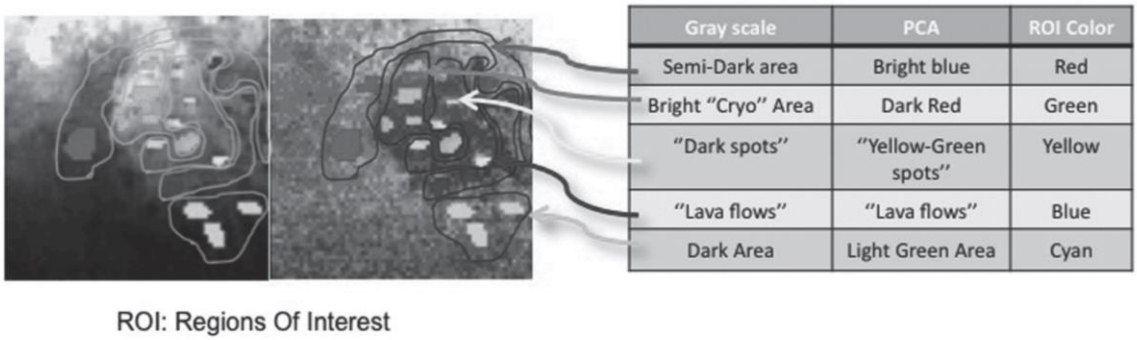

Fig. 11. Isolated areas with the use of visual color alterations, which suggest areas of spectral difference.

tra and brightness, suggesting alterations in surface composition. Thus, the area suggested to be cryovolcanic is distinguished from the surroundings. The only compatible figures with the surrounding area are the caldera-like structures (pointed by green lines, [b]), which probably reveal the primal surficial material, before resurfacing (i.e the surrounding area). The PCA images are compatible to gray scale (a) and RGB (b) projections of Hotei Regio.

Hotei Regio's spectral graph (Plot 2) indicates that the "Bright Cryovolcanic area'' presents the highest I/F values and remains brighter than the other areas at all wavelengths. In addition, the "Dark area'' remains darker with low values of I/F at all wavelengths. Surprisingly, the spectra from caldera-like structures present medium I/F values, lying almost in the average between the brighter ("volcanic area'') and the darker ("primal surface'') at most wavelengths. This is compatible with terrestrial caldera structures that consist partially of primary surficial components on which the volcano is being built, as well as new material coming from the interior.

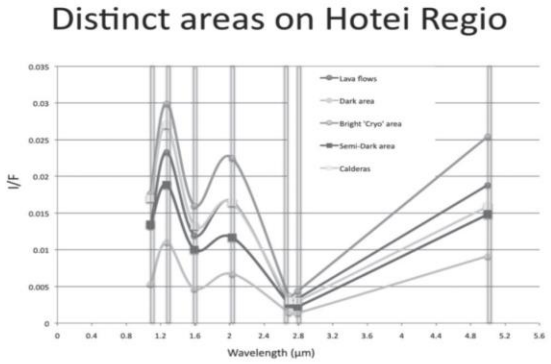

Plot 2. Spectral plot of five distinct areas at the seven atmospheric spectral windows.

DISCUSSION

Whilst it offers a particularly interesting opportunity for research, the existence of past or current cryovolcanic activity on Titan's surface, especially in areas with high reflectance, as observed by Cassini's VIMS instrument, is currently a highly controversial subject. This study has focused on evidence derived from Tui Regio and Hotei Regio, in order to analyze and interpret the data gathered from the VIMS instrument. The spectrographic analysis of VIMS data shows that the visually bright flow-like figure, seen in Tui Regio, has the highest I/F value from its surroundings, especially in the 2.03 μm, 2.8 μm and 5 μm spectral windows (Plot 1), suggests compositional variability in the material between the dark and the bright spots. Furthermore, the dark area presents the lowest I/F values at all wavelengths of the seven spectral windows. This suggests that the flow field has possibly been deposited over the initial (dark) material after single or multiple diachronic eruptions. If Tui Regio is a massive cryolava flow field, then it resembles the terrestrial Carrizozo flow field in New Mexico. Hotei Regio's field displays a low basin with flow-like features lying in the basin interior and at the margins. The flow field has higher I/F values at all wavelengths than the semi-dark and dark areas that either surround the field or lie within it (Plot 2). The dark areas present significantly lower I/F values. Even though the caldera-like structures are seeing as dark as the surrounding areas at VIMS images, they demonstrate medium I/F values suggesting altered chemical composition. The medium I/F values compared with the other areas, suggest that the calderas consist of the initial substrate (dark) material and the cryomagmatic (bright) new material. Such a combination could result in the formation of rough surfaces with high textural variability. The VIMS analysis for the caldera-like structure of Hotei Regio reinforces the theory that assumes the volcanic origin of the area's pattern. In addition, the area resembles the terrestrial volcanic terrain, Harrat Khaybar as well Enceladus' volcanic-tectonic zone of weakness, Tiger Stripes.

Further investigation and comparison of similar features from the three bodies, Titan-Enceladus-Earth, could provide information regarding their formation and future development. Titan, as described in detail hereabove, is perhaps one of the most intriguing objects in our Solar system. The combination of Titan's nitrogen atmosphere and the geologically complex and dynamic surface possesses the satellite as an

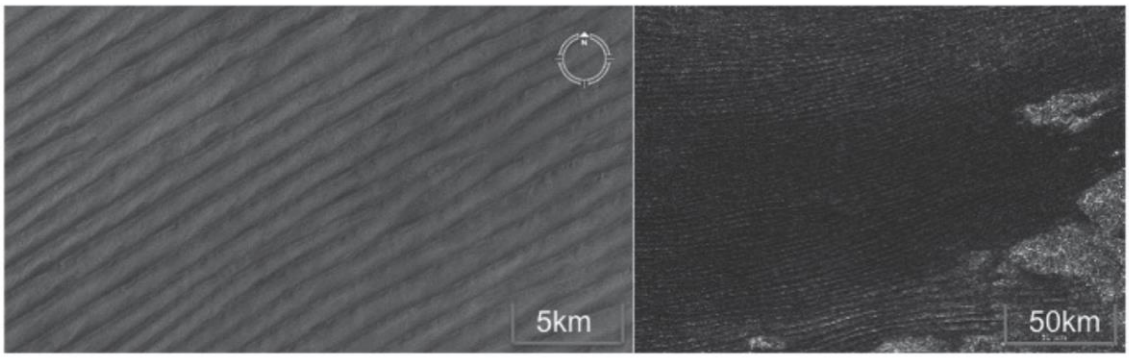

Fig. 12. (left) Longitudinal Sand dunes in Saudi Arabia (NASA). (right) Longitudinal equatorial dunes on Titan (RADEBAUGH *et al.,* 2009).

Earth-like body (COUSTENIS & TAYLOR, 2008). In addition, many atmospheric aspects such as the climate and the meteorology, as Titan displays a 'methanological' weather cycle of clouds, rainfall and evaporation that parallels the 'hydrological' cycle of the Earth, as well as, its complex morphology, make Titan an extremely important astrobiological place. Specifically, cryovolcanism has important astrobiological implications, as it provides a mechanism to expose Titan's organics to liquid water, transforming hydrocarbons and nitriles into more evolved and oxidized prebiotic species (NEISH *et al*., 2006). Also it has been suggested that life could exist in the lakes of liquid methane on Titan (MCKAY & SMITH, 2005). The existence of liquid bodies identified as lakes exposed on the surface (STOFAN *et al*., 2007), the equatorial dunes (Fig. 4c), dendritic flows, potential tectonics and volcanism, enhance Titan's resemblance to our own planet. Prior to this discovery, such combination of surface features and dense nitrogen atmosphere had only been identified on Earth.

All the aforementioned aspects, which mainly are the nitrogenic atmosphere, the liquid lakes, as well as the Earth-like geological structures, suggest that Titan resembles Earth more than any other body in the Solar System; despite the huge differences in temperature and other environmental conditions. Thus, an holistic understanding of Titan's system will help us better understand Earth's evolution starting with its primordial phase since early Earth probably looked much like Titan looks today (OWEN, 2005). In general, the activity of cryovolcanism might operate in analogy to terrestrial hydrovolcanic eruptions (SOLOMONIDOU *et al*., 2010). Fig. 13 shows the supervolcano of Lake Toba in North Sumatra, Indonesia, which is 100 km long and 30 km wide, in comparison with the possible supervolcanic structure called Ganesa Macula (50°N, 87°W) (LOPES *et al*., 2007b). The Volcanic Explosivity Index (VEI) for Lake Toba, which provides a relative measure of the explosiveness of volcanic eruptions (scale 0-8), was set to be 8 values and the total amount of erupted material volume of 2,800 km^3. Taking into consideration the amount of the erupted material, the size of the volcanic structure and the hazards that could affect the satellite, we can assume that supervolcanoes could be hosted in Titan's geological history. The candidate cryovolcanic figures Ganesa Macula, Tui Regio and Hotei Regio could resemble the supervolcanic structures seen on Earth.

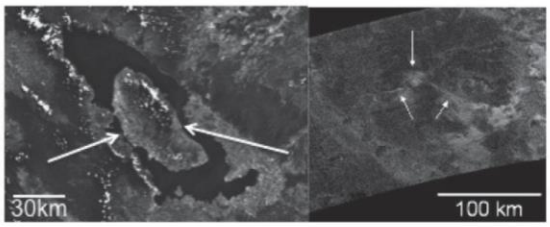

Fig. 13. (left) Supervolcano on Earth. Lake Toba (USGS). (right) Possible supervolcano on Titan. For both figures, the central part of calderas is indicated by the white arrows (LOPES *et al.,* 2007b).

In this study, we focus on the volcanological structures like the ones seen in Tui Regio and Hotei Regio that resemble terrestrial volcanic terrains and characteristics. Tui Regio is a massive (1,500 km) flow field-like figure that could possibly have formed after accumulation of cryolava flows erupted at different times, following the area's topography. On Earth, a massive edifice resembling Tui Regio, emerges in the Tularosa Basin in south-central New Mexico, USA. Carrizozo flow field (Fig. 14) is 75 km long and covers 328 km^2. The volume of eruptive material was 4.3 km^3 (BLEACHER *et al*., 2008). The field was probably formed from periodic deposition of eruptive material spewing from a source located 27 m

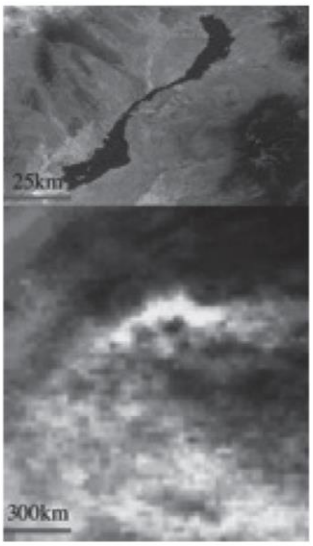

Fig. 14. (up) Carrizozo flow field, New Mexico, USA (USGS). (down) One of the largest candidate cryovolcanic flows on Titan, Tui Regio.

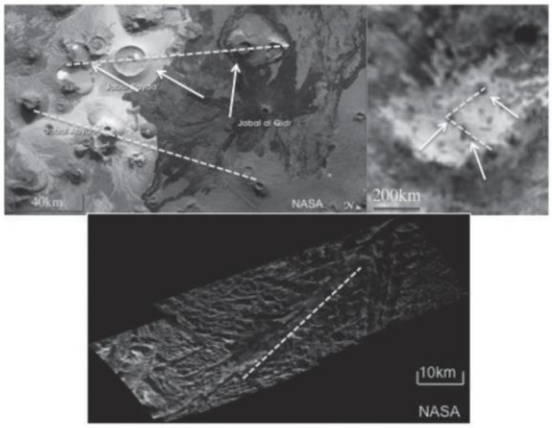

Fig. 15. (up left) Harrat Khaybar volcanic terrains, North of Medina, Saudi Arabia (NASA). (up right) Possible cryovolcanic terrain on Titan, Hotei Regio (SODERBLOM *et al.,* 2009). (down) Baghdad Sulcus, volcanic fracture on the south pole of Enceladus, Tiger Stripes (NASA). Pockets of heat have been appeared along the fracture. The white arrows indicate structures of tuffs, domes and calderas for Harrat Khaybar and possible dome and caldera formations for Hotei Regio. Additionally, the red arrows indicate lava flows and possible cryovolcanic flows within the volcanic terrain. The yellow dashed lines indicate areas that are possibly tectonic zones of weakness from which internal material may pass through.

high named Little Black Peak. The peak consists of three nested cinder cones and a solidified lava pond. The Titanian analogue (Fig. 14) is the possible cryovolcanic flow, Tui Regio; one of the largest seen on Titan. It presents similar shape as Carrizozo flow field (Fig. 14).

As indicated above, Hotei Regio is probably a massive cryovolcanic terrain that consists of caldera-like figures and depositional areas filled with lava flows. One terrestrial terrain that resembles Hotei Regio is the Harrat Khaybar volcanic field (Fig. 15), which is located at North of Medina in Saudi Arabia. The western half of the Arabian Peninsula contains extensive lava fields known as haraat (PINT, 2006). One such field is the 14,000 km^2 volcanic field that was formed by eruptions along a 100 km N-S vent system over the past 5 million years. The area contains a wide range of volcanic rock types, spectacular landforms and several generations of dark fluid basalt lava flows (PINT, 2006). Jabal Abyad, in the center of the image, was formed from more viscous, silica-rich lava classified as a rhyolite. While the 322 m high Jabal al Qidr exhibits stratovolcano, Jabal Abyad is a lava dome. To the west (image top center) is the impressive Jabal Bayda. This symmetric structure is a tuff cone, formed by eruption of lava in the presence of water. The combination produces wet, sticky pyroclastic deposits that can build a steep cone structure, particularly if the deposits consolidate quickly (PINT, 2006). In Fig. 15, we present a comparison between Earth's, Titan's and Enceladus' possible volcanic terrains and tectonic zones of weakness that consist the passage for internal material to deposit on the surfaces.

REFERENCES

BARNES, J.W. and 11 co-authors (2006). A 5-Micron-Bright Spot on Titan: Evidence for Surface Diversity. *Geophys. R. Lett*., 33, L16204.

BARNES, J.W. and 10 co-authors (2007). Global-scale surface spectral variations on Titan seen from Cassini/VIMS. *Icarus*, 186, 242-258.

BLEACHER, J.E., GARRY, W.B. & J.R. ZIMBELMAN (2008). Observations of surface textures that are indicative of lava sheet inflation in monogenetic flow fields: Insights from the McCartys and Carrizozo flow fields. *Geol. Society of America*, 40, 114.

BROWN, R.H. and 21 co-authors (2004). The Cassini Visual And Infrared Mapping Spectrometer (Vims) Investigation. *Space Science Reviews*, 115, 111-168.

BROWN, R.H. and 26 co-authors (2006). Composition and Physical Properties of Enceladus' Surface. *Science*, 311, 1425-1428.

COLLINS, G.C. & J.C. GOODMAN (2007). Enceladus' south polar sea. *Icarus*, 189, 72–82.

CONSOLMAGNO, G.J. & J.S. LEWIS (1978). The evolution of icy satellite interiors and surfaces. *Icarus*, 34, 280-293.

COUSTENIS, A., HIRTZIG, M., GENDRON, E., DROSSART, P., LAI, O., COMBES, M. & A. NEGRAO (2005). Maps of Titan's surface from 1 to 2.5 μm. *Icarus*, 177, 89-105.

COUSTENIS, A. & W.C. TAYLOR (2008). *Titan - Exploring an Earth-like World*. Scientific Publishing Company, Singapore, Eds.

DOUGHERTY, M.K., KHURANA, K.K., NEUBAUER, F.M., SAUR, C.T., LEISNER, J. & J.S. BURTON (2006). Identification of a Dynamic Atmosphere at Enceladus with the Cassini Magnetometer. *Science*, 311, 1406.

ELACHI, C. and 21 co-authors (2004). Radar: The Cassini Titan Radar Mapper. *Space Science Reviews*, 115, 71-110.

ELACHI, C. and 30 co-authors (2005). Cassini Radar Views the Surface of Titan. *Science*, 308, 970-974.

FORTES, A.D. (2000). Exobiological implications of a possible subsurface ocean inside Titan. *Icarus*, 146, 444–452.

FORTES, A.D., GRINDROD, P.M., TRICKETT, S.K. & L. VOCADLO (2007). Ammonium sulfate on Titan: Possible origin and role in cryovolcanism. *Icarus*, 188, 139–153.

FULCHIGNONI, M. and 41 co-authors (2005). In situ measurements of the physical characteristics of Titan's environment. *Nature*, 438, 785-791.

HANSEN, C.J., ESPOSITO, L., STEWART, A.I., COLWELL, J., HENDRIX, A., PRYIOR, W., SHEMANSKY, D. & R. WEST (2006). Enceladus' Water Vapor Plume. *Science*, 311, 1422.

HURFORD, T.A., BILLS, B.G., HELFENSTEIN, P., GREENBERG, R., HOPPA, G.V. & D.P. HAMILTON (2009). Geological implications of a physical libration on Enceladus. *Icarus*, 203, 541–552.

IVANOV, B.A., BASILEVSKY, A.T. & G. NEUKUM (1997). Atmospheric entry of large meteoroids: implication to Titan. *Planetary and Space Science*, 45. 993–1007.

JOHNSON, T. (2004). Geology of the Icy planets. *Space science reviews*, 166, 401-420.

JOLLIFFE, I.T. (2002). *Principal Component Analysis*. Springer series in statistics. New York: Springer.

KARGEL, J.S. (1994). Cryovolcanism on the icy satellites. *Earth, Moon, and Planets*, 67, 101-113.

KIEFFER, S.W., LU, X., BETHKE, C.M., SPENCER, J.R., MARSHAK, S. & A. NAVRITSKY (2006). A Clathrate Reservoir Hypothesis for Enceladus' South Polar Plume. *Science*, 314, 1764 - 1766.

LAMMER, H. and 16 co-authors (2009). What makes a planet habitable? *Astronomy and astrophysics review*, 17, 181-249.

LEWIS, J.S. (1971). Satellites of the Outer Planets: Their Physical and Chemical Nature. *Icarus*, 15, 174.

LEWIS, J.S. (1972). Metal/silicate fractionation in the Solar System. *Earth Planet. Sci. Lett*., 15, 286-290.

LINDAL, G.F., WOOD, G.E., HOTZ, H.B., SWEETNAM, D.N., ESHELMAN, V.R. & G.L. TYLER (1983). The atmosphere of Titan: An analysis of the Voyager 1 radio occultation measurements. *Icarus*, 53, 348-363.

LOPES, R.M.C. and 15 co-authors (2007a). The Lakes and Seas of Titan. *Eos, Transactions American Geophysical Union*, 88, 569-570.

LOPES, R.M.C. and 42 co-authors (2007b). Cryovolcanic features on Titan's surface as revealed by the Cassini Titan Radar Mapper. *Icarus*, 186, 395–412.

LOPES, R.M.C. and 24 co-authors and the Cassini Radar Team (2010). Distribution and interplay of geologic processes on Titan from Cassini radar data. *Icarus*, 205, 540–558.

LORENZ, R.D. & J. MITTON (2008). Titan Unveiled. Princeton University Press.

LORENZ, R.D. and 39 co-authors (2006). The sand seas of Titan: Cassini RADAR observations of longitudinal dunes. *Science*, 312, 724–727.

LORENZ, R.D. and 15 co-authors and the Cassini Radar Team (2008). Fluvial channels on Titan: Initial Cassini radar observations. *Planetary and Space Science*, 56, 1132-1144.

McCORD, T.B. and 16 co-authors and the Cassini VIMS Team (2006). Composition of Titan's Surface from Cassini VIMS. *Planetary Space Science*, 54, 1524–1539.

McCORD, T.B. and 13 co-authors (2008). Titan's surface: Search for spectral diversity and composition using the Cassini VIMS investigation. *Icarus*, 194, 212-242.

McKAY, C.P. & H.P. SMITH (2005). Possibilities for methanogenic life in liquid methane on the surface of Titan. *Icarus*, 178, 274-276.

NEISH, C.D., LORENZ, R.D., O' BRIEN, D.P and the Cassini Radar Team (2006). The potential for prebiotic chemistry in the possible cryovolcanic dome Ganesa Macula on Titan. *International Journal of Astrobiology*, 5(1), 57-65.

OWEN, T. (2005). Huygens rediscovers Titan. *Nature*, 438, 756-757.

PINT, J.J. (2006). Prospects for Lava-Cave Studies in Harrat Khaybar, Saudi Arabia. *AMCS Bulletin*, 19, 197-200.

PORCO, C.C. and 19 co-authors (2004). Cassini Imaging Science: Instrument Characteristics And Anticipated Scientific Investigations At Saturn. *Space Science Reviews*, 115, 363-497.

PORCO, C.C. and 35 co-authors (2005). Imaging of Titan from the Cassini spacecraft. *Nature*, 434, 159-168.

PORCO, C.C. and 24 co-authors (2006). Cassini Observes the Active South Pole of Enceladus. *Science*, 311, 1393-1401.

POSTBERG, F. and 7 co-authors (2009). Sodium salts in E-ring ice grains from an ocean below the surface of Enceladus. *Nature*, 459, 1098–1101.

RADEBAUGH, J., LORENZ, R., KIRK, R.L., LUNINE, J.I., STOFAN, E.R., LOPES, R.M.C., WALL, S.D. and the Cassini Radar Team (2007). Mountains on Titan observed by Cassini Radar. Icarus, 192, 77–91.

RADEBAUGH, J., LOPES, R.M.C., STOFAN, E.R., VALORA, P., LUNINE, J.I., LORENZ, R.D. and the Cassini Radar Team (2008). Mountains on Titan as Evidence of Global Tectonism and Erosion. *39th Lunar and Planetary Science Conference* XXXIX, 1391, 2206.

RADEBAUGH, J., LORENZ, R., FARR, T., PAILLOU, P., SAVAGE, C. & SPENCER, C. (2009). Linear dunes on Titan and earth: Initial remote sensing comparisons. *Geomorphology*, 121(1-2), 122-132.

RAULIN, F. (2008). Astrobiology and habitability of Titan. *Space Science Reviews*, 135, 37-48.

SODERBLOM, L.A. and 26 co-authors (2007). Correlations between Cassini VIMS spectra and RADAR SAR images: Implications for Titan's surface composition and the character of the Huygens Probe Landing Site. *Planetary and Space Science*, 55, 2025-2036.

SODERBLOM, L.A. and 12 co-authors (2009). The geology of Hotei Regio, Titan: Correlation of Cassini VIMS and RADAR. *Icarus*, 204, 610-618.

SOLOMONIDOU, A., COUSTENIS, A., BAMPASIDIS, G., KYRIAKOPOULOS, K. & X. MOUSSAS (2010). Possible cryovolcanic and tectonic processes on Titan and Enceladus: Similarities to terrestrial systems. *European Geosciences Union*, Vienna, 12, 4355.

SOTIN, C. and 25 co-authors (2005). Release of volatiles from a possible cryovolcano from near-infrared imaging of Titan. *Nature*, 435, 786-789.

STOFAN, E.R. and 37 co-authors (2007). The lakes of Titan. *Nature*, 445, 61-64.

THEKAEKARA, M.P. (1973). The Extraterrestrial Solar Spectrum. *Eds. Institute of Environmental Sciences, Mount Prospect Illinois*, 71-133.

TOBIE, G., JONATHAN, I.L. & C. SOTIN (2006). Episodic outgassing as the origin of atmospheric methane on Titan. *Nature*, 440, 61–64.

TOBIE, G., CADEKC, O. & C. SOTINA (2008). Solid tidal friction above a liquid water reservoir as the origin of the south pole hotspot on Enceladus. *Icarus*, 196, 642-652.

TOMASKO, M.G. and 39 co-authors (2005). Rain, winds and haze during the Huygens probe's descent to Titan's surface. *Nature*, 438, 765-778.

WAITE, J. H. and 14 co-authors (2009). Liquid water on Enceladus from observations of ammonia and ^{40}Ar in the plume. *Nature*, 460, 487–490.

WALL, S. D. and 16 co-authors (2009). Cassini RADAR images at Hotei Arcus and western Xanadu, Titan: Evidence for geologically recent cryovolcanic activity. *J. Geophys. Res*., 109, E06002.

WILSON, E.H. & S.K. ATREYA, (2004). Current state of modelling the photochemistry of Titan's mutually dependent atmosphere and ionosphere. *Geophys. Res. Lett.*, 36, L04203.

WOOD, C.A., LORENZ, R., KIRK, R., LOPES, R., MITCHELL, K., STOFAN, E. and the Cassini Radar Team (2009). Impact craters on Titan. *Icarus*, 206, 334-344.

ZARNECKI, J.C. and 25 co-authors (2005). A soft solid surface on Titan as revealed by the Huygens Surface Science Package. *Nature*, 438, 792-795.

Appendix A2

Water Oceans of Europa and Other Moons: Implications For Life in Other Solar Systems

Journal article published in *Journal of Cosmology* (2011),

Volume 13, pp. 4191-4211

Online publication: http://journalofcosmology.com/Planets103.html.

Journal of Cosmology, 2011, Vol 13. 4191-4211.

Water Oceans of Europa and Other Moons: Implications For Life in Other Solar Systems

Solomonidou, A.[1,2], Coustenis, A.[2], Bampasidis, G.[2,3], Kyriakopoulos, K.[1], Moussas, X.[3], Bratsolis, E.[3], Hirtzig, M.[2]

[1]Department of Geology and Geoenvironment, National & Kapodistrian University of Athens, Greece,
[2]LESIA, Observatoire de Paris-Meudon, 92195 Meudon Cedex, France,
[3]Department of Physics, National & Kapodistrian University of Athens, Greece.

Abstract

The icy satellites around Jupiter and Saturn have been revealed as recently or presently active bodies of high interest for geology and astrobiology. Several of them show promising conditions for internal structures involving liquid water oceans. The surface features observed on Jupiter's Europa and Ganymede as well as Saturn's Titan and Enceladus moons display interesting evidence and multicomplex geological figures, which resemble terrestrial geo-terrains in terms of structure and possibly followed similar formation mechanisms. All aforementioned satellites consist of differentiated interiors that are stratified into a high-density rocky core, a mantle and an icy crust. The confirmation of the presence of a liquid water ocean within these satellites would have important implications on the existence of solid bodies with internal liquid water in the outer Solar System well beyond the "habitable zone", with important astrobiological consequences. Indeed, an underground liquid ocean could provide a possible habitat by resembling terrestrial life-hosting environments like the deep oceans and the hydrothermal active vents. In this study we review the surficial aspects of Europa, Ganymede, Titan, and Enceladus and connect them to possible models of interior structure, with emphasis on the astrobiological implications.

Keywords: Icy satellites, internal ocean, planetary geology, Europa, Titan, Ganymede, Enceladus

Anezina Solomonidou
National & Kapodistrian University of Athens / Observatoire de Paris-Meudon
Panepistimiopolis, Zografou
15783 Athens, Greece
Email: asolomonidou@geol.uoa.gr
Phone: +30-2107276854
Fax: +30-2107276725

1. Introduction

Europa, Ganymede, Titan, Enceladus

Icy satellites of the gaseous giants, Jupiter and Saturn, at orbits beyond the ice-line, constitute extremely interesting planetary bodies due to – among other - their unique geological (Prockter et al. 2010) and surface composition characteristics (Dalton, 2010; Dalton et al. 2010; Fortes & Choukroun, 2010), the possible internal water ocean underneath their icy crust and the habitability potential (Schubert et al. 2010; Tobie et al. 2010; Hussmann et al 2010; Sohl et al. 2010). Two of the largest Jovian satellites, Ganymede and Europa, as well as Saturn's Enceladus and Titan, show not only surface features similar to the terrestrial planets and especially the Earth, but also internal heating and occasionally volcanism. Hereafter we summarize some of the characteristics of these moons.

In the neighborhood of Jupiter, two moons are good candidates for the internal liquid water ocean and together form today the main targets of the Europa Jupiter System Mission (EJSM), a concept studied by ESA and NASA for a launch in 2020.

Europa hosts one of the smoothest surface topographies in the Solar System, composed essentially of water ice and other (Dalton, 2010; Dalton et al. 2010), and displays structures like linear chains (lineae) (e.g. Figueredo & Greeley, 2004), which most likely are crack developments caused primarily by diurnal stresses (Prockter et al. 2010) and display the main characteristics of ridges. Other structures are domes (pits that are surface depressions), dark spots and very few craters (Pappalardo et al. 1998a) as the Galileo mission showed. Internal stratigraphic modeling suggests that the satellite is primarily composed of silicate rock (olivine-dominated mineralogy) (e.g. Schubert et al. 2004; Sohl et al. 2010) and most probably an iron-rich core (Anderson et al. 1998). It is also suggested that the icy crust is decoupled from the moon's deeper interior due to the presence of a subsurface liquid ocean (e.g. Schenk &Mckinnon, 1989; Zimmer et al. 2000; Schenk et al. 2004). The cracks, faults and lineae observed on the surface, have most probably been formed by endogenic processes that lead to tectonic movements and imply the presence of a subsurface ocean that interact with the crust. Also, Europa suffers heavily bombardment by charged particles from the Jovian magnetosphere that lead to surface material decomposition and form the tenuous atmosphere composed mainly of oxygen (Shematovich & Johnson, 2001; Coustenis et al. 2010).

On the other hand, Ganymede, the largest satellite of the Solar System, is the only known moon to possess a magnetosphere (Kivelson et al. 2002). Most of Ganymede's surface coverage displays dark and brighter regions. The former are filled with impact craters while the latter are covered by terrains curved by tectonic ridges and grooves (e.g. Pappalardo et al. 2004; Patterson et al. 2010). Its internal structure possibly consists of a relatively small iron-rich core, overlain by silicate rocky material, which is covered by an icy crust. It is believed that a liquid ocean exists within the mantle almost 200 km deep (e.g. McCord et al. 2001). The satellite possesses a thin oxygen atmosphere (Hall et al. 1998; Coustenis et al. 2010 and references therein).

The aforementioned information for Europa and Ganymede has been provided mostly from ground-based but also from *in situ* missions such as Pioneer 10 and 11, Voyager and more recently and efficiently Galileo. Taking into account the geological and structural elements of both satellites, they readily become promising worlds of astrobiological potential. The forthcoming Europa Jupiter System Mission (EJSM) which is composed of two orbiters, one dedicated to Europa and one to Ganymede, will provide detailed investigation of these satellites (e.g. Blanc et al. 2009).

Orbiting at circa 10 AU, the Kronian satellites Titan and Enceladus, stand as intriguing objects as the Jovian satellites. The Cassini-Huygens mission has unveiled the multivariable Earth-like geology of Titan since its arrival in 2004. Furthermore, Titan is the only one planetary object except the Earth that possesses a unique nitrogen and full of organics atmosphere (e.g. Coustenis & Taylor, 2008). Recently, a subsurface liquid ocean was suggested at Titan based on thermal and orbital calculations (e.g. Tobie et al. 2005) spin rate measurements and SAR reflectivity observations (Lorenz et al. 2008; Stiles et al. 2010; Hussmann et al. 2010). The surface investigation brought to light many geological expressions such as extensive mountains, ridges, dendritic networks, dunes, lakes, channels, canyons and riverbeds (Lopes et al. 2010). Furthermore, there is the possible existence of active zones on the satellite due to past or recent cryovolcanic and tectonic activity (e.g. Soderblom et al. 2007; Lorenz et al. 2008; Nelson et al. 2009a; 2009b).

Another Saturnian satellite, Enceladus, has been shown by Cassini to be one of the most active objects in the

Solar System despite its minor size. Indeed, jets from its southern polar region consisted mainly of water ice particles that reach over 435 km in height, enrich the E-ring of Saturn (Dougherty et al. 2006; Porco et al. 2006; Waite et al. 2006). The source of such activity could be a large internal liquid deposit, most likely an underground liquid ocean (e.g. Porco, 2008; Collins et al. 2007; Postberg et al. 2009). The surface expressions observed on Enceladus include craters and smooth terrains that consist of extensive linear cracks, scarps, troughs and belts of grooves.

Due to their complex surfaces and intriguing interiors, both Saturnian satellites, require new long-term missions with advanced instrumentation and possibly *in situ* elements. Such a concept was proposed within the Titan Saturn System Mission (TSSM), studied by ESA and NASA and could be launched after EJSM, around 2025. The mission consists in an orbiter, a Titan montgolfière hot air balloon and a Titan lake lander for simultaneous *in situ* and remote exploration of Titan and Enceladus.

A number of evidences, either surficial expressions or geophysical factors, endorse the existence of internal oceans beneath the four aforementioned satellites. The consideration of the possible implications from geological features on the surface and their possible relation to the interior is presented in the review hereafter.

2. Geology: Surface features and their implications

The diversity of geological features on Europa and Ganymede

Without doubt, the surface expressions observed on a planetary body are the signatures of both external and internal processes as occurred with time. Hence, although the environmental conditions and the working material are different from the terrestrial case, in the presence of similarities in the surface features observed, the heritage of Earth science can be used as a tool for their study on other bodies.

Europa and Ganymede present a major diversity in terms of appearance and surface geological structures and therefore in terms of the surface-shaping forces. Europa seems to be subject to active tectonism and cryovolcanism since it displays a young, smooth and active surface. On the contrary, Ganymede is heavily cratered on most of its surface and internal processes like cryovolcanism seem to have played only a minor role in the surface modification since there is little indication of resurfacing. In general, erosion as well as mass movement and landform degradation seem to play an important role in resurfacing as it reduces the topographic relief by moving surface materials to a lower gravitational potential (Moore et al. 2010).

The most distinct and characteristic morphotectonic features on Europa are the lineations that intersect the entire upper part of the satellite's crust (Fig. 1). These formations are probably the major resurfacing mechanism since their genesis is based on the intersection of any two parts of the surface by bedding or/and cleavage. Figure 2 displays a scheme of intersect lineae formation as seen on the Earth (Park, 1997). The tectonic activity that forms these edifices along with the heating from the subsurface diapirs (mobile material that was forced into more brittle surrounding rocks and follows an upward direction) composes the dominant dynamic potential of the satellite.

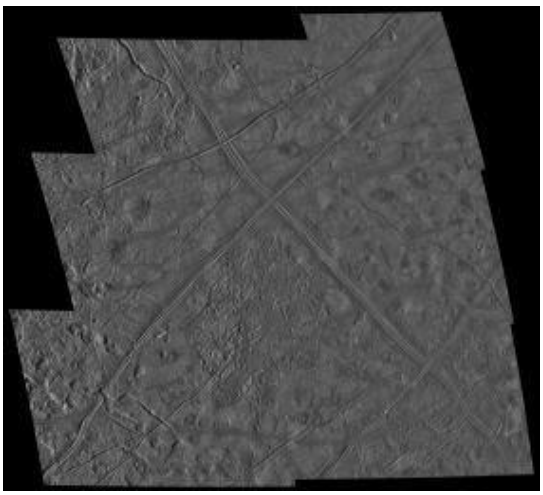

Fig. 1. Variety of interesting geologic features on Europa (NASA).

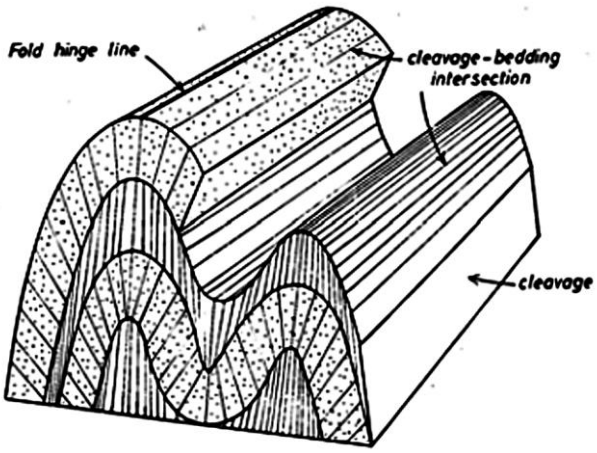

Fig. 2. Schematic formation of intersect lineation (Park, 1997).

Geissler et al. (1998) proposed four different classes of lineaments that vary with age and wipe out Europa's geologic history through time. Their size ranges from 1 to 20 km and they are separated into (a) incipient-simple colorless cracks, (b) ridges that are wider than the cracks, (c) multiple ridged triple bands and (d) ancient bands (Fig. 3). A distinct intersecting 1,500 km feature, Agenor Linea, is a candidate active region as found in photometric observations (Hoppa et al. 1998; Geissler et al. 1998).

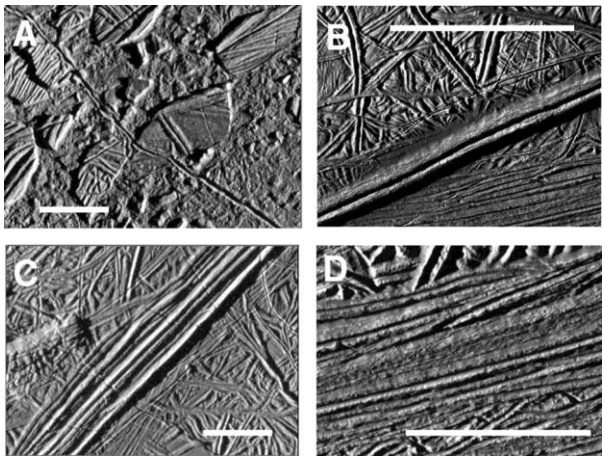

Fig. 3. Four classes of lineaments on Europa (Geissler et al. 1998).

Other geological expressions seen on Europa by Galileo are features that are called 'lenticulae' and 'chaos'. In terrestrial geology, a lenticulae feature is a depositional body that is thick in the middle and thin at the edges, resembling a convex lens in cross-section. Both features have probably formed by rising diapirs that produced partial melt. On Europa, the lenticulae are ovoidal features ranging from 5 to 20 km in diameter (Pappalardo et al. 1998) while the chaos structures, like Conamara Chaos (8°N, 274°W), are larger features presenting blocky material (Carr et al. 1998; Spaun et al. 1998; Sotin et al. 2002). Another hypothesis for the genesis of lenticulae features suggests a correlation between them and the chaos formations. This hypothesis by Greenberg (2008) assumes that the lenticulae are chaos formations in smaller dimension that low-resolution Galileo imaging interpreted wrongfully as distinct structures.

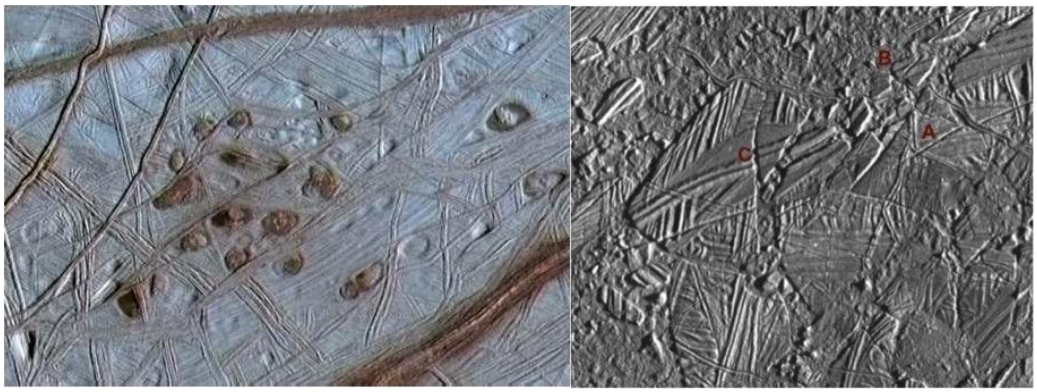

Fig. 4. (left) Lenticulae on Europa (reddish semi-circular spots in the middle of the image. (right) Conamara Chaos, area covered with big blocks of crust that are mixed and moved suggesting they floated on a liquid layer (Galilleo Project/NASA). The area of chaos terrain shows plate-like features (marked with A) with ridges and valleys, and regions lower than the plates (marked with B). Also, plate displacement is obvious with surface expressions like faults or ridges deviating from their linear structure (marked with C).

In contrast to Europa's flattened topography and homogeneous surface, Ganymede possesses two distinct types of terrain. The dominant terrain comprises the brighter regions marked with geological expressions such as extensive ridges, grooves and faults while its age considers as the youngest in comparison with the rest of the surface (Pappalardo et al. 1998) (Fig. 5).

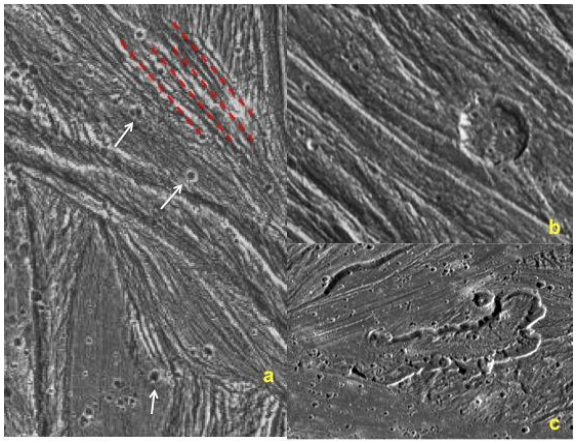

Fig. 5. Bright terrain's major geological features in Ganymede. (a) Uruk Sulcus region is filled with ridges (red dashed line), grooves, craters (white arrows) and generally displays a smooth area. (b) Nippur Sulcus region display an extensive crater overlying ridges and troughs. (c) Sippar Sulcus region contains a large curvilinear scarp or cliff or possibly a caldera. If this structure is identified as caldera then it is the basic evidence for a surficial edifice of active past or present cryovolcanism on Ganymede (NASA/JPL/Brown University).

The other geological terrain-type is the dark terrain (Prockter et al. 1998) (Fig. 6), which is the oldest one in terms of age, heavily cratered with astrobiological interest due to the existence of organic materials (McCord et al. 1998). Considering the fact that the satellite is heavily cratered and the dark terrain comprises one of the oldest terrains of the Galilean satellites (Zahnle et al. 1998), this surface is an indicator of the system's cratering history (Pappalardo et al. 1998).

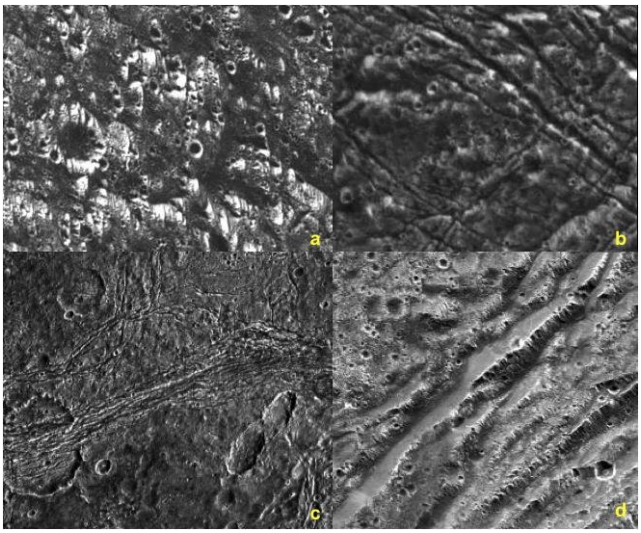

Fig. 6. Dark terrain's major geological features on Ganymede. (a) Ancient impact craters visible at the middle left. (b) Grooves – northwest to southeast sets of fractures that possibly traverse a chain of craters. (c) Tectonics in the dark terrain: sets of ridges and grooves and fault blocks traverse the extensive crater located at the lower left part of the image and deforms it. (d) Series of scarps cut through the heavily cratered and old dark terrain (NASA/JPL/Brown University).

The regions that are particularly interesting in terms of geology are the transitional regions (Fig. 7). Such regions correspond to surface areas that constitute a transition from the dark terrain to the bright grooved terrain of Ganymede. Even though cratering is present on both types of terrain, the dark ones seem heavily and more extensively bombarded (Showman & Malhotra, 1999) suggesting that they represent the oldest preserved (non-resurfaced) surfaces on Ganymede. Pappalardo et al. (2004) suggested that the modification of the dark terrain's material due to tectonic and cryovolcanic resurfacing formed the primary bright terrain.

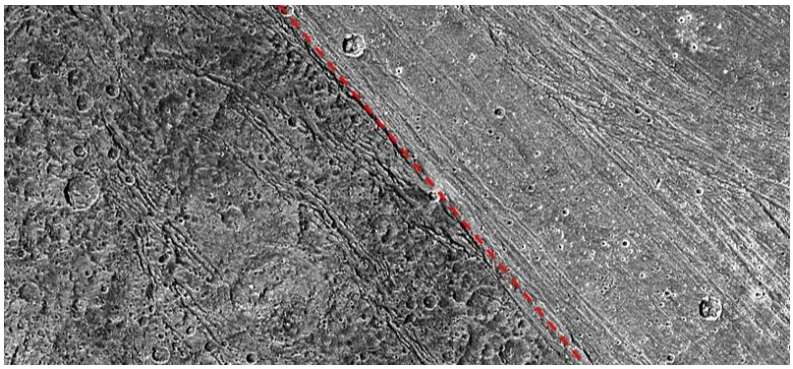
Fig. 7. Transitional region on Ganymede (dark terrain to bright terrain) separated by the red dashed line (NASA/JPL).

Another significant region on Ganymede is the Galileo Regio (Fig. 8), which has likely been formed during an active geologically period (Casacchia, 1984). The Galileo Regio is a heavily cratered area but not an impact crater. It seems to have been shaped under the influence of tectonic processes and young and bright material that arose from the interior (Harland, 2000).

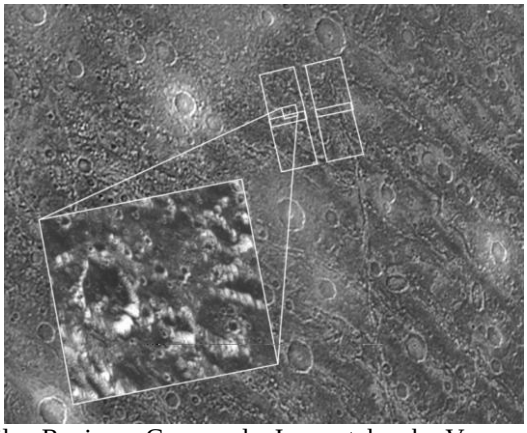

Fig. 8. Galileo Regio on Ganymede. Image taken by Voyager (NASA).

Both moons, Europa and Ganymede illustrate their own fascinating surface geology. Many factors contribute to their formation with the most influencing ones being the internal dynamics like tides, volcanism and tectonics as well as external factors like impact cratering.

Active worlds: Titan and Enceladus and their habitability

Even though Titan and Enceladus' surface expressions are very different in terms of composition, materials and size, they highly resemble the Earth's geomorphology. Titan's surface consists of structures like mountains, ridges, faults and canyons (Fig. 9), formed most probably by tectonic processes, as discovered by the Cassini-Huygens mission (Brown et al. 2009; Lopes et al. 2010; Mitri et al. 2010). Titan, other than its atmospheric uniqueness, is also the only among outer planet satellites where aeolian and fluvial processes operate to erode, transport, and deposit material (Moore et al. 2010).

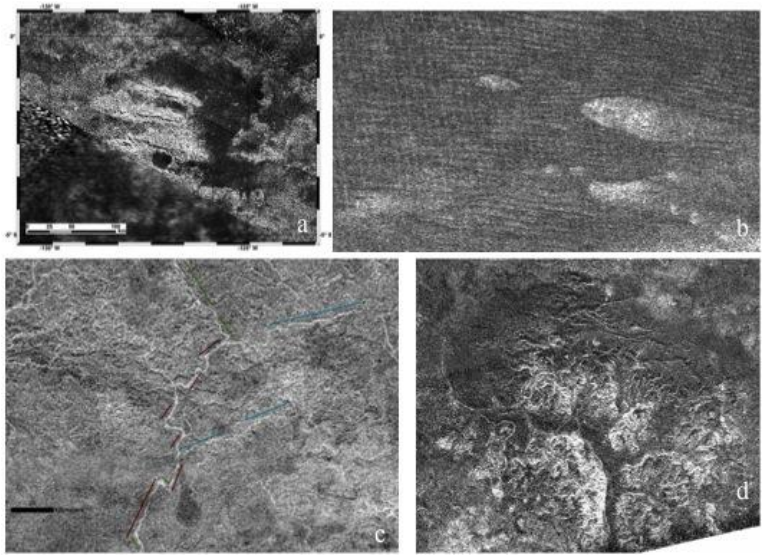

Fig. 9. Tectonic structures on Titan. (a) parallel mountains (NASA), (b) long, dark ridges spaced around one to two kilometers apart (NASA), (c) rectangular river network that possibly lie over faults that control the direction that methane can flow across the surface (NASA/JPL/Devon Burr), (d) canyon systems along with bedrocks, channels and high cliffs (NASA/JPL).

The phenomenon that most probably formed terrestrial-like volcanic structures like calderas, flows and domes on Titan, is cryovolcanism. Currently, there are three possible cryovolcanic regions. These are Tui Regio (20°S, 130°W), Hotei Regio (26°S, 78°W) and Sotra Facula (15°S, 40°W). The latter is considered as the most promising one with obvious surface expressions of peaks, flows and one caldera structure (Fig. 10).

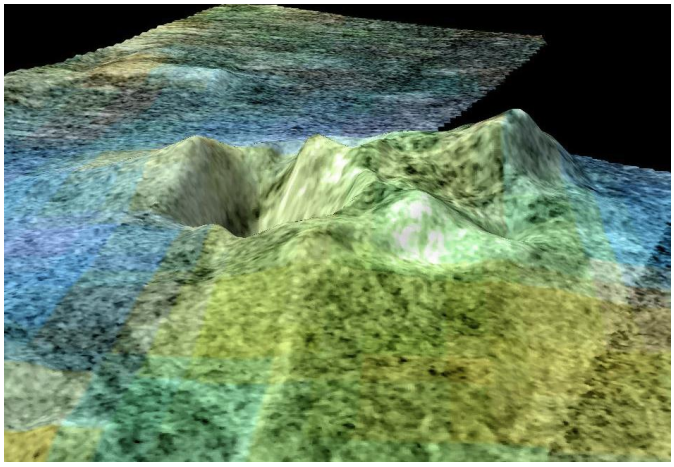

Fig. 10. Sotra Facula, a possible cryovolcano on Titan. The peaks are more than 1 km high and the craters-caldera almost 1.5 km deep. Furthermore, flow features about 100 meters thick are obvious following a radial pattern around the craters (NASA/JPL-Caltech/USGS/University of Arizona).

Furthermore, aeolian and fluvial processes acting on Titan's surface create edifices such as lakes, seas, riverbeds, sand dunes, shorelines, and dendritic drainage networks (Fig. 11). External impact phenomena like impact craters are rarely observed on the surface due to the resurface activity.

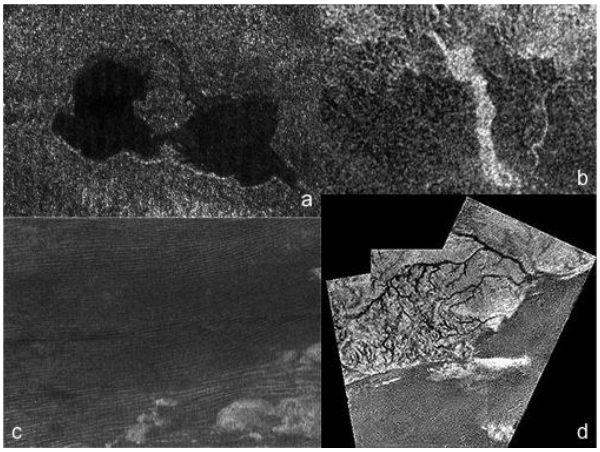

Fig. 11. Fluvial and aeolian features on Titan. (a) 'Connected' lakes (NASA/JPL), (b) riverbeds (NASA), (c) sand dunes (NASA/JPL), (d) dendritic drainage networks (NASA/JPL).

Similarly to Titan, Enceladus presents major tectonic features and active cryovolcanism. The most fascinating phenomenon occurs on Enceladus currently due to its tremendous internal dynamic convective forces that cause Geyser-like fountains at its southern pole that could reach more than 400-km in height (Porco et al. 2005). The rest of Enceladus' surface is covered by smooth and cratered terrains, rifts, ridges, grooves, escarpments and extensive linear fractures (Johnson, 2004). The geology of this tectonized moon is a field of active scientific research awaiting for new observations. Up to date, the observations and analysis showed two types of tectonic terrains. The north pole consists of heavily cratered landforms while the central region and southern pole of tectonic molded terrain with cryovolcanic features.

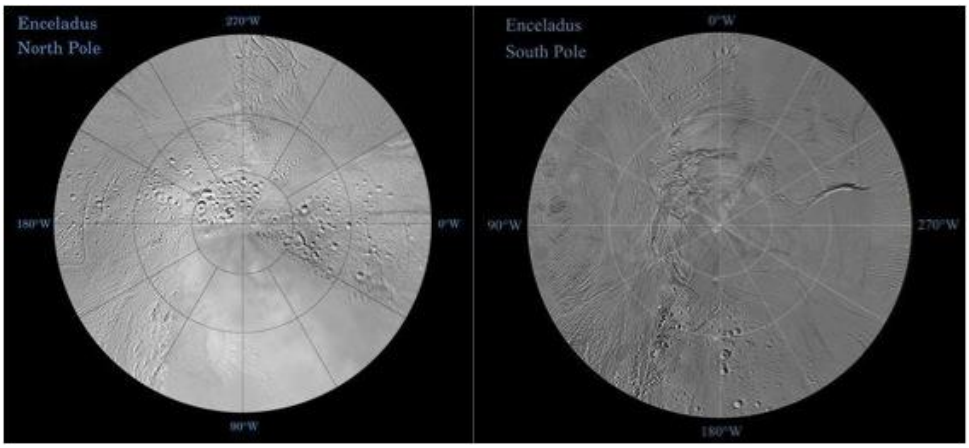

Fig. 12. Poles of Enceladus. (left) Heavily cratered terrain of the north pole. (right) Tectonized terrain (ridges, grooves, rifts) with fissures that emanate cryovolcanic material (NASA/JPL).

3. Interior models and liquid water subsurface oceans in giant planets' satellites

Our current knowledge of the icy moons' internal stratification and their composition is being built on a combination of spacecrafts data, laboratory experiments, and theoretical geophysical modeling. Resembling Earth's moon in terms of structure, icy moons consist of a core, a mantle, and a crust, with the specificity of the existence of a liquid ocean lying within the icy mantle (Fig. 13).

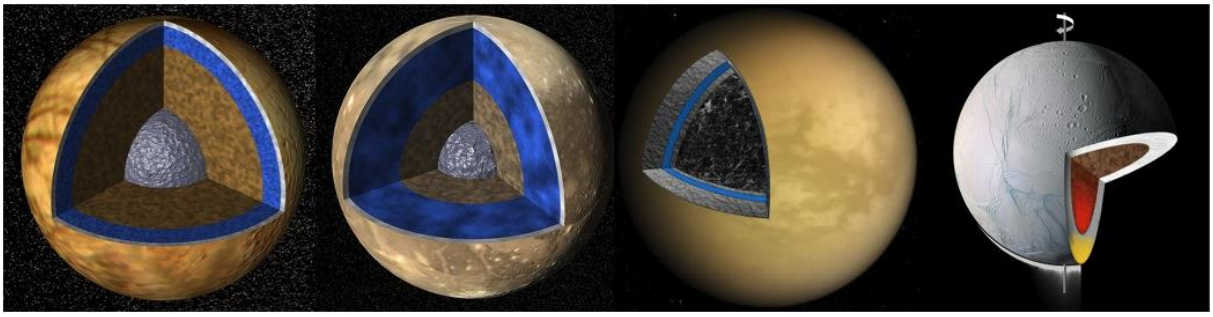
Fig. 13. From left to right: Europa, Ganymede, Titan and Enceladus' internal stratigraphic models (NASA/JPL).

According to current models of internal structure, the existence of subsurface oceans is expected for most of the icy moons of the Outer planets (e.g. Sohl et al. 2010; Schubert et al. 2010 and references therein). Even if an ocean is not currently hidden within the interior, it is suggested that a liquid layer was present in the past but cooled to ice over time. An example of such case is Neptune's moon Triton.

Evidence for hydrated sulfate salts on the surfaces of Europa and Ganymede from spectroscopic data support the possible existence of subsurface oceans (McCord et al. 1998; 2001; Cassidy et al. 2010; Fortes et al. 2010 and references therein) suggesting the deposition of minerals following internal hydrothermal events. In addition, Galileo's magnetometer (e.g. Khurana et al. 1998; Kivelson et al. 2002), detected induced magnetic fields at Europa and Ganymede that imply the presence of an electrically conductive subsurface layer (e.g. Sohl et al. 2010). Furthermore, the detection of a low viscosity layer underneath the icy crust again endorses the presence of a subsurface liquid ocean inducing recent geological activity (Stern & McKinnon, 1999; Ruiz & Fairen, 1999).

The common properties that need to be satisfied on all bodies in order to sustain a liquid subsurface ocean are:

(a) Heat production which mainly originates from radiogenic heating or other triggering mechanisms (e.g. McKinnon, 1999; Tobie et al. 2005). In the absence of an internal liquid layer, the tidal deformation of the ice shell remains very small as there is no decouple of the core and the mantle, thus the resulting stress and consequent heating is negligible (Moore & Schubert, 2000). Other possible heat sources are the dissipation of tidal energy due to orbital interaction between the satellites and their planets, or the exothermal geochemical

production of heat like hydration and crystallization of solids (e.g. Sohl et al. 2010; Hussmann et al. 2010).

(b) Efficiency of heat transfer, which is based on thermal diffusion and thermal convection (e.g. Hussmann et al. 2010).

(c) Components capable of decreasing the melting point of ice and supporting the ocean's liquid state (e.g. Sohl et al. 2010; Tobie et al. 2010). The composition of such oceans should offer an antifreeze constituent like a solution of water with ammonia, so that it remains in liquid state. The aqueous evolution of a possible internal ocean depends on the several chemical interactions between liquid water and rocks, on the hydrodynamic processes within the ocean (degassing), on the freezing of the expected plumes as well as on the presence of secondary organic and inorganic species (Sohl et al. 2010).

(d) Stability of the crust against convection, keeping the ocean subsurficial as well as preventing stagnant lid convection (e.g. McKinnon, 1998; Rainey & Stevenson, 2003).

The Voyager and Galileo missions data suggest that the internal stratification of Europa consists of an iron core (300 to 800 km) covered by a rocky mantle probably 100 km thick that it is overlain by a liquid water ocean less than ten kilometers thick. The ocean is covered by a surficial icy layer possibly 15 km thick (Fig. 13). The Galileo magnetometer's measurements that showed the crust had shifted by almost 80°, also indicated that the mantle is not attached to the crust, thus reinforcing the theory of an internal ocean (Kivelson et al. 2000; Greenberg, 2005). Nevertheless, the most convincing evidence for the liquid water ocean is the existence of the controversial 'chaos terrain' (Fig. 4) that possibly formed by melt-through from below (O'brien et al. 2002). The controversy debates on the mechanisms that formed the terrain, whether through induced impacts or cryovolcanic processes, as well as on the thickness and state of the ice shell. On one hand, one model (Fig. 14a) suggests that the ocean is a warm convective ice layer located several kilometers below the icy crust and on the other hand the other model (Fig. 14b) suggests a liquid ocean hidden more than 100 km below the crust.

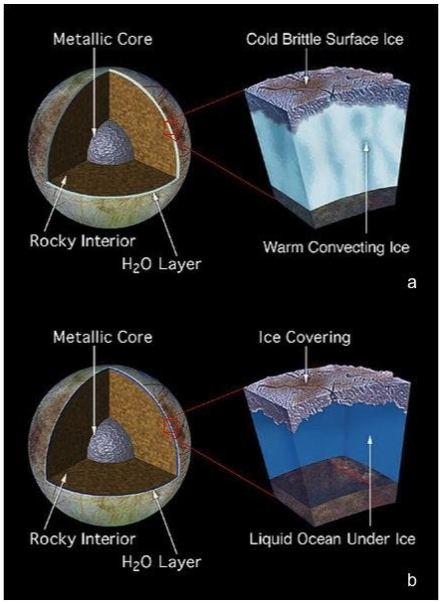

Fig. 14. Stratigraphic models of Europa's interior. Warm convective ice below the ice crust (a); Liquid ocean under the ice coverage (b) (NASA/JPL).

The radioactive decay cannot provide the amount of heat required to modify entirely the satellite surface, as observed on Europa. In this case, the surface temperature is limited to 110K at the equator and 50K at the poles; such cold temperatures make the ice locally as hard as terrestrial igneous granite (McFadden et al. 2007). On the other hand, hydrothermal activity has the potential to reshape the surface crust. Recent studies suggested that the influence of Jupiter on Europa due to its small but non-zero obliquity probably generates large tidal waves that keep the ocean warm (Tyler, 2008).

If the heat propagation and the buoyant oceanic currents are not intense then the ice shell will be thick and a warm ice layer will be formed at the bottom of the shell (Fig.15b). During the hydrothermal processes this warmer ice will rise and slide like the terrestrial glaciers. Such movements can cause surface modification and produce structures like the 'chaos terrain'. Other features supporting the existence of a thick ice layer are the large impact craters surrounded by concentric rings filled with ice. Geophysical models, associating the mere presence of these structures to the amount of heat generated by the tides, suggest an icy crust 10-30 km thick with a warm ice layer at the bottom and a liquid ocean probably 100 km thick (Schenk et al. 2004). Additionally, a scenario that consists of a thick icy crust of almost 15 km suggests a stratigraphic model with a 100 km deep ocean, which may be extremely deep, about10 times deeper than the deepest point of Earth's oceans, the Challenger Deep on the Mariana Trench, which is 11 km below sea level and the lowest elevation of the surface of the Earth's crust. The potential ocean of Europa would contain an amount of water twice the entire terrestrial surface hydrological system.

Alternatively to the previous model, if the heat flow and the plumes are intense then the ice shell is expected to be thin (Fig. 15a). The fragmentation of such a thin crust is most probably expressed with tectonic-like formations like the Conamara region. The debate regarding the thickness of Europa's crust gave birth to an alternative hypothesis regarding the thin ice model, which suggests a thin upper crust layer, almost 200-m thick, that behaves elastically and is in contact with the surface through zones of weakness like multiple linear ridges (Billings & Kattenhorn, 2005).

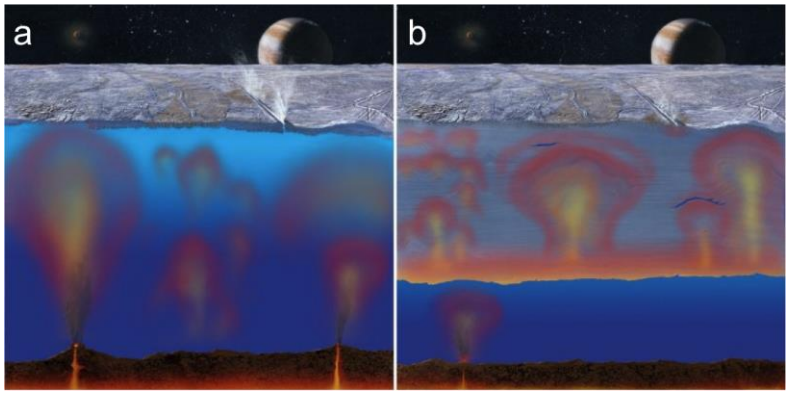

Fig. 15. Two models for the icy crust thickness. The thin ice model ~200m (a) the thick ice model ~15 km (b) (NASA/JPL).

Europa's case supports the existence of a stagnant lid underneath its crust (Fig. 16) (Showman & Han, 2004). The stagnant lid is a relatively cold and stiff conductive layer covering the warmer convective icy interior (Schubert et al. 2004). Since the expected activity within Europa's interior is upwelling thermal diapirism, the stagnant lid can prevent cold near-surface icy material from sinking towards the ocean.

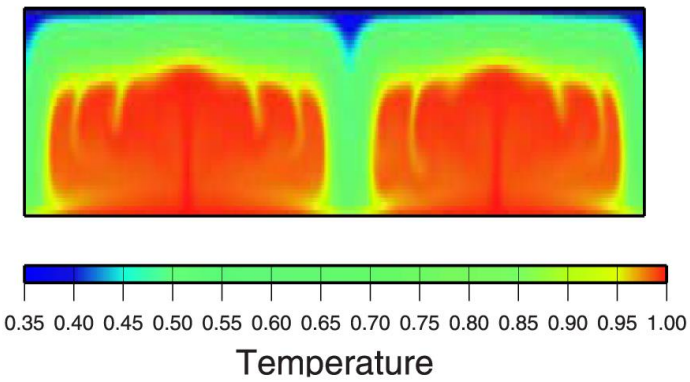

Fig. 16. Simulation of convection within Europa's ice shell (Showman and Han, 2004).

Compared to the Earth's oceans, the composition of Europa's hidden ocean should be significantly different. The Earth's ocean major component is sodium chloride while Europa's should be magnesium sulfate as indicated by Galileo data (e.g. Fanale et al. 2001). Indeed, Europa's weak magnetic moment is induced by the varying part of the Jovian magnetosphere (Schilling et al. 2007) and requires a highly conductive subsurface ocean. Such conductive materials candidates are the magnesium sulfate (e.g. McCord et al. 1998) or sulfuric acid hydrate (Carlson et al. 2005).

Similarly, Ganymede consists of a four-layer interior, based on measurements regarding its gravity field, mass, density and size. Geophysical models suggest two kinds of internal stratigraphy, one of an undifferentiated mixture of rock and ice and one of a differentiated body consisting of a rocky core, an extended icy mantle and an icy crust. We think the latter model is the most plausible as it is compatible with the gravity field measurements made by Galileo (e.g. Sohl et al. 2002). Such intrinsic magnetic field supports the existence of an iron-rich core (Hauk et al. 2006). The thickness of the layers in the interior depends on both the fraction of olivine and pyroxene and the amount of sulfur in the core (e.g. Sohl et al. 2002) (Fig. 17). Thus, the 2,634-km-radius Ganymede consists of an 800 km iron sulfide core, an almost 900-km thick outer ice mantle and a silicate-rich mantle 700 km thick (e.g. Kuskov et al. 2005).

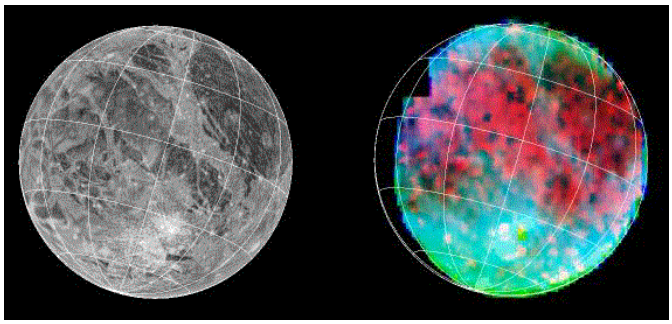

Fig. 17. Ice and mineral deposits on Ganymede. Surface features from Voyager in visible light (left); Minerals in red and ice grains in blue in infrared light from Galileo (NIMS, Galileo Mission, JPL, NASA).

Although the mechanisms that formed Ganymede's complex surface are still unidentified, multiple scenarios have been proposed. Most of the scenarios agree on a general mechanism that uses tectonism as the main chisel that formed and shaped the existing structures, especially the grooved terrain (Sohl et al. 2002). On the other hand, and in contrast with the other three aforementioned satellites, cryovolcanism does not seem to participate actively in the geodynamic processes. The radiogenic heating from within the satellite as well as tidal heating from past events are considered as the main forces that generate the stresses that lead to tectonic movements and eventually to tectonic structures.

Contrary to Ganymede, probably Titan but especially Enceladus provide evidence of past and current cryovolcanism that shapes their surfaces. The mechanisms that formed Titan's surface by endogenic factors are still unknown, although the central idea is focused on cryovolcanism and morphotectonism, with the latter being the short- and long-term surficial expressions of any tectonic activity originated from endogenic processes (Solomonidou et al. 2010). However, it is possible that Titan underwent a period of tectonism resembling those on Europa's and Ganymede's.

According to geophysical models, Titan's differentiated interior consists of a serpentinite core (~1,800 km), a high-pressure ice mantle (~400 km), a liquid layer of aqueous ammonium sulphate (50 to 150 km wide), and an externally heterogeneous icy few kilometers wide (Tobie et al. 2005; Fortes et al. 2007).

The subsurface instability due to the interactions within an interior liquid ocean causes the modification of extended features on Titan's surface, whether they derive from cryovolcanic or morphotectonic dynamic processes. Currently, all the geophysical models that try to explain the geodynamics of Titan support the existence of an oceanic layer that decouples the mantle from the icy crust. Additionally, the identification of a small but significant asynchronicity in Titan's rotation from Cassini SAR data favors the aforementioned decoupling (Lorenz et al. 2008). Internal geodynamic activity can transport effusively the explosive material from the oceanic layer to the surface and form the cryovolcanic structures like the lobate flows in Sotra Facula.

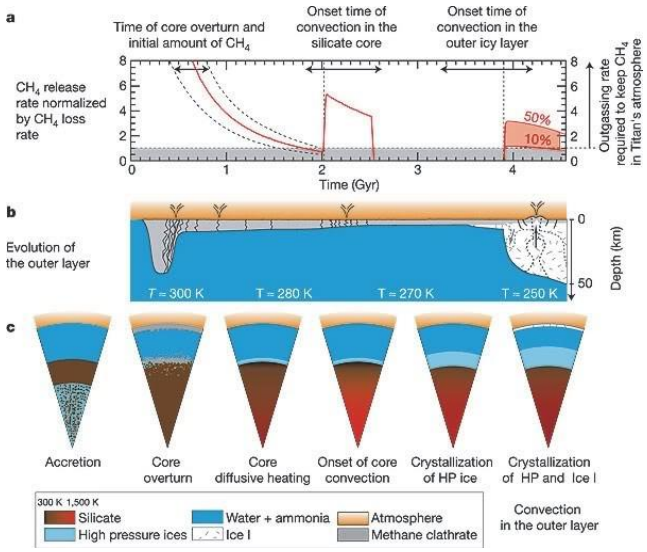

Fig. 18. Possible cryovolcanic events during Titan's history emerging from its internal liquid ocean (Tobie et al. 2006).

Tobie et al. (2006) suggested a cryovolcanic model for Titan's case to solve the mystery of Titan's methane replenishment since it is should vanish in 100 Ma. These authors suggested that episodic methane outgassing events occurred through three distinct episodes covering a chronological period from 2000 Ma ago until 500 Ma ago (Fig. 18). The internal ocean provides the 'magma' chamber by means of material, while convective processes are the triggering mechanisms that initiate the dynamic activity. A convective model of a stagnant lid is capable to explain such activities (Solomatov 1995) as explained for Europa's case earlier. However, the ice shell for Titan's case is expected to be thicker. In opposition, several studies suggest that Titan is not currently convective (Mitri et al. 2010; Nimmo and Bills, 2010).

The uniqueness of Titan's tectonism - even though not yet confirmed - lies in that the tectonic processes are contractional rather than extensional, setting Titan out as the only planetary body in the Solar System other than the Earth, where contractional deformation occurs.

Mitri et al. (2010) proposed an internal thermal model, focused on the changes in volume of a potential underground ocean caused by heat flux variations during freezing or melting. The authors suggest that the continuing cooling of the moon can develop global volume contraction, as described by Tobie et al. (2005; 2006).

Cassini's data proved that, despite its small size (about 505 km in diameter), Enceladus is an active planetary body that spews material through hydrothermal vents resembling terrestrial geysers. This moon is not in hydrostatic equilibrium (Schubert et al. 2007; Schubert et al. 2010), thus a simple and very general stratigraphic interior is being suggested: it consists of a 169 km rocky core overlain by an icy 82 km mantle (Barr and McKinnon, 2007; Fortes, 2007; Schubert et al. 2007). The subsurface ocean is lying between the two layers, and supplies the fountains observed at the south polar region through cracks called 'Tiger Stripes' (e.g. Porco, 2008; Postberg et al. 2009). The moon's tidal dissipation is proposed as the triggering mechanism as well as the cause of the dynamic phenomena like tectonics (convection-conduction, expansion contraction) and cryovolcanism (e.g. Mitri and Showman, 2008; Mitri et al. 2010) that formed the surface expressions described in the previous section.

4. Discussion: Internal activity and surface modification

The possible existence of subsurface liquid oceans underneath the crusts of the icy moons of Jupiter (Europa and Ganymede) and Saturn (Titan and Enceladus), places them in a potential group of planetary bodies where life could emerge and evolve. Other than data processing that provide evidence and information about the internal liquid layers, the surficial expressions that are related to the hydrothermal and dynamic processes occurring within these layers are the surface evidence that could lead to their identification. Specifically, the cryovolcanic and morphotectonic structures seen on the aforementioned satellites are the surface expressions of the internal activity while they are formed by modification of the crustal layer and deposition of material coming from the subsurface ocean. Therefore, investigating these surface exposures and associating them to terrestrial features where water is involved could shed some light on the investigation of internal liquid water oceans in the icy

moons. Trying to model the triggers of internal active phenomena, basic geophysical models usually propose liquid water reservoirs while the geodynamic models point at both radioactive decay and tidal stresses, caused by the giant planets Jupiter and Saturn. We shall herein try and reconcile both views.

The major and most significant structures on Europa's surface are the bunch lineae (e.g. Prockter et al. 2010) (Fig. 3). Data analysis showed that the geometry and the spectral properties vary depending on age, which indicates an evolutionary sequence (Geissler et al. 1998; Dalton, 2010). This means that persistent and drastic processes occur in order to form these features. Such processes seem to be different types of cryovolcanism in which multiple eruptions of ice (warmer than crustal ice) emerge through 'tectonic' crustal weaknesses (Figueredo & Greeley, 2004). This tectonic formation resembles the terrestrial mid-ocean ridges (MOR), which are the extensive opening seafloor terrains, and considered to be a global rather than a local phenomenon. MOR are dynamic and volcanically active structures that constantly provide and deposit new material from the mantle to create new oceanic crust. As seen in Figure 4, the red streaks, as well as the red spots called lenticulae, are most possibly evidence of upwelling warmer material emerging from the liquid layer while colder ice near the surface sinks downwards. After spectroscopic analysis, the red streaks are thought to be rich in magnesium sulfate, another hint in favor of their internal origin (McCord et al. 1998; Dalton et al. 2010). Furthermore, the lineament formations like the dark and red streaks present the basic resurfacing system that dominate on Europa's surface. Their formation is an indicator for current geological activity. Additionally, the thermal diapirism that most likely formed these structures, as well as the red spots, would imply that convective upwelling thermal plumes originate in the lower boundary of the convective system and gets in contact with the cold stagnant lid with the icy plumes (Showman & Han, 2004). Such temperature ranges indicate possible habitability at the upper part of the ice shell. Consequently, Europa's surface morphology is directly connected to the internal dynamic processes and provides evidence of a subsurface interactive ocean.

Unlike Europa's conflicting oceanic hydrothermal system that originates in a rocky sea layer, Ganymede's ocean lays between two icy layers that decouple it from the mantle. Barr et al. (2001; 2004) suggested that large magmatic events due to convective plumes could occur at Ganymede's rock – ice boundary. The surface expressions that are most possibly connected to tectonism are the deep fault structures like the horst-and-graben (resembling terrestrial continental rifts) as well as many cracks that are observed in Ganymede's bright terrain (Showman & Malhotra, 1999). Tidal heating events, either past or current, could cause dynamic forces that modify the icy lithosphere. The main mechanism that deforms tectonically the lithosphere is most likely warm liquid plumes that rise from the upper mantle to the surface, following a pattern similar to the plume-lithosphere interactions at the Hawaiian Swell which cause thinning and instabilities at the crust layer (Moore et al. 1998). Even though the plume theory indicates cryovolcanic processes, little evidence of such activity has been detected on Ganymede. Notably, the extreme morphological difference between the bright and the dark terrain as described in a previous section suggests a massive geological event or set of events that caused such large-scale geo-terrain alteration. Hence, it is possible that the extensive tectonic forces that fractured the dark terrain partially affected the bright terrain as well. Such tectonic weaknesses could display pathways to small cryovolcanic events that lead to resurface processes. However, tilt-block faulting and shears (Head et al. 2002) are some of the structures that appear bright within the dark terrain suggesting that tectonic cracks functioned as path for warm internal oceanic material to pass through like what occurred in the bright terrain. In terms of tectonics, and similarly to the other icy moons, there is no evidence of compressional deformation (Showman et al. 1997). Since the deformational pattern is extensional, the question is whether it is a global or a local phenomenon. Collins et al. (1998) studied observations of grooved terrains of specific stratigraphic ages that have consistent directions over hundreds of kilometers, something that indicates global stressing phenomena. On Earth stressing phenomena could occur where severe forces cause convective currents in the ocean. In a similar way, the plume convection within Ganymede's oceanic layer could create enough turbulence and temperature-pressure instabilities to cause global stressing phenomena with an impact on tectonism. Nevertheless, Ganymede presents styles of tectonism different from Europa's.

Following a pattern similar to the one mentioned for Ganymede, Enceladus' internal tidal stresses and radioenergetic decay produce warm pockets of material, the plumes, that subsequently form the geyser formations at the south polar region. The major and most valuable evidence of Enceladus' cryovolcanic activity, supporting as well the ocean existence, is this geyser formation or geyser accumulation that form a fountain of more than 400 km, as observed by Cassini. The jets initiate from four sub-parallel linear depressions, which are tectonic in origin. Other surface expressions are scarps, ridges, and shields (Collins et al. 2009). On the other hand, Titan's surface structures related to its dynamic interior that also support the existence of a subsurface ocean are the three cryovolcanic candidate regions Tui Regio, Hotei Regio and Sotra Facula and many morphotectonic structures like mountains, ridges and canyons (e.g. Solomonidou et al. 2010 and references therein). Generally, in the case of both moons it is thought that their ice shells transit from a conductive to a

convective state; since they probably overlay a pure liquid ocean (Tobie et al. 2005) this can have major effects on surface morphotectonics (Mitri and Showman, 2008). Indeed, thermodynamic oscillations within the ice shells may trigger repeated extensional and compressional events. In the presence of a subsurface ocean underneath Titan and as a consequence of local stress mechanisms, parts of the icy crust could behave like rigid ice floes due to lateral pressure gradients. If such floating occurs, many morphotectonic features like faults and canyons can relate their formation to this event. Furthermore, radial contraction of the internal high-pressure ice polymorphs could possibly amend the radial expansion caused during the cooling stage of the moon (Mitri and Showman, 2008), in which the existence of a liquid layer plays a significant role. As a result, the overall global contraction could form mountainous chains (Radebaugh et al. 2007).

These four satellites are dynamic planetary bodies and the internal ocean most likely plays an important role on the formation and modification of their surfaces. The properties on which the presence of an internal ocean depends were mentioned earlier (section 3). Another issue that should be taken under consideration is the set of properties that determine the possible exchange of material between the subsurface and the surface. These are the mechanical properties of the lithosphere as proposed by Tobie et al. (2010).

The formation of the surface signature of any upwelling activity depends on:

(a) the chemical interaction between the material in motion and the local environment, which travels through the conduit path from the source to the surface.
(b) the magnitude of the forces that triggers this motion.
(c) the complexity of the structure of the conduit path which could be an extensive tectonic zone of weakness. From such a structure, multiple cryovolcanic eruptions could emanate.
(d) the influence of the atmosphere on the surface as described in Tobie et al. (2010).

Titan and Enceladus display cryovolcanic expressions in specific regions. On Titan these zones appear on a latitudinal ring around 20°S - 30°S, while on Enceladus they lay at the southern pole. On the contrary, Europa and Ganymede do not host evidence of such large and localized structures. Considering these surface expressions, as well as the morphotectonic structures described earlier, we infer that different endogenic conditions occurred. Firstly, the upwelling material within Europa and Ganymede could spread throughout the lithosphere, while in Titan and Enceladus it would pass through more localize exsolution paths. On Titan and especially on Enceladus the cryovolcanic expressions illustrate instant energy relief of the hydrodynamic activity, while Europa and Ganymede could experience continuous relaxation. This can possibly explain the fractal development of lineae structures on Europa. Moreover, the gravitational field, as well as other heat and transfer mechanisms, play in each satellite a major role in the distribution of the upwelling material and the formation of the surface structures. In order to evaluate the above implications it is essential to record the spatial and temporal variations of the structures observed.

5. Habitability issues for outer planet satellites

The existence of an internal liquid ocean underneath the icy crusts of the giant planet satellites could serve as a potential abode for life. The location of the ocean close to the surface provides food for thought on habitability zones, and conditions for life in general, in the Solar System.

Indeed, the discovery of hydrocarbon surficial lakes on Titan and the possible existence of subsurface liquid oceans in Europa, Ganymede, Titan, and Enceladus reveal alternative concepts to the classical definition of the habitable zone, and suggest the need for reconsidering its limits (Lammer et al. 2009). Currently, more and more studies regarding the planetary habitability propose the icy moons with subsurface oceans as potential worlds for initiating and/or sustaining some sort of life forms (Fortes, 2000; Raulin, 2008; Raulin et al. 2010; Coustenis et al. 2011 and references therein). Figure 19 presents the possible locations of the liquid layers within the icy satellites of Jupiter as well as their habitability potential.

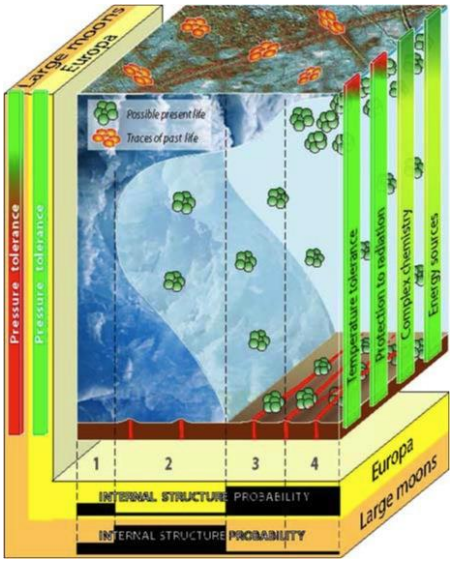

Fig. 19. Possible schematic location of oceans in the icy moons of Jupiter as a function of depth. Europa probably agrees with internal structures 3 (thick upper icy layer <10 km and a thick ocean) or 4 (very thin upper icy layer 3-4 km). Ganymede is closer to 1 (completely frozen) or 2 (three-layered structures impeding any contact between the liquid layer and the silicate floor) (Lammer et al. 2009). The color scales on the right side indicate the physical and chemical constraints on which habitability depends on.

For Europa, the assumed internal processes that trigger the geodynamic phenomena are the tidal stresses, which produce considerably less energy than radioenergetic decay. Europa is being compressed and stretched when affected by the gravitational forces of Jupiter and the other Galilean satellites and thus, the resulting tidal friction provides enough energy, as well as temperature, for an extensive ocean to exist underneath the crust. The provision of large amounts of energy at the bottom layer of an ocean can conceivably form hydrothermal vents like the ones seen on Earth. Notably, life could emerge around hydrothermal vents, which are important geological forms in terms of life propagation. Greenberg (2010) suggests that even ecology including complex organisms could exist on Europa. The author provided evidence of oxygen concentration within the ocean greater than that of the Earth's, which is suggested as an indicator for aerobic organisms. Nevertheless in the case where the concentration of salts is large, only extremophile organisms (like halophiles) could survive (Cooper et al. 2001; Marion et al. 2003).

Ganymede lays between structures 1 and 2 in the scheme shown on Fig. 19 indicating that it is much colder than Europa, a factor that lowers its habitability potential. On the other hand, reinforcing Ganymede's possibility for life to exist, Barr et al. (2001) imply that magmatic events could form pockets of liquid, which would then ascent buoyantly carrying nutrients to the internal ocean. Based on their calculations, a water plume could reach Ganymede's ocean and carry nutrient-rich material with an eruption time of 3 hours to 16 days. Additionally, Ganymede's system could provide the necessary tools to concentrate biological building block ingredients (Trinks et al. 2005) especially since it possesses a magnetic field that is able to protect life from harmful radiation and lies in a relatively quiet radio zone.
On Titan, terrestrial bacteria can absorb their energy and carbon needs from the tholins that exist in its thick atmosphere (Stoker et al. 1990). Furthermore, photochemically derived sources of free energy on the surface could maintain an exotic type of life, using liquid hydrocarbons as solvents (McKay & Smith, 2005). Other than the atmospheric properties that are favorable to life, the possible existence of an underground ocean might support terrestrial-type life that had been introduced previously or formed when liquid water was in contact with silicates early in Titan's history (Fortes, 2000). Furthermore, the possible amount of ammonia dissolved within the ocean is suggested to be ~10% (Lorenz et al. 2008), something that corresponds to a pH of 11.5, while at a depth of 200 km the pressure reaches ~ 5 kbars and hot plumes within the potential ocean could be generated (Coustenis et al. 2011 and references therein). The aforementioned conditions are not unfavorable to the emergence and maintenance of life (e.g. Fortes, 2000; Raulin, 2008).

Enceladus' extremely high temperatures at the south polar region are probably generated by the hydrodynamic processes that form the fountain, as previously described, and thus enhance the potential for habitability. The most convincing theory, after Cassini data analysis, suggests that a liquid ocean exists beneath the Tiger Stripes. There are standards for life that Enceladus' possible ocean is not consistent with: the sunlight, the oxygen compounds, and the organics produced on a surficial-crust environment. However, terrestrial regions like the

deep oceans that do no satisfy the aforementioned prerequisites for life, still function as active ecosystems (McKay et al., 2008; Muyzer and Stams, 2008). There, sulfur-reducing bacteria consume hydrogen and sulfate, produced by radioactive decay. Notably, the comparison with the terrestrial ecosystems suggests that plume's methane may be biological in origin (McKay et al., 2008). Hence, Enceladus displays an internal warm and chemically rich ocean that may facilitate complex organic chemistry and biological processes (Coustenis et al. 2011).

In conclusion, the confirmation of the existence of a subsurface liquid ocean underneath the crust of the icy moons of Jupiter and Saturn will revolutionise our perspective regarding the habitability potentials of such planetary bodies. Indeed, liquid water may exist well outside the traditional habitability zone, which is merely based on the presence of liquid water on the surface. For planetary habitability, the principal criteria are the presence of liquid water anywhere on the body, as well as the existence of environments able to assembly complex organic molecules and provide energy sources: this can well be underneath the surface in some cases, if stability conditions are met. The four satellites described in this study seem to fulfill some or all of the above requirements. However, it is of high priority to revisit these bodies with new missions and advanced instrumentation (such as gravitational and magnetic field sounding systems and in situ element detectors) in order to obtain altimetry and *in situ* monitoring of tidally-induced surface distortion data (Sohl et al. 2010) that could unveil in detail the internal stratigraphy of the moons and the specificity of the subsurface oceans. Future large missions, or smaller dedicated ones, to the Galilean and Khronian systems would allow us to better understand the mechanics behind the astrobiological potential of worlds with subsurface oceans, and shed some light on the emergence of life on our own planet.

6. Acknowledgement

A.Solomonidou is supported by the "HRAKLEITOS II" project, co-financed by Greece and the European Union.

7. References

Anderson, J. D., Schubert, G., Jacobson, R. A., Lau, E. L., Moore, W. B., Sjogren, W. L. (1998). Europa's Differentiated Internal Structure: Inferences from Four Galileo Encounters. Science, 281, 2019-2022.
Barr, A. C., Pappalardo, R. T.,Stevenson, D. J. (2001). Rise of deep melt into Ganymede's ocean and implications for astrobiology. Lunar and Planetary Science XXXII, 1781.
Barr, A. C., Pappalardo, R. T., Zhong, S. (2004). Convective instability in ice I with non-Newtonian rheology: Application to the icy Galilean satellites. Journal of Geophysical Research, 109, E12008.
Billings, S. E., Kattenhorn, S. A. (2005). The great thickness debate: Ice shell thickness models for Europa and comparisons with estimates based on flexure at ridges. Icarus, 177, 397-412.
Blanc, M., and 42 colleagues. (2009). LAPLACE: A mission to Europa and the Jupiter System for ESA's Cosmic Vision Programme. Experimental Astronomy, 23, 849-892.
Carlson, R. W., Anderson, M. S., Mehlman, R., Johnson, R. E. (2005). Distribution of hydrate on Europa: Further evidence for sulfuric acid hydrate. Icarus, 177, 461-471.
Carr, M. H., and 21 colleagues. (1998). Evidence for a subsurface ocean on Europa. Nature, 391, 363-365.
Casacchia, R., Strom, R. G. (1984). Geologic evolution of Galileo Regio, Ganymede. Journal of Geophysical Research, 89, B419-B428.
Cassidy, T., Coll, P., Raulin, F., Carlson, R. W., Johnson, R. E., Loeffler, M. J., Hand, K. P., Baragoila, R. A. (2010). Radiolysis and Photolysis of Icy Satellite Surfaces: Experiments and Theory. Space Science Reviews, 153, 299–315.
Collins, G. C., Head, J. W., Pappalardo, R. T. (1998). Formation of Ganymede grooved terrain by sequential extensional episodes: Implications of Galileo observations for regional stratigraphy, Icarus, 135, 345-359.
Collins, G.C., Goodman, J.C. (2007). Enceladus' south polar sea. Icarus, 189, 72-82.
Collins, G.C., McKinnon, W.B., Moore, J.M., Nimmo, F., Pappalardo, R.T., Prockter, L.M., Schenk, P.M., (2009). Tectonics of the outer planet satellites. Planetary Tectonics, Cambridge University Press.
Cooper, J. F., Johnson, R. E., Mauk, B. H., Garrett, H. B., Gehrels, N. (2001). Energetic Ion and Electron Irradiation of the Icy Galilean Satellites. Icarus, 149, 133-159.
Coustenis, A., Taylor, F.W. (2008). Titan: Exploring an Earth-like world. World Scientific
Publishing.
Coustenis, A., Tokano, T., Burger, M. H., Cassidy, T. A., Lopes, R. M. C., Lorenz, R. D., Retherford, K. D., Schubert, g. (2010). Atmospheric/Exospheric Characteristics of Icy Satellites. Space Science Reviews, 153, 155–184.
Coustenis, A., Raulin, P., Bampasidis, G., Solomonidou, A. (2011). Life in the Saturnian neighborhood, book chapter in Life on Earth and other planetary bodies, Springer Books, *Submitted for publication.*
Dalton, J. B. (2010). Spectroscopy of Icy Moon Surface Materials. Space Science Reviews, 153, 219–247.
Dalton, J. B., Cruikshank, D. P., Stephan, K., McCord, T. B., Coustenis, A., Carlson, R. W., Coradini, A. (2010). Chemical Composition of Icy Satellite Surfaces. Space Science Reviews, 153, 113–154.
Dougherty, M.K., Khurana, K.K., Neubauer, F.M., Russell, C.T., Saur, J., Leisner, J.S., Burton, M.E. (2006). Identification of a Dynamic Atmosphere at Enceladus with the Cassini Magnetometer. Science, 311, 1406 - 1409.
Fanale, F. P., Li, Y.-H., De Carlo, E., Farley, C., Sharma, S. K., Horton, K., Granahan, J. C. (2001). An experimental estimate of Europa's ``ocean'' composition-independent of Galileo orbital remote sensing. Journal of Geophysical Research, 106, 14595-14600.
Figueredo, P. H., Greeley, R. (2004). Geologic mapping of the northern leading hemisphere of Europa from Galileo solid-state imaging data. Journal of Geophysical Research, 105, 22629-22646.
Fortes, A.D. (2000). Exobiological Implications of a Possible Ammonia-Water Ocean inside Titan, Icarus, 146, 444-452.

Fortes, A.D., Grindrod, P.M., Trickett, S.K., Voc˘adlo, L. (2007). Ammonium sulfate on Titan: Possible origin and role in cryovolcanism. Icarus, 188, 139–153.
Fortes, A. D., Choukroun, M. (2010). Phase Behaviour of Ices and Hydrates. Space Science Reviews, 153, 185–218.
Geissler, P. E., and 14 colleagues. (1998). Evidence for non-synchronous rotation of Europa. Nature, 391, 368.
Greenberg, R., (2005). Europa: The Ocean Moon: Search for an Alien Biosphere, Springer Praxis Books.
Greenberg, R. (2008). Unmasking Europa In: The Search for Life on Jupiter's Ocean Moon. Springer.
Hall. D. T., Feldman, P. D., McGrath, M. A., Strobel, D. F. (1998). The Far-Ultraviolet Oxygen Airglow of Europa and Ganymede. Astrophysical Journal, 499, 475.
Harland, David M. (2000). Jupiter Odyssey: The Story of NASA's Galileo Mission. Springer.
Hauk, S. A., Aurnou, J. M., Dombard, A. J. (2006). Sulfur's impact on core evolution and magnetic field generation on Ganymede. Jour. Geophys. Res., 111, E09008.
Head, J. W., and 10 colleagues. (2002). Evidence for Europa-like tectonic resurfacing styles on Ganymede. Geophysical Research Letters, 29, 2151.
Hussmann, H., Choblet, G., Lainey, V., Matson, D. L., Sotin, C., Tobie, g., Van Hoolst, T. (2010). Implications of Rotation, Orbital States, Energy Sources, and Heat Transport for Internal Processes in Icy Satellites. Space Science Reviews, 153, 317–348.
Johnson, T.V., (2004). Geology of the icy satellites. Space Science Reviews 116, 401-420.
Khurana, K. K., Kivelson, M. G., Russel, C. T. (1998). Induced magnetic fields as evidence for subsurface oceans in Europa and Callisto. Nature, 395, 777-780.
Kivelson, M.G., Khurana, K. K., Russell, C. T., Volwerk, M., Walker, R. J., Zimmer, C. (2000). Galileo Magnetometer Measurements: A Stronger Case for a Subsurface Ocean at Europa. Science, 289, 1340–1343.
Kivelson, M.G., Khurana, K. K., Coroniti, F.V. (2002). The Permanent and Inductive Magnetic Moments of Ganymede. Icarus, 157, 507–522.
Kuskov, O. L., Kronrod, V. A. (1998). Models of Internal Structure of Jupiter Satellites: Ganymede, Europa, and Callisto. Astron. Vestn., 32, 49–57.
Lammer, H., Bredehöft, J. H., Coustenis, A., Khodachenko, M. L., Kaltenegger, L., Grasset, O., Prieur, D., Raulin, F., Ehrenfreund, P., Yamauchi, M. (2009). What makes a planet habitable? The Astronomy and Astrophysics Review, 17, 181-24.
Lopes, R.M.C., and 18 colleagues. (2010). Distribution and interplay of geologic processes on Titan from Cassini radar data. Icarus, 205, 540-558.
Lorenz, R.D., Stiles, B.W., Kirk, R.L., Allison, M.D., Persi del Malmo, P., Iess, L., Lunine, J.I., Ostro, S.J., Hensley, S. (2008). Titan's Rotation Reveals an Internal Ocean and Changing Zonal Winds. Science, 319, 1649 - 1651.
Marion, G. M., Fritsen, C. H., Eicken, H., Payne, M. C. (2003). The Search for Life on Europa: Limiting Environmental Factors, Potential Habitats, and Earth Analogues. Astrobiology, 3, 785-811.
McCord, T. B., and 11 colleagues. (1998). Salts on Europa's Surface Detected by Galileo's Near Infrared Mapping Spectrometer. Science, 280, 1242-1245.
McCord, T. B., and 12 colleagues. (1998). Non-water-ice constituents in the surface material of the icy Galilean satellites from the Galileo near-infrared mapping spectrometer investigation. Journal of Geophysical Research, 103, 8603-8626.
McCord, T. B., Hansen, G. B., Hibbits, C. A. (2001). Hydrated salt minerals on Ganymede's surface: Evidence of an ocean below. Science, 292, 1523-1525.
McFadden, L., Weissman, P., Johnson, T. V. (2007). The Encyclopedia of the Solar System. Elsevier, 432.
McKay, C. P., Smith, H. D. (2005), Icarus, 178, 274–276.
McKay, C.P., Porco, C., Altheide, T., Davis, W.L. and Kral, T.A. (2008). The Possible Origin and Persistence of Life on Enceladus and Detection of Biomarkers in the Plume, Astrobiology, 8, 909-919.
McKinnon, W.B. (1999). Convective instability in Europa's floating ice shell. Geophys. Res. Lett. 26, 951–954.
Mitri, G., Showman, A.P., (2008). Thermal convection in ice-I shells of Titan and Enceladus.
Icarus, 193, 387-396.
Mitri, G., Bland, M.T., Showman, A.P., Radebaugh, J., Stiles, B., Lopes, R.M.C., Lunine, J.I., Pappalardo, R.T. (2010). Mountains on Titan: Modeling and observations. J. Geophys. Res., 115, E10002.
Moore, W. B., Schubert, G., Tackley, P. (1998). Three-Dimensional Simulations of Plume-Lithosphere Interaction at the Hawaiian Swell. Science, 279, 1008-1011.
Moore, W. B., Schubert, G. (2000). The tidal response of Europa. Icarus, 147, 317-319.
Moore, J. M., Howard, A. D., Schenk, P., Wood, S. E. (2010). Erosion, Transportation, and Deposition on Outer Solar System Satellites: Landform Evolution Modeling Studies. American Geophysical Union, P31D-04.
Nelson, R. M., and 32 colleagues. (2009a). Photometric changes on Saturn's Titan: evidence for active cryovolcanism, Geophysical Research Letters, 36, L04202.
Nelson, R. M., and 28 colleagues. (2009b). Saturn's Titan: Surface change, ammonia, and implications for atmospheric and tectonic activity, Icarus, 199, 429-441.
Nimmo, F., Bills, B.G. (2010). Shell thickness variations and the long-wavelength topography
of Titan. Icarus, 208, 896–904.
Muyzer, G. and Stams, A.J.M. (2008) The ecology and biotechnology of sulphate-reducing bacteria, Nature Reviews. Microbiology, 6, 441-454.
O'Brien, D. P., Geissler, P., Greenberg, R. (2002). A Melt-through Model for Chaos Formation on Europa. Icarus, 156, 152-161.
Pappalardo, and 10 colleagues. (1998a). Geological evidence for solid-state convection in Europa's ice shell. Nature, 391, 365-368.
Pappalardo, R.T., and 14 colleagues. (1998b). Grooved Terrain on Ganymede: First Results from Galileo High-Resolution Imaging. Icarus, 135, 276-302.
Pappalardo, R.T., Collins, g. C., Head, J. W., Helfenstein, P., McCord, T. B., Moore, J. M., Prockter, L. M., Schenk, P. M., Spencer, J. (2004) Geology of Ganymede. In Jupiter: The Planet, Satellites & Magnetosphere, pp. 363-396.
Park, R.G. (1997). Foundations of Structural Geology. Routledge, pp. 216.
Patterson, G. W., Collins, G. C., Head, J. W., Pappalardo, R. T., Prockter, L. M., Lucchitta, B. K., Kaym J. P. (2010). Global geological mapping of Ganymede. Icarus, 207, 845-867.
Porco, C.C., and 35 colleagues. (2005). Imaging of Titan from the Cassini spacecraft, Nature, 434, 159-168.
Porco, C.C., and 24 colleagues. (2006). Cassini observes the active south pole of Enceladus. Science, 311, 1393–1401.
Porco, C. (2008). The restless world of Enceladus. Scientific American, 299, 26–35.
Postberg, F., Kempf, S., Schmidt, J., Brillantov, N., Beinsen, A., Abel, B., Buck, U., Srama, R. (2009). Sodium salts in E Ring ice grains from an ocean below Enceladus' surface. Nature, 459, 1098-1101.
Prockter, L. M., and 14 colleagues. (1998). Dark Terrain on Ganymede: Geological Mapping and Interpretation of Galileo Regio at High

Resolution. Icarus, 135, 317-344.
Prockter, L. M., Lopes, R. M. C., Giese, b., Jaumann, R., Lorenz, R. D., Pappalardo, R. T., Patterson, G. W., Thomas, P. C., Turtle, E. P., Wagner, R. J. (2010). Characteristics of Icy Surfaces. Space Science Reviews, 153, 63–111.
Radebaugh, J., Lorenz, R.D., Kirk, R.L., Lunine, J.I., Stofan, E.R., Lopes, R.M.C., Wall, S.D., the Cassini Radar Team, (2007). Mountains on Titan observed by Cassini Radar. Icarus 192, 77-91.
Raulin, F. (2008). Astrobiology and habitability of Titan. Space Science Reviews, 135, 37-48.
Raulin, F., Hand, K. P., McKay, C. P., Viso, M. (2010). Exobiology and Planetary Protection of icy moons. Space Science Reviews, 153, 511–535.
Ruiz, J., Fairen, A. G. (1999). Seas under ice: Stability of liquid-water oceans within icy worlds. In Earth, Moon, and Planets, 97, 79-90.
Schenk, P., McKinnon, W. (1989). Fault offsets and lateral crustal movement on Europa: Evidence for a mobile ice shell, Icarus, 79, 75-100.
Schenk, P. M., Chapman, C. R., Zahnle, K., Moore, J. M. (2004) Chapter 18: Ages and Interiors: the Cratering Record of the Galilean Satellites In Jupiter: The Planet, Satellites and Magnetosphere, Cambridge University Press.
Schilling, N., Neubauer, F., Saur, J. (2007). Time-varying interaction of Europa with the Jovian magnetosphere: Constraints on the conductivity of Europa's subsurface ocean. Icarus, 192, 41–55.
Schubert, G., Anderson, J.D., Spohn, T., McKinnon, W.B. (2004) Interior composition, structure and dynamics of the Galilean satellites. In: Jupiter. The planet, satellites and magnetosphere. Cambridge planetary science 1, pp. 281-306.
Schubert, G., Anderson, J.D., Travis, B.J., and Palguta, J. (2007). Enceladus: Present internal
structure and differentiation by early and long-term radiogenic heating. Icarus, 188, 345–355.
Schubert, G., Hussmann, H., Lainey, V., Matson, D. L., McKinnon, W. B., Sohl, F., Sotin, C., Tobie, G., Turrini, D., Van Hoolst, T. (2010). Evolution of Icy Satellites. Space Science Reviews, 153, 447-484.
Shematovich, V. I., Johnson, R. E. (2001). Near-surface oxygen atmosphere at Europa. Advances in Space Research, 27, 1881-1888.
Showman, A. P., Malhotra, R. (1997). Tidal Evolution into the Laplace Resonance and the Resurfacing of Ganymede. Icarus, 127, 93-111.
Showman, A. P., Malhotra, R. (1999). The Galilean Satellites. Science, 286, 77-84.
Showman, A. P., Han, L. (2004). Numerical simulations of convection in Europa's ice shell: Implications for surface features. J. Geophys. Res. 109.
Soderblom, L.A., and 18 colleagues. (2007). Topography and geomorphology of the Huygens landing site on Titan. Planetary and Space Science, 55, 2015-2024.
Sohl, F., Spohn, T., Breuer, D., Nagel, K. (2002). Implications from Galileo Observations on the Interior Structure and Chemistry of the Galilean Satellites. Icarus, 157, 104–119.
Sohl, F., Choukroun, M., Kargel, J., Kimura, J., Pappalardo, R., Vance, S., Zolotov, M. (2010). Subsurface Water Oceans on Icy Satellites: Chemical Composition and Exchange Processes. Space Science Reviews, 153, 485–510.
Solomatov, V.S. (1995). Scaling of temperature- and stress-dependent viscosity convection. Phys. Fluids, 7, 266–274.
Solomonidou, A., Bampasidis, g., Coustenis, A., Kyriakopoulos, K., Seymour, K. S., Hirtzig, M., Bratsolis, E., Moussas, X. (2010). Morphotectonics on Titan and Enceladus. Planetary and Space Sciences, *submitted.*
Sotin, C., Head, J. W., Tobie, G. (2001). Europa: Tidal heating of upwelling thermal plumes and the origin of lenticulae and chaos melting. Geophys. Res. Lett., 29, 74-1.
Spaun, N. A., Head, J. W., Collins, G. C., Prockter, L. M., Pappalardo R. T. (1998), Conamara Chaos Region, Europa: Reconstruction of mobile polygonal ice blocks, Geophys. Res. Lett., 25, 4277–4280.
Stern, S.A.,McKinnon, W.B., (1999). Triton's surface age and impactor population revisited (evidence for an internal ocean). In: Proc. Lunar Planet. Sci. Conf. 30th. Abstract 1766.
Stiles, B. W., and 14 colleagues. (2010). ERRATUM: "Determining Titan's Spin State from Cassini Radar Images". The Astronomical Journal, 139, 311.
Stoker, C. R., Boston, P. J., Mancinelli, R. L., Segal, W., Khare, B. N., Sagan, C. (1990). Icarus, 85, 241–256.
Tobie, G., Grasset, O., Lunine, J.I., Mocquet, A., and Sotin, C. (2005). Titan's internal structure inferred from a coupled thermal-orbital model. Icarus, 175, 496-502.
Tobie, G., Lunine, J.I., Sotin C. (2006). Episodic outgassing as the origin of atmospheric methane on Titan. Nature, 440, 61-64.
Tobie, G., and 10 colleagues. (2010). Surface, Subsurface and Atmosphere Exchanges on the Satellites of the Outer Solar System. Space Science Reviews, 153, 375–410.
Trinks, H., Schröder, W., Biebricher, C. (2005). Ice And The Origin Of Life, Origins of Life and Evolution of Biospheres, 35, 429-445.
Tyler, R. H. (2008). Strong ocean tidal flow and heating on moons of the outer planets. Nature, 456, 770–772.
Waite, J. H., and 13 colleagues. (2006). Cassini Ion and Neutral Mass Spectrometer: Enceladus Plume Composition and Structure. Science, 311, 1419-1422.
Zahnle, K., Dones, L. (1998). Cratering Rates on the Galilean Satellites. Icarus, 136, 202-222.
Zimmer, C., Khurana, K. K., Kivelson, M. G. (2000). Subsurface Oceans on Europa and Callisto: Constraints from Galileo Magnetometer Observations. Icarus, 147, 329-347.

Appendix A3

Morphotectonic features on Titan and their possible origin

Journal article published in *Planetary Space & Science* (2013),
Volume 77, pp. 104-117.

ARTICLE IN PRESS

Planetary and Space Science ▮ (▮▮▮▮) ▮▮▮–▮▮▮

Contents lists available at SciVerse ScienceDirect

Planetary and Space Science

journal homepage: www.elsevier.com/locate/pss

Morphotectonic features on Titan and their possible origin

Anezina Solomonidou [a,b,*], Georgios Bampasidis [b,c], Mathieu Hirtzig [b], Athena Coustenis [b], Konstantinos Kyriakopoulos [a], Karen St. Seymour [d,e], Emmanuel Bratsolis [c], Xenophon Moussas [c]

[a] Department of Geology and Geoenvironment, National & Kapodistrian University of Athens, 15784 Athens, Greece
[b] LESIA-Observatoire de Paris, CNRS, UPMC Univ. Paris 06, Univ. Paris-Diderot, 92195 Meudon Cedex, France
[c] Department of Physics, National & Kapodistrian University of Athens, 15784 Athens, Greece
[d] Department of Geology, University of Patras, 26504 Patras, Greece
[e] Concordia University, Department of Geography, H3G1M8 Montréal, Canada

ARTICLE INFO

Article history:
Received 26 December 2010
Received in revised form
12 January 2012
Accepted 3 May 2012

Keywords:
Titan
Morphotectonic features
Icy satellites
Cryovolcanism
Internal structure

ABSTRACT

Spectro-imaging and radar measurements by the Cassini–Huygens mission suggest that some of the Saturnian satellites may be geologically active and could support tectonic processes. In particular Titan, Saturn's largest moon, possesses a complex and dynamic geology as witnessed by its varied surface morphology resulting from aeolian, fluvial, and possibly tectonic and endogenous cryovolcanic processes. The Synthetic Aperture Radar (SAR) instrument on board Cassini spacecraft, indicates the possibility for morphotectonic features on Titan's surface such as mountains, ridges, faults and canyons. The mechanisms that formed these morphotectonic structures are still unclear since ensuing processes, such as erosion may have modified or partially obscured them. Due to the limitations of Cassini–Huygens in the acquisition of *in situ* measurements or samples relevant to geotectonics processes and the lack of high spatial resolution imaging, we do not have precise enough data of the morphology and topography of Titan. However we suggest that contractional tectonism followed by atmospheric modifications has resulted in the observed morphotectonic features. To test the possibility of morphotectonics on Titan, we provide in this work a comparative study between Cassini observations of the satellite versus terrestrial tectonic systems and infer suggestions for possible formation mechanisms.

1. Introduction

Tectonic or structural geology is the field of geological research that focuses on the study of features observed on the crust of the Earth and that of other planets investigating the processes, forces and movements that resulted in them. Tectonism encompasses geological events not caused by exogenous processes such as erosion and meteoritic impacts. Tectonism being compressional or extensional is related with important endogenous processes such as terrestrial volcanism and most probably with extraterrestrial cryovolcanism. Morphotectonics correlate landscape morphology to tectonism (Rosenau and Oncken, 2009; Scheidegger, 2004; Lidmar-Bergström, 1996) by studying landform evolution and degradation, since tectonic features are subsequently subjected to exogenous processes. Major morphotectonic features on Earth are represented by mountains, ridges, faults and escarpments, as well as by significant types of linear features such as rifts, grabens and other linear terrestrial terrains that are subjected to erosion subsequently to deformational events (e.g., Scheidegger, 2004). However, geology on Earth is dominated by active plate tectonics where rigid lithospheric plates float and move on a plastic asthenosphere.

Although the other planetary bodies in our Solar System possess different surface and internal conditions, bodies like Titan, Europa and Enceladus may possess a liquid water layer underneath their icy crust. If confirmed, then similarly to rocky plate tectonics on Earth, rigid ice plates may rupture and collide, floating over such a liquid substrate layer, resulting in surficial features, which may be reminiscent of terrestrial edifices. It is therefore possible that other planets and moons in the Solar System harbor "tectonic activity" in varying degrees and even exhibit morphotectonic features on their surfaces, which are subsequently modified by exogenous processes.

Venus appears to have no plate tectonics due to a high surface temperature and a higher density of its lithosphere compared to that of the mantle, which prevents a subduction regime, despite the fact that the mantle is convecting (Nimmo and McKenzie, 1998). However, the planet shows deformation and morphotectonic features such as faults, mountain crests and rifts, which probably originated from lithospheric movements in association with volcanism (Jull and Arkani-Hamed, 1995; Nimmo and McKenzie, 1998). In the case of Mars, two major regions are known to display morphotectonic features: the Tharsis volcanic plateau, which was possibly formed after crustal deformation in

* Corresponding author at: Department of Geology and Geoenvironment, National & Kapodistrian University of Athens, Greece. Tel.: +30 69 45 40 29 03.
E-mail addresses: asolomonidou@geol.uoa.gr, Anezina.Solomonidou@obspm.fr (A. Solomonidou).

0032-0633/$ - see front matter © 2012 Elsevier Ltd. All rights reserved.
http://dx.doi.org/10.1016/j.pss.2012.05.003

Please cite this article as: Solomonidou, A., et al., Morphotectonic features on Titan and their possible origin. Planetary and Space Science (2012), http://dx.doi.org/10.1016/j.pss.2012.05.003

association with active diapirism from the mantle (Mège and Masson, 1996) and the Elysium region, which was a result of volcanic activity (Hall et al., 1986). Io, Jupiter's moon, presents morphotectonic features with no apparent association to plate tectonic activity. The mountains of Io are formed by stresses at the bottom of the lithospheric layer and subsequent uplift through thrust faulting system (Schenk and Bulmer, 1998).

A good candidate for the study of morphotectonic features in the Solar System appears to be Titan. With a diameter of 5150 km (1/3 that of the Earth), Titan is the largest satellite of the Saturnian System and the second in the Solar System, after Ganymede the moon of Jupiter. The temperature and pressure conditions at the surface near the equator are 93.65 ± 0.25 K and 1.467 ± 1 hPa, as measured by the Huygens probe Atmospheric Structure Instrument (HASI) (Fulchignoni et al., 2005). Titan is recognized as a world bearing several resemblances to our own planet, with respect to its atmosphere and to its surface morphology. Titan's dense atmosphere consists mainly of nitrogen (~97%), methane (1.4%) and hydrogen (~0.2%) with traces of hydrocarbons, nitriles, oxygen compounds and argon (see table 6.4 in Coustenis and Taylor, 2008). This complex atmosphere renders the surface difficult to access and analyze, apart from within a few methane spectral windows in the near-infrared where the methane absorption is weak (Griffith et al., 1991). Thirty-two years after the Voyager encounter in 1980, Cassini is today able to probe Titan's surface with a spatial resolution reaching a few hundred meters per pixel (RADAR), while the Huygens probe achieved the first *in situ* measurements in 2005 (for instruments and resolutions see Section 2). Even though Titan's surface morphology resembles that of the Earth, it is made of materials and subjected to surface conditions very distinct from the terrestrial ones. Indeed, morphotectonic features such as mountains (e.g. Radebaugh et al., 2007; Lopes et al., 2010), ridges (Soderblom et al., 2007b; Mitri et al., 2010), faults (e.g., Radebaugh et al., 2011), rectangular drainage patterns and cryovolcanic structures are most likely controlled, at least in part, by tectonism (Burr et al., 2009).

Atmospheric processes, like cloud formation and precipitation create extensive fluvial features on the surface, as observed by Huygens near its landing site and constitute the visible part of an active methane cycle (Atreya et al., 2006; Coustenis and Taylor, 2008; Lorenz and Mitton, 2008; Raulin, 2008; Brown et al., 2009; Coustenis and Hirtzig, 2009; Lebreton et al., 2009). The preservation limit of 100 Myr for this atmospheric methane requires a reservoir that would replenish occasionally the atmosphere (Lunine and Atreya, 2008). One of the most predominant theories suggests that methane sources exist in Titan's interior (e.g., Tobie et al., 2006; Fortes et al., 2007). Since volcanism is a major process associated with the terrestrial carbon release (Bolin, 1981), cryovolcanism may play a similar role in the methane supply (Sotin et al., 2005), as well as significantly influence Titan's surface morphology.

Geophysical models suggest that Titan's partially differentiated interior consists of a silicate core (~1800 km thick), a high-pressure ice mantle (~400 km), a liquid layer of aqueous ammonium sulfate (50–150 km thick), and an external icy shell 100–170 km thick that possibly contains clathrate hydrates (Tobie et al., 2005; Fortes et al., 2007; Grindrod et al., 2008). Castillo-Rogez and Lunine (2010) suggested possible dehydration of the core's hydrated silicates, which impacts the geophysical structure of the satellite as well as the possible internal ocean. Regarding the icy shell, the methane stored as clathrate hydrates within the ice shell is a plausible methane reservoir that can replenish the atmosphere via cryovolcanism (Sotin et al., 2005). Indeed, surface discontinuities such as faults and fractures, which are probably the result of tectonic and volcanic-like processes, could provide the pathways of internal methane release to the atmosphere. The morphotectonic structures on Titan's surface provide good evidence of such a mechanism, in the same way as, over extensive zones of geological weaknesses, magma and volatiles are released on the Earth's surface.

In the last eight years, despite continuous observations by Cassini and the development of models and interpretations based on them, we still lack long-term *in situ* measurements and geophysical data of Titan's interior, in order to be in a position to accurately evaluate its endogenetic potential and how it affects morphotectonic features. However, in this work we attempt to use similarities between the surficial morphotectonic features on Titan and on Earth as the key for deciphering Titan's endogenetic processes, in spite of the fact that our understanding of Earth's endogenetic processes is rather recent (Wilson, 1973).

2. Titan surface observations

From the interpretation of Voyager 1 recordings, a global ocean of dissolved ethane and nitrogen, several kilometers deep, was first assumed to cover the entire surface of Titan (Flasar, 1983; Lunine et al., 1983). However, ground- and space-based observations refuted this assumption by unveiling, within the methane "windows" of weaker methane absorption (centered at 0.94, 1.08, 1.28, 1.59, 2.03, 2.8 and 5 μm), a solid surface with heterogeneous bright and dark features (Muhleman et al., 1990; Griffith, 1993; Smith et al., 1996; Gibbard et al., 1999; Meier et al., 2000; Coustenis et al., 2001). The Cassini orbiter arrived at the Saturnian System in 2004 equipped with two spectro-imagers capable to probe down to the surface via several of the near-infrared windows: the Visual and Infrared Mapping Spectrometer (VIMS—with a typical resolution of 10–20 km/pixel) and the Imaging Science Subsystem (ISS—with a typical resolution of 1 km/pixel). In the scope of this paper we also make use of the RADAR data from Cassini with a spatial resolution from 300 m to 1.5 km/pixel. In addition, Huygens probe measurements and observations by the Descent Imager Spectral Radiometer (DISR—Tomasko et al., 2005), the Surface Science Package (SSP—Zarnecki et al., 2005), and the Gas Chromatograph Mass Spectrometer (GCMS—Niemann et al., 2005, 2010) provided additional information of Titan's geology. The actual landing site on the Saturnian satellite appears to be a relatively soft surface similar to tar or dry sand, tinted by methane ready to evaporate and providing ample evidence for fluvial and aeolian processes.

2.1. Surface expressions

2.1.1. Geological features formed by non-tectonic processes

Endogenous, as well as exogenous dynamic processes have created diverse terrains with extensive ridges and grooves, impact units, icy flows, caldera-like structures, layered plains and stable liquid lakes (Mitri et al., 2007; Stofan et al., 2007). In addition, Cassini's radar has partially revealed the topography of Titan's surface, indicating several types of surficial expressions, which are non-tectonic. Features like dunes, lakes and drainage network are attributed solely to fluvial, aeolian and impact processes (Fig. 1). Thus, their formation is the result of exogenous processes with no influence of internal activity.

2.1.2. Morphotectonic features

Cassini's remote instrumentation and the Huygens lander brought evidence of many features on Titan's surface, which were probably formed by extension or compression of parts of the planetary solid crust due to endogenetic geological and geophysical processes (Radebaugh et al., 2007; Soderblom et al., 2007b;

Please cite this article as: Solomonidou, A., et al., Morphotectonic features on Titan and their possible origin. Planetary and Space Science (2012), http://dx.doi.org/10.1016/j.pss.2012.05.003

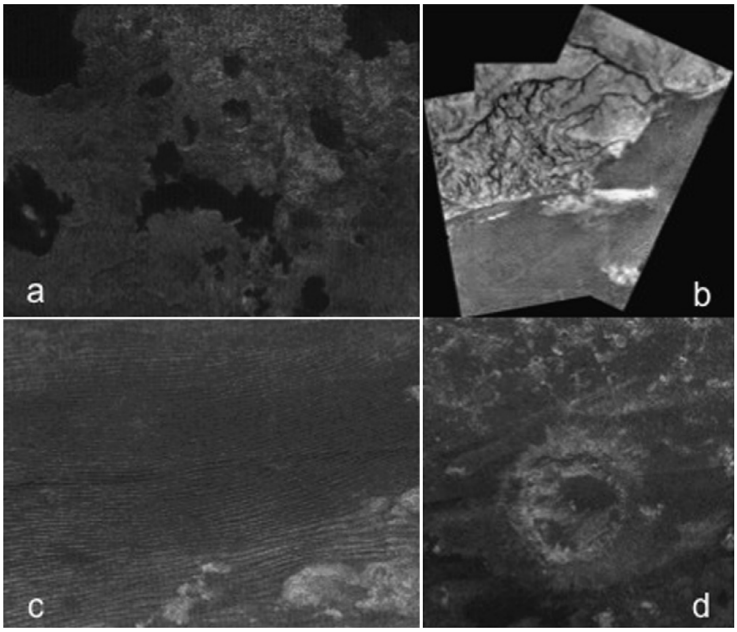

Fig. 1. Surface features on Titan. (a) Hydrocarbon liquid lakes at the North pole (Cassini Radar Mapper, JPL, ESA, NASA). (b) Complex network of narrow drainage channels formed by fluvial processes near the Huygens probe landing site (NASA/JPL). (c) Sand dunes formed by aeolian processes (NASA). (d) Afecan (26°N, 200°W) impact crater, discovered in 2008 (NASA/JPL).

Lopes et al., 2010). Furthermore, these features can be modified under the influence of exogenetic processes: the resultant morphotectonic structures are mainly mountains, ridges, faults, and structures of probable cryovolcanic origin as we will argue further down. Titan, despite its small size, displays surface features that resemble the structure of terrestrial volcanic fields albeit they are much more extensive. For example, Hotei Regio (see Section 4.2) covers an area of 140,000 km^2, which is an order of magnitude larger than Harrat Khaybar (14,000 km^2) in Saudi Arabia, which represents one of the most extensive volcanic fields on Earth (Camp et al., 1991).

2.2. Silicate and icy tectonism

A surface feature largely owes its shape to the material composing the planetary body's crust and to the forces that formed it. The response of the crustal material to the applied stresses, defines to a large extent the main topographic terrain of an area, along with the atmospheric conditions. Even though geological features such as mountains, faults and rifts on Titan present similar visual characteristics, the type of material that builds the features plays an important role. Indeed, the properties of the source material such as viscosity, elasticity and density in addition to the geological forces control the structural characteristics of the feature such as height, expansion and gradient slope.

On Titan, the surface should probably be composed mainly of mixtures of water and other ices, organics–tholins, nitriles (e.g. Soderblom et al., 2007a), while, most likely, its interior is composed of rock and high-pressure ice (Tobie et al., 2005). Since the well-known tectonic features of Earth are closely linked to silicate geology, we must first assess the similarities and differences between water ices and silicates, so that our comparative study can be based on reasonable assumptions. The icy crust of the outer system satellites possibly reacts in a brittle fashion to the application of stresses, similarly to the Earth's rocky upper crust (Collins et al., 2009). Both on Titan and Earth this reaction changes in proportion with depth. However, while water ice and silicate rock exhibit similar frictional strength (Beeman et al., 1988), when ductile yielding becomes important, ice is about ten times weaker than silicate rock (Melosh and Nimmo, 2011). The major differences and similarities between water ice and silicates are noted in Collins et al. (2009) and summarized in Table 1.

Table 1 shows that silicate materials, when compared to water ice, exhibit higher viscosity, Young modulus i.e. the ratio of linear stress to linear strain and melting temperature, but display lower density. As a result, the homologous temperature, on which rheology depends, is reached at greater depths in silicate environments while silicate magma eruptions are statistically more possible to occur than eruptions of ice (Collins et al., 2009). Nevertheless, both icy and silicate systems seem to follow some similar general deformation principles and mimic each other's behavior. Also, since ice topography could viscously relax over geologic time (e.g. Dombard and McKinnon, 2006) and elastic, brittle and ductile deformation could occur in the icy crust, tectonic-like movements, resembling the silicate plate behavior, are plausible.

3. Morphotectonic observations of mountains

3.1. Mountains and ridges

RADAR, VIMS as well as DISR data have provided some details of the characteristics of Titan's mountains and ridges. The term mountain describes large uplifted localized landforms while the term

Please cite this article as: Solomonidou, A., et al., Morphotectonic features on Titan and their possible origin. Planetary and Space Science (2012), http://dx.doi.org/10.1016/j.pss.2012.05.003

Table 1
Comparison between silicate and ice properties.

Properties	Water ice	Silicate	Similarity
Homologous temperature	0.4	0.4	Yes
Melting temperatures	273.15 K	950–1500 K	No
Density	Low (in solid state)	High	No
Young Modulus	~10 GPa	~100 GPa	No
Low stress and strain	Elastic deformation	Elastic deformation	Yes
High strain, low temperature	Brittle deformation	Brittle deformation	Yes
Low strain, high temperature	Ductile deformation	Ductile deformation	Yes

Table 2a
Major mountain and ridge features on Titan.

Location	Orientation	Heights	Characterization	Flyby/Time	Instrument (reference)
10°N, 15°W 15°N, 45°W		380–570 m	Blocks of mountains	T3/February 2005	RADAR (Radebaugh et al., 2007)
20°N, 87°W	E–W	~300 m	Ridges	T3/February 2005	RADAR (Williams et al., 2011)
40°S, 340°W			Hills	T7/September 2005	RADAR (Lunine et al., 2008)
5°S, 12.5°S 63°W, 67°W	E–W	~860–2000 m	Curvilinear mountains/Ridges	T8/October 2005	RADAR (Radebaugh et al., 2007; Mitri et al., 2010; Lopes et al., 2010)
10°S, 210°W		~400 m	Mountainous region	T9/December 2005 T13/April 2006	VIMS/RADAR (Barnes et al., 2007)
10.4°S, 192.4°W	W–E	100–150 m	Ridges	Huygens/January 2005	DISR (Tomasko et al., 2005; Soderblom et al., 2007b)
30°S, 315°W	NW–SE	~1500 m	Mountain ranges	T20/October 2006	VIMS (Sotin et al., 2007)
52°N, 347°W	E-W	~1400 m	Mountain block	T30/May 2007	RADAR (Stiles et al., 2009; Mitri et al., 2010)
30°S, 107°W	S–W	~800 m	Mountains	T43/May 2008	RADAR (Mitri et al., 2010)
2°S, 127°W	E–W	1930 m	Ridges	T43/May 2008	RADAR (Mitri et al., 2010)

Table 2b
Proposed mechanisms for the formation of mountains and ridges of Titan.

Proposed mechanism	Description	Observations	Terrestrial analog
Lithospheric shortening (Mitri et al., 2010)	Folding of the upper crust due to past high heat flux from the interior and high temperature gradients in the ice shell	Curvilinear mountains/ Ridges T8, T30, T43	Folded mountains: Rocky Mountains, North America
Tectonic stresses of the ice shell (Mitri and Showman, 2008)	Transitions of the ice shell over a liquid subsurface ocean, from a conductive state to a convective state, causes tectonic stresses and movements that influence the surface	Model	Rocky Mountains, North America
Crustal compression/ upthrust blocks (Radebaugh et al., 2007 scenario 1)	Localized compression due to thickening of the crust linked with the cooling of Titan at areas where fault structures exist	Linear mountains T8, T3 (15°N, 45°W)	Eroded mountains: Acadian Mountains, USA Mountain-building due to Sevier/Laramide Orogeny
Crustal stresses/upwelling of material (Sotin et al., 2007)	Generation of extensive stresses that penetrate the icy shell and create pathways for the internal material	High-standing mountain ranges T20	Tectonic and magmatic aspects on geological terrains: Mid Atlantic Ridge, Atlantic Ocean Ahaggar Mountains, North-central Sahara Desert
Crustal extension (Tobie et al., 2006; Radebaugh et al., 2007 scenario 2)	Recent crustal thickening due to localized extension	Blocks and grabens T8	Mountains due to extension: Basin and Range Province (Harcuvar Mountains, Gila Mountains, Maricopa Mountains) (Radebaugh et al., 2007)
Blocks of impact ejecta (Radebaugh et al., 2007 scenario 3)	Deposition of ejecta blocks around craters in a radial manner	Blocks of mountains T3	Ejecta patterns: Meteor crater, Arizona
Dissection and erosion (Radebaugh et al., 2007 scenario 4; Lunine et al., 2008)	Erosion and incision of terrains that form regional uplifted structures	Mountainous region T13	Erosional geomorphological structures: Colorado Plateau, USA (Lorenz and Lunine, 2005; Radebaugh et al., 2007). It is dissected by a number of long north–south trending normal faults while deep entrenchment of streams and differential erosion have formed high standing crustal blocks

mountain ridges (in this paper we will refer to mountain ridges as ridges), chains of elevated (uplifted) ground that extend for some distance. The major mountains and ridges on Titan are listed along with their location and observational characteristics in Table 2a.

Table 2a points at two intriguing aspects: mountain-like edifices exist at almost all latitudes on Titan; however, they are concentrated in the equatorial region at latitudes between 30°S and 30°N (Lopes et al., 2010). Their height is significantly lower than that of the terrestrial mountains ranging from 100 to 2000 m (Barnes et al., 2007; Radebaugh et al., 2007; Soderblom et al., 2007b; Sotin et al., 2007; Mitri et al., 2010). This may be partly due to erosional processes, as it is suggested by the blanket-like

Please cite this article as: Solomonidou, A., et al., Morphotectonic features on Titan and their possible origin. Planetary and Space Science (2012), http://dx.doi.org/10.1016/j.pss.2012.05.003

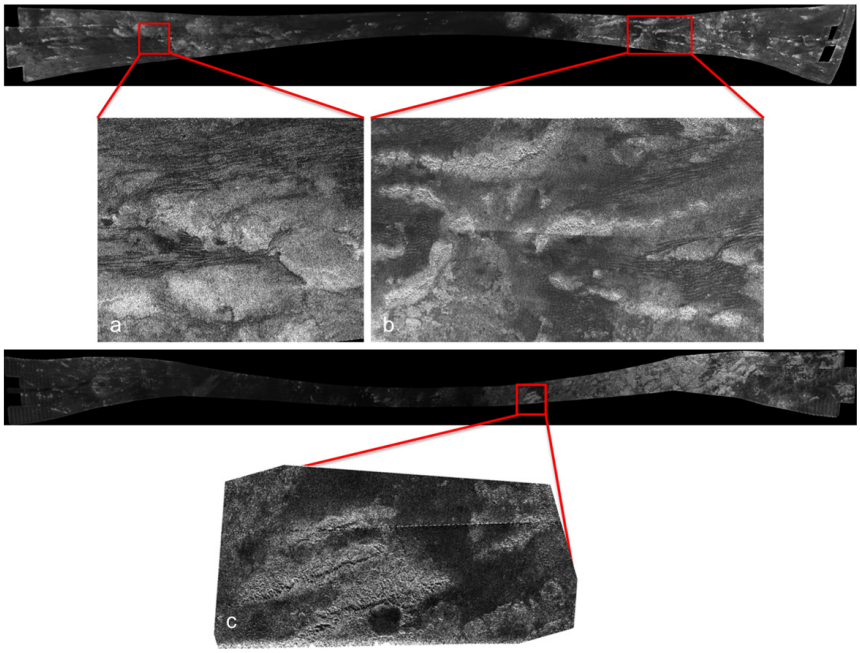

Fig. 2. Major mountainous regions on Titan. (a) Mountain extends for almost 240 km (NASA/JPL). (b) Long bright ridges with multiple mountain peaks were observed in T8 on October 28, 2005 (linear mountains extend from 13-5°S to 198-225°W) (e.g., Radebaugh et al., 2007; Lopes et al., 2010), and extend over 480 km (NASA/JPL). (c) Three radar bright parallel ridges (2°S, 127°W) within the mountainous area of Xanadu from T43 of May 12, 2008, the length of the image is almost 400 km (e.g., Mitri et al., 2010) (NASA/JPL/Space Science Institute).

materials that surround these structures (Radebaugh et al., 2007). Alternative hypotheses include the construction of Titan's mountains with materials with properties preventing height growth (Radebaugh et al., 2008) and the effects of high temperature gradients on the ice shell which, according to the calculations of Mitri et al. (2010), result in mountains from 100 to 2700 m high. Similarly to Earth where terrain topography is defined by the interaction of tectonism and erosion (Montgomery and Brandon, 2002), we suggest here that there is a strong connection between slope morphology and erosional rates on Titan due to its extreme conditions of hydrocarbon rainfall and/or winds.

Fig. 2 presents three portions of the T8 and T43 RADAR swaths that provide the most reliable evidence so far for the existence of mountains and ridges on Titan.

3.2. Related mechanisms and terrestrial analogs

The mechanisms for mountain formation on Titan are summarized in Table 2b and include pure extension (Tobie et al., 2006; Sotin et al., 2007; Radebaugh et al., 2007—scenario 2), pure compression (Radebaugh et al., 2007—scenario 1; Mitri et al., 2010) and transitions between compressional and extensional stresses (Mitri and Showman, 2008). Extensional deformation is observed on all icy moons, but if orogenesis on Titan can be attributed to compressional forces this will render Titan unique.

Orogenesis in the terrestrial analog is predominantly a compressional event due to the coming together of the lithospheric plates floating on the plastic asthenosphere. The phenomenon is attributed to global convection initiated from the liquid external core and might not be random but with peaks related to the orbit of our Solar System around the galactic center. Terrestrial orogenesis results in forms and tectonic structures such as folds and thrust faults. Such compressional structures are represented by the mountain chains of the Rocky Mountains, the Andes and the Himalayas. Fig. 3 shows the Rocky Mountains, an almost 5000 km long mountain chain, extending from Canada to the western United States. This region was formed by subduction of the Pacific plate beneath the North American plate (Bird, 1998), when two tectonic plates of different densities sank one beneath the other inducing internal compressive forces within the plates. Mitri et al. (2010) argued for Titan that ice floes of altered densities, moving on a liquid layer, could reproduce structures and simulate phenomena similar to subduction. If this hypothesis is confirmed in the near future by geophysical measurements and modeling, and under the assumption that ice floes would react exactly like silicate plates to the stresses simulating subduction, something not impossible as shown in Table 1, then we may infer that what we see on Titan is an Earth-like mountainous terrain with peaks and extensive ranges.

Formation of mountains due to extension on Earth is represented by the classical example of the Basin and Range area and other examples listed in Table 2b. The geomorphology of Basin and Range (Hawkesworth et al., 1995) consists of separate and semi-parallel mountain ranges as seen in Fig. 4. The formation of the area is attributed to crustal extension and associated development of large faults along which mountains were elevated and valleys have submerged. These endogenous tectonic processes resulted in a geological terrain characterized by morphotectonic

Please cite this article as: Solomonidou, A., et al., Morphotectonic features on Titan and their possible origin. Planetary and Space Science (2012), http://dx.doi.org/10.1016/j.pss.2012.05.003

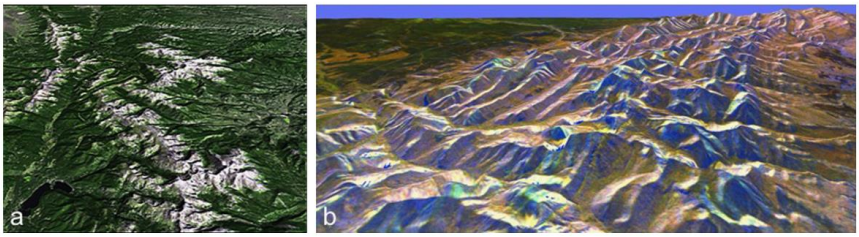

Fig. 3. Rocky Mountains, USA (a) in Landsat TM scene with DEM data (Credit: Federation American Scientists FAS). (b) 3-D perspective view by combining two spaceborne radar images (PIA01840 NASA/JPL).

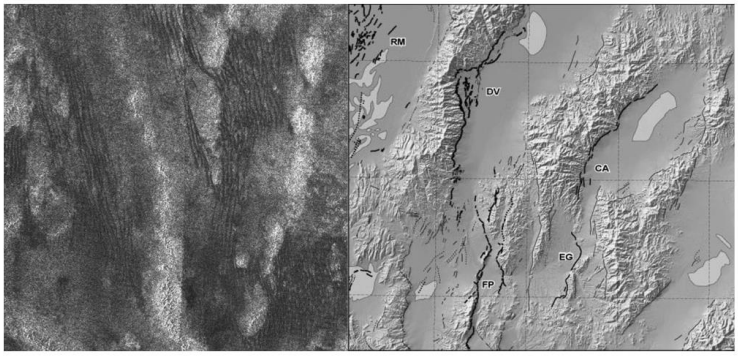

Fig. 4. (left) Fault-block mountains on Titan (portion of Fig. 2b) (PIA03566 NASA/JPL) formed possibly through crustal extension (Radebaugh et al., 2007). (right) Relief map of the Basin and Range province in west-central Nevada (USGS) displaying the parallel ranges and valleys created by crustal thinning and fracturing by extensive stresses.

features such as linear mountain ranges and valleys. Fluvial, aeolian and other exogenous processes subsequently modified these features.

However, convective stresses on silicate bodies tend to be larger and their rheological length scales are typically greater (Table 1). In Titan therefore it is essential to note that local/regional rather than global stress mechanisms are commonly suggested in the models for mountain building. Regional or local stress mechanisms invoked in these models include (a) convection, which depends in the ice shell thickness, (b) local gravity, and (c) ice viscosity, which depends on the temperature and mostly on the grain-size (Barr and Pappalardo, 2005; Collins et al., 2009). Indeed, on large icy satellites, layers of high- and low-pressure ice may convect separately (McKinnon, 1998).

Among the local stress mechanisms presented above, one can include lateral pressure gradients that may have as a consequence the lateral flow of floating ice shells on their low viscosity base. Rigid ice floes rupturing and colliding are reminiscent of plate tectonics albeit in a random fashion. This could lead to the creation of blocks of high-standing topography that would subsequently be subjected to erosional processes. Such elevated morphotectonic features on Titan, as mountains, ridges, hills and ranges, indicate a formation preference around the equatorial zone of the moon (Barnes et al., 2007; Radebaugh et al., 2007; Mitri et al., 2010).

4. Morphotectonics of faults and transverse processes

In this section, we describe Titan's morphotectonic features as a combination of a formation process and one or more superimposed "transverse processes" that occurred at the same time or subsequently, modifying the initial shape of the feature.

4.1. Tectonic control on Titan's linear features: Faults, fractures, canyons and drainage networks

In geology, a fault is a rupture that separates a rock unit into two parts, moving one relatively to another, in a microscale or a whole field in a macroscale. A variety of geological processes are associated with faults and therefore their analysis is very important. For instance, geologists consider the direct relation of earthquakes with faults, or the penetration of igneous rocks on Earth's crust along faults, or also the interaction of faults in the development of sedimentary basins. On the other hand, canyons are another type of crustal scars, formed on Earth by the accelerated erosion by rivers entrenched after tectonic activity and trying to reach base-line elevation (Schumm et al., 2002). On Titan the observed faults, fractures, canyons and ground lineaments are most likely the results of crustal movements due to tectonic and/or volcanic processes as well as structures associated with fluvial networks controlled by tectonism (Table 3). An investigation of canyon formation can augment our understanding of Titan's geology. A study in 2009 by Burr et al. (2009) provided evidence on the influence of subsurface tectonic activity on drainage patterns as observed by SAR data. Based on that, we can infer that these fluvial networks are morphotectonic features since there are indications that both tectonic and fluvial processes operate for their formation. Titan studies based on observations and mapping, have suggested the presence of fault formations. Table 3 summarizes their major observations by Cassini.

Please cite this article as: Solomonidou, A., et al., Morphotectonic features on Titan and their possible origin. Planetary and Space Science (2012), http://dx.doi.org/10.1016/j.pss.2012.05.003

As expected from the study of other icy satellites, the majority of formation mechanisms suggest extensional style tectonism. In the areas where fluvial networks seem to be controlled by tectonic patterns, the surface material seems to have the proper elasticity to create linear fractures. At the Huygens landing site, as proposed by Soderblom et al. (2007b), the linear structures can function as the ideal path for the hydrocarbon liquids to escape towards the surface. Furthermore, the observed radial fault system around the possible calderas of Hotei Regio (Soderblom et al., 2009), argue in favor of cryovolcanism since the identification of radial faults around caldera formations also on Earth, are indicators of ground elevation due to volcanic activity.

Fig. 5 displays a complex feature on Titan (71°S, 240°W), which — even if it is not confirmed by radar data processing yet — it appears to be a canyon-like morphotectonic feature since it consists of a sinuous dark, rather narrow feature with tributary-like off shoots and it is limited on all sides by high albedo i.e. elevated terrains (e.g. Radebaugh et al., 2007). The morphology of the bright and the dark shape of this region resembles the terrestrial analog, which is the Grand Canyon in the United States. This terrestrial feature is adjacent to the Basin and Range Province that was mentioned earlier. The formation of the Grand Canyon on Earth is the end result of the extensional tectonics that formed the Basin and Range Province and of continuous rifting and erosion (Sears, 1990).

From Table 3 we can distinguish a tendency for preferential formation of these features between 10°S and 26°S, that is, within the zone where mountains are formed. Such observations imply crustal movements are more frequent within this zone than around the poles, including compressional and extensional stresses. However, Titan's limited-coverage observations (less than 50% of the surface), with instruments incapable of precisely unveiling its geology, make this aspect a subject for future exploration.

4.2. Cryovolcanism and association with morphotectonics

Plate tectonics and volcanism are strongly associated on Earth (McDonald, 1982) and this can also be the case on Titan in the presence of tectonic features overlying a liquid water ocean. These can function as leading 'pathways' for the ammonia–water cryomagma to reach the surface and for the release of methane. Liquid pockets with methane clathrates and with a high ammonia mass concentration in a water solution can dissociate in the ice shell and eventually exsolve on the surface and in the atmosphere (Tobie et al., 2006; Mitri et al., 2008). Hence, cryovolcanism can also act as the dynamic force that deforms tectonic features. Cryovolcanism is believed to represent an important geological process in the history of several icy Saturnian satellites and other icy satellites, such as Triton (Kargel, 1994; Fagents, 2003; Lopes et al., 2007a). Gaidos (2001) stated that tectonic extension could trigger cryovolcanic eruptions by reducing the minimum normal stress in an aquifer to a value

Table 3
Major fault, fracture and canyon formations on Titan.

Location	Characterization	Proposed mechanism	Flyby/Time	Instrument (reference)
15°S, 155°W	Conjugate-like faults	i. Large scale tectonic modification of bedrock material. ii. Fluvial sapping of bedrock that enlarges tectonic zones of weakness.	T0/July 2004 TA/October 2004 TB/December 2004	ISS (Porco et al., 2005)
10°S, 145°W 0°N, 180°W	Joints and/or faults	Control by a subsurface tectonic structural fabric due to orbital processes (diurnal tides, non-synchronous rotation: tensional stresses)	T13/April 2006 T44/May 2008	RADAR (Burr et al., 2009)
10°S, 192°W	Linear fault patterns/ canyon-like formations	Preexisting faults reactivated from cryovolcanism and filled with deposited material and formed canyon-like systems	Huygens DISR/ January 2005	DISR (Soderblom et al., 2007b)
15°S, 100°W	Lithospheric fault-blocks	Extensional crustal stresses	Model	(Radebaugh et al., 2011)
26°S, 78°W	Radial fault system	i. Hot plume uplift and crust elevation-fault formation due to extension stresses. ii. Large ancient impact crater.	T47/November 2008	VIMS (Soderblom et al., 2009)

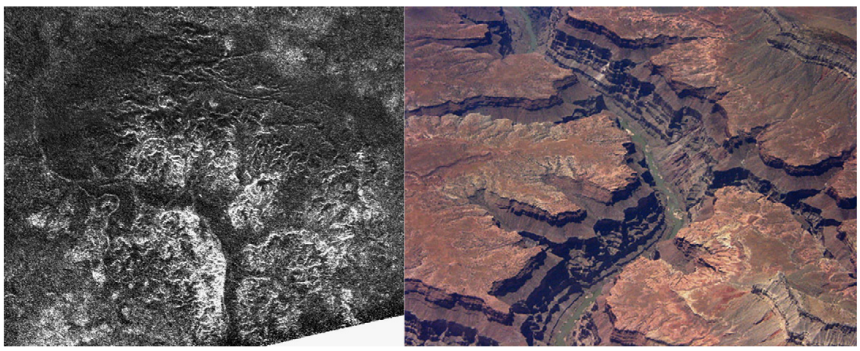

Fig. 5. (left) Radar image showing canyon-like systems on Titan (71°S, 240°W) (PIA12036 NASA/JPL). (right) Massive canyon formation on Earth, Grand Canyon, USA (USGS).

Please cite this article as: Solomonidou, A., et al., Morphotectonic features on Titan and their possible origin. Planetary and Space Science (2012), http://dx.doi.org/10.1016/j.pss.2012.05.003

below the pore pressure. On Titan, a few topographic features are candidates for large volcanic edifices (Table 4).

The mechanism of cryovolcanism resembles terrestrial type volcanism, however the cryomagma differs from the terrestrial magma in composition, texture and temperature. Indeed, the cryomagma i.e. aqueous solutions of ammonia, methane, salts, etc., can be found at temperatures well below the freezing point of pure water and degassing replaces the traditional silicate volcanism. Cryovolcanic structures are openings, or ruptures, on a planetary surface or crust, allowing for various internal products like water, other chemical components, gases and cryoclastic ash to escape from the planet's interior (Fortes et al., 2007).

On Titan, internal heating due to radiogenic decay and tidal forces along with pressure fluctuations may trigger cryomagma eruptions. The cryolava deposition would then happen at temperatures much lower than the terrestrial ones (Davies et al., 2010). In general, the temperatures of most terrestrial magma types range from 1150 to 1470 K while a plausible range of the Titan cryomagma temperatures is between 177 and 239 K (Mitri et al., 2008). Besides predictions from theoretical modeling we also have surface features indicating possible cryovolcanism on Titan. Indeed, lobate and fan shaped features seen in radar images have been interpreted as cryovolcanic in origin, as for instance, the lobate circular structure of Ganesa Macula (50°N, 87°W) (Lopes et al., 2007a). The structure contains bright rounded features, interpreted as cryovolcanic flows, while the curved or linear shapes are lineaments that could be caused by elevation of the crust due to cryovolcanic activity (Lopes et al., 2007a). Other such features like Tui Regio, Hotei Regio and Sotra Facula are more extensively discussed hereafter. The identification of cryovolcanic structures is rendered difficult mainly for two reasons: firstly, the masking of cryovolcanic features by the interaction with major exogenetic processes, e.g. by fluvial or aeolian deposits (Lopes et al., 2010). As an example of the latter case, Lopes et al. (2010) report in the Winia Fluctus (45°N, 30°W) a dune field, which has partially covered a cryovolcanic edifice. Secondly, the Cassini instrumentation with relevance to cryovolcanic investigations (SAR and VIMS) is not adequate on terms of spatial and spectral resolution (Elachi et al., 2004; Brown et al., 2004).

However, we have currently some cryovolcanic candidate features. The most probable ones are three areas located close to the equator. Tui Regio, as well as Hotei Regio, lie within the bright region of Xanadu (100°N, 15°S), a large, reflective equatorial area. Tui Regio presents relatively high 5-μm reflectivity and its size is 1500 km long and 150 km wide (McCord et al., 2006). It is a massive flow-like terrain, which resembles flow fields in volcanic areas on Earth. In 2006, Barnes et al. (2006) noted that there are two bright and long areas within Tui Regio that are filled with a material darker than the surrounding terrain, forming a trench. These areas, located within the northwestern portion of Tui Regio's flow and including the trending dark linear marks (Fig. 6), may have a regional tectonic origin (Barnes et al., 2006). Additionally, the latter authors pointed out a linear dark feature with similar spectral behavior which surrounds the southern bright region, suggesting that it might also be formed by regional tectonics. A recent and very reliable candidate for cryovolcanic activity is Sotra Facula; an area 235 km in diameter including a 1 km high mountainous peak next to a 1.5 km wide crater-like feature from which lobate flows seem to originate (Kirk et al., 2010; Lopes et al., 2010). Indeed, this area displays varying topography with adjacent uplifts and pit features suggesting probable tectonic control. Hotei Regio is also another candidate for the presence of tectonic features within a probable cryovolcanic region (Wall et al., 2009). Hotei Regio extends over 700 km and includes a 1 km wide topographic depression, characterized as a basin filled with flow-like features, a ridge-like mountainous terrain that surrounds the basin, dendritic channels, two caldera-like structures, dark blue patches (as seen in VIMS infrared images; a color that suggests enrichment in water ice), and possible alluvial deposits (Soderblom et al., 2009). Hotei Arcus, a bright arc in the southern margin of Hotei Regio, may represent a heavily eroded crater (Barnes et al., 2005). This assumption reinforces the hypothesis of interplay among the different types of processes. Soderblom et al. (2009) correlated VIMS and RADAR images in order to unveil the geological history of this area. Their interpretation suggests that a wide range of processes occurred — or are still occurring — in this varied terrain, including tectonism. Furthermore, they suggested that impact-induced faults created

Table 4
Candidates of major cryovolcanic features on Titan and their association with volcanotectonic processes.

Location	Name	Description	Possible tectonic features
20°S, 130°W	Tui Regio	Flow-like region	Trending dark linear marks on VIMS data (Barnes et al., 2006)
26°S, 78°W	Hotei Regio	Volcanic-like terrain	Circular tectonic features (Soderblom et al., 2009)
15°S, 42°W	Sotra Facula	Volcanic-like terrain	Topographic elevation, mountain-like structures (unidentified) (Lopes et al., 2007b)

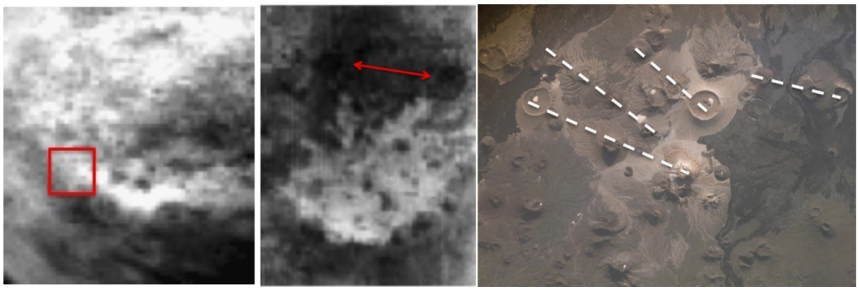

Fig. 6. Area on Tui Regio (left) with possible tectonic influence; two dark patches on Hotei Regio (middle) assumed to be volcanic caldera ridges (NASA/JPL/University of Arizona); Harrat Khaybar (right), massive volcanic terrain in western Saudi Arabia on Earth; the dashed lines indicate the linear trend of the volcanic vents suggesting tectonic control (NASA).

Please cite this article as: Solomonidou, A., et al., Morphotectonic features on Titan and their possible origin. Planetary and Space Science (2012), http://dx.doi.org/10.1016/j.pss.2012.05.003

zones of weakness on which volcanism and tectonism occurred. The two dark morphotectonic features (Fig. 6) north of Hotei Regio, are interpreted as cryovolcanic calderas by Soderblom et al. (2009).

A terrestrial region that appears to resemble the evolution of Hotei Regio is Harrat Khaybar, located in north of Medina in Saudi Arabia. It is a 14,000 km^2 volcanic field that was formed by eruptions along a 100 km N–S linear vent system. The area contains multiple volcanic rock types, lava flows, and volcanic structures such as calderas and domes (e.g., Baker et al., 1973). The internal mechanism that most likely formed the terrain is a mantle plume causing diffused lithospheric extension (Chang and Van der Lee, 2011). The association of the volcanic centers that lie over a linear zone of weakness with the Red Sea transform fault i.e. conservative plate boundary—where plates slide past each other along transform faults, characterizes them as geological structures that are presently active (Rehman, 2010). This suggests that local movements of parts of the crust, probably affect areas of great extent like Hotei Regio and Harrat Khaybar, even if they are not located precisely in the center of the active area. In the case of Harrat Khaybar, the adjacent Red Sea fault continues to propagate: its rifting causes seafloor spreading, triggering the volcanic centers of the region (Camp et al., 1991). Such a process illustrates the relation between the terrestrial volcanic terrains and tectonism, a relation that seems possible for Titan's case as well.

Tui Regio, Hotei Regio and Sotra Facula are all located in the 15°S–30°S latitudinal zone which is close to the southern margin of Xanadu (Soderblom et al., 2009), implying that the region might be an extensive zone of crustal weakness. The existence of possible volcanic and tectonic features within a specific area seem to be manifestations of the most active region of Titan like the boundaries of tectonic plates on Earth. Although still under investigation in Titan's case, the definite identification and understanding of morphotectonic features in these regions is crucial in order to determine the presence and origin of zones of crustal weakness, which will in turn impose additional constraints on cryovolcanism on Titan. Indeed, on Earth, as well as on other planetary bodies, the interplay of volcanism and tectonism causes the formation of extensive and distinct geological terrains.

The moons of Jupiter, Europa and Ganymede, possibly also display similarities with the morphotectonics of Earth (volcanism–tectonism) and of the Saturnian icy satellites (cryovolcanism–tectonism). Fig. 7a shows Europa's ridges, junctions and domes, as seen by the Galileo instrument Solid State Imager (SSI), which are typical geological expressions on this moon. The ridges are most likely formed by cryovolcanic processes probably causing deposition of subsurface materials over surface units, accompanied by tectonic movements, that formed the lineaments (Figueredo and Greeley, 2004). This extensional volcano-tectonic mechanism is similar to the terrestrial mid-oceanic rifting (Prockter et al., 2002). On Ganymede, volcanic processes may have occurred in the past, but current evidence suggests the presence of tectonic processes (e.g., Head et al., 2002). The linked tectonic–cryovolcanic hypothesis suggests graben rupture (depressed block of ice bordered by parallel faults) due to lithospheric extension and cryovolcanic deposition caused by flooding of the internal material (cryovolcanic resurfacing) (e.g., Schenk and McKinnon, 1985; Murchie et al., 1986). Also fault blocks operating as zones of weakness can act as pathways for the bright material onto the surface while the crustal movements could produce the bright ridges (e.g., Head et al., 1997, 2002) (Fig. 7b).

Ganymede, and partially Europa, are the targets of a future mission proposal to the Jovian system, which will, among others, could explore the icy moons' interior heat potential, as well as, the surface motion and morphology, with improved and enhanced instrumentation in order to better understand their surface composition, internal structure, dynamics and the morphotectonics. Further investigation and comparison of the morphotectonic features of many of the icy satellites will shed light on the potential different internal mechanisms that operate in the Solar System.

5. Discussion

The morphotectonic structures presented here are related to the most elevated, as well as the most fractured features observed on Titan. Major mountainous regions are concentrated in mid-latitudes between 30°S and 30°N and probable cryovolcanic areas are located within the same zone (20°S–30°S). Linear features are displayed also within the same region (10°S–26°S). Fig. 8 represents a location map of the major morphotectonic features presented in this study.

We have argued here that all these features are related to surface stress fields. In analogy with terrestrial morphotectonic structures, the shape, size and morphology of Titan's observed mountains, ridges, hills and linear features such as faults, major fractures and canyons probably originate through some form

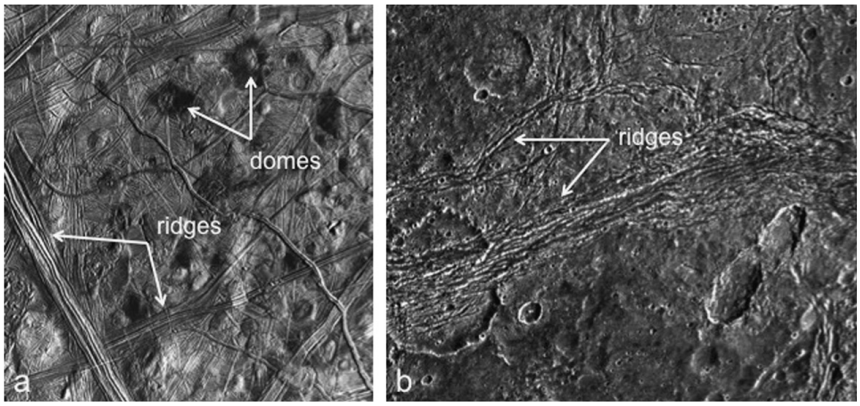

Fig. 7. (a) Europa's major geo-structures that may have formed due to volcanic and tectonic processes acting together (NASA/JPL-Caltech). (b) Ganymede's grooved and tectonic terrain (NASA/JPL/Brown University).

Please cite this article as: Solomonidou, A., et al., Morphotectonic features on Titan and their possible origin. Planetary and Space Science (2012), http://dx.doi.org/10.1016/j.pss.2012.05.003

compressional and extensional tectonic activity. Titan's rigid crust and the probable existence of a subsurface ocean create an analogy with terrestrial, at least surficial, plate tectonics.

If in future missions a number of Titan's surface features are definitely identified as a result of compressional processes, as it has been proposed here, and despite the fact that large stresses are required to form compressional features (Pappalardo and Davis, 2007), then this will render Titan unique among the rest of icy satellites where extensional features are dominant (Jaumann et al., 2009) and will ratify the thesis of Mitri et al. (2010) that some of Titan's mountains represent folds and/or thrusts.

On the other hand, in regard to the extensional features on Titan as compared to their terrestrial analogs one may question if there are some essential differences in the development and propagation of fractures in the icy crusts vis-à-vis the silicate crusts.

However, before addressing these questions, one should initially examine which factors control tectonism on a planetary body; essential stress mechanisms that can be either global, regional and local. Global stress mechanisms include tides, non-synchronous planetary rotation, polar wander, despinning, orbital recession and radiogenic decay. One major stress mechanism is provided by *convection*. Another array of mechanisms is due to volume changes up to the large density contrast between ice-I and water and is applicable to icy satellites (Collins et al., 2009). Finally, "impacts" represent another local stress mechanism. To global, regional or local stresses, Solar System bodies and particularly their crusts may react in a brittle, ductile or more rarely elastic fashion, producing corresponding landforms. In this respect it is essential to compare and contrast the mechanical properties of icy and silicate crusts, as well as, the order in which stress mechanisms occur, to find correlations between the morphotectonic features on Earth and those on Titan (Radebaugh et al., 2007; Collins et al., 2009).

Thus, a question arises: is there some essential difference in the development and propagation of faults in the icy crust with respect to a silicate crust? As indicated in Table 1, ice and silicates mainly share a similar crystal structure, differ in melting temperature but when ice involves water and methane, an additional similarity with the silicates is found in the three physical states of the material (solid, liquid, gas).

Earth and Titan share all the global stress mechanisms and sources of internal heat such as radiogenic decay, heating by applied tidal forces and primordial heat.

However the analogy probably stops here since Earth has preserved a capital of its primordial heat. The outer core of the Earth with a thickness of 2890–5150 km has a temperature range of 4400–6100 °C, similar to the photosphere of the Sun. Furthermore the total heat flux from Earth's interior ranges from 0.08 to 0.4 W m^{-2} (Pollack et al., 1993; Davies and Davies, 2010). Due to the state (liquid) and composition (Fe–Ni) of Earth's outer core, *thermal runaways* occur at the core–mantle interface and resurface as hot spots, causing local mantle convection and induce plate motion which implies the breaking of continents (Africa) or supercontinents (Pangea).

Hot spot volcanism is found in the middle of lithospheric plates and on the margins of extensional plates. Volcanism also occurs in compressional plate margins followed by orogenesis (mountain building). Titan's primordial heat flux from the satellite's interior is of the order of 0.02–0.06 W m^{-2} and Mitri et al. (2010) proposed that it can similarly result in crustal fold processes and mountain building.

On Titan, stress mechanisms even if global, as in the case of tides, can have very local effects: for instance Saturnian tidal forces result in a concentration of morphotectonic structures mainly around Titan's equator. It is not a random event that all the three candidates for cryovolcanic areas are concentrated in Titan's equatorial zone. Actually, it will be surprising if future detailed observations refute the case for cryovolcanism on Titan in this area, given positive indications from current studies (Lopes et al., 2010; Solomonidou et al., in preparation). Morphotectonic features resulting from tidal-induced convection have different ages, as can be shown from superposition and cross-cutting relationships. Mountains are old (20–100 million years—Radebaugh et al., 2007) and probable cryovolcanic areas are younger (less than 10,000 years for Hotei Regio—Soderblom et al., 2009). This is to be expected since tidal-induced convection will cause ice elevations with subsequent breaking of the surface ice and formation of fractures (extension). The ice floats may collide

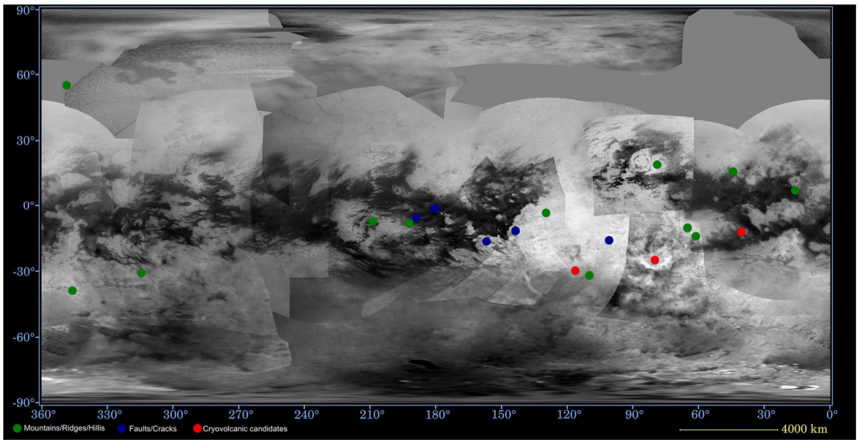

Fig. 8. Location map of the major morphotectonic features on Titan (background map credit: NASA/JPL). In green: mountains, ridges and hills; in blue: linear features, faults, fractures, canyons; in red: probable cryovolcanic regions. (For interpretation of the references to color in this figure legend, the reader is referred to the web version of this article.)

Please cite this article as: Solomonidou, A., et al., Morphotectonic features on Titan and their possible origin. Planetary and Space Science (2012), http://dx.doi.org/10.1016/j.pss.2012.05.003

against each other (compression) forming mountain- or ridge-like features. Subsequent extension of the so-formed fractures will provide the pathways for cryovolcanism, which will be the younger event.

Primordial heat, as well as, heat produced by radiogenic decay and heat induced by tidal forces can be dissipated both by conduction and/or convection. It has been shown that transitions from a conductive to a convective state for an ice shell, overlying a pure liquid ocean (Tobie et al., 2005), can have major effects on surface morphotectonics (Mitri and Showman, 2008). The same authors have shown that thermal convection can occur under a range of conditions in the ice-I shells of Titan and two possible scenarios can follow. A thin ice with a low viscosity base (I) and a thick ice with a high viscosity base (II). Thus, Mitri and Showman (2008) proposed oscillations in the thermal state of the ice-I shell of the Saturnian satellites, which may cause repeated episodes of extensional and compressional tectonism. Similarly on Earth, a current widely accepted internal evolution model suggests that expansion and contraction processes are due to internal thermal runaway cycles and can be important in controlling geotectonic mechanisms (Rice and Fairbridge, 1975; Fowler, 1986; Baumgardner, 1994, 2003; Benn et al., 2006).

Thermal stresses are responsible for updoming, weakening and subsequent fracturing of the crust of a planetary body. On Earth, such a paradigm is provided by the continent of Africa where hot spot activity has resulted in updoming, fracturing and volcanism (East African Rift, Ahaggar Mountains, Table 2a). On Titan, zones of tectonic weakness have probably formed in an analogous manner i.e. as a consequence of thermal stresses and weakening of the crust with concomitant formation of open fissures, which act as pathways for the ejection of material from the interior (cryovolcanism) as it has already been proposed for Enceladus and Europa (Manga and Wang, 2007).

Localized compression and crustal thickening can also lead to mountain building on Titan. Linear mountains in T3 and T8 swath, seen in radar data, probably have formed this way (Fig. 3a and b; Table 2b). A terrestrial analog can be provided by the Laramide Orogeny. The Laramide event that affected Western-North America during Late Cretaceous and Early Paleogene time, involved compressive forces, conductive heating and crustal thickening that eventually led to mountain building (orogeny) (Dickinson and Snyder, 1978). A similar example is provided by the Acadian Orogeny during middle Paleozoic, which has affected the Eastern-North America as the result of collision of Baltica plate with the Laurentia.

The proposed formation mechanism for Titan's mountains, mainly the ones observed during T8, T30 and T43 flybys (Fig. 2c), concerns folding of the upper crust due to high heat flows from the interior and high temperature gradients in the past (Table 2b). A terrestrial analog, the Rocky Mountains chain in Western-North America (Fig. 3), was formed over an area where high values of mantle heat flow occur (Bird, 1998).

For the high-standing ranges of the T20 radar swath a formation mechanism has been proposed by Sotin et al. (2007) involving the generation of stresses by tectonic extension that penetrate the icy shell and create pathways for the internal material. This finds a terrestrial analog in the formation of the Mid Atlantic Ridge in Atlantic Ocean where divergent tectonic plates are associated with magma upwelling due to partial melting of the upper mantle in the interior.

Other surface features on Titan that seem to be the result of intense forces of tectonic extension are the probable blocks and grabens seen in T8 radar swath (Tobie et al., 2006; Radebaugh et al., 2007). On Earth, the Basin and Range Province in USA (Fig. 4; Table 2b) is such a large terrain subjected to forces of tectonic extension. As it can be seen from Fig. 4 a striking structural similarity exists in the morphology of the T8 mountain range on Titan and the Basin and Range Province on Earth. Alternative proposed mechanisms for *mountain formation* on Titan do not involve crustal movements: Radebaugh et al. (2007) argue that blocks of mountains viewed in T3 swath could have been formed by *impact ejecta*. Such deposits resemble those of Meteor Crater in Arizona, USA where blocks of ejecta deposited 1200 m away from the rim create hilly features (Ramsey, 2002). Furthermore, two terrestrial analogs presented and described in this study that seem to have a major resemblance with *canyon-like* and *cryovolcanic* features seen on Titan, are the Grand Canyon (Fig. 5) and the Harrat Khaybar (Fig. 6). Both terrestrial terrains consist of a number of geological features that have been subject to multiple processes. Titan's surface seems to be as complex as the Earth's and may be the end result of the action of multiple processes as well.

The fact that the mountains and ridges seem to be concentrated around Titan's equatorial band is a very strong argument for tidal forces shaping these morphotectonics features. However, Lopes et al. (2010) showed that mountains exist at other latitudes, a possible sign for a global source of stress as well. It is plausible that radiogenic decay would heat uniformly the entire satellite, similarly to what occurs on Earth (Dickin, 1995), and lead to morphotectonic structures evenly distributed all over the body's crust. We argue, nevertheless, that mountain ranges are more extensive at the equator of the satellite as a result of tidal forces since the very geometry of tides causes local stresses larger at the equator than anywhere else, inducing convection and therefore enhancing mountain formation. This mountain formation can be contrasted with that on Earth where mountains occur globally along collisional plate boundaries. Furthermore, as noted hereabove, radiogenic heat production on small bodies like Titan or even Mars has significantly decreased over a long period of time (e.g., Schubert et al., 1986; Grasset and Sotin, 1996; Grott and Breuer, 2008). It should be noted here that Saturn's tides are still heating up Enceladus' interior (Hurford et al., 2007).

The existence of tectonism on Titan can provide significant insights on the internal structure of the Saturnian satellite. In reference to the terrestrial paradigm, where rigid lithospheric plates '*float*' on a weaker asthenosphere, it could provide indirect evidence for the existence of a subsurface ocean on Titan. The importance of deciphering morphotectonic features on Titan that can be linked to tectonism has also consequences in elucidating the methane cycle on Titan in analogy with the link between terrestrial tectonics and the global terrestrial carbon cycle (Bolin, 1981; Ruddiman, 1997). More specifically, Titan's tectonic activity can probably be directly related to the replenishment of the atmosphere in methane (Sotin et al., 2005; Atreya et al., 2006; Tobie et al., 2006; Coustenis and Taylor, 2008; Lunine and Atreya, 2008; Mitri et al., 2008).

Finally, the origin of some morphological features can be attributed to exogenous processes such as *meteorite impacts* (Moore and Pappalardo, 2011), *aeolian processes* (Stofan et al., 2006; Radebaugh et al., 2009) and *fluvial erosion* (Porco et al., 2005; Tomasko et al., 2005), especially *monsoonal rainfall* causing flooding mainly in the equatorial region (Tokano, 2011).

The Cassini–Huygens mission has significantly improved our understanding of Titan and the coupling of its atmosphere and surface. Since 2004 and for another five years, Titan is investigated by Cassini's flybys. However, only limited surface coverage will be achieved at high spatial resolution. Therefore, the composition and evolution of its diverse surface features will still demand extensive future investigation.

Acknowledgments

The authors are grateful to Julie Castillo, Ellen Stofan and an anonymous referee for extremely constructive and extensive

Please cite this article as: Solomonidou, A., et al., Morphotectonic features on Titan and their possible origin. Planetary and Space Science (2012), http://dx.doi.org/10.1016/j.pss.2012.05.003

comments that have immensely helped in improving the original manuscript. MH and AC acknowledge financial support from the French Agence Nationale de la Recherche (ANR Project: CH4@Titan, PI: Athena Coustenis).

Anezina Solomonidou has been co-financed by the European Union (European Social Fund—ESF) and Greek national funds through the Operational Program "Education and Lifelong Learning" of the National Strategic Reference Framework (NSRF)—Research Funding Program: Heracleitus II. Investing in knowledge society through the European Social Fund.

References

Atreya, S., Adams, E., Niemann, H., Demick-Montelara, J., Owen, T., Fulchignoni, M., Ferri, F., Wilson, E., 2006. Titan's methane cycle. Planetary and Space Science 54, 1177–1187.

Baker, P.E., Brosset, R., Gass, I.G., Neary, C.R., 1973. Jebel al Abyad: a recent alkalic volcanic complex in western Saudi Arabia. Lithos 6, 291–313.

Barnes, J.W., Brown, R.H., Turtle, E.P., McEwen, A.S., Lorenz, R.D., Janssen, M., Schaller, E.L., Brown, M.E., Buratti, B.J., Sotin, C., Griffith, C., Clark, R., Perry, J., Fussner, S., Barbara, J., West, R., Elachi, C., Bouchez, A.H., Roe, H.G., Baines, K.H., Bellucci, G., Bibring, J.P., 2005. A 5-micron-bright spot on Titan: evidence for surface diversity. Science 310, 92–95.

Barnes, J.W., Brown, R.H., Radebaugh, J., Buratti, B.J., Sotin, C., LeMouelic, S., Rodriguez, S., Turtle, E.P., Perry, J., Clark, R., Baines, K.H., Nicholson, P.D., 2006. Cassini observations of flow-like features in western Tui Regio, Titan. Geophysical Research Letters 33, L16204.

Barnes, J.W., Radebaugh, J., Brown, R.H., Wall, S., Soderblom, L., Lunine, J., Burr, D., Sotin, C., Lemouelic, S., Rodriguez, S., Buratti, B.J., Clark, R.N., Baines, K.H., Jaumann, R., Nicholson, P.D., Kirk, R.L., Lopes, R., Lorenz, R.D., Mitchell, K., Wood, C.A., 2007. Near-infrared spectral mapping of Titan's mountains and channels. Journal of Geophysical Research 112, E11006.

Barr, A.C., Pappalardo, R.T., 2005. Onset of convection in ice I with composite Newtonian and non-Newtonian rheology: application to the icy Galilean satellites. Journal of Geophysical Research 110, E12005.

Baumgardner, J.R., 1994. Runaway subduction as the driving mechanism for the Genesis Flood. In: Proceedings of the Third International Conference on Creationism, Technical Symposium Sessions. Creation Science Fellowship, Pittsburgh, pp. 63–75.

Baumgardner, J.R., 2003. Catastrophic plate tectonics: the physics behind the Genesis Flood. In: Proceedings of the Fifth International Conference on Creationism, pp. 113–126.

Beeman, M., Durham, W., Kirby, S., 1988. Friction of ice. Journal of Geophysical Research 93, 7625–7633.

Benn, K., Mareschal, J.-C., Condie, K.C., 2006. Archean geodynamics and environments. Geophysical Monograph Series, 164.

Bird, P., 1998. Formation of the Rocky Mountains, Western United States: a continuum computer model. Science 239, 1501–1507.

Bolin, B., 1981. Carbon Cycle Modelling. Plenum Press, New York.

Brown, R.H., Baines, K.H., Bellucci, G., Bibring, J.-P., Buratti, B.J., Capaccioni, F., Cerroni, P., Clark, R.N., Coradini, A., Cruikshank, D.P., Drossart, P., Formisano, V., Jaumann, R., Langevin, Y., Matson, D.L., McCord, T.B., Mennella, V., Miller, E., Nelson, R.M., Nicholson, P.D., Sicardy, B., Sotin, C., 2004. The Cassini Visual and Infrared Mapping Spectrometer (Vims) Investigation. Space Science Reviews 115, 111–168.

Brown, R.H., Lebreton, J.-P., Waite, J.H., 2009. Titan from Cassini–Huygens. Springer-Verlag, Berlin Heidelberg.

Burr, D.M., Jacobsen, R.E., Roth, D.L., Phillips, C.B., Mitchell, K.L., Viola, D., 2009. Fluvial network analysis on Titan: evidence for subsurface structures and west-to-east wind flow, southwestern Xanadu. Geophysical Research Letters 36, L22203.

Camp, V., Roobol, M., Hooper, P., 1991. The Arabian continental alkali basalt province: Part II. Evolution of Harrats Khaybar, Ithnayn, and Kura, Kingdom of Saudi Arabia. Geological Society of America Bulletin 103, 363–391.

Castillo-Rogez, J., Lunine, J.I., 2010. Evolution of Titan's rocky core constrained by Cassini observations. Geophysical Research Letters 37, L20205.

Chang, S.J., Van der Lee, S., 2011. Mantle plumes and associated flow beneath Arabia and East Africa. Earth and Planetary Science Letters 302, 448–454.

Collins, G.C., McKinnon, W.B., Moore, J.M., Nimmo, F., Pappalardo, R.T., Prockter, L.M., Schenk, P.M., 2009. Tectonics of the outer planet satellites. In: Schultz, R.A., Watters, T.R. (Eds.), Planetary Tectonics. Cambridge University Press, pp. 264–350.

Coustenis, A., Taylor, F.W., 2008. Titan: Exploring an Earth-Like World. World Scientific Publishing.

Coustenis, A., Hirtzig, M., 2009. Cassini–Huygens results on Titan's surface. Research in Astronomy and Astrophysics 9, 249.

Coustenis, A., Gendron, E., Lai, O., Veran, J.-P., Woillez, J., Combes, M., Vapillon, L., Fusco, T., Mugnier, L., Rannou, P., 2001. Images of Titan at 1.3 and 1.6 μm with adaptive optics at the CFHT. Icarus 154, 501–515.

Davies, A.G., Sotin, C., Matson, D., Castillo-Rogez, J., Johnson, T., Choukroun, M., Baines, K., 2010. Atmospheric control of the cooling rate of impact melts and cryolavas on Titan's surface. Icarus 208, 887–895.

Davies, J.H., Davies, D.R., 2010. Earth's surface heat flux. Solid Earth 1, 5–24.

Dickin, A.P., 1995. Radiogenic Isotope Geology. Cambridge University Press.

Dickinson, W.R., Snyder, W.S., 1978. Plate Tectonics of the Laramide Orogeny, 141. Geological Society of America Memoir, Boulder.

Dombard, A.J., McKinnon, W.B., 2006. Folding of Europa's icy lithosphere: an analysis of viscous-plastic buckling and subsequent topographic relaxation. Journal of Structural Geology 28, 2259–2269.

Elachi, C., Allison, M.D., Borgarelli, L., Encrenaz, P., Im, E., Janssen, M.A., Johnson, W.T.K., Kirk, R.L., Lorenz, R.D., Lunine, J.I., Muhleman, D.O., Ostro, S.J., Picardi, G., Posa, F., Rapley, C.G., Roth, L.E., Seu, R., Soderblom, L.A., Vetrella, S., Wall, S.D., Wood, C.A., Zebker, H.A., 2004. Radar: the Cassini Titan Radar Mapper. Space Science Reviews 115, 71–110.

Fagents, S.A., 2003. Considerations for effusive cryovolcanism on Europa: the post-Galileo perspective. Journal of Geophysical Research 108, E12.

Figueredo, P.H., Greeley, R., 2004. Resurfacing history of Europa from pole-to-pole geological mapping. Icarus 167, 287–312.

Flasar, F.M., 1983. Oceans on Titan? Science 221, 55–57.

Fortes, A.D., Grindrod, P.M., Trickett, S.K., Vocadlo, L., 2007. Ammonium sulfate on Titan: possible origin and role in cryovolcanism. Icarus 188, 139–153.

Fowler, A.C., 1986. Thermal runaways in the Earth's mantle. Studies in Applied Mathematics 74, 1–34.

Fulchignoni, M., Ferri, F., Angrilli, F., Ball, A.J., Bar-Nun, A., Barucci, M.A., Bettanini, C., Bianchini, G., Borucki, W., Colombatti, G., Coradini, M., Coustenis, A., Debei, S., Falkner, P., Fanti, G., Flamini, E., Gaborit, V., Grard, R., Hamelin, M., Harri, A.M., Hathi, B., Jernej, I., Leese, M.R., Lehto, A., Lion Stoppato, P.F., López-Moreno, J.J., Mäkinen, T., McDonnell, J.A.M., McKay, C.P., Molina-Cuberos, G., Neubauer, F.M., Pirronello, V., Rodrigo, R., Saggin, B., Schwingenschuh, K., Sieff, A., Simões, F., Svedhem, H., Tokano, T., Towner, M.C., Traunter, R., Withers, P., Zarnecki, J.C., 2005. In situ measurements of the physical characteristics of Titan's environment. Nature 438, 785–791.

Gaidos, E.J., 2001. Cryovolcanism and the recent flow of liquid water on Mars. Icarus 153, 218–223.

Gibbard, S.G., Macintosh, B., Gavel, D., Max, C.E., de Pater, I., Ghez, A.M., Young, E.F., McKay, C.P., 1999. Titan: high-resolution speckle images from the Keck Telescope. Icarus 139, 189–201.

Grasset, O., Sotin, C., 1996. The cooling rate of a liquid shell in Titan's interior. Icarus 123, 101–112.

Griffith, C.A., 1993. Evidence for surface heterogeneity on Titan. Nature 364, 511–513.

Griffith, C.A., Tobias, O., Wagener, R., 1991. Titan's surface and troposphere, investigated with ground-based, near-infrared observations. Icarus 93, 362–378.

Grindrod, P., Fortes, A., Nimmo, F., Feltham, D., Brodholt, J., Vocadlo, L., 2008. The long-term stability of a possible aqueous ammonium sulfate ocean inside Titan. Icarus 197, 137–151.

Grott, M., Breuer, D., 2008. Constraints on the radiogenic heat production rate in the Martian interior from viscous relaxation of crustal thickness variations. Geophysical Research Letters 35, L05201.

Hall, J., Solomon, S., Head, J., 1986. Elysium region, Mars: tests of lithospheric loading models for the formation of tectonic features. Journal of Geophysical Research 91, 11377–11392.

Hawkesworth, C., Turner, S., Gallagher, K., Hunter, A., Bradshaw, T., Rogers, N., 1995. Calc-alkaline magmatism, lithospheric thinning and extension in the basin and range. Journal of Geophysical Research 100, 10271–10286.

Head, J.W., Pappalardo, R.T., Collins, G., Greeley, R., 1997. Tectonic resurfacing on Ganymede and its role in the formation of the grooved terrain. In: Proceedings of the Lunar and Planetary Science Conference, XXIX. Houston, Texas, Abstract 535.

Head, J.W., Pappalardo, R., Collins, G., Belton, M., Giese, B., Wagner, R., Breneman, H., Spaun, N., Nixon, B., Neukum, G., Moore, J., 2002. Evidence for Europa-like tectonic resurfacing styles on Ganymede. Geophysical Research Letters 29, 2151.

Hurford, T.A., Helfenstein, P., Hoppa, G.V., Greenberg, R., Bills, B.G., 2007. Eruptions arising from tidally controlled periodic openings of rifts on Enceladus. Nature 447, 292–294.

Jaumann, R., Roger, C., Nimmo, F., Hendrix, A., Buratti, B., Tilmann, D., Moore, J., Schenk, P., Ostro, S., Srama, R., 2009. Icy satellites: geological evolution and surface processes. Saturn from Cassini–Huygens, 637. Springer.

Jull, M.G., Arkani-Hamed, J., 1995. The implications of basalt in the formation and evolution of mountains on Venus. Physics of the Earth and Planetary Interiors 89, 163–175.

Kargel, J.S., 1994. Cryovolcanism on the icy satellites. Earth, Moon and Planets 67, 101–113.

Kirk, R.L., Howington-Kraus, E., Barnes, J.W., Hayes, A.G., Lopes, R.M., Lorenz, R.D., Lunine, J.I., Mitchell, K.L., Stofan, E.R., Wall, S.D., 2010. La Sotra y las otras: topographic evidence for (and against) cryovolcanism on Titan. AGU, Fall Meet, Abstract P22A-03.

Lebreton, J.-P., Coustenis, A., Lunine, J.I., Raulin, F., Owen, T., Strobel, D., 2009. Results from the Huygens probe on Titan. Astronomy and Astrophysics Review 17, 149–179.

Lidmar-Bergström, K., 1996. Long term morphotectonic evolution in Sweden. Geomorphology 16, 33–59.

Lopes, R.M.C., Mitchell, K.L., Stofan, E.R., Lunine, J.I., Lorenz, R., Paganelli, F., Kirk, R.L., Wood, C.A., Wall, S.D., Robshaw, L.E., Fortes, A.D., Neish, C.D., Radebaugh, J., Reffet, E., Ostro, S.J., Elachi, C., Allison, M.D., Anderson, Y., Boehmer, R., Boubin, G., Callahan, P., Encrenaz, P., Flamini, E., Francescetti, G., Gim, Y., Hamilton, G., Hensley, S., Janssen, M.A., Johnson, W.T.K., Kelleher, K., Muhleman, D.O., Ori, G., Orosei, R., Picardi, G., Posa, F., Roth, L.E., Seu, R., Shaffer, S., Soderblom, L.A., Stiles, B., Vetrella, S., West, R.D., Wye, L.,

Please cite this article as: Solomonidou, A., et al., Morphotectonic features on Titan and their possible origin. Planetary and Space Science (2012), http://dx.doi.org/10.1016/j.pss.2012.05.003

Zebker, H.A., 2007a. Cryovolcanic features on Titan's surface as revealed by the Cassini Titan Radar Mapper. Icarus 186, 395–412.
Lopes, R.M.C., Stofan, E.R., Mitri, G., Robshaw, L.E., Mitchell, K.L., Wood, C.A., Radebaugh, J., Kirk, R.L., Wall, S.D., Lorenz, R., Lunine, J.I., Craig, J., Paganelli, F., Soderblom, L., The Cassini Radar Team, 2007b. Much like Earth: distribution of geologic processes on Titan from Cassini RADAR data. In: Proceedings of the 38th Lunar and Planetary Science Conference. Boulder, Colorado, Abstract 1357, pp. 78–79.
Lopes, R.M.C., Stofan, E.R., Peckyno, R., Radebaugh, J., Mitchell, K.L., Mitri, G., Wood, C.A., Kirk, R.L., Wall, S.D., Lunine, J.I., Hayes, A., Lorenz, R., Farr, T., Wye, L., Craig, J., Ollerenshaw, R.J., Janssen, M., LeGall, A., The Cassini RADAR Team, 2010. Distribution and interplay of geologic processes on Titan from Cassini radar data. Icarus 205, 540–558.
Lorenz, R.D., Lunine, J.I., 2005. Titan's surface before Cassini. Planetary and Space Science 53, 557–576.
Lorenz, R.D., Mitton, J., 2008. Titan Unveiled: Saturn's Mysterious Moon Explored. Princeton University Press.
Lunine, J.L., Atreya, S.K., 2008. The methane cycle on Titan. Nature Geosciences 1, 159–164.
Lunine, J.I., Stevenson, D.J., Yung, Y.L., 1983. Ethane ocean on Titan. Science 222, 1229–1230.
Lunine, J.I., Elachi, C., Wall, S.D., Janssen, M.A., Allison, M.D., Anderson, Y., Boehmer, R., Callahan, P., Encrenaz, P., Flamini, E., Franceschetti, G., Gim, Y., Hamilton, G., Hensley, S., Johnson, W.T.K., Kelleher, K., Kirk, R.L., Lopes, R.M., Lorenz, R., Muhleman, D.O., Orosei, R., Ostro, S.J., Paganelli, F., Paillou, P., Picardi, G., Posa, F., Radebaugh, J., Roth, L.E., Seu, R., Shaffer, S., Soderblom, L.A., Stiles, B., Stofan, E.R., Vetrella, S., West, R., Wood, C.A., Wye, L., Zebker, H., Alberti, G., Karkoschka, E., Rizk, B., McFarlane, E., See, C., Kazeminejad, B., 2008. Titan's diverse landscapes as evidenced by Cassini RADAR's third and fourth looks at Titan. Icarus 195, 415–433.
Manga, M., Wang, C.-Y., 2007. Pressurized oceans and the eruption of liquid water on Europa and Enceladus. Geophysical Research Letters 34, L07202.
McCord, T.B., Hansen, G.B., Buratti, B.J., Clark, R.N., Cruikshank, D.P., D'Aversa, E., Griffith, C.A., Baines, E.K.H., Brown, R.H., Dalle Ore, C.M., Filacchione, G., Formisano, V., Hibbits, C.A., Jaumann, R., Lunine, J.I., Nelson, R.M., Sotin, C., The Cassini VIMS Team, 2006. Composition of Titan's surface from Cassini VIMS. Planetary and Space Science 54, 1524–1539.
McDonald, K.C., 1982. Mid-ocean ridges: fine scale tectonic, volcanic and hydrothermal processes within the plate boundary zone. Annual Review of Earth and Planetary Sciences 10, 155.
McKinnon, W.B., 1998. Geodynamics of icy satellites. In: Schmitt, B., et al. (Eds.), Solar System Ices. Kluwer, Dordrecht, Netherlands, pp. 525–550.
Mège, D., Masson, P., 1996. A plume tectonics model for the Tharsis province, Mars. Planetary and Space Science 44, 1499–1546.
Meier, R., Smith, B.A., Owen, T.C., Terrile, R.J., 2000. The surface of Titan from NICMOS observations with the Hubble Space Telescope. Icarus 145, 462–473.
Melosh, H.J., Nimmo, F., 2011. Long-term strength of icy vs. silicate planetary bodies. In: Proceedings of the 42nd Lunar and Planetary Science Conference. The Woodlands, Texas, Abstract 2306.
Mitri, G., Showman, A.P., 2008. Thermal convection in ice-I shells of Titan and Enceladus. Icarus 193, 387–396.
Mitri, G., Showman, A.P., Lunine, J.I., Lorenz, R.D., 2007. Hydrocarbon lakes on Titan. Icarus 186, 385–394.
Mitri, G., Showman, A.P., Lunine, J.I., Lopes, R.M.C., 2008. Resurfacing of Titan by ammonia–water cryomagma. Icarus 196, 216–224.
Mitri, G., Bland, M.T., Showman, A.P., Radebaugh, J., Stiles, B., Lopes, R.M.C., Lunine, J.I., Pappalardo, R.T., 2010. Mountains on Titan: modeling and observations. Journal of Geophysical Research 115, E10002.
Montgomery, D.R., Brandon, M.T., 2002. Topographic controls on erosion rates in tectonically active mountain ranges. Earth and Planetary Science Letters 201, 481–489.
Moore, J.M., Pappalardo, R.T., 2011. Titan: an exogenic world? Icarus 212, 790–806.
Muhleman, D.O., Grossman, A.W., Butler, B.J., Slade, M.A., 1990. Radar reflectivity of Titan. Science 248, 975–980.
Murchie, S.L., Head, J.W., Helfenstein, P., Plescia, J.B., 1986. Terrain types and local-scale stratigraphy of grooved terrain on Ganymede. Journal of Geophysical Research 91, E222–E238.
Niemann, H.B., Atreya, S.K., Bauer, S.J., Carignan, G.R., Demick, J.E., Frost, R.L., Gautier, D., Haberman, J.A., Harpold, D.N., Hunten, D.M., Israel, G., Lunine, J.I., Kasprzak, W.T., Owen, T.C., Paulkovich, M., Raulin, F., Raaen, E., Way, S.H., 2005. The abundances of constituents of Titan's atmosphere from the GCMS instrument on the Huygens probe. Nature 438, 779–784.
Niemann, H.B., Atreya, S.K., Demick, J., Gautier, D., Haverman, J., Harpold, D., Kasprzak, W., Lunine, J., Owen, T., Raulin, F., 2010. Composition of Titan's lower atmosphere and simple surface volatiles as measured by the Cassini–Huygens probe gas chromatograph mass spectrometer experiment. Journal of Geophysical Research 115, E12006.
Nimmo, F., McKenzie, D., 1998. Volcanism and tectonics on Venus. Annual Review of Earth and Planetary Sciences 26, 23–51.
Pappalardo, R.T., Davis, D.M., 2007. Where's the compression? Explaining the lack of contractional structures on icy satellites. Workshop on Ices, Oceans, and Fire: Satellites of the Outer Solar System, vol. 1357, pp. 108–109.
Pollack, H.N., Hurter, S.J., Johnson, J.R., 1993. Heat flow from the Earth's interior: analysis of the global data set. Reviews of Geophysics 31, 267–280.
Porco, C.C., Baker, E., Barbara, J., Beurle, K., Brahic, A., Burns, J.A., Charnoz, S., Cooper, N., Dawson, D.D., Del Genio, A.D., Denk, T., Dones, L., Dyudina, U., Evans, R.A., Fussner, S., Giese, B., Grazier, K., Helfenstein, P., Ingersoll, A.P., Jacobson, R.A., Johnson, T.V., McEwen, A., Murray, C.D., Neukum, G., Owen, W.M., Perry, J., Roatsch, T., Spitale, J., Squyres, S., Thomas, P., Tiscareno, M., Turtle, E.P., Vasavada, A.R., Veverka, J., Wagner, R., West, R., 2005. Imaging of Titan from the Cassini spacecraft. Nature 434, 159–168.
Prockter, L.M., Head, J.W., Pappalardo, R.T., Sullivan, R.J., Clifton, A.E., Giese, B., Wagner, R., Neukum, G., 2002. Morphology of Europan bands at high resolution: a mid-ocean ridge-type rift mechanism. Journal of Geophysical Research 107, E5.
Radebaugh, J., Lorenz, R.D., Kirk, R.L., Lunine, J.I., Stofan, E.R., Lopes, R.M.C., Wall, S.D., The Cassini Radar Team, 2007. Mountains on Titan observed by Cassini Radar. Icarus 192, 77–91.
Radebaugh, J., Lorenz, R.D., Lunine, J.I., Wall, S.D., Boubin, G., Reffet, E., Kirk, R.L., Lopes, R.M., Stofan, E.R., Soderblom, L., Allison, M., Janssen, M., Paillou, P., Callahan, P., Spencer, C., 2008. Dunes on Titan observed by Cassini Radar. Icarus 194, 690–703.
Radebaugh, J., Lorenz, R.D., Farr, T., Paillou, P., Savage, C., Spencer, C., 2009. Linear dunes on Titan and earth: initial remote sensing comparisons. Geomorphology 121, 122–132.
Radebaugh, J., Lorenz, R.D., Wall, S.D., Kirk, R.L., Wood, C.A., Lunine, J.I., Stofan, E.R., Lopes, R.M.C., Valora, P., Farr, T.G., Hayes, A., Stiles, B., Mitri, G., Zebker, H., Janssen, M., Wye, L., LeGall, A., Mitchell, K.L., Paganelli, F., West, R.D., Schaller, E.L., The Cassini Radar Team, 2011. Regional geomorphology and history of Titan's Xanadu province. Icarus 211, 672–685.
Ramsey, M.S., 2002. Ejecta distribution patterns at Meteor Crater, Arizona: on the applicability of lithologic end-member deconvolution for spaceborne thermal infrared data of Earth and Mars. Journal of Geophysical Research 107, E8.
Raulin, F., 2008. Astrobiology and habitability of Titan. Space Science Reviews 135, 37–48.
Rehman, S., 2010. Saudi Arabian geothermal energy resources an update. In: Proceedings of the World Geothermal Congress, pp. 1–6.
Rice, A., Fairbridge, R.W., 1975. Thermal runaway in the mantle and neotectonics. Tectonophysics 29, 59–72.
Rosenau, M., Oncken, O., 2009. Fore-arc deformation controls frequency-size distribution of megathrust earthquakes in subduction zones. Journal of Geophysical Research 114, B10311.
Ruddiman, W.F., 1997. Tectonic Uplift and Climate Change. Plenum Press.
Scheidegger, A., 2004. Morphotectonics. Springer, Berlin.
Schenk, P., Bulmer, M., 1998. Origin of mountains on Io by thrust faulting and large-scale mass movements. Science 279, 1514–1518.
Schenk, P., McKinnon, W.B., 1985. Dark halo craters and the thickness of grooved terrain on Ganymede. Journal of Geophysical Research 90, 775–C783.
Schubert, G., Spohn, T., Reynolds, R.T., 1986. Thermal histories, compositions and internal structures of the moons of the solar system. Satellites, 224–292.
Schumm, S.A., Dumont, J.F., Holbrook, J.M., 2002. Active Tectonics and Alluvial Rivers. Cambridge University Press, New York.
Sears, J.W., 1990. Geological structure of the Grand Canyon supergroup, Grand Canyon Geology. University Press. (pp. 71–82).
Smith, P.H., Lemmon, M.T., Lorenz, R.D., Sromovsky, L.A., Caldwell, J.J., Allison, M.D., 1996. Titan's surface, revealed by HST imaging. Icarus 119, 336–349.
Soderblom, L.A., Kirk, R.L., Lunine, J.I., Anderson, J.A., Baines, K., Barnes, J., Barrett, J., Brown, R., Buratti, B., Clark, R., Cruikshank, D., Elachi, C., Janssen, M., Jaumann, R., Karkoschka, E., LeMouelic, S., Lopes, R., Lorenz, R., McCord, T., Nicholson, P., Radebaugh, J., Rizk, B., Sotin, C., Stofan, E., Sucharski, T., Tomasko, M., Wall, S., 2007a. Correlations between Cassini VIMS spectra and RADAR SAR images: implications for Titan's surface composition and the character of the Huygens Probe Landing Site. Planetary and Space Science 55, 2025–2036.
Soderblom, L.A., Tomasko, M.G., Archinal, B.A., Becker, T.L., Bushroe, M.W., Cook, D.A., Doose, L.R., Galuszka, D.M., Hare, T.M., Howington-Kraus, E., Karkoschka, E., Kirk, R.L., Lunine, J.I., McFarlane, E.A., Redding, B.L., Bashar, R., Rosiek, M.R., See, C., Smith, P.H., 2007b. Topography and geomorphology of the Huygens landing site on Titan. Planetary and Space Science 55, 2015–2024.
Soderblom, L.A., Brown, R.H., Soderblom, J.M., Barnes, J.W., Kirk, R.L., Sotin, C., Jaumann, R., Mackinnon, D.J., Mackowski, D.W., Baines, K.H., Buratti, B.J., Clark, R.N., Nicholson, P.D., 2009. The geology of Hotei Regio, Titan: correlation of Cassini VIMS and RADAR. Icarus 204, 610–618.
Solomonidou, A., Hirtzig, M., Bratsolis, E., Bampasidis, G., Coustenis, A., Kyriakopoulos, K., Le Mouelic, S., Stephan, K., Jaumann, R., Drossart, P., Sotin, C., Seymour, K., Moussas, X. New processing of Cassini/VIMS data on potentially geologically varying regions, in preparation.
Sotin, C., Jaumann, R., Buratti, B.J., Brown, R.H., Clark, R.N., Soderblom, L.A., Baines, K.H., Bellucci, G., Bibring, J.P., Capaccioni, F., Cerroni, P., Combes, M., Coradini, A., Cruikshank, D.P., Drossart, P., Formisano, V., Langevin, Y., Matson, D.L., McCord, T.B., Nelson, R.M., Nicholson, P.D., Sicardy, B., Le Moue'lic, S., Rodriguez, S., Stephan, K., Scholz, C.K., 2005. Release of volatiles from a possible cryovolcano from near-infrared imaging of Titan. Nature 435, 786–789.
Sotin, C., LeMouelic, S., Brown, R.H., Barnes, J., Soderblom, L., Jaumann, R., Buratti, B.J., Clark, R.N., Baines, K.H., Nelson, R.M., Nicholson, P., VIMS Science Team, 2007. Cassini/VIMS observatoire of Titan during the T20 flyby. In: Proceedings of the 37th Lunar and Planetary Science. League City, Texas, Abstract 2444.
Stiles, B.W., Hensley, S., Gim, Y., Bates, D.M., Kirk, R.L., Hayes, A., Radebaugh., J., Lorenz, R.D., Mitchell, K.L., Callahan, P.S., Zebker, H., Johnson, W.T.K., Wall, S.D., Lunine, J.I., Wood, C.A., Janssen, P.S., Pelletier, F., West, R.D., Veeramacheneni, C., The Cassini RADAR Team, 2009. Determining Titan surface topography from Cassini SAR data. Icarus 202, 584–598.

Please cite this article as: Solomonidou, A., et al., Morphotectonic features on Titan and their possible origin. Planetary and Space Science (2012), http://dx.doi.org/10.1016/j.pss.2012.05.003

Stofan, E.R., Lunine, J.I., Lopes, R., Paganelli, F., Lorenz, R.D., Wood, C.A., Kirk, R.L., Wall, S., Elachi, C., Soderblom, L.A., Ostro, S., Janssen, M., Wye, L., Zebker, H., Anderson, Y., Allison, M., Boehmer, R., Callahan, P., Encrenaz, P., Flamini, E., Francescetti, G., Gim, Y., Hamilton, G., Hensley, S., Johnson, W., Kelleher, K., Muhleman, D., Picardi, G., Posa, F., Roth, L., Seu, R., Shaffer, S., Stiles, B., Vetrella, S., West, R., 2006. Mapping of Titan: results from the first Titan radar passes. Icarus 185, 443–456.

Stofan, E.R., Elachi, C., Lunine, J.I., Lorenz, R.D., Stiles, B., Mitchell, K.L., Ostro, S., Soderblom, L., Wood, C., Zebker, H., Wall, S., Janssen, M., Kirk, R., Lopes, R., Paganelli, F., Radebaugh, J., Wye, L., Anderson, Y., Allison, M., Boehmer, R., Callahan, P., Encrenaz, P., Flamini, E., Francescetti, G., Gim, Y., Hamilton, G., Hensley, S., Johnson, W.T.K., Kelleher, K., Muhleman, D., Paillou, P., Picardi, G., Posa, F., Roth, L., Seu, R., Shaffer, S., Vetrella, S., West, R., 2007. The lakes of Titan. Nature 445, 61–64.

Tobie, G., Grasset, O., Lunine, J.I., Mocquet, A., Sotin, C., 2005. Titan's internal structure inferred from a coupled thermal-orbital model. Icarus 175, 496–502.

Tobie, G., Lunine, J.I., Sotin, C., 2006. Episodic outgassing as the origin of atmospheric methane on Titan. Nature 440, 61–64.

Tokano, T., 2011. Precipitation climatology on Titan. Science 331, 1393–1394.

Tomasko, M.G., Archinal, B., Becker, T., Bézard, B., Bushroe, M., Combes, M., Cook, D., Coustenis, A., de Bergh, C., Dafoe, L.E., Doose, L., Douté, S., Eibl, A., Engel, H.U., Gliem, F., Grieger, B., Holso, K., Howington-Kraus, E., Karkoschka, E., Keller, H.U., Kirk, R., Kramm, R., Küppers, M., Lanagan, P., Lellouch, E., Lemmon, M., Lunine, J., McFarlane, E., Moores, J., Prout, G.M., Rizk, B., Rosiek, M., Rueffer, P., Schröder, S.E., Schmitt, B., See, C., Smith, P., Soderblom, L., Thomas, N., West, R., 2005. Rain, winds and haze during the Huygens probe's descent to Titan's surface. Nature 438, 765–778.

Wall, S.D., Lopes, R.M.C., Stofan, E.R., Wood, C.A., Radebaugh, J.L., Horst, S.M., Stiles, B.W., Nelson, R.M., Kamp, L.W., Janssen, M.A., Lorenz, R.D., Lunine, J.I., Farr, T.G., Mitri, G., Paillou, P., Paganelli, F., Mitchell, K.L., 2009. Cassini RADAR images at Hotei Arcus and western Xanadu, Titan: evidence for geologically recent cryovolcanic activity. Geophysical Research Letters 36, L04203.

Williams, D.A., Radebaugh, J., Lopes, R.M.C., Stofan, E., 2011. Geomorphologic mapping of the Menrva region of Titan using Cassini RADAR data. Icarus 212, 744–750.

Wilson, T.Z., 1973. Mantle plumes and plate motions. Tectonophysics 19, 149–164.

Zarnecki, J.C., Leese, M.R., Hathi, B., Ball, A.J., Hagermann, A., Towner, M.C., Lorenz, R.D., McDonnell, J.A.M., Green, S.F., Patel, M.R., Ringrose, T.J., Rosenberg, P.D., Atkinson, K.R., Paton, M.D., Banaszkiewicz, M., Clark, B.C., Ferri, F., Fulchignoni, M., Ghafoor, N.A.L., Kargl, G., Svedhem, H., Delderfield, J., Grande, M., Parker, D.J., Challenor, P.G., Geake, J.E., 2005. A soft solid surface on Titan as revealed by the Huygens surface science package. Nature 438, 792–795.

Please cite this article as: Solomonidou, A., et al., Morphotectonic features on Titan and their possible origin. Planetary and Space Science (2012), http://dx.doi.org/10.1016/j.pss.2012.05.003

Appendix A4

Candidate regions on Titan as promising landing sites for future in situ missions

Journal article in press submitted in the proceedings of the *International Planetary Probe Workshop*-10 (2013)

CANDIDATE REGIONS ON TITAN AS PROMISING LANDING SITES FOR FUTURE IN SITU MISSIONS

Solomonidou Anezina (1,2), Coustenis Athena(1), Jaumann Ralf(3), Stephan Katrin(3), Sohl Frank(3), Hussmann Hauke(3), Hirtzig Mathieu(4,1), Bampasidis Georgios(1,5), Bratsolis Emmanuel(5), Moussas Xenophon(5), Kyriakopoulos Konstantinos(2).

(1) LESIA - Observatoire de Paris, CNRS, UPMC Univ. Paris 06, Univ. Paris-Diderot –Meudon, France, (Athena.Coustenis@obspm.fr)
(2) National and Kapodistrian University of Athens, Department of Geology and Geoenvironment, Athens, Greece, (asolomonidou@geol.uoa.gr)
(3) DLR, Institute of Planetary Research, Berlin, Germany, (Ralf.Jaumann@dlr.de)
(4) Fondation La Main à la Pâte, Montrouge, France, (mathieu.hirtzig@fondation-lamap.org)
(5) National and Kapodistrian University of Athens, Department of Physics, Athens, Greece, (xmoussas@phys.uoa.gr)

ABSTRACT

The highly successful and still on-going Cassini-Huygens mission to the Saturnian system points to the need for a return mission, with both remote and *in situ* instrumentation. The surface of Saturn's moon Titan, hosts a complex environment in which many processes occur shaping its landscape. Several of its geological features resemble terrestrial ones, albeit constructed from different material and reflecting the interior-surface-atmosphere exchanges. The resulting observed morphotectonic features and cryovolcanic candidate regions could benefit from further extensive exploration by a return mission that would focus on these aspects with adapted state-of-the-art instrumentation affording higher spectral and spatial resolution and *in situ* capabilities. We suggest that some features on Titan are more promising candidate locations for future landing and we present the case for Tui Regio, Hotei Regio and Sotra Patera as to why they could provide a wealth of new scientific results.

1. INTRODUCTION

Data retrieved from the Visual and Infrared Mapping Spectrometer (VIMS) [1], the Synthetic Aperture Radar (SAR) and RADAR [2] and the Imaging Science Subsystem (ISS) [3] aboard Cassini and the instruments on board the Huygens probe supplied information regarding Titan's atmosphere, surface composition and morphology. This detailed approach on Titan's geological environment has classified it as extremely interesting due to its complex surface composition. A combination with unique geological features [4, 12, 20] make Titan a prime candidate for geological, internal and surface *in situ* investigation. Multiple flybys (91 to this date) of the NASA/ESA Cassini-Huygens spacecraft, which is still in commission, brought into light surficial expressions that were not expected to be observed on an icy surface. Many of them have counterparts in Earth geology, but the materials in play are different. The diversity of surface formational mechanisms include potential cryovolcanism on a number of areas such as Tui Regio (20°S, 130°W), Hotei Regio (26°S, 78°W) and Sotra Patera (15°S, 42°W) [4]. In this work, we actually focus on these areas from VIMS and RADAR data. The two cameras of Cassini/VIMS have observed the surface of the candidate areas at visible and infrared wavelengths, giving insights about their composition. Furthermore, the Cassini/RADAR with SAR acquires topographic pictures using microwaves, penetrating Titan's hazy thick atmosphere. Combined investigations specifically of Hotei Regio and Sotra Patera suggest that both instruments are in agreement with results pointing to a variety of geological processes having occurred in the past [4, 5] or recently [6], possibly indicating cryovolcanism. Indeed, data correlation and analysis from VIMS and RADAR provided us with images and mosaics combining both spectral and morphological information [4]. However, the problem of atmospheric haze scattering and particle absorption is still present, making surficial imaging ambiguous unless a complete and accurate modelling of the atmospheric contribution is performed. In our processing VIMS and RADAR data, we take into account the atmospheric effect and photometric corrections, as well as filtering with a view to produce constraints on the surficial chemical composition and morphology. The evidence of such interesting areas like Tui Regio, Hotei Regio and Sotra Patera as it will be shown hereafter, enhances the significance of a future mission to Titan with *in situ* capabilities [7,8].

2. GEOLOGY OF AREAS OF INTEREST

In general, Titan's surface appears to host diverse types of both smooth and rough areas of various relief types, which - among other - include volcanic-like features and impact craters that are intermittently filled by atmospheric precipitations which have been reported [9, 10]. In addition, Titan exhibits topographic features such as mountains, ridges, faults, and aeolian and fluvial features such as dunes and lakes. Chronologically, the surficial geological features are young and unique for a celestial satellite [11].

The geological terrains of Tui Regio, Hotei Regio, and Sotra Patera are the main focus of this study and they are proposed as interesting candidates for future landing sites. The wealth of data acquired from VIMS and RADAR on board Cassini spacecraft and their analysis with specific software provide the evidence as to why [4, 5, 21, 24]. These candidate regions consist of diverse geomorphology, possible surface albedo changes with time and a correlation with the interior's high zones of tidal potential. Not only have the data revealed the uniqueness of all three areas by means of morphological aspects such as caldera-like features, a deep crater, high mountains and lobate flows, but also depicted the variability in composite component. Moreover, Tui, Hotei and Sotra are the only ones among the cryovolcanic candidate regions as in [4] that appear anomalously bright at 5μm and have been observed adequately by VIMS for a temporal variation study. The candidate regions for *in situ* investigations should combine atmospheric, surficial, near sub-surficial and deep internal investigations [12]. If

the cryovolcanic origin of Tui, Hotei and Sotra is identified, they will stand as case study areas for all the aforementioned investigations.

a) **Tui Regio**

Tui Regio (20°S-130°W) is one of the areas which was observed as anomalously bright at 5μm wavelength and therefore constitutes a component of the most reliable evidence yet obtained concerning the activity of cryovolcanism on Titan's surface (Fig. 1). Tui Regio consists of a flow-like figure 150 km-wide and extends for 1,500 km in an East-West direction [13]. Theories suggest that it may be geologically young and that the resembling lava flows could be deposits of cryovolcanic activity. The analysis of Cassini ISS and mainly VIMS data suggest that the area is a massive flow field since at least three long lobate spectrally distinct tendrils [13] have been observed and have possibly being effused from a main point like a caldera-like structure, fracture or fissure. The observed geological surficial expressions such as calderas, ejecta deposits, alluvial terrains, flows, the low basin and more, depict the imprints of dynamic activities. The area has been characterized by [14] as a spectrally distinct unit in composition, especially because of its anomalous brightness at 5 μm, which has been confirmed by using updated VIMS maps from [15]. Reference [16] proposed that Tui Regio could be an active centre of cryovolcanism. Reference [13] suggested that a flow-like feature in the western part of Tui Regio could represent past cryovolcanic activity based on its morphology, relative age and chemical composition.

b) **Hotei Regio**

Hotei Regio is a 700 km-wide area that is probably volcanic in origin [4, 5] (Fig. 1). The Cassini SAR images confirm the interpretation that the area is a low basin surrounded by higher terrains with possible calderas, fault features and extensive cryovolcanic flows. Reference [5] have studied the area and indicated significant geological features that resemble terrestrial volcanic features. These are viscous flow-like figures, a 1 km mountainous terrain (ridge-like) that surrounds the basin as well as dendritic channels, caldera-like features, dark blue patches (in RGB coloring) and possibly alluvial deposits. Processing of RADAR images showed that Hotei Regio is a low basin depression, (as expected to be observed in a volcanic terrain) one km deep. It is filled with terrestrial volcanic-like flows that are 100 to 200 km thick. The peripheral area lying at higher altitudes has rough as well as smooth texture. This means the surrounded formations are probably alluvial deposits [5]. The ring-fault-like structures seen within the basin present possibly a caldera-like feature. Hotei Regio is the first Titan area that has been reported to exhibit changes in brightness with time from July 2004 until March 2006 [6]. Reference [6] described evidence for photometric variability on Hotei Regio by analyzing VIMS data, which could be linked to cryovolcanism and ammonia deposits.

Alternatively, Tui and Hotei Regio have been suggested to be sites of large low latitude paleolakes based on estimations of Titan's topography [17]. In addition, reference [19] suggested the presence of dry lakebeds at Titan's north pole with spectral characteristics similar to Tui and Hotei Regio, suggesting a common evaporitic origin. Recent studies [18] also suggested that the areas are the result of exogenic deposits, either fluvial or lacustrine.

c) **Sotra Patera** (formerly known as Sotra Facula)

Sotra Patera, a 235 km in diameter area, has recently been identified as an additional potential cryovolcanic feature [4] and is currently under investigation by means of endogenic processes that might have shaped it (Fig. 1). Reference [4] have found that there are two peaks more than 1-km high and one deep volcanic crater (1-km deep) and finger-like lobate flows.

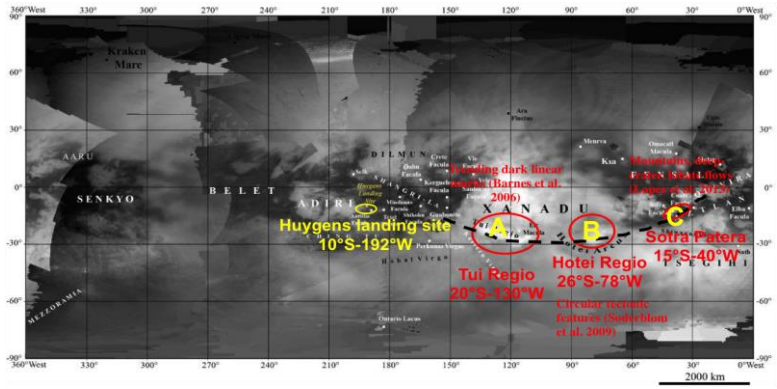

Fig. 1. Map of Titan's indicating three promising landing sites: Tui Regio (A), Hotei Regio (B), Sotra Patera (C) [21].

3. IMAGE PROCESSING

In order to understand Titan's geology and evolution, it is critical to investigate and identify the chemical composition of the areas of interest. The VIMS instrument acquired many spectral images from several flybys in the interest of chemical composition analysis. Even though many images captured parts of the surface, the fact that Titan possesses an extended, hazy and dense atmosphere suggests a major constraint on data accuracy. As mentioned earlier for our study case, observations from VIMS in 352 wavelengths have indicated three anomalously bright areas, Tui Regio, Hotei Regio and Sotra Patera. All three areas are imaged in narrow spectral windows centered at 0.93, 1.08, 1.27, 1.59, 2.03, 2.8 and 5 μm, through Titan's thick atmosphere. Despite the weak atmospheric methane absorption within theses windows, the surficial imaging is still ambiguous due to haze scattering and particle absorption. Our goal is to obtain relatively clear surface images without the interference of the atmospheric contribution. Atmospheric scattering and absorption need to be clearly evaluated before we can extract the surface properties.

We are sequentially using two methods in order to acquire the optimal result from the data set [21]. First, the Principal Component Analysis (PCA), which is a statistical method, de-correlates the features visible on many similar images into a new set of images that show the main features only, sorted by frequency of appearance. We have tested this method on the previously studied Sinlap crater [22], delimitating compositional heterogeneous areas compatible with the published conclusions. Secondly, the radiative transfer method is a 1-D multi-stream radiative transfer (RT from now on) code based on the open-source solver SHDOMPP [23]. We have used as inputs most of the Huygens Atmospheric Structure Instrument (HASI) and the Descent Imager/Spectral Radiometer (DISR) measurements, as well as new methane absorption coefficients, which are important to evaluate the atmospheric contribution and to allow us to better constrain the real surface alterations, by comparing the spectra of these regions [21]. Figure 2 presents the surface albedo ratios from RT as selected with PCA (Regions of Interest –RoI) of the brightest (red) and the darkest (green) RoIs.

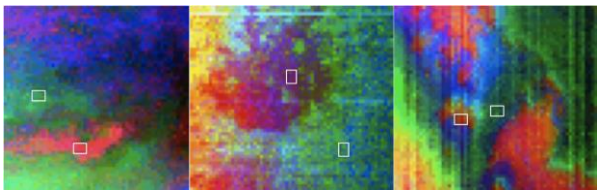

Fig. 2. PCA on VIMS data (the red spot marks the brightest RoI and the green the darkest) using specific Principal Components (PCs) for each data cube [21].

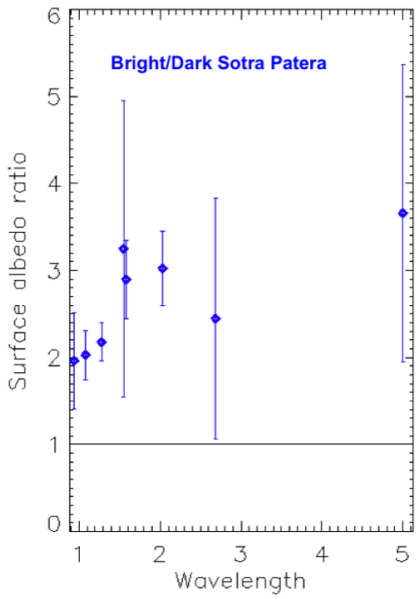

Fig. 3. Retrieval of surface albedo ratios with radiative transfer between the brightest and the darkest Sotra Patera RoIs with respect to the Huygens landing site albedo -HLS (black horizontal line) [21].

Furthermore, we study the temporal surface variations of the three regions at all wavelengths (Fig. 4). In order to validate our results we applied the same method for the same periods of time on two dark dunes fields as test cases and did not find any changes in surface albedo.

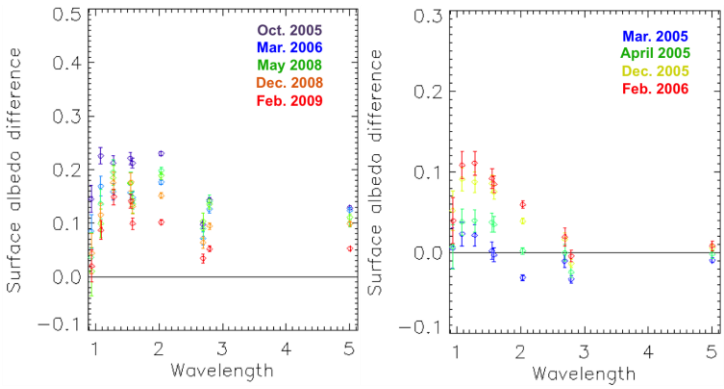

Fig. 4. Temporal variation of the average surface albedo of Tui Regio (2005-2009) (left) and the Sotra Patera area (2005-2006) (right) [24]. The surface albedo differences (with respect to HLS) with time from radiative transfer application on VIMS data from 2005 (purple points) to 2009 (red points) showing that within 3.5 years Tui Regio has decreased in brightness while from 2005 (blue points) to 2006 (red points) Sotra Patera has increased in brightness. The dark line always corresponds to HLS surface albedo [24].

4. RESULTS

We have isolated 2 regions (RoIs) in Tui Regio, Hotei Regio and Sotra Patera with PCA that have different spectral response as shown by the radiative transfer simulation [21]. The dynamical range in surface albedo within the three areas indicates that the bright RoIs are always brighter than the dark ones by significant amounts. For Tui Regio and Hotei Regio the largest differences in surface albedo are in the longer wavelengths while for Sotra Patera the offsets are rather homogenously distributed throughout the spectrum with the largest ones at 5μm. We then study the temporal surface variations of the three regions.

Our findings indicate a significant darkening for Tui Regio from 2005-2009 (at all wavelengths). For Sotra Patera a brightening is observed from 2005-2006 (Fig. 4) [24]. On the contrary, the dunes fields' test cases did not change with time. Hotei Regio has been previously suggested to present brightness variations over a two-year period (2004-2005) [6]. However, we find that to-date available observations of that region present issues (e.g. geometry) prevent an accurate application of our RT model to infer surface information with the desired

accuracy. The surface albedo variations together with the presence of volcanic-like morphological features suggests that the cryovolcanic candidate features are connected to the satellite's deep interior, which could have important implications for the satellite's astrobiological potential. This idea has been recently augmented by the construction of new interior structure models of Titan and corresponding calculations of the spatial pattern of maximum tidal stresses at the satellite's surface [25]. Tui Regio, and Sotra Patera are found to be situated in most prominent tidally flexed zones (yellow) on Titan's, thereby enhancing the possibility of tide-induced weakening and the generation of cryovolcanically 'active' zones (Fig. 5).

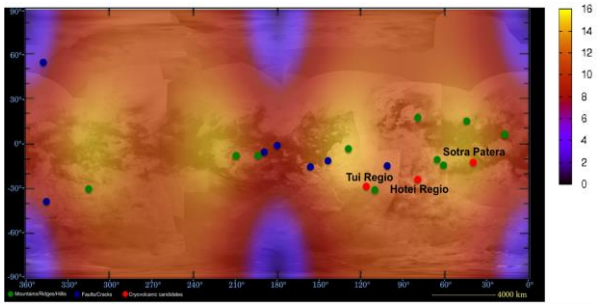

Fig. 5. Map showing the correlation between cryovolcanic candidate regions and the maximum tidal stress pattern (color-coded)[25].

5. LANDING SITES

The suggestion of Tui Regio, Hotei Regio and Sotra Patera as landing sites (Fig. 6) is based on their geomorphological variability as well as the expected compositional alterations of all areas. A crucial point of such selection is the determination of investigation and sampling after landing. A potential lander, like the Huygens probe should be capable to land on a solid surface and carry a fully instrumented robotic laboratory down to the surface. The lander's principal function is to sample and analyze grains attributed from regions of the surface within the areas of interest that lie at the margins of alternative structures (i.e. the area where two geological edifices/plains conjunct). Since all three areas have been suggested to be cryovolcanic in origin, the sampling process should be treated similarly as on terrestrial volcanic terrains. Tui Regio is possibly an accumulation of cryolava flows forming a massive flow. Ideal *in situ* and remote imaging of the Tui Regio area should comprise sampling from diverse regions by means of chemical composition and morphology. Such regions could be the main part of the flow, the marginal areas, and the surrounding terrain, which is considered as the primary material on which possible cryovolcanic material deposited. Since *in situ* imaging of multiple areas, which are considerably distant between them, is impossible, then the selection of a landing area is restricted to an area that presents spectral scientific interest. Such area could be the margin between the flow-like feature and the "old" spectrally dark terrain (Fig. 6 -left).

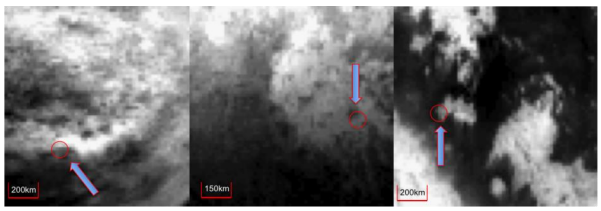

Fig. 6. Areas of potential landing on Tui Regio (left), Hotei Regio (middle) and Sotra Patera (right).

Hotei Regio presents a more complex geological terrain than Tui Regio in terms of morphology as seen from the current data. As mentioned before (Section 2), central Hotei Regio is a low basin consisting of caldera-like figure, flows, channels, and faults while mountains surround it. Data processing showed that the area suggested to be cryovolcanic is different from its surroundings in terms of surface albedo [21]. This is compatible with terrestrial caldera structures that consist partially of primal surficial components on which the volcano is being build as well as newly fresh material coming from the interior. Potential sampling and identification of the chemical composition of both the surrounding dark area and the material from the caldera-like feature could bring into light significant information regarding internal processing on Titan. Thus, the landing region proposed is the margin area lying between the largest caldera within Hotei Regio's terrain and the bright component that surrounds the caldera (Fig. 6 -middle).

For Sotra Patera, that consists of a topographically diverse terrain with a 1-km crater (Sotra Patera), two mountains (Doom and Erebor Monters) and a lobate flow region (Mohini Fluctus) [4] a potential landing site option should be carefully selected having in mind the safety of the landing (Fig. 6 -right). Thus, it seems that the lobate flow region is a safe and scientifically interesting option since the *in situ* identification of the material covering such feature will provide insights regarding the unknown material of the 5μm anomalously bright regions.

6. FUTURE EXPLORATION – SOME TITAN MISSION CONCEPTS

Undoubtedly, the Cassini-Huygens mission has provided us with valuable data that have expanded our knowledge. However, there are still aspects, especially regarding the surface that are not yet covered, along with several unanswered questions. The revelation of Titan's surface will be a key point to unveil the atmosphere and the interior but also a major contribution to icy moons' understanding. After having evaluated Cassini-Huygens mission's data, it is now clear how important it is to acquire direct sampling of the surface and have mobility in the near-surface environment. Thus, we should have the opportunity to map Titan on a global scale from orbit and visit other targets in the Saturn system. The geological objectives request landing site measurements of the *in situ* geological context, chemical composition by several types of spectroscopy, mineralogy provided by infrared data and petrological properties such as porosity, grain size, permeability and more [12]. This could be achieved with measurements from close range of scientifically interesting areas with a montgolfière which could explore close-up the surface and also perhaps crash onto the surface and get measurements [26]; and/or a lander that will descend in an equatorial or polar region and make measurements of solid ground or a liquid.

Therefore, a future mission focusing on this Earth-like world is important, with a dedicated orbiter and *in situ* elements. Such concepts have been proposed in the past, like Titan Explorer [28], TandEM [7], the Titan Saturn System Mission (TSSM) [26], the Titan Aerial Explorer (TAE) [30], the Aerial Vehicle for In-situ and Airborne Titan Reconnaissance (AVIATR) [29] and the Titan Mare Explorer (TiME) [32].

The TSSM mission was a merge of the Titan explorer [31] and the Titan and Enceladus Mission [7] concepts, which had been selected respectively by NASA and ESA for studies. TSSM was studied in 2008 [26]. It has to do an in-depth long-term exploration of Titan's atmospheric and surface environment and in situ measurements in one of Titan's lakes with the goals to explore Titan as an Earth-like System, examine Titan's organic inventory and explore also Enceladus and Saturn's magnetosphere. To achieve these goals, a dedicated orbiter would carry two in situ elements: the Titan montgolfière (hot air balloon) and the Titan Lake Lander, which would combine to provide data and analyses directly in the atmosphere, on the surface and sound the interior of Titan. The mission would launch in the 2023-2025 timeframe on a trajectory using Solar Electric Propulsion (SEP), as well as gravity assists, to arrive ~9 years later for a 4-year mission in the Saturn system. Soon after arrival at Saturn, the montgolfière would be delivered to Titan. The TSSM three elements would operate as follows:

a) The orbiter, using nuclear power, would perform 7 close-up Enceladus' flybys and then enter into orbit around Titan for 2 years of dedicated observations.

b) The hot air balloon would probe both Titan's atmosphere and surface from above the equator and a low altitude orbit of 10 km for at least six months using MMRTGs.

c) The Lake Lander would perform the first extraterrestrial oceanographic experiment by landing in one of the Titan's lakes, the Kraken Mare at approximately 75° N.

The TSSM concept was designed to carry the adapted instrumentation in order to study the atmosphere, the surface as well as the subsurface. The surface exploration payload included specific instruments on-board the orbiter, such as a high-resolution imager and spectrometer that is capable to acquire spectra at 1–6 μm and perform global mapping at 50 m/pixel in three colors, which would greatly improve the spectral data to an extremely high extend, considering that the current resolution from images acquired from Cassini/VIMS observations of Tui Regio, Hotei Regio and Sotra Patera range between 12-150 km/pixel. Another important part of the payload would be the Penetrating Radar and Altimeter instrument that could obtain global mapping of subsurface reflectors with 10 m altitude resolution in altimetry mode and more than 10 m depth resolution with roughly 1 km x 10 km spatial resolution. Furthermore, a montgolfière travelling over 10,000 km in linear

distance could image and map Titan's diverse landscapes at close range. The TSSM montgolfière would contain instrumentation such as a Balloon Imaging Spectrometer, a Visual Imaging System and also a Titan Radar Sounder (>150 MHz) for more than a year. In addition to topography, the radars on both the orbiter and the montgolfière will provide information on the tectonics and stratigraphy of the crust with different and complementary resolution. TSSM is planned to have the ability to examine in detail the lakes and their surrounding environment through the probe entry, descent and landing of a lake lander, which could also include efficient electronic equipment focusing on the study of the liquid its self, like MEMS (Micro-Electro-Mechanical Systems) instrumentation. The proposal of MEMS as part of the science surface properties package on board of a future Lake Lander on Titan, reinforces such kind of research [27]. MEMS devices offer a low cost and reduced size of instrumentation in order to accomplish the 3D sounding of the liquid deposit and detect the presence of any biomarkers in a broader area. By dramatically reducing the production cost without decreasing the efficacy, these micro devices can execute scientific investigations in places and micro scales never imagined before.

This mission came second in the decision by the agencies and was abandoned, however it inspired several other proposed concepts for smaller size missions, like the following.

- Titan Aerial Explorer (TAE) was an M3 candidate for ESA's Cosmic Vision call [30]. TAE was a balloon, which was planned to fly in the lower atmosphere of Titan at an altitude of 8 km from 3 to 6 months on Titan's equatorial latitudes, with Direct to Earth transmission and no need for an orbiter.

- The Aerial Vehicle for In-Situ and Airborne Titan Reconnaissance (AVIATR) was an alternative idea to the Titan balloon. In Titan's low gravity and a dense atmosphere, a nuclear powered airplane could fly more easily than on Earth and could sample directly the atmosphere over large swaths of Titan's surface [29].

- The Titan Mare Explorer (TiME), a Discovery candidate, is a probe focusing on exploring Titan's lakes and especially the Ligeia mare. This lake lander could study the chemical composition and the geological characteristics of the hydrocarbon pools [32]. Adjacent to this idea, was the Titan Lake Probe which included a submarine [33].

- Another Discovery candidate was the Journey to Enceladus and Titan (JET), a simple orbiter with two instruments only and radio science that would explore the plumes of Enceladus and the atmosphere and surface of Titan [34].

- A seismic network proposed as part of the geophysical payload of such missions [28], resembling a geophone array widely used on the Earth, capable of detecting ground motions caused by natural or controlled sources.

Discussions on future missions to Titan, beyond the end of the *Cassini* mission in 2017, are already underway with proposals for aerial explorers, such as airplanes or balloons (as discussed here above), and dune and lake landers that will more thoroughly investigate this complex world.

7. SUMMARY

Titan's spectacular surficial terrain requires further and deeper investigation. The identification of ongoing processes on the surface will reveal the internal, sub-surficial and atmospheric processes as well, giving an holistic view on Titan's evolution. Tui Regio, Sotra Patera and Hotei Regio are some of Titan's cryovolcanic candidates [4] with the first two probably subject to changes in surface albedo with time. The indications of multivariable processes occurring in all three areas, identifies them as desirable candidate landing sites for a lander that could measure the chemical composition as well as detect the geological properties of each area. Future in situ explorations with landers and close-up *in situ* elements would be the way to go for such investigations.

8. REFERENCES

[1] Brown R. H et al. The Cassini Visual And Infrared Mapping Spectrometer (Vims) Investigation. Space Sci. Rev., Vol. 115, 111-168, 2004.

[2] Elachi C., et al. Radar: The Cassini Titan Radar Mapper. Spa. Sci. Reviews, Vol. 115, 71-110, 2004.

[3] Porco C. C., et al. Cassini Imaging Science: Instrument Characteristics And Anticipated Scientific Investigations At Saturn. Space Sci. Rev., Vol. 115, 363-497, 2004.

[4] Lopes R. M. C., et al. Cryovolcanism on Titan: New results from Cassini RADAR and VIMS. J. of Geophys. Res., Vol. 118, 416-435, 2013.
[5] Soderblom, L. A., et al. The geology of Hotei Regio, Titan: Correlation of Cassini VIMS and RADAR. Icarus, Vol. 204, 610-618, 2009.
[6] Nelson R. M., et al. Saturn's Titan: Surface change, ammonia, and implications for atmospheric and tectonic activity. Icarus, Vol. 199, 429-441, 2009.
[7] Coustenis A et al. TandEM: Titan and Enceladus mission. *Exp. Astronomy,* Vol. 23, 893, 2009.
[8] Reh K., et al. Titan Saturn System Mission Study. *Bull. Americam Astr. Soc.,* Vol. 41, 9, 2008.
[9] Tokano T., et al. Methane drizzle on Titan. *Nature,* Vol. 442, 432, 2006.
[10] Tomasko M. G., et al. Rain, winds and haze during the Huygens probe's descent to Titan's surface. *Nature,* Vol. 438, 765 – 778, 2005.
[11] Mahaffy R. Intensive Titan Exploration Begins. *Science,* Vol. 308, 969, 2005.
[12] Jaumann R., Scientific Objectives and Engineering Constraints of Future Titan Landing Sites. *IPPW-7 Workshop*, Barcelona, 2010.
[13] Barnes J. W., et al. Cassini observations of flow-like features in western Tui Regio, Titan. *Geophys. Res. Lett.,* 33, L16204, 2006.
[14] McCord T. B., et al. Titan's surface: Search for spectral diversity and composition using the Cassini VIMS investigation. *Icarus,* Vol. 194, 212-242, 2008.
[15] Vixie G., et al. Mapping Titan's surface features within the visible spectrum via Cassini VIMS. *Planet. Space Sci.*, Vol. 60, 52-61, 2012.
[16] Hayne P., et al. Titan's Surface Composition: Constraints from Laboratory Experiments and Cassini/VIMS Observations. *LPSC XXXIX,* 9093, 2008.
[17] Moore J. M., and A. D. Howard. Are the basins of Titan's Hotei Regio and Tui Regio sites of former low latitude seas? *Geophys. Res. Lett.,* Vol. 37, L22205, 2010.
[18] Moore J. M., and R. T. Pappalardo. Titan: an exogenic world? *Icarus,* Vol. 212, 790-806, 2011.
[19] Barnes J. W., et al. Organic sedimentary deposits in Titan's dry lakebeds: Probable evaporite. *Icarus,* Vol. 216, 136-140, 2011.
[20] Solomonidou A., et al. Morphotectonic features on Titan and their possible origin. *Planet. Space. Sci.*, Vol. 77, 104-117, 2013.
[21] Solomonidou A., et al. Surface albedo spectral properties of geologically interesting areas on Titan. *Submitted.*
[22] Le Mouélic S., et al. Mapping and interpretation of Sinlap crater on Titan using Cassini VIMS and RADAR data. *J. Geophys. Res.*, Vol. 113, E04003, 2008.
[23] Hirtzig M., et al. Titan's surface and atmosphere from Cassini/VIMS data with updated methane opacity. *Icarus, in press.*
[24] Solomonidou A., et al. Temporal Variations Of Titan's Surface Regions With Cassini/VIMS. *In prep.*
[25] Sohl F., et al. Tides on Titan. *AOGS 10th Annual Meeting, Brisbane, Australia*, PS09-A001, 2013.
[26] TSSM NASA/ESA Joint Summary Report, ESA-SRE(2008)3, *JPL D-48442, NASA Task Order* NMO710851, 2009.
[27] Bampasidis, G., et al. Sounding the interior of Titan's lakes by using Micro-Electro-Mechanical Systems (MEMS). *Proceedings of the International Conference on Space Technology*, 2011.
[28] Lorenz R., et al. The Case for a Titan Geophysical Network Mission. White paper, *Solar System Decadal Survey*, 2009.
[29] Barnes J.W., et al. **AVIATR – Aerial Vehicle for In-situ and Airborne Titan Reconnaissance. A Titan airplane mission concept. *Experimental Astronomy*, Vol. 33, 55-127, 2012.**
[30] Hall J., et al. Titan Aerial Explorer (TAE): Exploring Titan By Balloon. *JPL report*, 2011.
[31] Leary J.C., et al. Titan Explorer Flagship Mission Study. *NASA's Planetary Science Division*, 2008.
[32] Stofan E., et al., Titan Mare Explorer (TiME): First In Situ Exploration of an Extraterrestrial Sea, LPSC, Woodlands, TX, USA, 2011.
[33] Waite H., et al. Titan Lake Probe: The Ongoing NASA Decadal Study Preliminary Report. *EGU*, Vienna, Austria, 2010.
[34] Sotin C., et al. JET (Journey to Enceladus and Titan, *JPL report*, 2010.

Appendix B

A despeckle filter for the Cassini synthetic aperture radar images of Titan's surface

Journal article published in *Planetary Space & Science* (2012),
Volume 61, pp. 108-113.

Planetary and Space Science 61 (2012) 108–113

Contents lists available at ScienceDirect

Planetary and Space Science

journal homepage: www.elsevier.com/locate/pss

A despeckle filter for the Cassini synthetic aperture radar images of Titan's surface

Emmanuel Bratsolis [a,*], Georgios Bampasidis [a,b], Anezina Solomonidou [b,c], Athena Coustenis [b]

[a] Faculty of Physics, University of Athens, Athens GR-15784, Greece
[b] LESIA, Observatoire de Paris - Meudon, 92195 Meudon Cedex, France
[c] Faculty of Geology and Geoenvironment, University of Athens, Athens GR-15784, Greece

ARTICLE INFO

Article history:
Received 24 December 2010
Received in revised form
30 March 2011
Accepted 7 April 2011
Available online 18 May 2011

Keywords:
Titan
Lakes
Radar imaging
Filtering
Segmentation

ABSTRACT

Cassini synthetic aperture radar (SAR) images of Titan, the largest satellite of Saturn, reveal surface features with shapes ranging from quasi-circular to more complex ones, interpreted as liquid hydrocarbon deposits assembled in the form of lakes or seas. One of the major problems hampering the derivation of meaningful texture information from SAR imagery is the speckle noise. It overlays real structures and causes gray value variations even in homogeneous parts of the image. We propose a filtering technique which can be applied to obtain restored SAR images. Our technique is based on probabilistic methods and regards an image as a random element drawn from a prespecified set of possible images. The despeckle filter can be used as an intermediate step for the extraction of regions of interest, corresponding to structured units in a given area or distinct objects of interest, such as lake-like features on Titan. This tool can therefore be used, among other, to study seasonal surficial changes of Titan's polar regions. In this study we also present a segmentation technique that allows us to separate the lakes from the local background.

1. Introduction

Cassini–Huygens, the extremely successful NASA/ESA joint mission to the Saturnian system, has already accomplished six years of extended investigation. Titan being one of the most intriguing objects in the Solar system, hosting an Earth-like environment, is one of the main targets of this mission. Titan's landscape has been observed by multiple flybys that examine the surface expressions through Cassini's infrared and radar instrumentation.

Cassini's RADAR instrument operates in the Ku-band (13.78 GHz, $\lambda = 2.17$ cm), at both high and low resolution, viewing Titan's surface in four modes: imaging, altimetry, scatterometry and radiometry (Elachi et al., 2004).

The SAR mode is used at altitudes lower than 4000 km, resulting in spatial resolution ranging from about 350 m to more than 1 km. Images are acquired either left or right of nadir using 1–5 looks while a swath, 120–450 km in width, is created from five antenna beams. SAR coverage is dependent on spacecraft range and orbital geometry (Elachi et al., 2004) and radar backscatter variations in SAR images can be interpreted in terms of variations of surface geometry (incidence angle, azimuth angle, and the polarization vector), near-surface roughness, or near-surface dielectric properties.

The images obtained using SAR revealed that Titan hosts a very complex surface formed with features such as lakes, mountains, fluvial river networks, possible volcanic-like features and dunes (Jaumann et al., 2008; Lopes et al., 2010 and references therein) which resemble Earth-like geomorphological structures (Coustenis and Hirtzig, 2009). However, both the material and the environmental conditions shaping their respective surfaces are considerably different. Despite these differences, the exogenic mechanisms forming the surficial expressions may be similar. Indeed, one dominating terrestrial surface-affecting procedure is the water cycle while on Titan an active methane cycle is at play (Atreya et al., 2006). The impact of the endogenic processes in the surface construction on Titan is still under investigation through geophysical interior models (e.g. Tobie et al., 2005). Radar images provided evidence of drainage and branching channel networks with subdivided channels (Perron et al., 2006; Soderblom et al., 2007; Lorenz et al., 2008; Burr et al., 2009), as well as distinct fluvial erosional patterns (Jaumann et al., 2008) that indicate dynamic and evolved surface processes. Additionally, SAR imagery observed lake-like features in several swaths (Stofan et al., 2007; Turtle et al., 2009; Hayes et al., 2010; Wye et al., 2010).

Other features, identified by radar, are the potentially volcanic in origin structures (Elachi et al., 2005; Lopes et al., 2007a; Soderblom et al., 2009; Nelson et al., 2009; Wall et al., 2009), the impact craters

* Corresponding author. Tel.: +30 2105813069.
E-mail address: ebrats@phys.uoa.gr (E. Bratsolis).

0032-0633/$ - see front matter © 2011 Published by Elsevier Ltd.
doi:10.1016/j.pss.2011.04.003

(Wood et al., 2010), the mountain chains (e.g. Radebaugh et al., 2007) and the linear dunes (Elachi et al., 2006; Radebaugh et al., 2008).

2. Lacustine features of Titan's surface

The thermodynamical conditions dominating Titan as well as its chemical profile allow the hydrocarbon liquid phase to exist on its surface (Kouvaris and Flasar, 1991; Thompson et al., 1992; Atreya et al., 2006). Indeed, the temperature of its icy surface has been measured in situ (10.34°S, 192.34°W) (Tomasko et al., 2005) by Huygens at 93.7 K (Fulchignoni et al., 2005), while the Cassini composite infrared spectrometer (CIRS) found by remote observations an average temperature of 92 K between 2004 and 2008 (Jennings et al., 2009).

Cassini RADAR instrumentation confirmed the presence of lake-like features on the surface of Titan. Several models have suggested organic precipitation on Titan (Toon et al., 1988; Lorenz, 1993; Graves et al., 2008) either violently through torrential storms (Hueso and Sanchez-Lavega, 2006) or smoothly through drizzle at the lower atmosphere (Tokano et al., 2006) and rainfalls originated from occasional short-lived clouds (Griffith et al., 2000, 2005; Lorenz et al., 2005), such phenomena have not been recorded yet.

The first recording of organic liquid pools was accomplished during the T16 flyby at the northern polar locations, where more than 75 lake candidate features were identified (Sotin, 2007; Stofan et al., 2007). In 2008, the Cassini/RADAR swaths counted in both north and south polar regions, above 50°N and 50°S, respectively, more than 655 lake-like features (Hayes et al., 2008). SAR imaging shows lake-like features separated into three classes: dark lakes, granular lakes, and bright lakes (Hayes et al., 2008). Dark lakes are interpreted as liquid filled, while bright lakes are interpreted as empty basins and granular lakes are inferred as transitional between dark and bright lake features. From a geomorphological aspect the lakes on Titan span over the range of observed morphologies on Earth (Stofan et al., 2007; Mitri et al., 2007; Hayes et al., 2008). They are rimmed features, from circular to irregular and some with distinct edges, steep margins and smooth surfaces (Stofan et al., 2007) and they show very low microwave backscatter. Some of them are surrounded by a drainage network of dark channels, which may supply them with liquid (Stofan et al., 2007), while some are not.

It is suggested that this liquid is a methane/ethane mixture, with smaller concentrations of nitrogen and higher order hydrocarbons/nitriles (Lunine et al., 1983; Mitri et al., 2007; Brown et al., 2008; Raulin, 2008).

The lakes' radiometric brightnesses which appear to be warmer than the surrounding region (Janssen et al., 2009) are consistent with the high emissivity expected for a smooth surface with the real part of the low dielectric constant between 1.7 and 1.9 of liquid ethane–methane solutions (Lopes et al., 2007b) with most possible value the 1.9. However, the imaginary part is still under investigation (Notarnicola et al., 2009).

This study provides a qualitative method of recognition of lake-like features from Cassini SAR images. The intended goal is to label regions in an image into three classes (dark lakes, granular lakes and the local background). First, a filtering technique is applied to obtain the restored image. Then, a method of supervised segmentation is used. The segmentation method based on the minimum Euclidean distance is used here.

3. Filtering

Strip mapping SAR consists of a large antenna which is synthesized from many small antennas and remains fixed with respect to the radar platform, so that the large antenna illuminates a strip of the ground. This technique is used to improve the azimuthal resolution. As the platform moves, a sequence of closely spaced pulses is emitted and the returned waveforms are recorded. An image is computed after the coherent sum of reflected monochromatic microwaves. The image is distorted by a strong granulation, called speckle. Speckle noise exists in all types of coherent imaging systems and its presence reduces the resolution of the image and the detectability of the target. Speckle noise is not only signal dependent but is also spatially correlated and reduces the effectiveness of image reduction. The Cassini RADAR measures the normalized backscatter cross-section (σ_0) of Titan's surface (Ulaby et al., 1982). The SAR textures are generally affected by multiplicative speckle noise. In order to reduce the speckle noise, the multilook technique, based on incoherently averaging the independent neighboring pixels, is used to estimate the characteristics of the same ground area.

The statistical characteristics of multilook data depart considerably from those of single-look data. Multilook data tend to mix some physical and statistical properties of the terrain. The terrain appears more homogeneous and the multilook averaging will tend to be close to the Gaussian statistics (Chitroub et al., 2002).

Speckle noise overlays real structures and causes gray value variations even in homogeneous parts of the image and also makes automatic segmentation of such images difficult. We propose here a filtering technique that can be applied to obtain the SAR restored images. After filtering the structured parts of the image can be much better separated. The total sum preserving regularization (TSPR) filter, is based on a membrane model Markov random field approximation optimized by a synchronous local iterative method (Bratsolis and Sigelle, 2003). The final form of despeckling gives a sum-preserving regularization for the pixel values of the image.

Image formation is the process of computing (or refining) an image both from raw sensor data that is related to that image and from prior information about that image. Information about the image is contained in the raw sensor data, and the task of image formation is to extract this information so as to compute the image.

Image space is the set $\mathcal{F}$ of model images that represent the true, underlying physical distributions that are measured by the sensors.

Working in a probabilistic imaging problem, an a priori knowledge about an image is most naturally incorporated through the use of a prior probability distribution (or prior) $P(f)$ on the image space. Our objective here is to reconstruct the original (or true) image from its degraded version.

A random field is an appropriate model for image values. Random variables characterized by conditional priors that account for local interactions are often used as natural and convenient priors in imaging problems. These priors are placed directly on the image space. However, the fundamental probability distribution on the field is the joint probability distribution $P(f)$, and this is difficult or impossible to specify directly. One needs to verify that the chosen specification of conditional distributions is sufficient and consistent in the sense that a unique joint probability distribution corresponds to this set of conditional probability distributions.

Assume that an image is formed on a finite rectangular lattice when the sensors of this lattice select one scene from $\mathcal{F}$. Let us note the finite lattice of sites as $S=\{s\}_{s=1\ldots N}$ with $S\subset Z^2$. Each site $s\in S$ has a set of neighbors r noted $\mathcal{N}_s$. If $s=(i,j)$ four-connectivity is assumed in the following : $\mathcal{N}_s=\{(i-1,j);(i+1,j);(i,j-1);(i,j+1)\}$.

A random process $\{f_s|s\in S\}$ with f_s random variables following the joint probability function $P(f)$ is a "random field". In the special case where $P(f_s|\{f_r\neq s\})=P(f_s|\{f_r\}_{r\in\mathcal{N}_s})$ the random field is

called a "Markov random field" (MRF). By the Hammersley–Clifford theorem MRFs and Gibbs random fields on a finite lattice are equivalent under the positivity condition (Besag, 1974).

Let g be the degraded observed image and f the restored image. The general problem is now to estimate f from a set of input data g.

The Bayes theorem allows us to obtain the a posteriori probability for the field f given the data g:

$$P(f|g)=\frac{P(g|f)P(f)}{P(g)} \tag{1}$$

where $P(f)$ is the a priori probability for the field f, $P(g|f)$ is the conditional probability for the data g given f and $P(g)$ is the probability of g, which is independent of f.

Considering a multilook image, we assume for the conditional probability $P(g|f)$ a Gaussian distribution (Chitroub et al., 2002) and we have

$$P(g|f)=\frac{\exp-\left[\sum_s \frac{(f_s-g_s)^2}{2\sigma^2}\right]}{C_1} \tag{2}$$

where σ is the standard deviation of the Gaussian distribution and C_1 a normalization constant.

The probability $P(f)$ is given by

$$P(f)=\frac{\exp-\left[\beta\sum_{(r,s)}(f_s-f_r)^2\right]}{C_2} \tag{3}$$

where β is a smoothness factor, C_2 a normalization constant, and the sum runs on all pairs of neighboring sites. From (1) we obtain

$$P(f|g)=\frac{1}{Z}\exp-U(f) \tag{4}$$

where Z, also called the a posteriori partition function, is a normalization constant and $U(f)$ is the total a posteriori potential function, which is written as

$$U(f)=\sum_s \frac{(f_s-g_s)^2}{2\sigma^2}+\beta\sum_{(r,s)}(f_s-f_r)^2 \tag{5}$$

The related local conditional potential functions are given by

$$V_s(f)=\frac{(f_s-g_s)^2}{2\sigma^2}+\beta\sum_{r\in N_s}(f_s-f_r)^2 \tag{6}$$

The a posteriori usual maximum (MAP) estimate is assigned to the value f which maximizes (4), i.e. which minimizes the a posteriori energy $U(f)$ (Bratsolis and Sigelle, 2003). We accept as a fast method of optimization a synchronous minimization of the local potential energies which we named synchronous local iterative method.

Our final TSPR filter is an iterative filter which uses the equation given by

$$f^{(n+1)}=\lambda g+(1-\lambda)\mathcal{R}*f^{(n)} \quad \forall n\geq 1 \tag{7}$$

where $*$ is the 2-D convolution operation. Thus, at each step the current pixel value will depend in a regularizing manner on its neighboring ones, according to the magnitude of parameter λ. It is also obvious that positivity is preserved when $0\leq\lambda\leq 1$. $\mathcal{R}$ is a normalized matrix given by

$$\mathcal{R}=\begin{bmatrix}0 & 0.25 & 0\\ 0.25 & 0 & 0.25\\ 0 & 0.25 & 0\end{bmatrix}$$

According to the notation of our method, it is evident that $\sigma_0=g_s$ and $\langle\sigma_0\rangle=\langle g_s\rangle=\langle f_s\rangle$. The TSPR method preserves the mean values of local homogeneous regions and decreases the standard deviation up to six times (Bratsolis and Sigelle, 2003).

4. The segmentation method

The purpose of segmentation is to divide the image into specific regions that correspond to structural units in the scene or distinguish objects of interest. These regions are characterized by spatially connected, non-overlapping sets of pixels sharing common properties.

In general, image segmentation is a classification problem. A classification problem can be formalized as a pair $(\mathcal{O},\mathcal{C})$, where $\mathcal{O}$ denotes a set of objects and $\mathcal{C}$ a collection of disjoint subsets $\mathcal{C}_1,\ldots,\mathcal{C}_l$ that partitions $\mathcal{O}$. The problem is to determine the subset $\mathcal{C}_j\subset\mathcal{C}$ to which a given object $o\in\mathcal{O}$ belongs. The supervised method of minimum Euclidean distance uses the mean values (or vectors) of each member and calculates the Euclidean distance from each classified object to the nearest class segmenting the image into different regions of interest or different labels (Richards, 1999). In our case we choose three regions of interest: dark lakes (black label), granular lakes (dark gray label) and local background (light gray label). The TSPR filter can be used as an intermediate step before the extraction of the regions of interest.

As Euclidean distance here, we define the distance

$$d_e=\sqrt{(f_s-\mu_i)^2} \tag{8}$$

where μ_i with $i=1,\ldots,3$ presents the mean values ($\langle\sigma_0\rangle$) corresponding to three sampled regions of interest. The algorithm is applied for every site s and for every value f_s of the restored (filtered) image. The value μ_i which minimize the distance d_e gives the characteristic label (black, dark gray or light gray) to the segmented image of Fig. 4, where μ_1 corresponds to -20.27 db, μ_2 to -18.64 db and μ_3 to -13.78 db.

We begin our analysis with the Cassini SAR image (PIA08630, NASA/JPL) acquired during the T16 flyby on July 22, 2006, at high latitudes near the north pole. This image is centered near 80°N, 92°W. Our image has dimensions 750×3100 in pixel size and the pixel scale is set to 175.558 m per pixel ($\sim 256^{*}$), but the actual SAR resolution is around 350 m per pixel and the image has been subjected to some interpolation. Cassini SAR images across this region contain numerous very dark splotches with sharp-edged boundaries, which may be filled with hydrocarbon liquid.

After using the despeckling filter TSPR we apply the segmentation method. Figs. 1 and 2 illustrate the initial image derived form the Cassini SAR while Fig. 3 is the filtering result of the previous image. The despeckling TSPR filter is used to smooth out the multiplicative

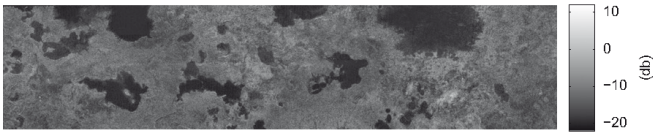

Fig. 1. Initial image of lakes (PIA08630, NASA/JPL) after subtraction of negative σ_0.

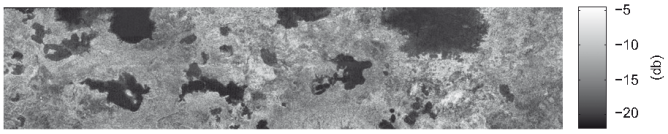

Fig. 2. Initial image of lakes (PIA08630, NASA/JPL) after subtraction of negative σ_0 and subtraction of values greater than $\langle\sigma_0\rangle+3\,std(\sigma_0)$.

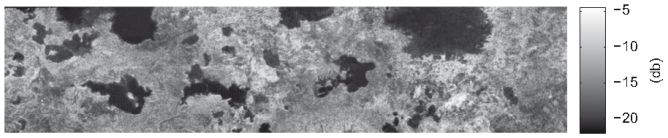

Fig. 3. Filtered image.

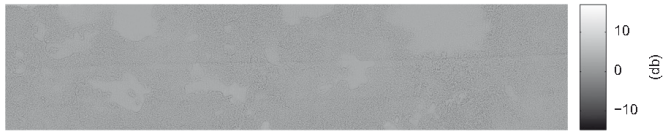

Fig. 4. Image ratio between the initial (Fig. 2) and the despeckled (Fig. 3) image.

Table 1
Characteristics of the sampled regions of interest.

Regions of interest	Before filtering $\langle\sigma_0\rangle \pm std(\sigma_0)$ (db)	After filtering $\langle\sigma_0\rangle \pm std(\sigma_0)$ (db)
Region 1 (black)	-20.27 ± 0.44	-20.26 ± 0.13
Region 2 (dark gray)	-18.64 ± 2.03	-18.53 ± 0.69
Region 3 (light gray)	-13.78 ± 3.57	-13.19 ± 1.32

noise of SAR images without missing important textural details from the regions of interest. Consequently, Fig. 3 seems smoother than Fig. 2. Fig. 4 depicts the ratio between the initial and the despeckle image. In this figure the lakes' interior is presented smoother than the surrounding area. This can be explained as the dark lakes are not really speckled regions. From the initial data (and σ_0 in non-dimensional values) the samples of the region 2 (granular lake) and the region 3 (local background) we take a value for the ratio $std(\sigma_0)/\langle\sigma_0\rangle$ equal to 0.4 and for the region 1 (dark lakes) equal to 0.05 which means that the region 1 is flatter than we were waiting.

The characteristics of the sampled regions of interest are listed in Table 1.

We can see the segmentation results in Fig. 5, where the black area corresponds to the dark lakes, the dark gray to the granular lakes and the light gray to the local background.

5. Discussion

Titan is indeed an active planetary body and both endogenic and exogenic processes have most possibly left their marks on the surface. Hence, one should focus on the surface geomorphology in order to identify any local tectonic field and estimate the importance as well as influence of each forming mechanism.

The TSPR filter, in combination with the minimum Euclidean distance method of supervised segmentation, can be used to extract regions of interest on the surface of Titan, such as lakes or seas using Cassini SAR images. Such despeckle filter can be applied in studying other surface features on Titan like the drainage networks, the equatorial dunes and the impact craters, where different textures appear.

Our approach allows to isolate each distinct surface feature from its surroundings and to study their distribution through out the surface. Then, in combination with radiative transfer modeling using Cassini visual and infrared mapping spectrometer (VIMS) data, we can infer about the relation between surface composition and morphotectonic structures. When we determine in a more accurate way the shapes of several surface structures, we will be able to study their global distribution and perform effectively classifications.

Since the Cassini mission extended its operational duration, new swaths, overlapping the liquid areas, have shown that the lakes have been evolving during the past years. Recent studies, focused on lake Ontario, the largest lake of the southern hemisphere, showed a significant recession of its shoreline (Turtle et al., 2009; Hayes et al., 2010; Wall et al., 2010) and support the hypothesis that these liquid deposits are not stable structures but evolve with time by expanding in winter and shrinking in the summer (Sotin, 2007). Applying the segmentation method on the same area at various periods of time, we can identify possible enhancements or reductions of the liquid coverage of the region. In particular, the temporal variation of the dark spots can provide information on the evolution of the lake system and consequently help us to better understand the methane cycle on Titan and therefore the mechanisms linked with the lake surface features, their origin and fate, through a global temporal and spatial coverage.

The passage from qualitative to quantitative results, requires to apply the aforementioned method in the same regions of interest with the same observational characteristics at different time periods in order to measure the surface each time.

Using this temporal dataset will help us evaluate the volume variation through time and estimate the hydrocarbon loss rate,

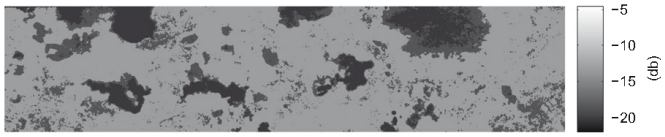

Fig. 5. Segmented image after filtering.

a critical parameter for the global methane cycle (Atreya et al., 2006).

Cassini evolves in the Saturnian system since 2004 and will continue returning data until at least 2017 in the extended mission. Although Cassini SAR recordings have unveiled new characteristics of Titan's surface, more advanced instrumentation with higher resolution is necessary to give a full picture of this complex environment.

A new long-term mission to Titan which will perform efficient in situ experiments in order to study widely the nature and the dynamics of its environment would be required.

Several proposals have been studied to this end. Recently, the 2008 study of a flagship mission, Titan Saturn System Mission (TSSM), focused on Titan and Enceladus exploration (Reh et al., 2008; Coustenis et al., 2009). TSSM consists of an orbiter, a lake lander and a balloon (montgolfière) and aims to a complete investigation scrutinizing thoroughly the whole satellite from the exosphere to its interior. The montgolfière would contain advanced instrumentation such as the Titan radar sounder ($>$ 150 MHz), which could perform a detailed surface investigation. In addition to topography, the radars on both the orbiter and the montgolfière would provide extended information regarding the lakes coverage. The proposed filtering and segmentation method in this paper would be a helpful tool in enhancing the return of the analysis of all SAR data acquired on Titan and other objects as well as in the exploitation of future missions to Titan.

Acknowledgments

The authors would like to gratefully acknowledge the assistance of Dr. Alexander Hayes in providing us with raw SAR Cassini data and with a thorough and constructive review of the manuscript and subsequent fruitful discussions. We are also grateful to another anonymous referee for helpful comments and suggestions.

A. Solomonidou is supported by the "HRACLEITOS II" project, co-financed by Greece and the European Union.

References

Atreya, S.K., Adams, E.Y., Niemann, H.B., Demick-Montelara, J.E., Owen, T.C., Fulchignoni, M., Ferri, F., Wilson, E.H., 2006. Titan's methane cycle. Planetary and Space Science 54, 1177–1187.

Besag, J., 1974. Spatial interaction and the statistical analysis of lattice systems (with discussion). Journal of the Royal Statistical Society Series B 36, 192–236.

Bratsolis, E., Sigelle, M., 2003. Fast SAR image restoration, segmentation and detection of high-reflectance regions. IEEE Transactions on Geoscience and Remote Sensing 41, 2890–2899.

Brown, R.H., Soderblom, L.A., Soderblom, J.M., Clark, R.N., Jaumann, R., Barnes, J.W., Sotin, C., Buratti, B., Baines, K.H., Nicholson, P.D., 2008. The identification of liquid ethane in Titan's Ontario Lacus. Nature 454, 607–610.

Burr, D.M., Jacobsen, R.E., Roth, D.L., Phillipis, C.B., Mitchell, K.L., Viola, D., 2009. Fluvial network analysis on Titan: evidence for subsurface structures and west-to-east wind flow, southwestern Xanadu. Geophysical Research Letters 36, L22203.

Chitroub, S., Houacine, A., Sansal, B., 2002. Statistical characterization and modeling of SAR images. Signal Processing 82, 69–92.

Coustenis, A., Hirtzig, M., 2009. Cassini–Huygens results on Titan's surface. Research in Astronomy and Astrophysics 9, 249–268.

Coustenis, A., Atreya, S., Balint, T., Brown, R., Dougherty, M., Ferri, F., Fulchignoni, M., Gautier, D., Gowen, R., Griffith, C., Gurvits, L., Jaumann, R., Langevin, Y., Leese, M., Lunine, J., McKay, C., Moussas, X., Muller-Wodarg, I., Neubauer, F., Owen, T., Raulin, F., Sittler, E., Sohl, F., Sotin, C., Tobie, G., Tokano, T., Turtle, E., Wahlund, J.E., Waite, J., Baines, K., Blamont, J., Coates, A., Dandouras, I., Krimigis, T., Lellouch, E., Lorenz, R., Morse, A., Porco, C., Hirtzig, M., Saur, J., Spilker, T., Zarnecki, J., Choi, E., Achilleos, N., Amils, R., Annan, P., Atkinson, D., Benilan, Y., Bertucci, C., Bezard, B., Bjoraker, G., Blanc, M., Boireau, L., Bouman, J., Cabane, M., Capria, M., Chassefière, E., Coll, P., Combes, M., Cooper, J., Coradini, A., Crary, F., Cravens, T., Daglis, I., de Angelis, E., de Bergh, C., de Pater, I., Dunford, C., Durry, G., Dutuit, O., Fairbrother, D., Flasar, F., Fortes, A., Frampton, R., Fujimoto, Galand, M., Grasset, O., Grott, M., Haltigin, T., Herique, A., Hersant, F., Hussmann, H., Ip, W., Johnson, R., Kallio, E., Kempf, S., Knapmeyer, M., Kofman, W., Koop, R., Kostiuk, T., Krupp, N., Kuppers, M., Lammer, H., Lara, L.M., Lavvas, P., Le Moulic, S., Lebonnois, S., Ledvina, S., Li, J., Livengood, T., Lopes, R., Lopez-Moreno, J.J., Luz, D., Mahaffy, P., Mall, U., Martinez-Frias, J., Marty, B., McCord, T., MenorSalvan, C., Milillo, A., Mitchell, D., Modolo, R., Mousis, O., Nakamura, M., Neish, C., Nixon, C., Nna Mvondo, D., Orton, G., Paetzold, M., Pitman, J., Pogrebenko, S., Pollard, W., Prieto-Ballesteros, O., Rannou, P., Reh, K., Richter, L., Robb, F., Rodrigo, R., Rodriguez, S., Romani, P., Ruiz Bermejo, M., Sarris, E., Schenk, P., Schmitt, B., Schmitz, N., Schulze-Makuch, D., Schwingenschuh, K., Selig, A., Sicardy, B., Soderblom, L., Spilker, L., Stam, D., Steele, A., Stephan, K., Strobel, D., Szego, K., Szopa, C., Thissen, R., Tomasko, M., Toublanc, D., Vali, H., Vardavas, I., Vuitton, V., West, R., Yelle, R., Young, E., 2009. TandEM: Titan and Enceladus mission. Experimental Astronomy 23, 893–946.

Elachi, C., Allison, M.D., Borgarelli, L., Encrenaz, P., Im, E., Janssen, M.A., Johnson, W.T.K., Kirk, R.L., Lorenz, R.D., Lunine, J.I., Muhleman, D.O., Ostro, S.J., Picardi, G., Posa, F., Rapley, C.G., Roth, L.E., Seu, R., Soderblom, L.A., Vetrella, S., Wall, S.D., Wood, C.A., Zebker, H.A., 2004. Radar: the Cassini Titan Radar Mapper. Space Science Reviews 115, 71–110.

Elachi, C., Wall, S., Allison, M., Anderson, Y., Boehmer, R., Callahan, P., Encrenaz, P., Flamini, E., Franceschetti, G., Gim, Y., Hamilton, G., Hensley, S., Janssen, M., Johnson, W., Kelleher, K., Kirk, R., Lopes, R., Lorenz, R., Lunine, J., Muhleman, D., Ostro, S., Paganelli, F., Picardi, G., Posa, F., Roth, L., Seu, R., Shaffer, S., Soderblom, L., Stiles, B., Stofan, E., Vetrella, S., West, R., Wood, C., Wye, L., Zebker, H., 2005. Cassini Radar views the surface of Titan. Science 308, 970–974.

Elachi, C., Wall, S., Janssen, M., Stofan, E., Lopes, R., Kirk, R., Lorenz, R., Lunine, J., Paganelli, F., Soderblom, L., Wood, C., Wye, L., Zebker, H., Anderson, Y., Ostro, S., Allison, M., Boehmer, R., Callahan, P., Encrenaz, P., Flamini, E., Francescetti, G., Gim, Y., Hamilton, G., Hensley, S., Johnson, W., Kelleher, K., Muhleman, D., Picardi, G., Posa, F., Roth, L., Seu, R., Shaffer, S., Stiles, B., Vetrella, S., West, R., 2006. Titan Radar Mapper observations from Cassini's T3 fly-by. Nature 441, 709–713.

Fulchignoni, M., Ferri, F., Angrilli, F., Ball, A.J., Bar-Nun, A., Barucci, M.A., Bettanini, C., Bianchini, G., Borucki, W., Colombatti, G., Coradini, M., Coustenis, A., Debei, S., Falkner, P., Fanti, G., Flamini, E., Gaborit, V., Grard, R., Hamelin, M., Harri, A.M., Hathi, B., Jernej, I., Leese, M.R., Lehto, A., Lion Stoppato, P.F., Lpez-Moreno, J.J., Mkinen, T., McDonnell, J.A.M., McKay, C.P., Molina-Cuberos, G., Neubauer, F.M., Pirronello, V., Rodrigo, R., Saggin, B., Schwingenschuh, K., Seiff, A., Simes, F., Svedhem, H., Tokano, T., Towner, M.C., Trautner, R., Withers, P., Zarnecki, J.C., 2005. In situ measurements of the physical characteristics of Titan's environment. Nature 438, 785–791.

Graves, S.D.B., McKay, C.P., Griffith, C.A., Ferri, F., Fulchignoni, M., 2008. Rain and hail can reach the surface of Titan. Planetary and Space Science 56, 346–357.

Griffith, C.A., Hall, J.L., Geballe, T.R., 2000. Detection of daily clouds on Titan. Science 290, 509–513.

Griffith, C.A., Penteado, P., Baines, K., Drossart, P., Barnes, J., Bellucci, G., Bibring, J., Brown, R., Buratti, B., Capaccioni, F., Cerroni, P., Clark, R., Combes, M., Coradini, A., Cruikshank, D., Formisano, V., Jaumann, R., Langevin, Y., Matson, D., McCord, T., Mennella, V., Nelson, R., Nicholson, P., Sicardy, B., Sotin, C., Soderblom, L.A., Kursinski, R., 2005. The evolution of Titan's mid-latitude clouds. Science 310, 474–477.

Hayes, A., Aharonson, O., Callahan, P., Elachi, C., Gim, Y., Kirk, R., Lewis, K., Lopes, R., Lorenz, R., Lunine, J., Mitchell, K., Mitri, G., Stofan, E., Wall, S., 2008. Hydrocarbon lakes on Titan: distribution and interaction with a porous regolith. Geophysical Research Letters 35, L09204.

Hayes, A., Wolf, A., Aharonson, O., Zebker, H., Lorenz, R., Kirk, R., Paillou, P., Lunine, J., Wye, L., Callahan, P., Wall, S., Elachi, C., 2010. Bathymetry and absorptivity of Titan's Ontario Lacus. Journal of Geophysical Research 115, E09009.

Hueso, R., Sanchez-Lavega, A., 2006. Methane storms on Saturn's moon Titan. Nature 442, 428–431.

Jaumann, R., Brown, R.H., Stephan, K., Barnes, J.W., Soderblom, L.A., Sotin, C., Le Mouelic, S., Clark, R.N., Soderblom, J., Buratti, B.J., Wagner, R., McCord, T.B., Rodriguez, S., Baines, K.H., Cruikshank, D.P., Nicholson, P.D., Griffith, C.A.,

Langhans, E., Lorenz, R.D., 2008. Fluvial erosion and post-erosional processes on Titan. Icarus 197, 526–538.
Janssen, M.A., Lorenz, R.D., West, R., Paganelli, F., Lopes, R.M., Kirk, R.L., Elachi, C., Wall, S.D., Johnson, W.T.K., Anderson, Y., Boehmer, R.A., Callahan, P., Gim, Y., Hamilton, G.A., Kelleher, K.D., Roth, L., Stiles, B., Le Gall, A., 2009. the Cassini Radar Team, 2009. Titan's surface at 2.2-cm wavelength imaged by the Cassini Radar radiometer: calibration and first results. Icarus 200, 222–239.
Jennings, D.E., Flasar, F.M., Kunde, V.G., Samuelson, R.E., Pearl, J.C., Nixon, C.A., Carlson, R.C., Mamoutkine, A.A., Brasunas, J.C., Guandique, E., Achterberg, R.K., Bjoraker, G.L., Romani, P.N., Segura, M.E., Albright, S.A., Elliott, M.H., Tingley, J.S., Calcutt, S., Coustenis, A., Courtin, R., 2009. Titan's surface brightness temperatures. Astrophysical Journal 691, L103–L105.
Kouvaris, L.C., Flasar, F.M., 1991. Phase equilibrium of methane and nitrogen at low temperatures: application to Titan. Icarus 91, 112–124.
Lopes, R.M.C., Mitchell, K.L., Stofan, E.R., Lunine, J.I., Lorenz, R., Paganelli, F., Kirk, R.L., Wood, C.A., Wall, S.D., Robshaw, L.E., Fortes, A.D., Neish, C.D., Radebaugh, J., Reffet, E., Ostro, S.J., Elachi, C., Allison, M.D., Anderson, Y., Boehmer, R., Boubin, G., Callahan, P., Encrenaz, P., Flamini, E., Francescetti, G., Gim, Y., Hamilton, G., Hensley, S., Janssen, M.A., Johnson, W.T.K., Kelleher, K., Muhleman, D.O., Ori, G., Orosei, R., Picardi, G., Posa, F., Roth, L.E., Seu, R., Shaffer, S., Soderblom, L.A., Stiles, B., Vetrella, S., West, R.D., Wye, L., Zebker, H.A., 2007a. Cryovolcanic features on Titan's surface as revealed by the Cassini Titan Radar Mapper. Icarus 186, 395–412.
Lopes, R.M.C., Mitchell, K.L., Wall, S.D., Mitri, G., Janssen, M., Ostro, S.J., Kirk, R.L., Hayes, A., Stofan, E.R., Lunine, J.I., Lorenz, R., Wood, C.A., Radebaugh, J., Paillou, P., Zebker, H.A., Paganelli, F., 2007b. the Cassini RADAR Team, 2007. The lakes and seas of Titan. Transactions of EOS, American Geophysical Union 88, 569–576.
Lopes, R.M.C., Stofan, E.R., Peckyno, R., Radebaugh, J., Mitchell, K.L., Mitri, G., AWood, C.A., Kirk, R.L., Wall, S.D., Lunine, J.I., Hayes, A., Lorenz, R., Farr, T., Wye, L., Craig, J., Ollerenshaw, R.J., Janssen, M., Legall, A., Paganelli, F., West, R., Stiles, B., Callahan, P., Anderson, Y., Valora, P., Soderblom, L., 2010. the Cassini RADAR Team, 2010. Distribution and interplay of geologic processes on Titan from Cassini radar data. Icarus 205, 540–558.
Lorenz, R.D., 1993. The life, death and afterlife of a raindrop on Titan. Planetary and Space Science 41, 647–655.
Lorenz, R.D., Griffith, C.A., Lunine, J.I., McKay, C.P., Renn, N.O., 2005. Convective plumes and the scarcity of Titan's clouds. Geophysical Research Letters 32, L01201.
Lorenz, R.D., Lopes, R.M., Paganelli, F., Lunine, J.I., Kirk, R.L., Mitchell, K.L., Soderblom, L.A., Stofan, E.R., Ori, G., Myers, M., Miyamoto, H., Radebaugh, J., Stiles, B., Wall, S.D., Wood, C.A., Team, T.C.R., 2008. Fluvial channels on Titan : initial Cassini radar observations. Planetary and Space Science 56, 1132–1144.
Lunine, J.I., Stevenson, D.J., Yung, Y.L., 1983. Ethane ocean on Titan. Science 222, 1229–1230.
Mitri, G., Showman, A.P., Lunine, J.I., Lorenz, R.D., 2007. Hydrocarbon lakes on Titan. Icarus 186, 385–394.
Nelson, R.M., Kamp, L.W., Lopes, R.M.C., Matson, L., Kirk, R., Hapke, B., Wall, S.D., Boryta, M.D., Leader, F.L., Smythe, W.D., Mitchell, K., Baines, K.H., Jaumann, R., Sotin, C., Clark, R.N., Cruickshank, D.P., Drossart, P., Lunine, J., Combes, M., Bellucci, G., Bibring, J.-P., Capaccioni, F., Cerroni, P., Coradani, A., Formasiano, V., Filacchione, G., Langevin, Y., McCord, T., Menella, V., Nicholson, P.D., Sicardy, B., Itrwin, P.J., Pearl, J.C., 2009. Photometric changes on Saturn's Titan: evidence for active cryovolcanism. Geophysical Research Letters 36, L04202.
Notarnicola, C., Ventura, B., Casarano, D., Posa, F., 2009. Cassini radar data: estimation of Titan's lake features by means of Bayesian inversion algorithm. IEEE Transactions on Geoscience and Remote Sensing 47, 1503–1511.
Perron, J.T., Lamb, M.P., Koven, C.D., Fung, I.Y., Yager, E., Adamkovics, M., 2006. Valley formation and methane precipitation rates on Titan. Journal of Geophysical Research 111, E11001.
Radebaugh, J., Lorenz, D., Kirk, R.L., Lunine, J.I., Stofan, E.R., Lopes, R.M.C., Wall, S.D., 2007. the Cassini Radar Team, 2007. Mountains on Titan observed by Cassini Radar. Icarus 192, 77–91.
Radebaugh, J., Lorenz, R.D., Lunine, J.I., Wall, S.D., Boubin, G., Reffet, E., Kirk, R.L., Lopes, R.M., Stofan, E.R., Soderblom, L., Allison, M., Janssen, M., Paillou, P., Callahan, T., Spencer, C., The Cassini Radar, T., 2008. Dunes on Titan observed by Cassini Radar. Icarus 194, 690–703.
Raulin, F., 2008. Planetary science: organic lakes on Titan. Nature 454, 587–589.
Reh, K., Lunine, J., Matson, D., Magner, T., Lebreton, J.-P., Coustenis, A., 2008. TSSM Final Report on the NASA Contribution to a Joint Mission with ESA, JPL D-48148, NASA Task Order NMO710851.
Richards, J.A., 1999. Remote Sensing Digital Image Analysis. Springer-Verlag, Berlin, p. 240.
Soderblom, L.A., Tomasko, M.G., Archinal, B.A., Becker, T.L., Bushroe, M.W., Cook, D.A., Doose, L.R., Galuszka, D.M., Hare, T.M., Howington-Kraus, E., Karkoschka, E., Kirk, L., Lunine, J.I., McFarlane, E.A., Redding, B.L., Rizk, B., Rosiek, M.R., See, C., Smith, P.H., 2007. Topography and geomorphology of the Huygens landing site on Titan. Planetary and Space Science 55, 2015–2024.
Soderblom, L.A., Brown, R.H., Soderblom, J.M., Barnes, J.W., Kirk, R.L., Sotin, C., Jaumann, R., Mackinnon, d.J., Mackowski, D.W., Baines, K.H., Buratti, B.J., Clark, R.N., Nicholson, P.D., 2009. The geology of Hotei Regio, Titan: correlation of Cassini VIMS and RADAR. Icarus 204, 610–618.
Sotin, C., 2007. Planetary science: Titan's lost seas found. Nature 445, 29–30.
Stofan, E.R., Elachi, C., Lunine, J.I., Lorenz, R.D., Stiles, B., Mitchell, K.L., Ostro, S., Soderblom, L., Wood, C., Zebker, H., Wall, S., Janssen, M., Kirk, R., Lopes, R., Paganelli, F., Radebaugh, J., Wye, L., Anderson, Y., Allison, M., Boehmer, R., Callahan, P., Encrenaz, P., Flamini, E., Francescetti, G., Gim, Y., Hamilton, G., Hensley, S., Johnson, W.T.K., Kelleher, K., Muhleman, D., Paillou, P., Picardi, G., Posa, F., Roth, L., Seu, R., Shaffer, S., Vetrella, S., West, R., 2007. The lakes of Titan. Nature 445, 61–64.
Thompson, W.R., Zollweg, J.A., Gabis, D.H., 1992. Vapor–liquid equilibrium thermodynamics of N_2 + CH_4—model and Titan applications. Icarus 97, 187–199.
Tobie, G., Grasset, O., Lunine, J.I., Mocquet, A., Sotin, C., 2005. Titans internal structure inferred from a coupled thermal-orbital model. Icarus 175, 496–502.
Tokano, T., McKay, C.P., Neubauer, F.M., Atreya, S.K., Ferri, F., Fulchignoni, M., Niemann, H.B., 2006. Methane drizzle on Titan. Nature 442, 432–435.
Tomasko, M.G., Archinal, B., Becker, T., Bezard, B., Bushroe, M., Combes, M., Cook, D., Coustenis, A., de Bergh, C., Dafoe, L.E., Doose, L., Doute, S., Eibl, A., Engel, S., Gliem, F., Grieger, B., Holso, K., Howington-Kraus, E., Karkoschka, E., Keller, H.U., Kirk, R., Kramm, R., Kuppers, M., Lanagan, P., Lellouch, E., Lemmon, M., Lunine, J., McFarlane, E., Moores, J., Prout, G.M., Rizk, B., Rosiek, M., Rueffer, P., Schroder, S.E., Schmitt, B., See, C., Smith, P., Soderblom, L., Thomas, N., West, R., 2005. Rain, winds and haze during the Huygens probe's descent to Titan's surface. Nature 438, 765–778.
Toon, O.B., McKay, C.P., Courtin, R., Ackerman, T.P., 1988. Methane rain on Titan. Icarus 75, 255–284.
Turtle, E.P., Perry, J.E., McEwen, A.S., DelGenio, A.D., Barbara, J., West, R.A., Dawson, D.D., Porco, C.C., 2009. Cassini imaging of Titan's high-latitude lakes, clouds, and south-polar surface changes. Geophysical Research Letters 36, L02204.
Ulaby, F.T., Moore, R.K., Fung, A.K., 1982. Microwave Remote Sensing: Active and Passive, vol. 2. Artech House, Norwood, Mass.
Wall, S.D., Lopes, R.M.C., Stofan, E.R., Wood, C.A., Radebaugh, J.L., Horst, S.M., Stiles, B.W., Nelson, R.M., Kamp, L.W., Janssen, M.A., Lorenz, R.D., Lunine, J.I., Farr, T.G., Mitri, G., Paillou, P., Paganelli, F., Mitchell, K.L., 2009. Cassini RADAR images at Hotei Arcus and western Xanadu, Titan: evidence for geologically recent cryovolcanic activity. Geophysical Research Letters 36, L04203.
Wall, S., Hayes, A., Bristow, C., Lorenz, R., Stofan, E., Lunine, J., Le Gall, A., Janssen, M., Lopes, R., Wye, L., Soderblom, L., Paillou, P., Aharonson, O., Zebker, H., Farr, T., Mitri, G., Kirk, R., Mitchell, K., Notarnicola, C., Casarano, D., Ventura, B., 2010. Active shoreline of Ontario Lacus, Titan: a morphological study of the lake and its surroundings. Geophysical Research Letters 37, L05202.
Wood, C.A., Lorenz, R., Kirk, R., CLopes, R.M., Mitchell, K.L., Stofan, E., 2010. Impact craters on Titan. Icarus 206, 334–344.
Wye, L., Zebker, H.A., Hayes, A.G., Lorenz, R.D., Notarnicola, C., Ventura, B., Casarano, D., the Cassini Radar Team, 2010. Constraining depths and wave heights for Titan's lakes with Cassini RADAR Data. In: American Geophysical Union, Fall Meeting 2010, abstract P31C-1552.

Appendix C

Life in the Saturnian Neighborhood

Book Chapter published in the book *Life on Earth and other Planetary Bodies* (2012),
Series: Cellular Origin, Life in Extreme Habitats and Astrobiology,
Volume 24, pp. 485-522
Hanslmeier, Arnold; Kempe, Stephan; Seckbach, Joseph (Eds.)
Springer Books

LIFE IN THE SATURNIAN NEIGHBORHOOD

ATHENA COUSTENIS[1], FRANCOIS RAULIN[2], GEORGIOS BAMPASIDIS[1,3], AND ANEZINA SOLOMONIDOU[1,3]
[1]LESIA, Observatoire de Paris, CNRS, UPMC Univ Paris 06, Univ. Paris-Diderot–Meudon, France
[2]LISA-IPSL, CNRS/UPEC & Univ. Paris Diderot, 61 Avenue Général de Gaulle, F-94000 Créteil, France
[3]National & Kapodistrian University of Athens, Athens, Greece

1. Introduction and Context

Charles Darwin's vision, in 1859, of the origin and evolution of life on Earth, paved the way for future biological searches and studies on our planet and on other planetary bodies. The DNA decoding by James Watson and Francis Crick (1953) confirmed both the complexity and the symmetry of living particles. Following their strides, astrobiology, the study of evidence for life outside the Earth, is not only the research of the origin, distribution, and evolution of life in the whole universe but also that of structures and processes related to life and its destiny (Raulin, 2007). In general, astrobiology brings together different scientific disciplines such as astrophysics, geology, chemistry, geochemistry, biology, and more in order to shed light on the many aspects regarding the creation of our solar system as well as the initiation of life. Starting with the terrestrial paradigm, astrobiology focuses on extraterrestrial environments, posing the unanswered question on the origins of life on Earth and elsewhere, while investigating the more easily accessible organic compounds—and in particular the prebiotic chemistry—on other celestial bodies.

It is generally admitted today that life arose on Earth as the derivative of a long chemical evolution, implying three major raw ingredients: liquid water, carbonaceous matter, and energy, working together over time. Since life primitive structures should be able to emerge, evolve, and develop in suitable environments, the quest for possible habitats outside our planet is focused on places where these ingredients are or have been present.

With the discovery of planets beyond our solar system and the search for current living organisms or for favorable conditions for past and future life in exotic places such as Mars, Europa, Titan, and Enceladus, the notion of habitability takes a new dimension. In this chapter, we focus on habitability issues and possible living forms around Saturn. Saturn has 62 known natural satellites to this date, and the discoveries from the Cassini–Huygens mission, which started in 2004, have revolutionized our perception about whether these bodies could harbor life

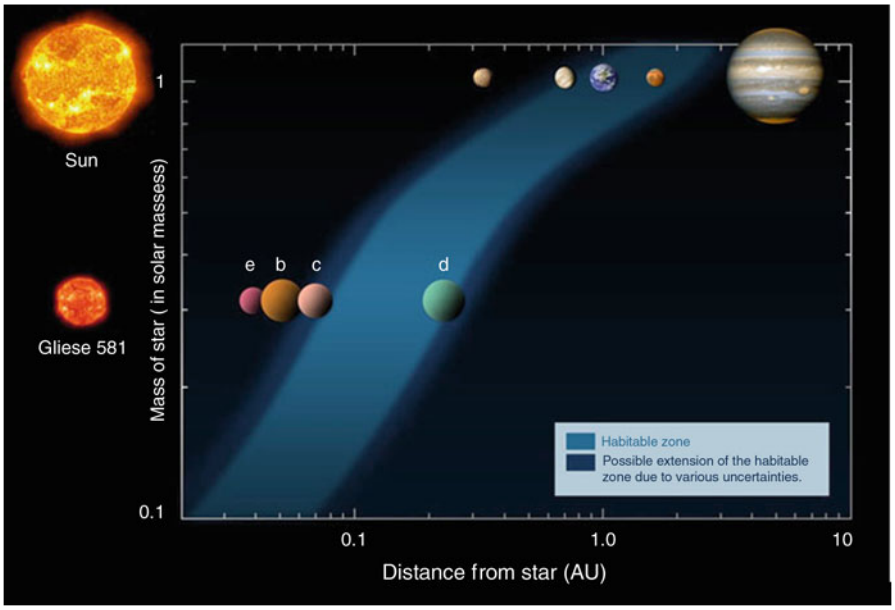

Figure 1. Map of the habitable zone's (*HZ*) limits. Earth is in the middle of the HZ for the solar system while Mars and Venus lie in its boundaries. The planetary bodies *e*, *b*, *c*, and *d* are exoplanets. Gliese 581 is *red dwarf* star 20.3 light years from Earth (NASA).

(now or in the future) or at least provide us with valuable information on the origin and evolution of life in the solar system. In the latter case, at least two of the Kronian satellites, Titan and Enceladus, can certainly offer a lot.

Discovered in 1655 by the Dutch astronomer Christiaan Huygens, Titan is the largest satellite of Saturn, bigger than planet Mercury, at 5,152 km in diameter. Titan rotates around the Sun within 29.5 years following Saturn on its trek. As a result, Titan experiences seasons, each of which lasts about 7.5 terrestrial years. Moreover, Titan orbits around Saturn within 16 Earth-days almost synchronously; thus, its solid surface rotates very slowly. Instead, due to strong zonal winds (Bird et al., 2005; Lorenz et al., 2008b), its atmosphere is in super-rotation. Due to Titan's distance from the Sun of about 9.5 astronomical units (AU), the satellite receives slightly more than 1% of the solar flux that the Earth registers at the top of its atmosphere at 1 AU (Fig. 1). In addition, Titan revolves far enough from the giant planet (about 20 Saturnian radii), to avoid any critical interactions with the rings or the magnetosphere. Although sometimes Titan moves close enough to Saturn to allow its atmosphere to interact with the energetic particles of the magnetosphere of Saturn. Together with the solar photons, these interactions play a key role in Titan's chemical evolution. Indeed, Titan possesses an extensive atmosphere made mostly of N_2 with a column density ten times that of Earth's (Fig. 2). Furthermore, Titan's astrobiological potential is enhanced by the presence

Figure 2. (*left*) Titan's thick, orange, and smoggy atmosphere (NASA); (*right*) Earth's atmosphere as seen from space (NASA); the cloudy nature of both atmospheric envelopes and also commonalities. Both Titan and Earth experience a greenhouse effect and complex photochemical reactions in their upper atmospheric layers.

of a rich organic chemistry which is produced in its atmosphere, thanks to the presence of its second most abundant gas, methane (about 1.4% in the stratosphere and 5% on the ground), and on the surface from the interactions among the various constituents.

Thus, Titan's unique and dense atmosphere harbors a whole host of organic trace gases: hydrocarbons and nitriles (e.g., Coustenis et al., 2007, 2010b). Its surface presents many morphological similarities with the Earth's, which surprisingly show similar structural diversity, but the raw materials are different from those on our own planet. With an environment very rich in organics, Titan, along with comets, is thus often considered as one of the best targets to search for prebiotic chemistry at a full planetary scale and a possible habitat for extraterrestrial life in all probability different from the terrestrial one. More importantly, our understanding of the origin of life on Earth could greatly benefit from studying Titan, where the low solar influx, the composition of the atmosphere, and the possible presence of an internal water ocean give us the opportunity to study the conditions prevailing on the primitive Earth.

After more than 8 years of close observations by remote sensing and *in situ* instruments on board the Cassini–Huygens mission, Titan is revealed as an evolving planet, geologically active, not only from erosional processes in the face of the lack of impact craters (Lopes et al., 2010) but also because of its possible cryovolcanism (Tobie et al., 2005; Barnes et al., 2006; Nelson et al., 2009a, b; Soderblom et al., 2009) and morphotectonism (Solomonidou et al., 2012), aeolian and fluvial erosion (Fulchignoni et al., 2005; Israel et al., 2005; Niemann et al., 2005; Owen, 2005; Tomasko et al., 2005; Zarnecki et al., 2005; Jaumann et al., 2008;

Lorenz and Mitton, 2008; Raulin, 2008; Lebreton et al., 2009), clouds and precipitations, and a methane cycle very similar to the water cycle on Earth (Bird et al., 2005; Atreya et al., 2006; Coustenis and Taylor, 2008; Brown et al., 2009a; Coustenis and Hirtzig, 2009). The organic chemistry products are found on Titan all the way from the upper atmosphere to the surface and possibly in the interior, indicating close exchanges between the different elements and planetary layers (interior-surface-atmosphere).

Enceladus, first observed by Sir Frederick William Herschel in 1789, is another intriguing moon of Saturn. Although it is quite small compared to Titan, with a mean radius of 252 km, the large plumes ejected from its south-polar region, as first discovered by the Cassini–Huygens mission magnetometer (Dougherty et al., 2006), make it very important for astrobiology. These geyser-like features mainly consist of water vapor and ice and include organic compounds (Dougherty et al., 2009; Waite et al., 2009). This strongly suggests the potential presence of a complex organic chemistry ongoing in the interior and the presence of liquid water, providing grounds for the search of a liquid ocean at short distances under the surface.

Enceladus is an unambiguous example of a cryovolcanically active icy satellite identified in the outer solar system and can be used to understand active processes that are thought to have once played and/or are still possibly playing (e.g., Titan's case) a role in shaping the surfaces of other icy moons. These processes include tidal heating, possible internal convection, cryovolcanism, and ice tectonics, which all can be studied as they currently happen on Enceladus. Moreover, the plume source region on Enceladus samples a warm, chemically rich, environment that may facilitate complex organic chemistry and biological processes.

What is the level of complexity reached by the organic chemistry in Titan and Enceladus? What is the correlation between the interior, the surface, and the atmosphere, especially regarding the biological aspects? What are the habitability potentialities in the Kronian environment, in particular for Titan? Such are the questions that further exploration of Titan and Enceladus should answer in the coming years (Brown et al., 2009b). After all, Darwin's evolutionary ideas could also be successfully applied *sensu lato* in the Saturnian neighborhood.

2. Habitability Issues for Outer Planetary Satellites

Liquid water is established as the necessary solvent in which life emerges and evolves. Water, as an abundant compound in our galaxy, can be found in various places, from cold dense molecular clouds to hot stellar atmospheres (e.g., Cernicharo and Crovisier, 2005; Hanslmeier, 2010). The thermodynamic behavior of water, which enables it to remain liquid in a large range of temperatures and pressures and to be a strong polar–nonpolar solvent, makes it essential for maintaining stable biomolecular and cellular structures (Des Marais et al., 2002).

A large number of organisms are capable of living in water. However, in a deposit of pure water, life will probably never spontaneously originate and evolve,

since while there are many organisms living in water, none we know of is capable of living on water alone, because life requires other essential elements such as nitrogen and phosphorus in addition to hydrogen and oxygen. Moreover, no known organism is made entirely of water. "Just water" is therefore not an auspicious place for the emergence and evolution of life.

The concept of the habitable zone (Fig. 1) is, of course, based on our understanding of life on Earth and is related to the presence of liquid water on a body's surface. But the requirements for extraterrestrial life do not have to be the same, suggesting that life could exist outside the habitable zone (Cohen and Stewart, 2002), in particular if liquid water exists underneath the surface. Furthermore, the changes that occurred on Earth's primordial atmosphere under the influence of early primitive plant life (Wolstencroft and Raven, 2002) require that diachronic alternation be taken into account regarding the habitability opportunities of a planetary body. In addition, internal processes such as volcanic activity, hydrothermal movements, and radioactive decay that possibly occur within satellites located outside the habitable zone could affect the radiation and thermal level of the body and thus change significantly the environmental conditions favoring life (Horneck, 2008).

Of the large satellites of the gas giants, there are those that may house underground water deposits in direct contact with heat sources below their icy crust and those expected to have either liquid water layers encapsulated between two ice layers or liquids above ice. In the study for the emergence of life elements on such satellites, the timescale is of essence. If it is long enough, the liquid water underground ocean may host life. Thus, the icy satellites of the outer planets of the solar system, as well as the recently discovered exoplanets, host unique conditions which may inhibit the emergence of life precursors in isolating environments that can prevent the concentration of the ingredients necessary for life or the proper chemical inventory for the relevant biochemical reactions. Conversely, according to Trinks et al. (2005), a coupled sea/ice system could in theory provide the necessary conditions for life emergence in the primitive Earth. Additional laboratory experiments and *in situ* studies of deep subglacial isolated lakes in Antarctica (Kapitsa et al., 1996) would improve our understanding in this field, as the physical properties of deep subglacial lakes resemble those found on both Jupiter's moon Europa and Saturn's moon Enceladus (Bulat et al., 2009).

As a consequence, the satellites of the giant planets like Europa, Enceladus, Ganymede and Titan are possible habitable environments and valid targets in the research for life with space missions and/or telescopes. However, life structures that do not influence the atmosphere of their host planet on a global scale will not be remotely detectable. In the solar system's neighborhood, such potential habitats can only be investigated with appropriate designed space missions, as in the case of Europa, where the Europa Jupiter Space Mission (Clark et al., 2009) will attempt to look for the hypothesized internal liquid water ocean. In the case of the Saturnian satellites (see hereafter), proposed future missions shall also address this question.

3. Titan: Organic Factory and Habitat

Retracing the processes, which allowed for the emergence of life on Earth around 4 billion years ago, is a difficult challenge. Our planet has drastically evolved since that time, and most of the traces of what were the initial environmental conditions have been erased as a consequence of plate tectonics and erosion. It is thus crucial for astrobiologists to find extraterrestrial locales with similarities to our planet's early stages. This will provide a way to study in the present time some of the processes, which occurred on the primitive Earth, when prebiotic chemistry was in its young stages (Fig. 3). For instance, a subsurface ocean in the interior of the satellite of a gas giant (as on Europe, Enceladus, Titan, etc.) may be habitable for some kind of life form—even though not necessarily an Earth analogue-but also information on the terrestrial-like atmospheric and surface conditions on any planetary body can provide valuable information.

Titan is a good candidate in this instance as its atmosphere exhibits more similarities with the Earth's today—and even more so in the past than any other solar system body (e.g., Coustenis and Taylor, 2008). Recent Cassini–Huygens findings have revolutionized our understanding of Titan's system and its potential for harboring the "ingredients" necessary for life (Coustenis and Taylor, 2008;

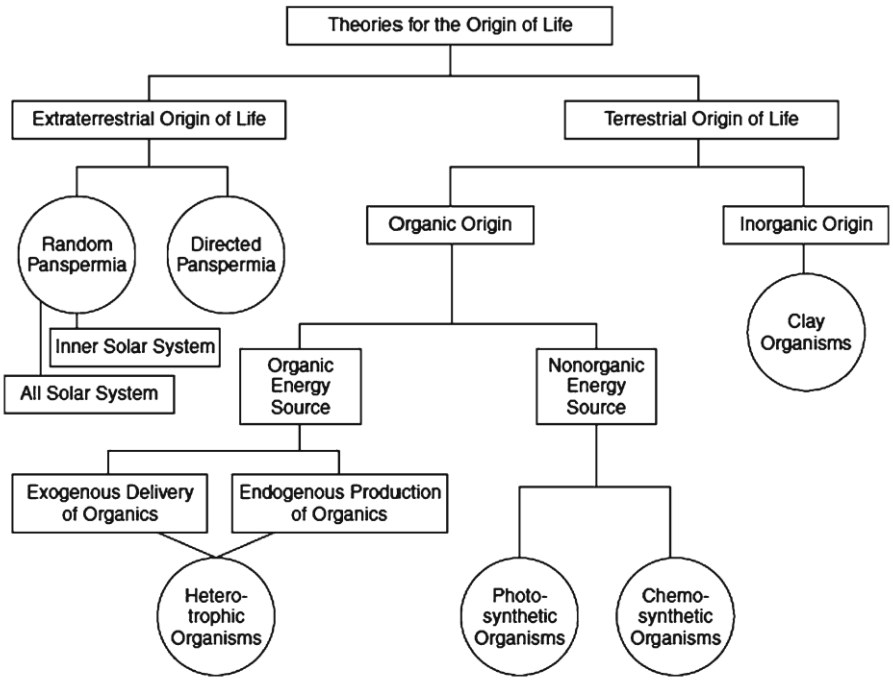

Figure 3. A scheme of possible theories on the origin of terrestrial and extraterrestrial life. The chemistry of the raw materials as well as energy sources plays key roles to each evolutionary path (From Davis and McKay (1996) and McKay et al. (2008)).

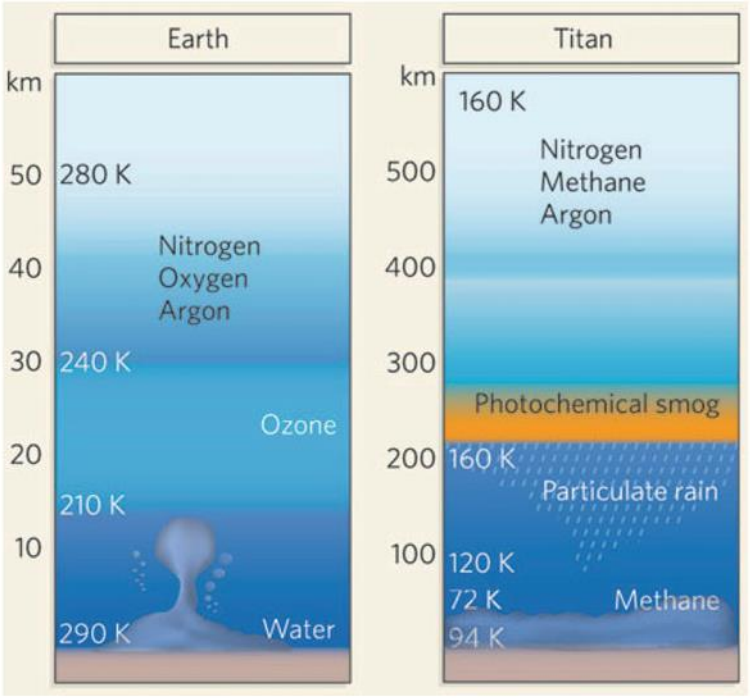

Figure 4. Atmospheric structure comparison of Earth and Titan. Both atmospheres are nitrogen-dominated, but on Titan, methane plays the role of water on Earth. Both atmospheres have an important haze content, and condensation processes are expected similarly on both bodies (Owen, 2005).

Lorenz and Mitton, 2008). Recent discoveries reveal that beyond its rich organic budget, and sufficient energy sources to drive chemical evolution, Titan also probably contains a vast subsurface ocean (Lorenz et al., 2008b).

Titan is indeed a very complex world much as our own planet. It is the only one other than Earth, that possesses a thick nitrogen-based atmosphere, four times denser than on our own atmosphere, with a rich organic chemistry (Fig. 4). It also has a geologically complex and active surface including lake-like features filled with organic liquid (e.g., Stofan et al., 2007). The physical processes within this world invite further close-up investigation that will provide a better understanding of the terrestrial processes as well.

Current investigations have shown that Titan fulfills many of life's prerequisites for a carbonaceous portfolio. Due to its nitrogen atmosphere, which is not in chemical equilibrium but like a chemical factory initiates the formation of complex positive and negative ions in the high thermosphere as a consequence of induced magnetospheric–ionospheric–atmospheric interactions involving EUV, UV radiation, energetic ions, and electrons (as recently demonstrated by the Cassini Ion and Neutral Mass Spectrometer, INMS). In this dynamic evolving environment, the second most abundant atmospheric constituent, methane, is dissociated irreversibly to produce a variety of trace gases such as hydrocarbons

(e.g., ethane, acetylene, and propane) and in combination with the nitrogen, nitriles (e.g., hydrogen, cyanide, acetonitrile, cyanoacetylene), which are detected in the stratosphere (between 70 and 500 km in altitude) by the Composite Infrared Spectrometer (CIRS) onboard Cassini (e.g., Coustenis et al., 2007, 2010b). Literally, some of these gases would be considered as signs of life if they were on our planet (HCN is considered a prebiotic molecule, a precursor of life). Hence, finding how they form on Titan could give us clues on how life began on Earth.

The Cassini–Huygens mission has revealed the essential details of the organic and methane hydrologic cycles that we see today on Titan (Raulin et al., 2008; Brown et al., 2009b; Lebreton et al., 2009). Methane on Titan seems to play the role of water on Earth, with a similar complex cycle as shown in Fig. 5 (Atreya et al., 2006). On Titan, where methane is photodissociated and forms ethane and other organic products in the atmosphere, it should have disappeared after 10–100 million years, with around 34 Myrs as a nominal period (Atreya et al., 2006).

The intriguing question then is of how methane gets replenished in the atmosphere. On Earth today, it is life itself that refreshes the methane supply since methane is a by-product of the metabolism of many organisms. Hence, could this mean there is life on Titan? However, the Huygens Gas Chromatograph Mass Spectrometer (GCMS) data have shown that methane is not of biogenic origin, because the isotopic ratios are compatible with inorganic values (Niemann et al., 2005, 2010). Thus, the sinks of atmospheric methane on Titan are relatively well understood, but the major sources of replenishment are still very model dependent, as will be discussed later.

3.1. THE ATMOSPHERIC ORGANIC-RICH ENVIRONMENT OF TITAN

Although Titan's atmosphere is much colder than Earth's, it presents many direct similarities with our planet (Fig. 4), at different levels which have been pointed out since Voyager days. To begin with, both are made of the same main constituent, dinitrogen. A similar vertical structure from the troposphere to the ionosphere is also present, as well as a surface pressure of 40% larger than that of the Earth's (Fulchignoni et al., 2005). This is the only case of an extraterrestrial planetary atmospheric pressure so similar to that of Earth. Furthermore, a very exciting and complex organic chemistry takes place in Titan's atmosphere.

The direct analysis of the ionosphere by the Cassini Ion and Neutral Mass Spectrometer (INMS) instrument during the low-altitude Cassini flybys of Titan shows the presence of many organic species at detectable levels, at very high altitudes (1,100–1,300 km). Extrapolation of the INMS measurements (limited to mass up to 100 Da) and of Cassini Plasma Spectrometer (CAPS) data strongly suggests that high molecular weight species (up to several 1,000 Da) may be present in the ionosphere (Waite et al., 2007). These observations open a fully new vision of the organic processes occurring in Titan's atmosphere, with a strong implication of the ionospheric chemistry in the formation of complex organic

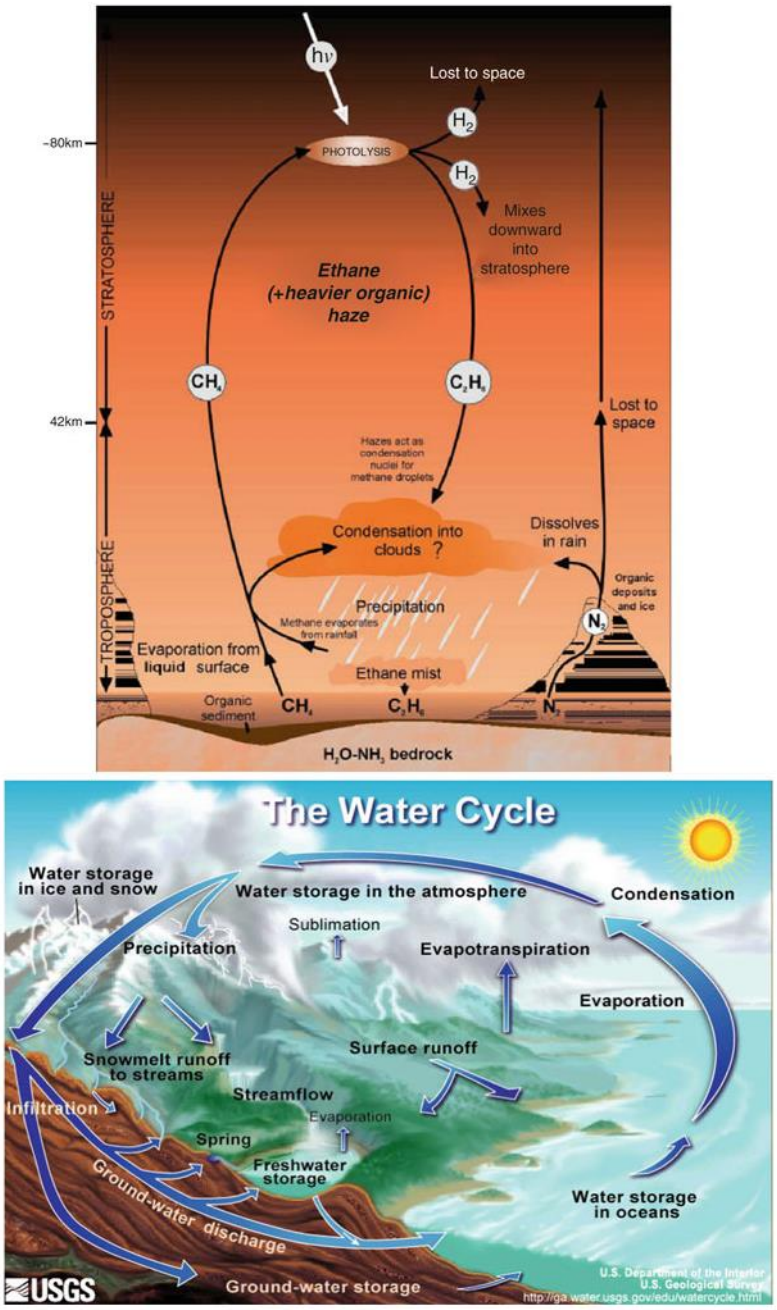

Figure 5. Titan's methane (*upper*) and Earth's water (*lower*) cycles in the atmosphere (USGS). Titan has a methane cycle resembling Earth's water cycle in its processes.

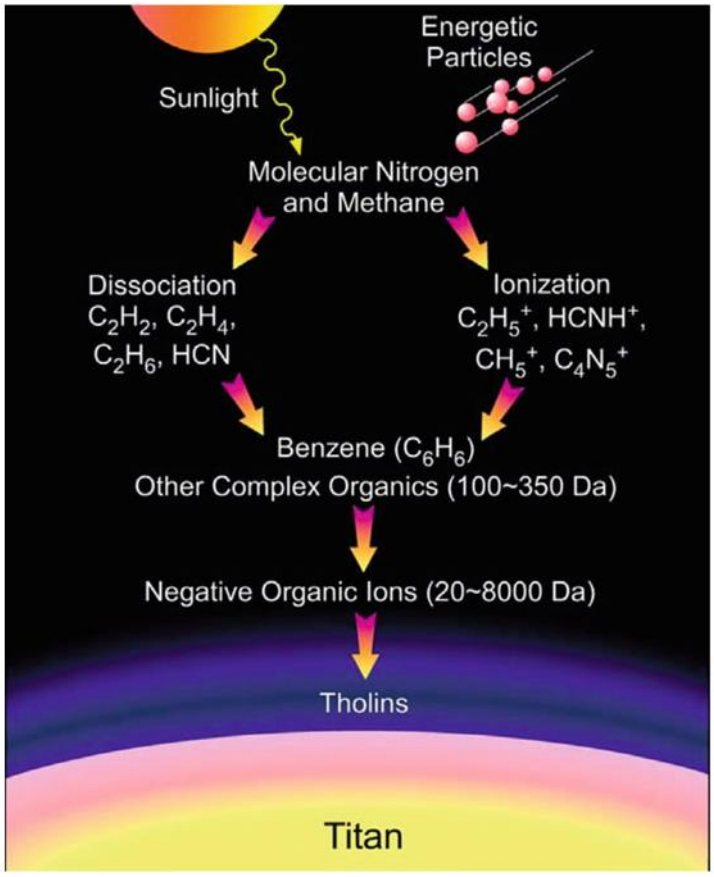

Figure 6. Organic chemistry in Titan's upper atmosphere. At the upper layers of the atmosphere, sunlight and energetic particles from Saturn's magnetosphere destroy CH_4 and N_2 and produce complex organic molecules that assemble to form negative ions from which tholins (hydrocarbon–nitrile aerosols) possibly form and diffuse in the lower parts of the atmosphere. Cassini/INMS measurements showed evidence for their formation around 1,000 km in altitude (Waite et al., 2007), and the Cassini/CIRS instrument detects the neutral chemistry in the stratosphere (Flasar et al., 2005).

compounds in Titan's environment (Fig. 6), which was not envisaged before. These compounds are detectable in solar and stellar UV occultations and initiate the process of haze formation starting at about 950 km (Waite et al., 2007) to finally condense out.

In the neutral atmosphere of Titan (between roughly 100 and 500 km), as we mentioned above, CH_4 chemistry is coupled with N_2 chemistry producing the formation of many organics in gas and particulate phase: hydrocarbons, nitriles, and complex refractory organics. Several photochemical models describing the chemical and physical pathways involved in the chemical evolution of the atmosphere of Titan have been published for the last 20 years (Yung et al., 1984;

Toublanc et al., 1995; Wilson and Atreya, 2004; Lavvas et al., 2008). These papers estimate the resulting vertical concentration profiles of the different molecules. Based on these models, the cycling of volatile chemicals starts with the dissociation of N_2 and CH_4 through electron, photon, and cosmic rays impacts in Titan's atmosphere. The primary processes allow for the formation of acetylene (C_2H_2) and hydrogen cyanide (HCN) in the high atmosphere. These molecules play a key role in the general chemical scheme: once they are formed, they diffuse down to the lower levels where they allow the formation of higher hydrocarbons and nitriles and perhaps aromatic compounds. Additionally, methane dissociation probably also occurs in the low stratosphere through photocatalytic processes involving acetylene and polyynes. The end products of the chemical evolution of methane in the atmosphere are complex refractory organic compounds and ethane.

As these aerosols and haze particles fall through the atmosphere and grow, they become detectable with imaging systems such as the Cassini Imaging Science Subsystem (ISS) at about 500 km altitude and are ubiquitous throughout the stratosphere (Porco et al., 2005). They are strong absorbers of solar UV and visible radiation and play a fundamental role in heating Titan's stratosphere and driving wind systems in the middle atmosphere, much as ozone does in the Earth's middle atmosphere.

Experiments that simulate the reactions taking place in Titan's atmosphere (such as the Miller-Urey experiment) produce refractory organics, usually named tholins (Sagan and Khare, 1979) ("tholins" are solid products in the laboratory mimicking complex refractory organics: Nguyen et al. (2007); and references therein). Tholins represent laboratory analogues of Titan's aerosols and are useful to interpret many observational data which require information on the aerosols. As being experimental analogues of Titan's atmospheric particles, tholins also allow the study of the aerosols behavior in Titan's conditions with the tools available in the laboratory. Several organic compounds have already been detected in Titan's upper and lower atmosphere (Waite et al., 2007; Coustenis et al., 2010b). The list includes hydrocarbons (both with saturated and unsaturated chains) and nitrogen-containing organic compounds, exclusively nitriles, as expected from laboratory simulation experiments (Fig. 6). Moreover, since the Cassini arrival in the Saturnian system in 2004, the presence of water vapor and benzene has been unambiguously confirmed by the CIRS instrument.

3.2. TITAN'S PREBIOTIC RELEVANCE

Several of the organic processes that are occurring today on Titan form some of the organic compounds which are considered as key molecules in terrestrial prebiotic chemistry, such as hydrogen cyanide (HCN), cyanoacetylene (HC_3N), and cyanogen (C_2N_2). In fact, with several percent of methane in dinitrogen, the atmosphere of Titan is one of the most favorable atmospheres for prebiotic synthesis, although it almost lacks both oxygen and hydrogen. Concerning the hydrocarbon trace budget, photochemical models imply that light hydrocarbons are destroyed mostly

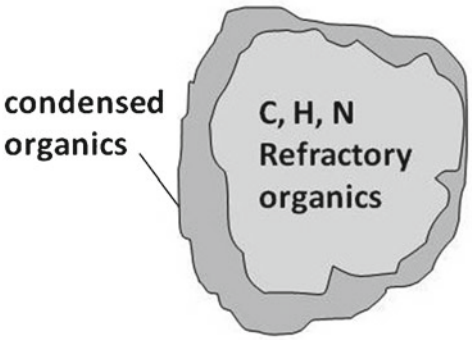

Figure 7. Composition of Titan's aerosols.

by reactions with OH^- and Cl^- radicals. Contrary to the very short lifetime of C_2H_2 on Earth (Rudolph et al., 1984), acetylene on Titan shows a seasonal variation during a Titan year (29.5 terrestrial years) and reaches almost the abundances recorded by Voyager 1 in 1980 (Coustenis et al., 2010a).

The Aerosol Collector Pyrolyser (ACP) experiment on Huygens provided the first direct *in situ* chemical analysis of Titan's aerosols. It collected haze particles from the stratosphere and the troposphere, heated them at different temperatures, and sent the produced gases for analysis to the GCMS instrument. The obtained results indicated that the aerosols are made of a refractory nucleus, composed of H, C, and N atoms (Fig. 7) and producing NH_3 and HCN after pyrolysis at 600°C (Israel et al., 2005). This strongly supports the tholin hypothesis. It also strongly suggests that Titan's aerosols may evolve once in contact with water ice on the surface and may produce a variety of organics of biological interest, such as amino acids (Neish et al., 2010; Ramirez et al., 2010).

Analogies are thus obvious between the organic chemistry activity currently occurring on Titan and the prebiotic chemistry which was once active on the primitive Earth, prior to the emergence of life (e.g., McKay and Smith, 2005). Indeed, in spite of the absence of permanent bodies of liquid water on Titan's surface, both chemistries are similar. As noted earlier, many resemblances can also be made between the role of methane on Titan and that of water on the Earth, with a complex cycle that has yet to be fully understood. Indeed, on Titan, methane can exist as a gas, liquid, and solid, since the mean surface temperature is almost 94 K (Fulchignoni et al., 2005), approaching the triple point of methane.

The atmosphere we enjoy today on Earth is probably radically different from the primitive one dating back to 4.6 billion years ago when our planet was nothing more than a molten ball of rock surrounded by an atmosphere of hydrogen and helium. In the absence of a magnetic field at those early stages, the intense solar wind from the young Sun blew this early atmosphere away. Then, as Earth cooled enough to form a solid crust, it was covered with active volcanoes, ejecting

water vapor, carbon dioxide, and ammonia to form an early toxic atmosphere. Eventually, light from the Sun broke down the ammonia molecules exsolved by the volcanoes, releasing nitrogen into the atmosphere. Over billions of years, the quantity of nitrogen built up to the levels we see today. Although life formed just a few hundred million years later, it was not until the evolution of bacteria, 3.3 billion years ago, that the early Earth atmosphere changed into the one we know today. During the period from 2.7 to 2.2 billion years ago, these early bacteria—known as cyanobacteria—used energy from the Sun for photosynthesis and released oxygen as a by-product. They also trapped carbon dioxide in organic molecules. In just a few hundred million years, these bacteria completely changed the Earth's atmosphere composition, bringing us to the current mixture of 21% oxygen and 78% nitrogen. Schaefer and Fegley (2007) predict that Earth's early atmosphere contained CH_4, H_2, H_2O, N_2, and NH_3, similar to the components used in the Miller–Urey synthesis of organic compounds, often related to Titan's and Enceladus's atmospheric inventory. Furthermore, Trainer et al. (2006) looked at the processes that formed haze on Titan and on early Earth and found many similarities for what could have served as a primary source of organic material to the surface.

Before the rise of the atmospheric oxygen in the terrestrial atmosphere 2.5 Gy ago, it considered possible that the abundance of methane gas was 10–20 times higher than the today's value of 1.6×10^{-6} (Pavlov et al., 2003). Hence, if the atmospheric CO_2/CH_4 ratio had become equal to 10 at the mid-Achaean era, an organic haze could have formed on this early environment (Pavlov et al., 2000; DeWitt et al., 2009). This hydrocarbon haze produced the anti-greenhouse effect which reduced the temperature of the atmosphere (Kasting and Howard, 2006). Titan also hosts a thick methane-induced organic haze, similar to the one predicted for the early Earth and, consequently, experiences the same anti-greenhouse effect (McKay et al., 1999). The absence of vast amounts of CO_2 on Titan is one of the major differences between the two atmospheric envelopes. On the other hand, hydrogen cyanide and other prebiotic molecules are among the starting materials for biosynthesis. The existence of hydrocarbons, and in particular acetylene and benzene, has really enlarged the borders of photochemical organic products.

Especially, the presence of benzene (C_6H_6) seems extremely interesting, as it is the only polycyclic aromatic hydrocarbon (PAHs) discovered on Titan today. The presence of PAHs on Titan's atmosphere is very important as they could contribute to the synthesis of biological building blocks. Moreover, the combination of the liquid deposits on the surface of Titan and the low temperature could host the proper environment for this biosynthesis. Recent laboratory experiments showed that aromatic compounds could be plausibly produced on icy surfaces (Menor-Salván et al., 2008). Benzene was first detected at 674 cm^{-1} based on Infrared Space Observatory (ISO/SWS) data (Coustenis et al., 2003) with the mixing ratio of 4×10^{-10} and was then also detected in the thermosphere (950–1,150 km) from the analysis of Cassini/INMS data (Waite et al., 2007) and firmly in the stratosphere (100–200 km) at all latitudes by Cassini/CIRS

measurements (Flasar et al., 2005; Coustenis et al., 2007, 2010b). Moreover, benzene has been tentatively identified on Titan's surface by Huygens/CGMS measurements (Niemann et al., 2005).

As Titan lacks oxygen and sufficiently high temperatures, as did primitive Earth, different evolutionary pathways from Earth must have been followed on Titan, and polyphenyls may possibly be created (Delitsky and McKay, 2010). The abundances of hydrocarbons are higher on Titan than those on Earth by a factor of about 10^2–10^4. Moreover, the temporal variations of the hydrocarbon traces on Titan experience a full cycle during the Titan year (Coustenis et al., 2010a) and are probably influenced by local or regional sources and sinks. Photochemical models are trying to reproduce these phenomena. Taking into account all the above-described characteristics, the prebiotic potential of Titan is enormous, and a huge effort in astrobiological studies is focused on its environment. Eventually, Titan still seems to be the ideal planet-size laboratory for increasing our knowledge of the evolution of the Earth's atmosphere.

3.3. ORGANIC CHEMISTRY AND MORPHOLOGY OF TITAN'S ACTIVE SURFACE

The Cassini–Huygens mission has significantly enhanced our understanding of Titan as the largest abiotic organic factory in the solar system. The abundance of methane and its organic products in the atmosphere, seas, and dunes exceeds the carbon inventory in the Earth's ocean, biosphere, and fossil fuel reservoirs by more than an order of magnitude (Lorenz et al., 2008a). As discovered by the Cassini/INMS, in the high atmosphere, heavy ions are formed (Waite et al., 2007).

Measurements throughout the atmosphere, both remote and *in situ*, have indicated the presence of numerous hydrocarbon and nitrile gases, as well as a complex layering of organic aerosols that persists all the way down to the surface of the moon (Tomasko et al., 2005; Coustenis et al., 2007; de Kok et al., 2007). Radar observations suggest that the ultimate fate of this aerosol "rain" is the generation of expansive organic dunes that produce an equatorial belt around the surface. Condensation of these species on aerosol particles is a probable explanation for these atmospheric characteristics. These particles, for which no direct data on their chemical composition were previously available, were analyzed by the Aerosol Collector and Pyrolyser instrument aboard Huygens probe. ACP results show that the aerosol particles are made of refractory organics which release HCN and NH_3 during pyrolysis.

This supports the tholin hypothesis (as described in section 3.1). From these new *in situ* measurements, it seems very likely that the aerosol particles are made of a refractory organic nucleus, covered with condensed volatile compounds (Israel et al., 2005). However, Huygens/GCMS did not detect a large variety of organic compounds in the low atmosphere (Niemann et al., 2005).

Figure 8. Linear dunes on Titan (Radebaugh et al., 2010). Titan's dunes are believed to be composed of ice and organics grains that possibly derive from a combination of the surface ice and the organic chemicals that fall through in Titan's atmosphere.

Moreover, the nature and abundances of the condensates have not been measured. Even more importantly for astrobiology, neither the elemental composition nor the molecular structure of the refractory part of the aerosols has been determined.

Eventually, these complex organic molecules are deposited on Titan's surface in large quantities, where data from Cassini's instruments hint at their existence. Hence, the upper thermosphere is linked intimately with the surface and the intervening atmosphere. In spite of the low surface temperature, the organics reaching the surface are probably evolving once in contact with water ice and may form organic molecules of biological interest.

Radar observations suggest that the ultimate fate of this aerosol "rain" is the generation of expansive organic dunes that produce an equatorial belt around the surface. Indeed, the surface of Titan shows also the presence of sedimentological and meteorological processes, as we see on Earth: There are many large dune areas (Lorenz et al., 2006; Radebaugh et al., 2008, 2010) (Fig. 8) where the terrestrial silica sand is probably replaced, once more, by water ice particles, mixed with the organic material of the aerosols.

Cassini's radar instrument finally unveiled what appears to be a land of lakes in Titan's northern polar regions (see Fig. 9) (Stofan et al., 2007). Cassini/ISS images also show a kidney-shaped dark feature about 200 km in length, named Ontario Lacus, that is outside the area of radar coverage and has recently been confirmed by the Cassini Visual and Infrared Mapping Spectrometer (VIMS)

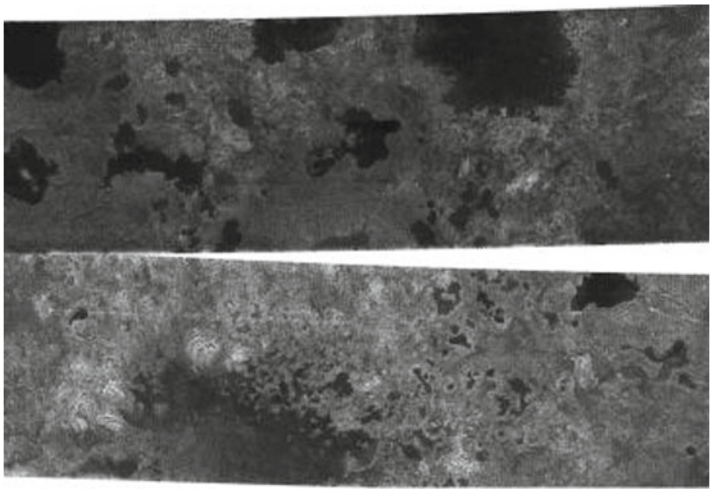

Figure 9. Lakes discovered in Titan's north-polar region by the Synthetic Aperture Radar (SAR) on board Cassini–Huygens mission (NASA/JPL). The dark patches are believed to be filled with hydrocarbon liquid.

not only to be a lake but also to be composed of ethane liquid (Brown et al., 2008). In the absence of a massive surface ocean but with analogues to all other terrestrial hydrological phenomena present, Titan's methane cycle is very exotic.

The liquid bodies are one of the main astrobiological aspects of Titan. Cassini's cameras (ISS) have allowed scientists to compile a nearly global surface map and to monitor the surface and atmosphere for activity. Intriguingly, repeated south-polar imaging by ISS revealed differences consistent with ponding of hydrocarbon liquids on the surface due to precipitation from a large storm. More recent ISS images of high northern latitudes illustrate the full extents (>500,000 km^2) of hydrocarbon seas, also observed by Cassini's radar. These observations demonstrate dynamic processes at work on Titan and indicate that the poles harbor liquid-hydrocarbon reservoirs, the extents of which differ from pole to pole and which may be coupled to seasonally varying circulation (Turtle et al., 2009).

The lakes and seas observed on Titan in the polar regions (Mitri et al., 2007; Stofan et al., 2007) make Titan the only body in the solar system having large liquid bodies on its surface. These very dark features at the high northern latitudes of Titan were finally shown to be liquid-filled (most probably with ethane-rich mixtures (Brown et al., 2008)) basins—classifying them as lakes.

The features range in size from less than 10 km^2 to at least 100,000 km^2. They are limited to the region poleward of 55°N. Currently, Cassini's instruments have identified and mapped almost 655 geological structures referred as lakes and/or basins (Fig. 10) (Hayes et al., 2008). Titan is thus the only planetary body, other than the Earth, with long-standing bodies of liquid on its surface (although direct observational evidence of the longevity of Titan's surface liquids remains

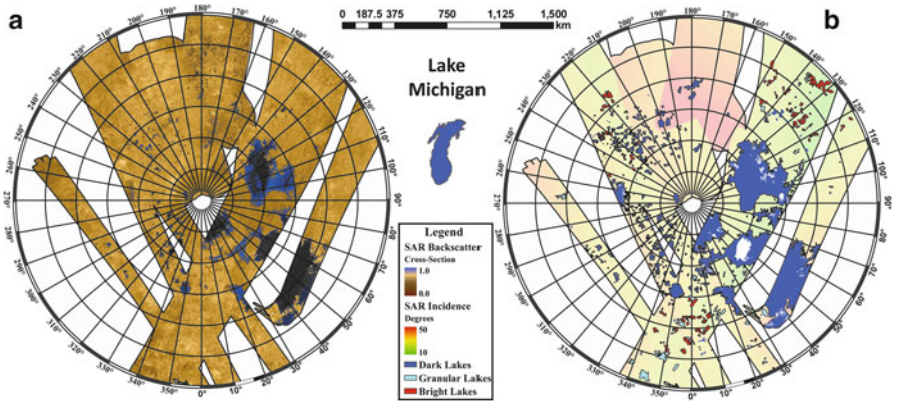

Figure 10. Map of almost 655 lakes and sea features by the Cassini radar system in azimuthal projection at the north pole of Titan. Map A (*left*) shows the radar swath mosaic up to May 2007 flybys. Map B (*right*) represents the spatial distribution of mapping units. Lake Michigan is illustrated for scale purposes (Hayes et al., 2008).

to be obtained). All of this suggests that Titan maybe even more similar to primitive Earth than we thought. However, the degree of complexity which can be reached from such an organic chemistry in absence of permanent liquid water bodies on Titan's surface is still unknown, although it could be quite high.

McKay and Smith (2005) noted the astrobiological importance of these geological features that are filled with liquid hydrocarbons, since there is a possibility for a different form of life to exist in such environments. It has been hypothesized that such a methanogenic life form consumes H_2 instead of O_2 that could be measured in the lower atmosphere. Two papers, by Strobel (2010) and Clark et al. (2010), based on data from the Cassini orbiter focus on the complex chemical activity on the surface of Titan. Strobel (2010) shows that hydrogen flows down through Titan's atmosphere and then somehow disappears on the surface. One of the most interesting phenomena occurring on Titan is that important quantities of atmospheric hydrogen precipitates and disappears when reach the surface. Such process resembles the oxygen consumption as occurring on Earth although in Titan's case, the element is hydrogen (Strobel, 2010).

Even though this is not supportive to the Titan's terrestrial-type life theory, it represents a hypothetical second form of life independent from water-based life we know on Earth. Strobel (2010) describes densities of hydrogen in different parts of the atmosphere and the surface. Previous models had predicted that hydrogen molecules, a by-product of ultraviolet sunlight breaking apart acetylene and methane molecules in the upper atmosphere, should be distributed fairly evenly throughout the atmospheric layers. The authors found a disparity in the hydrogen densities that lead to a flow down to the surface at a rate of about 10,000 trillion hydrogen molecules per second. This is about the same rate at which the molecules escape out of the upper atmosphere. Strobel (2010) states

that it is not likely for hydrogen to be stored in a cave or underground space on Titan. Titan's surface is also so cold that a chemical process that involved a catalyst would be needed to convert hydrogen molecules and acetylene back to methane, even though overall there would be a net release of energy. The energy barrier could be overcome if there were an unknown mineral acting as the catalyst on Titan's surface.

Another possible indicator for life on Titan is the lack of acetylene on the surface since there is no clear evidence of this compound in the received data to date, while it is expected to have been deposited through the atmosphere. It has been suggested that this could be due to the fact that some form of life on the surface is using acetylene as an energy source (Clark et al., 2010). This theory is largely debated and controversial among the scientific community, especially due to suggestions of nonbiological origin of this phenomenon; however, it has the merit to propose new interesting astrobiological theories. In detail, Clark et al. (2010) map hydrocarbons on the surface from Cassini/VIMS data and find a lack of acetylene. McKay and Smith (2005) had identified acetylene as the best energy source for methane-based life on Titan. While nonbiological chemistry offers one possible explanation, these authors believe these chemical signatures bolster the argument for a primitive, exotic form of life or precursor to life on Titan's surface. According to one theory put forth by astrobiologists, the signatures fulfill two important conditions necessary for a hypothesized "methane-based life", which would consume not only methane but also hydrogen. However, one other possibility is that sunlight or cosmic rays are transforming the acetylene in icy aerosols in the atmosphere into more complex molecules that would fall to the ground with no acetylene signature.

To date, methane-based life forms are only hypothetical. Scientists have not yet detected this form of life anywhere, though there are liquid-water-based microbes on Earth that thrive on methane or produce it as a waste product. At Titan's low temperatures, a methane-based organism would have to use a substance that is liquid as its medium for living processes, but not water itself. Water is frozen solid on Titan's surface and much too cold to support life as we know it. The list of liquid candidates includes liquid methane and related molecules like ethane. While liquid water is widely regarded as necessary for life, there has been extensive speculation published in the scientific literature that this is not a strict requirement. The new hydrogen findings are consistent with conditions that could produce an exotic, methane-based life form, but do not prove its existence.

3.4. INTERIOR MODELS FOR TITAN AND ITS POSSIBLE SUBSURFACE OCEAN

Regarding Titan's interior structure, since the only *in situ* data from its surface are the Huygens probe recordings, only modeling assumptions can be presented. Structural models for planetary interiors suggest that Titan, like Europa, Ganymede,

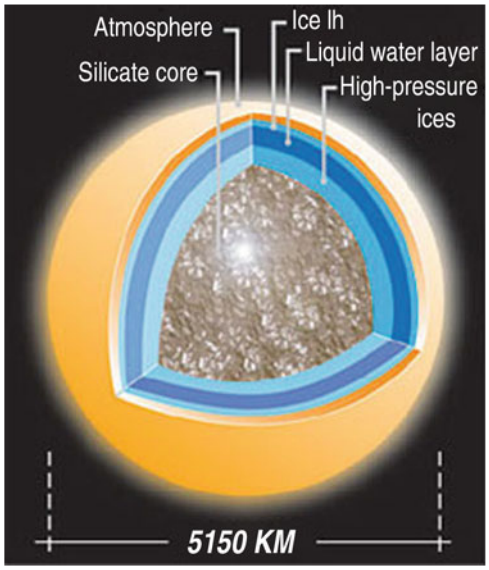

Figure 11. Illustration of Titan's internal structure with a liquid ocean between two subsurface ice layers (From Tobie et al., 2005). Cassini–Huygens recorded extremely low-frequency radio waves which supports the existence of this liquid subsurface layer (NASA/LPGN).

and Callisto, has maintained internal liquid water reservoirs, probably mixed with some ammonia and more speculatively sulfur and possibly entrained methane clathrates (Fig. 11).

Another possible location to look for life on Titan would be in an undersurface liquid water ocean. The presence of such an internal ocean is supported by Titan internal structure models (Tobie et al., 2005; Mitri et al., 2008), radar and gravity Cassini measurements (Lorenz et al., 2008b), and the Huygens Atmospheric Structure Instrument (HASI) experiment. Beghin et al. (2009) thus interpreted the extremely low-frequency electric signal recorded by HASI as a Schumann resonance between the ionosphere and a modestly conducting ocean (since the ice is not conductive) roughly 30–50 km below the surface. Thermal evolution models suggest that Titan may have an ice crust between 50 and 150 km thick, lying atop a liquid water ocean a couple of 100 km deep, with some amount (a few to 30%, most likely ~10%) of ammonia dissolved in it, acting as an antifreeze material (Lorenz et al., 2008b). This correspond to a pH around 11.5. The pressure reaches~5 kbars at 200 km depth, and it could include hot spots reaching −20 °C. Such conditions are not incompatible with life as we know it on Earth (Fortes, 2000; Raulin, 2008; Raulin et al., 2009).

Tobie et al. (2005) suggested a layered interior structure of Titan, consisting of a rocky core overlaid by high-pressure ice, a liquid layer overlaid by low pressure ice, and finally a solid icy crust (Fig. 11). An earlier model by Fortes (2000)

noted that underneath Titan's icy crust, at a depth of approximately 200 km, there lies an ammonia–water solution ocean in which life could survive. Another, more recent model by Mitri et al. (2008) suggests pockets of methane clathrates trapped within an ammonia–water ocean which could exsolute and produce overpressure and consequently the ammonia–water can erupt to the surface leading to cryovolcanic phenomena.

With regard to Titan's morphology and internal dynamic geology, it has been suggested that there may be active cryovolcanoes on Titan (Sotin et al., 2005; Lopes et al., 2007) since traces of former flows have been found across parts of the surface. A wide variety of Cassini data support the presence of cryovolcanism on Titan. Indeed, at least two regions have been observed to change reflectance on Titan's surface (Tui Regio 20°S, 130°W; Hotei Regio 26°S, 78°W) (Barnes et al., 2006; Nelson et al., 2009a, b), and one of them (Hotei Regio) in addition to a recent discovery (Sotra Facula 15°S, 42°W) in radar images exhibit lobate "flow" forms (Soderblom et al., 2009; Lopes et al., 2010), consistent with the morphology of volcanic terrain, supporting the hypothesis of cryovolcanic eruptions (Sotin et al., 2005).

However, on Titan, fluid water mobilized and made buoyant by ammonia and other materials could replace terrestrial melted silicates. Cryovolcanism suggests a dynamic process than involves the interior, the surface, and the atmosphere as well. It is a multi-complex activity that resembles terrestrial volcanic processes as it follows a similar pattern although in extremely altered conditions and different initial and depositional products. Cryovolcanism on Titan is believed to be a significant source of the methane in the atmosphere (Tobie et al., 2006). An underground liquid ocean, several hundred kilometers deep at the surface of Titan, is suggested to be the source of cryomagma, hence outgassing methane into the atmosphere and thus replenishing the destroyed amounts.

There are indeed studies suggesting the presence of an internal ammonia–water ocean (Grasset and Sotin, 1996; Grasset et al., 2000; Tobie et al., 2005; Mitri et al., 2007) while another study has modeled and suggested an ocean filled with methane clathrate pockets that lead to explosive cryovolcanism (Fortes et al., 2007).

The theory of trapped methane clathrates in the potential liquid ocean is of a major astrobiological interest. The presence of methane clathrates in an aqueous environment is attached to the "clathrate gun" hypothesis. This hypothesis suggests that potential movement and rise of the temperature in an underground liquid reservoir could trigger the sudden release of methane from methane clathrate compounds buried in permafrost or seabeds (Kennett et al., 2003) or an ocean like on Titan's case. The initiation of such process leads to further temperature rise and further methane clathrate destabilization that could easily cause and trigger cryovolcanic eruptions (Kennett et al., 2003). For Titan, a dynamic process like the one suggested by the clathrate gun hypothesis could result to increase of temperature values, creating an environment more favorable for life to exist.

With respect to the astrobiological interest, there is a controversy about the effectiveness of methane as a medium for life compared to water or ammonia. Water has higher solubility than methane, enabling easier transport of substances in a cell, while methane's lesser chemical reactivity allows for the easier formation of large structures corresponding to proteins (Benner et al., 2004). In addition, the cryovolcanic activity suggests higher temperatures within the ocean and the volcanic conduit where heat transfer between the interior and upper layers would be critical in sustaining any subsurface oceanic life (Grasset et al., 2000).

Thus, the possibility of life in this ocean cannot be excluded. Moreover, models also predict that during the first tens millions of years after Titan's formation, the ocean was in direct contact with the atmosphere on one side and with the bedrock on the side. This could have provided conditions very favorable for an efficient prebiotic chemistry toward the emergence of life, with the possible involvement of hydrothermal vents. Thus, the internal ocean of Titan not only is habitable but could be inhabited.

Hence, in spite of the low temperature, Titan is not a congealed Earth: The chemical system is not frozen. Titan is an evolving planetary body and so is its chemistry. Once deposited on Titan's surface, the aerosols and their complex organic content may follow a chemical evolution of astrobiological interest. Laboratory experiments show that, once in contact with liquid water, Titan tholins can release many compounds of biological interest, such as amino acids (Khare et al., 1986). Such processes could be particularly favorable in zones of Titan's surface where cryovolcanism may occur. The N_2–CH_4 by-products in Titan's atmosphere eventually end up as sediments on the surface, where they accumulate presently at a rate of roughly 0.5 km in 4.5 Gyr.

Long-term chemical evolution is impossible to study in the laboratory: *In situ* measurements of Titan's surface thus offer a unique opportunity to study by a ground-truth approach some of the many processes which could be involved in prebiotic chemistry, including isotopic and enantiomeric fractionation (Nguyen et al., 2007).

There are suggestions that Titan is presently geologically active on the surface (Nelson et al., 2006, 2009a, b) and in its interior. If Titan is currently active, then these results raise the following questions: What is the full extent of current geologic activity? What are the ongoing processes? Are Titan's chemical processes today supporting a prebiotic chemistry similar to that under which life evolved on Earth?

Although the chemical reactions that lead to life on Earth take place in liquid water, the reactions themselves are almost entirely between organics. The study of organic chemistry is therefore an important, and arguably richer, adjunct to the pursuit of liquid water in the solar system. Titan's organic inventory is impressive, and carbon-bearing compounds are widespread across the surface in the form of lakes, seas, dunes, and, probably, sedimentary deltas at the mouths of channels.

4. Enceladus: Liquid Water Far Away from the Sun

Discovered by William Herschel in 1789, Enceladus is arguably a place in the solar system where a demonstrably habitable environment already occurs and evaluating its astrobiological potential should be an overarching goal of Enceladus research. Although Enceladus is a relative small planetary body (500 km in diameter), significant chemical processes could produce primitive life structures. Obviously, oxidation/reduction reactions necessitate supporting redox-based life (Gaidos et al., 1999). Fe- and Ni-bearing dust particles can operate as reducing agents on Enceladus, which exist since planetary formation from the ancient solar nebula.

As concerns oxidant agents on Enceladus, Gaidos et al. (1999) also noted their production through E-ring particles, charged from the Saturnian magnetospheric environment. Then, some suitable geological process is needed to mix the reducing and oxidizing compounds. In a model by Cooper et al. (2009), the astrobiological parameters that support life on Enceladus are evaluated as higher than for Europa due to a less extreme state of oxidation and greater residual abundance of organics.

Indeed, Enceladus, Saturn's most active moon as observed from Cassini, presents a mystery in the studies of planetary science and, more specifically, in geophysics. The enigma evolves around how a small moon can possess sufficient dynamical energy to drive a geyser plume rising 600 miles in space out of the moon's south pole, eventually feeding its material to the outer E-ring of Saturn (Postberg et al., 2009). The heat source for Enceladus is still an open question, as is the possibility for life to exist on this small satellite if an underground liquid water ocean or liquid water subsurface pockets exist to explain the plumes (Kieffer and Jakosky, 2008).

The geyser plumes arise from the warm surface surrounding and including four parallel faults located at the moon's south pole, the "Tiger Stripes" fractures (Porco et al., 2006; Spencer et al., 2006), spewing a series of jets more than 600 km high (Fig. 12). The mass production rate of the plume gas has been estimated to be ~150 kg/s from occultation data (Tian et al., 2007). This value is surprisingly high, sufficient to remove a significant fraction (~20%) of Enceladus's mass over the age of the solar system (Kargel, 2006).

Data obtained by the VIMS instrument on board Cassini indicate CO_2 and organics as possible components (Brown et al., 2006). Data processing showed components that Cassini's INMS identified H_2O as the predominant component, CO_2 as the second most abundant, methane, and trace quantities of acetylene and propane (Waite et al., 2009). During the 9th of October 2008 flyby, Cassini dived into the south-polar plume, and INMS reported the presence of ammonia and other various organic compounds like deuterium and ^{40}Ar, as well as complex organics like benzene and other probable species such as methanol and formaldehyde (Waite et al., 2009). The chemical composition of the plume and surface material of Enceladus suggests the presence of a heat source in its interior, hot

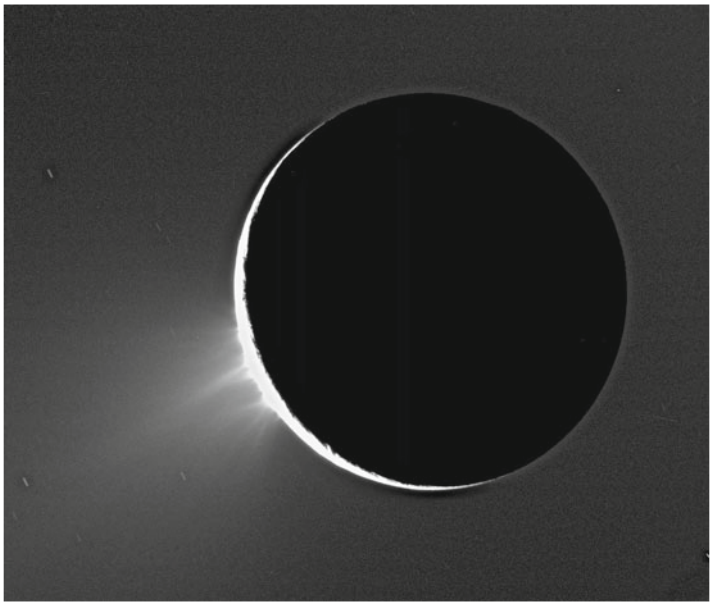

Figure 12. Enceladus's plumes ejected from the south-polar region captured by Cassini/ISS (Porco et al., 2006).

enough to decompose ammonia into N_2 and to drive reactions with hydrocarbons, implying internal temperatures on the order of 500–800 K (Matson et al., 2007).

There is a plethora of competing theories regarding the triggering and exsolution of geysers from the Tiger Stripes. The main controversy lies on as to whether the plumes are formed by a massive underground ocean (Tobie et al., 2008; Postberg et al., 2009) (Fig. 13a) or if the material generates from ice warmed, melted, or crushed by tectonic-like motions (Nimmo et al., 2007) (Fig. 13b).

Given the aforementioned observations and analysis, it is now known that Enceladus contains enough heat to drive complex and dynamic geologic activity. Interpretation of Cassini data with a view to explain the major internal reservoir that triggers and feeds this dynamic process points to a possible underground liquid ocean beneath the icy crust. Since the prerequisites for life to emerge are the simultaneous existence of energy, organic compounds, and liquid water that have been found on Enceladus, it seems that it possesses all the necessary components to support life.

In general, as described above, the south-polar region of Enceladus presents extremely high temperatures while the exsoluted vapor has also been shown to contain simple organic compounds. Most theories regarding the origin of this active region suggest that it is very likely for a liquid water environment to exist beneath the Tiger Stripes. This hypothesis enables the parallelism between potential biological ecosystems on Enceladus and the already existing on Earth (Fig. 14).

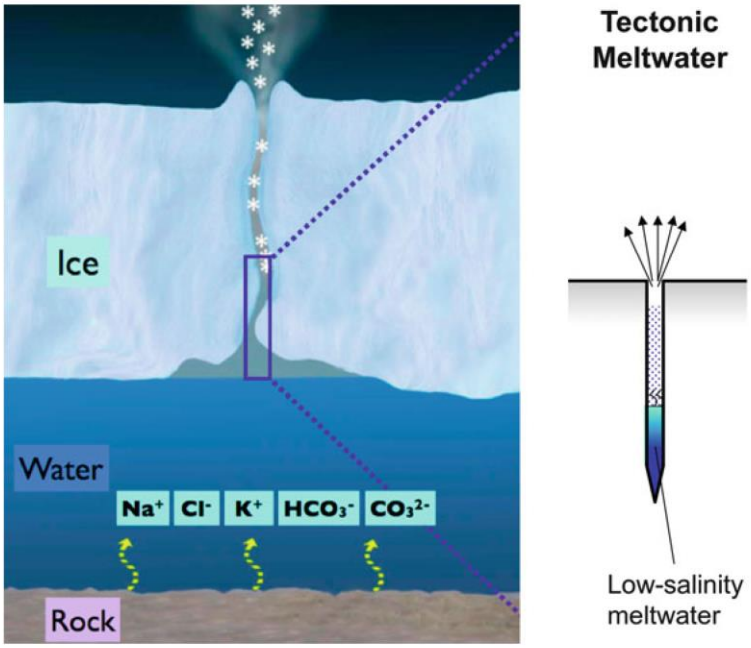

Figure 13. (*left*) Modeling of a possible internal ocean on Enceladus filled with water and chemical compounds. This model tries to explain the significant abundance of sodium salts of Saturn's E-ring, probably originating in Enceladus plumes (Postberg et al., 2006). (*right*) Internal model of Enceladus based on tectonic meltwater. Heating along fractures is caused by tidal flexing (Nimmo et al., 2007).

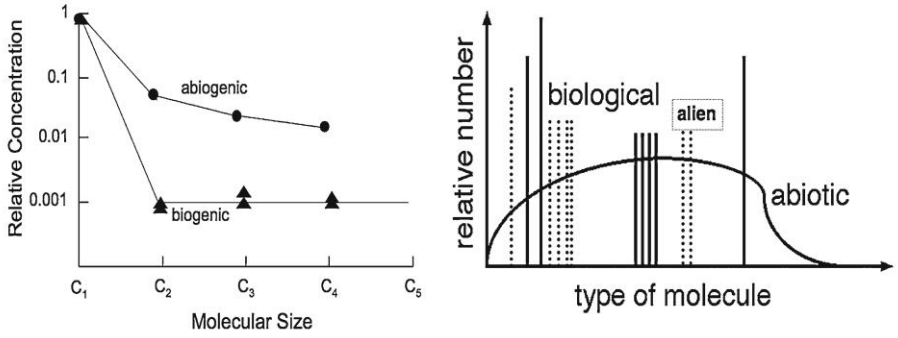

Figure 14. Indications for biological and nonbiological processes in relation to molecular parameter (*left*) terrestrial abiogenic production of hydrocarbons from McCollom and Simoneit (1999) and its biogenic pendant from Devai and Delaune (1996). (*right*) Organic distribution for abiotic, biological, and possible alien life on Enceladus (Both figures from McKay et al., 2008).

The standards for life that Enceladus' possible ocean does not fall into are the sunlight, the oxygen compounds, and the organics produced on a surficial-crust environment. Environments and ecosystems that do not meet the aforementioned prerequisites exist and evolve on Earth as well. Such an environment is located deep inside South Africa's surface, where sulfur-reducing bacteria consume hydrogen and sulfate, produced by radioactive decay (McKay et al., 2008; Muyzer and Stams, 2008). In addition, other analogous to Enceladus ecosystems are found within the magmatic volcanic rocks, which are produced through the activity of metasomatism. The metasomatosis of the volcanic rocks under the reaction of water produces methanogens of hydrogen on which the primary productivity is based on (McKay et al., 2008). Cassini's data showed that methane is present in the plumes. The terrestrial comparison regarding the ecosystems suggests that plume's methane may be biological in origin (McKay et al., 2008).

Specific questions relevant to the goal of understanding habitability on Enceladus include: Is liquid water present on Enceladus, either in a subsurface ocean, in the plume vent regions, or elsewhere? How extensive and long lived is the water, if present, and what is its chemistry? How does the liquid reservoir communicate with the surface? How thick is the ice crust and how uniform is that thickness? What energy sources are available for life? Is life present there now?

VIMS observations of several other satellites of Saturn, in the near-infrared region, show that their surface is covered by dark materials. This is particularly the case with Dione but also with Phoebe, Iapetus, Hyperion, Epimetheus and even with the F-ring (Clark et al., 2009). This dark material could be made of cyanide compounds and could be of cometary origin (Clark et al., 2009).

Spectral signatures of hydrocarbons have also been found from VIMS data on Iapetus and Phoebe suggesting the presence of organic compounds such as PAH's, kerogen-, or coal-like structure compounds (Cruishank et al., 2008).

Some of these satellites may also have internal liquid water pockets and thus may present the requisite essential for the emergence and development of life: liquid water and organic compounds. The solstice mission may be able to discover such properties and thus extend drastically the list of planetary bodies of important astrobiological interest in the Saturnian system.

5. Discussion: What Can Titan and Enceladus Tell Us About Life?

The complex mechanisms that have led to the emergence and development of life on Earth are still under investigation. Despite the great strides on biological sciences, the roots, the sources, and the initial conditions of life still remain unknown. Some answers can be found in extraterrestrial environments, hopefully in our solar system neighborhood or in exoplanets orbiting Sun-type stars. Without doubt, every planetary body, with a possible astrobiological potential, is a target for further investigations. Currently, after years of explorations, extended missions, and data analysis, it appears that among the main candidates for finding signs of

past or current life within our solar system are Mars, Enceladus, Europa, and Titan (not in any particular order of priority or importance).

In this context, Titan and Enceladus, both orbiting Saturn, seem ideal locations for further investigation. As said before, their astrobiological importance is obvious, because they propose uniquely all the necessary ingredients for life emerging and evolution. Not surprisingly, scientists expect that their study will provide some important insights on the origin of life.

The surface of Titan appears, like the surface of Mars or Europa, as an unlikely location for extant life, at least for terrestrial-type life. Even though Titan presents terrestrial-type geology with complex structures formed mostly from dynamic processes, the absence of water on the surface makes it unlikely to support terrestrial-type life. Liquid water, if it exists, is not presently in contact with a silicate core, which is isolated from the subsurface ocean by a layer of a high-pressure ice phase (Tobie et al., 2005). However, Fortes (2000) noted that Titan's internal water ocean might support terrestrial-type life that had been introduced there previously or formed when liquid water was in contact with silicates early in Titan's history. According to McKay and Smith (2005), photochemically derived sources of free energy on Titan's surface could maintain an exotic type of life, using liquid hydrocarbons as solvents. Similarly, Stoker et al. (1990) stressed that terrestrial bacteria can in fact satisfy their energy and carbon needs by "eating" tholin. In this sense, a methane-rich atmosphere may act as a "poor planet's photosynthesis," providing a means to capture the free energy from ultraviolet light and make it available for metabolic reactions.

Consequently, it cannot be excluded that life may have emerged on or in Titan. In spite of the extreme conditions in this environment, life may have been able to adapt and to persist. Even though the possible current conditions (pH, temperature, pressure, salt concentrations) are not incompatible with life, as we know it on Earth (Fortes, 2000), the detection of a potential biological activity in the putative liquid mantle seems very challenging. Furthermore, as mentioned above, another possible location to look for life on Titan would be in a possible subsurface liquid water ocean, and thus, it seems astrobiologically essential to confirm its presence.

Marine geologists and Marine biologists are nowadays close to confirm after many years of research and analysis that in the lower part of Earth's ocean, below the thermocline, where the environmental conditions are extremely different than on the surface, life exists. In deep oceanic layers that suffer from low temperature and high pressure, there are two extreme environments where life is abundant. Such environments are the cold seeps (vents) (e.g., Ritt et al., 2010) and the hydrothermal vents. Cold seeps are areas resembling brine pools, from which methane and hydrogen sulfide and other hydrocarbon-rich fluid seepage are released into the ocean. In such conditions, types of life exist, feeding on single-cell Archaea and Eubacteria microbes that consume the methane and hydrogen sulfide from the seep. The environmental and living conditions described above resemble that of Titan's hypothesized internal liquid ocean. Similarly, the temperature is low,

the pressure is high, and possible hydrovolcanic events exist, releasing methane and sulfides in the liquid ocean. Thus, there are many aspects of Titan that might argue for the presence of some sort of very basic life on Titan.

6. Future Exploration of the Kronian Satellites

Could Titan be providing us with hints as to the future of our own planet? Indeed, in addition to the past, Titan appears to be an analogue, albeit with different working materials, of the future state of the Earth when surface conditions preclude stable equatorial/midlatitude oceans. If we are to focus on the Earth and its climate, as well as on its organic chemistry, we need in the future to concentrate on another object in the solar system that sustains an active hydrologic cycle with surface liquids, meteorology, and climate change. The Cassini–Huygens mission has firmly established that Titan is such a body, in which the active working fluid of the hydrologic cycle is methane. The cycle is active but different from the Earth because Titan lacks a surface methane ocean. It possesses, however, methane lakes and seas, fluvial erosion, rounded pebbles, and liquid methane in the soil at the Huygens site.

With Titan, we are observing an active hydrologic cycle subjected to seasonal, annual, and longer term changes, as on the Earth. Moreover, the future increase in the solar luminosity make it almost inevitable that eventually water on the Earth will no longer be trapped in our ocean and troposphere but will escape rapidly in a process we see today for methane on Titan. The late stages of this evolution—an Earth with liquid water in the polar regions, in the crust, but no longer in an ocean—may be echoed by the configuration we see today in Titan's methane hydrologic cycle.

Our understanding of the future of living beings on Earth (and hence the habitability in many ways of our planet) may then have something to gain from a thorough exploration of Titan's current state.

Enceladus, on the other hand, may hold the key to understanding an important source of energy, plate tectonics, and volcanism. Indeed, many tectonic features on Enceladus may be analogous to features observed on other icy satellites such as Europa, Ganymede, and perhaps Titan. Thus, the study of the tectonics of Enceladus, which is currently active, can be used as a natural laboratory to investigate the response to stresses of the other surfaces of the outer solar system. Moreover, Enceladus possesses a warm, chemically rich, environment that may facilitate complex organic chemistry and biological processes.

The Cassini–Huygens mission has enormously advanced our knowledge of the Saturnian system and the satellites within. As far as Titan and Enceladus are concerned, the wealth of data retrieved by the Cassini–Huygens mission will definitely be the reference point for future planetary investigation. However, the key contribution to planetary science of Cassini may be the questions raised rather than those answered. Some drawbacks of the mission, such as insufficient

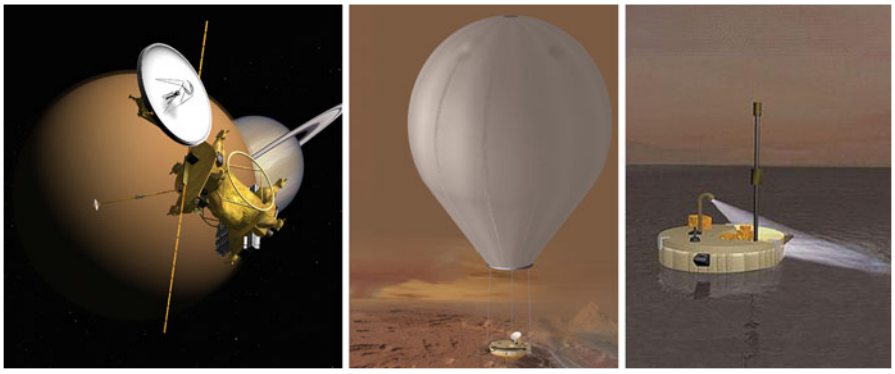

Figure 15. The TSSM basic concept. The orbiter (*left*), the balloon (*center*), and the lake lander (*right*) (Reh et al., 2008).

global coverage which has inhibited a full mapping of the atmospheric structure, composition, and temporal variations as well as the surface features of Titan and Enceladus, point to the need for further studies. Similarly, the part of the Titan's atmosphere between 400 and 950 km will remain unexplored (Coustenis et al., 2009). In addition, we will lack *in situ* measurements since the Cassini orbiter can only perform flybys of Titan and Enceladus, and the single vertical profile of the atmosphere taken by Huygens probe is limited to its landing site.

It is clear that Titan's organic chemistry and the possible subsurface ocean (among other) remain to be investigated. In particular, joint measurements of large-scale and mesoscale topography and gravitational field anomalies on Titan from an orbiter and from an aerial platform would impose important constraints on the thickness of the "lithosphere", the presence of mass anomalies at depth, and any lateral variation of the ice mantle thickness. As discussed above, it is astrobiologically crucial to confirm the presence of such an internal ocean, even though the water layer may not be in contact with the silicate core, like on Europa.

Lessons from Huygens will be used in the future to go back to Titan and explore in details its surface, in many locations. The intriguing discoveries of geological activity, excess warmth, and outgassing on Enceladus (due perhaps to the ejection of water and organics from subsurface pockets bathed in heat or by some other mechanism) mandate a follow-up investigation of that tiny Saturnian world that can only be achieved with high-resolution remote observations and detailed in situ investigations of the near-surface south-polar environment.

Among other options, a flagship (large) mission, TSSM (for Titan/Saturn System Mission), was proposed (Reh et al., 2008; Coustenis et al., 2009), jointly studied by NASA and ESA. TSSM could explore extensively one of the Titan's lakes and study for several months Titan's atmospheric and surface environment (Fig. 15).

This concept would also investigate the astrobiological perspective of Titan and Enceladus. In particular, since hydrocarbon lakes on Titan's surface may harbor evidence for present or past life, the proposed lake lander would play a crucial role. Similarly, the balloon platform would be responsible for understanding how volatile-rich worlds evolve and how organic chemistry and planetary evolution interact on large spatial and temporal scales.

The primary science goals of TSSM are to understand Titan's and Enceladus' atmospheres, surfaces, and interiors; to determine the pre- and proto-biotic chemistry that may be occurring on both objects; and to derive constraints on the satellites' origin and evolution, both individually and in the context of the complex Saturnian system as a whole. Many internal processes play crucial roles in the evolution of Titan and Enceladus. The formation and replenishing of Titan's atmosphere and the jet activity at Enceladus' south pole are intimately linked to the satellite's interior structure and dynamics. Open issues are listed below:

1. To determine their present-day structure and levels of activity
2. To determine whether the satellites underwent significant tidal deformation and whether they possess intrinsic or induced magnetic fields and significant seismicity
3. To identify heat sources, internal reservoirs of volatiles (in particular methane and ammonia), and eruptive processes
4. To detect plausible evidence for life by analysis of hydrocarbons in the plume during close encounters

A mission like TSSM would answer important astrobiological questions with precise measurements as follows:

1. What degree of complexity is reached by Titan's organic chemistry in the different parts of the geological system?
2. Is Titan a habitable world? Does it have an undersurface liquid water ocean or episodical liquid water bodies on the surface?
3. Is there currently, has there been or will there be biological activity on Titan?

To answer these questions and complement the Cassini–Huygens exploration of Titan, a dedicated orbiter and in situ elements would help by providing data and analyses directly in the atmosphere, on the surface, and the interior of Titan. The exchanges among the different media and the external processes that affect Titan on time lapses of days, years, or seasons beg for further investigation, even beyond the solstice Cassini mission which will be operating until 2017. Besides TSSM, other concepts for future missions to return to Titan have been proposed

Such as a simple orbiter to perform close-up investigations of the surface and the atmosphere of Titan (JET, C. Sotin, PI). Further more, several in situ elements have been proposed like:

The Aerial Vehicle for In-Situ and Airborne Titan Reconnaissance (AVIATR), an alternative proposal to a Titan balloon mission. Since Titan experiences low gravity and a dense atmosphere, such a nuclear-powered airplane

could fly more than 20 times easier than on Earth. It could sample directly the atmosphere and cover huge swaths of Titan's landscape (Barnes et al., 2010; McKay et al., 2010).

Titan Mare Explorer (TiME) is a proposed probe focusing on exploring Titan's lakelike features. This lake lander could study the chemical composition and the geological characteristics of the hydrocarbon pools (Lorenz et al., 2009; Stofan et al., 2009).

Similarly, Titan lake probe is a lake lander which could be considered as part of the TSSM mission or as a stand-alone mission. The main objective of this proposal is to investigate the lake deposit and the physical properties of the liquids like the TiME concept (Waite et al., 2010).

Future exploration of the Saturnian neighborhood shall no doubt bring forth extremely important insights on our quest for the possibility of life and habitable sites elsewhere.

7. References

Atreya SK, Adams EY, Niemann HB, Demick-Montelara JE, Owen TC, Fulchignoni M, Ferri F, Wilson EH (2006) Titan's methane cycle. Planet Space Sci 54:1177–1187

Barnes JW, Brown RH, Radebaugh J, Buratti BJ, Sotin C, Le Mouelic S, Rodriguez S, Turtle EP, Perry J, Clark R, Baines KH, Nicholson PD (2006) Cassini observations of flow-like features in western Tui Regio, Titan. Geophys Res Lett 33:16204–16204

Barnes JW, McKay C, Lemke L, Beyer RA, Radebaugh J, Atkinson D (2010) AVIATR: Aerial Vehicle for In-Situ and Airborne Titan Reconnaissance. In: 41st Lunar and planetary science conference, vol 41, Texas, 1–5 Mar, p 2551

Béghin C, Canu P, Karkoschka E, Sotin C, Bertucci C, Kurth WS, Berthelier JJ, Grard R, Hamelin M, Schwingenschuh K, Simoes F (2009) New insights on Titan's plasma-driven Schumann resonance inferred from Huygens and Cassini data. Planet Space Sci 57: 1872–1888

Benner R, Benitez-Nelson B, Kaiser K, Amon RMW (2004) Export of young terrigenous dissolved organic carbon from rivers to the Arctic Ocean. Geophys Res Lett 31:05305–05305

Bird MK, Allison M, Asmar SW, Atkinson DH, Avruch IM, Dutta-Roy R, Dzierma Y, Edenhofer P, Folkner WM, Gurvits LI, Johnston DV, Plettemeier D, Pogrebenko SV, Preston RA, Tyler GL (2005) The vertical profile of winds on Titan. Nature 438:800–802

Brown RH, Clark RN, Buratti BJ, Cruikshank DP, Barnes JW, Mastrapa RME, Bauer J, Newman S, Momary T, Baines KH, Bellucci G, Capaccioni F, Cerroni P, Combes M, Coradini A, Drossart P, Formisano V, Jaumann R, Langevin Y, Matson DL, McCord TB, Nelson RM, Nicholson PD, Sicardy B, Sotin C (2006) Composition and physical properties of Enceladus' surface. Science 311:1425–1428

Brown RH, Soderblom LA, Soderblom JM, Clark RN, Jaumann R, Barnes JW, Sotin C, Buratti B, Baines KH, Nicholson PD (2008) The identification of liquid ethane in Titan's Ontario Lacus. Nature 454:607–610

Brown ME, Schaller EL, Roe HG, Chen C, Roberts J, Brown RH, Baines KH, Clark RN (2009a) Discovery of lake-effect clouds on Titan. Geophys Res Lett 36:01103–01103

Brown R, Lebreton J-P, Waite H (eds) (2009b) Titan from Cassini-Huygens. Springer, New York, p 535

Bulat S, Alekhina I, Petit JR (2009) Life detection strategy for subglacial Lake Vostok, Antarctica: lessons for Jovian moon Europa. Goldschmidt conference, Davos, Switzerland, p 173

Cernicharo J, Crovisier J (2005) Water in space: the Water World of ISO. Space Sci Rev 119:29–69

Clark RN, 11 co-authors (2008) Compositional mapping of Saturn's satellite Dione with Cassini VIMS and implications of dark material in the Saturn system. Icarus 193:372–386

Clark K, Stankov A, Pappalardo RT, Greeley R, Blanc M, Lebreton J-P (2009) Europa Jupiter system mission. Joint summary report, NASA/ESA. JPL D-48440 and ESA-SRE(2008)1

Clark RN, Curchin JM, Barnes JW, Jaumann R, Soderblom L, Cruikshank DP, Brown RH, Rodriguez S, Lunine J, Stephan K, Hoefen TM, Le Mouelic S, Sotin C, Baines KH, Buratti BJ, Nicholson PD (2010) Detection and mapping of hydrocarbon deposits on Titan. J Geophys Res 115:E10005

Cohen J, Stewart I (2002) Evolving the Alien: The Science of Extraterrestrial Life. Ebury Press.

Cooper JF, Cooper PD, Sittler EC, Sturner SJ, Rymer AM (2009) Old faithful model for radiolytic gas-driven cryovolcanism at Enceladus. Planet Space Sci 57:1607–1620

Coustenis A, Hirtzig M (2009) Cassini-Huygens results on Titan's surface. Res Astron Astrophys 9:249–268

Coustenis A, Taylor FW (2008) Titan: exploring an earthlike world, Series on atmospheric, oceanic and planetary physics, vol 4. World Scientific, Singapore

Coustenis A, Salama A, Schulz B, Ott S, Lellouch E, Encrenaz TH, Gautier D, Feuchtgruber H (2003) Titan's atmosphere from ISO mid-infrared spectroscopy. Icarus 161:383–403

Coustenis A, Achterberg RK, Conrath BJ, Jennings DE, Marten A, Gautier D, Nixon CA, Flasar FM, Teanby NA, Bezard B, Samuelson RE, Carlson RC, Lellouch E, Bjoraker GL, Romani PN, Taylor FW, Irwin PGJ, Fouchet T, Hubert A, Orton GS, Kunde VG, Vinatier S, Mondellini J, Abbas MM, Courtin R (2007) The composition of Titan's stratosphere from Cassini/CIRS mid-infrared spectra. Icarus 189:35–62

Coustenis A, Atreya S, Balint T, Brown R, Dougherty M, Ferri F, Fulchignoni M, Gautier D, Gowen R, Griffith C, Gurvits L, Jaumann R, Langevin Y, Leese M, Lunine J, McKay C, Moussas X, Muller-Wodarg I, Neubauer F, Owen T, Raulin F, Sittler E, Sohl F, Sotin C, Tobie G, Tokano T, Turtle E, Wahlund JE, Waite J, Baines K, Blamont J, Coates A, Dandouras I, Krimigis T, Lellouch E, Lorenz R, Morse A, Porco C, Hirtzig M, Saur J, Spilker T, Zarnecki J, Choi E, Achilleos N, Amils R, Annan P, Atkinson D, Benilan Y, Bertucci C, Bezard B, Bjoraker G, Blanc M, Boireau L, Bouman J, Cabane M, Capria M, ChassefiŠre E, Coll P, Combes M, Cooper J, Coradini A, Crary F, Cravens T, Daglis I, de Angelis E, de Bergh C, de Pater I, Dunford C, Durry G, Dutuit O, Fairbrother D, Flasar F, Fortes A, Frampton R, Fujimoto M, Galand M, Grasset O, Grott M, Haltigin T, Herique A, Hersant F, Hussmann H, Ip W, Johnson R, Kallio E, Kempf S, Knapmeyer M, Kofman W, Koop R, Kostiuk T, Krupp N, Kuppers M, Lammer H, Lara LM, Lavvas P, Le Mouélic S, Lebonnois S, Ledvina S, Li J, Livengood T, Lopes R, Lopez-Moreno JJ, Luz D, Mahaffy P, Mall U, Martinez-Frias J, Marty B, McCord T, Menor Salvan C, Milillo A, Mitchell D, Modolo R, Mousis O, Nakamura M, Neish C, Nixon C, Nna Mvondo D, Orton G, Paetzold M, Pitman J, Pogrebenko S, Pollard W, Prieto-Ballesteros O, Rannou P, Reh K, Richter L, Robb F, Rodrigo R, Rodriguez S, Romani P, Ruiz Bermejo M, Sarris E, Schenk P, Schmitt B, Schmitz N, Schulze-Makuch D, Schwingenschuh K, Selig A, Sicardy B, Soderblom L, Spilker L, Stam D, Steele A, Stephan K, Strobel D, Szego K, Szopa C, Thissen R, Tomasko M, Toublanc D, Vali H, Vardavas I, Vuitton V, West R, Yelle R, Young E (2009) TandEM: Titan and Enceladus mission. Exp Astron 23:893–946

Coustenis A, Bampasidis G, Nixon C, Vinatier S, Achterberg R, Jennings D, Teanby N, Carlson R, Lavvas P, Flasar FM (2010a) Titan's atmospheric chemistry and its variations. Titan through time; A workshop on Titan's past, present and future, NASA Goddard Space Flight Center, USA, p 68

Coustenis A, Jennings DE, Nixon CA, Achterberg RK, Lavvas P, Vinatier S, Teanby N, Bjoraker GL, Carlson RC, Bampasidis G, Flasar F, Romani PN (2010b) Titan's meridional stratospheric composition: CIRS observations and modelling. Icarus 207:461–476

Cruikshank DP, 26 co-authors (2008) Hydrocarbons on Saturn's satellites Iapetus and Phoebe. Icarus 193:334–343

Darwin CR (1859) On the origin of species by means of natural selection, or the preservation of favoured races in the struggle for life. John Murray, London

Davis WL, McKay CP (1996) Origins of life: a comparison of theories and application to Mars. Orig Life Evol Biosph 26:61–73

de Kok R, Irwin P, Teanby N, Nixon C, Jennings D, Fletcher L, Howett C, Calcutt S, Bowles N, Flasar F (2007) Characteristics of Titan's stratospheric aerosols and condensate clouds from Cassini CIRS far-infrared spectra. Icarus 191:223–235

Delitsky ML, McKay CP (2010) The photochemical products of benzene in Titan's upper atmosphere. Icarus 207:477–484

Des Marais DJ, Harwit MO, Jucks KW, Kasting JF, Lin DNC, Lunine JI, Schneider J, Seager S, Traub WA, Woolf NJ (2002) Remote sensing of planetary properties and biosignatures on extrasolar terrestrial planets. Astrobiology 2:153–181

Devai I, Delaune RD (1996) Light hydrocarbon production in freshwater marsh soil as influenced by soil redox conditions. Water Air Soil Pollut 88:39–46

DeWitt HL, Trainer MG, Pavlov AA, Hasenkopf CA, Aiken AC, Jimenez JL, McKay CP, Toon OB, Tolbert MA (2009) Reduction in haze formation rate on prebiotic Earth in the presence of hydrogen. Astrobiology 9:447–453

Dougherty MK, Khurana KK, Neubauer FM, Russell CT, Saur J, Leisner JS, Burton ME (2006) Identification of a dynamic atmosphere at Enceladus with the Cassini Magnetometer. Science 311:1406–1409

Dougherty MK, Esposito LW, Krimigis SM (eds) (2009) Saturn from Cassini-Huygens. Springer, New York, p 805

ESA (2010) Web site on Huygens probe. http://sci.esa.int/huygens/

Flasar FM, Achterberg RK, Conrath BJ, Gierasch PJ, Kunde VG, Nixon CA, Bjoraker GL, Jennings DE, Romani PN, Simon-Miller AA, Bezard B, Coustenis A, Irwin PGJ, Teanby NA, Brasunas J, Pearl JC, Segura ME, Carlson RC, Mamoutkine A, Schinder PJ, Barucci A, Courtin R, Fouchet T, Gautier D, Lellouch E, Marten A, Prange R, Vinatier S, Strobel DF, Calcutt SB, Read PL, Taylor FW, Bowles N, Samuelson RE, Orton GS, Spilker LJ, Owen TC, Spencer JR, Showalter MR, Ferrari C, Abbas MM, Raulin F, Edgington S, Ade P, Wishnow EH (2005) Titan's atmospheric temperatures, winds, and composition. Science 308:975–978

Fortes AD (2000) Exobiological implications of a possible ammonia-water ocean inside Titan. Icarus 146:444–452

Fortes AD, Grindrod PM, Trickett SK, Vočadlo L (2007) Ammonium sulfate on Titan: possible origin and role in cryovolcanism. Icarus 188:139–153

Fulchignoni M, Ferri F, Angrilli F, Ball AJ, Bar-Nun A, Barucci MA, Bettanini C, Bianchini G, Borucki W, Colombatti G, Coradini M, Coustenis A, Debei S, Falkner P, Fanti G, Flamini E, Gaborit V, Grard R, Hamelin M, Harri AM, Hathi B, Jernej I, Leese MR, Lehto A, Lion Stoppato PF, Lopez-Moreno JJ, Makinen T, McDonnell JAM, McKay CP, Molina-Cuberos G, Neubauer FM, Pirronello V, Rodrigo R, Saggin B, Schwingenschuh K, Seiff A, Simoes F, Svedhem H, Tokano T, Towner MC, Trautner R, Withers P, Zarnecki JC (2005) In situ measurements of the physical characteristics of Titan's environment. Nature 438:785–791

Gaidos EJ, Nealson KH, Kirschvink JL (1999) Biogeochemistry: life in ice-covered oceans. Science 284:1631–1633

Grasset O, Sotin C (1996) The cooling rate of a liquid shell in Titan's interior. Icarus 123:101–112

Grasset O, Sotin C, Deschamps F (2000) On the internal structure and dynamics of Titan. Planet Space Sci 48:617–636

Hanslmeier A (2010) Water in the universe. Springer, London/New York, p 239

Hayes A, Aharonson O, Callahan P, Elachi C, Gim Y, Kirk R, Lewis K, Lopes R, Lorenz R, Lunine J, Mitchell K, Mitri G, Stofan E, Wall S (2008) Hydrocarbon lakes on Titan: distribution and interaction with a porous regolith. Geophys Res Lett 35:09204–09204

Horneck G (2008) Astrobiology. In: Artmann GM, Chien S (eds) Bioengineering in cell and tissue research. Springer, Berlin/Heidelberg, pp 641–666

Israel G, Szopa C, Raulin F, Cabane M, Niemann HB, Atreya SK, Bauer SJ, Brun JF, Chassefiére E, Coll P, Cond E, Coscia D, Hauchecorne A, Millian P, Nguyen MJ, Owen T, Riedler W, Samuelson RE, Siguier JM, Steller M, Sternberg R, Vidal-Madjar C (2005) Complex organic matter in Titan's atmospheric aerosols from in situ pyrolysis and analysis. Nature 438:796–799

Jaumann R, Brown RH, Stephan K, Barnes JW, Soderblom LA, Sotin C, Le Mouélic S, Clark RN, Soderblom J, Buratti BJ, Wagner R, McCord TB, Rodriguez S, Baines KH, Cruikshank DP, Nicholson PD, Griffith CA, Langhans M, Lorenz RD (2008) Fluvial erosion and post-erosional processes on Titan. Icarus 197:526–538

JPL/NASA (2010) Web site on Cassini mission. http://saturn.jpl.nasa.gov/index.cfm
Kapitsa AP, Ridley JK, de Q. Robin G, Siegert MJ, Zotikov IA (1996) A large deep freshwater lake beneath the ice of central East Antarctica. Nature 381:684–686
Kargel JS (2006) Enceladus: cosmic gymnast, volatile miniworld. Science 311:1389–1391
Kasting JF, Howard MT (2006) Atmospheric composition and climate on the early Earth. Philos Trans R Soc B Biol Sci 361:1733–1742
Kennett JP, Cannariato KG, Hendy IL, Behl RJ (2003) Methane hydrates in quaternary climate change: the clathrate gun hypothesis. American Geophysical Union, Washington, DC
Khare BN, Sagan C, Ogino H, Nagy B, Er C, Schram KH, Arakawa ET (1986) Amino acids derived from Titan tholins. Icarus 68:176–184
Kieffer SW, Jakosky BM (2008) Enceladus – oasis or ice ball? Science 320:1432–1433
Lavvas PP, Coustenis A, Vardavas IM (2008) Coupling photochemistry with haze formation in Titan's atmosphere, Part I: Model description. Planet Space Sci 56:27–66
Lebreton J-P, Coustenis A, Lunine J, Raulin F, Owen T, Strobel D (2009) Results from the Huygens probe on Titan. Astron Astrophys Rev 17:149–179
Lopes RMC, Mitchell KL, Stofan ER, Lunine JI, Lorenz R, Paganelli F, Kirk RL, Wood CA, Wall SD, Robshaw LE, Fortes AD, Neish CD, Radebaugh J, Reffet E, Ostro SJ, Elachi C, Allison MD, Anderson Y, Boehmer R, Boubin G, Callahan P, Encrenaz P, Flamini E, Francescetti G, Gim Y, Hamilton G, Hensley S, Janssen MA, Johnson WTK, Kelleher K, Muhleman DO, Ori G, Orosei R, Picardi G, Posa F, Roth LE, Seu R, Shaffer S, Soderblom LA, Stiles B, Vetrella S, West RD, Wye L, Zebker HA (2007) Cryovolcanic features on Titan's surface as revealed by the Cassini Titan Radar Mapper. Icarus 186:395–412
Lopes RMC, Stofan ER, Peckyno R, Radebaugh J, Mitchell KL, Mitri G, Wood CA, Kirk RL, Wall SD, Lunine JI, Hayes A, Lorenz R, Farr T, Wye L, Craig J, Ollerenshaw RJ, Janssen M, LeGall A, the Cassini RADAR Team (2010) Distribution and interplay of geologic processes on Titan from Cassini radar data. Icarus 205: 540–558
Lorenz R, Mitton J (2008) Titan unveiled: Saturn's mysterious moon explored. Princeton University Press, Princeton
Lorenz RD, Wall S, Radebaugh J, Boubin G, Reffet E, Janssen M, Stofan E, Lopes R, Kirk R, Elachi C, Lunine J, Mitchell K, Paganelli F, Soderblom L, Wood C, Wye L, Zebker H, Anderson Y, Ostro S, Allison M, Boehmer R, Callahan P, Encrenaz P, Ori GG, Francescetti G, Gim Y, Hamilton G, Hensley S, Johnson W, Kelleher K, Muhleman D, Picardi G, Posa F, Roth L, Seu R, Shaffer S, Stiles B, Vetrella S, Flamini E, West R (2006) The sand seas of Titan: Cassini RADAR observations of longitudinal dunes. Science 312:724–727
Lorenz RD, Mitchell KL, Kirk RL, Hayes AG, Aharonson O, Zebker HA, Paillou P, Radebaugh J, Lunine JI, Janssen MA, Wall SD, Lopes RM, Stiles B, Ostro S, Mitri G, Stofan ER (2008a) Titan's inventory of organic surface materials. Geophys Res Lett 35:02206
Lorenz RD, Stiles BW, Kirk RL, Allison MD, del Marmo PP, Iess L, Lunine JI, Ostro SJ, Hensley S (2008b) Titan's rotation reveals an internal ocean and changing zonal winds. Science 319:1649–1651
Lorenz RD, Stofan ER, Lunine JI, Kirk RL, Mahaffy PR, Bierhaus B, Aharonson O, Clark BC, Kantsiper B, Ravine MA, Waite JH, Harri A, Griffith CA, Trainer MG (2009) Titan Mare Explorer (TiME): a discovery mission to Titan's hydrocarbon lakes. AGU Fall Meet Abstr 51:1199–1199
Matson DL, Castillo JC, Lunine J, Johnson TV (2007) Enceladus' plume: compositional evidence for a hot interior. Icarus 187:569–573
McCollom TM, Simoneit BRT (1999) Abiotic formation of hydrocarbons and oxygenated compounds during thermal decomposition of iron oxalate. Orig Life Evol Biosph 29:167–186
McKay CP, Smith HD (2005) Possibilities for methanogenic life in liquid methane on the surface of Titan. Icarus 178:274–276
McKay CP, Lorenz RD, Lunine JI (1999) Analytic solutions for the antigreenhouse effect: Titan and the early Earth. Icarus 137:56–61
McKay CP, Porco Carolyn C, Altheide T, Davis WL, Kral TA (2008) The possible origin and persistence of life on Enceladus and detection of biomarkers in the plume. Astrobiology 8:909–919

McKay C, Barnes JW, Lemke L, Beyer RA, Radebaugh J, Atkinson D, Flasar FM (2010) Titan's atmosphere and surface in 2026: the AVIATR Titan Airplane Mission, Titan Through Time, NASA Goddard Space Flight Center, 6–8 Apr, p 31

Menor-Salván C, Ruiz-Bermejo M, Osuna-Esteban S, Muñoz-Caro G, Veintemillas-Verdaguer S (2008) Synthesis of polycyclic aromatic hydrocarbons and acetylene polymers in ice: a prebiotic scenario. Chem Biodivers 5:2729–2739

Mitri G, Showman AP, Lunine JI, Lorenz RD (2007) Hydrocarbon lakes on Titan. Icarus 186:385–394

Mitri G, Showman AP, Lunine JI, Lopes RMC (2008) Resurfacing of Titan by ammonia-water cryomagma. Icarus 196:216–224

Muyzer G, Stams AJM (2008) The ecology and biotechnology of sulphate-reducing bacteria. Nature Rev Microbiology 6:441–454

Neish CD, Somogyi A, Smith MA (2010) Titan's primordial soup: formation of amino acids via low-temperature hydrolysis of tholins. Astrobiology 10:337–347

Nelson RM, Brown RH, Hapke BW, Smythe WD, Kamp L, Boryta MD, Leader F, Baines KH, Bellucci G, Bibring JP, Buratti BJ, Capaccioni F, Cerroni P, Clark RN, Combes M, Coradini A, Cruikshank DP, Drossart P, Formisano V, Jaumann R, Langevin Y, Matson DL, McCord TB, Mennella V, Nicholson PD, Sicardy B, Sotin C (2006) Photometric properties of Titan's surface from Cassini VIMS: relevance to titan's hemispherical albedo dichotomy and surface stability. Planet Space Sci 54:1540–1551

Nelson RM, Kamp LW, Lopes RMC, Matson DL, Kirk RL, Hapke BW, Wall SD, Boryta MD, Leader FE, Smythe WD, Mitchell KL, Baines KH, Jaumann R, Sotin C, Clark RN, Cruikshank DP, Drossart P, Lunine JI, Combes M, Bellucci G, Bibring J-P, Capaccioni F, Cerroni P, Coradini A, Formisano V, Filacchione G, Langevin Y, McCord TB, Mennella V, Nicholson PD, Sicardy B, Irwin PGJ, Pearl JC (2009a) Photometric changes on Saturn's Titan: evidence for active cryovolcanism. Geophys Res Lett 36:04202–04202

Nelson RM, Kamp LW, Matson DL, Irwin PGJ, Baines KH, Boryta MD, Leader FE, Jaumann R, Smythe WD, Sotin C, Clark RN, Cruikshank DP, Drossart P, Pearl JC, Hapke BW, Lunine J, Combes M, Bellucci G, Bibring JP, Capaccioni F, Cerroni P, Coradini A, Formisano V, Filacchione G, Langevin RY, McCord TB, Mennella V, Nicholson PD, Sicardy B (2009b) Saturn's Titan: surface change, ammonia, and implications for atmospheric and tectonic activity. Icarus 199:429–441

Nguyen MJ, Raulin F, Coll P, Derenne S, Szopa C, Cernogora G, Israël G, Bernard JM (2007) Carbon isotopic enrichment in Titan's tholins? Implications for Titan's aerosols. Planet Space Sci 55:2010–2014

Niemann HB, Atreya SK, Bauer SJ, Carignan GR, Demick JE, Frost RL, Gautier D, Haberman JA, Harpold DN, Hunten DM, Israel G, Lunine JI, Kasprzak WT, Owen TC, Paulkovich M, Raulin F, Raaen E, Way SH (2005) The abundances of constituents of Titan's atmosphere from the GCMS instrument on the Huygens probe. Nature 438:779–784

Niemann HB, Atreya SK, Demick JE, Gautier D, Haberman JA, Harpold DN, Kasprzak WT, Lunine JI, Owen TC, Raulin F (2010) The composition of Titan's lower atmosphere and simple surface volatiles as measured by the Cassini-Huygens probe gas chromatograph mass spectrometer experiment. J Geophys Res-Planets 115:22

Nimmo F, Spencer JR, Pappalardo RT, Mullen ME (2007) Shear heating as the origin of the plumes and heat flux on Enceladus. Nature 447:289–291

Owen T (2005) Planetary science: Huygens rediscovers Titan. Nature 438:756–757

Pavlov AA, Kasting JF, Brown LL, Rages KA, Freedman R (2000) Greenhouse warming by CH4 in the atmosphere of early Earth. J Geophys Res 105:11981–11990

Pavlov AA, Hurtgen MT, Kasting JF, Arthur MA (2003) Methane-rich proterozoic atmosphere? Geology 31:87–90

Porco CC, Baker E, Barbara J, Beurle K, Brahic A, Burns JA, Charnoz S, Cooper N, Dawson DD, Del Genio AD, Denk T, Dones L, Dyudina U, Evans MW, Fussner S, Giese B, Grazier K, Helfenstein P, Ingersoll AP, Jacobson RA, Johnson TV, McEwen A, Murray CD, Neukum G, Owen WM, Perry J, Roatsch T, Spitale J, Squyres S, Thomas P, Tiscareno M, Turtle EP,

Vasavada AR, Veverka J, Wagner R, West R (2005) Imaging of Titan from the Cassini spacecraft. Nature 434:159–168

Porco CC, Helfenstein P, Thomas PC, Ingersoll AP, Wisdom J, West R, Neukum G, Denk T, Wagner R, Roatsch T, Kieffer S, Turtle E, McEwen A, Johnson TV, Rathbun J, Veverka J, Wilson D, Perry J, Spitale J, Brahic A, Burns JA, Del Genio AD, Dones L, Murray CD, Squyres S (2006) Cassini observes the active south pole of Enceladus. Science 311:1393–1401

Postberg F, Kempf S, Schmidt J, Brilliantov N, Beinsen A, Abel B, Buck U, Srama R (2009) Sodium salts in E-ring ice grains from an ocean below the surface of Enceladus. Nature 459:1098–1101

Radebaugh J, Lorenz RD, Lunine JI, Wall SD, Boubin G, Reffet E, Kirk RL, Lopes RM, Stofan ER, Soderblom L, Allison M, Janssen M, Paillou P, Callahan P, Spencer C, The Cassini Radar Team (2008) Dunes on Titan observed by Cassini Radar. Icarus 194:690–703

Radebaugh J, Lorenz R, Farr T, Paillou P, Savage C, Spencer C (2010) Linear dunes on Titan and earth: Initial remote sensing comparisons

Ramirez SI, Coll P, Buch A, Brassé C, Poch O, Raulin F (2010) The fate of aerosols on the surface of Titan. Faraday Discuss 147:419–427

Raulin F (2007) Question 2: why an astrobiological study of Titan will help us understand the origin of life. Orig Life Evol Biosph 37:345–349

Raulin F (2008) Planetary science: organic lakes on Titan. Nature 454:587–589

Raulin F, Gazeau MC, Lebreton JP (2008) Latest news from Titan. Planet Space Sci 56:571–572

Raulin F, McKay CP, Lunine J, Owen T (2009) Titan's astrobiology. In: Brown R, Lebreton J-P, Waite H (eds) Titan from Cassini-Huygens, Springer, New York, pp 215–233

Reh K, Lunine J, Matson D, Magner T, Lebreton J-P, Coustenis A (2008) TSSM final report on the NASA contribution to a joint mission with ESA, JPL D-48148, NASA Task Order NMO710851

Ritt B, Sarrazin J, Caprais J-C, Noel P, Gauthier O, Pierre C, Henry P, Desbruyeres D (2010) First insights into the structure and environmental setting of cold-seep communities in the Marmara Sea. Deep-Sea Res I Oceanogr Res Pap 57:1120–1136

Rudolph J, Ehhalt DH, Khedim A (1984) Vertical profiles of acetylene in the troposphere and stratosphere. J Atmos Chem 2:117–124

Sagan C, Khare BN (1979) Tholins – organic chemistry of interstellar grains and gas. Nature 277:102–107

Schaefer L, Fegley B (2007) Outgassing of ordinary chondritic material and some of its implications for the chemistry of asteroids, planets, and satellites. Icarus 186:462–483

Soderblom LA, Brown RH, Soderblom JM, Barnes JW, Kirk RL, Sotin C, Jaumann R, MacKinnon DJ, Mackowski DW, Baines KH, Buratti BJ, Clark RN, Nicholson PD (2009) The geology of Hotei Regio, Titan: correlation of Cassini VIMS and RADAR. Icarus 204:610–618

Solomonidou A, Bampasidis G, Hirtzig M, Coustenis A, Kyriakopoulos K, Seymour K, Bratsolis E, Moussas X (2012) Morphotectonic features on Titan and their possible origin. Planet Space Sci in press

Sotin C, Jaumann R, Buratti BJ, Brown RH, Clark RN, Soderblom LA, Baines KH, Bellucci G, Bibring JP, Capaccioni F, Cerroni P, Combes M, Coradini A, Cruikshank DP, Drossart P, Formisano V, Langevin Y, Matson DL, McCord TB, Nelson RM, Nicholson PD, Sicardy B, Lemouelic S, Rodriguez S, Stephan K, Scholz CK (2005) Release of volatiles from a possible cryovolcano from near-infrared imaging of Titan. Nature 435:786–789

Spencer JR, Pearl JC, Segura M, Flasar FM, Mamoutkine A, Romani P, Buratti BJ, Hendrix AR, Spilker LJ, Lopes RMC (2006) Cassini encounters Enceladus: background and the discovery of a south polar hot spot. Science 311:1401–1405

Stoker CR, Boston PJ, Mancinelli RL, Segal W, Khare BN, Sagan C (1990) Microbial metabolism of tholins. Icarus 85: 241–256

Stofan ER, Elachi C, Lunine JI, Lorenz RD, Stiles B, Mitchell KL, Ostro S, Soderblom L, Wood C, Zebker H, Wall S, Janssen M, Kirk R, Lopes R, Paganelli F, Radebaugh J, Wye L, Anderson Y, Allison M, Boehmer R, Callahan P, Encrenaz P, Flamini E, Francescetti G, Gim Y, Hamilton G, Hensley S, Johnson WTK, Kelleher K, Muhleman D, Paillou P, Picardi G, Posa F, Roth L, Seu R, Shaffer S, Vetrella S, West R (2007) The lakes of Titan. Nature 445:61–64

Stofan ER, Lunine J, Lorenz R, Aharonson O, Bierhaus E, Clark B, Kirk R, Kantsiper B, Morse B (2009) Titan Mare Explorer (time): a discovery mission to a Titan sea. American Astronomical Society, DPS meeting #41, Puerto Rico, USA, vol 41

Strobel DF (2010) Molecular hydrogen in Titan's atmosphere: implications of the measured tropospheric and thermospheric mole fractions. Icarus 208:878–886

Tian F, Stewart AIF, Toon OB, Larsen KW, Esposito LW (2007) Monte Carlo simulations of the water vapor plumes on Enceladus. Icarus 188:154–161

Tobie G, Grasset O, Lunine JI, Mocquet A, Sotin C (2005) Titan's internal structure inferred from a coupled thermal-orbital model. Icarus 175:496–502

Tobie G, Lunine JI, Sotin C (2006) Episodic outgassing as the origin of atmospheric methane on Titan. Nature 440:61–64

Tobie G, Čadek O, Sotin C (2008) Solid tidal friction above a liquid water reservoir as the origin of the south pole hotspot on Enceladus. Icarus 196:642–652

Tomasko MG, Archinal B, Becker T, Bézard B, Bushroe M, Combes M, Cook D, Coustenis A, de Bergh C, Dafoe LE, Doose L, Douté S, Eibl A, Engel S, Gliem F, Grieger B, Holso K, Howington-Kraus E, Karkoschka E, Keller HU, Kirk R, Kramm R, Küppers M, Lanagan P, Lellouch E, Lemmon M, Lunine J, McFarlane E, Moores J, Prout GM, Rizk B, Rosiek M, Rueffer P, Schröder SE, Schmitt B, See C, Smith P, Soderblom L, Thomas N, West R (2005) Rain, winds and haze during the Huygens probe's descent to Titan's surface. Nature 438:765–778

Toublanc D, Parisot JP, Brillet J, Gautier D, Raulin F, McKay CP (1995) Photochemical modeling of Titan's atmosphere. Icarus 113:2–26

Trainer MG, Pavlov AA, DeWitt HL, Jimenez JL, McKay CP, Toon OB, Tolbert MA (2006) Organic haze on Titan and the early Earth. Proc Natl Acad Sci USA 103:18035–18042

Trinks H, Schröder W, Biebricher C (2005) Ice and the origin of life. Orig Life Evol Biosph 35:429–445

Turtle EP, Perry JE, McEwen AS, DelGenio AD, Barbara J, West RA, Dawson DD, Porco CC (2009) Cassini imaging of Titan's high-latitude lakes, clouds, and south-polar surface changes. Geophys Res Lett 36:02204–02204

Waite JH, Young DT, Cravens TE, Coates AJ, Crary FJ, Magee B, Westlake J (2007) The process of tholin formation in Titan's upper atmosphere. Science 316:870–875

Waite JH, Lewis WS, Magee BA, Lunine JI, McKinnon WB, Glein CR, Mousis O, Young DT, Brockwell T, Westlake J, Nguyen MJ, Teolis BD, Niemann HB, McNutt RL, Perry M, Ip WH (2009) Liquid water on Enceladus from observations of ammonia and 40Ar in the plume. Nature 460:487–490

Waite JH, Brockwell T, Elliot J, Reh K, Spencer J, Outer Planets Satellites Decadal S (2010) Titan lake probe: the ongoing NASA Decadal Study Preliminary Report, EGU General Assembly, vol 12, Vienna, Austria, 2–7 May, p 14762

Watson JD, Crick FHC (1953) A structure for deoxyribose nucleic acid. Nature 171:737–738

Wilson EH, Atreya SK (2004) Current state of modeling the photochemistry of Titan's mutually dependent atmosphere and ionosphere. J Geophys Res (Planets) 109:06002–06002

Wolstencroft RD, Raven JA (2002) Photosynthesis: likelihood of occurrence and possibility of detection on Earth-like planets. Icarus 157:535–548

Yung YL, Allen M, Pinto JP (1984) Photochemistry of the atmosphere of Titan – comparison between model and observations. Astrophys J Suppl Ser 55:465–506

Zarnecki JC, Leese MR, Hathi B, Ball AJ, Hagermann A, Towner MC, Lorenz RD, McDonnell JAM, Green SF, Patel MR, Ringrose TJ, Rosenberg PD, Atkinson KR, Paton MD, Banaszkiewicz M, Clark BC, Ferri F, Fulchignoni M, Ghafoor NAL, Kargl G, Svedhem H, Delderfield J, Grande M, Parker DJ, Challenor PG, Geake JE (2005) A soft solid surface on Titan as revealed by the Huygens Surface Science Package. Nature 438:792–795

Appendix D1

Seismometers on the satellites of the Outer Solar System

IEEE Electronic Refereed Conference Proceedings, (2011)
DOI: 10.1109/ICSpT.2011.6064647.

Seismometers on the Satellites of the Outer Solar System

Georgios Bampasidis, Anezina Solomonidou, Emmanuel Bratsolis, Konstantinos Kyriakopoulos, Xenophon Moussas, Panagiota Preka-Papadema
National & Kapodistrian University of Athens
Athens, Greece
gbabasid@phys.uoa.gr

Mathieu Hirtzig, Athena Coustenis
LESIA
Observatoire de Paris-Meudon
Meudon, France

Abstract— **The icy moons of the Outer Solar System are extremely interesting planetary bodies since they possess evidence about the origin and evolution of their systems and the Solar System in general. In terms of surface morphology, internal structure as well as their environmental uniqueness, Saturn's moons Titan and Enceladus and Jupiter's Europa and Io are the best representatives in that perspective. In this study, we propose a seismic experiment for the icy moons as a payload of future missions' landers. This suite of instruments comprises a gas monitoring sensor (micro Gas-Chromatograph) which will operate along with the seismic sensor. Data from the micro Gas-Chromatograph will give us the opportunity to correlate each time the recorded seismic data of the current gas-relief activity. We also suggest possible target areas with internal dynamic potential and multivariable surface expressions. Hence, it will be possible to identify active regions on the satellites, which will provide important information regarding the fluid transfer processes towards the surface as well as the presence of a subsurface liquid deposit.**

Keywords: Seismometer; Future mission; Icy moons; Titan; Enceladus; Europa; Io.

I. INTRODUCTION

Since 2004, the Cassini-Huygens mission has made exciting discoveries in the Saturnian system and especially with regard to its satellites Titan, the largest one, as well as the enigmatic Enceladus. Not only have their observations furthered our understanding of the complexity of these harsh environments, but many questions about their surface and interior have also been raised e.g. [1, 2].

Titan, the second largest moon of the Solar System may be representative of many planetary bodies and consequently, the understanding of its internal geology may allow scientists to enlighten the inner structure of an entire class of planets and moons [3]. Similarly, Enceladus, although it has minor dimensions (radius of 252 km), it is extremely interesting due its huge geysers which mainly feed the E-ring of Saturn. These plumes show that the moon is geologically active hosting a possible internal water ocean, the source of its vents [4, 5].

Likewise, the Galilean satellites of Jupiter present many similarities with rocky planetary bodies in terms of their surface features and atmospheric environments. Europa, the smallest of the Galilean satellites, hosts a relatively stable environment, a putative internal ocean in combination with a young evolving surface, and therefore the moon houses a great astrobiological potential [6]. On the other hand Io seems to be the most geologically active planetary moon through the solar system considering its huge volcanic activity occurring at the time of observation [7].

Without doubt, the icy satellites orbiting outer planets can significantly contribute to the study of geological processes across the solar system. Comparative Planetology can enlighten fundamental mysteries concerning the origin and the evolution of Earth and the solar system in general and predict future geological events. However, the internal geological structure of each planet or moon can only be determined by *in situ* measurements.

The local or global tectonic field, meteoroid impacts and moon's tidal deformations induced by Jupiter/Saturnian's gravity field as well as temperature and pressure fluctuations may cause ground vibrations within the icy moons. Such ground vibrations provide information about the nature of the subsurface material, its fracture and its chemical composition.

Therefore, the Cassini-Huygens mission heritage encourages scientists to discuss about launching future missions towards the outer planets' satellites. For that reason, two large L-Class missions set these moons as primary targets: Europa Jupiter System Mission (EJSM) [8] will investigate the subsurface, surfaces and atmospheres of Jupiter's satellites, while the Titan Saturn System Mission (TSSM) [9] will advance our current knowledge regarding the Saturnian icy moons. For further information the reader is referred to visit the NASA's website of the Outer Planet Flagship Mission (http://opfm.jpl.nasa.gov).

This paper examines the possibility of installing seismic experiments on icy satellites of the outer planets, setting the minimum technical requirements and describing scientific achievements and possible problems. The sections II and III contain a brief description of such space seismic equipment and the micro Gas Chromatograph (μGC) for gas sampling respectively, while in section IV the risks of such an instrument are discussed. Finally, the major goals of the proposed experiment are depicted in section V.

Data obtained by a seismic experiment, in combination with the analysis results of the μGC will provide us with details

about the interiors of the moons and their connection with the observed surface features.

II. Description Of The Seismic Instrument

The seismograph is the basic instrument for measuring any ground vibration. It mainly contains the seismometer and the unit which records the signal. The seismometer consists of three sensors placed in the same sealed case. Each sensor can be described as a pendulum that moves from its equilibrium position triggered by the ground movement. The sensors can measure any ground motion within a frequency range of 0.001 Hz to 100 Hz usually, at the north/south, east/west and vertical component in orthogonal system.

Both low and high frequencies can be recorded by broadband seismometers on Earth. Newer seismographs measure ground movements smaller than 1 nm. There are several kinds of these instruments depending from the surface's location.

By using seismic instruments we extend our knowledge of planets' interior at the Solar System. Additionally, both these space and telluric observations will help us understand better the origin and the evolutionary path of our own planet.

A. Instrument's specifications – technical requirements

The Table I below indicates the main seismic instrument's requirements considering the specifications of the shortest modern seismic instruments which operate in extreme conditions on Earth like the deep ocean floor [10]. Similar sensors can be easily found in the global market.

TABLE I. Seismic Instrument's Specifications

Power	Seismic Sensors		
	Mass	*Velocity Bandwidth*	*Operational temperature*
0.32 W	0.200g each	0.001-100Hz	below 100K

Future mission's instruments on the icy satellites' surface of the outer planets will operate in abnormal physical conditions during the entry descent and after landing of their carrier. To achieve the seismograph's accuracy in such a location the environmental factors (mainly temperature and pressure) should be considered.

B. System Hardware Architecture

The ground vibration is the input signal to the system. If the ground vibrates within a range of 0.001 Hz to 100 Hz, it will be recorded by each one of the three sensors. The sensor system contains a transducer, the device that converts the mechanical motion into electrical signal. A piezoelectric accelerometer can be used as a transducer to sense any weak or strong ground motion in a low frequency range (up to 100 Hz) without using extra power to operate [11].

Once the sensor records a motion, a signal will be sent at the Main Processor Unit (MPU) of the system. The MPU is responsible for the operation, the administration and the maintenance of the instrument and contains the core of the application software. After receiving and recording the signal from the MPU, it will be transferred at the next component of the instrument, the Multiplexer (MUX) by using a line interface circuit, which provides the connectivity between MPU and MUX.

At the MUX, data files will be compressed, converted to the right format and prepared for transmission. Because of the continuous function of the seismograph, a service for bulky data needed. The transmission frame protocols will be defined similar to the protocols of the lander's instrumentation.

Fig. 1 shows the basic functional procedure of a seismic instrument on icy moons according to the requirements mentioned above. The configuration of the system is illustrated in a simplified plot. All the components inside the dashed line in Fig. 1 are parts of the same physical equipment, the seismograph.

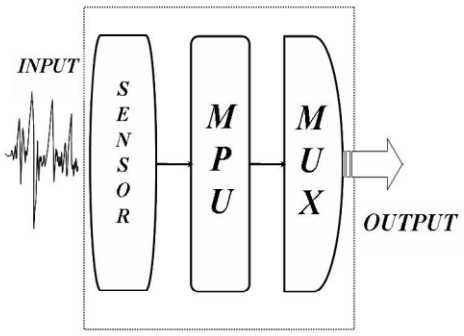

Figure 1. Functional procedure of the seismic instrument

III. Description Of The micro Gas Chromatograph

The purpose of the micro Gas Chromatograph (μGC) is to provide accurate information about the composition of the local gaseous environment. A successful relative experiment with the Gas Chromatograph Mass Spectrometer (GC-MS), was performed by the Huygens probe during its descent phase [12]. This instrument on Huygens only made measurements during the descent from 170 km to the surface and it provided us with valuable data in harsh environmental conditions. We propose the micro-GC as a payload of the lander to operate during the descent phase of the probe like in the Huygens case as well as after the touchdown. During terrestrial earthquakes close to volcanoes, amounts of gas are released, triggered by the ground vibration. In some cases this relief is used for earthquake prediction. Such instrumentation can be extremely useful on the surface of icy moons' locations where gas relief has been identified, like the tiger stripes of the Enceladus' South Pole.

The μGC tube/column mounted on the probe hosting the seismograph will be triggered when any vibration will be recorded by the seismic sensors. A presentation of a low power μGC column can be found in [13]. The instrument will also take samples of the local atmospheric envelope in several

specific times which will enable us to determine any temporal variations in chemical composition due to any recorded vibration as well as during in the descent phase of the lander. Such measurements can be extremely useful in the case of Enceladus if the probe landed close to the tiger stripes, the great linear surface fractures from where its plumes spread out.

In fig. 2 the procedure of the operation of the μGC is depicted.

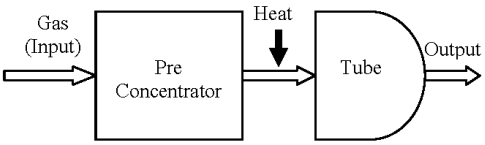

Figure 2. Operational flow diagram of the micro Gas Chromatograph

Briefly, the instrument will collect the sample from the local gas and collected material will be droved into the pre concentrator device where the concentration will be increased. Then, the sample will be heated in order to release the gas and it will be passed through the tube. This is the separation phase, critical to the analysis procedure where each component of the sampled gas needs its specific time to traverse the tube. Eventually, the identification stage follows this separation. The design of the signal condition circuit which converts the content of the separated gas to electric signal can follow the standards of [14]. The μGC will perform batch sampling like the Huygens/GC-MS did during Huygens Descent phase [15]. Hydrogen will be selected as the carrier gas like in the Huygens/GC-MS case [12].

By correlating the seismic soundings with the gas composition, we can infer about the significance of the internal gases and the mechanism beyond their relief. These measurements can help us solve the puzzle of icy moons interiors.

IV. Problems And Risks Of A Future Seismic Experiment On Outer Solar System

Terms and Conditions of the implementation of seismic instrumentation on icy moons and the possibly emerged problems and difficulties are listed in the Table II below.

TABLE II. Scientific And Technical Problems And Difficulties

Terms and Conditions	Possible Problems and Difficulties		
	Science	***Engineering***	***Precautions***
Fluctuations in temperature	Accuracy affected	Malfunction of the sensors	Special thermal shield
Surface characteristics	Sensors' deformation	Loose the equilibrium position	Special installation and stabilization needed
Dense atmosphere	Chemical Corrosion	Insufficient solar power to recharge batteries	Shield case
Stability of the apparatus	First time in space exploration	Orientation lost	Robotic installation of the seismometer
Maintenance	No recordings	Impossible to repair	Autonomous System
Data transmission	Radio frequency signals	A permanent link needed	Orbiter and large ground radiotelescopes
Exact recordings	3D plotting	Different devices	Seismic network needed
Ground/wind noise	Low Signal to Noise ratio	Stable structure	A shallow hole needed for installation
Power	Continuous operation	Batteries	Radioisotope thermoelectric Generator (RTG)

Since we lack any knowledge of seismic events on icy moons, data from a seismic instrument and global radar mapping for long periods of time will be of extreme importance. Obviously, due to power limitations, any instrument on these surfaces will operate continuously from the touchdown until its battery discharging. Therefore, a more durable energy source is necessary. A radioisotope thermoelectric generator (RTG) is to be considered.

An appropriate location for the placement of a seismic equipment will ensure that its recordings will represent accurately and separately every ground vibration. For this purpose, on Earth the seismic instruments should be placed in a hole of approximately 0.5 m depth. Thus, less ground noise will be recorded. Noise on an icy surface can be originated by the atmosphere due to its seasonal and diurnal effects as described in [16] for the Titan case. Noise can be produced also from the local wind and meteor impacts.

In the case of Titan, its dense atmosphere protects the surface from meteoroid impacts - few craters have been observed [17] – therefore, the seismometers will record merely interior events. On the other hand the same instrumentation on Enceladus, Io and Europa will also measure vibrations caused by external sources.

The proper contact between the feet of the seismograph and the local surface at the landing area stands for another issue to be confronted. Any particles and dust can easily perturb the seismic sensors during their function and cause random errors at the sensor's record. This type of surface features has already found on Titan. The Huygens probe landed on a relatively soft solid surface whose properties consisting of analogous to wet clay, lightly packed snow and wet or dry sand [18]. Moreover, the Descent Imager and Spectral Radiometer's (DISR) surface images showed rounded stones approximately 15 cm in diameter to lie on top of a finer-grained surface in variable spatial distribution [19]. If the icy pebbles lying over the instrument's feet move or/and melt, the equilibrium position of the seismic equipment will disturbed and the sensors will lose their orientation. The measurements should be corrected if such a micro-movement of the probe is noticed.

Experience gained from the Apollo Passive Seismic Experiment (PSE) on the Moon will be extremely useful for

such an ambitious effort. PSE was the first extraterrestrial network of seismic instruments and it consisted of four seismometers deployed by the astronauts on the lunar surface between 1969 and 1972 while Earth-based stations received data for eight years. The Apollo seismometers recorded 12,558 events and these seismic data have been recently reanalyzed [20]. A seismic experiment has also been performed on Mars as part of the Viking mission payload [21]. The Viking seismograph performed a long-term operation and measured ground vibrations without any significant seismic signals. The primary source of the recorded noise was the local wind. The dimensions of the equipment were 12x15x12 cm, weighted 2.2 kg and needed 3.5 W to operate.

V. Major Scientific Goals-Discussion

Icy moons of the outer planets seem to be or have been active like our own planet, as far as their atmospheric circulation, surface geological processes and tectonics are concerned. Each moon has its own atmospheric and geological record and therefore it should be treated separately. The internal structure of these satellites may be involved in some surface processes. Hence, since only the seismic instrumentation can map the subsurface layers, determine their composition and structure and measure their thickness, we will consider mounting it in a future mission as part of a landing probe payload.

Seismic waves from distant events travel deeper into the interior of a planetary body than waves from nearby events. Hence, measuring events at various distances by seismometers can provide the variance with depth of seismic velocities within icy moons.

Future missions to the outer planets icy moons will be a great opportunity for comparative planetology providing proofs of active planetary systems. A seismic experiment can identify the existence of liquid internal deposits, with a great astrobiological potential. Such isolated environments that consist of water and organics, components that have already been identified on most icy satellites, provide ideal conditions for the survival of biological building blocks. Table III lists the main benefits and advances in short terms of mounting seismic equipment in the surface of icy moons.

TABLE III. The Benefits Of Future Seismic Instrumentation

Features	Benefits of space seismic experiments	
	Icy moons	***Engineering***
Completed scientific experiment	Regional scale geology	New science– Planetary Seismology
Small size	Ideal as a payload for a space mission lander	Low power consumption
Continuous operation	Improve modeling for the three-dimensional internal structure	Service for bulky data needed
Evolution of seismic	Earthquake prediction Tidal effects caused by	No special software needs to be developed
instruments and applications	Jupiter/Saturn	

References

[1] A. Coustenis and M. Hirtzig, "Cassini-Huygens results on Titan's surface," *Research in Astronomy and Astrophysics*, vol. 9, pp. 249-268, 2009.

[2] R. H. Brown et al, "Composition and Physical Properties of Enceladus' Surface," *Science*, vol. 311, pp. 1425-1428, 2006.

[3] A. Coustenis and F. W. Taylor, "Titan: exploring an Earthlike World," *Series on atmospheric, oceanic and planetary physics, vol 4. World Scientific, Singapore*, 2008.

[4] M. K. Dougherty et al, "Identification of a Dynamic Atmosphere at Enceladus with the Cassini Magnetometer," *Science*, vol. 311, pp. 1406-1409, 2006.

[5] G. C. Collins and J. C. Goodman, "Enceladus' south polar sea," *Icarus*, vol. 189, pp. 72-82, 2007.

[6] J. S. Kargel et al, "Europa's Crust and Ocean: Origin, Composition, and the Prospects for Life," *Icarus*, vol. 148, pp. 226-265, 2000.

[7] R. Lopes and J. Spencer, "Io After Galileo: A view of Jupiter's volcanic moon," *Berlin, Springer*, 2006.

[8] EJSM, *NASA/ESA Final Report*, 30 January 2009.

[9] TSSM, *NASA/ESA Final Report*, 30 January 2009.

[10] B. Romanowicz et al, "The Monterey Bay broadband ocean bottom seismic observatory," *ANNALS OF GEOPHYSICS*, vol. 49, 2006.

[11] F. Garcia, E. L. Hixsom, C. I. Huerta, and H. Orozco, "Seismic Accelerometer," *Instrumentation and Measurement Technology Conference, IMTC/99, Proceedings of the 16th IEEE*, vol. 3, pp. 1342-1346,

[12] H. B. Niemann et al, "The Gas Chromatograph Mass Spectrometer for the Huygens Probe," *Space Science Reviews*, vol. 104, pp. 553-591, 2002. 1999.

[13] J. A. Potkay, G. R. Lambertus, R. D. Sacks, and K. D. Wise, "A Low-Power Pressure- and Temperature-Programmable Micro Gas Chromatography Column," *Journal of Microelectromechanical Systems*, vol. 16, pp. 1071-1078, 2007.

[14] L. Hongfei, L. Chaoli, and C. Zhong, "Signal Conditioning Circuit Design for Micro Gas Chromatograph," *International Forum on Computer Science-Technology and Applications*, vol. 3, pp. 86-89, 2009.

[15] H. B. Niemann et al, "The abundances of constituents of Titan's atmosphere from the GCMS instrument on the Huygens probe," *Nature*, vol. 438, pp. 779-784, 2005.

[16] M. Hirtzig, T. Tokano, S. Rodriguez, S. le Mouelic, and C. Sotin, "A review of Titan's atmospheric phenomena," *Astronomy and Astrophysics Review*, vol. 17, pp. 105-147, 2009.

[17] C. Elachi et al, "Cassini Radar Views the Surface of Titan," *Science*, vol. 308, pp. 970-974, 2005.

[18] J. C. Zarnecki et al, "A soft solid surface on Titan as revealed by the Huygens Surface Science Package," *Nature*, vol. 438, pp. 792-795, 2005.

[19] M. G. Tomasko et al, "Rain, winds and haze during the Huygens probe's descent to Titan's surface," *Nature*, vol. 438, pp. 765 - 778, 2005.

[20] R. C. Bulow, C. L. Johnson, and P. M. Shearer, "New events discovered in the Apollo lunar seismic data," *Journal of Geophysical Research (Planets)*, vol. 110, pp. 10003, 2005.

[21] D. L. Anderson et al, "Seismology on Mars", *Journal of Geophysical Research*, vol. 82, pp. 4524-4546, 1977.

Appendix D2

Sounding the interior of Titan's lakes by using Micro-Electro-Mechanical Systems

IEEE Electronic Refereed Conference Proceedings, (2011)
DOI: 10.1109/ICSpT.2011.6064648.

Sounding the interior of Titan's lakes by using Micro-Electro-Mechanical Systems (MEMS)

Georgios Bampasidis, Anezina Solomonidou, Emmanuel Bratsolis, Konstantinos Kyriakopoulos, Xenophon Moussas, Panagiota Preka-Papadema
National & Kapodistrian University of Athens
Athens, Greece
gbabasid@phys.uoa.gr

Mathieu Hirtzig, Athena Coustenis
LESIA
Observatoire de Paris-Meudon
Meudon, France

Abstract—**The Synthetic Aperture Radar (SAR) instrumentation on board the Cassini orbiter has identified large hydrocarbon liquid deposits on the surface of Titan [e.g. 1], distributed mainly around its northern polar regions. Recent studies [2] suggest that the rims of these structures display seasonal changes, where the lakes appear to be shrinking. However, the precise depth, evolution and composition of these lake-like features are still unknown. The physical and chemical characteristics of the Titan lakes will be one of the major objectives of a future space mission to Titan [e.g. 3, 4]. We propose here the application of Micro-Electro-Mechanical Systems (MEMS) as part of a science surface properties package aboard a future Lake Lander. MEMS devices offer a low cost and reduced size of instrumentation in order to accomplish the 3-D sounding of the liquid deposit and detect the presence of any biomarkers in a broader area.**

Keywords: MEMS; Future mission; Titan.

I. INTRODUCTION

The Cassini-Huygens mission has been investigating the Saturnian System since July 2004 when it performed the Saturn Orbit Insertion (SOI). Titan, the largest satellite of Saturn, is one of the major targets of the mission mainly due to its dense atmosphere. Indeed, the Cassini-Huygens mission has revealed the complex organic nitrogen-dominated atmosphere of Titan, rich in methane (1.48% [5]) and the diversity of its multivariable surface [e.g. 6].

The temperature on Titan's surface has been measured *in situ* at almost 94 K [7], which is close to the triple point of methane, meaning that methane on the satellite can exist as liquid, gas and ice [8]. Literally, Titan hosts a complex and active organic global chemistry where methane plays a critical role in a cycle resembling the terrestrial hydrological one [9].

The presence of large hydrocarbon liquid deposits on Titan's surface was assumed before the Cassini-Huygens mission, considering the thermodynamics which dominate the satellite globally [e.g. 10, 11]. Although the existence of a planetary-scale ocean has been rejected, the Cassini orbiter has unveiled concentrations of large organic pools close to both poles [1, 12, 13]. However, the Cassini RADAR beams are not able to penetrate through the liquid surfaces hindering sounding their interior. Therefore such features can be described only by modeling [e.g. 14]. However, it is crucial to understand how these hydrocarbon liquids contribute in the active methane cycle. According to the contemporary photo-dissociation rate of methane, it should be vanished within a period of 10-100 Myrs [9], since currently no methane source has been identified to replenish it. Towards this direction, as well as the necessity of the thorough investigation of these features, a lake touchdown by a probe has been proposed, carried by a future mission [3].

The usage of Micro-Electro-Mechanical-Systems (MEMS) devices as infrared emitters has been recently proposed [15], as part of the science surface properties package of a future probe to Titan like the TSSM Lake Lander or the Titan Lake Explorer [3, 4]. In this paper we suggest MEMS devices to operate as micro-laboratories by including also radio frequency RF wavelength emitters and temperature and pressure sensors. Thus, these micro-machines could obtain the 3D sounding of the liquid deposit, its chemical composition and detect the presence of any biological building blocks within the liquid. Likewise, the temperature and pressure micro-sensors could provide the vertical pressure, temperature and density profile of the liquid deposit.

The MEMS pattern, owing to their very small shape and size without reducing their operational performance, seems ideal payload for a lake lander probe on Titan as well as outer planetary space missions in general. MEMS implementation in Titan's exotic environment is a great challenge for science, engineering and space physics.

In section II we present the advantages of MEMS devices, while in section III we report MEMS already used in space applications. The experiment concept and the MEMS technology embedded is described in Section IV and Section V contains the concluding remarks.

II. MICRO-ELECTRO-MECHANICAL-SYSTEMS (MEMS) DEVICES

Any small-size product within the range of a micron to a centimeter, which also combines mechanical and electrical structures, can be identified as a MEMS device. Although the first device was constructed by H. C. Nathanson in late 1960s [16], the industrial techniques were unable to produce such minor integrated circuits and only after the 1980s did start the massive production in microscopic scale [17].

Due to their small size (20 μm to 1 mm) and shape, MEMS present properties that increase the performance of every scientific experiment for a wide range of uses and applications. In general, they provide an excellent rate of the optimum shape to the rendering performance relation. Micro-devices can now be included in every part of any experiment and also visit impossibly approachable places by traditional instrumentation. They can successfully replace quite larger devices giving the user the opportunity to explore the micro-structure of the nature. Therefore, due to the minimization of the cost both in their manufacture and operation, MEMS instruments are preferable for scientific use by improving the quality and the amount of the obtained data range.

III. MEMS Devices In Space Scene

The benefit of implementing MEMS techniques in Aerospace and Space systems is obvious especially due to the reduced requirements in size, mass, power issues of many Aerospace/Space applications [18]. In order to overcome portability and consumption limitations in any future outer planetary missions, new alternative technologies have to be implemented. The minimization of the embedded electronic instrumentation is a promising approach when it employs MEMS Systems. Therefore, the presence of MEMS in space systems offers important monetary advantages to space agencies by severely shrinking the cost of any mission, while they are reducing the weight of future spacecrafts.

Among many other applications, MEMS devices have already been used on the adaptive optics imaging technology in major telescopes [19-22]. Moreover, JPL has already developed a new MEMS deformable mirror (DM) system for NASA's adaptive space-based telescopes and in particular for Terrestrial Planet Finding (TPF) mission [23]. Likewise, several proposals have recently been submitted for future space missions and telescopes, exploiting the new leading edge of MEMS technology. Especially, MEMS techniques have been incorporated as detectors, a spectrophotometer and an IR camera of the new proposed telescope called MTEL (MEMS Telescope for Extreme Lightning) in order to observe the extreme lightning occurring in the upper atmosphere [24]. MEMS devices seem also appropriate for observing fast moving objects and transient events by the proposed space-based telescope called Obscura [25]. Moreover, MEMS have also been implemented in Space Infrared telescope for Cosmology and Astrophysics (SPICA), the Japanese coronagraph which is planned for a launch in 2017 [26].

Without doubt, although the use of MEMS in space applications is in fairly early stage, they will certainly optimize the scientific potential of any future mission.

IV. Experiment Description

MEMS as components of the science surface properties package of a future Lake Lander probe to Titan are being discussed hereafter. We propose MEMS machines to operate as (a) infrared emitters inside the liquid and (b) micro-laboratories by including also radio frequency RF wavelength emitters as well as temperature and pressure sensors.

During the last stages of the descent of a probe in Titan's atmosphere and a few meters before landing on a liquid surface, the probe will release the MEMS devices (Fig. 1). This procedure will be continued after the landing, when the probe will release more MEMS directly into the liquid. From this point, they commence their operation by transmitting instantly as IR and RF emitters. Some of these devices will float on the surface of the liquid and other will dive without stopping transmitting depending on their weight and exterior design. Schematically, the proposed experiment will be consistent of two phases:

A. Phase One: The Deployment

Few meters before the touchdown of the vehicle, MEMS capsules will be released into the atmosphere and begin simultaneously to operate as micro-laboratories. Another group of MEMS can be also released after the landing of the lake vehicle inside the liquid environment (Fig. 1).

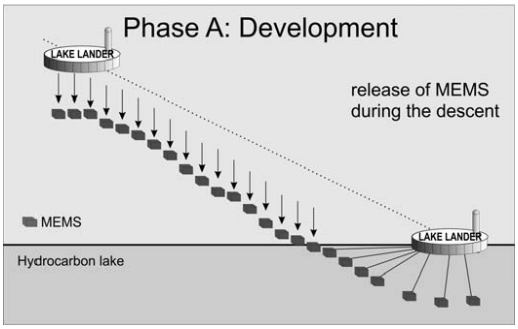

Figure 1: The deployment of the MEMS network during the entry descent and landing (EDL) procedure of the Lake Lander.

B. Phase Two: The Operation

Subsequently to Phase One, these devices will flow or dive into the liquid hydrocarbons and continuously transmit data to the Lander depending on the duration of their power supplies (Fig. 2).

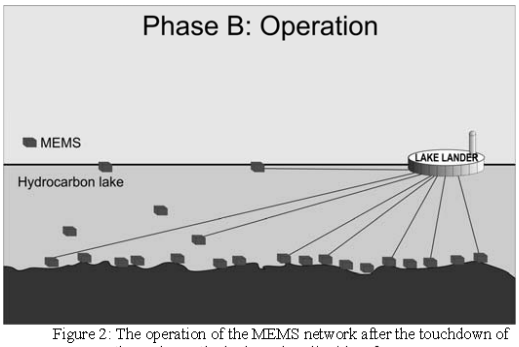

Figure 2: The operation of the MEMS network after the touchdown of the probe on the hydrocarbon liquid surface.

This deployment will provide a broad network of surface and submarine IR and RF sources, while the signal receiver sensor will be aboard the Lake Lander. The MEMS micro-

probes will follow the swarm pattern [27] in which each apparatus single operation is a component of a large group of similar devices. Apparently, their combination will enhance the results.

C. MEMS components

As mentioned before, each MEMS device will include a combination of scientific instruments in micro scale. In particular, one pair of infrared (IR) and radio frequency (RF) emitters and two sensors for measuring the temperature and the pressure will be enclosed in each micro-shell. Additionally, MEMS technology can be part of the IR spectrometer's equipment aboard the Lake Lander.

1) Infrared Sources

Apart from traditional IR sources, micro-machined infrared emitters have been constructed, comprised of a photonic crystal modified micro-hotplate that emits thermally stimulated infrared radiation in a narrow band. As far as the performance of the device is concerned, it exhibits efficiencies in excess of 10 % greater than competitive technologies. These applications are like the deposited filament emitter, with the advantage of minimization of the filament which reduces the thermal mass of the system and enhances the modulated performance [28].

2) Micro-mirror

MEMS technology can be implemented at the IR spectrometer's architecture of a classical Michelson interferometer, being a transducer of the IR sensor. MEMS translational mirrors, covering an area of 1.1x1.5 mm^2 have been already tested giving reliable measurements at high scanning speed -in milliseconds- which enhances signal-to-noise ratio, suspended on a two long bending springs pattern [29]. A recent approach is the pantograph, which even though it exhibits less stability, it covers a surface mirror of 7 mm^2 providing a spectral resolution of 20 cm^{-1} [30]. The IR source can be based on silicon structure, a pattern which is already in long-term use for detecting gas in oil platforms without a failure recording [31]. In Titan's case, the target gases are mainly hydrocarbons, nitriles and carbon dioxide.

The surface temperature in Titan's environment is approximately 94 K, as it has been determined by the Huygens probe [7]. MEMS devices, released by the Lake Lander at low height and inside the liquid, have to be subjective to such low temperatures. In fact, micro-devices are already adaptable in cryogenic conditions. In the SPICA coronagraph [26] the included micro-scale machines are designed to operate in cryogenic conditions, while the whole telescope will be cooled down to 4.5 K [32]. This cryogenic environment can cause serious damage to the mirrors such as deformation and flaking. To achieve robust function in this harsh temperature conditions these micro-mirrors can be based on a silicon-on-insulator wafer, while their back surface can be made of polycrystalline silicon [33].

3) RF transmitter

The exact composition of the lake as well as its physical parameters are still unknown. If the liquid material behaves as a partial conductor (when consisting of i.e. ionic contaminants), it will prevent RF propagation in long distances. Such liquid conductors set the independent operation of these RF emitters inside the liquid under discussion, since their high permittivity and permeability cause strong attenuation of the signal power. For this reason the capsules which will be designed to dive in the lake can be connected by a wire with the mother ship as it shown in Figs 1, 2. This pattern can also support the micro probes with energy originated by the carrier. An overview of RF MEMS transmit/receive switches can be found in [34, 35]

4) Temperature and pressure sensors

The temperature and pressure sensors have the functional difference that they should interact with the environment surrounding the MEMS capsule.

Any temperature measurement is correlated on the variance of an attribute of the exposed material with any ambient temperature change. MEMS resonator-based oscillators have been proposed to be used as Complementary metal-oxide-semiconductor (CMOS) temperature sensor with a resolution of 0.008°C [36].

The MEMS pressure sensing technique is based on the silicon piezoresistive effect, where any pressure change will cause deflection and internal stain change, which will result output voltage variation [e.g. 37, 38]. Usually, a Wheatstone bridge circuit delivers such voltage measurements, in order to correlate them with the applied pressure.

V. CONCLUSION

The MEMS experiment will vertically measure the temperature and the pressure of the liquid deposit of an hydrocarbon lake on Titan's surface during a future mission, while at the same time it will operate as an internal source of infrared wavelengths giving the opportunity to the Lake Lander to analyze the composition of the lake by receiving its IR signals. Moreover, the recorded reflections of the RF signal emitted by MEMS will construct the topographical map of the bottom of the lake.

Although it is intentional to have many devices in order to construct a network, the major issue of portability comes up. However, micro-electro-mechanical devices suit perfectly in this kind of requirements because of their small shape, size and weight. Obviously, the utilization of any innovative instrumentation requires complete knowledge of the environmental issues and parameters and of course the deep understanding of their complexity.

In the contemporary market, MEMS can be easily found combining low cost and high reliability. These devices feature low power consumption, high-modulation depth, high emissivity and a long lifetime.

In a sense, this ambitious experiment can easily accomplish both the 3D sounding of the lake as well as its chemical composition.

MEMS devices combine:

1) Very small size (20 μm to 1 mm)
2) Fast pulsing (thanks to low mass of the emitter)
3) Limitation of low output power (450mW)

4) Reduction of the thermal mass of the system

5) Enhancement of the modulated performance

6) Extremely low cost.

ACKNOWLEDGMENT

The authors would like to thank Mr Dimosthenis Kouritis for fruitful discussions concerning the concept of the proposed experiment and Mr Theodosios Chatzistergos who provided valuable assistance with the figures. Anezina Solomonidou is financially supported by the European Union (European Social Fund – ESF) and Greek national funds through the Operational Program "Education and Lifelong Learning" of the National Strategic Reference Framework (NSRF) - Research Funding Program: Heracleitus II. Investing in knowledge society through the European Social Fund.

REFERENCES

[1] E. R. Stofan et al., "The lakes of Titan," *Nature*, vol. 445, pp. 61-64, 2007.

[2] E. P. Turtle et al., "Rapid and extensive surface changes near Titan's equator: evidence of April showers," *Science*, vol. 331, pp. 1414-1417, 2011.

[3] Stofan, E., et al., "The Titan Mare Explorer Mission : A Discovery mission to a Titan sea", EPSC-DPS 2011 Assembly, Nantes 3-8 Oct. 2011.

[4] TSSM, *NASA/ESA Final Report*, 30 January 2009.

[5] H. B. Niemann et al., "Composition of Titan's lower atmosphere and simple surface volatiles as measured by the Cassini-Huygens probe gas chromatograph mass spectrometer experiment," *Journal of Geophysical Research (Planets)*, vol. 115, pp. E12006, 2010.

[6] A. Coustenis and F. W. Taylor, "Titan: exploring an Earthlike World," *Series on atmospheric, oceanic and planetary physics, vol 4. World Scientific, Singapore*, 2008.

[7] M. Fulchignoni et al., "In situ measurements of the physical characteristics of Titan's environment," *Nature*, vol. 438, pp. 785-791, 2005.

[8] L. C. Kouvaris and F. M. Flasar, "Phase equilibrium of methane and nitrogen at low temperatures: Application to Titan," *Icarus*, vol. 91, pp. 112-124, 1991.

[9] S. K. Atreya et al., "Titan's methane cycle," *Planetary and Space Science*, vol. 54, pp. 1177-1187 2006.

[10] F. M. Flasar, "Oceans on Titan?," *Science*, vol. 221, pp. 55-57, 1983.

[11] J. I. Lunine, D. J. Stevenson, and Y. L. Yung, "Ethane ocean on Titan," *Science*, vol. 222, pp. 1229-1230, 1983.

[12] A. Hayes et al., "Hydrocarbon lakes on Titan: distribution and interaction with a porous regolith," *Geophysical Research Letters*, vol. 35, pp. E09204, 2008.

[13] G. Mitri, A. P. Showman, J. I. Lunine, and R. D. Lorenz, "Hydrocarbon lakes on Titan," *Icarus*, vol. 186, pp. 385-394, 2007.

[14] C. Notarnicola, B. Ventura, D. Casarano, and F. Posa, "Cassini radar data: estimation of Titan's lake features by means of a Bayesian inversion algorithm," *IEEE Transactions on Geoscience and Remote Sensing*, vol. 47, pp. 1503-1511, 2009.

[15] G. Bampasidis, A. Coustenis, A. Solomonidou, and X. Moussas, "MEMS techniques for sounding the interior of Titanic lakes," *European Planetary Science Congress, EPSC2009-722*, vol. Vol. 4, 2009.

[16] H. C. Nathanson, W. E. Newell, R. A. Wickstrom, and J. Davis, J. R., "The resonant gate transistor," *IEEE Transactions on Electron Devices*, 1967.

[17] B. Stark and J. Bernstein, "Reliability overview," *in MEMS reliability assurance guidelines for space applications (ed. B. Stark), JPL Publication 99-1*, 1999.

[17] S. W. Janson, H. Helvajian, and K. Breuer, "MEMS, microengineering and aerospace systems," *AIAA 99-3502*, 1999.

[19] D. Dayton et al., "Demonstration of new technology MEMS and liquid crystal adaptive optics on bright astronomical objects and satellites," *Optics Express*, vol. 10, pp. 1508-1508, 2002.

[20] R. Krishnamoorthy and T. Bifano, "MEMS arrays for deformable mirrors," *SPIE*, vol. 2641, 1995.

[21] M. C. Roggemann, V. M. Bright, B. M. Welsh, W. D. Cowan, and M. Lee, "Micro-electro-mechanical deformable mirrors for aberration control in optical systems," *Optical and Quantum Electronics*, vol. 31, pp. 451-468, 1999.

[22] Y. Zhou and T. G. Bifano, "Characterization of contour shapes achievable with a MEMS deformable mirror," *Proc. of SPIE*, vol. 6113, 2006.

[23] J. B. Stewart, T. G. Bifano, P. Bierden, S. Cornelissen, T. Cook, and B. M. Levine, "Design and development of a 329-segment tip-tilt piston mirrorarray for space-based adaptive optics," *Proc. of SPIE*, vol. 6113, pp. 181-189, 2006.

[24] S. Nam et al., "A telescope for observation from space of extreme lightnings in the upper atmosphere," *Nuclear Instruments and Methods in Physics Research Section A: Accelerators, Spectrometers, Detectors and Associated Equipment*, vol. 588, pp. 197-200, 2008.

[25] J. H. Park et al., "Obscura telescope with a MEMS micromirror array for space observation of transient luminous phenomena or fast-moving objects," *Optics Express*, vol. 16, pp. 20249-20249, 2008.

[26] B. Swinyard et al., "The space infrared telescope for cosmology and astrophysics: SPICA A joint mission between JAXA and ESA," *Experimental Astronomy*, vol. 23, pp. 193-219, 2009.

[27] W. Truszkowski, H. Hallock, C. Rouff, J. Karlin, J. Rash, and M. Hinchey, *Autonomous and autonomic systems: with applications to NASA intelligent spacecraft operations and exploration systems*. London: Springer-Verlag, 2009.

[28] B. Elias, "Match the emitter to the task," *Photonics Spectra*, vol. 42, 2008.

[29] M. Kraft, A. Kenda, T. Sandner, and H. Schenk, "MEMS-based compact FT-spectrometers - a platform for spectroscopic mid-infrared sensors," *IEEE Sensors*, pp. 130-133, 2008.

[30] A. Tortschanoff, M. Lenzhofer, A. Frank, A. Kenda, T. Sandner, and H. Schenk, "Improved MEMS based FT-IR spectrometer," *Int. Symposium on Optomechatronic Technologies*, pp. 116-121, 2009.

[31] R. W. Bernstein, A. Ferber, I. Johansen, S. T. Moe, H. Rogne, and D. T. Wang, "Optical MEMS for infrared gas sensors," *IEEE/LEOS Int. Conf. on Optical MEMS*, pp. 137-138, 2000.

[32] K. Enya, H. Kataza, and P. Bierden, "A Micro Electrical Mechanical Systems (MEMS)-based cryogenic deformable mirror," *Publications of the Astronomical Society of the Pacific*, vol. 121, pp. 260-265, 2009.

[33] S. Waldis, F. Zamkotsian, P. Lanzoni, W. Noell, and N. de Rooij, "Packaged MEMS micromirrors for cryogenic environment," *IEEE 21st Int. Conf. on Micro Electro Mechanical Systems*, pp. 758-761, 2008.

[34] K. Van Caekenberghe, "RF MEMS on the radar," *Microwave Magazine, IEEE*, vol. 10, pp. 99-116, 2009.

[35] S. K. Lahiri, H. Saha, and A. Kundu, "RF MEMS SWITCH: An overview at- a-glance," *4th Int. Conf. on Computers and Devices for Communication*, pp. 1-5, 2009.

[36] C. M. Jha et al., "Cmos-Compatible dual-resonator MEMS temperature sensor with milli-degree accuracy," *Int. Solid-State Sensors, Actuators and Microsystems Conf., TRANSDUCERS*, pp. 229-232, 2007.

[37] L. Lin and W. Yun, "MEMS pressure sensors for aerospace applications," *IEEE Aerospace Conf. Proc.* vol. 1, pp. 429-436, 1998.

[38] B. Li, G. Q. Zhang, D. G. Yang, H. Fengze, and H. Yang, "The effect of diaphragm on performance of MEMS pressure sensor packaging," *11th Int. Conf. on Electronic Packaging Technology & High Density Packaging*, pp. 601-606, 2010.

References

Achilleos, N., Arridge, C. S., Bertucci, C., Jackman, C. M., Dougherty, M. K., Khurana, K. K., Russell, C. T. (2008). Large-scale dynamics of Saturn's magnetopause: Observations by Cassini. Journal of Geophysical Research 113, A11209-A11209.

Achterberg, R. K., Conrath, B. J., Gierasch, P. J., Flasar, F. M., Nixon, C. A. (2008). Titan's middle-atmospheric temperatures and dynamics observed by the Cassini Composite Infrared Spectrometer. Icarus 194, 263-277.

Abdi, H. and L. J. Williams (2010). Principal component analysis. Wiley Interdisciplinary Reviews: Computational Statistics 2, 433-459.

Adámkovics, M., de Pater, I., Hartung, M., Barnes, J. W. (2009). Evidence for condensed-phase methane enhancement over Xanadu on Titan. Planetary and Space Science 57, 1586-1595.

Albert, S., Bauerecker, S., Boudon, V., Brown, L.R., Champion, J.-P., Loëte, M., Nikitin, A., Quack, M. (2009). Global analysis of the high resolution infrared spectrum of methane 12CH4 in the region from 0 to 4800 cm-1. Chem. Phys. 356, 131-146.

Allison, M. L. and Clifford, S. M. (1978). Ice-covered water volcanism on Ganymede. Journal of Geophysical Research 92, 7865-7876.

Anderson, J. D., Lau, E. L., Sjogren, W. L., Schubert, G., Moore, W. B. (1997). Europa's Differentiated Internal Structure: Inferences from Two Galileo Encounters. Science 276, 1236-1239.

Anderson, J. D., Schubert, G., Jacobson, R. A., Lau, E. L., Moore, W. B., Sjogren, W. L. (1998). Europa's Differentiated Internal Structure: Inferences from Four Galileo Encounters. Science 281, 2019-2019.

Anderson, J. D., Jacobson, R. A., McElrath, T. P., Moore, W. B., Schubert, G., Thomas, P. C. (2001). Shape, Mean Radius, Gravity Field, and Interior Structure of Callisto. Icarus 153, 157-161.

Arridge, C. S., Khurana, K. K., Russell, C. T., Southwood, D. J., Achilleos, N., Dougherty, M. K., Coates, A. J. and Leinweber, H. K. (2008). Warping of Saturn's magnetospheric and magnetotail current sheets. Journal of Geophysical Research 113. A08217-A08217.

Artemieva, N. and Lunine, J. (2003). Cratering on Titan: impact melt, ejecta, and the fate of surface organics. Icarus 164, 471-480.

Atreya, S. K., Adams, E. Y., Niemann, H. B., Demick-Montelara, J. E., Owen, T. C., Fulchignoni, M., Ferri, F., Wilson, E. H (2006). Titan's methane cycle. Planetary and Space Science 54, 1177-1187.

Atreya, S. K. (2010). The significance of trace constituents in the solar system. Faraday Discuss.,147, 9–29.

Backes, H., Neubauer, F. M., Dougherty, M. K., Achilleos, N., Andre, N., Arridge, C. S., Bertucci, C., Jones, G. H., Khurana, K. K., Russell, C. T. and Wennmacher, A. (2005). Titan's Magnetic Field Signature During the First Cassini Encounter. Science 308, 992-995.

Baker, P.E., Brosset, R., Gass, I.G., Neary, C.R. (1973). Jebel al Abyad: A recent alkalic volcanic complex in western Saudi Arabia. Lithos 6, 291-313.

Bampasidis, G., Coustenis, A., Solomonidou, A. and Moussas, X. (2009). MEMS Techniques for Sounding the Interior of Titanic Lakes. European Planetary Science Congress, EPSC2009-722 Vol. 4.

Bampasidis, G., Solomonidou, A., Bratsolis, E., Kyriakopoulos, K., Moussas, X., Preka-Papadema, P., Hirtzig, M., Coustenis, A. (2011a). Seismometers on the satellites of the Outer Solar System. 2nd International Conference on Space Technology (ICST) Athens, Greece, 15-17 Sept., 10.1109/ICSpT.2011.6064647.

Bampasidis, G., Solomonidou, A., Bratsolis, E., Kyriakopoulos, K., Moussas, X., Preka-Papadema, P., Hirtzig, M., Coustenis, A. (2011b). Sounding the interior of Titan's lakes by using Micro-Electro-Mechanical Systems (MEMS). 2nd International Conference on Space Technology (ICST), Athens, Greece, 15-17 Sept.,10.1109/ICSpT.2011.6064648.

Bampasidis, G. (2013). Study of the environment of Titan: The stratosphere and the surface of the satellite, future mission experiments & educational activities. PhD Thesis.

Barnash, A.N., Rathbun, J.A., Turtle, E.P., Squyres, S.W. (2006). Interactions Between Impact Craters and Tectonic Fractures on Enceladus. Bulletin of the American Astronomical Society 38, 522.

Barnes, J.W., R. H. Brown, E. P. Turtle, A. S. McEwen, R. D. Lorenz, M. Janssen, E. L. Schaller, M.E. Brown, B.J. Buratti, C. Sotin, C. Griffith, R. Clark, J. Perry, S. Fussner, J. Barbara, R. West, C. Elachi, A. H. Bouchez, H. G. Roe, K.H. Baines, G. Bellucci, and J.P. Bibring (2005). A 5-micron-bright spot on Titan: Evidence for surface diversity. Science 310, 92-95.

Barnes, J. W., R. H. Brown, J. Radebaugh, B. J. Buratti, C. Sotin, S. Le Mouélic, S. Rodriguez, E. P. Turtle, J. Perry, R. Clark, K. H. Baines, and P. D. Nicholson (2006). Cassini observations of flow-like features in western Tui Regio, Titan. Geophys. Res. Lett. 33, L16204.

Barnes, J. W., Brown, R. H., Soderblom, L., Buratti, B. J., Sotin, C., Rodriguez, S., Le Mouelic, S., Baines, K. H., Clark, R. and Nicholson, P. (2007a). Global-scale surface spectral variations on Titan seen from Cassini/VIMS. Icarus 186, 242-258.

Barnes, J. W., Radebaugh, J., Brown, R. H., Wall, S., Soderblom, L., Lunine, J., Burr, D., Sotin, C., Mouelic, S. L., Rodriguez, S., Buratti, B. J., Clark, R., Baines, K. H., Jaumann, R., Nicholson, P. D., Kirk, R. L., Lopes, R., Lorenz, R. D., Mitchell, K. and Wood, C. A. (2007b). Near-infrared spectral mapping of Titan's mountains and channels. Journal of Geophysical Research 112, E11006-E11006.

Barnes, J. W., Brown, R. H., Soderblom, L., Sotin, C., Le Mouelic, S. p., Rodriguez, S., Jaumann, R., Beyer, R. A., Buratti, B. J., Pitman, K., Baines, K. H., Clark, R. and Nicholson, P. (2008). Spectroscopy, morphometry, and photoclinometry of Titan's dunefields from Cassini/VIMS. Icarus 195, 400-414.

Barnes, J. W., Brown, R. H., Soderblom, J. M., Soderblom, L. A., Jaumann, R., Jackson, B., Le Mouelic, S., Sotin, C., Buratti, B. J., Pitman, K. M., Baines, K. H., Clark, R. N., Nicholson, P. D., Turtle, E. P., Perry, J. (2009). Shoreline features of Titan's Ontario Lacus from Cassini/VIMS observations. Icarus 201, 217-225.

Barnes, J. W., Soderblom, J. M., Brown, R. H., Soderblom, L. A., Stephan, K., Jaumann, R., Mouelic, S. L., Rodriguez, S., Sotin, C., Buratti, B. J., Baines, K. H., Clark, R. N. and Nicholson, P. D. (2011). Wave constraints for Titan's Jingpo Lacus and Kraken Mare from VIMS specular reflection lightcurves. Icarus 211, 722-731.

Barnes, J. W., Lemke, L., Foch, R., McKay, C. P., Beyer, R. A., Radebaugh, J., Atkinson, D. H., Lorenz, R. D., Le Mouelic, S., Rodriguez, S., Gundlach, J., Giannini, F., Bain, S., Flasar, F. M., Hurford, T., Anderson, C. M., Merrison, J., Adamkovics, M., Kattenhorn, S. A., Mitchell, J., Burr, D. M., Colaprete, A., Schaller, E., Friedson, A. J., Edgett, K. S., Coradini, A., Adriani, A., Sayanagi, K. M., Malaska, M. J., Morabito, D. and Reh, K. (2012). AVIATR-Aerial Vehicle for In-situ and Airborne Titan Reconnaissance. A Titan airplane mission concept. Experimental Astronomy 33, 55-127.

Barr, A. C., Pappalardo, R. T., Stevenson, D. J. (2001). Rise of Deep Melt into Ganymede's Ocean and Implications for Astrobiology. 32nd Annual Lunar and Planetary Science Conference, 1781.

Barr, A.C. (2008). Mobile lid convection beneath Enceladus' south polar terrain. J. Geophys. Res. 113, E07009.

Barr, A.C., McKinnon, W.B. (2007). Convection in Enceladus' ice shell: conditions for initiation. Geophys. Res. Lett. 34, L09202.

Barr, A.C. and Pappalardo, R.T. (2005). Onset of convection in ice I with composite Newtonian and non-Newtonian Rheology: Application to the icy Galilean satellites. J. Geophys. Res. 110, E12005.

Barth, E. L. (2010). Cloud formation along mountain ridges on Titan. Planetary and Space Science 58, 1740-1747.

Baum, W. A., Kreidl, T., Westphal, J. A., Danielson, G. E., Seidelmann, P. K., Pascu, D., Currie, D. G. (1981). Saturn's E-ring. Icarus 47, 84-96.

Baumgardner, J.R. (1994). Runaway subduction as the driving mechanism for the Genesis Flood. Proceedings of the Third International Conference on Creationism, Technical Symposium Sessions, Creation Science Fellowship, Pittsburgh, 63–75.

Baumgardner, J.R. (2003). Catastrophic Plate Tectonics: The Physics Behind the Genesis Flood. Proceedings of the Fifth International Conference on Creationism 113-126.

Beeman, M., Durham, W., Kirby, S. (1988). Friction of ice. J. Geophys. Res. 93, 7625-7633.

Beghin, C., Canu, P., Karkoschka, E., Sotin, C., Bertucci, C., Kurth, W. S., Berthelier, J. J., Grard, R., Hamelin, M., Schwingenschuh, K. and SimΓμes, F. (2009). New insights on Titan's plasma-driven Schumann resonance inferred from Huygens and Cassini data. Planetary and Space Science 57, 1872-1888.

Beghin, C., Randriamboarison, O. l., Hamelin, M., Karkoschka, E., Sotin, C., Whitten, R. C., Berthelier, J.-J., Grard, R. j. and SimΓμes, F. (2012). Analytic theory of Titan's Schumann resonance: Constraints on ionospheric conductivity and buried water ocean. Icarus 218, 1028-1042.

Behounkova, M., Tobie, G., Choblet, G. and Cadek, O. (2012). Tidally-induced melting events as the origin of south-pole activity on Enceladus. Icarus 219, 655-664.

Benn, K., Mareschal, J-C., Condie, K.C. (2006). Archean Geodynamics and Environments. Geophysical Monograph Series 164.

Bertucci, C., Achilleos, N., Dougherty, M. K., Modolo, R., Coates, A. J., Szego, K., Masters, A., Ma, Y., Neubauer, F. M., Garnier, P., Wahlund, J. E. and Young, D. T. (2008). The Magnetic Memory of Titan's Ionized Atmosphere. Science, 1475-1478.

Bird, P. (1988). Formation of the Rocky Mountains, Western United States: A Continuum Computer Model. Science 239, 1501-1507.

Bird, M. K., Dutta-Roy, R., Heyl, M., Allison, M., Asmar, S. W., Folkner, W. M., Preston, R. A., Atkinson, D. H., Edenhofer, P., Plettemeier, D., Wohlmuth, R., Iess, L. and Tyler, G. L. (2002). The Huygens Doppler Wind Experiment - Titan Winds Derived from Probe Radio Frequency Measurements. Space Science Reviews 104, 613-640.

Bird, M. K., Allison, M., Asmar, S. W., Atkinson, D. H., Avruch, I. M., Dutta-Roy, R., Dzierma, Y., Edenhofer, P., Folkner, W. M., Gurvits, L. I., Johnston, D. V., Plettemeier, D., Pogrebenko, S. V., Preston, R. A. and Tyler, G. L. (2005). The vertical profile of winds on Titan. Nature 438, 800-802.

Black, B. A., Perron, J. T., Burr, D. M., Drummond, S. A. (2012). Estimating erosional exhumation on Titan from drainage network morphology. Journal of Geophysical Research 117, E08006.

Blanc, M., Kallenbach, R., Erkaev, N. (2005). Solar System Magnetospheres. Space Science Reviews 116, 227-298.

Blanc, M., Alibert, Y., André, N., Atreya, S., Beebe, R., Benz, W., Bolton, S., Coradini, A., Coustenis, A., Dehant, V., Dougherty, M., Drossart, P., Fujimoto, M., Grasset, O., Gurvits, L., Hartogh, P., Hussmann, H., Kasaba, Y., Kivelson, M., Khurana, K., Krupp, N., Louarn, P., Lunine, J., McGrath, M., Mimoun, D., Mousis, O., Oberst, J., Okada, T., Pappalardo, R., Prieto-Ballesteros, O., Prieur, D., Regnier, P., Roos-Serote, M., Sasaki, S., Schubert, G., Sotin, C., Spilker, T., Takahashi, Y., Takashima, T., Tosi, F., Turrini, D., Van Hoolst, T. and Zelenyi, L. (2009). LAPLACE: A mission to Europa and the Jupiter System for ESA's Cosmic Vision Programme. Experimental Astronomy 23, 849-892.

Bland, M.T., Singer, K.N., McKinnon, W.B., Schenk, P.M. (2012). Enceladus' extreme heat flux as revealed by its relaxed craters. Geophys. Res. Lett. 39, L17204.

Bleacher, J. E., Garry, W. B., Zimbelman, J. R. (2008). Observations of surface textures that are indicative of lava sheet inflation in monogenetic flow fields: Insights from the McCartys and Carrizozo flow fields. Geol. Society of America 40, 114.

Boudon, V., Rey, M., Loete, M. (2006). The vibrational levels of methane obtained from analyses of high-resolution spectra. J. Quant. Spectrosc. Radiat. Transfer 98, 394–404.

Brandt, P. C., Dialynas, K., Dandouras, I., Mitchell, D. G., Garnier, P. and Krimigis, S. M. (2012). The distribution of Titan's high-altitude (out to 50,000 km) exosphere from energetic neutral atom (ENA) measurements by Cassini/INCA. Planetary and Space Science 60, 107-114.

Bratsolis, E. and Sigelle, M. (2003). Fast SAR image restoration, segmentation, and detection of high-reflectance regions. IEEE Transactions on Geoscience and Remote Sensing 41, 2890-2899.

Bratsolis, E., Bampasidis, G., Solomonidou, A. and Coustenis, A. (2012). A despeckle filter for the Cassini synthetic aperture radar images of Titan's surface. Planetary and Space Science 61, 108-113.

Brown, R. H., Baines, K. H., Bellucci, G., Bibring, J. P., Buratti, B. J., Capaccioni, F., Cerroni, P., Clark, R. N., Coradini, A., Cruikshank, D. P., Drossart, P., Formisano, V., Jaumann, R., Langevin, Y., Matson, D. L., McCord, T. B., Mennella, V., Miller, E., Nelson, R. M., Nicholson, P. D., Sicardy, B. and Sotin, C. (2004). The Cassini Visual And Infrared Mapping Spectrometer (Vims) Investigation. Space Science Reviews 115, 111-168.

Brown, R.H., Clark, R.N., Buratti, B.J., Cruikshank, D.P., Barens, J.W., Mastrapa, R.M.E., Bauer, J., Newman, S., Momary, T., Baines, K.H., Bellucci, G., Capaccioni, P., Cerroni, P., Combes, M., Coradini, A., Drossart, P., Formisano, V., Jaumann, R., Langevin, Y., Matson, D.L., McCord, T.B., Nelson, R.M., Nicholson, P.D., Sicardy, B., and Sotin, C. 2006. Composition and physical properties of Enceladus' surface. Science 311, 1425-1428.

Brown, R. H., Soderblom, L. A., Soderblom, J. M., Clark, R. N., Jaumann, R., Barnes, J. W., Sotin, C., Buratti, B., Baines, K. H. and Nicholson, P. D. (2008). The identification of liquid ethane in Titan's Ontario Lacus. Nature 454, 607-610.

Brown, R. H., Barnes, J. W., Melosh, H. J. (2011). On Titan's Xanadu region. Icarus 214, 556-560.

Buratti, B. J., Sotin, C., Brown, R. H., Hicks, M. D., Clark, R. N., Mosher, J. A., McCord, T. B., Jaumann, R., Baines, K. H., Nicholson, P. D., Momary, T., Simonelli, D. P., Sicardy, B. (2006). Titan: Preliminary results on surface properties and photometry from VIMS observations of the early flybys. Planetary and Space Science 54, 1498-1509.

Buratti, B. J., Sotin, C., Lawrence, K., Brown, R. H., Le Mouélic, S., Soderblom, J. M., Barnes, J., Clark, R. N., Baines, K. H., Nicholson, P. D. (2012). A newly discovered impact crater in Titan's Senkyo: Cassini VIMS observations and comparison with other impact features. Planetary and Space Science 60, 18-25.

Burr, D. M., Jacobsen, R. E., Roth, D. L., Phillips, C. B., Mitchell, K. L. and Viola, D. (2009). Fluvial network analysis on Titan: Evidence for subsurface structures and west-to-east wind flow, southwestern Xanadu. Geophysical Research Letters 36, 22203-22207.

Burr, D. M., Taylor P. J., Lamb, M. P., Irwin, R. P., Collins, G. C., Howard, A. D., Sklar, L. S., Moore, J. M., Adamkovics, M., Baker, V. R. (2013). Fluvial features on Titan: Insights from morphology and modeling. Geological Society of America Bulletin 125, 299-321.

Caldwell, J. (1977). Thermal radiation from Titan's atmosphere. IAU Colloq. 28: Planetary Satellites. J. A. Burns, 438-450.

Calvin, W. M. and Spencer, J. R. (1997). Latitudinal Distribution of O2 on Ganymede: Observations with the Hubble Space Telescope. Icarus 130, 505-516.

Cameron, A.G.W. (1973). History of the solar system. Earth-Science reviews 9, 125–137.

Camp, V., Roobol, M., Hooper, P. (1991). The Arabian continental alkali basalt province: Part II. Evolution of Harrats Khaybar, Ithnayn, and Kura, Kingdom of Saudi Arabia. Geological Society of America Bulletin 103, 363-391.

Campargue, A., Wang, L., Mondelain, D., Kassi, S., Bézard, B., Lellouch, E., Coustenis, A., de Bergh, C., Hirtzig, M., Drossart. P. (2012). An empirical line list for methane in the 1.26-1.71 μm region for planetary investigations (T=80-300 K]. Application to Titan. Icarus 219, 110-128.

Campbell, D. B., Black, G. J., Carter, L. M., Ostro, S. J. (2003). Radar Evidence for Liquid Surfaces on Titan. Science 302, 431-434.

Carlson, R. W. (1999). A Tenuous Carbon Dioxide Atmosphere on Jupiter's Moon Callisto. Science 283, 820-821.

Cassidy, T.A., Johnson, R.E. (2010). Collisional spreading of Enceladus' neutral cloud. Icarus 209, 696–703.

Castillo-Rogez, J. and Lunine, J. I. (2010). Evolution of Titan's rocky core constrained by Cassini observations.
Geophysical Research Letters 37, L20205.

Chang, S.J., Van der Lee, S. (2011). Mantle plumes and associated flow beneath Arabia and East Africa. Earth Planet. Sci. Lett. 302, 448-454.

Chen, C. W. and Hensley, S. (2008) .Amplitude-based height-reconstruction techniques for synthetic aperture ladar systems. Optical Society of America Journal 22, 529-538.

Chen, E.M.A. and Nimmo, F. (2011). Obliquity tides do not significantly heat Enceladus. Icarus 214, 779–81.

Chitroub, S., Houacine, A. and Sansal, B. (2002). Statistical characterisation and modelling of SAR images. Signal Processing 82, 69-92.

Choukroun, M. and Grasset, O. (2007), Thermodynamic model for water and high-pressure ices up to 2.2 GPa and down to the metastable domain. J. Chem. Phys. 127, 124, 506.

Choukroun, M. and Grasset, O (2010), Thermodynamic data and modeling of the water and ammonia-water phase diagrams up to 2.2 GPa for planetary geophysics. J. Chem. Phys., 133, 144, 502.

Choukroun, M. and Sotin, C. (2012). Is Titan's shape caused by its meteorology and carbon cycle? Geophysical Research Letters 39, 04201-04201.

Choukroun, M., Grasset, O., Tobie, G., Sotin, C. (2010). Stability of methane clathrate hydrates under pressure: Influence on outgassing processes of methane on Titan. Icarus 205, 581-593.

Clark, R. N. and McCord, T. B. (1980). The Galilean satellites - New near-infrared spectral reflectance measurements /0.65-2.5 microns/ and a 0.325-5 micron summary. Icarus 41, 323-339.

Clark, R. N., Curchin, J. M., Hoefen, T. M., Swayze, Gregg A. (2009). Reflectance spectroscopy of organic compounds: 1. Alkanes. Journal of Geophysical Research 114, E03001.

Cloos, H. (1936). Einführung in die Geologie : ein Lehrbuch der inneren Dynamik. Borntraeger, Berlin.

Coates, A. J., Crary, F. J., Lewis, G. R., Young, D. T., Waite, J. H. and Sittler, E. C. (2007). Discovery of heavy negative ions in Titan's ionosphere. Geophysical Research Letters 34, 22103-22103.

Coates, A. J., Jones, G. H., Lewis, G. R., Wellbrock, A., Young, D. T., Crary, F. J., Johnson, R. E., Cassidy, T. A. and Hill, T. W. (2010). Negative ions in the Enceladus plume. Icarus 206, 618-622.

Consolmagno, G. J. and Lewis, J. S. (1978). The evolution of icy satellite interiors and surfaces. Icarus,34, 280-293.

Collins, G. C. and Goodman, J. C. (2007). Enceladus' south polar sea. Icarus 189, 72-82.

Collins, G. C., Head, J. W., Pappalardo, R. T. (1998). Formation of Ganymede Grooved Terrain by Sequential Extensional Episodes: Implications of Galileo Observations for Regional Stratigraphy. Icarus 135, 345-359.

Collins, G.C., McKinnon, W.B., Moore, J.M., Nimmo, F., Pappalardo, R.T., Prockter, L.M., Schenk, P.M. (2009). Tectonics of the outer planet satellites. Planetary Tectonics, Cambridge University Press.

Comas Solá, J. (1908). Observations des satellites principaux de Jupiter et de Titan. Astronomische Nachrichten 4290, 289 - 290.

Combes, M., Vapillon, L., Gendron, E., Coustenis, A., Lai, O., Wittemberg. R., Sirdey. R. (1997). Spatially Resolved Images of Titan by Means of Adaptive Optics. Icarus 129, 482-497.

Cook, C., Barnes, J. W., Kattenhorn, S. A., Radebaugh, J., Hurford, T., Stiles, B. (2013). Evidence for Global Contraction on Titan from Patterns of Tectonism. 44th Lunar and Planetary Science Conference 1719, 2509.

Cooper, J. F., Johnson, R. E., Mauk, B. H., Garrett, H. B., Gehrels, N. (2001). Energetic Ion and Electron Irradiation of the Icy Galilean Satellites."Icarus 149, 133-159.

Cooper, J.F., Cooper, P.D., Sittler, E.C., Sturner, S.J., Rymer, A.M. (2009). Old Faithful model for radiolytic gas-driven cryovolcanism at Enceladus. Planetary and Space Science 57, 1607-1620.

Cordier, D., Mousis, O., Lunine, J. I., Lebonnois, S., Rannou, P., Lavvas, P., Lobo, L. Q., Ferreira, A. G. M. (2013). Titan's lakes chemical composition: Sources of uncertainties and variability. Planetary and Space Science 61, 99-107.

Cornet, T., Bourgeois, O., Le Mouélic, S., Rodriguez, S., Lopez Gonzalez, T., Sotin, C., Tobie, G., Fleurant, C., Barnes, J. W., Brown, R. H., Baines, K. H., Buratti, B. J., Clark, R. N., Nicholson, P. D. (2012). Geomorphological significance of Ontario Lacus on Titan: Integrated interpretation of Cassini VIMS, ISS and RADAR data and comparison with the Etosha Pan (Namibia). Icarus 218, 788-806.

Coustenis, A. (1989). L' atmosphere de Titan a partir des observations infrarouges de Voyager. PhD Thesis, L' Universite de Paris VII.

Coustenis, A. and Encrenaz, Th. (2013). Life beyond Earth: the search for habitable worlds in the Universe. Cambridge Univ. Press.

Coustenis, A. and Hirtzig, M. (2009). Cassini-Huygens results on Titan's surface. Research in Astronomy and Astrophysics 9, 249-268.

Coustenis, A. and Taylor, F. W. (2008). Titan: exploring an Earthlike World. Series on atmospheric, oceanic and planetary physics, vol 4. World Scientific, Singapore.

Coustenis, A., Bezard, B., Gautier, D., Marten, A., Samuelson, R. (1991). Titan's atmosphere from Voyager infrared observations. III - Vertical contributions of hydrocarbons and nitriles near Titan's north pole. Icarus 89, 152-167.

Coustenis, A., Lellouch, E., Maillard, J. P., McKay, C. P. (1995). Titan's surface: composition and variability from the near-infrared albedo. Icarus 118, 87-104.

Coustenis, A., Salama, A., Lellouch, E., Encrenaz, T., Bjoraker, G. L., Samuelson, R. E., de Graauw, T., Feuchtgruber, H., Kessler, M. F. (1998). Evidence for water vapor in Titan's atmosphere from ISO/SWS data. Astronomy and Astrophysics 336, L85-L89.

Coustenis, A., Gendron, E., Lai, O., Veran, J.-P., Woillez, J., Combes, M., Vapillon, L., Fusco, T., Mugnier, L. and Rannou, P. (2001). Images of Titan at 1.3 and 1.6 μm with Adaptive Optics at the CFHT. Icarus 154, 501-515.

Coustenis, A., Salama, A., Schulz, B., Ott, S., Lellouch, E., Encrenaz, T. H., Gautier, D. and Feuchtgruber, H. (2003). Titan's atmosphere from ISO mid-infrared spectroscopy. Icarus 161, 383-403.

Coustenis, A., Hirtzig, M., Gendron, E., Drossart, P., Lai, O., Combes, M. and Negrao, A. (2005). Maps of Titan's surface from 1 to 2.5 μm. Icarus 177, 89-105.

Coustenis, A., Negrao, A., Salama, A., Schulz, B., Lellouch, E., Rannou, P., Drossart, P., Encrenaz, T., Schmitt, B., Boudon, V. and Nikitin, A. (2006). Titan's 3-micron spectral region from ISO high-resolution spectroscopy. Icarus 180, 176-185.

Coustenis, A., Achterberg, R. K., Conrath, B. J., Jennings, D. E., Marten, A., Gautier, D., Nixon, C. A., Flasar, F. M., Teanby, N. A., Bezard, B., Samuelson, R. E., Carlson, R. C., Lellouch, E., Bjoraker, G. L., Romani, P. N., Taylor, F. W., Irwin, P. G. J., Fouchet, T., Hubert, A., Orton, G. S., Kunde, V. G., Vinatier, S., Mondellini, J., Abbas, M. M. and Courtin, R. (2007). The composition of Titan's stratosphere from Cassini/CIRS mid-infrared spectra. Icarus 189, 35-62.

Coustenis, A., Atreya, S., Balint, T., Brown, R., Dougherty, M., Ferri, F., Fulchignoni, M., Gautier, D., Gowen, R., Griffith, C., Gurvits, L., Jaumann, R., Langevin, Y., Leese, M., Lunine, J., McKay, C., Moussas, X., Muller-Wodarg, I., Neubauer, F., Owen, T., Raulin, F., Sittler, E., Sohl, F., Sotin, C., Tobie, G., Tokano, T., Turtle, E., Wahlund, J. E., Waite, J., Baines, K., Blamont, J., Coates, A., Dandouras, I., Krimigis, T., Lellouch, E., Lorenz, R., Morse, A., Porco, C., Hirtzig, M., Saur, J., Spilker, T., Zarnecki, J., Choi, E., Achilleos, N., Amils, R., Annan, P., Atkinson, D., Benilan, Y., Bertucci, C., Bezard, B., Bjoraker, G., Blanc, M., Boireau, L., Bouman, J., Cabane, M., Capria, M., ChassefiŠre, E., Coll, P., Combes, M., Cooper, J., Coradini, A., Crary, F., Cravens, T., Daglis, I., de Angelis, E., de Bergh, C., de Pater, I., Dunford, C., Durry, G., Dutuit, O., Fairbrother, D., Flasar, F., Fortes, A., Frampton, R., Fujimoto, M., Galand, M., Grasset, O., Grott, M., Haltigin, T., Herique, A., Hersant, F., Hussmann, H., Ip, W., Johnson, R., Kallio, E., Kempf, S., Knapmeyer, M., Kofman, W., Koop, R., Kostiuk, T., Krupp, N., Kuppers, M., Lammer, H., Lara, L. M., Lavvas, P., Le Mou,lic, S., Lebonnois, S., Ledvina, S., Li, J., Livengood, T., Lopes, R., Lopez-Moreno, J. J., Luz, D., Mahaffy, P., Mall, U., Martinez-Frias, J., Marty, B., McCord, T., Menor Salvan, C., Milillo, A., Mitchell, D., Modolo, R., Mousis, O., Nakamura, M., Neish, C., Nixon, C., Nna Mvondo, D., Orton, G., Paetzold, M., Pitman, J., Pogrebenko, S., Pollard, W., Prieto-Ballesteros, O., Rannou, P., Reh, K., Richter, L., Robb, F., Rodrigo, R., Rodriguez, S., Romani, P.,

Ruiz Bermejo, M., Sarris, E., Schenk, P., Schmitt, B., Schmitz, N., Schulze-Makuch, D., Schwingenschuh, K., Selig, A., Sicardy, B., Soderblom, L., Spilker, L., Stam, D., Steele, A., Stephan, K., Strobel, D., Szego, K., Szopa, C., Thissen, R., Tomasko, M., Toublanc, D., Vali, H., Vardavas, I., Vuitton, V., West, R., Yelle, R. and Young, E. (2009). TandEM: Titan and Enceladus mission. Experimental Astronomy 23, 893-946.

Coustenis, A., Tokano, T., Burger, M. H., Cassidy, T. A., Lopes, R. M., Lorenz, R. D., Retherford, K. D., Schubert, G. (2010). Atmospheric/Exospheric Characteristics of Icy Satellites. Space Science Reviews 153, 155-184.

Coustenis, A., Hirtzig, M., Bampasidis, G., Solomonidou, A., Bratsolis, E., Kyriakopoulos, K., Moussas, X. and Preka-Papadema, P. (2011). Exploring the satellites of the outer planets with in situ elements. 2nd International Conference on Space Technology (ICST), Athens, Greece, 15-17 Sept.,10.1109/ICSpT.2011.6064652.

Coustenis, A., Raulin, F., Bampasidis, G., Solomonidou, A. (2012). Life in the Saturnian Neighborhood. Life on Earth and other Planetary Bodies. A. Hanslmeier, S. Kempe and J. Seckbach, Springer 24, 522.

Cravens, T. E., Robertson, I. P., Waite, J. H., Yelle, R. V., Kasprzak, W. T., Keller, C. N., Ledvina, S. A., Niemann, H. B., Luhmann, J. G., McNutt, R. L., Ip, W.-H., De La Haye, V., Mueller-Wodarg, I., Wahlund, J.-E., Anicich, V. G., Vuitton, V. (2006). Composition of Titan's ionosphere. Geophysical Research Letters 33, L07105.

Crow-Willard, E. and Pappalardo, R.T. (2011). Global geological mapping of Enceladus. EPSC--DPS Jt. Meet., Oct. 2–7, Nantes, Fr. (Abstr. EPSC-DPS2011-635-1).

Cyr, K.E., Sears, W.D., Lunine, J.I. (1998). Distribution and Evolution of Water Ice in the Solar Nebula: Implications for Solar System Body Formation. Icarus 135, 537-548.

Dalton, J. B. (2010). Spectroscopy of Icy Moon Surface Materials. Space Science Reviews 153, 219-247.

Dalton, J. B., Cruikshank, D. P., Stephan, K., McCord, T. B., Coustenis, A., Carlson, R. W. and Coradini, A. (2010). Chemical Composition of Icy Satellite Surfaces. Space Science Reviews 153, 113-154.

Dandouras, I., Garnier, P., Mitchell, D. G., Roelof, E. C., Brandt, P. C., Krupp, N. and Krimigis, S. M. (2009). Titan's exosphere and its interaction with Saturn's magnetosphere. Philosophical Transactions of the Royal Society A: Mathematical, Physical and Engineering Sciences 367, 743-752.

Danielson, R. E., Caldwell, J. J., Larach, D.R. (1973). An Inversion in the Atmosphere of Titan. Icarus 20, 437-437.

Davies, J. H. and Davies, D. R. (2010). Earth's surface heat flux. Solid Earth 1, 5–24.

Davies, A.D., Sotin, C., Matson, D.L., Castillo-Rogez, J., Johnson, T.V., Choukroun, M., Baines, K.H. (2010). Atmospheric control of the cooling rate of impact melts and cryolavas on Titan's surface. Icarus 208, 887–895.

Daumont, L. Nikitin, A. V., Thomas, X., Régalia, L., Von der Heyden, P., Tyuterev, Vl. G., Rey, M., Boudon, V., Wenger, Ch., Loëte, M., Brown, L. R. (2013). New assignments in the 2 μm transparency window of the 12CH4 Octad band system. J. Quant. Spectrosc. Radiat. Transfer 116, 101-109.

de Bergh, C., Courtin, R., Bezard, B., Coustenis, A., Lellouch, E., Hirtzig, M., Rannou, P., Drossart, P., Campargue, A., Kassi, S., Wang, L., Boudon, V., Nikitin, A., Tyuterev. V. (2012). Applications of a new set of methane line parameters to the modeling of Titan's spectrum in the 1.58 μm window. Planet. Spa. Sci., 61, 85-98.

de Kok, R., Irwin, P., Teanby, N., Lellouch, E., Bézard, B., Vinatier, S., Nixon, C., Fletecher, L., Howett, C., Calcutt, S., Bowles, N., Flasar, F. M., Taylor. F. (2007). Oxygen compounds in Titan's stratosphere observed by Cassini CIRS. Icarus, 186, 354-363.

Des Marais, D. J., Harwit, M. O., Jucks, K. W., Kasting, J. F., Lin, D. N. C., Lunine, J. I., Schneider, J., Seager, S., Traub, W. A. and Woolf, N. J. (2002). Remote Sensing of Planetary Properties and Biosignatures on Extrasolar Terrestrial Planets. Astrobiology 2, 153-181.

Dermott, S. F. and Sagan, C. (1995). Tidal effects of disconnected hydrocarbon seas on Titan. Nature 374, 238-240.

Dickinson, W.R. and Snyder, W.S. (1978). Plate Tectonics of the Laramide Orogeny. Geological Society of America Memoir 141, Boulder.

Dombard, A. J., McKinnon, W.B. (2006). Folding of Europa's icy lithosphere: An analysis of viscous-plastic buckling and subsequent topographic relaxation. J. Structur. Geol. 28, 2259–2269.

Dorofeeva, V. A. and Ruskol, E. L. (2010). On the thermal history of Saturn's satellites Titan and Enceladus. Solar System Research 44, 192-201.

Dougherty, M. K., Kellock, S., Southwood, D. J., Balogh, A., Smith, E. J., Tsurutani, B. T., Gerlach, B., Glassmeier, K. H., Gleim, F., Russell, C. T., Erdos, G., Neubauer, F. M. and Cowley, S. W. H. (2004). The Cassini Magnetic Field Investigation. Space Science Reviews 114, 331-383.

Dougherty, M. K., Khurana, K. K., Neubauer, F. M., Russell, C. T., Saur, J., Leisner, J. S., Burton, M. E. (2006). Identification of a Dynamic Atmosphere at Enceladus with the Cassini Magnetometer. Science 311, 1406-1409.

Duncan, M., Quinn, T., Tremaine, S. (1987). The formation and extent of the solar system comet cloud. Astronomical Journal 94, 1330-1338.

Easterbrook, D.J. (1999). Surface Processes and Landforms. Prentice Hall, New Jersey, USA.

Elachi, C., Allison, M. D., Borgarelli, L., Encrenaz, P., Im, E., Janssen, M. A., Johnson, W. T. K., Kirk, R. L., Lorenz, R. D., Lunine, J. I., Muhleman, D. O., Ostro, S. J., Picardi, G., Posa, F., Rapley, C. G., Roth, L. E., Seu, R., Soderblom, L. A., Vetrella, S., Wall, S. D., Wood, C. A. and Zebker, H. A. (2004). Radar: The Cassini Titan Radar Mapper. Space Science Reviews 115, 71-110.

Elachi, C., Wall, S., Allison, M., Anderson, Y., Boehmer, R., Callahan, P., Encrenaz, P., Flamini, E., Franceschetti, G., Gim, Y., Hamilton, G., Hensley, S., Janssen, M., Johnson, W., Kelleher, K., Kirk, R., Lopes, R., Lorenz, R., Lunine, J., Muhleman, D., Ostro, S., Paganelli, F., Picardi, G., Posa, F., Roth, L., Seu, R., Shaffer, S., Soderblom, L., Stiles, B., Stofan, E., Vetrella, S., West, R., Wood, C., Wye, L., Zebker, H. (2005). Cassini Radar Views the Surface of Titan. Science 308, 970-974.

Elachi, C., Wall, S., Janssen, M., Stofan, E., Lopes, R., Kirk, R., Lorenz, R., Lunine, J., Paganelli, F., Soderblom, L., Wood, C., Wye, L., Zebker, H., Anderson, Y., Ostro, S., Allison, M., Boehmer, R., Callahan, P., Encrenaz, P., Flamini, E., Francescetti, G., Gim, Y., Hamilton, G., Hensley, S., Johnson, W., Kelleher, K., Muhleman, D., Picardi, G., Posa, F., Roth, L., Seu, R., Shaffer, S., Stiles, B., Vetrella, S. and West, R. (2006). Titan Radar Mapper observations from Cassini's T3 fly-by. Nature 441, 709-713.

Emery, J.P., Burr, D.M., Cruikshank, D.P., Brown, R.H., Dalton, J.B. (2005). Near-infrared (0.8–4.0 mu m) spectroscopy of Mimas, Enceladus, Tethys, and Rhea. Astron. Astrophys. 435, 353–62.

Esposito, L. W., Barth, C. A., Colwell, J. E., Lawrence, G. M., McClintock, W. E., Stewart, A. I. F., Keller, H. U., Korth, A., Lauche, H., Festou, M. C., Lane, A. L., Hansen, C. J., Maki, J. N., West, R. A., Jahn, H., Reulke, R., Warlich, K., Shemansky, D. E. and Yung, Y. L. (2004). The Cassini Ultraviolet Imaging Spectrograph Investigation. Space Science Reviews 115, 299-361.

Esposito, L. W., Colwell, J. E., Hansen, C. J., Hallett, J. T., Hendrix, A. R., Larsen, K., McClintock, W. E., Pryor, W. R., Shemansky, D. E., Stewart, A. I., West, R. A. (2005). Cassini UVIS Results from Saturn, Titan, Icy Satellites and Rings. American Geophysical Union, Spring Meeting 2005, abstract #P13A-02.

Evans, K.F. (2007). SHDOMPPDA: A Radiative Transfer Model for Cloudy Sky Data Assimilation. J. Atmos. Sci., 64, 3854–3864.

Eviatar, A. and Podolak, M. (1983). "Titan's gas and plasma torus." Journal of Geophysical Research 88: 833-840.

Fagents, S.A., 2003. Considerations for effusive cryovolcanism on Europa: The post-Galileo perspective. J. Geophys. Res. 108, E12.

Fink, U. and Larson, H. P. (1979). The infrared spectra of Uranus, Neptune, and Titan from 0.8 to 2.5 microns. Astrophysical Journal 233, 1021-1040.

Fimmel, R. O., Swindell, W., Burgess, E. (1974). Pioneer odyssey: Encounter with a giant. NASA SP. 349.

Figueredo, P. H. and Greeley, R. (2004). Resurfacing history of Europa from pole-to-pole geologimapping. Icarus 167, 287-312.

Flasar, F. M. (1983). Oceans on Titan? Science 221, 55-57.

Flasar, F. M., Kunde, V. G., Abbas, M. M., Achterberg, R. K., Ade, P., Barucci, A., Bezard, B., Bjoraker, G. L., Brasunas, J. C., Calcutt, S., Carlson, R., Cesarsky, C. J., Conrath, B. J., Coradini, A., Courtin, R., Coustenis, A., Edberg, S., Edgington, S., Ferrari, C., Fouchet, T., Gautier, D., Gierasch, P. J., Grossman, K., Irwin, P., Jennings, D. E., Lellouch, E., Mamoutkine, A. A., Marten, A., Meyer, J. P., Nixon, C. A., Orton, G. S., Owen, T. C., Pearl, J. C., Prange, R., Raulin, F., Read, P. L., Romani, P. N., Samuelson, R. E., Segura, M. E., Showalter, M. R., Simon-Miller, A. A., Smith, M. D., Spencer, J. R., Spilker, L. J., Taylor, F. W. (2004). Exploring The Saturn System In The Thermal Infrared: The Composite Infrared Spectrometer. Space Science Reviews 115, 169-297.

Flasar, F. M., Achterberg, R. K., Conrath, B. J., Gierasch, P. J., Kunde, V. G., Nixon, C. A., Bjoraker, G. L., Jennings, D. E., Romani, P. N., Simon-Miller, A. A., Bezard, B., Coustenis, A., Irwin, P. G. J., Teanby, N. A., Brasunas, J., Pearl, J. C., Segura, M. E., Carlson, R. C., Mamoutkine, A., Schinder, P. J., Barucci, A., Courtin, R., Fouchet, T., Gautier, D., Lellouch, E., Marten, A., Prange, R., Vinatier, S., Strobel, D. F., Calcutt, S. B., Read, P. L., Taylor, F. W., Bowles, N., Samuelson, R. E., Orton, G. S., Spilker, L. J., Owen, T. C., Spencer, J. R., Showalter, M. R., Ferrari, C., Abbas, M. M., Raulin, F., Edgington, S., Ade, P. and Wishnow, E. H. (2005). Titan's Atmospheric Temperatures, Winds, and Composition. Science 308, 975-978.

Fortes, A. D. (2000). Exobiological Implications of a Possible Ammonia-Water Ocean inside Titan. Icarus 146, 444-452.

Fortes, A. D. (2012). Titan's internal structure and the evolutionary consequences. Planetary and Space Science 60, 10-17.

Fortes, A. D., Grindrod, P. M., Trickett, S. K. and Vočadlo, L. (2007). Ammonium sulfate on Titan: Possible origin and role in cryovolcanism. Icarus 188, 139-153.

Fowler, A.C. (1986). Thermal runaways in the Earth's mantle. Studies in applied Mathematics 74, 1-34.

Franceschetti, G. and Lanari, R. (1999). Synthetic Aperture Radar Processing. CRC Press.

Fulchignoni, M., Ferri, F., Angrilli, F., Bar-Nun, A., Barucci, M. A., Bianchini, G., Borucki, W., Coradini, M., Coustenis, A., Falkner, P., Flamini, E., Grard, R., Hamelin, M., Harri, A. M., Leppelmeier, G. W., Lopez-Moreno, J. J., McDonnell, J. A. M., McKay, C. P., Neubauer, F. H., Pedersen, A., Picardi, G., Pirronello, V., Rodrigo, R., Schwingenschuh, K., Seiff, A., Svedhem, H., Vanzani, V. and Zarnecki, J. (2002). The Characterisation of Titan's Atmospheric Physical Properties by the Huygens Atmospheric Structure Instrument (Hasi). Space Science Reviews 104, 395-431.

Fulchignoni, M., Ferri, F., Angrilli, F., Ball, A. J., Bar-Nun, A., Barucci, M. A., Bettanini, C., Bianchini, G., Borucki, W., Colombatti, G., Coradini, M., Coustenis, A., Debei, S., Falkner, P., Fanti, G., Flamini, E., Gaborit, V., Grard, R., Hamelin, M., Harri, A. M., Hathi, B., Jernej, I., Leese, M. R., Lehto, A., Lion Stoppato, P. F., Lopez-Moreno, J. J., Makinen, T., McDonnell, J. A. M., McKay, C. P., Molina-Cuberos, G., Neubauer, F. M., Pirronello, V., Rodrigo, R., Saggin, B., Schwingenschuh, K., Seiff, A., Simoes, F., Svedhem, H., Tokano, T., Towner, M. C., Trautner, R., Withers, P. and Zarnecki, J. C. (2005). In situ measurements of the physical characteristics of Titan's environment. Nature 438, 785-791.

Gault, D. E., Guest, J. E., Murray, J. B., Dzurisin, D., Malin, M. C. (1975). Some comparisons of impact craters on Mercury and the moon. Journal of Geophysical Research 80, 2444-2460.

Gautier, D. and Hersant, F. (2004). Formation and composition of planetesimals – trapping volatiles by clathration. Space Science Reviews 116, 25-52.

Gibbard, S. G., Macintosh, B., Gavel, D., Max, C. E., de Pater, I., Ghez, A. M., Young, E. F. and McKay, C. P. (1999). Titan: High-Resolution Speckle Images from the Keck Telescope. Icarus 139, 189-201.

Gibbard, S. G., Macintosh, B., Gavel, D., Max, C. E., de Pater, I., Roe, H. G., Ghez, A. M., Young, E. F. and McKay, C. P. (2004). Speckle imaging of Titan at 2 microns: surface albedo, haze optical depth, and tropospheric clouds 1996-1998. Icarus 169, 429-439.

Geissler, P. E., Greenberg, R., Hoppa, G., Helfenstein, P., McEwen, A., Pappalardo, R., Tufts, R., Ockert-Bell, M., Sullivan, R., Greeley, R. (1998). Evidence for non-synchronous rotation of Europa. Nature, 391, 368.

Gendron, E., Coustenis, A., Drossart, P., Combes, M., Hirtzig, M., Lacombe, F., Rouan, D., Collin, C., Pau, S., Lagrange, A. M., Mouillet, D., Rabou, P., Fusco, T. and Zins, G. (2004). VLT/NACO adaptive optics imaging of Titan. Astronomy and Astrophysics 417, L21-L24.

Giese, B., Hussmann, H., Roatsch, T., Helfenstein, P., Thomas, P.C., Neukum, G. (2011). Enceladus: evidence for librations forced by Dione. Presented at EPSC-DPS Jt. Meet., Oct. 2–7, Nantes, Fr. (Abstr. 6:EPSC- DPS2011-976).

Goldstein, R. M and Morris, G. A. (1973). Radar Observations of the rings of Saturn. Icarus 20, 250-252.

Goodman, J. W. (1976). Some fundamental properties of speckle." Journal of the Optical Society of America (1917-1983) 66, 1145-1150.

Graniczny, M., Kowalski, Z., Czarongorska, M., Reczka, J., Pivtkowska, A. (2006). Potential of SAR Interferometery for identification of ground motions., in Abstracts Living Morphotectonic of the European Lowland. 28–30 August 2006, Cedynia, Poland.

Grasset, O. and Sotin, C. (1996). The Cooling Rate of a Liquid Shell in Titan's Interior. Icarus 123, 101-112.

Grasset, O., Sotin, C., Deschamps, F. (2000). On the internal structure and dynamics of Titan. Planetary and Space Science 48, 617-636.

Grasset, O., Dougherty, M. K., Coustenis, A., Bunce, E. J., Erd, C., Titov, D., Blanc, M., Coates, A., Drossart, P., Fletcher, L. N., Hussman, H., Jaumann. R., Krupp, N., Lebreton, J.-P., Prieto-Ballesteros, O., Tortora, P., Tosi, F., Van Hoolst. T. (2013). JUpiter ICy moons Explorer (JUICE): An ESA mission to orbit Ganymede and to characterise the Jupiter system. Planetary and Space Science 78, 1-21.

Graves, S. D. B., McKay, C. P., Griffith, C. A., Ferri, F. and Fulchignoni, M. (2008). Rain and hail can reach the surface of Titan. Planetary and Space Science 56, 346-357.

Gray, D. F. (1992). Observation & Analysis of Stellar Photospheres. Cambridge University Press.

Greeley, R., Klemaszewski, J. E., Wagner, R. (2000). Galileo views of the geology of Callisto. Planetary and Space Science 48, 829-853.

Greenberg, R. (2010). Transport Rates of Radiolytic Substances into Europa's Ocean: Implications for the Potential Origin and Maintenance of Life. Astrobiology 10, 275-283.
Greenberg, R., Geissler, P., Hoppa, G., Tufts, B. R., Durda, D. D., Pappalardo, R., Head, J. W., Greeley, R., Sullivan, R., Carr, M. H. (1998). Tectonic Processes on Europa: Tidal Stresses, Mechanical Response, and Visible Features. Icarus 135, 64-78.
Griffith, C. A., Owen, T., Wagener, R. (1991). Titan's surface and troposphere, investigated with ground-based, near-infrared observations. Icarus 93, 362-378.
Griffith, C. A. (1993). Evidence for surface heterogeneity on Titan. Nature 364, 511-513.
Griffith, C. A. and Zahnle, K. (1995). Influx of cometary volatiles to planetary moons: The atmospheres of 1000 possible Titans. Journal of Geophysical Research 100, 16907-16922.
Griffith, C. A., Owen, T., Geballe, T. R., Rayner, J. and Rannou, P. (2003). Evidence for the Exposure of Water Ice on Titan's Surface. Science 300, 628-630.
Griffith, C. A., Owen, T., Geballe, T. R., Rayner, J., Rannou, P. (2003). Evidence for the Exposure of Water Ice on Titan's Surface. Science 300, 628-630.
Griffith, C. A., Doose, L., Tomasko, M. G., Penteado, P. F., See, C. (2012). Radiative transfer analyses of Titan's tropical atmosphere. Icarus 218, 975–988.
Grossman, L. and Larimer. W. (2010). Early chemical history of the solar system 12, 71-101.
Guillot, T., Atreya, S., Charnoz, S., Dougherty, M.K., Read, P. (2009). Saturn's Exploration Beyond Cassini-Huygens. In Dougherty, M.K., Esposito, L.W., Krimigis, S.:Saturn from Cassini-Huygens. Springer Science.
Gurnett, D. A., Kurth, W. S., Kirchner, D. L., Hospodarsky, G. B., Averkamp, T. F., Zarka, P., Lecacheux, A., Manning, R., Roux, A., Canu, P., Cornilleau-Wehrlin, N., Galopeau, P., Meyer, A., BostrΓ¶m, R., Gustafsson, G., Wahlund, J. E., Γ…hlen, L., Rucker, H. O., Ladreiter, H. P., Macher, W., Woolliscroft, L. J. C., Alleyne, H., Kaiser, M. L., Desch, M. D., Farrell, W. M., Harvey, C. C., Louarn, P., Kellogg, P. J., Goetz, K. and Pedersen, A. (2004). The Cassini Radio and Plasma Wave Investigation. Space Science Reviews 114, 395-463.
Iess, L., Jacobson, R.A., Ducci, M., Stevenson, D.J., Lunine, J.I., Armstrong, J.W., Asmar, S.W., Racioppa, P., Rappaport, N.J., Tortora, P. (2012). The tides of Titan. Science, 337, 457.
Haff, P. K., Siscoe, G. L., Eviatar, A. (1983). Ring and plasma - The enigmae of Enceladus. Icarus 56, 426-438.
Hall, D.K. and Martinec, J. (1985), Remote sensing of ice and snow. Chapman and Hall, New York, 189 pp.
Hall, D. T., Strobel, D. F., Feldman, P. D., McGrath, M. A. and Weaver, H. A. (1995). Detection of an oxygen atmosphere on Jupiter's moon Europa. Nature 373, 677-679.
Hall, J., L., Lunine, J., Sotin, C., Reh, K., Vargas, A. and Couzin, P. (2011). Titan Aerial Explorer (TAE): Exploring Titan By Balloon. Interplanetary Probe Workshop 8, Portsmouth, VA.
Han, L., Tobie, G., Showman, A.P. (2012). The impact of a weak south pole on thermal convection in Enceladus' ice shell. Icarus 218, 320–30.
Hanel, R., Conrath, B., Flasar, F. M., Kunde, V., Maguire, W., Pearl, J. C., Pirraglia, J., Samuelson, R., Herath, L., Allison, M., Cruikshank, D. P., Gautier, D., Gjerasch, P. J., Horn, L., Koppany, R., Ponnamperuma, C. (1981). Infrared observations of the Saturnian system from Voyager 1. Science 212, 192-200.
Hanel, R., Conrath, B. J., Jennings. D. E., Samuelson, R. E. (2003). Exploration of the Solar System by infrared remote sensing. Cambridge University Press.
Hansen, C. J., Esposito, L., Stewart, A. I. F., Colwell, J., Hendrix, A., Pryor, W., Shemansky, D., West, R. (2006). Enceladus' Water Vapor Plume. Science 311, 1422-1425.
Hayes, A., Aharonson, O., Callahan, P., Elachi, C., Gim, Y., Kirk, R., Lewis, K., Lopes, R., Lorenz, R., Lunine, J., Mitchell, K., Mitri, G., Stofan, E. and Wall, S. (2008). Hydrocarbon lakes on Titan: Distribution and interaction with a porous regolith. Geophysical Research Letters 35, E09204.
Hayes, A., Aharonson, O., Lunine, J., Wolf, A., Wye, L., Zebker, H., Lorenz, R., Turtle, E., Kirk, R., Wall, S. and Elachi, C. (2010). Cassini RADAR Observations of the Nature and Seasonal Varibility of Titan's Lakes. 38th COSPAR Scientific Assembly (18-15 July), Bremen, Germany.
Hayes, A. G., Aharonson, O., Lunine, J. I., Kirk, R. L., Zebker, H. A., Wye, L. C., Lorenz, R. D., Turtle, E. P., Paillou, P., Mitri, G., Wall, S. D., Stofan, E. R., Mitchell, K. L. and Elachi, C. (2011). Transient Surface Liquid in Titan's Polar Regions from Cassini. Icarus 211, 655-671.
Hayes, A. G., Lorenz, R. D., Donelan, M. A., Manga, M., Lunine, J. I., Schneider, T., Lamb, M. P., Mitchell, J. M., Fischer, W. W., Graves, S. D., Tolman, H. L., Aharonson, O., Encrenaz, P. J., Ventura, B., Casarano, D., Notarnicola, C. (2013). Wind driven capillary-gravity waves on Titan's lakes: Hard to detect or non-existent? Icarus 225, 403-412.
Hawkesworth, C., Turner, S., Gallagher, K., Hunter, A., Bradshaw, T., Rogers, N. (1995). Calc-alkaline magmatism, lithospheric thinning and extension in the Basin and Range. Journal of Geophysical Research 100, 10271-10286.

Head, J. W., Pappalardo, R., Collins, G., Belton, M., Giese, B., Wagner, R., Breneman, H., Spaun, N., Nixon, B., Neukum, G., Moore, J. (2002). Evidence for Europa-like tectonic resurfacing styles on Ganymede. Geophys. Res. Lett., 29, 2151.

Hedman, M. M., Gosmeyer, C. M., Nicholson, P. D., Sotin, C., Brown, R. H., Clark, R. N., Baines, K. H., Buratti, B. J., Showalter, M. R. (2013). An observed correlation between plume activity and tidal stresses on Enceladus. Nature 500, 182-184.

Helfenstein, P., Thomas, P., Veverka, J., Porco, C., Giese, B., Wagner, R., Roatsch, T., Denk, Tillmann, Neukum, G. (2006). Surface Geology and Tectonism on Enceladus. American Geophysical Union, P22B-02.

Henry, C. A. (2002). An Introduction to the Design of the Cassini Spacecraft. Space Science Reviews 104, 129-153.

Herschel, W. (1795) Description of a Forty-feet Reflecting Telescope, Philosophical Transactions of the Royal Society of London 85, 347–409.

Hess, H.H. (1965). Mid-oceanic ridges and tectonics of the sea floor, in Whit- tard, W.F., and Bradshaw, R., eds.. Submarine Geology and Geophysics, 317-344.

Hirtzig, M., Bézard, B., Lellouch, E., Coustenis, A., de Bergh, C., Drossart, P., Campargue, A., Boudon, V., Tyuterev, V., Rannou, P., Cours, T., Kassi, S., Nikitin, A., Mondelain, D., Rodriguez, S., Le Mouélic, S. (2013). Titan's surface and atmosphere from Cassini/VIMS data with updated methane opacity. Icarus 226, 470-486.

Hoffman, K.M. and Kunze, R. (1971). Linear Algebra. Pearson publisher.

Howard, M., Goldman, N., Vitello, P. A. (2006). Comet Impacts as a Source of Methane on Titan. American Astronomical Society, DPS meeting #38, #27.32; Bulletin of the American Astronomical Society 38, 1296.

Howett, C.J.A., Spencer, J.R., Pearl, J., Segura, M. (2010). Thermal inertia and bolometric Bond albedo values for Mimas, Enceladus, Tethys, Dione, Rhea and Iapetus as derived from Cassini/CIRS measurements. Icarus 206, 573–93.

Howett, C.J.A., Spencer, J.R., Pearl, J., Segura, M. (2011). High heat flow from Enceladus' south polar region measured using 10–600 cm−1 Cassini/CIRS data. J. Geophys. Res. 116, E03003.

Huang, S.-S. (1959). Occurrence of Life in the Universe. American Scientist 47, 397-402.

Hubbard, W. B. and Marley, M. S (1989). Optimized Saturn, Jupiter and Uranus interior models. Icarus 78, 102–118.

Hueso, R. and Sanchez-Lavega, A. (2006). Methane storms on Saturn's moon Titan. Nature 442, 428-431.

Hunten, D. M. (1977). Titan's atmosphere and surface. IAU Colloq. 28, Planetary satellites, Tucson, University of Arizona Press.

Huntoon, P. W. (1990). Phanerozoic structural geology of the Grand Canyon, in Beus, S. S. University Press, 261-309.

Hurford, T.A., Helfenstein, P., Hoppa, G.V., Greenberg, R., Bills, B.G. (2007). Eruptions arising from tidally controlled periodic openings of rifts on Enceladus. Nature 447, 292-294.

Hurford, T. A., Bills, B. G., Helfenstein, P., Greenberg, R., Hoppa, G. V., Hamilton, D. P. (2009). Geological implications of a physical libration on Enceladus. Icarus 203, 541-552.

Hussmann, H., Sohl, F., Oberst, J. (2011), Measuring tidal de- formations at Europa's surface, Adv. Space Res., 48, 718–724.

Iess, L., Rappaport, N. J., Jacobson, R. A., Racioppa, P., Stevenson, D. J., Tortora, P., Armstrong, J. W., Asmar, S. W. (2010). Gravity Field, Shape, and Moment of Inertia of Titan. Science 327, 1367.

Iess, L., Jacobson, R.A., Ducci, M., Stevenson, D.J., Lunine, J.I., Armstrong, J.W., Asmar, S.W., Racioppa, P., Rappaport, N.J., Tortora, P. (2012). The tides of Titan. Science, 337, 457.

Imura, R. (1992). Eruptive history of the Kirishima volcano during the past 22,000 years. Geogr. Rep. Tokyo Metropl. Univ. 27, 73-91.

Ingersoll, A.P. and Ewald, S.P. (2011). Total particulate mass in Enceladus plumes and mass of Saturn's E ring inferred from Cassini ISS images. Icarus 216, 492–506.

Ingersoll, A.P. and Porco, C.C. (1978). Solar Heating and Internal Heat Flow on Jupiter. Icarus 35, 27–43.

Irwin, P. G. J., Sromovsky, L. A., Strong, E. K., Sihra, K., Teanby, N. A., Bowles, N., Calcutt, S. B., Remedios, J. J. (2006). Improved near-infrared methane band models and k-distribution parameters from 2000 to 9500 cm -1 and implications for interpretation of outer planet spectra. Icarus 181, 309-319.

Israel, G., Cabane, M., Brun, J. F., Niemann, H., Way, S., Riedler, W., Steller, M., Raulin, F. and Coscia, D. (2002). Huygens Probe Aerosol Collector Pyrolyser Experiment. Space Science Reviews 104, 433-468.

Israel, G., Szopa, C., Raulin, F., Cabane, M., Niemann, H. B., Atreya, S. K., Bauer, S. J., Brun, J. F., Chassefire, E., Coll, P., Cond, E., Coscia, D., Hauchecorne, A., Millian, P., Nguyen, M. J., Owen, T., Riedler, W., Samuelson, R. E., Siguier, J. M., Steller, M., Sternberg, R. and Vidal-Madjar, C. (2005). Complex organic matter in Titan's atmospheric aerosols from in situ pyrolysis and analysis. Nature 438, 796-799.

Jacquemart, D., E. Lellouch, B. Bézard, C. de Bergh, C. Coustenis, A. Lacome, B. Schmitt, and M. G. Tomasko (2008). New laboratory measurements of CH4 in Titan's conditions and a reanalysis of the DISR near-surface spectra at the Huygens landing site. Planet. Space Sci. 56, 613-623.

Jara-Orue, H. M. and Vermeersen, B. L. A. (2011), Effects of low-viscous layers and a non-zero obliquity on surface stresses induced by diurnal tides and non-synchronous rotation: The case of Europa, Icarus 215, 417–438.

Jaumann, R.; Stephan, K.; Brown, R. H.; Buratti, B. J.; Clark, R. N.; McCord, T. B.; Coradini, A.; Capaccioni, F.; Filacchione, G.; Cerroni, P.; Baines, K. H.; Bellucci, G.; Bibring, J.-P.; Combes, M.; Cruikshank, D. P.; Drossart, P.; Formisano, V.; Langevin, Y.; Matson, D. L.; Nelson, R. M.; Nicholson, P. D.; Sicardy, B.; Sotin, C.; Soderbloom, L. A.; Griffith, C.; Matz, K.-D.; Roatsch, Th.; Scholten, F.; Porco, C. C. (2006). High-resolution CASSINI-VIMS mosaics of Titan and the icy Saturnian satellites. Planetary and Space Science 54, 1146-1155.

Jaumann, R., Brown, R. H., Stephan, K., Barnes, J. W., Soderblom, L. A., Sotin, C., Le Mouelic, S., Clark, R. N., Soderblom, J., Buratti, B. J., Wagner, R., McCord, T. B., Rodriguez, S., Baines, K. H., Cruikshank, D. P., Nicholson, P. D., Griffith, C. A., Langhans, M. and Lorenz, R. D. (2008). Fluvial erosion and post-erosional processes on Titan. Icarus 197, 526-538.

Jaumann, R., Kirk, R., Lorenz, R., Lopes, R., E. Stofan, Uwe Keller, H., Wood, C., Turtle, E., Sotin, C., Soderblom, L.A., Tomasko, M. (2009). Geology and Surface Processes on Titan. In: Titan after Cassini-Huygens. Springer Netherlands 75-140.

Jeans, J. (1925). The dynamical theory of gases, republished by Dover Publisher 1954.

Johnson, T.V. (2004). Geology of the icy satellites. Space Science Reviews 116, 401-420.

Jolliffe, I. T. (1986). Principal Component Analysis, Springer-Verlag, New York.

Jolliffe, I. T. (2002). Principal Component Analysis, second edition, Springer-Verlag, New York.

Jolliffe, I. T. (2005). Principal Component Analysis. Encyclopedia of Statistics in Behavioral Science.

Jones, T. D. and Lewis, J. S. (1987). Estimated impact shock production of N2 and organic compounds on early Titan. Icarus 72, 381-393.

Joreskog, K. G., Klovan, J. E., Reyment, R. A. (1976). Geological factor analysis. Elsevier, Amsterdam, 178.

Jurac, S.; Johnson, R. E.; Richardson, J. D. (2001). Saturn's E Ring and Production of the Neutral Torus. Icarus 149, 384-396.

Kargel, J.S. (1994). Cryovolcanism on the icy satellites. Earth Moon Plan. 67, 101-113.

Kargel, J. S. and Pozio, S. (1996). The Volcanic and Tectonic History of Enceladus. Icarus 119, 385-404.

Kargel, J. S., Croft, S. K., Lunine, J. I., Lewis, J. S. (1991). Rheological properties of ammonia-water liquids and crystal-liquid slurries - Planetological applications. Icarus 89, 93-112.

Kargel, J. S. (2006). Enceladus: Cosmic Gymnast, Volatile Miniworld. Science 311, 1389-1391.

Karkoschka, E. (1998). Methane, Ammonia, and Temperature Measurements of the Jovian Planets and Titan from CCD-Spectrophotometry. Icarus 133, 134-146.

Karkoschka, E. and Tomasko, M.G. (2010). Methane absorption coefficients for the jovian planets from laboratory, Huygens, and HST data. Icarus 205, 674-694.

Kasting, J. F. (1988). Runaway and moist greenhouse atmospheres and the evolution of earth and Venus. Icarus 74, 472-494.

Kattenhorn, S.A. and Patthoff, D.A. (2009). A History of Old Tiger Stripe Fracture Sets in the South-Polar Region of Enceladus. American Astronomical Society 41, 38.11.

Kempf, S., Beckmann, U., Schmidt, J. (2010). How the Enceladus dust plume feeds Saturn's E ring. Icarus 206, 446–57.

Kennett, J. P., Cannariato, K. G., Hendy, I. L., Behl, R. J. (2003). Methane Hydrates in Quaternary Climate Change: the Clathrate Gun Hypothesis, American Geophysical Union.

Khare, B. N., Thompson, W. R., Cheng, L., Chyba, C., Sagan, C., Arakawa, E. T., Meisse, C., Tuminello, P. S. (1993). Production and optical constraints of ice tholin from charged particle irradiation of (1:6) C2H6/H2O at 77 K. Icarus 103, 290-300.

Khurana, K. K., Kivelson, M. G., Stevenson, D. J., Schubert, G., Russell, C. T., Walker, R. J., Polanskey, C. (1998). Induced magnetic fields as evidence for subsurface oceans in Europa and Callisto. Nature 395, 777-780.

Kieffer, S. W., Lu, X., Bethke, C. M., Spencer, J. R., Marshak, S., Navrotsky, A. (2006). A Clathrate Reservoir Hypothesis for Enceladus' South Polar Plume. Science 314, 1764-1764.

Kim, S. J., Trafton, L. M., Geballe, T. R. (2008). No Evidence of Morning or Large-Scale Drizzle on Titan. The Astrophysical Journal 679, L53-L56.

Kirchoff, M.R., Schenk, P. (2009). Crater modification and geologic activity in Enceladus' heavily cratered plains: evidence from the impact crater distribution. Icarus 202, 656–68.

Kious, J.W. and Tilling, R.I. (1996). This Dynamic Earth: The Story of Plate Tectonics. USGS General Interest Publication.

Kirk, R. L., Howington-Kraus, E., Stiles, B., Hensley, S., Cassini RADAR Team (2008). Digital Topographic Models of Titan Produced by Radargrammetry with a Rigorous Sensor Model. 39th Lunar and Planetary Science Conference, (Lunar and Planetary Science XXXIX). LPI Contribution 1391, 2320.

Kirk, R. L., Howington-Kraus, E., Redding, B. L., Becker, T. L., Lee, E. M., Stiles, B. W., Hensley, S., Cassini RADAR Team (2009). Three-Dimensional views of Titan. EGU General Assembly 2009, 10296.

Kirk, R. L., Howington-Kraus, E., Barnes, J. W., Hayes, A. G., Lopes, R. M., Lorenz, R. D., Lunine, J. I., Mitchell, K. L., Stofan, E. R., Wall, S. D. (2010). La Sotra y las otras: Topographic evidence for (and against) cryovolcanism on Titan. American Geophysical Union, Fall Meeting 2010, abstract #P22A-03.

Kivelson, M. G., Khurana, K. K., Russell, C. T., Volwerk, M., Walker, R. J., Zimmer, C. (2000). Galileo Magnetometer Measurements: A Stronger Case for a Subsurface Ocean at Europa. Science 289, 1340-1343.

Kliore, A. J., Anderson, J. D., Armstrong, J. W., Asmar, S. W., Hamilton, C. L., Rappaport, N. J., Wahlquist, H. D., Ambrosini, R., Flasar, F. M., French, R. G., Iess, L., Marouf, E. A. and Nagy, A. F. (2004). Cassini Radio Science. Space Science Reviews 115, 1-70.

Knapmeyer, M., Akito, A., Bampasidis, G., Banerdt, W. B., Coustenis, A., Fouch, M. J., Garnero, E. J., Khavroshkin, O., Kobayashi, N., Moussas, X., Pike, W. T., Seidensticker, K. J., Solomonidou, A., Yu, H. and Zakharov, A. (2012). Planetary Seismometers: An Overview. EGU 2012, Vienna, Austria.

Korycansky, D.G, Bodenheimer, P. and Pollack, J.B. (1991). Numerical models of giant planet formation with rotation. Icarus 92, 234-251.

Kress, M. E. and McKay, C. P. (2004). Formation of methane in comet impacts: implications for Earth, Mars, and Titan. Icarus 168, 475-483.

Krimigis, S. M., Mitchell, D. G., Hamilton, D. C., Livi, S., Dandouras, J., Jaskulek, S., Armstrong, T. P., Boldt, J. D., Cheng, A. F., Gloeckler, G., Hayes, J. R., Hsieh, K. C., Ip, W. H., Keath, E. P., Kirsch, E., Krupp, N., Lanzerotti, L. J., Lundgren, R., Mauk, B. H., McEntire, R. W., Roelof, E. C., Schlemm, C. E., Tossman, B. E., Wilken, B. and Williams, D. J. (2004). Magnetosphere Imaging Instrument (MIMI) on the Cassini Mission to Saturn/Titan. Space Science Reviews 114, 233-329.

Krimigis, S. M., Mitchell, D. G., Hamilton, D. C., Krupp, N., Livi, S., Roelof, E. C., Dandouras, J., Armstrong, T. P., Mauk, B. H., Paranicas, C., Brandt, P. C., Bolton, S., Cheng, A. F., Choo, T., Gloeckler, G., Hayes, J., Hsieh, K. C., Ip, W. H., Jaskulek, S., Keath, E. P., Kirsch, E., Kusterer, M., Lagg, A., Lanzerotti, L. J., LaVallee, D., Manweiler, J., McEntire, R. W., Rasmuss, W., Saur, J., Turner, F. S., Williams, D. J. and Woch, J. (2005). Dynamics of Saturn's Magnetosphere from MIMI During Cassini's Orbital Insertion. Science 307, 1270-1273.

Kunde, V. G., Aikin, A. C., Hanel, R. A., Jennings, D. E., Maguire, W. C., Samuelson, R .E (1981). "C4H2, HC3N and C2N2 in Titan's atmosphere." Nature 292: 686-688.

Kuiper, G. P. (1957). Infrared observations of planets and satellites. The Astronomical Journal 62, 245-245.

Kuskov, O. L. and Kronrod, V. A. (2005). Internal structure of Europa and Callisto. Icarus 177, 550-569.

Lammer, H., Bredehoft, J., Coustenis, A., Khodachenko, M., Kaltenegger, L., Grasset, O., Prieur, D., Raulin, F., Ehrenfreund, P., Yamauchi, M., Wahlund, J. E., Grießmeier, J. M., Stangl, G., Cockell, C., Kulikov, Y., Grenfell, J. and Rauer, H. (2009). What makes a planet habitable? Astronomy and Astrophysics Review 17, 181-249.

Lancaster, N. (2006). Linear dunes on Titan. Science 312, 702-703.

Langhans, M. H., Jaumann, R., Stephan, K., Brown, R. H., Buratti, B. J., Clark, R. N., Baines, K. H., Nicholson, P. D., Lorenz, R. D., Soderblom, L. A., Soderblom, J. M., Sotin, C., Barnes, J. W., Nelson, R. (2012). Titan's fluvial valleys: Morphology, distribution, and spectral properties. Planetary and Space Science 60, 34-51.

Lange, C., Sohl, F., Coustenis, A., Jaumann, R., Karatekin, O., Schmitz, N., Solomonidou, A., Wagenbach, S., Rosta, R. and van Zoest, T. (2011). Concept Study for a Titan Geophysical Network. EGU, Vienna, Austria.

Lavvas, P. P., Coustenis, A. and Vardavas, I. M. (2008). Coupling photochemistry with haze formation in Titan's atmosphere, Part I: Model description. Planetary and Space Science 56, 27-66.

Leary, J., Strain, R., Lorenz, R. and Waite, J. H. (2008). Titan explorer flagship mission study, Public Report. http://www.lpi.usra.edu/opag/Titan_Explorer_Public_Report.pdf.

Lebreton, J.-P., Witasse, O., Sollazzo, C., Blancquaert, T., Couzin, P., Schipper, A.-M., Jones, J. B., Matson, D. L., Gurvits, L. I., Atkinson, D. H., Kazeminejad, B., Perez-Ayucar, M. (2005). An overview of the descent and landing of the Huygens probe on Titan. Nature 438m 758-764.

Lebreton, J.-P., Coustenis, A., Lunine, J., Raulin, F., Owen, T. and Strobel, D. (2009). Results from the Huygens probe on Titan. Astronomy and Astrophysics Review 17, 149-179.

Le Corre, L., Le Mouélic, S., Sotin, C., Combe, J.-P., Rodriguez, S., Barnes, J. W., Brown, R. H., Buratti, B. J., Jaumann, R., Soderblom, J., Soderblom, L. A., Clark, R., Baines, K. H., Nicholson, P. D. (2009). Analysis of a cryolava flow-like feature on Titan. Planetary and Space Science 57, 870-879.

Le Gall, A., Hayes, A. G., Ewing, R., Janssen, M. A., Radebaugh, J., Savage, C., Encrenaz, P., the Cassini Radar Team (2012). Latitudinal and altitudinal controls of Titan's dune field morphometry. Icarus 217, 231-242.

Lellouch, E., Coustenis, A., Sebag, B., Cuby, J. G., Lopez-Valverde, M., Schmitt, B., Fouchet, T. and Crovisier, J. (2003). Titan's 5-μm window: observations with the Very Large Telescope. Icarus 162, 125-142.

Lemmon, M. T., Karkoschka, E. and Tomasko, M. (1993). Titan's Rotation: Surface Feature Observed. Icarus 103, 329-332.

Lemmon, M. T., Karkoschka, E. and Tomasko, M. (1995). Titan's rotational light-curve. Icarus 113, 27-38.

Lemmon, M. T., Smith, P. H., Lorenz, R. D. (2002). Methane Abundance on Titan, Measured by the Space Telescope Imaging Spectrograph. Icarus 160, 375-385.

Le Mouélic, S., Rannou, P., Rodriguez, S., Sotin, C., Griffith, C. A., Le Corre, L., Barnes, J. W., Brown, R.H., Baines, K. H., Buratti, B. J., Clark, R. N., Nicholson, P. D., Tobie, G. (2012). Dissipation of Titan's north polar cloud at northern spring equinox. Planetary and Space Science 60, 86-92.

Lewis, J. S. (1971). Satellites of the Outer Planets: Their Physical and Chemical Nature. Icarus 15, 174-174.

Lewis, J. S. (1971). Metal/silicate fractionation in the Solar System. Earth Planet. Sci. Lett., 15, 286-290 .

Lidmar-Bergström, K. (1996). Long-term morphotectonic evolution in Sweden. Geomorphology 16, 33-59.

Lindal, G. F., G. E. Wood, Hotz, H. B., Sweetnam, D. N., Eshleman, V. R., Tyler, G. L. (1983). The atmosphere of Titan: An analysis of the Voyager 1 radio occultation measurements. Icarus 53, 348-363.

Litwin, K. L., Zygielbaum, B. R., Polito, P. J., Sklar, L. S.; Collins, G. C. (2012). Influence of temperature, composition, and grain size on the tensile failure of water ice: Implications for erosion on Titan. Journal of Geophysical Research 117, E08013.

Lopes, R. M. C., K. L. Mitchell, E. R. Stofan, J. I. Lunine, R. Lorenz, F. Paganelli, R. L. Kirk, C. A. Wood, S. D. Wall, L. E. Robshaw, A. D. Fortes, C. D. Neish, J. Radebaugh, E. Reffet, S. J. Ostro, C. Elachi, M. D. Allison, Y. Anderson, R. Boehmer, G. Boubin, P. Callahan, P. Encrenaz, E. Flamini, G. Francescetti, Y. Gim, G. Hamilton, S. Hensley, M.A. Janssen, W. T. K. Johnson, K. Kelleher, D. O. Muhleman, G. Ori, R. Orosei, G. Picardi, F. Posa, L. E. Roth, R. Seu, S. Shaffer, L. A. Soderblom, B. Stiles, S. Vetrella, R. D. West, L. Wye, and H. A. Zebker (2007). Cryovolcanic features on Titan's surface as revealed by the Cassini Titan Radar Mapper. Icarus 186, 395–412.

Lopes, R. M. C., E. R. Stofan, R. Peckyno, J. Radebaugh, K. L. Mitchell, G. Mitri, C. A. Wood, R. L. Kirk, S. D. Wall, J. I. Lunine, A. Hayes, R. Lorenz, T. Farr, L. Wye, J. Craig, R. J. Ollerenshaw, M. Janssen, A. LeGall, and the Cassini RADAR Team (2010). Distribution and interplay of geologic processes on Titan from Cassini radar data. Icarus 205, 540-558.

Lopes, R. M. C., R. L. Kirk, K. L. Mitchell, A. LeGall, J. W. Barnes, A. Hayes, J. Kargel, L. Wye, J. Radebaugh, E. R. Stofan, M. Janssen, C. Neish, S. Wall, C.A. Wood, J. I. Lunine, and M. Malaska (2013). Cryovolcanism on Titan: New results from Cassini RADAR and VIMS. J. of Geophys. Res. 118, 416-435.

Lorenz, R. D. (1993). The life, death and afterlife of a raindrop on Titan. Planetary and Space Science 41, 647-655.

Lorenz, R. D. and Mitton, J. (2002). Lifting Titan's Veil: Exploring the Giant Moon of Saturn, Cambridge University Press.

Lorenz, R. D. and Radebaugh, J. (2009). Global pattern of Titan's dunes: Radar survey from the Cassini prime mission. Geophysical research Letters 36, L03202.

Lorenz, R. D., Wall, S., Radebaugh, J., Boubin, G., Reffet, E., Janssen, M., Stofan, E., Lopes, R., Kirk, R., Elachi, C., Lunine, J., Mitchell, K., Paganelli, F., Soderblom, L., Wood, C., Wye, L., Zebker, H., Anderson, Y., Ostro, S., Allison, M., Boehmer, R., Callahan, P., Encrenaz, P., Ori, G. G., Francescetti, G., Gim, Y., Hamilton, G., Hensley, S., Johnson, W., Kelleher, K., Muhleman, D., Picardi, G., Posa, F., Roth, L., Seu, R., Shaffer, S., Stiles, B., Vetrella, S., Flamini, E. and West, R. (2006a). The Sand Seas of Titan: Cassini RADAR Observations of Longitudinal Dunes. Science 312, 724-727.

Lorenz, R. D., Niemann, H. B., Harpold, D. N., Way, S. H. and Zarnecki, J. C. (2006b). Titan's damp ground: Constraints on Titan surface thermal properties from the temperature evolution of the Huygens GCMS inlet. Meteoritics and Planetary Science 41, 1705-1714.

Lorenz, R. D., Wood, C. A., Lunine, J. I., Wall, S. D., Lopes, R. M., Mitchell, K. L., Paganelli, F., Anderson, Y. Z., Wye, L., Tsai, C., Zebker, H. and Stofan, E. R. (2007). Titan's young surface: Initial impact crater survey by Cassini RADAR and model comparison. Geophysical Research Letters 34, 07204-07204.

Lorenz, R. D., Lopes, R. M., Paganelli, F., Lunine, J. I., Kirk, R. L., Mitchell, K. L., Soderblom, L. A., Stofan, E. R., Ori, G., Myers, M., Miyamoto, H., Radebaugh, J., Stiles, B., Wall, S. D., Wood, C. A. and Team, t. C. R. (2008). Fluvial channels on Titan: Initial Cassini radar observations. Planetary and Space Science 56, 1132-1144.

Lorenz, R. D., Stofan, E. R., Lunine, J. I., Kirk, R. L., Mahaffy, P. R., Bierhaus, B., Aharonson, O., Clark, B. C., Kantsiper, B., Ravine, M. A., Waite, J. H., Harri, A., Griffith, C. A. and Trainer, M. G. (2009). "Titan Mare Explorer (TiME): A Discovery Mission to Titan's Hydrocarbon Lakes." AGU Fall Meeting Abstracts 51: 1199-1199.

Lorenz, R. D., Turtle, E. P., Stiles, B., Le Gall, A., Hayes, A., Aharonson, O., Wood, C. A., Stofan, E., Kirk, R. (2011). Hypsometry of Titan. Icarus 211, 699-706.

Lorenz, R.D., Stiles, B.W., Aharonson, O., Lucas, A., Hayes, A.G., Kirk, R.L., Zebker, H.A., Turtle, E.P., Neish, C.D., Stofan, E.R., Barnes, J.W. (2013). A global topographic map of Titan. Icarus 225, 367-377.

Lunine, J.L., Atreya, S.K., 2008. The methane cycle on Titan. Nature Geoscience 1, 159-164.

Lunine, J. I., Stevenson D. J., Yung. Y. L. (1983). Ethane ocean on Titan. Science 222, 1229-1230.

Lunine, J. I., Yung, Y. L., Lorenz, R. D. (1999). On the volatile inventory of Titan from isotopic abundances in nitrogen and methane. Planetary and Space Science 47, 1291-1303.

Lunine, J. I., Elachi, C., Wall, S. D., Janssen, M. A., Allison, M. D., Anderson, Y., Boehmer, R., Callahan, P., Encrenaz, P., Flamini, E., Franceschetti, G., Gim, Y., Hamilton, G., Hensley, S., Johnson, W. T. K., Kelleher, K., Kirk, R. L., Lopes, R. M., Lorenz, R., Muhleman, D. O., Orosei, R., Ostro, S. J., Paganelli, F., Paillou, P., Picardi, G., Posa, F., Radebaugh, J., Roth, L. E., Seu, R., Shaffer, S., Soderblom, L. A., Stiles, B., Stofan, E. R., Vetrella, S., West, R., Wood, C. A., Wye, L., Zebker, H., Alberti, G., Karkoschka, E., Rizk, B., McFarlane, E., See, C., Kazeminejad, B. (2008). Titan's diverse landscapes as evidenced by Cassini RADAR's third and fourth looks at Titan. Icarus 195, 415-433.

MacLachlan, J. (1997). Galileo Galilei: First Physicist by James MacLachlan. Oxford University Press.

Manga, M. and Wang, C. Y. (2007). Geophys. Res. Lett. 34, 7202.

Marcus, M. and Minc, H. (1988). Introduction to Linear Algebra. Courier Dover Publications.

Marion, G. M., Fritsen, C. H., Eicken, H. and Payne, M. C. (2003). The Search for Life on Europa: Limiting Environmental Factors, Potential Habitats, and Earth Analogues. Astrobiology 3, 785-811.

Matson, D. L., Castillo, J. C., Lunine, J. and Johnson, T. V. (2007). Enceladus' plume: Compositional evidence for a hot interior. Icarus 187, 569-573.

Matson, D.L., Castillo-Rogez, J.C., Davies, A.G., Johnson, T.V. (2012). Enceladus: a hypothesis for bringing both heat and chemicals to the surface. Icarus 221, 53–62.

McCord, T. B., G. B. Hansen, R. N. Clark, P. D. Martin, C. A. Hibbitts, F. P. Fanale, J. C. Granahan, M. Segura, D. L. Matson, T. V. Johnson, R. W. Carlson, W. D. Smythe, G. E. Danielson, and The NIMS Team (1998), Non-water-ice constituents in the surface material of the icy Galilean satellites from the Galileo near-infrared mapping spectrometer investigation, Journal of Geophysical Research-Planets 103, 8603-8626.

McCord, T. B., Hansen, G. B., Hibbitts, C. A. (2001). Hydrated Salt Minerals on Ganymede's Surface: Evidence of an Ocean Below. Science 292, 1523-1525.

McCord, T. B., Hansen, G. B., Buratti, B. J., Clark, R. N., Cruikshank, D. P., D'Aversa, E., Griffith, C. A., Baines, E. K. H., Brown, R. H., Dalle Ore, C. M., Filacchione, G., Formisano, V., Hibbitts, C. A., Jaumann, R., Lunine, J. I., Nelson, R. M., Sotin, C. and the Cassini, V. T. (2006). Composition of Titan's surface from Cassini VIMS. Planetary and Space Science 54, 1524-1539.

McCord, T. B., Hayne, P., Combe, J.-P., Hansen, G. B., Barnes, J. W., Rodriguez, S., Le Mouélic, S., Baines, E. K. H., Buratti, B. J., Sotin, C., Nicholson, P., Jaumann, R., Nelson, R. and The Cassini Vims, T. (2008). Titan's surface: Search for spectral diversity and composition using the Cassini VIMS investigation. Icarus 194, 212-242.

McDonald, K.C. (1982). MID-OCEAN RIDGES: Fine Scale Tectonic, Volcanic and Hydrothermal Processes Within the Plate Boundary Zone. Ann. Rev. Earth Planet. Sci. 10, 155.

McKay, C. P., Pollack, J. B. and Courtin, R. G. (1989). The thermal structure of Titan's atmosphere. Icarus 80, 23-53.

McKay, C.P., Pollack, J.B., Courtin, R. (1991). The greenhouse and antigreenhouse effects on Titan. Science 253, 1118-1121.
McKay, C. P., Porco Carolyn, C., Altheide, T., Davis, W. L. and Kral, T. A. (2008). The Possible Origin and Persistence of Life on Enceladus and Detection of Biomarkers in the Plume. Astrobiology 8; 909-919.
McKinnon, W.B. (1998). Geodynamics of icy satellites, in: Schmitt, B., et al. (Eds.), Solar System Ices. Kluwer, Dordrecht, Netherlands, 525–550.
Means, W.D. and Park, Y. (1994). New experimental approach to understanding igneous texture. Geology, 22, 324-326.
Meier, R., Smith, B. A., Owen, T. C. and Terrile, R. J. (2000). The surface of Titan from NICMOS observations with the Hubble Space Telescope. Icarus 145, 462-473.
Melosh, H.J., Nimmo, F. (2011). Long-term strength of icy Vs silicate planetary bodies. Abstract 2306. 42nd Lunar and Planetary Science Conference, The Woodlands, Texas.
Michaud, R.L., Pappalardo, R.T., Collins, G.C. (2008). Pit chains on Enceladus: A discussion of their origin. Lunar Planet. Sci. XXXIX. Abst. #1678.
Mihalas, D. (1978). Stellar Atmospheres. W.H Freeman publisher.
Miller, E. A.; Klein, G., Juergens, D. W., Mehaffey, K., Oseas, J. M., Garcia, R. A., Giandomenico, A., Irigoyen, R. E., Hickok, R., Rosing, D., Sobel, H. R., Bruce, C. F., Flamini, E., Devidi, R., Reininger, F. M., Dami, M., Soufflot, A., Langevin, Y., Huntzinger, G. (1996). The Visual and Infrared Mapping Spectrometer for Cassini. Proc. SPIE 2803, 206-220.
Mingalev I.V., Mingalev V.S., Mingalev O.V., Kazeminejad B., Lammer H., Biernat H.K., Lichtenegger H.I.M., Schwingenschuh K., Rucker H.O. (2006) First simulation results of Titan's atmosphere dynamics with a global 3-D non-hydrostatic circulation model. Ann. Geophys. 24, 1–5.
Mitchell, K. L. and Malaska, M. (2011). Karst on Titan. First International Planetary Caves Workshop: Implications for Astrobiology, Climate, Detection, and Exploration. LPI Contribution 1640, 18.
Mitri, G., Showman, A.P., Lunine, J.I., Lorenz, R.D. (2007). Hydrocarbon lakes on Titan. Icarus 186, 385-394.
Mitri, G., Showman, A.P., 2008. Thermal convection in ice-I shells of Titan and Enceladus. Icarus 193, 387-396.
Mitri, G., Showman, A.P., Lunine, J.I., Lopes, R.M.C (2008). Resurfacing of Titan by ammonia-water cryomagma. Icarus 196, 216–224.
Mitri, G., Showman, A.P., Lunine, J.I., Lopes, R.M.C. (2008). Resurfacing of Titan by ammonia-water cryomagma. Icarus 196, 216-224.
Mitri, G., M. T. Bland, A. P. Showman, J. Radebaugh, B. Stiles, R. M. C. Lopes, J. I. Lunine, and R. T. Pappalardo (2010). Mountains on Titan: Modeling and observations. J. Geophys. Res. 115, E10002.
Montgomery, D. R. and Brandon, M. T. (2002). Topographic controls on erosion rates in tectonically active mountain ranges. Earth and Planetary Science Letters 201, 481-489.
Montmerle, T., Augereau, J,-C., Chaussidon, M., Gounelle, M., Marty, B., Morbidelli, A. (2006). Solar System Formation and Early Evolution: the First 100 Million Years. Earth, Moon, and Planets 98, 39-95.
Moore, J. M., and Howard, A. D. (2010). Are the basins of Titan's Hotei Regio and Tui Regio sites of former low latitude seas? Geophys. Res. Lett. 37, L22205.
Moore, J. M., and Pappalardo, R. T. (2011). Titan: an exogenic world? Icarus 212, 790-806.
Moore, W. B. and Schubert, G. (2000). The Tidal Response of Europa. Icarus 147, 317-319.
Moore, W. B., Schubert, G., Tackley, P. (1998). Three-Dimensional Simulations of Plume-Lithosphere Interaction at the Hawaiian Swell. Science, 279, 1008-1011.
Morabito, L. A., Synnott, S. P., Kupferman, P. N., Collins, S. A. (1979). Discovery of currently active extraterrestrial volcanism. Science 204, 972.
Moussas, X., Bampasidis, G., Solomonidou, A. and colleagues (2010). The Antikythera Mechanism as an educational device. European Planetary Science Congress (EPSC). Rome, Italy.
Moussas, X., Coustenis, A., Solomonidou, A., Bampasidis, G., Bratsolis, E. and Stamogiorgos, S. (2012). The oldest computer in today's education: The great attractor of children to science, the Antikythera Mechanism, as an educational instrument. EGU General Assembly, 22-27 April, Vienna, Austria.
Mousis, O., Lunine, J.I., Pasek, M., Cordier, D., Hunter W.J., Mandt, K.E., Lewis, W.S., Nguyen, M (2009). A primordial origin for the atmospheric methane of Saturn’s moon Titan. Icarus 204, 749-751.
Muhleman, D. O., Grossman, A. W., Butler, B. J., Slade, M.A (1990). Radar reflectivity of Titan. Science 248, 975-980.
Mumma, M. J., DiSanti, M. A., Dello Russo, N., Magree-Sauer, K., Gibb, E., and Novak, R. (2003). Remote infrared observations of parent volatiles in comets: A window on the early solar system. Adv. Space Res., 31, 2563.
Muyzer, G. and Stams, A. J. M. (2008). The ecology and biotechnology of sulphate-reducing bacteria. Nature Reviews. Microbiology 6, 441-454.

Nagel, K., Breuer, D., Spohn, T. (2004). A model for the interior structure, evolution, and differentiation of Callisto. Icarus 169, 402-412.

Nakagawa, Y., Sekiya, M., Hayashi C. (1986). Settling and Growth of Dust Particles in a Laminar Phase of a Low-mass Solar Nebula. Icarus 67, 375-390.

Negrao, A., Coustenis, A., Lellouch, E., Maillard, J. P., Rannou, P., Schmitt, B., McKay, C. P. and Boudon, V. (2006). Titan's surface albedo variations over a Titan season from near-infrared CFHT/FTS spectra. Planetary and Space Science 54, 1225-1246.

Neish, C. D. and Lorenz, R. D. (2012). Titan's global crater population: A new assessment. Planetary and Space Science 60, 26-33.

Nelson, R. M., Brown, R. H., Hapke, B. W., Smythe, W. D., Kamp, L., Boryta, M. D., Leader, F., Baines, K. H., Bellucci, G., Bibring, J. P., Buratti, B. J., Capaccioni, F., Cerroni, P., Clark, R. N., Combes, M., Coradini, A., Cruikshank, D. P., Drossart, P., Formisano, V., Jaumann, R., Langevin, Y., Matson, D. L., McCord, T. B., Mennella, V., Nicholson, P. D., Sicardy, B., Sotin, C. (2006). Photometric properties of Titan's surface from Cassini VIMS: Relevance to titan's hemispherical albedo dichotomy and surface stability. Planetary and Space Science 54, 1540-1551.

Nelson, R. M., Kamp, L. W., Matson, D. L., Irwin, P. G. J., Baines, K. H., Boryta, M. D., Leader, F. E., Jaumann, R., Smythe, W. D., Sotin, C., Clark, R. N., Cruikshank, D. P., Drossart, P., Pearl, J. C., Hapke, B. W., Lunine, J., Combes, M., Bellucci, G., Bibring, J. P., Capaccioni, F., Cerroni, P., Coradini, A., Formisano, V., Filacchione, G., Langevin, R. Y., McCord, T. B., Mennella, V., Nicholson, P. D. and Sicardy, B. (2009a). Saturn's Titan: Surface change, ammonia, and implications for atmospheric and tectonic activity. Icarus 199, 429-441.

Nelson, R. M., Kamp, L. W., Lopes, R. M. C., Matson, D. L., Kirk, R. L., Hapke, B. W., Wall, S. D., Boryta, M. D., Leader, F. E., Smythe, W. D., Mitchell, K. L., Baines, K. H., Jaumann, R., Sotin, C., Clark, R. N., Cruikshank, D. P., Drossart, P., Lunine, J. I., Combes, M., Bellucci, G., Bibring, J.-P., Capaccioni, F., Cerroni, P., Coradini, A., Formisano, V., Filacchione, G., Langevin, Y., McCord, T. B., Mennella, V., Nicholson, P. D., Sicardy, B., Irwin, P. G. J. and Pearl, J. C. (2009b). Photometric changes on Saturn's Titan: Evidence for active cryovolcanism. Geophysical Research Letters 36, 04202-04202.

Ness, N. F., Acuna, M. H. and Behannon, K. W. (1982). The induced magnetosphere of Titan. Journal of Geophysical Research 87, 1369-1381.

Newman, S.F., Buratti, B.J., Brown, R.H., Jaumann, R., Bauer, J., Momary, T. 2008. Photometric and spectral analysis of the distribution of crystalline and amorphous ices on Enceladus as seen by Cassini. Icarus 193, 397–406.

Newman, S.F., Buratti, B.J., Jaumann, R., Bauer, J.M., Momary, T.W. 2007. Hydrogen peroxide on Enceladus. Astrophys. J. 670, L143–46.

Niemann, H. B., Atreya, S., Bauer, S.J., Biemann, K.; Block, B.; Carignan, G.; Donahue, T.; Frost, L.; Gautier, D.; Harpold, D.; Hunter, D., Israel, G., Lunine, J., Mauersberger, K., Owen, T., Raulin, F., Richards, J., Way, S. (1997). The Gas Chromatograph Mass Spectrometer Aboard Huygens. Huygens: Science, Payload and Mission, Proceedings of an ESA conference. Edited by A. Wilson, 85.

Niemann, H. B., Atreya, S. K., Bauer, S. J., Carignan, G. R., Demick, J. E., Frost, R. L., Gautier, D., Haberman, J. A., Harpold, D. N., Hunten, D. M., Israel, G., Lunine, J. I., Kasprzak, W. T., Owen, T. C., Paulkovich, M., Raulin, F., Raaen, E. and Way, S. H. (2005). The abundances of constituents of Titan's atmosphere from the GCMS instrument on the Huygens probe. Nature 438, 779-784.

Niemann, H. B., Atreya, S. K., Demick, J., Gautier, D., Haverman, J., Harpold, D., Kasprzak, W., Lunine, J., Owen, T., Raulin, F. (2010). Composition of Titan's lower atmosphere and simple surface volatiles as measured by the Cassini-Huygens probe gas chromatograph mass spectrometer experiment. J. Geophys. Res. 115, E12006.

Nikitin, A.V., Mikhailenko, S., Morino, I., Yokota, T., Kumazawa, R., Watanabe, T. (2009). Isotopic substitution shifts in methane and vibrational band assignment in the 5560–6200 cm-1 region. J. Quant. Spectrosc. Radiat. Trans. 110, 964–73.

Nikitin, A.V., Lyulin, O. M., Mikhailenko, S. N., Perevalov, V. I., Filippov, N. N., Grigoriev, I. M. et al., 2010. GOSAT-2009 methane spectral linelist in the 5550–6236 cm-1 range. J. Quant. Spectrosc. Radiat. Trans., 111, 2211-2224.

Nikitin, A.V., Thomas, X., Régalia, L., Daumont, L., Von der Heyden, P., Tyuterev, Vl. G., Wang, L., Kassi, S., Campargue, A., 2011. Assignment of the 5ν4 and ν2+4ν4 band systems of 12CH4 in the 6287-6550 cm-1 region. J. Quant. Spectrosc. Radiat. Trans. 112, 28-40.

Nikitin, A. V., Brown, L. R., Sung, K., Tyuterev, Vl. G., Smith M. A. H., Mantz, A. W. (2013). Preliminary modeling of CH3D from 4000 to 4550 cm-1. J. Quant. Spectrosc. Radiat. Trans. 114, 1-12.

Nimmo, F., Spencer, J. R., Pappalardo, R. T. and Mullen, M. E. (2007). Shear heating as the origin of the plumes and heat flux on Enceladus. Nature 447, 289-291.
Nimmo, F. and Bills, B. G. (2010). Shell thickness variations and the long-wavelength topography of Titan. Icarus 208, 896-904.
Nimmo, F., Bills, B. G., Thomas, P. C. (2011). Geophysical implications of the long-wavelength topography of the Saturnian satellites. Journal of Geophysical Research 116, E11001.
Oberbeck, V. R., Quaide, W. L., Arvidson, R. E., Aggarwal, H. R. (1977). Comparative studies of Lunar, Martian, and Mercurian craters and plains. Journal of Geophysical Research 82, 1681-1698.
O'Neill, C. and Nimmo, F. (2010). The role of episodic overturn in generating the surface geology and heat flow on Enceladus. Nat. Geosci. 3, 88–91.
Paganelli, F., Elachi, C., Lopes, R.M., Stofan, E., Wood, C.A., Janssen, M.A., Stiles, B., West, R., Roth, L., Wall, S.D., Lorenz, R.D., Lunine, J.I., Kirk, R.L., Soderblom, L., Cassini Radar Team (2005). Channels and fan-like features on Titan's surface imaged by the Cassini RADAR. Lunar Planet. Sci. 36. Abstract 2150.
Palomba, E., Zinzi, A., Cloutis, E.A., D'Amore, M., Grassi, D., Maturilli, A. (2009). Evidence for Mg-rich carbonates on Mars from a 3.9 μm absorption feature. Icarus 203, 58-65.
Pang, K. D., Voge, C. C., Rhoads, J. W., Ajello, J. M. (1984). The E ring of Saturn and satellite Enceladus. Journal of Geophysical Research 89, 9459-9470.
Pappalardo, R. T., Head, J. W., Collins, G. C., Kirk, R. L., Neukum, G., Oberst, J., Giese, B., Greeley, R., Chapman, C. R., Helfenstein, P., Moore, J. M., McEwen, A., Tufts, B. R., Senske, D. A., Breneman, H. H. and Klaasen, K. (1998). Grooved Terrain on Ganymede: First Results from Galileo High-Resolution Imaging. Icarus 135, 276-302.
Passey, Q. R. (1983). Viscosity of the lithosphere of Enceladus. Icarus 53, 105-120.
Perrillat, J.P., Daniel, I., Koga, K.T., Reynard, B., Cardon, H., Crichton, W.A. (2005). Kinetics of antigorite dehydration: A real-time X-ray diraction study. Earth Planet. Sci. Lett. 236, 899.
Perron, J. T., Lamb, M. P., Koven, C. D., Fung, I. Y., Yager, E., Adamkovics, M. (2006). Valley formation and methane precipitation rates on Titan. Journal of Geophysical Research 111, E11001.
Perron, J. T., Kirchner, J. W., Dietrich, W. E. (2009), Formation of evenly spaced ridges and valleys, Nature 460, 502–505.
Pike, R. J. and Spudis, P. D. (1987). Basin-ring spacing on the moon, Mercury, and Mars. Earth, Moon, and Planets 39, 129-194.
Pollack, J. B. (1973). Greenhouse Models of the Atmosphere of Titan. Icarus 19, 43-43.
Poirier, J. P., Boloh, L., Chambon, P. (1983). Tidal dissipation in small viscoelastic ice moons - The case of Enceladus. Icarus 55, 218-230.
Porco, C. C., West, R. A., Squyres, S., McEwen, A., Thomas, P., Murray, C. D., Delgenio, A., Ingersoll, A. P., Johnson, T. V., Neukum, G., Veverka, J., Dones, L., Brahic, A., Burns, J. A., Haemmerle, V., Knowles, B., Dawson, D., Roatsch, T., Beurle, K. and Owen, W. (2004). Cassini Imaging Science: Instrument Characteristics And Anticipated Scientific Investigations At Saturn. Space Science Reviews 115, 363-497.
Porco, C. C., Baker, E., Barbara, J., Beurle, K., Brahic, A., Burns, J. A., Charnoz, S., Cooper, N., Dawson, D. D., Del Genio, A. D., Denk, T., Dones, L., Dyudina, U., Evans, M. W., Fussner, S., Giese, B., Grazier, K., Helfenstein, P., Ingersoll, A. P., Jacobson, R. A., Johnson, T. V., McEwen, A., Murray, C. D., Neukum, G., Owen, W. M., Perry, J., Roatsch, T., Spitale, J., Squyres, S., Thomas, P., Tiscareno, M., Turtle, E. P., Vasavada, A. R., Veverka, J., Wagner, R. and West, R. (2005). Imaging of Titan from the Cassini spacecraft. Nature 434, 159-168.
Porco, C. C., Helfenstein, P., Thomas, P. C., Ingersoll, A. P., Wisdom, J., West, R., Neukum, G., Denk, T., Wagner, R., Roatsch, T., Kieffer, S., Turtle, E., McEwen, A., Johnson, T. V., Rathbun, J., Veverka, J., Wilson, D., Perry, J., Spitale, J., Brahic, A., Burns, J. A., Del Genio, A. D., Dones, L., Murray, C. D. and Squyres, S. (2006). Cassini Observes the Active South Pole of Enceladus. Science 311, 1393-1401.
Porco, C. (2008). The restless world of Enceladus. Scientific American 299, 26–35.
Postberg, F., Kempf, S., Schmidt, J., Brilliantov, N., Beinsen, A., Abel, B., Buck, U. and Srama, R. (2009). Sodium salts in E-ring ice grains from an ocean below the surface of Enceladus. Nature 459, 1098-1101.
Postberg, F., Schmidt, J., Hillier, J., Kempf, S. and Srama, R. (2011). A salt-water reservoir as the source of a compositionally stratified plume on Enceladus. Nature 474, 620-622.
Poulet, F., Cuzzi, J. N., Cruikshank, D.P., Roush, T., Dalle Ore, C.M. (2002). Comparison between the Shkuratov and Hapke Scattering Theories for Solid Planetary Surfaces: Application to the Surface Composition of Two Centaurs. Icarus 160, 313-324.

Prinn, R. G., Larson, H. P., Caldwell, J. J., and Gautier, D. (1984). Composition and Chemistry of Saturn's Atmosphere, in Gehrels, T., and Matthews, M. S. (eds.), Saturn, University of Arizona Press, Tucson, pp. 88–149.

Prockter, L. M., Lopes, R. M. C., Giese, b., Jaumann, R., Lorenz, R. D., Pappalardo, R. T., Patterson, G. W., Thomas, P. C., Turtle, E. P., Wagner, R. J. (2010). Characteristics of Icy Surfaces. Space Science Reviews 153, 63–111.

Pye, K. and Tsoar, H. (2009). Aeolian Sand and Sand Dunes. Springer.

Radebaugh, J., Lorenz, R.D., Kirk, R.L., Lunine, J.I., Stofan, E.R., Lopes, R.M.C., Wall, S.D., the Cassini Radar Team, (2007). Mountains on Titan observed by Cassini Radar. Icarus 192, 77-91.

Radebaugh, J., Lorenz, R.D., Lunine, J.I., Wall, S.D., Boubin, G., Reffet, E., Kirk, R.L., Lopes, R.M., Stofan, E.R., Soderblom, L., Allison, M., Janssen, M., Paillou, P., Callahan, P., Spencer, C. (2008). Dunes on Titan observed by Cassini Radar, Icarus 194, 690-703.

Radebaugh, J., Lorenz, R.D., Farr, T., Paillou, P., Savage, C., Spencer, C. (2009). Linear dunes on Titan and earth: Initial remote sensing comparisons. Geomorphology 121, 122-132.

Radebaugh, J., Lorenz, R. D., Wall, S. D., Kirk, R. L., Wood, C. A., Lunine, J. I., Stofan, E. R., Lopes, R. M. C., Valora, P., Farr, T. G., Hayes, A., Stiles, B., Mitri, G., Zebker, H., Janssen, M., Wye, L., Legall, A., Mitchell, K. L., Paganelli, F., West, R. D., Schaller, E. L. and Cassini, R. T. (2011). Regional geomorphology and history of Titan's Xanadu province. Icarus 211, 672-685.

Rannou, P., Montmessin, F., Hourdin, F., Lebonnois, S. (2006). The Latitudinal Distribution of Clouds on Titan. Science 311, 201-205.

Rannou, P., Cours, T., Le Mouelic, S., Rodriguez, S., Sotin, C., Drossart, P, Brown, R. (2010). Titan haze distribution and optical properties retrieved from recent observations. Icarus 208, 850-867.

Rannou, P., Le Mouélic, S., Sotin, C., Brown, R. H. (2012). Cloud and Haze in the Winter Polar Region of Titan Observed with Visual and Infrared Mapping Spectrometer on Board Cassini. The Astrophysical Journal, 748, 6.

Rappaport, N., Bertotti, B., Giampieri, G. and Anderson, J. D. (1997). Doppler Measurements of the Quadrupole Moments of Titan. Icarus 126, 313-323.

Rappaport, N. J., Iess, L., Tortora, P., Anabtawi, A., Asmar, S. W., Somenzi, L. and Zingoni, F. (2007). Mass and interior of Enceladus from Cassini data analysis. Icarus 190, 175-178.

Rathbun, J.A., Turtle, E.P., Helfenstein, P., Squyres, S.W., Thomas, P., Veverka, J., Denk, T., Neukum, G., Roatsch, T., Wagner, R., Perry, J., Smith, D., Johnson, T.V., Porco, C. (2005). Enceladus' global geology as seen by Cassini ISS. American Geophysical Union, P32A-03.

Raulin, F. (2007). Question 2: Why an Astrobiological Study of Titan Will Help Us Understand the Origin of Life. Origins of Life and Evolution of Biospheres 37, 345-349.

Raulin, F. (2008). Astrobiology and habitability of Titan. Space Science Reviews 135, 37-48.

Raulin, F. and Owen, T. (2002). Organic Chemistry and Exobiology on Titan. Space Science Reviews 104, 377-394.

Raulin, F., Frere, C., Do, L., Khlifi, M., Paillous, P. and de Vanssay, E. (1992). Organic chemistry on Titan versus terrestrial prebiotic chemistry: Exobiological implications. In ESA, Symposium on Titan, 149-160.

Raulin, F., Gazeau, M. C. and Lebreton, J. P. (2008). Latest news from Titan. Planetary and Space Science 56: 571-572.

Reh, K., Erd, C., Matson, D., Coustenis, A., Lunine, J. and Lebreton, J.-P. (2008). TSSM NASA/ESA Joint Summary Report. ESA-SRE(2008)3, JPL D-48442 NASA Task Order NMO710851.

Ricard, Y., Sramek, O., Dubuffet, F. (2009). A multi- phase model of runaway core-mantle segregation in planetary embryos. Earth Planet. Sci. Lett. 284, 144–150.

Rice, A. and Fairbridge, R.W. (1975). Thermal runaway in the mantle and neotectonics. Tectonophysics 29, 59-72.

Richardson, J. D. (1998). Thermal plasma and neutral gas in Saturn's magnetosphere. Reviews of Geophysics 36, 501-524.

Ripmeester, J.A., Tse, J.S., Ratcliffe, C.I., Powell, B.M. (1987). A new clathrate hydrate structure. Nature 325, 135-136.

Ringwood, A. E. and Anderson, D. L. (1977). Earth and Venus - A comparative study. Icarus 30, 243-253.

Rivkin, A. S., Brown, R. H., Trilling, D. E. et al. (2002). Near-Infrared Spectrophotometry of Phobos and Deimos. Icarus 156, 64-75, 2002.

Roberts, J. H. amd Nimmo, F. (2008). Tidal heating and the long-term stability of a subsurface ocean on Enceladus. Icarus 94, 675-689.

Rodriguez, S., Le Mouélic, S., Sotin, C., Clenet, H., Clark, R. N., Buratti, B., Brown, R. H., McCord, T. B., Nicholson, P. D., Baines, K. H., the VIMS Science Team (2006). Cassini/VIMS hyperspectral observations of the Huygens landing site on Titan. Planet. Spa. Sci. 54, 1510–1523.

Rodriguez S., A. Garcia, Lucas, A., Appéré, T., Le Gall, A., Reffet, E., Le Corre, L., Le Mouélic, S., Cornet, T., Courrech du Pont, S., Narteau, C., Bourgeois, O., Radebaugh, J., Arnold, K., Barnes, J. W., Sotin, C., Brown, R. H., Lorenz, R. D., Turtle, E. P. (2013). Global mapping and characterization of Titan's dune fields with Cassini: correlation between RADAR and VIMS observations. Submitted to Icarus.

Roe, H. G., de Pater, I., Gibbard, S. G., Macintosh, B. A., Max, C. E., Young, E. F., Brown, M. E. and Bouchez, A. H. (2004). A new 1.6-micron map of Titan's surface. Geophys. Res. Lett. 31, 17-20.

Rosenau, M. and Oncken, O. (2009). Fore-arc deformation controls frequency-size distribution of megathrust earthquakes in subduction zones. J. Geophys. Res. 114, B10311.

Rothery, D.A. (1999). Satellites of the Outer Planets: Worlds in their own right. Oxford University Press.

Rubin, D. M. and Hesp, P. A. (2009). Multiple origins of linear dunes on Earth and Titan. Nature Geoscience 2, 653-658.

Sachs, A. (1974). Babylonian Observational Astronomy. Philosophical Transactions for the Royal Society of London. Series A, Mathematical and Physical Sciences 276, 43-50.

Saumon, D. and Guillot, T. (2004). Shock Compression of Deuterium and the Interiors of Jupiter and Saturn. The Astrophysical Journal, 609,1170-1180.

Savage, C. J. (2011). Implications of Dune Pattern Analysis for Titan's Surface History. PhD Thesis.

Scheidegger, A. (2004). Morphotectonics. Springer, Berlin.

Schenk, P. M. and McKinnon, W. B. (2009). One-hundred-km-scale basins on Enceladus: Evidence for an active ice shell. Geophysical Research Letters 36, L16202.

Schenk, P.M. and Moore, J.M. (1995). Volcanic constructs on Ganymede and Enceladus: Topographic evidence from stereo images and photoclinometry. J. Geophys. Res. 100, 19,009-19,022.

Schenk, P.M. and Moore, J.M. (2007). Impact Crater Topography and Morphology on Saturnian Mid-Sized Satellites. 38th Lunar and Planetary Science Conference 1338, 2305.

Schenk, P.M. and Seddio, S. (2006). Geologic and Cratering History of Enceladus. Bulletin of the American Astronomical Society 38, 513.

Schenk, P. M. and Pappalardo, R. T. (2004). Topographic variations in chaos on Europa: Implications for diapiric formation. Geophysical Research Letters 31, 16703-16703.

Schenk, P., Hamilton, D.P., Johnson, R.E., McKinnon, W.B., Paranicas, C. et al. (2011). Plasma, plumes and rings: Saturn system dynamics as recorded in global color patterns on its midsize icy satellites. Icarus 211, 740–57.

Schmidt, J., Brilliantov, N., Spahn, F. and Kempf, S. (2008). Slow dust in Enceladus' plume from condensation and wall collisions in tiger stripe fractures. Nature 451, 685-688.

Schmidt, B. E., Blankenship, D. D., Patterson, G. W., Schenk, P. M. (2011). Active formation of 'chaos terrain' over shallow subsurface water on Europa. Nature 479, 502-505.

Schneider, N.M., Burger, M.H., Schaller, E.L., Brown, M.E., Johnson, R.E. et al. (2009). No sodium in the vapour plumes of Enceladus. Nature 459, 1102–4.

Schubert, G., Anderson, J.D., Spohn, T., McKinnon, W.B. (2004). Interior composition, structure and dynamics of the Galilean satellites. In: Jupiter. The planet, satellites and magnetosphere. Cambridge planetary science 1, 281 - 306.

Schubert, G., Anderson, J.D., Travis, B.J., Palguta, J. (2007). Enceladus: present internal structure and differentiation by early and long-term radiogenic heating. Icarus 188, 345–55.

Schubert, G., Hussmann, H., Lainey, V., Matson, D. L., McKinnon, W. B., Sohl, F., Sotin, C., Tobie, G., Turrini, D., van Hoolst, T. (2010). Evolution of Icy Satellites. Space Science Reviews 153, 447-484.

Sears, J.W. (1990). Geological structure of the Grand Canyon Supergroup. Grand Canyon Geology, University Press, 71–82.

Shemansky, D.E., Matheson, P., Hall, D.T., Hu, H.-Y., Tripp, T.M. (1993). Detection of the hydroxyl radical in the Saturn magnetosphere. Nature 363, 329–331.

Shemansky, D. E., Stewart, A. I. F., West, R. A., Esposito, L. W., Hallett, J. T. and Liu, X. (2005). The Cassini UVIS Stellar Probe of the Titan Atmosphere. Science 308, 978-982.

Showman, A. P. and Han, L. (2004). Numerical simulations of convection in Europa's ice shell: Implications for surface features. Journal of Geophysical Research 109, E01010.

Showman, A. P. and Malhorta, R. (1999). The Galilean satellites. Science 296, 77 – 84.

Simon, S., Wennmacher, A., Neubauer, F. M., Bertucci, C. L., Kriegel, H., Saur, J., Russell, C. T. and Dougherty, M. K. (2010). Titan's highly dynamic magnetic environment: A systematic survey of

Cassini magnetometer observations from flybys TA, T62. Planetary and Space Science 58, 1230-1251.
Singh, A. and Harrison, A. (1985). Standardized Principal Components, Inl. J. Remote Sensing, 6, 885-8S6.
Smith, B. A., Soderblom, L., Batson, R., Bridges, P., Inge, J. A. Y., Masursky, H., Shoemaker, E., Beebe, R., Boyce, J., Briggs, G., Bunker, A., Collins, S. A., Hansen, C. J., Johnson, T. V., Mitchell, J. L., Terrile, R. J., Cook, A. F., Cuzzi, J., Pollack, J. B., Danielson, G. E., Ingersoll, A. P., Davies, M. E., Hunt, G. E., Morrison, D., Owen, T., Sagan, C., Veverka, J., Strom, R., Suomi, V.E. (1982). A New Look at the Saturn System: The Voyager 2 Images. Science 215, 504-537.
Smith, D.E., Turtle, E.P., Melosh, H.J., Bray, V.J. (2007). Viscous relaxation of craters on Enceladus. Lunar Planet. Sci. XXXVIII. Abst. #2237.
Smith, L. I. (2002). A tutorial on principal components analysis. Cornell University, USA, 51, 52.
Smith, P. H. (1980). The radius of Titan from Pioneer Saturn data. Journal of Geophysical Research 85, 5943-5947.
Smith, P. H., Lemmon, M. T., Lorenz, R. D., Sromovsky, L. A., Caldwell, J. J., Allison, M. D. (1996). Titan's Surface, Revealed by HST Imaging. Icarus 119, 336-349.
Soderblom, L. A., Becker, T. L., Kieffer, S. W., Brown, R. H., Hansen, C. J., Johnson, T. V. (1990). Triton's geyser-like plumes - Discovery and basic characterization. Science 250, 410-415.
Soderblom, L. A., R. L. Kirk, J. I. Lunine, J. A. Anderson, K. Baines, J. Barnes, J. Barrett, R. Brown, B. Buratti, R. Clark, D. Cruikshank, C. Elachi, M. Janssen, R. Jaumann, E. Karkoschka, S. Le Mouélic, R. Lopes, R. Lorenz, T. McCord, P. Nicholson, J. Radebaugh, B. Rizk, C. Sotin, E. Stofan, T. Sucharski, M. Tomasko, and S. Wall (2007a). Correlations between Cassini VIMS spectra and RADAR SAR images: Implications for Titan's surface composition and the character of the Huygens Probe Landing Site. Planet. Space Sci. 55, 2025–2036.
Soderblom, L.A., Tomasko, M.G., Archinal, B.A., Becker, T.L., Bushroe, M.W., Cook, D.A., Doose, L.R., Galuszka, D.M., Hare, T.M., Howington-Kraus, E., Karkoschka, E., Kirk, R.L., Lunine, J.I., McFarlane, E.A., Redding, B.L., Bashar, R., Rosiek, M.R., See, C., Smith, P.H., (2007b). Topography and geomorphology of the Huygens landing site on Titan. Planetary and Space Science 55, 2015-2024.
Soderblom, L.A., Brown, R.H., Soderblom, J.M., Barnes, J.W., Kirk, R.L., Sotin, C., Jaumann, R., Mackinnon, d.J., Mackowski, D.W., Baines, K.H., Buratti, B.J., Clark, R.N., Nicholson, P.D. 2009. The geology of Hotei Regio, Titan: Correlation of Cassini VIMS and RADAR. Icarus 204, 610-618.
Sohl, F., Hussmann, H., Schwentker, B., Spohn, T. and Lorenz, R. D. (2003). Interior structure models and tidal Love numbers of Titan. Journal of Geophysical Research (Planets) 108, 5130.
Sohl, F., Solomonidou, A., Wagner, F. W., Coustenis, A., Hussmann, H., Schulze-Makuch. D. (2013). Tidal stresses on Titan and implications for its geology and habitability. Submitted for publication.
Solomatov, V.S. (1995). Scaling of temperature- and stress-dependent viscosity convection. Phys. Fluids 7, 266–274.
Solomonidou, A., Bampasidis, G., Kyriakopoulos, K., Bratsolis, E., Hirtzig, M., Coustenis, A. and Moussas, X. (2010). Imaging of potentially active geological regions on Saturn's moons Titan and Enceladus, using Cassini-Huygens data: With emphasis on cryovolcanism. Hellenic Journal of Geosciences 45, 257-268.
Solomonidou, A., Coustenis, A., Bampasidis, G., Kyriakopoulos, K., Moussas, X., Bratsolis, E. and Hirtzig, M. (2011). Water Oceans of Europa and Other Moons: Implications For Life in Other Solar Systems. Journal of Cosmology 13, 4191-4211.
Solomonidou, A., Moussas, X., Coustenis, A., Lebreton, J. P., Bampasidis, G., Kyriakopoulos, K., Kouloumvakos, A., Xystouris, G., Sigala, E. and Patsou, I. (2012). Cassini Scientist for a Day: an international contest in Greece. EGU General Assembly, 22-27 April, Vienna, Austria.
Solomonidou, A., Bampasidis, G., Hirtzig, M., Coustenis, A., Kyriakopoulos, K., St. Seymour, K., Bratsolis, E., Moussas, X. (2013a). Morphotectonic features on Titan and their possible origin. Planetary and Space Science 77, 104-117.
Solomonidou, A., Hirtzig, M., Coustenis, A., Bratsolis, E., Le Mouélic, S., Rodriguez, S., Stephan, K., Drossart, P., Sotin, C., Jaumann, R., Brown, R.H., Kyriakopoulos, K., Lopes, R.M.C., Bampasidis, G., Stamatelopoulou-Seymour, K., Moussas, X. (2013b). Surface albedo spectral properties of geologically interesting areas on Titan. Submitted for publication.
Solomonidou, A., Coustenis, A., Hirtzig, M., Rodriguez, S., Stephan, K., Le Mouélic, S., Drossart, P., Bratsolis, E., Jaumann, R., Lopes, R.M.C., Kyriakopoulos, K., Sotin, C., Brown, R.H. (2013c). Temporal variations of Titan's surface regions with Cassini/VIMS. Submitted for publication.
Solomonidou, A., Coustenis, A., Jaumann, R., Stephan, K., Sohl, F., Hussmann, H., Hirtzig, M., Bampasidis, G., Bratsolis, E., Moussas, X., Kyriakopoulos, K. (2013d). Candidate regions on Titan as promising landing sites for future in situ missions. Submitted for publication.

Sotin, C., Jaumann, R., Buratti, B. J., Brown, R. H., Clark, R. N., Soderblom, L. A., Baines, K. H., Bellucci, G., Bibring, J. P., Capaccioni, F., Cerroni, P., Combes, M., Coradini, A., Cruikshank, D. P., Drossart, P., Formisano, V., Langevin, Y., Matson, D. L., McCord, T. B., Nelson, R. M., Nicholson, P. D., Sicardy, B., Lemouelic, S., Rodriguez, S., Stephan, K. and Scholz, C. K. (2005). Release of volatiles from a possible cryovolcano from near-infrared imaging of Titan. Nature 435, 786-789.

Sotin, C., Le Mouélic, S., Brown, R. H., Barnes, J., Soderblom, L., Jaumann, R., Buratti, B. J., Clark, R. N., Baines, K. H., Nelson, R. M., Nicholson, P., the VIMS Science team (2007). Cassini VIMS observation of Titan during flyby T20. Lunar and Planetary Science XXXVIII, 2444.

Sotin, C., Mielke, R., Choukroun, M., Neish, C., Barmatz, M., Castillo, J., Lunine, J., Mitchell, K. (2009). Ice-Hydrocarbon Interactions Under Titan-like Conditions: Implications for the Carbon Cycle on Titan. 40th Lunar and Planetary Science Conference, (Lunar and Planetary Science XL), 2088.

Sotin, C., Lawrence, K. J., Reinhardt, B., Barnes, J. W., Brown, R. H., Hayes, A. G., Le Mouélic, S., Rodriguez, S., Soderblom, J. M., Soderblom, L. A., Baines, K. H., Buratti, B. J., Clark, R. N., Jaumann, R., Nicholson, P. D., Stephan, K. (2012). Observations of Titan's Northern lakes at 5 μm: Implications for the organic cycle and geology. Icarus 221, 768-786.

Spahn, F., Schmidt, J., Albers, N., Kempf, S., Krivov, A. V., Sremcevic, M. (2006). Dust Sources of Saturn's E Ring. European Planetary Science Congress 2006. Berlin, Germany, 18 - 22 September 2006, 533.

Spencer, J. R., Pearl, J. C., Segura, M., Flasar, F. M., Mamoutkine, A., Romani, P., Buratti, B. J., Hendrix, A. R., Spilker, L. J., Lopes, R. M. C. (2006). Cassini Encounters Enceladus: Background and the Discovery of a South Polar Hot Spot. Science 311, 1401-1405.

Spencer, J.R., Barr, A.C., Esposito, L.W., Helfenstein, P., Ingersoll, A.P. et al. (2009). Enceladus: an active cryovolcanic satellite, 683–724.

Spencer, J.R., Howett, C.J.A., Verbiscer, A.J., Hurford, T.A., Segura, M.E., Pearl, J.C. (2011). High-resolution observations of thermal emission from the south pole of Enceladus. Presented at Lunar Planet. Sci. Conf., 42nd, The Woodlands, Tex. (LPI Contrib. 1608, Abstr. 2553).

Spencer, J. and Grinspoon, D. (2007). Planetary science: Inside Enceladus. Nature 445, 376-377.

Spencer, J. R. and Nimmo, F. (2013). Enceladus: An Active Ice World in the Saturn System. Annual Review of Earth and Planetary Sciences 41, 693-717.

Spitale, J.N., Porco, C.C. (2007). Association of the jets of Enceladus with the warmest regions on its south polar fractures. Nature 449, 695–97.

Spohn, T. and Schubert, G. (2003). Oceans in the icy Galilean satellites of Jupiter? Icarus 161, 456-467.

Squyres, S. W., Reynolds, R. T., Cassen, P. M. (1983). The evolution of Enceladus. Saturn Conference 53, 319-331.

Srama, R., Ahrens, T. J., Altobelli, N., Auer, S., Bradley, J. G., Burton, M., Dikarev, V. V., Economou, T., Fechtig, H., Gurlich, M., Grande, M., Graps, A., Grun, E., Havnes, O., Helfert, S., Horanyi, M., Igenbergs, E., Jessberger, E. K., Johnson, T. V., Kempf, S., Krivov, A. V., Kruger, H., Mocker-Ahlreep, A., Moragas-Klostermeyer, G., Lamy, P., Landgraf, M., Linkert, D., Linkert, G., Lura, F., McDonnell, J. A. M., Muhlmann, D., Morfill, G. E., Muller, M., Roy, M., SchΓ¤fer, G., Schlotzhauer, G., Schwehm, G. H., Spahn, F., Stubig, M., Svestka, J., Tschernjawski, V., Tuzzolino, A. J., Wusch, R. and Zook, H. A. (2004). The Cassini Cosmic Dust Analyzer. Space Science Reviews 114, 465-518.

Sromovsky, L. A., Suomi, V. E., Pollack, J. B., Krauss, R. J., Limaye, S. S., Owen, T., Revercomb, H. E., Sagan, C. (1981). Implications of Titan's north-south brightness asymmetry. Nature 292, 698-702.

Stark, B. and Bernstein, J. (1999). Reliability Overview. In MEMS Reliability Assurance Guidelines for Space Applications (ed. B. Stark), JPL Publication 99-1.

Stephan, K., Hibbitts, C. A., Hoffmann, H., Jaumann. R. (2008). Reduction of instrument-dependent noise in hyperspectral image data using the principal component analysis: Applications to Galileo NIMS data. Planet. Space Sci. 56, 406-419.

Stephan, K., Jaumann, R., Karkoschka, E., Kirk, R. L., Barnes, J. W., Tomasko, M. G., Turtle, E. P., Corre, L. L., Langhans, M., Mouelic, S. L., Lorenz, R. D. and Perry, J. (2009). Mapping Products of Titan's Surface. Titan from Cassini-Huygens. R. H. Brown, J.-P. Lebreton and J. H. Waite, Springer, 489-489.

Stevenson, R.J. (1987). An evolutionary framework for the Jovian and Saturnian satellites. Earth, Moon and Planets 39, 225-236.

Stevenson, D. J. (1992). Interior of Titan. In ESA, Symposium on Titan (SEE N92-32348 23-91).

Stiles, B. W., Kirk, R. L., Lorenz, R. D., Hensley, S., Lee, E., Ostro, S. J., Allison, M. D., Callahan, P. S., Gim, Y., Iess, L., del Marmo, P. P., Hamilton, G., Johnson, W. T. K., West, R. D. and Cassini Radar Team, T. (2008). DETERMINING TITAN'S SPIN STATE FROM CASSINI RADAR IMAGES. The Astronomical Journal 135, 1669-1680.

Stiles, B. W., Hensley, S., Gim, Y., Bates, D. M., Kirk, R. L., Hayes, A., Radebaugh, J., Lorenz, R. D., Mitchell, K. L., Callahan, P. S., Zebker, H., Johnson, W. T. K., Wall, S., Lunine, J. I., Wood, C. A., Janssen, M., Pelletier, F., West, R. D., Veeramacheneni, C., The Radar Team (2009). Determining Titan surface topography from Cassini SAR data. Icarus 202, 584-598.

Stofan, E. R., Lunine, J. I., Lopes, R., Paganelli, F., Lorenz, R. D., Wood, C. A., Kirk, R., Wall, S., Elachi, C., Soderblom, L. A., Ostro, S., Janssen, M., Radebaugh, J., Wye, L., Zebker, H., Anderson, Y., Allison, M., Boehmer, R., Callahan, P., Encrenaz, P., Flamini, E., Francescetti, G., Gim, Y., Hamilton, G., Hensley, S., Johnson, W. T. K., Kelleher, K., Muhleman, D., Picardi, G., Posa, F., Roth, L., Seu, R., Shaffer, S., Stiles, B., Vetrella, S. and West, R. (2006). Mapping of Titan: Results from the first Titan radar passes. Icarus 185, 443-456.

Stofan, E. R., Elachi, C., Lunine, J. I., Lorenz, R. D., Stiles, B., Mitchell, K. L., Ostro, S., Soderblom, L., Wood, C., Zebker, H., Wall, S., Janssen, M., Kirk, R., Lopes, R., Paganelli, F., Radebaugh, J., Wye, L., Anderson, Y., Allison, M., Boehmer, R., Callahan, P., Encrenaz, P., Flamini, E., Francescetti, G., Gim, Y., Hamilton, G., Hensley, S., Johnson, W. T. K., Kelleher, K., Muhleman, D., Paillou, P., Picardi, G., Posa, F., Roth, L., Seu, R., Shaffer, S., Vetrella, S. and West, R. (2007). The lakes of Titan. Nature 445: 61-64.

Stofan, E. R., Lunine, J. I., Lorenz, R. D., Aharonson, O., Bierhaus, E., Clark, B., Griffith, C., Harri, A. M., Karkoschka, E., Kirk, R., Kantsiper, B., Mahaffy, P., Newman, C., Ravine, M., Trainer, M., Waite, H. and Zarnecki, J. (2011). Exploring the Seas of Titan: The Titan Mare Explorer (TiME) Mission. 41st Lunar and Planetary Science Conference, The Woodlands, Texas.

Strobel, D. F. (1974). The Photochemistry of Hydrocarbons in the Atmosphere of Titan. Icarus 21, 466-466.

Strobel, D. F., Atreya, S. K., Bezard, B., Ferri, F., Flasar, F. M., Fulchignoni, M., Lellouch, E. and Muller-Wodarg, I. (2009). Atmospheric Structure and Composition. Titan from Cassini-Huygens. B. R., 235-257.

Teanby, N. A., Irwin, P. G. J., de Kok, R., Nixon, C. A., Coustenis, A., Royer, E., Calcutt, S. B., Bowles, N. E., Fletcher, L., Howett, C. and Taylor, F. W. (2008). Global and temporal variations in hydrocarbons and nitriles in Titan's stratosphere for northern winter observed by Cassini/CIRS. Icarus 193, 595-611.

Teanby, N. A., Irwin, P. G. J., de Kok, R. and Nixon, C. A. (2009). Dynamical implications of seasonal and spatial variations in Titan's stratospheric composition. Royal Society of London Philosophical Transactions Series A 367, 697-711.

Terrile, R. J., Cook, A. F. (1981). Enceladus: Evolution and Possible Relationship to Saturn's E-Ring. Lunar and Planetary Science XII, LPI Contribution 428, published by the Lunar and Planetary Institute, 3303 Nasa Road 1, Houston, TX 77058, 1981, p.10.

Thekaekara, M. P. (1973). The Extraterrestrial Solar Spectrum. A.J Drummond and M.P. Thekaekara, Eds. Institute of Environmental Sciences, Mount Prospect Illinois, 71-133.

Thomas, P.C. (2010). Sizes, shapes and derived properties of the Saturnian satellites after the Cassini nominal mission. Icarus 208, 395–401.

Thomas-Osip, J. E., Gustafson, B. Å. S., Kolokolova, L., Xu, Y.-L. (2005). An investigation of Titan's aerosols using microwave analog measurements and radiative transfer modeling. Icarus 179, 511-522.

Thommes, E. W., Duncan, M. J., and Levison, H. F. (1999). The formation of Uranus and Neptune in the Jupiter-Saturn region of the Solar System. Nature, 402, 635.

Tian, F., Stewart, A.I.F., Toon, O.B., Larsen, K.W., Esposito, L.W. (2007). Monte Carlo simulations of the water vapor plumes on Enceladus. Icarus 188, 154-161.

Tobie, G., Grasset, O., Lunine, J. I., Mocquet, A. and Sotin, C. (2005). Titan's internal structure inferred from a coupled thermal-orbital model. Icarus 175, 496-502.

Tobie, G., Lunine, J. I. and Sotin, C. (2006). Episodic outgassing as the origin of atmospheric methane on Titan. Nature 440, 61-64.

Tobie, G., Čadek, O. and Sotin, C. (2008). Solid tidal friction above a liquid water reservoir as the origin of the south pole hotspot on Enceladus. Icarus 196, 642-652.

Tobie, G., Lunine, J. I., Monteux, J., Mousis, O., Nimmo, F. (2010a).The Origin and Evolution of Titan. Titan from Cassini-Huygens. Springer Science+Business Media B.V., 35.

Tobie, G., Giese, B., Hurford, T. A., Lopes, R. M., Nimmo, F., Postberg, F., Retherford, K. D., Schmidt, J., Spencer, J. R., Tokano, T. and Turtle, E. P. (2010b). Surface, Subsurface and Atmosphere Exchanges on the Satellites of the Outer Solar System. Space Science Reviews 153, 375-410.

Tobie, G., Gautier, D., Hersant, F. (2012). Titan's Bulk Composition Constrained By Cassini-Huygens: Implication For Internal Outgassing. The Astrophysical Journal 752, 125-135.

Tobie, G. and Teanby, N. (2013). The science goals and mission concept for a future exploration of Titan and Enceladus. White paper submitted to ESA for the definition of the L2 and L3 missions in the ESA Science Programme.

Tokano, T. (2009). Limnological Structure of Titan's Hydrocarbon Lakes and Its Astrobiological Implication. Astrobiology 9, 147-164.
Tokano, T., 2011. Precipitation Climatology on Titan. Science 331, 1393-1394.
Tokano, T., McKay, C. P., Neubauer, F. M., Atreya, S. K., Ferri, F., Fulchignoni, M., Niemann, H. B. (2006). Methane drizzle on Titan. Nature 442, 432-435.
Tomasko, M. G., Smith, P. H. (1982). Photometry and polarimetry of Titan - Pioneer 11 observations and their implications for aerosol properties. Icarus 51, 65-95.
Tomasko, M. G., Doose, L.R., Smith, P.H., West, R.A., Soderblom, L.A., Combes, M., Bézard, B., Coustenis, A., de Bergh, C., Lellouch, E., Rosenqvist, J., Saint-Pe, O., Schmitt, B., Keller, H. U., Thomas, N., Gliem, F. (1997). The Descent Imager/spectral Radiometer Aboard Huygens. Huygens: Science, Payload and Mission, Proceedings of an ESA conference. Edited by A. Wilson, 109.
Tomasko, M. G., Buchhauser, D., Bushroe, M., Dafoe, L. E., Doose, L. R., Eibl, A., Fellows, C., Farlane, E. M., Prout, G. M., Pringle, M. J., Rizk, B., See, C., Smith, P. H. and Tsetsenekos, K. (2002). The Descent Imager/Spectral Radiometer (DISR) Experiment on the Huygens Entry Probe of Titan. Space Science Reviews 104, 469-551.
Tomasko, M. G., Archinal, B., Becker, T., Bézard, B., Bushroe, M., Combes, M., Cook, D., Coustenis, A., de Bergh, C., Dafoe, L. E., Doose, L., Douté, S., Eibl, A., Engel, S., Gliem, F., Grieger, B., Holso, K., Howington-Kraus, E., Karkoschka, E., Keller, H. U., Kirk, R., Kramm, R., Küppers, M., Lanagan, P., Lellouch, E., Lemmon, M., Lunine, J., McFarlane, E., Moores, J., Prout, G. M., Rizk, B., Rosiek, M., Rueffer, P., Schröder, S. E., Schmitt, B., See, C., Smith, P., Soderblom, L., Thomas, N. and West, R. (2005). Rain, winds and haze during the Huygens probe's descent to Titan's surface. Nature 438, 765 - 778.
Tomasko, M. G., Bezard, B., Doose, L., Engel, S., Karkoschka, E. and Vinatier, S. (2008). Heat balance in Titan's atmosphere. Planetary and Space Science 56, 648-659.
Tomasko, M. G., Doose, L. R., Dafoe, L. E., See, C. (2009). Limits on the size of aerosols from measurements of linear polarization in Titan's atmosphere. Icarus 204, 271-283.
Toon, O. B., McKay, C. P., Courtin, R. and Ackerman, T. P. (1988). Methane rain on Titan. Icarus 75, 255-284.
Tso, M. and Mather, P. M. (2009). Classification Methods for Remotely Sensed Data. CRC Press.
Toublanc, D., Parisot, J. P., Brillet, J., Gautier, D., Raulin, F. and McKay, C. P. (1995). Photochemical modeling of Titan's atmosphere. Icarus 113, 2-26.
Trinks, H., Schröder, W., Biebricher, C. (2005). Ice And The Origin Of Life. Origins of Life and Evolution of Biospheres 35, 429-445.

Turtle, E. P., Perry, J. E., McEwen, A. S., West, R. A., Del Genio, A. D., Barbara, J., Dawson, D. D. and Porco, C. C. (2008). Cassini Imaging Observations of Titan's High-Latitude Lakes. Bull. Amer. Astron. Soc. 40, 428-428.
Turtle, E. P., Perry, J. E., McEwen, A. S., DelGenio, A. D., Barbara, J., West, R. A., Dawson, D. D. and Porco, C. C. (2009). Cassini imaging of Titan's high-latitude lakes, clouds, and south-polar surface changes. Geophysical Research Letters 36, 02204-02204.
Turtle, E. P., Perry, J. E., Hayes, A. G., McEwen, A. S (2011a). Shoreline retreat at Titan's Ontario Lacus and Arrakis Planitia from Cassini Imaging Science Subsystem observations. Icarus 212, 957-959.
Turtle, E. P., Perry, J. E., Hayes, A. G., Lorenz, R. D., Barnes, J. W., McEwen, A. S., West, R. A., Del Genio, A. D., Barbara, J. M., Lunine, J. I., Schaller, E. L., Ray, T. L., Lopes, R. M. C. and Stofan, E. R. (2011b). Rapid and Extensive Surface Changes Near Titan's Equator: Evidence of April Showers. Science 331, 1414-1417.
Verbiscer, A., French, R., Showalter, M., Helfenstein, P. (2007). Science 315, 815.
Vinatier, S., Bezard, B., Fouchet, T., Teanby, N. A., de Kok, R., Irwin, P. G. J., Conrath, B. J., Nixon, C. A., Romani, P. N., Flasar, F. M. and Coustenis, A. (2007). Vertical abundance profiles of hydrocarbons in Titan's atmosphere at 15ºS and 80ºN retrieved from Cassini/CIRS spectra. Icarus 188: 120-138.
Vinatier, S., Bezard, B., de Kok, R., Anderson, C. M., Samuelson, R. E., Nixon, C. A., Mamoutkine, A., Carlson, R. C., Jennings, D. E., Guandique, E. A., Bjoraker, G. L., Michael Flasar, F. and Kunde, V. G. (2010). Analysis of Cassini/CIRS limb spectra of Titan acquired during the nominal mission II: Aerosol extinction profiles in the 600-1420 cm-1 spectral range. Icarus 210, 852-866.
Vixie, G., Barnes, J. W., Bow, J., Le Mouélic, S., Rodriguez, S., Brown, R. H., Cerroni, P., Tosi, F., Buratti, B., Sotin, C., Filacchione, G., Capaccioni, F., Coradini, A (2012). Mapping Titan's surface features within the visible spectrum via Cassini VIMS. Planet. Space Sci. 60, 52-61.
Vuitton, V., Yelle, R. V. and McEwan, M. J. (2007). Ion chemistry and N-containing molecules in Titan's upper atmosphere. Icarus 191, 722-742.

Vuitton, V., Yelle, R. V. and Cui, J. (2008). Formation and distribution of benzene on Titan. Journal of Geophysical Research (Planets) 113, 05007-05007.

Waite, J. H., Lewis, W. S., Kasprzak, W. T., Anicich, V. G., Block, B. P., Cravens, T. E., Fletcher, G. G., Ip, W. H., Luhmann, J. G., McNutt, R. L., Niemann, H. B., Parejko, J. K., Richards, J. E., Thorpe, R. L., Walter, E. M. and Yelle, R. V. (2004). The Cassini Ion and Neutral Mass Spectrometer (INMS) Investigation. Space Science Reviews 114, 113-231.

Waite, J. H., Combi, M. R., Ip, W.-H., Cravens, T. E., McNutt, R. L., Kasprzak, W., Yelle, R., Luhmann, J., Niemann, H., Gell, D., Magee, B., Fletcher, G., Lunine, J. and Tseng, W.-L. (2006). Cassini Ion and Neutral Mass Spectrometer: Enceladus Plume Composition and Structure. Science 311, 1419-1422.

Waite, J. H., Young, D. T., Cravens, T. E., Coates, A. J., Crary, F. J., Magee, B. and Westlake, J. (2007). The Process of Tholin Formation in Titan's Upper Atmosphere." Science 316, 870-875.

Waite, J. H., Lewis, W. S., Magee, B. A., Lunine, J. I., McKinnon, W. B., Glein, C. R., Mousis, O., Young, D. T., Brockwell, T., Westlake, J., Nguyen, M. J., Teolis, B. D., Niemann, H. B., McNutt, R. L., Perry, M. and Ip, W. H. (2009). Liquid water on Enceladus from observations of ammonia and 40Ar in the plume. Nature 460, 487-490.

Waite, J. H., Brockwell, T., Elliot, J., Reh, K., Spencer, J. and Outer Planets Satellites Decadal, S. (2010). Titan Lake Probe: The Ongoing NASA Decadal Study Preliminary Report. EGU General Assembly, 2-7 May, Vienna, Austria 12, 14762.

Walessa, M. and Datcu, M. (2000). Model-based despeckling and information extraction from SAR images. IEEE Transactions on Geoscience and Remote Sensing 38, 2258-2269.

Wall, S. D., Lopes, R. M. C., Stofan, E. R., Wood, C. A., Radebaugh, J. L., Horst, S. M., Stiles, B. W., Nelson, R. M., Kamp, L. W., Janssen, M. A., Lorenz, R. D., Lunine, J. I., Farr, T. G., Mitri, G., Paillou, P., Paganelli, F., Mitchell, K. L. (2009). Cassini RADAR images at Hotei Arcus and western Xanadu, Titan: Evidence for geologically recent cryovolcanic activity. Geophys. Res. Lett. 36, L04203.

Wall, S., Hayes, A., Bristow, C., Lorenz, R., Stofan, E., Lunine, J., Le Gall, A., Janssen, M., Lopes, R., Wye, L., Soderblom, L., Paillou, P., Aharonson, O., Zebker, H., Farr, T., Mitri, G., Kirk, R., Mitchell, K., Notarnicola, C., Casarano, D. and Ventura, B. (2010). Active shoreline of Ontario Lacus, Titan: A morphological study of the lake and its surroundings. Geophysical Research Letters 37, 5.

Wang, L., Kassi, S., Campargue, A. (2010a). Temperature dependence of the absorption spectrum of CH4 by high resolution spectroscopy at 81 K: (I) The region of the 2n3 band at 1.66 mm. J. Quant. Spectrosc. Radiat. Trans. 111, 1130-1140.

Wang, L., Kassi, S., Liu, A. W., Hu, S. M., Campargue, A. (2010b). High sensitivity absorption spectroscopy of methane at 80 K in the 1.58-μm transparency window: temperature dependence and importance of the CH3D contribution. J. Mol. Spectrosc. 261, 41-52.

Wang, L., Kassi, S., Liu, A. W., Hu, S. M., Campargue, A. (2011). The 1.58-μm transparency window of methane (6150-6750 cm-1): Empirical line list and temperature dependence between 80 K and 296 K. J. Quant. Spectrosc. Radiat. Trans. 112, 937-951.

Wang, L., Mondelain, D., Kassi, S., Campargue, A. (2012). The absorption spectrum of methane at 80 K and 294 K in the icosad (6717–7589 cm-1): Improved empirical line lists, isotopologue identification and temperature dependence. J. Quant. Spectrosc. Radiat. Trans. 113, 47–57.

Wasiak, F. C., Androes, D., Blackburn, D. G., Tullis, J. A., Dixon, J., Chevrier, V. F. (2013). A geological characterization of Ligeia Mare in the northern polar region of Titan. Planetary and Space Science 84, 141-147.

Weidenschilling, S. J. (1977). The distribution of mass in the planetary system and solar nebula. Astrophysics and Space Science 51, 153-158.

Wellman, J. B., Duval, J., Juergens, D., Voss, J. (1987). Visible and infrared maping spectrometer (VIMS): a facility instrument for planetary missions. Conference on Imaging Spectroscopy, 213 – 221.

Williams, D.A., Radebaugh, J., Lopes, R.M.C., Stofan, E. (2011). Geomorphologic mapping of the Menrva region of Titan using Cassini RADAR data. Icarus 212, 744-750.

Wilson, E. H. and Atreya, S. K. (2004). Current state of modeling the photochemistry of Titan's mutually dependent atmosphere and ionosphere. Journal of Geophysical Research (Planets) 109, 06002-06002.

Witasse, O., Lebreton, J.-P., Bird, M. K., Dutta-Roy, R., Folkner, W. M., Preston, R. A., Asmar, S. W., Gurvits, L. I., Pogrebenko, S. V., Avruch, I. M., Campbell, R. M., Bignall, H. E., Garrett, M. A., van Langevelde, H. J., Parsley, S. M., Reynolds, C., Szomoru, A., Reynolds, J. E., Phillips, C. J., Sault, R. J., Tzioumis, A. K., Ghigo, F., Langston, G., Brisken, W., Romney, J. D., Mujunen, A., Ritakari, J., Tingay, S. J., Dodson, R. G., van't Klooster, C. G. M., Blancquaert, T., Coustenis, A., Gendron, E., Sicardy, B., Hirtzig, M., Luz, D., Negrao, A., Kostiuk, T., Livengood, T. A.,

Hartung, M., de Pater, I., Adamkovics, M., Lorenz, R. D., Roe, H., Schaller, E., Brown, M., Bouchez, A. H., Trujillo, C. A., Buratti, B. J., Caillault, L., Magin, T., Bourdon, A., Laux, C. (2006). Overview of the coordinated ground-based observations of Titan during the Huygens mission. Journal of Geophysical Research (Planets) 111, E07S01.

Wood, C. A., Lorenz, R., Kirk, R., Lopes, R., Mitchell, K., Stofan, E. and Cassini, R. T. (2010). Impact craters on Titan. Icarus 206, 334-344.

Wye, L. C., Zebker, H. A. and Lorenz, R. D. (2009). Smoothness of Titan's Ontario Lacus: Constraints from Cassini RADAR specular reflection data. Geophysical Research Letters 36,16.

Wyrick, D.Y., Buczkowski, D.L., Bleamaster, L.F., Collins, G.C. (2010). Pit Crater Chains Across the Solar System. 41st Lunar and Planetary Science Conference 1533, 1413.

Young, R. S. (1973). The beginning of comparative planetology. Space life Sciences 4, 505-515.

Young, D. T., Berthelier, J. J., Blanc, M., Burch, J. L., Coates, A. J., Goldstein, R., Grande, M., Hill, T. W., Johnson, R. E., Kelha, V., McComas, D. J., Sittler, E. C., Svenes, K. R., SzegΓ¶, K., Tanskanen, P., Ahola, K., Anderson, D., Bakshi, S., Baragiola, R. A., Barraclough, B. L., Black, R. K., Bolton, S., Booker, T., Bowman, R., Casey, P., Crary, F. J., Delapp, D., Dirks, G., Eaker, N., Funsten, H., Furman, J. D., Gosling, J. T., Hannula, H., Holmlund, C., Huomo, H., Illiano, J. M., Jensen, P., Johnson, M. A., Linder, D. R., Luntama, T., Maurice, S., McCabe, K. P., Mursula, K., Narheim, B. T., Nordholt, J. E., Preece, A., Rudzki, J., Ruitberg, A., Smith, K., Szalai, S., Thomsen, M. F., Viherkanto, K., Vilppola, J., Vollmer, T., Wahl, T. E., WΓOest, M., Ylikorpi, T. and Zinsmeyer, C. (2004). Cassini Plasma Spectrometer Investigation. Space Science Reviews 114, 1-112.

Yung, Y. L., Allen, M. and Pinto, J. P. (1984). Photochemistry of the atmosphere of Titan - Comparison between model and observations. Astrophysical Journal Supplement Series 55, 465-506.

Zahnle, K., Pollack, J. B., Grinspoon, D., Dones, L. (1992). Impact-generated atmospheres over Titan, Ganymede, and Callisto. Icarus 95, 1-23.

Zarnecki, J. C., Leese, M. R., Garry, J. R. C., Ghafoor, N. and Hathi, B. (2002). Huygens' Surface Science Package. Space Science Reviews 104, 593-611.

Zarnecki, J. C., Leese, M. R., Hathi, B., Ball, A. J., Hagermann, A., Towner, M. C., Lorenz, R. D., McDonnell, J. A. M., Green, S. F., Patel, M. R., Ringrose, T. J., Rosenberg, P. D., Atkinson, K. R., Paton, M. D., Banaszkiewicz, M., Clark, B. C., Ferri, F., Fulchignoni, M., Ghafoor, N. A. L., Kargl, G., Svedhem, H., Delderfield, J., Grande, M., Parker, D. J., Challenor, P. G., Geake, J. E. (2005). A soft solid surface on Titan as revealed by the Huygens Surface Science Package. Nature 438, 792-795.

Zimmer, C., Khurana, K.K., Kivelson, M.G. (2000). Subsurface Oceans on Europa and Callisto: Constraints from Galileo Magnetometer Observations. Icarus 147, 329-347.

Zolotov, M.Y. (2007). An oceanic composition on early and today's Enceladus. Geophys. Res. Lett. 34, L23203.